Agriculture Automation and Control

Minzan Li
Chenghai Yang
Qin Zhang *Editors*

Soil and Crop Sensing for Precision Crop Production

Springer

Agriculture Automation and Control

Series Editor
Qin Zhang, CPAAS
Washington State University
Prosser, WA, USA

The ultimate goal of agricultural research and technology development is to help farmers produce sufficient foods, feeds, fibers, or biofuels while at the same time, minimize the environmental impacts caused by these large scale activities. Automation offers a potential means by which improved productivity, resource optimization, and worker health and safety, can be accomplished. Although research on agricultural automation can be found in the published literature, there lacks a curated source of reference that is devoted to the unique characteristics of the agricultural system. This book series aims to fill the gap by bringing together scientists, engineers, and others working in these areas, and from around the world, to share their success stories and challenges. Individual book volume will have a focused theme and will be guest-edited by researchers/scientists renowned for their work within the respective sub-discipline.

Minzan Li • Chenghai Yang • Qin Zhang
Editors

Soil and Crop Sensing for Precision Crop Production

Springer

Editors
Minzan Li
College of Information and Electrical Engineering
China Agricultural University
Haidian, Beijing, China

Chenghai Yang
Agricultural Research Service
United States Department of Agriculture
College Station, TX, USA

Qin Zhang
Center for Precision and Automated Agricultural Systems
Washington State University
Prosser, WA, USA

ISSN 2731-3492 ISSN 2731-3506 (electronic)
Agriculture Automation and Control
ISBN 978-3-030-70431-5 ISBN 978-3-030-70432-2 (eBook)
https://doi.org/10.1007/978-3-030-70432-2

This Springer imprint is published by the registered company Springer Nature Switzerland AG
The registered company address is: Gewerbestrasse 11, 6330 Cham, Switzerland

Foreword

Agriculture is a very large-scale social and economic engine. The "engine" needs to be sustainable and profitable for many obvious reasons. Agriculture involves human activities in producing food, feed, fiber, fuel, and furnishing by utilizing natural resources. It has evolved with the advances in science, engineering, and technologies in its own right and with other economic sectors. Agricultural modernization has been, and will continue to be, a very important subject for agricultural researchers and practitioners. In today's modernized agriculture, human-like machine capabilities (aka. automation), including perception, reasoning, learning, communication, task planning/execution, and systems integration, have been key enablers. Machine perception, reasoning, and communication are the starting points for the other capabilities to be meaningful.

One of the ultimate purposes for agricultural automation is to assist, extend, and expand human's ability in managing agricultural production to achieve planned objectives. Precision crop production has been viewed as a promising form of modern agriculture, where input resources and cultural tasks are precisely managed and executed. Perception is the understanding of situations and happenings that are fundamentally useful in planning, designing, implementing, managing, and operating devices, tasks, or the entire system. A commonly used term to describe the action of perception is sensing. To make sensing functional, it frequently includes the capabilities of reasoning and communication. Soil is one of the most impactful factors that influence the performance of a crop's growth and development. Sensing of soil and crop, as well as their interactions, is key to successful precision crop production.

Minzan Li, Chenghai Yang, and Qin Zhang, the editors of this book on "soil and crop sensing for precision crop production," are well-known researchers and educators in providing engineering solutions to agricultural production. They have invited active and knowledgeable authors, specializing in the state-of-the-art methodologies for monitoring soil and crop, to write the nine chapters. The chapters address essential topics that are systematically covered and logically organized in this book. The information on science and practical use of soil and crop sensing as applied to the management of precision crop production has been assembled in one integrated volume. The opportunities and challenges of developing smart agriculture based on

the current and future successes in sensing technologies are also presented. This book provides a comprehensive and timely information source for readers who are interested in learning about the important subject area of sensing and management of agricultural crops.

K. C. Ting

Professor and Head Emeritus,
Department of Agricultural and Biological Engineering
University of Illinois at Urbana-Champaign
Champaign IL USA

Professor and Vice Dean,
International Campus Zhejiang University
Hangzhou China
August 2020

Contents

About the Editors

Minzan Li is Professor of Agricultural Informatics in the College of Information and Electrical Engineering at China Agricultural University. He is currently the director of the Key Laboratory on Precision Agriculture, Ministry of Education, China. He has published more than 200 refereed papers and filed more than 20 patents in agricultural informatics and spectroscopy. He is a vice-chairperson of the Committee of Basic Technologies, Chinese Society for Agricultural Machinery (CSAM), and a vice-chairperson of the Committee of Agricultural Aviation, Chinese Society of Agricultural Engineering (CSAE). He has served as an associate editor for the journals of the *Transaction of the Chinese Academy of Engineering* (*Agriculture Edition*, *Frontiers of Agricultural Science and Engineering*), *International Journal of Agricultural and Biological Engineering*, *Transactions of the CSAE*, *Transactions of the CSAM*, *Journal of China Agricultural University*, and *Journal of Zhejiang University*. His research interests include the development of soil nutrient sensors with spectroscopy, soil EC measurement system, sensing system on crop growth status with spectral analysis and remote sensing, yield monitor and yield mapping system, and application of agricultural IoT. He received his BS and MS degrees in agricultural engineering from China Agricultural University in China and his PhD degree in agricultural engineering in 2000 from Tokyo University of Agriculture and Technology (TUAT), Japan.

Chenghai Yang is a research agricultural engineer with the U.S. Department of Agriculture, Agricultural Research Service's (USDA-ARS) Aerial Application Technology Research Unit in College Station, Texas. Dr. Yang has been conducting research on the development and application of remote sensing technologies for precision agriculture and pest management since 1995. He has authored or coauthored over 160 peer-reviewed journal articles and 16 books or book chapters. Dr. Yang has served several professional societies, including the American Society of Agricultural and Biological Engineers (ASABE) for which he has chaired the Precision Agriculture Committee and four other technical committees. He has also served as a division editor or associate editor for five technical journals, including the *International Journal of Agricultural and Biological Engineering*, *Transactions*

of the ASABE, and *Computers and Electronics in Agriculture*. Dr. Yang received his BS and MS degrees in agricultural engineering from Northwest A&F University in China and his PhD in agricultural engineering from the University of Idaho. He is an ASABE Fellow and serves as an adjunct professor at Texas A&M University and a guest professor at multiple universities.

Qin Zhang is the director of the Center for Precision and Automated Agricultural Systems (CPAAS) of Washington State University (WSU) and Professor of Agricultural Automation in the Department of Biological Systems Engineering, WSU. His research interests are in the areas of agricultural cybernetics, agricultural robotics, and off-road equipment mechatronics. Prior to his current position, he was a faculty member at the University of Illinois at Urbana-Champaign, worked at Caterpillar Inc., and taught at Zhejiang Agricultural University in China. Based on his research outcomes, he has authored/edited 8 books, edited 3 conference proceedings, written more than 20 book chapters, published over 180 peer reviewed journal articles, and been awarded 11 US patents. He is currently serving as the editor-in-chief of *Computers and Electronics in Agriculture*. Dr. Qin Zhang received his BS degree in engineering from Zhejiang Agricultural University, China; MS degree from the University of Idaho; and PhD degree from the University of Illinois at Urbana-Champaign. Dr. Qin Zhang is a member of the Washington State Academy of Sciences, an ASABE Fellow, and is serving or served as a guest or an adjunct professor for nine other universities in different countries.

Contributors

Liping Chen National Engineering Research Center of Intelligent Equipment for Agriculture, Beijing, China

Daming Dong National Engineering Research Center of Intelligent Equipment for Agriculture, Beijing, China

Xiantao He Zhejiang University, Hangzhou, China

Yong He Zhejiang University, Hangzhou, China

Masakazu Kodaira Tokyo University of Agriculture and Technology, Tokyo, Japan

Han Li China Agricultural University, Beijing, China

Minzan Li China Agricultural University, Beijing, China

Lili Yao Nanjing Agricultural University, Nanjing, China

Fei Liu Zhejiang University, Hangzhou, China

Yanlong Miao China Agricultural University, Beijing, China

Eiji Morimoto Tottori University, Tottori, Japan

Jun Ni Nanjing Agricultural University, Nanjing, China

Quan Qiu National Engineering Research Center for Information Technology in Agriculture, Beijing, China

Ruicheng Qiu China Agricultural University, Beijing, China

Sakae Shibusawa Tokyo University of Agriculture and Technology, Tokyo, Japan

Hong Sun China Agricultural University, Beijing, China

Nikolaos Sygrimis Agricultural University of Athens, Athens, Greece

Ning Wang Oklahoma State University, Stillwater, OK, USA

Chenghai Yang Agricultural Research Service, United States Department of Agriculture, College Station, TX, USA

Guijun Yang National Engineering Research Center for Information Technology in Agriculture, Beijing, China

Wei Yang China Agricultural University, Beijing, China

Man Zhang China Agricultural University, Beijing, China

Qin Zhang Washington State University, Prosser, WA, USA

Yao Zhang China Agricultural University, Beijing, China

Yan Zhu Nanjing Agricultural University, Nanjing, China

Chapter 1
Soil and Crop Sensing for Precision Crop Production: An Introduction

Han Li, Minzan Li, Nikolaos Sygrimis, and Qin Zhang

Abstract The development of agriculture has experienced the transformation from Agriculture 1.0 to Agriculture 4.0, or from traditional agriculture to smart agriculture. Agriculture 1.0 is the traditional agriculture using human and animal labor as its main resource. With the development of industrial revolution, agricultural machines were emerging, which directly resulted in Agriculture 2.0, featured by agricultural mechanization. With the increasing application of computers, electronics, communication technology, and automation equipment in agriculture, agriculture has stepped into the 3.0 era, characterized by digital agriculture or precision agriculture. Agriculture 4.0, also called smart agriculture or precision agriculture V2.0, is characterized by the application of IoT (Internet of Things), big data, cloud computing, and robots in agriculture. Precision agriculture or smart agriculture relies on the acquisition of field information including the environment, crops, and soil, and the accuracy of sensing data is the cornerstone of smart agriculture applications. Soil and crop sensing technology involves the exploration of sensing mechanism, spectroscopy, biology, microelectronics, remote sensing, sensors, and information processing methods. The platforms of soil and crop sensing are also constantly upgrading and improving. Multidimensional perception fusion is realized by using platforms of different scales, such as satellites, unmanned aerial vehicles (UAVs), and ground vehicles integrated with multiple sensors. Intelligent, convenient, accurate, and energy-saving information acquisition technology will continue to be the research hotspots in the field of smart agriculture.

H. Li · M. Li (✉)
China Agricultural University, Beijing, China
e-mail: gpac@cau.edu.cn

N. Sygrimis
Agricultural University of Athens, Athens, Greece

Q. Zhang
Washington State University, Prosser, WA, USA

M. Li et al. (eds.), *Soil and Crop Sensing for Precision Crop Production*,
Agriculture Automation and Control, https://doi.org/10.1007/978-3-030-70432-2_1

Keywords Precision agriculture · Smart agriculture · Crop sensing · Soil sensing · ICT

1.1 History of Agriculture, from Agriculture 1.0 to Agriculture 4.0

Agriculture is an industry that uses the growth and development law of plants and animals to obtain products through artificial cultivation. The objects of agricultural production are plants and animals. Due to the different geographical distributions of animals and plants, as well as the regional differences in natural and socioeconomic conditions, there are many types of agricultural regions in the world, such as tropical rainforest migration agriculture, commodity grain agriculture, dairy industry, and animal husbandry. Agriculture is the primary industry to support the construction and development of a national economy.

Agriculture has experienced the transition eras from Agriculture 1.0 to Agriculture 4.0. The development of the human society is a process of constantly creating new labor tools, understanding nature, adapting to nature, and transforming nature. In different historical periods, the human society has expanded and enhanced human's own functions by using different functional tools, which have become one of the basic standards to distinguish human social formations. Therefore, the evolution of labor tools reflects the evolution from Agriculture 1.0 to Agriculture 4.0 (De Clercq et al. 2018; Li 2018; Rose and Chilvers 2018). Agriculture 1.0 is a traditional agriculture using human labor and animal power as its main tools. Agriculture 2.0 is a mechanized agriculture using agricultural machinery as its production means. Agriculture 3.0 is a digital agriculture or precision agriculture using information as its production factors, and it is characterized by the application of the Internet, automation, and other information and communication technologies (ICT). Agriculture 4.0, also called smart agriculture, applies Internet of Things (IoT), big data, cloud computing, and intelligent robot in agriculture to realize agricultural informatization and intellectualization.

Agriculture 1.0 is a traditional agriculture using human and animal labor as its main resource, which belongs to the agricultural society (Huang and Han 2012; Li 2018). In the long development of the agricultural society, the most important tools were all kinds of simple hand tools and animal power, which were used in development of land resources. Those hand tools and animal power could relieve human physical labor to some extent, but they did not fundamentally liberate human production activities from heavy physical labor. In the agricultural society, although the production tools had developed from the early stone tools and bronzes to the later iron tools, they were still primary and only a limited extension of the part functions of the human body.

As the invention and use of steam engines in 1765, human societies have made the revolutionary development of production tools. With the development of industrial revolution, agricultural machines were emerging, which directly resulted in

Agriculture 2.0, featured by agricultural mechanization. Compared with the manual and animal labor tools of Agriculture 1.0, Agriculture 2.0 is a large-scale agriculture characterized by large-scale farms and mechanized production using advanced and applicable agricultural machinery to replace human and animal production tools. It transforms backward and inefficient traditional production mode into advanced and efficient large-scale production mode, which greatly improves labor productivity and agricultural productivity.

With the increasing application of computers, electronics, communication technology, and automation equipment in agriculture, agriculture has stepped into the 3.0 era. Agriculture 3.0, namely, digital agriculture or precision agriculture, is characterized by the application of modern ICT. Supported by ICT, it enables the effective integration of information technology and all aspects of agriculture and implements modern agricultural operations and management at the right position, the right time, and the right amount according to the spatial variation (Marucci et al. 2017), so as to achieve the purpose of rational utilization of agricultural resources, reduction of production costs, improvement of ecological environments, and enhancement of crop products and quality.

With the wide application of modern information technology in agriculture, the fourth revolution of agriculture, Agriculture 4.0 (smart agriculture or precision agriculture V2.0), has come. It is characterized by the application of IoT, big data, cloud computing, and intelligent robots, which deeply integrates modern information technology with agriculture (O'Grady and O'Hare 2017; Ozdogan et al. 2017; Wolfert et al. 2017; Adnan et al. 2018; Braun et al. 2018). Agriculture 4.0 uses the systematic method and standardization system to manage agricultural production in a unified way, with all processes controllable and efficient, to realize unmanned operation. Equal connection between agricultural service providers and agricultural producers is realized through agricultural standardization platform, so as to strengthen the interaction in the whole process.

1.2 Modern Agriculture Technologies

1.2.1 Precision Agriculture

The studies related to precision agriculture, or precision farming, originated in the United States in the 1980s (McKinion and Lemmon 1985; Schueller and Bae 1987; Searcy et al. 1989; Stafford and Hendrick 1988). It was proposed and started to be studied and practiced by agronomists in the United States who were engaged in crop cultivation, soil fertility, and crop disease and grass pest control. In the end of the 1980s and early 1990s, the word "precision agriculture" or "precision farming" had not been popular, and there were several words to describe this new agronomic technology, such as farming by soil, spatially prescriptive farming, computer-aided farming, farming by satellite, site-specific farming, site-specific crop management (SSCM), and so on. Robert et al. (1995) proposed the definition of SSCM as

follows: site-specific crop management is an information- and technology-based agricultural management system to identify, analyze, and manage site soil spatial and temporal variability within fields for optimum profitability, sustainability, and protection of the environment.

Since the late 1990s, the word "precision agriculture" or "precision farming" was accepted by the scientists in this field. With the development of agricultural engineering technology, agricultural information technology, geographic information systems (GIS), continuous data acquisition sensors (CDS), remote sensing, variable rate technology (VRT), intelligent agricultural equipment, and decision support systems, the United States, the United Kingdom, Germany, the Netherlands, Italy, and other developed countries applied precision agriculture to automatic navigation, automatic yield monitoring, fruit picking, farmland irrigation, field weeding, and other applications (Baker et al. 1996; Blackmore 2000; Stafford 2000).

The concept of precision agriculture is also evolving. The International Society of Precision Agriculture (ISPA, https://www.ispag.org/) adopted the following new definition of precision agriculture in 2019: "Precision agriculture is a management strategy that gathers, processes and analyzes temporal, spatial and individual data and combines it with other information to support management decisions according to estimated variability for improved resource use efficiency, productivity, quality, profitability and sustainability of agricultural production."

In essence, precision agriculture is a management strategy for agricultural production, which completely changes the technical system of extensive production mode. Its emphasis is to use modern information technology to greatly improve the level of production and management of traditional agriculture, so that all aspects of agricultural production are more rigorous and meticulous, in order to achieve the purpose of optimizing the utilization efficiency of various resources. In terms of technical equipment, the yield monitor assembled on the combine harvester can be used to generate yield map, and the soil sensors can be used to generate the map of soil parameters or fertilizer prescription map. Moreover, the variable fertilizer applicators, intelligent seeders, automatic mechanical weeding, automated steering tractor, etc., are used to perform VRT farming. In terms of management strategy, it adopts precise agricultural production technologies, such as variable input technology, block-by-block differentiated management, tillage by soil, water-saving irrigation, and personalized planting schemes.

1.2.2 Digital Agriculture

With the concept of digital earth that was put forward in 1998 in the United States, the concept of digital agriculture had also aroused great concern from that time (Gore 1998). The original meaning of digital agriculture refers to the intensive and informationized agricultural technology supported by geoscience space and information technology. Specifically, digital agriculture combines remote sensing (RS); GIS; global positioning systems (GPS); computer technology; communication and

network technology; and automation technology with geography, agronomy, ecology, plant physiology, soil science and other basic disciplines to achieve the purposes of optimizing the use of agricultural resources, reducing production costs, improving the ecological environment, and improving the quality of crop products (Liang et al. 2002). As the development of mobile Internet and big data technology, the connotation of digital agriculture is gradually developing, and it extends to agricultural research, agricultural management, agricultural product circulation, sales, security, and other aspects (Ozdogan et al. 2017).

Digital agriculture can be regarded as the upgrade and expansion of precision agriculture. First of all, in the application links, digital agriculture extends to the whole process of agricultural production, circulation, and sales, while precision agriculture is mainly concentrated in the agricultural production links. Second, in terms of technology and equipment, compared with precision agriculture, there are more types of digital agriculture, which rely more on integrated technologies such as remote communication, IoT. Third, precision agriculture is still the core of digital agriculture. All the technological progress should ultimately be reflected in the improvement of the quality and efficiency of agricultural production. The final result of digital agriculture should be embodied by precision agriculture.

The Food and Agriculture Organization (FAO) of the United Nations also attaches great importance to digital agriculture (Trendov et al. 2019). It indicates that the ubiquity, portability, and mobility of digital technologies are transforming agriculture and food production. Specifically, in the agriculture and food sector, the spread of mobile technologies, remote sensing services, and distributed computing are already improving smallholders' access to information, inputs, and markets, increasing production and productivity, streamlining supply chains, and reducing operational costs.

1.2.3 Smart Agriculture

ICT technology promotes agriculture to a more advanced stage after precision agriculture and digital agriculture, which is smart agriculture or Agriculture 4.0. Smart agriculture is a new agricultural production mode formed by introducing the organization mode, management concept, and advanced technology of modern industry into agriculture. Through the application of the Internet, computer, modern communication technology, IoT, modern agricultural machines, and other new technologies, the perception of agricultural production environmental conditions is enhanced, and the intelligent management of remote diagnosis, remote control, and disaster warning is performed (Brown 2018). Smart agriculture can realize more complete information-based support, more thorough agricultural information perception, more centralized data resources, more extensive connectivity, more in-depth intelligent control, and more intimate public services. Smart agriculture can not only improve crop yield and land resource utilization efficiency but also reduce the damage of agricultural production to the natural environment, which plays an important

role in the development of resource-intensive and environment-friendly green agriculture. In addition to accurate perception, control, and decision-making management, smart agriculture also includes agricultural e-commerce, food traceability and anti-counterfeiting, agricultural leisure tourism, agricultural information services, agricultural industrial policy management, and other aspects.

At present, many countries in the world attach great importance to the promotion and application of smart agriculture (Zhao 2019). Smart agriculture is the general trend of global agriculture, and many countries have launched their smart agriculture development plans. Japan launched the implementation of the "Cross-ministerial Strategic Innovation Promotion Program (SIP)" in 2014 and launched the "next generation of agricultural, forestry and aquaculture creation technology" based on the "intelligent machinery + modern information" technology in 2015, the goals of which were to develop a highly productive and labor-saving smart agriculture model by innovative technologies such as robotics, IT, big data, and artificial intelligence (AI) and to add high value to agricultural and forest products by differentiation focusing on functionality and developing new materials from unutilized resources (Noguchi 2017). The European Agricultural Machinery Industry Association (CEMA) held a summit of Farming 4.0 on October 12, 2017, and stated that under the background of information technology, the digital revolution in agriculture was coming and the future development direction of European agriculture was Farming 4.0, that is, smart agriculture (CEMA 2017). The National Centre for Precision Farming (NCPF), UK, supported by the European Union FP7 program, is implementing the Future Farm project, developing a weeding robot to carry out weeding operations, in order to replace the use of chemical pesticides (NCPF 2018). The Policy Horizons Canada published a report in 2014 named "Meta Scan 3: Emerging Technologies" (Policy Horizons Canada 2014). According to the report, technologies such as soil and crop sensors, livestock biometric technology, variable speed harvesting control, agricultural robots, mechanized farm network, closed ecosystems, and vertical (factory) agriculture will enter into production application in the next 5–10 years to change traditional agriculture. The United States is moving toward smart agriculture after mechanization, chemistry, and biotechnology. It is predicted that IoT will be widely used in agriculture in the United States after 2020 (Erickson and David 2015).

The Research and Market, an international consulting agency, has released a report on the smart agriculture market to 2025 (Research and Markets 2017). The report focuses on an in-depth segmentation of the market based on product type and application. The geographic segmentation of the report covers six major regions including North Americas, Europe, Asia-Pacific (APAC), Middle East and Africa (MEA), and South America (SA). The largest adopter of smart agriculture is APAC, followed by Europe, while the Middle East and Africa region with rising adoption of digital farming methods is anticipated to be one of the most promising regions in terms of the smart agriculture market. According to the report, it is predicted that by 2025, the global smart agriculture market is expected to grow from US$ 11.30 billion in 2016 to US$ 30.01 billion by 2025 at a compound annual growth rate of 11.5% from 2017 to 2025 in main fields such as precision agriculture, intelligent

animal husbandry, intelligent fishery, and intelligent greenhouse. The main technologies include remote sensing and sensor technology, agricultural big data and cloud computing service technology, intelligent agricultural equipment (such as UAV and robot), and so on.

1.3 New Challenges in Agriculture

1.3.1 IoT in Agriculture

In 2008, IBM (International Business Machines Corporation) proposed a new concept of "Smarter Planet" in the United States, which emphasizes timeliness, real-time perception, and timely feedback (IBM 2008). After that, as a powerful tool of information perception, IoT has been developing rapidly in the world and is called the third wave of information technology development.

Agricultural IoT is a complex system, involving electronics, communications, computers, agronomy, and other disciplines and fields. According to the basic research content of informatics, that is, the acquisition, processing, transmission, and utilization of information, the key technologies of agricultural IoT can be divided into four levels, physical layer, transmission layer, processing layer, and application layer, focusing on solving the problems of agricultural individual identification, situational awareness, heterogeneous equipment networking, multisource heterogeneous data processing, knowledge discovery, and decision support (Khanna and Kaur 2019). In the agricultural IoT, different kinds of agricultural equipment and sensors break through the barrier of data sharing and share operation parameters through machine-to-machine (M2M) communication technology and conduct the optimal automatic control of the whole agricultural process based on big data and AI. The agricultural IoT will create a production mode that is mainly based on machines and technology, which will greatly improve the transparency of agricultural product quality and logistics, and comprehensively reduce the production and operation costs of agricultural products. Nowadays, agricultural IoT has been used in the fields of agricultural monitoring and control, controlled-environment agriculture, open-field agriculture, livestock applications, food supply chain tracking, middleware and interoperability in agriculture, multilayer deployments, and commercial solutions (Tzounis et al. 2017).

With the continuous upgrading of information technology, the process of agricultural modernization has entered a new information era. The upgrading process of traditional agriculture puts forward new requirements for the agricultural IoT. The IoT platforms have been built one after another, but they are still independent of each other, leading to the phenomenon of data island. Big data technology and cloud computing technology provide solutions for data management and analysis, and many well-known technology companies have begun to work on cloud computing infrastructure construction. They provide access platforms to farmers and, at the same time, get the spatial and temporal agricultural data to establish production and

practice models for farmers including plant monitoring information, environmental information, and nutrient information. For example, the use of historical environmental information and plant growth information can be used to establish the early warning system for field or greenhouse crop disease, to guide farmers to take preventive measures in advance.

In addition, the characteristics of agricultural production environments and the technical needs of low power consumption sensors put forward higher requirements for data transmission of agricultural IoT. Due to the lack of standards and specifications, the standardized application of IoT in the field is restricted. Therefore, the agricultural IoT technology must be upgraded in an all-round way to further improve its universality, reliability, and intelligence level, while reducing costs and promoting its wider application.

1.3.2 Big Data in Agriculture

With the continuous popularization of information technology and the rapid development of computer storage technology, the amount of data has stepped into the ZB (1.024 × 1021 B) era. For example, the growing application of sensing techniques, such as RGB, thermal, near-infrared (NIR), multispectral, and hyperspectral imaging, has resulted in large amounts of data, which have to be analyzed to derive value from the collective farm information. The efficient storage and analytic solutions need to be developed to handle those numerous data (Ip et al. 2018). Since the amount of information to be processed exceeds the amount of memory that can be used by general computers when processing data, the big data analysis is needed, and the new distributed system architecture Hadoop and the computing model "MapReduce" have emerged. New technical conditions make the integration, clustering, and regression of massive data feasible. The main characteristics of big data can be summarized as "4V" characteristics, that is, volume, velocity, variety, and veracity (Chen and Zhang 2014). The complexity of agricultural big data is determined by its volume and variety, and the quality is determined by its velocity and veracity.

Agricultural data is large in volume, complex in structure, changeable in mode, strong in real time, and highly correlated (Li and Yang 2018). The main way to solve the problem of high-dimensional and strong coupling of agricultural variables is to obtain value relationship from massive agricultural data through big data analysis technology. The essence of agricultural big data is to analyze the relationship between data variables and develop solutions based on large-scale agricultural data and processing methods for specific agricultural problems. With regard to what role big data plays in smart agriculture, Wolfert et al. (2017) indicated that the big data is changing the scope and organization of agriculture through a pull-push mechanism, and the global issues such as food security and safety, sustainability, and as a result efficiency improvement are tried to be addressed by big data applications. It is also stated that the IoT development, wirelessly connecting all kinds of objects,

devices, sensors, and robots in farming and the supply chain, is producing many new data that can be real-time accessible, and these big amounts of data provide access to explicit information and decision-making capabilities at a level that was impossible before. Based on the agricultural big data technology, in-depth analysis of agricultural data and discovery of potential value are the research focus. The application of big data mainly focuses on the reliable decision support system for precision agriculture, the national rural comprehensive information service system, the agricultural data monitoring and early warning system, the agricultural production environment monitoring and control system, etc.

Agricultural data is mainly an objective reflection of various agricultural objects, relationships, and behaviors. Agricultural big data technology is an abstract mathematical description of multisource heterogeneous massive agricultural data. At present, there have been breakthroughs in agricultural knowledge models, agricultural pattern recognition, agricultural knowledge representation, and machine learning of agricultural business models. On the other hand, some models and algorithms are not accurate enough to reflect the objective reality for use in precision agriculture. The challenges are how to mine the valuable information of the whole chain, such as agricultural production, processing, sales, resources, environment, and process, and how to quantify the agricultural objects, relationships, and behaviors through statistical methods, so that the big data can be transformed into intelligent data, which are easy to be accepted and used by farmers, and provide knowledge support for the research and implementation of precision agriculture and smart agriculture. In addition, with the maturity of big data technology and the continuous accumulation of massive basic data technology, the studies and applications of deep learning algorithms are thriving. Deep learning is a kind of machine learning based on the mathematical principle of artificial neural network, with multilayer parameter learning systems as the structure and massive data as the training parameters. Its characteristic is that it can automatically extract the features contained in the data and express the relationship between high-dimensional and complex variables mathematically. How to apply deep learning to big data mining and establish crop physiological models and environmental models in agricultural production is also a challenge to be approached.

1.3.3 Cloud Computing in Agriculture

Cloud computing is a new network service mode. It transforms the traditional task processing with desktop as the core into the task with network as the core. It uses the Internet to transfer services and computing power and information to achieve on-demand computing and network collaboration. It is a high-performance parallel computing technology. Cloud computing technology has the advantages of superscale, virtualization, distributed storage, high reliability, and high performance. The characteristics of flexibility and expandability provide good technical support for solving the problems in rural agricultural information construction. In terms of

agricultural cloud services, there are different types of cloud computing applications worldwide in the recent years. In the field of agriculture, the Fujitsu Limited, Japan, launched the cloud computing service "F & AGRIPACK" to serve the development of Japanese agricultural industry in 2010 (Fujitsu 2010). The National Engineering Research Center for Information Technology in Agriculture (NERCITA) of China has used the cloud storage for the management of massive agricultural knowledge resources and realized the effective management of 3.2 TB agricultural resources. In the aspect of information resource management of agricultural cloud platform, extensive research has been carried out in the aspects of agricultural information resource representation, resource organization management, agricultural intelligent system development platform, construction of agricultural domain ontology database, and agricultural knowledge collaboration and service, and a large number of software and functional modules have been formed for the application characteristics of the field.

FAO proposed climate-smart agriculture (CSA) in 2013, which is an approach to help the people who manage agricultural systems respond effectively to climate change. The CSA approach pursues the triple objectives of sustainably increasing productivity and incomes, adapting to climate change, and reducing greenhouse gas emissions where possible (FAO 2013). CSA is a field which is highly benefited with the applications of cloud computing with regard to resource sharing, cost saving, and efficient agro system construction. Moreover, the integration of agricultural processes with cloud computing has given a significant impetus to production, marketing, and sales of agricultural goods. The features provided in CSA through cloud computing technology include data acquisition and remote storage, low-cost access to ICT resources, online agriculture expert consultation, land record automation, and weather forecasting (Symeonaki et al. 2017).

Zamora-Izquierdo et al. (2019) proposed a flexible platform which is able to cope with soilless culture needs in full recirculation greenhouses using moderately saline water. The platform was supported by a three-tier open-source software at local, edge, and cloud planes. The edge plane of the platform was in charge of monitoring and managing main PA tasks near the access network to increase system reliability against network access failures, while the cloud platform collected current and past records and hosts data analytic modules.

In the aspect of agricultural cloud platform architecture research and development, the emergence and development of grid technology promote the effective aggregation and full sharing of distributed and heterogeneous agricultural information resources. However, in terms of transparent user services and on-demand access, it cannot meet the requirements of many agricultural users and significant demand differences. Cloud computing takes users as the center and provides users with transparent computing, storage, and information services in the way of resource pool. Cloud computing architecture, distributed storage, security management, cloud monitoring, resource scheduling, cloud computing programming model, and other key technologies have been widely studied. How to combine with domain application to realize resource aggregation and on-demand service has become an important trend in the development of cloud computing technology.

1.4 Overview of Soil and Crop Sensing Technologies for Precision Crop Production

1.4.1 Information of Soil and Crop for Precision Crop Production

As described in 1.2.1 Precision Agriculture, ISPA suggested the new definition of precision agriculture in 2019 as "Precision agriculture is a management strategy that gathers, processes and analyzes temporal, spatial and individual data and combines it with other information to support management decisions according to estimated variability for improved resource use efficiency, productivity, quality, profitability and sustainability of agricultural production." Information (or data) is the basis of precision agriculture.

The agricultural information in precision agriculture mainly includes six elements: geographical environment, soil environment, microclimate, water environment, information related to crop growth, and management information (Luo et al. 2006). The information has the characteristics of large amount, multidimensional (various information), dynamic, uncertain (system noise or random noise), incomplete, sparse, strong spatiotemporal variability, and so on. As soil and crop are the most important elements in agricultural production, it is the priority of soil and crop information acquisition in precision agriculture.

Soil is the basis for human survival, and the fertility is the essential attribute of soil. Soil fertility indexes include various soil physical indexes, chemical and nutrient indexes, and biological indexes (Zheng et al. 2004). Soil physical indicators include soil moisture content, soil hardness (soil compaction), soil texture (the proportion of clay, silt, and sand particles in the soil), topsoil layer thickness, bulk density, soil porosity, soil aggregate structure, and soil temperature. Soil water is the main source of water absorbed by plants, and it is indispensable for seed germination and soil nutrient absorption. Soil moisture content is the most important soil physical parameter. In different growth stages of crops, water requirements are different, so it is necessary to monitor soil moisture content frequently. Soil chemical and nutrient indicators include pH, CEC (cation exchange capacity), EC (electrical conductivity), total nitrogen, total phosphorus, total potassium, available nitrogen (ammonium nitrogen, nitrate nitrogen), available phosphorus, available potassium, and total amount and availability of micronutrients (Ca, Mg, S, Cu, Fe, Zn, Mn). These chemical and nutrient indicators are the key indexes to grasp soil fertility. Soil organic matter (SOM) is the most important biological index of soil, which plays a variety of roles in soil fertility, including water retention, fertilizer conservation, and buffering, providing crop nutrients, promoting the formation of aggregate structure, improving soil physical properties, and reducing or eliminating pesticide residues and heavy metal pollution in soil.

Precision crop management focuses on crop growth status and crop yield information. Crop growth status can be described by individual and population characteristics, that is, crop growth characteristic parameters (Clevers et al. 1994). A

reasonable population composed of strong individuals is a good growing crop. Crop growth monitoring refers to the macroscopic monitoring of crop seedling situation, growing status, and its changes, which can be divided into temporal monitoring and spatial monitoring. Taking winter wheat as an example, the individual characteristics of winter wheat can be described by the characteristics of stem, leaf, root, and spike, such as plant height, number of tillers, and number, shape, and color of leaves, and development of roots. Population characteristics can be described by population density, LAI (leaf area index), layout, and dynamics. The commonly used parameters are population density and LAI. The data and information of crop diseases, insect pests, and weeds are also important information related to crop growth. It is necessary to record the damage degree and distribution of crop diseases, insect pests, and weeds. Especially, it will be more meaningful to detect the relevant information and issue early warning in the early stage of damage.

Crop yield monitoring is divided into yield estimation based on growth season information and yield automatic measurement in harvest season. There are many methods for crop yield estimation, including three models: meteorological model, agronomic model, and remote sensing model (Doraiswamy et al. 2004). Due to the complex factors affecting crop yield, the precision of meteorological model and agronomic model fluctuates greatly in a large range of crop yield prediction. Remote sensing model is to estimate crop yield by establishing the relationship between crop information (spectral information) and yield measured by remote sensing, which has higher generality and prediction accuracy. The real-time measurement of crop yield is to use the sensor mounted on the combine harvester to measure the grain yield in real time and to generate the yield spatial distribution map with DGPS, which is used to guide the precision agricultural production in the coming year (Grisso et al. 2009).

Another hot topic of crop information acquisition is plant phenotyping (Walter et al. 2015; Zhou et al. 2018; Pieruschka and Schurr 2019). It generally refers to the observable morphological characteristics of an individual or group of organisms under specific conditions (such as various environments and growth stages). It is considered to be the result of complex interaction between genetic types and environmental factors. Automatic and rapid acquisition of phenotypic parameters is of great significance for genetic breeding and crop precise management.

1.4.2 Soil and Crop Sensing Technologies for Precision Crop Production

Before the introduction of machine and electronic technology, farmers used their five senses to perceive the characteristics of soil and crops and used manual tools to measure some characteristic parameters of soil and crops. Since the development of precision agriculture requires accurate and rapid sensing and processing of farmland information, the optical, acoustic, electrical, and magnetic technologies are

used in the sensing of soil and crop parameters. With the development of information and communication technology (ICT), wireless sensor network (WSN), mobile Internet technology, and UAV technology are introduced to further improve the ubiquitous and real-time performance of information acquisition (Wang et al. 2006; Jiang et al. 2020).

Visible light and near-infrared spectroscopy (NIRS) have become an important means to obtain the biological environment information of farmland due to their advantages of simplicity, rapidity, high precision, and nondestructive measurement and play an important role in the development of precision agriculture (Pasquini 2003). Soil moisture content, soil organic matter content, and soil nutrient content can be analyzed by spectral analysis (Li et al. 2013). Based on the spectral characteristics of crops, farmers can automatically analyze crop growth, diagnose crop nutritional status, monitor crop diseases and insect pests, estimate yield and quality, etc. According to the information obtained, farmers can evaluate the interaction between crop growth and environment, improve crop management level, and realize site-specific crop management and prescription farming.

Using satellite as the platform of spectral sensor, remote sensing provides a powerful tool for soil and crop information acquisition. It can be used in monitoring and diagnosing of crop nutrient status, crop sown area, crop growth, crop yield, agricultural disaster, agricultural climate, agricultural ecological environment, and agricultural water. Among them, crop growth is closely related to the final quality and actual yield of crops. Crop growth detection based on remote sensing plays an important role in precision agriculture and mainly refers to the macro monitoring of crop seedlings, growth, and changes (Yang and Pei 1999; Wu et al. 2004). For different crops, their development period and growth trend are different, so they have different spectral reflectance. According to the characteristics of crop canopy reflectance in different wavebands, scientists have designed a variety of crop spectral indexes (vegetation indexes), which have a strong linear relationship with crop growth parameters, such as LAI, leaf nitrogen content, leaf water content, and crop yield (Bannari et al. 1995; Tian and Min 1998). Using these vegetation indexes, the crop growth and nutrition parameters can be accurately obtained, so that the crop growth situation can be monitored and the yield can be estimated.

With the development of computer technologies, image processing and analysis technology has also been rapidly developed. Using computer image processing technology to monitor crop growth has the characteristics of nondestructive, fast, and real time. It can not only measure the geometric parameters of plant organs, such as the length, width, perimeter, area, and angle of root, stem, and leaf, but also measure the area, diameter, and shape factor of irregular leaves, which are difficult to be measured by conventional methods. Through the analysis of the images obtained in different periods of crops, the dynamics of crop growth can be reflected, such as leaf aging process, seedling growth rate, crop water shortage, and fertilizer shortage. Automatic identification and determination of diseases, insect pests, and weeds in crop growth are also the important application areas of image processing and analysis in crop production.

Soil or crop detection based on ground spectra (also known as ground-based remote sensing) has high spectral resolution, but its detection range is small and its efficiency is low. Satellite remote sensing has a wide range and high efficiency, but its spatial resolution and spectral resolution are limited. UAV remote sensing has higher spectral resolution and spatial resolution and a wider range of optical measurement area and efficiency. With the development and popularization of UAV technology, UAV remote sensing has been more and more widely used, and some multispectral and hyperspectral cameras for UAV remote sensing have been developed.

With the development of ICT technology, some modern spectral analysis technologies for farmland information perception have emerged, including fluorescence spectroscopy, terahertz spectral analysis, and laser-induced breakdown spectroscopy (LIBS). There are also some sensing technologies based on dielectric properties of materials, biosensor technology, and so on. After widely using artificial neural network (ANN), wavelet analysis, and support vector machine (SVM), some new information processing technologies in the network era have been introduced such as big data technology and machine learning including deep learning. The application of modern information perception and processing technology provides a solid foundation for the development of precision agriculture.

1.5 Summary

From traditional agriculture to smart agriculture, information acquisition is indispensable. Modern information acquisition technology will continue playing an increasingly important role. With the rapid development of sensor technology, modern communication technology, and IoT technology, modern information acquisition technology has made rapid progress. For example, in recent years, new sensors are characterized by miniaturization, digitization, intelligence, multifunction, and networking. In the aspect of communication, low-power wide area networks (LPWAN) such as LoRa and NBIoT, which are characterized by low power consumption, low operation cost, and large node capacity, are the main approaches for agricultural sensor networks to connect in the future. As the supplement of LPWAN transmission rate, 4G and 5G mobile communication technology will make the large file transmission represented by agricultural images and audio become reality and further expand the dimension of agricultural information. In the future, intelligent, convenient, accurate, and energy-saving information acquisition technology will continue to be one of the research hotspots in the field of smart agriculture.

References

Adnan N, Nordin SM, Rahman I, Noor A (2018) The effects of knowledge transfer on farmers decision making toward sustainable agriculture practices, in view of green fertilizer technology. World J Sci Technol Sustain Dev 15:98–115

Baker J, Colvin TS, Jaynes DB (1996) Potential environmental benefits of adopting precision agriculture. In: Proceedings of the 3rd international conference. Minneapolis, Minnesota, June 23–26, 1996, pp 1051–1052

Bannari A, Morin D, Bonnr F, Huete AR (1995) A review of vegetation indices. Remote Sens Rev 13(1–2):95–120

Blackmore BS (2000) Developing the principles of precision farming. In: Proceeding of international conference on engineering and technological sciences. Beijing, China. October 11, 2000, pp 133–136

Braun A, Colangelo E, Steckel T (2018) Farming in the era of industrie 4.0. Proc CIRP 72:979–984

Brown M (2018) Smart farming – automated and connected agriculture. https://www.engineering.com/DesignerEdge/DesignerEdgeArticles/ArticleID/16653/Smart-FarmingAutomated-and-Connected-Agriculture.aspx

CEMA (2017) A revolution in the making: EU should lend stringent support to Digital Farming and become a 'world-leader'. 2017 CEMA Summit – FARMING 4.0, (2017-10-12). https://www.cema-agri.org/images/publications/press_releases/Press_Release_2017_CEMA_Summit_12_October_2017.pdf

Chen CP, Zhang CY (2014) Data-intensive applications, challenges, techniques and technologies: a survey on Big Data. Inf Sci 275:314–347

Clevers JGPW, Büker C, van Leeuwen HJC, Bouman BAM (1994) A framework for monitoring crop growth by combining directional and spectral remote sensing information. Remote Sens Environ 50(2):161–170

De Clercq M, Vats A, Biel A (2018) Agriculture 4.0: the future of farming technology. World Government Summit, February, 2018. https://www.worldgovernmentsummit.org/api/publications/document?id=95df8ac4-e97c-6578-b2f8-ff0000a7ddb6

Doraiswamy PC, Hatfield JL, Jackson TJ, Akhmedov B, Prueger J, Stern A (2004) Crop condition and yield simulations using Landsat and MODIS. Remote Sens Environ 92:548–559

Erickson B, David AW (2015) 2015 precision agricultural services dealership survey results. Purdue University, West Lafayette

FAO (2013) Climate-smart agriculture sourcebook. Food and Agriculture Organization of the United Nations, pp 27–30. http://www.fao.org/3/i3325e/i3325e.pdf

Fujitsu (2010) Cloud services for agricultural industry. 2010-04-05, Fujitsu Limited. https://www.fujitsu.com/global/about/resources/news/press-releases/2010/0405-02.html

Gore A (1998) The digital earth: understanding our planet in the 21st century. Los Angeles. http://www.digitalearth.net.cn

Grisso R, Alley M, McClellan P (2009) Precision farming tools: yield monitor. Virginia Cooperative Extension, publication, pp 442–502. https://vtechworks.lib.vt.edu/bitstream/handle/10919/51375/442-502.pdf

Huang T, Han P (2012) Rediscussion on the relationship between production relation and productivity as well as production mode. West Forum 22(3):47–54

IBM (2008) Smarter Planet, 2008-11-06. https://www.ibm.com/ibm/history/ibm100/us/en/icons/smarterplanet/

Ip RHL, Ang LM, Seng KP, Broster JC, Pratley JE (2018) Big data and machine learning for crop protection. Comput Electron Agric 151:376–383

Jiang R, Wang P, Xu Y, Zhou ZY, Luo XW, Lan Y, Zhao GP, Sanchez-Azofeifa A, Laakso K (2020) Assessing the operation parameters of a low-altitude UAV for the collection of NDVI values over a paddy rice field. Remote Sens 12:1850. https://doi.org/10.3390/rs12111850

Khanna A, Kaur S (2019) Evolution of Internet of Things (IoT) and its significant impact in the field of Precision Agriculture. Comput Electron Agric 157:218–231

Li DL (2018) Agriculture 4.0, the approaching age of intelligent agriculture. J Agric 8(1):207–214
Li DL, Yang H (2018) State-of-the-art review for Internet of Things in agriculture. Trans Chin Soc Agric Machine 49(1):1–20
Li MZ, Zheng LH, An XF, Sun H (2013) Fast measurement and advanced sensors of soil parameters with NIR spectroscopy. Trans CSAM 44(3):73–87
Liang Y, Lu XS, Zhang DG, Liang F (2002) The main content, technical support and enforcement strategy of digital agriculture. Geo-Spatial Inf Sci 5(1):68–73
Luo X, Zang Y, Zhou ZY (2006) Research progress in farming information acquisition technique for precision agriculture. Trans CSAE 22(1):167–173
Marucci A, Colantoni A, Zambon I, Egidi G (2017) Precision farming in hilly areas: the use of network RTK in GNSS technology. Agriculture 7(7):60
McKinion JM, Lemmon HE (1985) Expert systems for agriculture. Comput Electron Agric 1:31–40
NCPF (2018) National Centre for Precision Farming/UK. (2018-07-11). https://www.harper-adams.ac.uk/research/ncpf/
Noguchi N (2017) Smart agriculture toward society 5.0: SIP "Technologies for Creating Next-Generation Agriculture, Forestry and Fisheries". 2017-07. http://jastip.org/sites/wp-content/uploads/2017/07/prof.Noguchi.pdf
O'Grady MJ, O'Hare GM (2017) Modelling the smart farm. Inf Process Agric 4(3):179–187
Ozdogan B, Gacar A, Aktas H (2017) Digital agriculture practices in the context of agriculture 4.0. J Econ Finance Account 4(2):186–193
Pasquini C (2003) Near infrared spectroscopy: Fundamentals, practical aspects and analytical applications. J Braz Chem Soc 14(2):198–219
Pieruschka R, Schurr U (2019) Plant phenotyping: past, present, and future. Plant Phenomics, Article ID 7507131. https://doi.org/10.34133/2019/7507131
Policy Horizons Canada (2014) MetaScan 3-emerging technologies. (2014-03-01). https://horizons.gc.ca/en/2014/03/01/metascan-3-emerging-technologies/
Research and Markets (2017) Smart agriculture market to 2025-Global analysis and forecast. (2017-01). https://www.researchandmarkets.com/reports/4375555/smart-agriculture-market-to-2025-global
Robert PC, Rust RH, Larson WE (1995) Site-specific management for agricultural systems. ASA-CSSA-SSSA, Madison, pp 13–14
Rose DC, Chilvers J (2018) Agriculture 4.0: broadening responsible innovation in an era of smart farming. Front Sustain Food Syst 2(87). https://doi.org/10.3389/fsufs.2018.00087
Schueller JK, Bae YH (1987) Spatially-attributed automatic combine date acquisition. Comput Electron Agric 2:119–127
Searcy SW, Schueller JK, Bae YH, Borgelt SC, Stout BA (1989) Mapping of spatially variable yield during grain combining. Trans Am Soc Agric Eng 32(3):826–829
Stafford JV, Hendrick JG (1988) Dynamic sensing of soil pans. Trans Am Soc Agric Eng 31(1):9–13
Stafford JV (2000) Implementing precision agriculture in the 21st century. J Agric Eng Res 76:267–275
Symeonaki E, Arvanitis K, Piromalis D (2017) Review on the trends and challenges of cloud computing technology in climate-smart agriculture. In: Proceedings of the 8th international conference on information and communication technologies in agriculture, food and environment (HAICTA 2017), Chania, Greece, 21–24 September, 2017
Tian QJ, Min XJ (1998) Advances in study on vegetation indices. Adv Earth Science 13(4):327–333
Trendov NM, Varas S, Zeng M (2019) Digital technologies in agriculture and rural areas, briefing paper. Food and Agriculture Organization of the United Nations, Rome, p 2019
Tzounis A, Katsoulas N, Bartzanas T, Kittas C (2017) Internet of Things in agriculture, recent advances and future challenges. Biosyst Eng 164:31–48
Walter A, Liebisch F, Hund A (2015) Plant phenotyping: from bean weighing to image analysis. Plant Methods 11:14. https://doi.org/10.1186/s13007-015-0056-8
Wang N, Zhang N, Wang MH (2006) Wireless sensors in agriculture and food industry – recent development and future perspective. Comput Electron Agric 50(1):1–14

Wolfert S, Ge L, Verdouw C, Bogaardt MJ (2017) Big data in smart farming – a review. Agric Syst 153:69–80

Wu BF, Zhang F, Liu CL, Zhang L, Luo ZM (2004) An integrated method for crop condition monitoring. J Remote Sens 8(6):498–514

Yang BJ, Pei ZY (1999) Definition of crop condition and crop monitoring using remote sensing. Trans CSAE 15(3):214–218

Zamora-Izquierdo MA, Santa J, Martínez JA, Martínez V, Skarmeta AF (2019) Smart farming IoT platform based on edge and cloud computing. Biosyst Eng 177:4–17

Zhao CJ (2019) State-of-the-art and recommended developmental strategic objectives of smart agriculture. Smart Agric 1(1):1–7

Zheng LC, Yu WT, Ma Q, Wang YB (2004) Advances in the integrated evaluation of farmland fertility. Chin J Ecol 23(5):156–161

Zhou J, Tardieu F, Pridmore T, Doonan J, Reynold D, Hall N, Griffiths S, Cheng T, Zhu Y, Wang X, Jiang D, Ding Y (2018) Plant phenomics: history, present status and challenges. J Nanjing Agric University 41(4):580–588

Chapter 2
Sensing Technology of Soil Physical Properties

Wei Yang, Yao Zhang, and Minzan Li

Abstract Soil physical properties mainly refer to various physical phenomena and processes produced in the three-phase system of soil solid, liquid, and gas. It mainly includes the color, texture, density, structure, porosity, moisture, compaction, heat (thermal property), air condition, and cation exchange capacity (CEC) of soil, as well as the mechanical and physical properties and electromagnetic properties of soil. Among these properties, texture, porosity, moisture, compaction, and CEC of soil are very important for crops and need to be quickly and accurately sensed and automatically controlled in precision agriculture. The laser diffraction (LD) method is used as a fast detection method of texture. Dielectric parameters, neutron meter, and near-infrared spectroscopy are used as a main detection method of soil moisture. Frequency domain reflection (FDR), standing wave ratio (SWR), and time domain reflection (TDR) are effective methods based on dielectric parameters. Image processing is used on soil bulk density online detection. Penetrometers and on-the-go measurement are popular in the detection of soil compaction. Visible and near-infrared (vis-NIR) spectroscopy has become the most promising measurement technique to provide accurate and meaningful data on soil CEC for successful decision support on soil fertility management. The determination of soil physical properties provides the basis for soil studying, soil improvement, and soil scientific management. The rapid and accurate measurement of soil physical parameters can promote water-saving irrigation and precise fertilization and improve the yield and quality of crops.

Keywords Soil texture · Soil porosity · Soil moisture · Soil compaction · Soil CEC

W. Yang · Y. Zhang · M. Li (✉)
China Agricultural University, Beijing, China
e-mail: gpac@cau.edu.cn

M. Li et al. (eds.), *Soil and Crop Sensing for Precision Crop Production*,
Agriculture Automation and Control, https://doi.org/10.1007/978-3-030-70432-2_2

Soil is made up of weathered rock particles (mineral substance) and decayed plant and animal matter (organic matter), and it refers to the top layer material on the Earth's surface and constitutes the outer most layer of the Earth's crust. Soil has two main functions, storing nutrients and supplying water to crops and maintaining the healthy growth of crop roots. Soil physical properties mainly refer to various physical phenomena and processes produced in the three-phase system of soil solid, liquid, and gas. It mainly includes the color, texture, density, structure, porosity, moisture, compaction, heat (thermal property), air condition, and cation exchange capacity (CEC) of soil, as well as the mechanical and physical properties and electromagnetic properties of soil. Among these properties, texture, porosity, moisture, compaction, and CEC of soil are very important for crops and need to be fast and accurately sensed and automatically controlled in precision agriculture.

2.1 Sensing Technology of Soil Texture

2.1.1 Introduction of Soil Texture

Soil texture is one of the physical properties of soil and specifically refers to the combination of mineral particles of different sizes and diameters in the soil. At the same time, some important indexes can be used to characterize soil texture, such as soil bulk density, soil roughness, soil porosity, and so on. Soil texture is closely related to soil aeration, fertilizer conservation, water conservation, and cultivation. It is an important basis for soil utilization, management, and improvement and reflects the soil type according to the particle composition of soil. Soil texture is very important to crop growth, which greatly affects the maturity and yield of crops in the field.

Soil texture is mainly divided into three types: sand, loam, and clay. Among them, sandy soil has poor water retention, fertilizer retention, and drought resistance. Quick acting fertilizer is easy to be lost along with the rain and irrigation water flow. Therefore, it is necessary to increase the application of organic fertilizer, make timely topdressing, and master the principle of frequent thin application. Loam has good water conservation, fertilizer conservation, drought resistance, and rich organic matter. It is an ideal soil because of its good plowing ability. Clay soil is rich in nutrients and high in organic matter. Therefore, most of the soil nutrients are not easy to be leached by rainwater and irrigation water, so that the clay soil has good fertilizer retention performance. However, due to rain or irrigation, water is often difficult to infiltrate into the soil, resulting in drainage difficulties, affecting the growth of crop roots and hindering the absorption of soil nutrients by roots. For this kind of soil in production, it is necessary to pay attention to trenching and drainage in order to reduce the underground water level and avoid or reduce the waterlogging damage. It is also necessary to select intensive cultivation under the appropriate soil water content conditions in order to improve the soil structure and arability, and

promote the release of soil nutrients. The acquisition of soil texture information is of great significance to land management, fertilization, and irrigation.

Although the properties and characteristics of soil texture are mainly determined by the type of parent material, which is relatively stable, the texture of the cultivated layer can still be adjusted through cultivation, fertilization, and other activities. The international soil texture grading standards are shown in Table 2.1.

2.1.2 Sensing Technology for Soil Texture and Particle Size

The determination technique of soil texture by pipette is simple and easy, and it has been used by many researchers (Miller and Miller 1987; Muller et al. 2009). But it also has some great disadvantages and takes a long time to obtain results. The settling speed will become slow if the particle size is small. When the particle size is less than 1 μm, the settling time will be more than 30 h, and the relative error of the measured data is large, which limits its usage.

With the development of science and technology, the laser diffraction (LD) method, which uses laser to measure the distribution of soil particles, has been proposed. The determination principle of the LD method is based on Fraunhofer diffraction theory and Mie scattering theory (Konert and Vandenderghe 1997).

At present, there are also other many related studies on the analysis of soil texture information by means of electrical conductivity, spectral technology, and compactness, but most of them have some problems such as single detection means, isolated target parameters, and limited information interpretation. Most of the studies on the determination of soil texture by the LD method focus on the comparative analysis between the LD method and the traditional pipette method as well as the relationship between the two methods (Taubner et al. 2009; Muller et al. 2009).

Table 2.1 International soil texture grading standards. (Wu and Zhao 2019)

Texture name	Sand (2~0.002 mm, %)	Silty sand (0.02~0.002 mm, %)	Clay particle (<0.002 mm, %)
1 Loamy sand	85~100	0~15	0~15
2 Sandy loam	55~85	0~45	0~15
3 Loam	40~55	30~45	0~15
4 Silty loam	0~55	45~100	0~15
5 Sandy clay loam	55~85	0~30	15~25
6 Clay loam	30~55	20~45	15~25
7 Silty clay loam	0~40	45~85	15~25
8 Sandy clay	55~75	0~20	25~45
9 Loam clay	10~55	0~45	25~45
10 Silty clay	0~30	45~75	25~45
11 Clay	0~55	0~55	45~65

The principle of the LD method is laser dispersion. When it encounters particles in the process of propagation, it will interact with them, and some of them will deviate from the original direction. This physical phenomenon is called light scattering (diffraction). When a beam of parallel light encounters an obstacle particle in the process of propagation, the light wave deflects, and the deflection angle is related to the particle size. The larger particle size will result in smaller deflection angle of light wave and vice versa. The principle structure of laser particle sizer is shown in Fig. 2.1. A certain wavelength (633 nm) laser emitted by He-Ne laser tube is transformed into a single parallel beam through a filter. The scattering phenomenon occurs when the light beam irradiates the particle sample transmitted from the dispersion system. The angle of the scattering light is inversely proportional to the particle diameter. The scattering light intensity is logarithmically attenuated with the increase of the angle. After the Fourier lens, the image is formed on the focal plane with multiple detectors arranged. The energy distribution of the scattering light is directly related to the particle diameter distribution. The particle size distribution characteristics can be obtained by receiving and measuring the energy distribution of scattered light, and then the soil texture can be estimated.

In recent years, because of its advantages of simple operation, high resolution, high precision, and short detection time, laser particle sizer is gradually regarded as the standard instrument of soil particle size distribution. It can disperse the soil particles into the solution and then uses the refractive index and other optical properties of the measured particles and the dispersing medium, to reflect the particle size distribution data according to the scattering light intensity of different sizes of particles in different angles. After the measurement of soil samples, according to the needs of the measurement results, the "international soil texture classification standard" or "Katschinski soil texture classification standard" can be used to classify the texture of soil samples.

Mccave et al. (1986) first applied LD method to particle analysis and compared the two methods. Loizeau et al. (1994) and Konert and Vandenderghe (1997) began to study the application of LD method in soil particle analysis. After the twenty-first century, many scientific research institutes in China have introduced laser particle analyzer, and the research in this field has gradually increased (Chen et al. 2002,

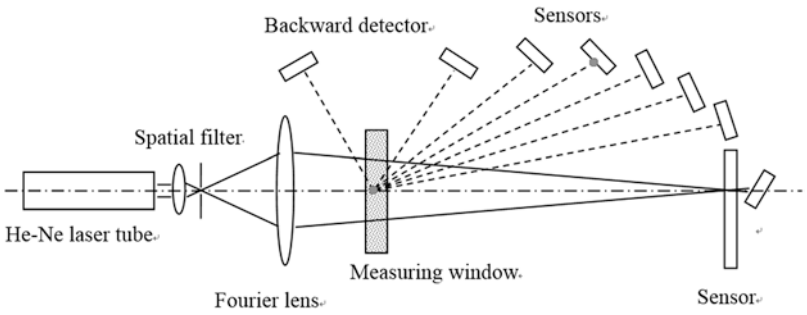

Fig. 2.1 Principle structure of the laser particle sizer

2004). Yang's group selected 265 soil samples from six major soil classes in China (Yang et al. 2009) and clay-rich iron soil with clay content more than 40% in Jinxian red soil (Yang et al. 2008) to measure particle size distribution (PSD), respectively, by LS230 laser particle analyzer. It was found that the clay content measured by LD method was lower than that measured by pipette method, while the silt content was higher than that measured by pipette method. There is a significant linear correlation among clay, silt, and sand. In addition, the results of laser particle sizer can be used to classify soil texture after correction. Most researchers think that compared with pipette method, LD method underestimates the clay part and overestimates the powder part, and the sand part has little difference. In order to realize the wide application of LD method, it is important to establish the correction relationship between the two results. In order to find the relationship between LD method and pipette method, two methods were used to analyze and compare the cinnamon soil. It was found that the data of <2 μm, 2–20 μm, and 20–50 μm grain size determined by the two methods had a good correlation and the correlation coefficient was greater than 0.95. LD method can better reflect the particle composition of cinnamon soil by linear transformation (Liu and Gao 2012).

There are great differences between the results of LD and pipette methods. There are mainly two aspects: First, the principle is different. The pipette method follows Stoke law (ISO 13320-1:1999(E)). According to the research results of Stokes in 1851, the settling rate of the spherical particles in still water is directly proportional to the square of the sphere radius and inversely proportional to the viscosity coefficient of the medium. Therefore, the equivalent particle size of the soil is measured, and the settling rate of the particles is reflected. As mentioned before, LD method is based on the optical principle and reflects the cross-sectional characteristics of particles (Pang et al. 2003; Eshel et al. 2004; Cheng et al. 2001). In the application of Stokes law, it is assumed that the soil particles are spherical; in fact, the soil particles are irregular objects with complex structures or flat, rectangular, and so on (Dixon and Weed 1977), which leads to a great difference between the results and the actual results (Gee and Bauder 1986). For LD method, the diameter of the cross section that the laser irradiates randomly is taken as the diameter of the particles, so there is a certain difference between the two methods for the nonspherical particles. Second, there are different shapes for soil particles. The soil particles themselves are irregular. When the pipette method is used to screen the soil, the large particles, such as the long particles passing through the sieve hole and the small end particles passing through the sieve hole, will cause the measurement value of the small particles to be larger. The settling speed of particles is also affected by the shape. When the maximum cross section of particles is 90° with the settling direction, the settling speed of the same particles is the slowest (Matthews 1991). For this reason, many studies have concluded that the sand content obtained by pipette method is lower than the true value, while the content of silt and clay is higher (Eshel et al. 2004).

Another reason is that the particle composition measured by the pipette method is the percentage of the total weight of soil particles at all levels, but different soil densities are different, and the density of soil particles with different particle sizes is also different. In the actual calculation, the density of soil is assumed to be 2.65 g

cm^{-3}. The PSD (power spectral density) measured by LD method is independent. Because the laser can measure any cross section of the particles in the random operation of the particles, the diameter obtained is the average diameter, and the final calculation result is the spherical volume of the soil particles. However, due to various changes in the shape of the soil particles, the measured results may be larger or smaller. Because the kaolinite and montmorillonite of clay soil are mostly flat type, it is likely that small particles will be calculated in large particles (Jonasz 1991), resulting in the low content of clay particles measured by LD method and the high content of silt and sand particles, just opposite to the situation of pipette method, so there is a significant difference between the two methods (Konert and Vandenderghe 1997).

At present, there are many reports about LD and pipette methods, and there is a great controversy on the feasibility of LD method used to determine soil particles. The determination of PSD and the determination of soil texture type are of great significance for the analysis of various physical and chemical properties of soil. The methods to determine the texture type are all based on the pipette method, that is, through the percentage division of grain quality. LD method is used to calculate the volume percentage of soil particles. The results measured by LD method are quite different from the data measured by pipette method, so it is impossible to directly determine the texture type of soil by traditional methods. It is necessary to establish a conversion model between the two to convert the LD data into the mass percentage content or establish the soil texture division method based on the volume percentage content according to LD method. The current research focuses on the former. Eshel et al. measured the PSD of 42 soil samples. Results showed that the conversion relationship of clay particles is good, but the data consistency of silt and sand particles is poor. One hundred fifty-eight soil samples were measured by Konert and Vandenderghe (1997). The conversion relationship between the two methods is $y = 0.361x-0.232$ ($r = 0.95$), where y is the volume percentage determined by LD method and x is the mass percentage determined by pipette method. Matthews (1991) proposed that the results of the two methods have reasonable consistency. Liu and Gao (2012) studied the conversion relationship between clay particles as $y = 0.85x + 11.54$ ($r = 0.99$). Beuselinck et al. (1998) and others used laser method and pipette method to study the conversion relationship between clay particles as $y = 2.74x-7.77$ ($r = 0.98$). One of the important reasons for this result is soil density. The difference of density will inevitably lead to the failure to establish a good linear correlation between the two results. In addition, there are also other possible reasons such as soil types and types of measuring methods and instruments.

Compared with optical microscope, scanning electron microscopy(SEM)has the advantages of high resolution, wide magnification, large depth of field, and strong sense of three-dimensional and simple sample preparation, which can be observed and analyzed from multiple angles. It has been widely used in the fields of soil genesis, soil investigation and mapping, soil fertility evaluation, and soil cultivation and improvement.

The principle of SEM is shown in Fig. 2.2. The electron beam spot is emitted by electron gun cathode. Under the action of accelerating electric field, the electron beam is focused by electromagnetic lens and reaches the surface of the sample. Under the action of double deflection coil, the surface of the sample is scanned orderly by grating, and the secondary electrons, backscattered electron, and X-ray are generated by the interaction between the electron and the sample. These signals are amplified after being detected by the corresponding detector and output to the display system to form an image.

Soil belongs to a kind of heterogeneous porous media material. The small scanning area selected in the observation may lead to the unrepresentative and universal results. It is recommended to select the scanning area where the distribution of soil particles and pores is relatively uniform. In order to reduce the analysis error, for the same soil, multiple samples and scanning points should be studied. When using SEM to analyze soil structure, a large magnification does not necessarily mean a good result. The selection of magnification should be determined according to the research purpose. For the conventional microstructure research of soil, the magnification should be within 300–3000. The image of SEM is a two-dimensional gray-scale image with 256 levels of gray. The threshold reflects the proportion relationship between pores and particles on the surface of soil. Scientific and reasonable selection of appropriate threshold is an important step in the process of extracting soil microstructure information. The threshold selection should be adjusted according to the research objectives and objects, and the selection method should be combined with the average method, the median method, and the maximum variance method for comprehensive evaluation. Generally speaking, a relatively small threshold should be selected for the quantitative study of soil pore structure, and a relatively large threshold should be selected for the study of soil particle shape characteristics.

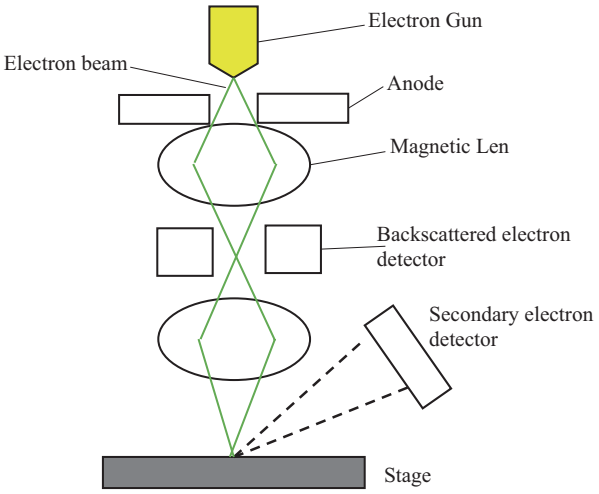

Fig. 2.2 Principle of scanning electron microscopy(SEM)

Scholars have made great achievements in the fields of soil formation, evolution, degradation, fertility, and land use. Hua et al. (2012) used SEM and polarizing microscope to study the relationship between the formation of soil crust and response to soil erosion. It is observed that soil crust is composed of a layer of closely combined smooth surface and high-density particles. Its surface is smooth, with continuous pattern of spots or clusters, and the soil crust is thin. Its characteristics are high density, high shear strength, small porosity, and low saturated hydraulic conductivity. In addition, raindrop impact is the most important factor in the formation of soil crust. Aranda et al. (2011) studied the effect of soil type and management on its organic matter content. SEM technology was used to observe that soil samples collected from the river mud lime base have more pores and structural systems, showing more biological activities.

2.2 Sensing Technology of Soil Water Content

Soil is the foundation of land resources and the basic natural resources of agricultural production. It can provide nutrients and water for plant. Soil water content (SWC), as one of the key components of the soil, is the basic premise and condition for all crops and an important factor to determine crop planting and production. SWC can have a greater impact on the regional soil temperature, heat balance, and agricultural moisture and can maintain regional ecological environment stability too. SWC is one of the most active factors of soil fertility. The lack of water is easy to restrict the dissolution and transfer of nutrients in soil and the activities of most microorganisms. In addition, SWC affects the physical properties of soil. It can affect the soil structure and arable property, control the soil respiration, and change the composition and distribution of soil gas, heat, and nutrients. Therefore, SWC is used as an important basis for agricultural production departments to provide farming measures and evaluate and judge soil fertility.

There are two parameters used to evaluate SWC level: soil volume water content and soil mass water content. Soil volume water content refers to the ratio of the volume of water in the soil to the total volume of the soil:

$$\theta_{\mathrm{V}} = V_{\mathrm{W}} / V_{\mathrm{S}} \times 100\% \tag{2.1}$$

where θ_{V} is the soil volume water content, V_{W} is the volume of water in the soil, and V_{S} is the total volume of the soil.

There are two kinds of soil mass water content, dry base and wet base. Soil mass water content in dry base refers to the ratio of the mass of water in the soil to the mass of corresponding solid substances:

$$\theta_{\mathrm{M}}\left(\mathrm{db}\right) = M_{\mathrm{W}} / M_{\mathrm{S}} \times 100\% \tag{2.2}$$

where θ_M (db) is the soil mass water content in dry base, M_W is the mass of water in the soil, and M_S is the mass of corresponding solid substances. In some case, θ_M (db)>100%. Soil mass water content in wet base refers to the ratio of the mass of water in the soil to the mass of total substances including solid and liquid:

$$\theta_M(\text{wb}) = M_W / M_T \times 100\% \tag{2.3}$$

where θ_M (wb) is the soil mass water content in wet base, M_W is the mass of water in the soil, and M_T is the mass of total substances. Usually θ_M (db) is used in agriculture and here it is abbreviated to θ_M.

In summary, soil physics, chemistry, mineralogy, mechanics, geology, hydrology, and biology properties are largely determined by SWC. At present, a variety of SWC sensors have been developed based on different measuring principles. Several typical methods are neutron method, near-infrared spectroscopy method, and dielectric parameter-based method, including frequency domain reflection (FDR) method, standing wave ratio (SWR) method, and time domain reflection (TDR) method.

2.2.1 Measurement of Soil Water Content with Dielectric Parameters

The soil water content in soil has a significant effect on the dielectric properties of soil (Williams and Baker 1982). Based on this principle, the dielectric constant method uses the dielectric constant of soil to reflect its value. At present, the handheld SWC meter mostly measures the dielectric properties of water-bearing soil by sensing. When the soil moisture changes, the dielectric constant of the soil characterization changes, resulting in the change of the electromagnetic properties of water-bearing soil. The change of soil water content can be inferred by detecting the change of electrical parameters in the circuit. This method is fast, accurate, and easy to integrate. It has gradually become the main method of soil moisture measurement.

1. Frequency Domain Reflection (FDR) Method

In the three-phase media composition of soil, the dielectric constant of soil particles (ε_s = 3~4, 20 °C) and air (ε_a = 1, 20 °C) is very low, while the dielectric constant of water (ε_w = 80, 20 °C) is far greater than that of soil and air, which is dominant. Therefore, the dielectric constant of soil mainly depends on the content of water, so the SWC can be obtained indirectly according to the dielectric constant of soil. The principle of FDR SWC monitoring is shown in Fig. 2.3. The monitoring equipment uses the oscillation of LC circuit to measure the dielectric constant of the medium according to the change of the oscillation frequency of electromagnetic wave in different medium and then reversely displays the soil moisture status

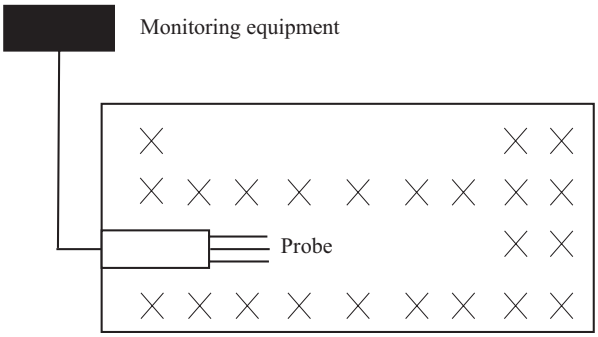

Fig. 2.3 Schematic diagram of the FDR soil moisture monitor

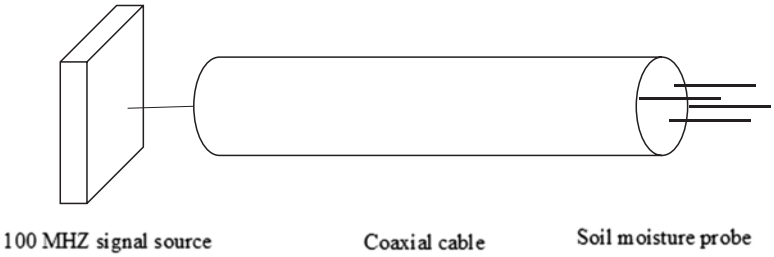

Fig. 2.4 Diagram of SWR measurement device

through a certain corresponding relationship. The frequency F of LC oscillation circuit is expressed as

$$F = \frac{2\pi}{\sqrt{LC}} \tag{2.4}$$

where L is the inductance and C is the capacitance.

The frequency F of LC oscillation circuit is mainly affected by the change of inductance and capacitance, because the inductance value of SWC monitoring instrument is the same. The change of oscillation frequency only depends on the change of capacitance, while the change of capacitance depends on the influence of soil. When the dielectric properties of soil change, the capacitance of LC oscillation circuit changes. From Eq. (2.4), it can be seen that the frequency F of LC oscillation circuit changes with the capacitance change. Therefore, there is a certain relationship between the oscillation frequency F and the SWC outside the pipe sleeve. By analyzing the frequency of LC oscillation circuit, the SWC can be reflected. The sensor of soil water content based on frequency domain reflection method is shown in Fig. 2.3.

2. Standing Wave Ratio (SWR) Method

SWR (standing wave ratio) measuring instrument is mainly composed of signal generator, coaxial transmission line, and soil probe and precision detection circuit,

as shown in Fig. 2.4. The signal generated by the signal source is transmitted to the soil probe along the transmission line. Because the probe impedance does not match the transmission line impedance, part of the signal is reflected back along the transmission line, and the other part continues to propagate along the probe. In the transmission line, the incident wave and the reflected wave will be superposed to form standing wave, which will change the voltage value of each point on the transmission line, while the impedance of the soil probe depends on the dielectric property of the soil, and the dielectric constant of the soil mainly depends on the soil water content, so the soil water content can be obtained by measuring the voltage variation on the transmission line.

3. Time Domain Reflection (TDR) Method

According to the physical phenomenon that the traveling speed of electromagnetic wave will change when it propagates in the medium with different dielectric constants, the time domain reflectometry (TDR) method is proposed. TDR is a high-speed measurement technology in dielectric measurement. It is developed on the basis of the research on dielectric properties of many liquids (Fellner-Feldegg 1969) and originally used to locate defects in communication cables. TDR is a system similar to radar system, which has strong independence. Topp et al. (1980) introduced them into the study of SWC measurement. SWC has a great influence on the dielectric properties of soil. Under the action of external electric field, the polarization degree of water is much greater than that of other substances. In the microwave frequency band, different wavelengths correspond to different dielectric constants of water. The dielectric constant of water is much larger than that of air, and the dielectric constant of soil water in soil matrix is absolutely dominant. A TDR sensor is composed of pulse signal generator, coaxial transmission line, and probe and high-frequency oscilloscope, as shown in Fig. 2.5.

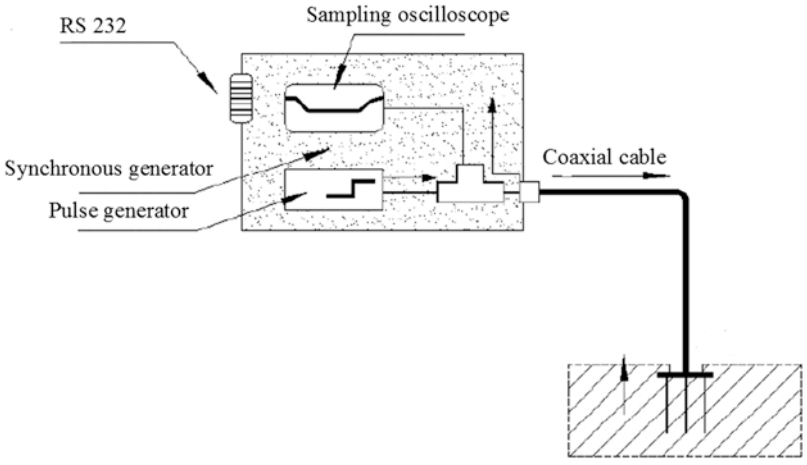

Fig. 2.5 TDR organization chart

2.2.2 Measurement of Soil Water Content with Neutron Meter

The neutron method uses radium as the radiation source. The neutrons with high energy (fast neutrons) are emitted into the soil. They collide with atoms in a series and lose enough energy, and this kind of slow neutron energy can be counted by the counter. When the neutron collides with the atom, the lighter the atomic weight is, the greater the energy loss is. The hydrogen atom in the soil mainly comes from the soil water. Therefore, when the SWC is high, there will be the more hydrogen atoms, and the more slow neutrons return to the counter. The density of slow neutrons has a certain relationship with SWC. Therefore, the SWC can be calculated by measuring the slow neutron density reflected by the soil. The main types of neutron water meter for SWC measurement are embedded type, surface type, transmission type, and scattering type. The working process of the embedded neutron water meter is to embed the neutron source into the soil to be measured. The neutron source continuously and stably emits fast neutrons, which enter the soil medium and collide with the nuclei of various atomic ions, so that the fast neutrons lose energy and slow it down. The SWC is determined by measuring the relationship between the density of slow neutron cloud and water molecules.

The neutron instrument system includes a neutron source probe and a counter for recording the number of slow neutrons. Both of them can be placed in one device or opened separately. When they are together, only one tube is needed to be driven into the soil. When they are separated, two tubes are needed. When the probe is placed at the depth of boron fluoride, the soil water content at different depths can be measured.

The advantage of neutron method is that it provides a rapid method to determine the soil water content. The soil sample is undisturbed and can be continuously observed at the same measuring point for many times. The disadvantage is that the precision of soil with more organic matter content is poor and the cost is high, so additional devices are needed for the determination of soil water in surface layer of soil (0.3 m).

To measure SWC with neutron meter, the operation procedure must be strictly standardized. During the operation, the following problems should be paid attention to:

1. Before using the neutron SWC meter, the operators should have special training and operation training and should be familiar with the usage and maintenance methods, radiation protection methods, and national regulations on the use and storage of radioactive sources.
2. In the representative area of the representative plot, the measuring points and depth shall be arranged according to the observation requirements, and the neutron SWC meter tube shall be buried. Once the monitoring points are set, they shall not be changed at random to ensure the consistency of SWC.
3. The material of neutron meter tube is aluminum alloy or hard plastic tube. When using plastic tube, PVC tube and plastic tube with high hydrogen content shall

be avoided. The tube should have certain strength and corrosion resistance to prevent the deformation and corrosion of the tube wall.

4. During the installation of the pipe, the pipe shall not be squeezed excessively by the soil and external forces, and the poor contact between the pipe wall and the soil shall be prevented to form a channel for water to flow into the lower soil. The soil around the pipe wall near the surface shall be compacted to prevent the inflow of irrigation water and rainwater runoff. During the installation of the neutron SWC meter tube, the diameter of the borehole shall be the same as the outer diameter of the tube, so that the tube is in close contact with the soil. The outer diameter of the tube shall be the same as the diameter of the socket at the bottom of the neutron meter, and the top of the tube shall be 10cm higher than the ground.
5. The lower end of the neutron meter tube is sealed with a cone to prevent the underground water from entering, and the upper end of the tube is sealed with a rubber plug to prevent the surface water from entering.
6. After the installation of the pipeline, check whether the pipeline leaks or accumulates water after water filling or dewatering. If there is any of the above phenomena, the pipeline shall be reinstalled.
7. If the neutron source of the instrument is replaced, the calibration shall be carried out again.
8. When observing the SWC in the field, the recording time of the counting or neutron SWC meter can be set according to the SWC level. When the SWC is large, the counting time can be longer. Generally, take the mean value of two close readings as the reading of this point. If the difference between the two readings is large, take the third count, and take the mean value of two close readings as the reading.

As a whole, the neutron instrument can measure large volume soil samples. Relatively speaking, it is fast, accurate, and representative. However, it is expensive and radioactive, which limits the promotion of its use. The vertical resolution of neutron instrument is poor, so it is difficult to obtain surface moisture of soil.

2.2.3 Measurement of Soil Water Content with Near-Infrared Spectroscopy

It was observed that when the natural soil was wet, the spectral reflectance of the soil would decrease. The reason for this phenomenon is that the soil particles are covered with a water film and the total reflectance of the water film makes part of the energy reflected back to the soil particles, and part of it is absorbed. Bowers and Hanks (1965) and Planet (1970) conducted a series of soil spectra reflectance measurement and the result showed that soil reflectance decreased with the increase of SWC. Stoner and Baumgardner (1981) confirmed that there was a phenomenon that soil spectral reflectance decreased with the increase of SWC. They pointed out that

the shape of soil spectral reflectance curve changed, especially in the brightly colored soil and the short wave near-infrared region, which was more obvious because of the soil moisture absorption. Bedidi et al. (1992) also pointed out that the main reason why water had a great impact on soil spectral reflectance was that the spectral reflectance of soil was determined by the band, the absorption intensity, and the absorption location of soil solid components. Therefore, the change of SWC has an effect on the spectral reflectance of the whole band, especially in the absorption band, which is most sensitive and violent to the change of SWC. Therefore, effective acquisition of soil moisture-sensitive spectral information is an important basis for accurate estimation of SWC.

After obtaining data of soil moisture-sensitive spectrum, the model is built based on the selected band or full band information of soil moisture-sensitive spectrum to predict SWC. At present, two kinds of soil spectral modeling techniques, linear model and nonlinear model, are mainly used. At first, the stepwise multivariate linear regression (SMLR) model with high reliability under controllable conditions or the principal component regression analysis (PCA) method widely used in the statistical analysis and modeling of visible and near-infrared spectral data are used by most of the researches. Moreover, the partial least square (PLS) regression analysis method with reference to the common multiple regression, PCA, and typical correlation analysis ideas with the development of data mining technology, support vector machine (SVM), artificial neural network (ANN), random forest (RF), and other nonlinear models are also used to estimate SWC. These models are much more complex than linear model, but with the development and revolution of computer technology, nonlinear model parameter estimation, nonlinear optimization, and other problems have been solved, which have become a research hotspot. According to the current research, both linear model and nonlinear model have their own advantages and disadvantages and applicable conditions. The hyperspectral estimation methods for SWC need to be further studied and compared to determine the more applicable modeling methods.

In order to quickly measure SWC, a portable SWC sensor was developed and consisted of two parts, optical part and control part, as shown in Fig. 2.6 (An 2013). The optical part included seven wavelengths of near-infrared light source, light source driving circuit, Y-type incident/reflected optical fiber, and probe and photoelectric sensor. The used seven wavelengths are 940 nm, 1050 nm, 1100 nm, 1200 nm, 1300 nm, 1450 nm, and 1550 nm, part of which (1050 nm and 1450 nm) are used to measure SWC and the other wavelengths are used to detect other soil parameters. The sensor was designed to penetrate into the soil to measure the relevant parameters of the soil. The single band optical signal provided by near-infrared light source was transmitted to the underground soil through Y-type optical fiber for spectral reflectance measurement. InGaAs was used as the photoelectric material to convert the light signal into electric signal. The electric signal was amplified, filtered, and A/D converted and finally sent to the microcomputer system. After the data were processed by the system, the detection results were displayed on LCD, and the data were easily transmitted with the upper computer or stored on the U-disk through the serial port.

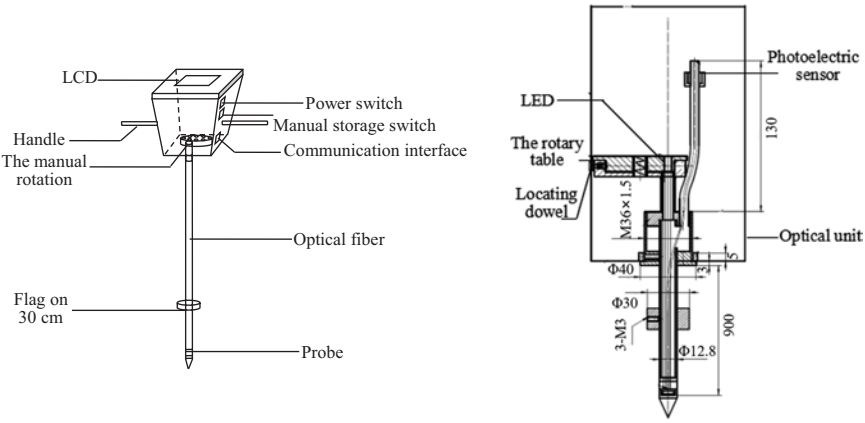

(a) General schematic (b) Optical unit

Fig. 2.6 Portable SWC sensor. (An 2013)

Table 2.2 Statistical table of data of soil sample

Parameter	Range/%	Average value/%	Standard deviation/%
Modeling set	3.15~14.19	8.79	2.41
Validation set	4.54~12.09	8.03	2.09

The field experiment of the portable SWC sensor was conducted in a farmland. The soil was loam and belonged to the typical soil in the North China. The soil mass water content (dry base) data for calibration was obtained by drying in the laboratory. As shown in Table 2.2, 48 samples were divided into 2 groups, with 3/4 as the calibration set and 1/4 as the verification set; 3.15~14.19% covered most of the distribution range of soil, and the validation set distribution was 4.54~12.09%, the average value was 8.03%, and the standard deviation was 2.09%, which met the modeling requirements.

1. Linear Model of SWC

Simple linear regression is the most basic and simple modeling method, which describes the linear correlation between an objective function and an independent variable. Because of its simple modeling method and reliable model, simple linear regression is widely used in near-infrared spectrum detection.

In the experiment, the soil absorbance data were measured by the portable soil sensor and the correlation coefficient between the absorbance value of soil at 1450nm and the SWC was 0.89.

2. Nonlinear Modeling of Soil Moisture

Since the soil reflectance was obtained in an open field, it cannot fully satisfy the Beer-Lambert law. A nonlinear SWC model based on BP neural network method was tried. Because the absorption coefficients of soil water were higher at 1450 nm

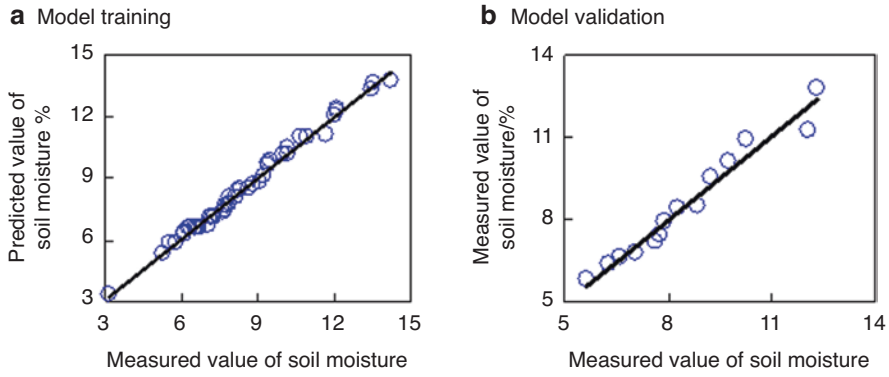

Fig. 2.7 Prediction model of soil moisture. (An 2013)

and 1050 nm, the absorbance values at 1050 nm and 1450 nm were used as input parameters.

In the process of BP neural network modeling, because the absorption of soil moisture is more obvious, the hidden layer factor and training times can choose a lower value to reduce the complexity of the model and improve the stability of the model. Forty-eight soil samples were divided into test set and verification set, 34 samples were used as training modeling, and 14 samples were used for prediction verification.

The result of the program shows that the network can reach the target value after 90 steps of learning training, and the fitting accuracy of the network is shown in Fig. 2.7. The correlation coefficient of training set is 0.99, and the correlation coefficient of verification set is 0.94.

The matrix of weight for input layer, the matrix of weight for the middle layer, and the threshold vector of the network are recorded, which are saved as the network technical data, so that the function of using the network model to predict soil moisture can be realized by programming these values.

2.3 Sensing Technology of Soil Porosity and Bulk Density

2.3.1 Introduction of Soil Porosity and Bulk Density

The spaces between the soil particles or aggregates and within the aggregates are called soil pores. Soil pore structure refers to the shape, size, quantity matching, and spatial distribution of soil pores, including the shape and quantity characteristics of porosity, pore number, pore radius, pore size distribution, and roundness rate as well as the spatial distribution characteristics of pores, such as the spatial distribution, interconnection, and correlation between pores. The pore structure of soil directly affects the way and mode of water migration on the surface and in the soil, which is

closely related to the runoff and permeability on the surface of soil, and also has many effects on soil fertility.

Soil's specific gravity refers to the ratio of the weight of solid dry soil particles per unit volume to the weight of water in the same volume, excluding soil pores. The main factors determining the size of soil's specific gravity are the content of soil organic matter and the composition of soil minerals. Correction Soil bulk density, also called "apparent specific gravity of soil", is the ratio of the weight of a certain volume of soil (including soil particles and pores between particles) after drying to the weight of the same volume of water is the same as the unit weight of the dry soil of one cubic centimeter, including pores, expressed in grams. Generally, the proportions of soil volume are between 1.4 and 1.7 for the soil with many minerals and poor structure (such as sandy soil) and between 1.1 and 1.4 for the soil with many organic materials and good structure (such as agricultural soil). The soil bulk density can be used to calculate the weight and porosity of a certain area of arable soil. It can also be used as one of the indicators of the degree of soil ripening. The soil bulk density with a higher degree of ripening is often smaller. Soil bulk density is determined by the number of soil pores and soil solids. The weight of any unit of soil can be calculated according to the soil bulk density. The formula is soil weight = volume ×soil bulk density. Through the measurement of soil bulk density, the organic matter content of soil, texture, and soil structure can be roughly estimated. The capacity of soil water permeability and water conservation can be evaluated by soil bulk density and soil porosity.

There are many methods to measure soil bulk density, among which the most classical method is the ring cutter method. When measuring soil bulk density with ring cutter, the expressions of soil water content and soil bulk density are as follows:

$$b = g \times 100 / \left[v \times \left(100 + w \right) \right] \tag{2.5}$$

$$w = \frac{g - g_1}{g_1} \times 100\% \tag{2.6}$$

where b represents soil bulk density (g/cm^3), g represents the total weight of wet soil in ring cutter (g), v represents the volume of ring cutter (cm^3), w represents the soil mass water content (%), and g represents the total weight of dry soil in ring cutter (g). Other methods to measure soil bulk density include wax seal method, mercury removal method, sand filling method, drainage method, soil bulk density prediction based on BP neural network, time domain reflectometer combined with soil drilling method, volume replacement method, gamma ray and visible near-infrared spectroscopy, and so on. The research of measurement method is mainly reflected on how to measure soil bulk density and soil water content quickly, accurately, and economically, which is of great significance to detect soil water status in time, so as to make scientific decisions or take reasonable measures in time.

The time domain reflectometer combined with the soil drill method is usually used to measure soil bulk density. It uses the metal probe to measure the soil dielectric constant and converts it into the soil volume moisture content. This method

combined with the soil drilling method to determine the weight and water content of the soil can also obtain the ratio of the volume and mass water content of the soil which is the soil bulk density. Using time domain reflectometer to measure soil volume water content is almost not affected by soil type, soil density, soil temperature, and soil pore water conductivity. Generally, these factors are not calibrated in practical application, so a lot of additional work is saved and the reliability of measurement results can be guaranteed. This method has the advantages of fast, accurate, and continuous measurements. It does not damage the soil structure, can basically maintain the original soil, and is more suitable for long-term continuous monitoring.

The volume replacement method is based on the assumption of a certain density of soil particles. After a certain volume of standard sampling ring cutter is used to obtain the soil sample, the soil is saturated by adding water to the soil to be measured, and the air void in the soil is replaced by a certain volume of water until the soil sample reaches the saturation state. Then, the volume of the replaced air void is calculated, and then the soil mass moisture content and soil bulk density are calculated. The experimental equipment system mainly includes the ring cutter for soil sampling, stacked soil sample saturator, balance (accuracy is 0.1g, water content measurement accuracy is 1/1000), permeable rock, and filter paper. This measurement operation is simple, but the time for saturation depends on the soil properties and generally takes 10 h, and the time for cohesive soil is slightly longer.

2.3.2 Sensing Instruments of Soil Porosity and Bulk Density

The traditional method of measuring soil bulk density has a long and tedious process, which is difficult to be used in a wide range of different texture soil bulk density measurements. In order to estimate soil bulk density online in real time, a camera can be used to obtain the image features of soil surface and then predict soil bulk density combining the image processing analysis modeling (Liu 2019).

A Canon camera was used to take photo of soil surface and then image processing was conducted. The gray level co-occurrence matrix (GLCM) was applied to extract 12 texture eigenvalues of soil surface images, namely, energy value, entropy value, uniformity, homogeneity, variance, sum average, sum variance, sum entropy, difference variance, difference average, difference entropy, and inertia moment, which were correlated with the soil bulk density obtained by the ring cutter method, respectively. Eighty-six samples of soil surface images were analyzed, and the correlation analysis was made between the soil bulk density obtained by the ring cutter soil sampling experiment and each of the 12 texture eigenvalues of soil surface images. Finally, 12 correlation coefficients r were calculated between the soil bulk density and each of the 12 texture eigenvalues of soil surface images, which were 0.8418, 0.8195, 0.5501, 0.8510, 0.5661, 0.6353, 0.5807, 0.3755, 0.5244, 0.6348, 0.6165, and 0.8595. The results show that energy (0.8418), homogeneity (0.8195), entropy (0.8510), and moment of inertia (0.8595) had a high correlation with soil bulk density.

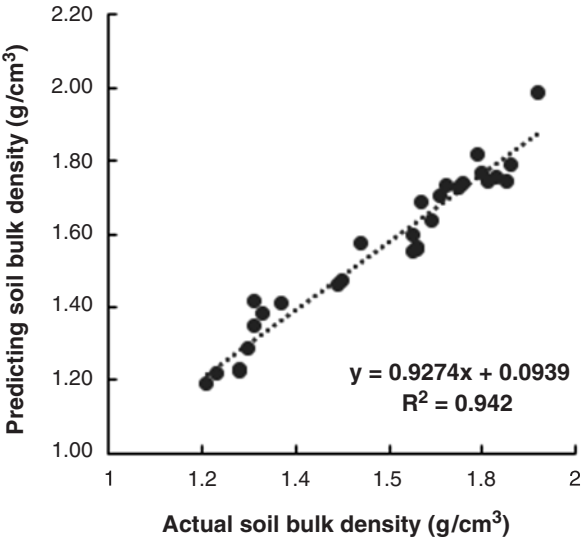

Fig. 2.8 Prediction result of the soil bulk density by BP model. (Liu 2019)

Since four texture characteristic values of energy, homogeneity, entropy, and moment of inertia had higher correlation with the soil bulk density, using those texture characteristic values as input, a generalized neural network algorithm was used to predict soil bulk density. The advantage of this method was that the experimental process was simple, it was an easy-to-follow-up analysis, and the measurement accuracy was high. The coefficient of determination (R^2) of the prediction model was 0.9420. The model result is shown in Fig. 2.8.

2.4 Sensing Technology of Soil Compaction

Soil compaction or soil compactness, also known as soil hardness, refers to the resistance of soil to tools inserted into the soil. It is one of the soil physical properties and a comprehensive performance of soil mechanical composition, porosity, bulk density, water content, and other characteristics. It has an important influence on plant growth and microbial activities, such as soil aeration and water permeability, nutrient existing form, and transformation. Therefore, it is one of the necessary items in the agricultural and forestry production practice. In farmland ecosystem, soil compactness is mainly affected by rainwater, agricultural equipment, and planting methods. Rainwater often forms a layer of soil shell on the soil surface, which makes the topsoil hard. The parameters of agricultural machines (seeder, harvester, rotary cultivator, etc.), such as weight, area of contact between wheel and ground, material and shape of tire, and inflation condition, will have different effects on soil compaction. The heavier the machine, the smaller the contact area and the greater the soil compactness is. The increase of soil compactness is a process in which soil

particles rearrange to reduce soil porosity and increase bulk density. Soil compactness is usually measured by bulk density and porosity. However, when using those indexes to measure soil compactness, the result will be affected by soil expansion and contraction. Therefore, it is necessary to point out the soil water content when describing soil compactness. Soil texture and organic matter content can also affect the size of soil bulk density, so the comparability of using soil bulk density to represent different types of soil compactness is poor.

Except for bulk density and porosity, the traditional methods of measuring soil compactness also include multichannel surface wave analysis and soil compactor. The multichannel surface wave analysis and measurement method need to bombard the soil with air gun source for many times, causing serious damage to the soil, which is time-consuming and labor-consuming. The measurement of soil compactor is greatly affected by soil water content and human factors. The results of traditional soil compaction measurement method are relatively rough, and the repeated application is poor, which are not suitable to precision agriculture. At present, penetrometer, ground-penetrating radar, and on-the-go measurement device are recommended and utilized in agricultural practice, because they can measure soil compaction fast and accurately.

2.4.1 Measurement of Soil Compaction with Penetrometer

The improved measurement method of soil compaction is penetrometer based on cone index meter. The parameters measured by the penetrometer are cone index (CI), which is defined as the ratio of the resistance of the cone probe to the cross-sectional area of the upper end of the cone. According to ASAE S313.3 FEB1999ED(R2013)standard, the soil cone index meter is used as the measuring device to characterize the soil compactness. The force required to press a 30° cone into the soil, in kilopascals, is the index of soil strength, known as the taper index. The manual soil cone indexer has a tapered and graduated drive shaft. The standard recommends the use of two tapered base sizes as follows. For soft soil, 323 mm^2, the diameter of cone is 20.27 mm, and the shaft diameter is 15.88 mm. For hard soil, 129 mm^2, the diameter of cone is 12.83 mm, and the diameter of the shaft is 9.53 mm.

AISI416 stainless steel is recommended by the American Iron and Steel Association to be produced into a tapered surface with a maximum smoothness of 1.6 μm. If the length of the shaft does not exceed 457 mm, the cone with 129 mm^2 base is suitable for hard soil. In very hard soil, because the driving shaft is stronger, cone with 323 mm^2 base driven by machinery is used. The scale on the drive shaft is 25.4mm apart to identify the depth of the hand device. In order to adapt to most agricultural soil conditions, the measuring device of manual operation unit shall have a cone index capacity of about 2MPa for 323 mm reference area penetrometer and not more than 5MPa for 129mm^2. The taper index needs to be read directly. In some cases, smaller diameter shafts may be required. When the base diameter is

worn more than 3%, the spherical cone should be replaced; otherwise, the taper index will have 5% error. The 1.5 mm shoulder at the bottom of the cone provides longer cone life without seriously affecting the accuracy of readings. The most important thing is in order to eliminate the friction in the process, it is necessary to ensure that the cone rod penetrates into the soil at a constant speed of 30 mm/s.

At present, many products of handheld soil compactors have been sold on the market, for example, SC-900 digital soil compactor (Spectrum Enterprise, California, USA). When using handheld soil cone index meter, the operator keeps it perpendicular to the soil surface, inserts the tip part into the soil at the speed of 30 mm/s, and reads the sensor value to calculate the soil cone index.

2.4.2 On-the-Go Measurement of Soil Compaction

The cone penetrometer has been the standard tool for quantifying soil compaction in situ by using cone index (CI). In order to automatically map the soil compaction fast and accurately, on-the-go measurement system of soil compaction is necessary. Various on-the-go soil sensor systems have been developed. Liu et al. (1996) designed a multi-sensor device to continuously detect the soil mechanical resistance. A vertical blade with multiple strain gages mounted on a tractor equipped with a GPS was developed. It can simultaneously measure soil mechanical resistance continuously with several depths. The correlation coefficient between the measured value of the device and the standard cone measurement was 0.95 (Adamchuk et al. 2001). Sirjacobs et al. (2002) designed a system that uses octagonal ring sensors as force-sensing elements to measure the horizontal force, vertical force, and bending moment of the soil tillage tool simultaneously. The correlation coefficient between the cone index and the three measured parameters is 0.81. An integrated soil physical properties mapping system (ISPPMS) was developed. It was comprised of an optical sensor, a capacitance sensor, and an instrumented blade. The system was used to determine parameters of a second-order polynomial model representing the change of soil mechanical resistance with depth. However, based on field evaluation, it was concluded that in most cases, the second-order coefficient was not significant. Therefore, the assumption of a linear relationship may be appropriate (Adamchuk and Christenson 2005).

An approach to quantify soil compaction is to measure soil strength, since soil strength is strongly associated with compactness and drainable porosity (Chung 2004; Chung et al. 2008). Furthermore, since the soil strength can be calculated by measured soil resistance (Chung et al. 2006), several on-the-go measurement systems of soil compaction were developed (Chung and Sudduth, 2004; Chung et al. 2006).

1. On-the-Go Soil Strength Profile Sensor (SSPS) (Chung et al. 2006)

The overall objective was to design an on-the-go soil strength profile sensor (SSPS) that could measure “CI-like” soil strength at multiple depths while traveling

across a field. The SSPS design concept enabled measurement of soil strength at multiple depths (Fig. 2.9). Each force-sensing tip interfaced with a load cell located inside a narrow soil-cutting blade and was extended in front of the blade edge. The main blade was mounted to a frame using a shear bolt mechanism, and the frame was attached to a tractor through the three-point hitch. Major design issues were (1) soil strength sensing, (2) data acquisition and calibration, (3) selection of materials for the main blade and sensing tip, and (4) tractor attachment and overload protection.

Maximum sensing depth, expected maximum soil strength, and sensing resolution were selected as 50 cm, 10 MPa, and 0.1 MPa, respectively, based on examination of CI profiles from a Missouri clay pan soil field. Higher loads due to dynamic operation of the sensor, along with a safety factor, were considered for appropriate load cell selection and sensor design. The desired maximum vertical sensing interval was 10 cm, contingent on being able to obtain accurate strength data from tips on that spacing.

High-resolution and high-frequency data acquisition was needed to capture variability in soil strength. Assuming a 2 ms^{-1} normal operating speed, a minimum sampling frequency of 4 Hz was selected to detect repeating spatial patterns in CI (e.g., wheel traffic patterns). Faster data acquisition would be desirable for more reliable measurements and would allow application of filtering techniques such as a moving average.

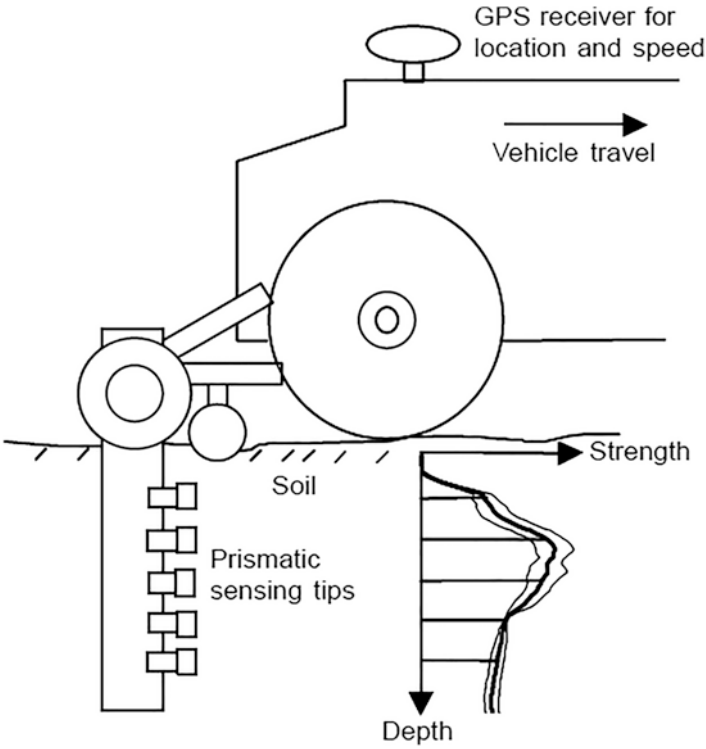

Fig. 2.9 Operational concept of the on-the-go soil strength profile sensor. (Chung et al. 2006)

A prismatic tip with a 60° cutting or apex angle was selected as the sensing tool to reduce soil disturbance and avoid extreme force measurements for most soils, based on modeling and simulation of soil failure mechanisms.

2. Subsoiler-Based Measurement System of Soil Compaction

When a farm implement, for example, subsoiler, moves forward in the soil, it will be affected by the soil mechanical resistance, which is closely related to soil strength or soil compactness. Therefore, a subsoiler-based measurement system of soil compaction was developed (Zheng 2019). The measurement system included two parts of measurement units, the pressure sensor and three sets of strain gauges as shown in Fig. 2.10a. When the subsoiler shovel moves forward in the soil, the tip is the first part under the press. Then, the mechanical resistance makes the strain gauges sense the tiny deformation of the subsoiler shovel. Through the leverage of force, the soil mechanical resistance is transformed to the pressure sensor.

The system shown in Fig. 2.10a can be simplified as an equivalent diagram shown in Fig. 2.10b.

According to the equivalent diagram, soil surface mechanical resistance can be calculated as Eq. 2.7:

$$P_0 = f\left(F_s, \varepsilon_i, u, v\right) \tag{2.7}$$

where P_0 is the soil surface mechanical resistance (N), F_s is the force of the pressure sensor (N), ε_i (i = 1, 2, 3) is the ith depth force of the strain gauges (N), u is the distance between the frame and the soil surface (cm), and v is the forward speed (km/h).

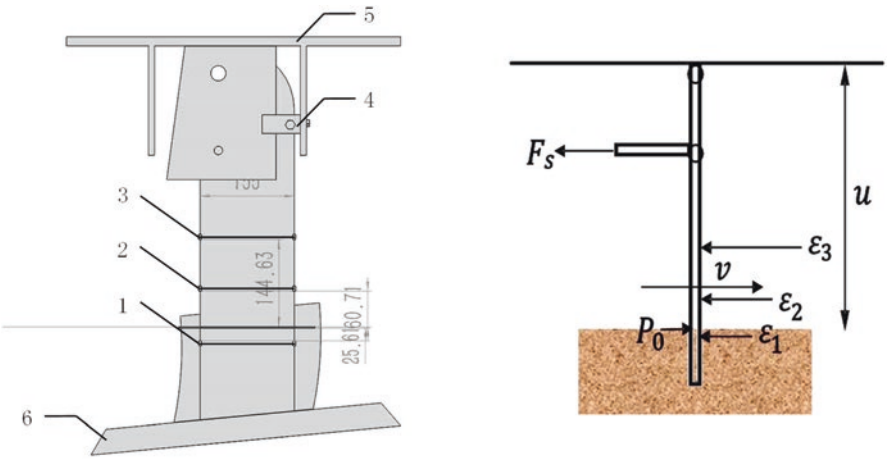

(a) Measurement unit (b) Simplified equivalent diagram

Fig. 2.10 Subsoiler-based measurement system of soil compaction. (Zheng 2019)

The field experiments were conducted to verify the feasibility of the system, and a linear model was established to estimate the soil mechanical resistance system. The result showed that the on-the-go soil mechanical resistance system could realize the measurement accurately. The deviation is no more than ±5%.

2.5 Sensing Technology of Soil Cation Exchange Capacity

2.5.1 Introduction of Soil Cation Exchange Capacity

The soil cation exchange capacity (CEC) refers to the capacity of cation adsorbed and exchanged by the soil colloid (soil particles with a diameter of 1–1000 nm) under certain pH conditions. The CEC value is expressed as the amounts of various cations per kilogram of soil, that is, mol/kg.

Soil colloids can be divided into inorganic colloids, organic colloids, and organic-inorganic composite colloids. Inorganic colloids include hydrous silicon oxide, iron aluminum, and layered aluminum silicate. Organic colloids include humus, protein, and cellulose. In agricultural soil, organic colloids rarely exist alone, about 50–90% of which are combined with mineral colloids to form organic and inorganic complex (also known as absorbent complex).

With its huge specific surface area and surface energy, soil colloids make the soil adsorbent. The adsorption and ion exchange properties of soil make it the main destination of heavy metal pollutants. It can regulate the concentration of soil solution and ensure the diversity of soil solution components, thereby ensuring the "physiological balance" of the soil solution, while also maintaining nutrients from being lost by rain.

Soil CEC is a very important soil characteristic in agriculture. It is closely related to the content of colloidal particles and organic matter, soil type (different clay minerals), soil pH value, soil texture, etc. For example, (1) when the content of colloidal particles is high and soil humus is rich, CEC value is also high. (2) For different types of clay minerals, the CEC value of the soil with 2:1 (montmorillonite) is greater than that of soil with 1:1 (kaolin). (3) When pH value is high, the variable negative charge of soil increases, resulting in the increase of CEC. (4) When the pH value and humus content of the soil are approximately equal, the CEC depends on the texture of the soil. Therefore, soil exchange performance is an indicator of soil characteristics. The determination of CEC can evaluate the soil water and fertilizer conservation capacity and can be used as an important basis for soil improvement and rational fertilization.

2.5.2 Sensing Method of Soil Cation Exchange Capacity

In the laboratory measurement method, the determination of soil CEC is to use an exchange agent (also known as a saturator) to exchange the ions adsorbed on the soil colloidal particles and then carry out the determination. This exchange reaction is carried out with equal mass. A large number of different experimental methods have been proposed, and they could be summarized into four groups, namely, summation methods, direct displacement of the saturating salt, displacement of index cation after washing out excess salt, and radioactive tracer methods (Bache 1976). Whether the exchange is complete mainly depends on the selected exchange agent and exchange method. The exchange methods include multiple leaching (or centrifugation) exchange methods and one-time equilibrium exchange method. Among them, multiple leaching (or centrifugation) exchange methods are used to rinse (or centrifuge) the soil multiple times according to the chemical equilibrium movement law to complete the exchange. This method is complete but time-consuming. The one-time equilibrium exchange method is to add the exchanger to the soil sample and filter after shaking. The exchange of this method is not complete, but it is simple and fast.

At present, the widely used measurement methods in laboratory of soil CEC mainly include neutral ammonium acetate method and barium chloride-sulfuric acid-forced exchange method. With the continuous development and application of new reagents and new instruments, many researchers are continuously exploring methods to improve efficiency and accuracy of soil CEC determination, such as ammonium fluoride exchange difference method, EDTA (ethylenediaminetetraacetic acid) ammonium salt rapid method, and ICP-AES (inductively coupled plasma optical emission spectroscopy) (Shen and Xing 2016).

The determination methods of soil CEC mentioned above all require sample preparation (drying, grinding, weighing, washing, and centrifugation) in laboratory, which is time-consuming and is destructive to the sample when it is examined. As such, CEC is not presently easily field determinable. Therefore, researchers have attempted to find alternative methods that are simple, fast, cost-effective, and even in situ.

In a review of the application of proximal soil sensing to assess soil properties, it is identified that visible and near-infrared (vis-NIR) spectroscopy has become the most promising measurement technique to supply accurate and meaningful data on soil CEC for successful decision support on soil fertility management. This is because vis-NIR spectra of soils contain large sets of spectral information representing broad bands of overtones and combinations of fundamental vibrations occurring in the range of the electromagnetic spectrum. Quantitative information on CEC can be extracted with suitable multivariate regression methods, which have an advantage over simple bivariate relationships and are suitable for peak intensity measurements. So far, the use of vis-NIR spectroscopy for the determination of soil CEC has achieved varying degrees of success, depending on the conditions, under which the evaluations are carried out (e.g., in the laboratory or online in the field).

Apart from the vis-NIR spectroscopy methods, the combination of optical soil sensor and electrical conductivity (EC) sensing unit and portable X-ray fluorescence (PXRF) spectrometry are all used to estimate soil CEC and proved effective.

2.5.3 Sensing Technologies of Soil Cation Exchange Capacity

1. In Situ Determination of Soil CEC with vis-NIR Spectroscopy

The in situ determination system of soil CEC with vis-NIR spectroscopy was developed based on the online soil sensor, which consisted of an optical sensor and a subsoiler as shown in Fig. 2.11 (Mouazen et al. 2005). The subsoiler with the optical probe, which was used as a soil-cutting tool, was installed on a frame, which had been manufactured by Mouazen's group at Uludag University (Ulusoy et al. 2016). For field measurements, the online sensor was mounted on the three-point linkage of a tractor. An AgroSpec mobile, fiber-type vis-NIR spectrophotometer (Tec5 Technology for Spectroscopy, Germany) with the spectral range of 350–2200 nm was used in this study (Quraishi and Mouazen 2013).

After preprocessing of the original spectral signals, the spectra within wavelengths of 421–1745 nm were selected for the calibration. Partial least square (PLS) regression analyses with full cross-validation were carried out to establish CEC models. Results of the CEC prediction using online measurement gave acceptable prediction results, with averaged R^2 values around 0.7, root mean squared errors of prediction (RMSEP) around 3 cmol kg^{-1}, and residual prediction deviations (RPD) around 1.5 (Ulusoy et al. 2016).

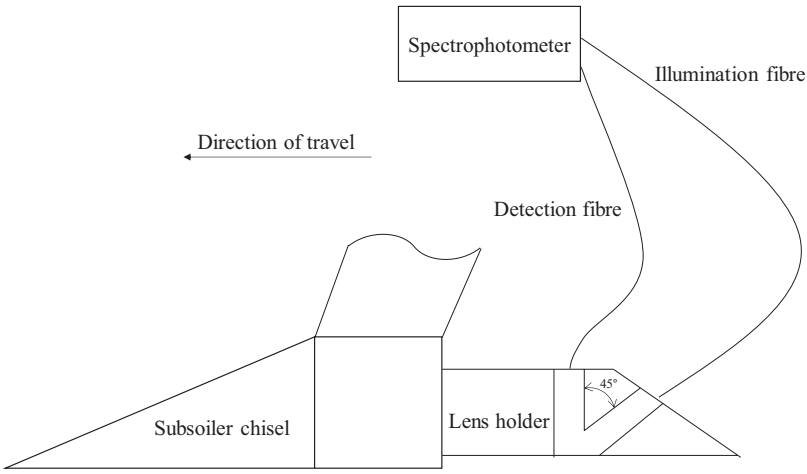

Fig. 2.11 Illustration of the subsoiler and optical sensor. (Mouazen et al. 2005)

2. Soil CEC Sensing with On-the-Go Soil Electrical Conductivity and Optical Sensors

The Veris Technologies has developed a commercially available dual-wavelength on-the-go soil optical sensor (OpticMapper™, Veris Technologies, Salina, KS, USA) for SOM and CEC measurements with high-density and full-field coverage at a relatively low cost. Soil electrical conductivity (EC) and optical data were collected for the purpose of mapping with multiple soil sensors (Kweon et al. 2013). The sensor modules consist of six coulter electrodes for EC measurements, and a specially configured row unit for optical measurements, which were used to determine the soil CEC and SOM separately. The module is mounted between two disks, which are used to control sensing depth. Data were collected approximately 4 cm below the soil surface at a 1 Hz rate on 15–20 m transects with speed of 10–15 km/h.

With the sensor moving, the electrical current travels two feet into the rooting zone. These readings provide soil depth and water-holding capacity information, which has significant implications on CEC determination. Therefore, Veris soil CEC readings are gathered by measuring the EC of the soil.

To estimate soil CEC in fields, a calibration routine was programmed by the LabVIEW (National Instruments Corp., Austin, TX, USA). For the calibration, each red and NIR reflectance reading and optical reading ratio (NIR/red), shallow EC (EC_SH) and deep EC (EC_DP) values, and EC ratio (EC_DP/EC_SH), slope, curvature, and elevation were used as independent variables. For calibration between sensed data and lab-analyzed values, a multivariate linear regression (MLR) with leave-one-out cross-validation was performed on fields with more than ten lab samples, and a single variable linear regression was performed on fields with less than ten samples. From the CEC calibration results, six of nine fields had good results with R^2 of 0.86 or higher and RPD of 2.78 or greater.

3. Portable X-Ray Fluorescence Spectrometer for Soil CEC Determination

Portable X-ray fluorescence (PXRF) spectrometry is a proximal sensing technique which provides elemental data in situ, in seconds (Sharma et al. 2015). Recently, some scientists tried to examine the potential of using PXRF for soil CEC prediction. They employed ADP-6000 Delta Premium PXRF (Olympus, Waltham, MA, USA) featuring an Rh X-ray tube operated at 15–40 keV to scan the soil samples. Elemental quantification was accomplished using the integrated ultrahigh resolution (b165 eV) silicon drift detector. Prior to sample analysis, the PXRF was standardized using a stainless steel “316” alloy clip containing 16.130% Cr, 1.780% Mn, 68.760% Fe, 10.420 % Ni, 0.200% Cu, and 2.100% Mo tightly fitted over the aperture. The instrument was operated in a proprietary software configuration known as Soil Mode which offers quantitative analysis of the following elements: V, Cr, Fe, Co, Ni, Cu, Zn, Hg, As, Se, Pb, Rb, Sr, Zr, Mo, Ag, Cd, Sn, Sb, Ti, Mn, P, S, Cl, K, and Ca. Sequential scanning was conducted for 30s per beam (three-beam operation), such that total scanning time was 90s per sample. The PXRF was repositioned between each scan. The aperture of the instrument was cleaned by air blowing to prevent soil or dust from contaminating the aperture window after each scan. Each sample was scanned in duplicate, with data subsequently averaged for analysis.

Subsequently, multiple linear regression was applied to a modeling dataset to establish the relationship between lab-determined CEC and PXRF elemental data. The model showed good performance with R^2 of 0.908 and RMSE of 2.498 cmol kg^{-1}. Therefore, PXRF was able to predict soil CEC accurately, which could minimize the need for lab-based CEC data for many applications.

References

Adamchuk VI, Christenson PT (2005) An integrated system for mapping soil physical properties on-the-go: the mechanical sensing component. In: Stafford JV (ed) Precision agriculture, vol 5. Wageningen Academic Publishers, The Netherlands, pp 449–456

Adamchuk VI, Morgan MT, Sumali H (2001) Application of a strain gauge array to estimate soil mechanical impedance on-the-go. Trans ASAE 44(6):1377–1383

An XF (2013) Real-time portable sensing device of soil total nitrogen content based on spectroscopy. PhD dissertation, China Agricultural University, Beijing

Aranda V, Ayora-Cañada MJ, Domínguez-Vidal A, Martín-García JM, Calero J, Delgado R, Verdejo T, González-Vila FJ (2011) Effect of soil type and management (organic vs. conventional) on soil organic matter quality in olive groves in a semi-arid environment in Sierra Mágina Natural Park (S Spain). Geoderma 164:54–63

ASAE Standards, 2013S313.3, FEB1999ED. Soil cone penetrometer. ASABE, St. Joseph

Bache BW (1976) The measurement of cation exchange capacity of soils. J Sci Food Agri 27(3):273–280

Bedidi A, Cervelle B, Madeira J (1992) Moisture effects on spectral characteristic (visible) of lateritic soils. Soil Sci 153(2):129–141

Beuselinck L, Govers G, Poesen J (1998) Grain-size analysis by laser diffractometry: comparison with the sieve-pipette method. Catena 32:193–208

Bowers SA, Hanks RJ (1965) Reflection of radiant energy from soils. Soil Sci 100(2):130–138

Chen XF, Feng XL, Liu DY, Zhuang ZY, Wu ZL, Zhao M (2002) Correlation comparison between laser method and pipette-sieve method of grain size. J Ocean Univ Qingdao 32(4):68–614

Chen ST, Wang J, Zhu ZK, Lou YJ (2004) Comparison of the grain size measured by the laser diffract instrument with that by the hydrometer–a case study of beach silts. J Sediment Res 3:64–68

Cheng P, Gao S, Li XS (2001) Evaluation of a wide range laser particle size analyses and comparison with pipette and sieving methods. Acta Sedimentologica Sinica 19(3):449–455

Chung SO (2004) On-the-go soil strength profile sensor. PhD dissertation, University of Missouri, Columbia

Chung SO, Sudduth KA (2004) Characterization of cone index and tillage draft data to define design parameters for an on-the-go soil strength profile sensor. Agric Biosyst Eng 5(1):10–20

Chung SO, Sudduth KA, Hummel JW (2006) Design and validation of an on-the-go soil strength profile sensor. Trans ASABE 49(1):5–14

Chung SO, Sudduth KA, Plouffe C, Kitchen NR (2008) Soil bin and field tests of an on-the-go soil strength profile sensor. Trans ASABE 51(1):5–18

Dixon JB, Weed SB (1977) Minerals in soil environment. Soil Science Society of America, Madison, p 1188

Eshel G, Levy GJ, Mingelgrin U (2004) Critical evaluation of the use of laser diffraction for particle size distribution analysis. Soil Sci Soc Am J 68:736–743

Fellner-Feldegg H (1969) The measurement of dielectrics in the time domain. J Phys Chem 73(3):616–623

Gee GW, Bauder JW (1986) Particle-size analysis. In: Klute A (ed) Methods of soil analysis: Part 1–physical and mineralogical methods. American Society of Agronomy, Madison, pp 383–411

Hua X, Liu LY, Li SJ (2012) Development of soil crusts under simulated rainfall and crust formulation on a loess soil as influenced by polyacrylamide. Pedosphere 22(3):415–424
ISO 13320-1:1999(E) (1999) Particle size analysis-laser diffraction methods-part 1. International Organization for Standardization, Geneva
Jonasz M (1991) Size, shape, composition, and structure of microparticles from light scattering. In: Syvitski J. P. M. ed. Principles, Methods, and Applications of Particle Size Analysis. Cambridge: Cambridge Univ. Press: 143–162
Konert M, Vandenderghe J (1997) Comparison of laser grain size analysis with pipette and sieve analysis: a solution for the underestimation of the clay fraction. Sedimentology 44:523–535
Kweon G, Lund E, Maxton C (2013) Soil organic matter and cation-exchange capacity sensing with on-the-go electrical conductivity and optical sensors. Geoderma 199:80–89
Liu Z (2019) Image-based prediction of soil roughness and soil bulk density. Master dissertation, China Agricultural University, Beijing
Liu T, Gao XF (2012) Comparison of determination on grain size of cinnamon soil by laser diffraction particle size analyzer and pipette method. Res Soil Water Conserv 19(1):16–18, 22
Liu W, Upadhyaya SK, Kataoka T, Shibusawa S (1996) Development of a texture/soil compaction sensor. In: Proceedings of the 3rd international conference in precision agriculture, Minneapolis, p 617–630
Loizeau J-L, Arbouille D, Santiago S, Vernet J-P (1994) Evaluation of a wide range laser diffraction grain size analyzer for use in sediments. Sedimentology 41(2):353–361
Matthews MD (1991) The effect of grain shape and density on the size measurement. In: Syvitski JPM (ed) Principles, methods, and applications of particle size analysis. Cambridge University Press, Cambridge, pp 22–33
McCave IN, Bryant RS, Cook HF (1986) Evaluation of a laser-diffraction-size analyzer for use with natural sediments. J Sediment Res 56(4):561–564
Miller WP, Miller DM (1987) A micro-pipette method for soil mechanical analysis. Commun Soil Sci Plant Anal 18(1):1–15
Mouazen AM, De Baerdemaeker J, Ramon H (2005) Towards development of on-line soil moisture content sensor using a fiber-type NIR spectrophotometer. Soil Tillage Res 80:171–183
Muller HW, Dohrmann R, Klosa D, Rehder S, Eckelmann W (2009) Comparison of two procedures for particle-size analysis: Kohn pipette and X-ray granulometry. J Plant Nutr Soil Sci 172:172–179
Pang JL, Huang CC, Jia YF (2003) Comparison grain size analytical results in loess, soil between laser and hydrometer method. J Shaanxi Norm Univ (Natural Science Edition) 31(04):87–92
Planet WG (1970) Some comments on reflectance measurements of wet soils. Remote Sensing of Environment, 1(2), 127–129
Quraishi MZ, Mouazen AM (2013) Calibration of an on-line sensor for measurement of topsoil bulk density in all soil textures. Soil Tillage Res 126:219–228
Sharma A, Weindorf DC, Wang DD, Chakraborty S (2015) Characterizing soils via portable X-ray fluorescence spectrometer: 4. Cation exchange capacity (CEC). Geoderma 239–240:130–134
Shen CY, Xing WY (2016) Research on the rapid determination of cation exchange capacity in soil. Soil Fertil Sci China 5:144–147
Sirjacobs D, Hanquet B, Lebeau F, Destain M-F (2002) Online soil mechanical resistance mapping and correlation with soil physical properties for precision agriculture. Soil Tillage Res 64(3–4):231–242
Stoner ER, Baumgardner MF (1981) Characteristic variations in reflectance of surface soil. Soil Sci Am J 45(6):1161–1165
Taubner H, Roth B, Tippkotter R (2009) Determination of soil texture: comparison of the sedimentation method and the laser-diffraction analysis. J Plant Nutr Soil Sci 172:161–171
Topp GC, Davis JL, Anna AP (1980) Electromagnetic determination of soil water content: measurements in coaxial transmission lines. Water Resour Res 16:574–582
Ulusoy Y, Tekin Y, Tümsavaş Z, Mouazen AM (2016) Prediction of soil cation exchange capacity using visible and near infrared spectroscopy. Biosyst Eng 152:79–93

Wu KN, Zhao R (2019) Soil texture classification and its application in China. Acta Pedologica Sinica 56(1):227–241

Yang YF, Li DC, Yang JL, Zhang GL, Zhao YG, Zhao WJ (2008) Comparison between laser diffraction and pipette methods in analyses of PSD of clayey ferrosol. Acta Pedologica Sinica 45(3):405–412

Yang JL, Zhang GL, Li DC, Pan JH (2009) Relationships of soil particle size distribution between sieve-pipette and laser diffraction methods. Acta Pedologica Sinica 46(5):772–780

Zheng J (2019) Design of an on-the-go soil tillage resistance measurement system. Master dissertation, China Agricultural University, Beijing

Chapter 3
Theories and Methods for Soil Nutrient Sensing

Fei Liu, Xiantao He, and Yong He

Abstract Soil provides the essential nutrient elements for plant growth. Soil nutrients include soil macronutrients such as nitrogen, phosphorus, and potassium, as well as soil micronutrients such as calcium, magnesium, sulfur, iron, and boron. Precision agriculture is a technology of applying precise and right amounts of inputs such as water, fertilizer, and pesticides at the right time to the crop for increasing the productivity and maximizing the yields. Therefore, it is necessary to obtain soil nutrient information quickly and accurately. Near-infrared spectroscopy (NIRS) with high-efficiency and nondestructive characteristics has great potential in soil nutrition detection. According to the NIR absorption of the hydrogen bonds, soil total nitrogen content and soil organic matter content can be estimated. Multiple linear regression, partial least square regression (PLSR), and principal component analysis (PCA) are commonly used to establish the estimation models of soil nutrient contents based on NIRS. Moreover, the modern algorithms of wavelet algorithm (WA), genetic algorithm (GA), uninformative variable elimination (UVE), support vector machine (SVM), etc., are used to reduce the multicollinearity of the NIR spectra to improve estimation accuracy. Laser-induced breakdown spectroscopy (LIBS) is a promising spectral detection technology with high sensitivity, fast speed, and the ability to measure multiple elements simultaneously. It can also be used to detect both soil macronutrients and micronutrients. At present, scientists have developed various forms of soil testing instruments based on spectral technology, such as portable, vehicle-mounted, and remote sensing devices. Through these devices, it is convenient to implement comprehensive, full-range, all-weather, and real-time soil sensing for soil and crop precision management.

Keywords Soil nutrients · Soil sensing · Near-infrared spectroscopy (NIRS) · Laser-induced breakdown spectroscopy (LIBS) · Soil sensors

F. Liu (✉) · X. He · Y. He
Zhejiang University, Hangzhou, China
e-mail: fliu@zju.edu.cn

M. Li et al. (eds.), *Soil and Crop Sensing for Precision Crop Production*,
Agriculture Automation and Control, https://doi.org/10.1007/978-3-030-70432-2_3

Soil serves as a medium for nurturing plants, and its nutrients have a great influence on the healthy growth and yield improvement of crops. Precision agriculture is a technology to precisely input right amount of agricultural means of production such as water, fertilizer, and pesticides at the right time to the crop for increasing its productivity and maximizing its yield. To achieve expected crop production, it is necessary to obtain soil information quickly and accurately. Soil nutrients mainly include nitrogen, phosphorus, potassium, and organic matter content, and obtaining the information of those soil nutrients is beneficial to farmland management and decision-making, as well as prediction of crop yields.

Traditional soil sampling technology for acquiring soil information is costly, time-consuming, and poor in real time and is not suitable to large-scale farmland. Thus, it is necessary to detect the characteristic information of the soil rapidly and accurately in large-scale areas. In recent years, a lot of studies have been conducted on the method of rapid nondestructive detection of soil information, and great progress has been made.

3.1 Laboratory Measurement of Soil Nutrients

The traditional chemical analysis method of soil nutrients is to extract a specific element in a soil sample through a specific extraction solution, thereby realizing quantitative detection of the soil nutrient content. In this traditional analysis method, the complex procedures of soil sampling and nutrient extracting and measuring are the main reasons for cost reduction and speed improvement of soil nutrient detection.

3.1.1 Detection of Soil Nitrogen Content in Laboratory

Nitrogen is an important building block of proteins, nucleic acids, and other cellular constituents which are essential for all forms of life. Therefore, soil nitrogen is a key nutrient element for plants so that it warrants careful management. Soil nitrogen absorbed by plants is available nitrogen, which is easily hydrolyzed as a part of the soil solution or the cation exchange complex when applied to moist soils. Available nitrogen is mainly from most of the commonly applied inorganic sources, such as ammonia, ammonium nitrate, ammonium phosphate, ammonium sulfate, calcium nitrate, nitric phosphate, potassium nitrate, and sodium nitrate.

The commonly used method for the determination of soil available nitrogen content is the alkali-nitrogen hydrolysis method. The principle of this method is to use sodium hydroxide of 1 ~ 2 mol/L for hydrolyzing soil samples and to decompose the inorganic nitrogen and easily decomposed organic nitrogen in the soil into ammonia nitrogen, which is absorbed with boric acid and standard acid to titrate. The detailed operation process is as follows: weighing 2 g of soil sample into the outer chamber of the Conway diffusion dish firstly and then adding 2 mL of boric

acid solution to the inner chamber of the diffusion dish and 100 mL of 1 mol/L sodium hydroxide to the outer chamber and finally sealing it with Vaseline for 48 hours and titrating it with standard concentration of sulfuric acid at 0.005 mol/L. The end of the titration is when the solution turns purple. The formula for calculating nitrogen content is shown in Eq. 3.1:

$$N = \frac{c \times (v - v_0) \times 14.0}{m} \times 10^3 \tag{3.1}$$

where N is the available nitrogen (mg/kg), c is the concentration of 0.005 mol/L (1/2 H_2SO_4) standard solution (mol/L), v is the volume of the 0.005 mol/L (1/2 H_2SO_4) standard solution used for sample titration (mL), v_0 is the volume of the 0.005 mol/L (1/2 H_2SO_4) standard solution used in the blank test titration (mL), 14.0 is the molar mass of the nitrogen atom (g/mol), m is the mass of the sample for testing (g), and 10^3 is the conversion factor of mass units.

3.1.2 Detection of Soil Phosphorus Content in Laboratory

There are many methods for determining soil available phosphorus, and the results are inconsistent due to different extraction reagents used. The selection of extractant methods is mainly based on the properties of the soil to be tested. Neutral and calcareous soils are extracted by sodium bicarbonate reagent, while acid paddy soils are extracted by hydrochloric acid, and acid dry soils are extracted by hydrochloric acid-sodium fluoride method.

The hydrochloric acid extraction method for acid paddy soil is specifically introduced here (Fig. 3.1). First, a 2.5 g soil sample is weighed into a 250 mL Erlenmeyer flask, and then a teaspoon of phosphorus-free activated carbon is added for decolorization, and 0.1 mol/L hydrochloric acid is added to the 250 mL scale mark for extracting available phosphorus in soil. After shaking the Erlenmeyer flask for about 30 minutes and then filtering the available phosphorus from the solution, 10 mL of filter solution is taken in a tube, and then 5 mL of molybdate-antimony-scandium color agent is added to maintain constant volume. After the solution stands for 15 min, a colorimetry at 700 nm is used to obtain the absorbance value of the test solution, and then the concentration of available phosphorus is determined by the calibration curve of phosphorus solution, and the content of available phosphorus in soil is calculated by Eq. 3.2:

$$P = \frac{\rho \times V \times T_s \times 1000}{m \times 1000 \times k} \tag{3.2}$$

where P is the available phosphorus (mg/kg), ρ is the concentration of available phosphorus (μg/mL), V is the volume of maintaining constant volume during color

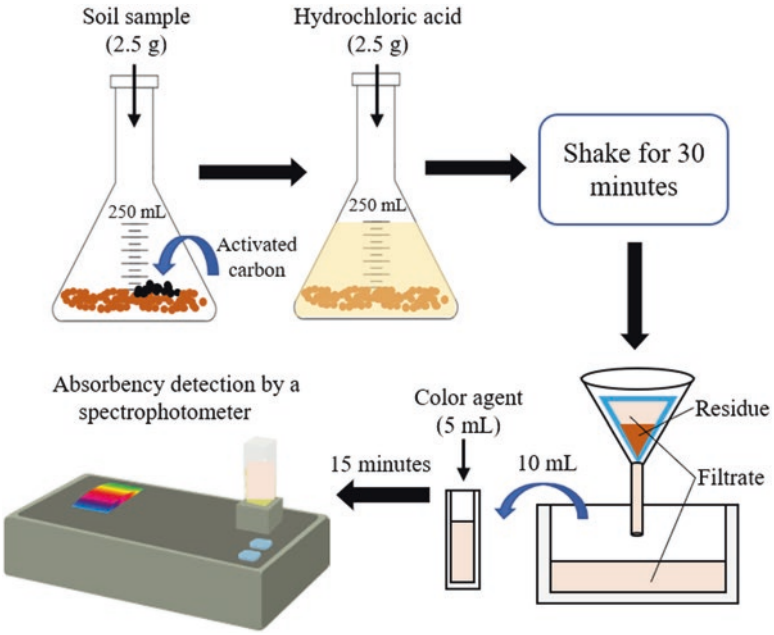

Fig. 3.1 Hydrochloric acid extraction method for detecting phosphorus in soil

rendering (mL), T_s is the ratio of the total volume of the extract solution to the volume of the extract solution absorbed during color rendering, m is the mass value of air-dried soil (g), and k is the mass coefficient of air-dried soil converting into oven-dried soil.

The process of drawing the calibration curve is as follows: accurately take 5 μg/mL phosphorus standard solution of 0, 1, 3, 7, and 10 ml into volumetric flasks, respectively, and add 5 ml molybdate-antimony-scandium color agent in each flask, and then slowly rotate the volumetric flask to shake well and add water to the flasks to obtain standard solutions with phosphorus contents of 0.0, 0.1, 0.3, 0.5, 0.7, and 1.0 μg/mL, respectively. After standing for 30 min, perform colorimetric measurement at a wavelength of 700 nm to obtain the absorbance of the standard solutions, and then draw the calibration curve of the standard phosphorus solution with the phosphorus concentration (μg/mL) as the abscissa and the absorbance (Abs) as the ordinate.

3.1.3 Detection of Soil Kalium Content in Laboratory

Along with nitrogen and phosphorus, kalium is also one of the essential nutrients for crop growth. The kalium in soil can be classified as mineral kalium (insoluble kalium), non-exchangeable kalium (slow-acting kalium), exchangeable kalium, and

water-soluble kalium (quick-acting kalium). The kalium that can be absorbed by plants is water-soluble and exchangeable kalium.

The method of chemical determination for available kalium in soil is similar to the method shown in Fig. 3.1. It uses the acetic acid as the extracting solution to extract the available kalium from the soil, and then the content of kalium is determined by flame photometer according to the characteristics of kalium element. The detailed processes are as follows: weighing 5 g of air-dried soil sample into a 100 mL test tube, adding 50 mL of 1 mol/L neutral ammonium acetate solution, and then plugging the tube with a rubber stopper and shaking for 30 minutes, filtering the solution and measuring the filtrate directly on a flame photometer with a 766.5 nm filter, and then recording the galvanometer reading and obtaining the concentration of test solution from a calibration curve of the standard kalium solution. The specific formula for calculating kalium content in soil is shown in Eq. 3.3:

$$K = C \times \frac{v}{m_d} \tag{3.3}$$

where K is the available kalium (mg/kg), v is the volume of acetic acid added, C is the concentration of test solution (μg/mL), and m_d is the mass value of oven-dried soil (g).

3.1.4 Detection of Soil Organic Matter Content in Laboratory

Soil organic matter, as a sign of fertility formation, is an important indicator for identifying soil fertility. The content and composition of organic matter will change regularly with the changes of the climate and biological conditions. Therefore, the detection of organic matter is also an important part in the detection of soil nutrients. The potassium dichromate method is an important method for the determination of soil organic matter in laboratory. The testing principle is to use potassium dichromate-sulfuric acid solution to oxidize organic matter during heating process, and the remaining potassium dichromate is titrated with a standard solution of ferrous sulfate using o-phenanthroline as an indicator, and then the amount of potassium dichromate consumed is used to calculate the carbon content.

The detailed process of detecting soil organic matter by the potassium dichromate method is shown in Fig. 3.2: accurately weighing 0.5 g of soil sample into a 250 mL flask, adding 5 mL of potassium dichromate standard solution and 5 mL of concentrated sulfuric acid into the flask with a pipette, and then carefully shaking the solution to uniform, heating a thermostatic oil bath to 185-degree Celsius, and then placing the flask in the constant temperature oil bath, boiling the solution in the flask for 5 minutes, moving the flask from the oil bath and cool the solution to room temperature, finally adding three drops of o-phenanthroline indicator to the flask, and then titrating it with a 0.1 mol/L standard ferrous sulfate solution. When the

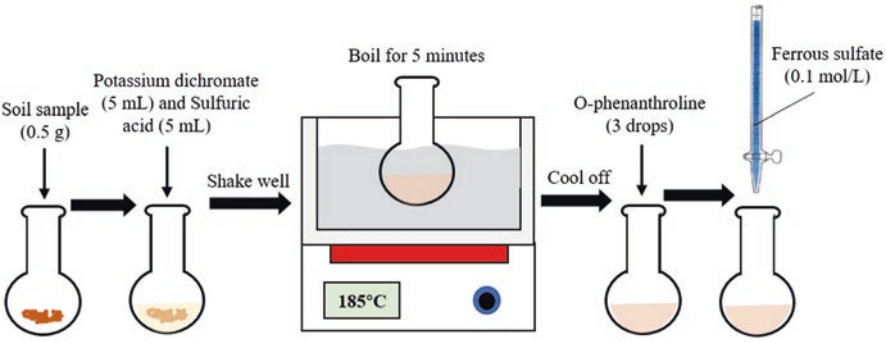

Fig. 3.2 Method of chemical determination for soil organic matter content

color of the solution in the flask changes from orange yellow to green and then mutates to brown red, the titration will be stopped. For each batch of samples, quartz is used instead of soil sample for blank test. The calculation method of carbon content is shown in Eq. 3.4:

$$TC = \frac{c\left(V_0 - V\right) \times 0.003 \times 1.724}{m \times D} \times 100\% \tag{3.4}$$

where TC is the organic carbon content (%), c is the concentration of a standard solution of ferrous sulfate (mol/L), V_0 is the volume of ferrous sulfate used in blank test (mL), V is the volume of sulfuric acid solution consumed during measurement (mL), 0.003 is the molar mass of 1/4 carbon atom (kg/mol), m is the sample mass used for testing (g), and D is the dilution ratio. There is a certain conversion relationship between the organic matter content in the soil and the organic carbon content. The content of organic matter in the soil can be obtained by multiplying the measured organic carbon content with a conversion factor of 1.724: organic matter (%) = TC(%) × 1.724.

3.2 Spectral Technology for Soil Nutrient Sensing

Using laboratory chemical analysis to obtain farmland soil nutrient information can accurately obtain soil nutrient information at a single point in the field, but it is cumbersome, time-consuming, labor-intensive, costly, and poor in real time. Meanwhile, the number of samples is too little to reflect objectively the distributed situation of actual soil nutrients in large areas of farmland. In addition, the method for determining soil nutrient in laboratory will produce chemical waste and cause secondary pollution to the environment. The spectral analysis methods for detecting soil fertility can shorten analysis time, reduce detection costs, and improve testing efficiency. Moreover, the in situ detection for soil fertility based on spectroscopy

will help achieve real-time measurement of soil fertility properties, which can facilitate the global application of the technology of on-demand fertilizer management.

3.2.1 Vis/NIR Spectral Sensing Technology for Soil Nutrients

Vis/NIR spectroscopy to sense soil nutrients is a mature technique for detecting soil moisture, organic matter, nitrogen, phosphorus, kalium, etc. Yu et al. (2002) measured total nitrogen, organic matter, and alkali-hydrolyzed nitrogen in soil by near-infrared spectroscopy. The NIR spectra of 2 mm and 0.15 mm air-dried soil were obtained, and a partial least square (PLS) method was used to establish a mathematical model for predicting soil nutrition content. The results showed that NIR spectra had a good correlation for detecting soil organic matter, total nitrogen, and alkali-hydrolyzed nitrogen. Zhu et al. (2008) used near-infrared spectroscopy to detect organic matter in untreated soil. In the experiment, near-infrared spectra in the range of 4000~12,500 cm^{-1} was applied to detect organic matter in the soil that had not been pulverized and sieved, and the quantitative relationship between the spectral absorbance and the organic matter content was established by the methods of first-order differential pretreatment and PLS regression analysis. The experiment has obtained good results. The predicted correlation coefficient of organic matter is 0.818, the standard deviation is 0.069, and the root mean square error is 0.085.

The team from China Agricultural University has been working on the spectroscopic detection methods of soil nutrients since the 2000s (Sun et al. 2006; Sun et al. 2007). The research objects were mainly black soil in Northeast China and Chao (aquic cambisols) soil in North China. The spectral data of soil samples were collected without pretreatment, and then the correlation between soil parameters and spectral characteristics was analyzed and a predictive model for soil nutrient was established. Meanwhile, the effects of soil moisture content and particle size on soil spectrum by using wavelet transform were studied (An et al. 2013). The results showed that the change trend of the soil spectral curve was affected by the soil moisture content, and the instantaneous fluctuation of the spectral curve was mainly caused by the soil particle size. A filtering process was performed to a certain extent, which eliminated high-frequency oscillation of the spectral curve caused by uneven particle size of soil (Li et al. 2013).

The principle of spectral detection of soil nutrition is the multiple frequency absorption of near-infrared spectrum to nutrients in the soil. The mass information of the spectral bands for different substances overlaps heavily, so that the full-band spectrum contains a lot of redundant information and noise data, which affects the prediction accuracy of the model. This is the main reason of low stability and accuracy of spectral measurements for soil nutrition in earlier studies. In order to reduce a large amount of useless information in the full-band spectral information, it is necessary to extract the truly effective bands from the full band to reduce the amount of calculation and increase the speed of detection. The main wavelength extraction methods are wavelet algorithm (WA), genetic algorithm (GA), uninformative

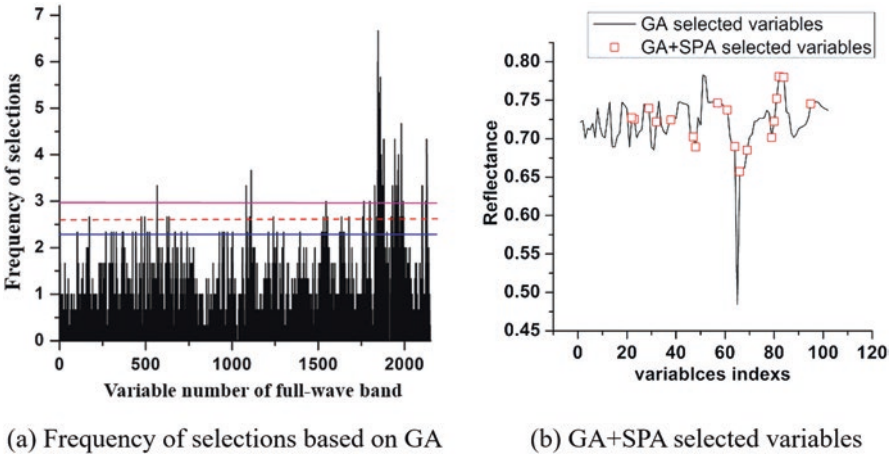

Fig. 3.3 Result of spectral feature selection (Zhang 2015) (**a**) Frequency of selections based on GA (**b**) GA + SPA selected variables

variable elimination (UVE), principal component analysis (PCA), successive projection algorithm (SPA), etc. The application of these methods to the spectral detection of soil nutrients combined with advanced modeling methods will greatly improve the speed of spectral determination of nutrients in soil. The result of spectral feature selection for soil organic matter based on GA is shown in Fig. 3.3a (Zhang 2015). There are three horizontal lines in the figure, and the numbers of the wavelengths corresponding to the lines from top to bottom are 64, 102, and 169, with the accumulative contribution rate of 79.51%, 81.99%, and 81.97%, respectively. Therefore, 102 was selected as the number of the wavelengths in the next analysis. A SPA algorithm was used to select 18 characteristic wavelengths from the 102 wavelengths (Fig. 3.3b), and the prediction model was established using PLS. The prediction set achieved a determination coefficient (R^2) of 0.83 and root mean square error (RMSE) of 0.20, while R^2 and RMSE were 0.84 and 0.20, respectively, when using 102 wavelengths for prediction model. It is observed that the prediction accuracy was almost not reduced when the number of wavelengths dropped to 18, indicating that the combination of GA and SPA can greatly simplify the prediction model.

3.2.2 Mid-infrared Spectral Sensing Technology for Soil Nutrients

The principle of sensing soil nutrients by mid-infrared (MIR) spectroscopy (2500 ~ 25,000 nm) is absorptions of fundamental frequency related to molecular structures of soil constituents. Different compounds have specific infrared absorption spectra, and the intensity, position, shape, and number of bands are related to

the type of compound and its state. Compared with near-infrared spectroscopy, mid-infrared spectroscopy has more specificity in detecting soil nutrients.

Jia et al. (2017) applied diffuse reflectance spectroscopy, including visible and near-infrared (VNIR) and MIR radiation, to rapidly estimate soil organic carbon (SOC). The absorbance spectra in the VNIR and MIR regions at different depths of soil profile of shrub meadow are shown in Fig. 3.4. The SOC concentrations usually decreased with depth, and the absorbance curves reduced overall with increasing soil depths. A comparison of the field-moist intact and air-dried ground spectra in the range of 400 ~ 2450 nm indicated that the soil moisture and structural integrity also affected the soil absorbance spectra. The strong absorptions near 1400 and 1900 nm in the VNIR spectra were caused by the O–H functional group of free water, and the absorptions near 2200 nm were caused by the organic matter. In the MIR region, the spectra information mainly responded to mineral properties, such as quartz, kaolin, and montmorillonite. Preprocessed spectra were used to predict the SOC in the soil cores using partial least square regression (PLSR) and support vector machine (SVM) algorithm. The SVM models (average values of RMSEP and R^2 of 8.31 g·kg^{-1} and 0.84, respectively) performed better in predicting the SOC concentration under different land cover types than the PLSR models (average values of RMSEP and R^2 of 12.41 g·kg^{-1} and 0.70, respectively). The prediction of forest soil had the highest prediction accuracy, followed by the total dataset and finally the shrub meadow subset.

Janik et al. (2007) applied MIR spectroscopy and partial least square analysis to predict the concentration of soil organic carbon. The PLS calibrations were derived from a standard set of soils that had been analyzed for total organic carbon (TOC), particulate organic carbon (POC), and charcoal carbon (char-C) using physical and chemical means. PLS calibration models from this soil standard set allowed the prediction of TOC, POC, and char-C fractions with a coefficient of determination (R^2) of measured and predicted data ranging between 0.97 and 0.73. For the POC fraction, the coefficient of determination could be improved (R^2 = 0.94) by using local calibration sets. The capacity to estimate soil fractions such as char-C rapidly

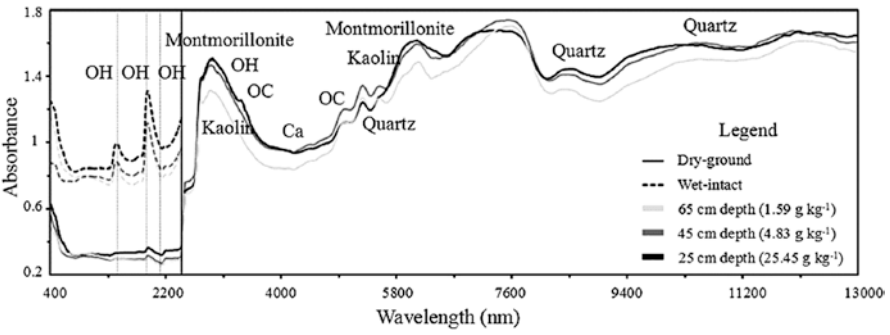

Fig. 3.4 Absorbance spectra at different depths with different contents in one soil core of shrub meadow in the VNIR and MIR regions. (Jia et al. 2017)

and inexpensively makes this approach highly attractive for studies where large numbers of analyses are required. Inclusion of a set of soils from Kenya demonstrated the robustness of the method for total organic carbon and charcoal carbon prediction. Baldock et al. (2013) combined diffuse reflection MIR spectra with PLSR analysis to predict soil carbon content and composition. Total organic and inorganic carbon contents were determined with MIR spectra acquired for 20,495 soil samples collected from 4526 locations from soil depths to 1 m within Australia's agricultural regions. It was found that the degree of soil dryness and grinding of soil samples had a great impact on the test results. Therefore, the grinding time was standardized in the study, and prediction of total carbon, organic carbon, and inorganic carbon was achieved. Compared with the traditional laboratory method, the MIR method provided a faster and more economical method for detecting the soil carbon and total nitrogen content in soil.

3.2.3 LIBS Sensing Technology for Soil Nutrients

1. Working Principle of LIBS.

Laser-induced breakdown spectroscopy (LIBS) is a promising spectral detection technology with high sensitivity, fast speed, and the ability to measure multiple elements simultaneously. As early as 1994, scientists at the International Association for Remote Sensing Science announced that they had successfully detected As, Cd, Cr, Hg, Pb, Zn, and other metal elements in soil using LIBS technology (Alexander et al. 1994). In the soil nutrient detection, it can be used for the detection of metal nutrient elements, such as potassium, calcium, and cuprum. At present, in the process of detecting heavy metals in the soil by LIBS, a single pulsed laser is generally used to excite soil samples to generate plasma, and the detection sensitivity obtained is generally tens of mg/kg, and some metals with high sensitivity can reach several mg/kg.

The working principle of LIBS is to use high-energy laser pulses to directly hit the surface of the sample, forming a high-intensity laser spot (plasma) on the surface of the analysis material and exciting the elements to be tested to a high-energy state. When outer electrons of the element atoms move into the ground state, their characteristic spectra will be emitted and then detected by a spectrometer. By comparing the detected spectrum to elemental spectrograms in the standard spectral library, the content of elements contained in the soil sample can be obtained.

In the calculation process, it is generally considered that the content of each element in the plasma is the same as that in the sample before ablation. The intensity of the radiation spectrum when an atom transitions from the k-level to the i-level (I_{ki}) is

$$I_{ki} = \frac{h\nu_{ki}}{4\pi} N \frac{g_k A_{ki}}{U_S(T)} e^{-E_k/(kT)} \tag{3.5}$$

where h is the Planck constant, v_{ki} is the frequency of spectral lines, N is the number of excited particles, g_k is the k-level statistical weight, A_{ki} is the probability of atomic transition from k-level to i-level, $U_s(T)$ is the distribution function of elements at temperature T, E_k is the k-level potential energy, K is the Boltzmann's constant, and T is the Calcination temperature. When the characteristic spectral line of the specified element is detected, the v_{ki}, g_k, A_{ki}, T, $U_s(T)$, E_k, and k have certain values, and the number of excited particles N is proportional to the content of the test element in the sample (C), so the above formula can be rewritten as

$$I = aC^b \tag{3.6}$$

where a is proportionality coefficient and b is self-absorption coefficient, which is related to the content of the element to be measured. According to this formula, the element content in the soil sample can be calculated by the intensity of the characteristic line of the element, providing a theoretical basis for the quantitative detection of the element in soil.

2. Theoretical Basis of Soil Nutrient Detection with LIBS.

A typical experimental platform system for LIBS is mainly composed of a laser, a spectral information acquisition system (a spectrometer and a detector), digital pulse delay generators, and accessory devices (sample stage, energy meter, computer, etc.). Figure 3.5a shows the composition of a typical LIBS system (Yu 2016; Yu et al. 2019). The laser is the energy source of the LIBS system and can provide energy to excite the sample and generate plasma. The acquisition system consisting of a spectrometer and a detector is used to collect the radiation spectrum of laser-induced plasma and perform photoelectric conversion for digital analysis. The digital pulse delay generator is used to control the delay time of the spectrometer detector relative to the laser pulse, and the computer is applied to conduct the setup of working parameters and subsequent data processing of each component. Yu (2016) obtained that a spectral curve of soil added some heavy metals in the range of 270~850 nm by the experiments (Fig. 3.5b). It can be seen that the emission lines of most metal elements are distributed in the range of 270~450 nm. The emission spectrum of elements such as Fe, Mg, Si, Ca, Ti, Al, Pb, Cd, Na, Li, N, K, H, and O can be observed in the entire spectrum, and the wavelengths of the atomic spectrum and the ion spectrum correspond to specific elements, and the spectral signal intensity has a certain quantitative relationship with the corresponding element content. Generally, the same element produces multiple emission lines with different wavelength positions and different intensities. However, the quantitative prediction of an element is mainly based on data analysis in a single band in practical applications, that is, only the intensity data of a certain spectral line needs to be selected to predict the element content in the soil.

In addition, there are also O and N emission lines in the spectrum diagram, some of which are due to the breakdown of a large amount of O_2 and N_2 in the air and others are due to the presence of O and N in the soil. For the low content of elements, although characteristic spectral lines are detected under this test condition,

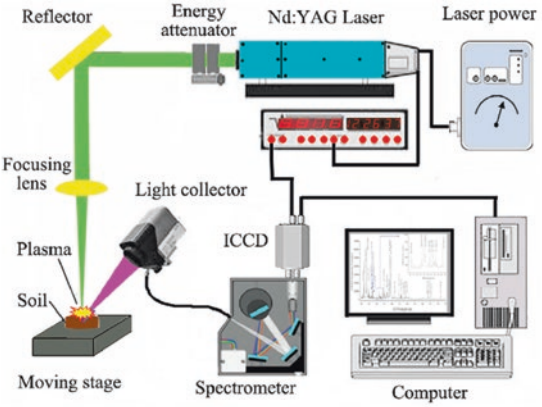

(a) Representative LIBS analytical system for soil analysis

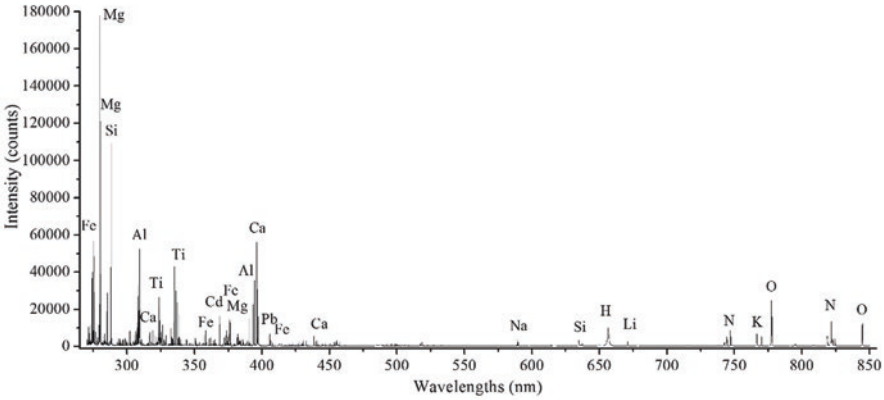

(b) Spectral curve of soil added some heavy metals in 270-850 nm

Fig. 3.5 Soil analysis based on LIBS analytical system (Yu 2016; Yu et al. 2019) (**a**) Representative LIBS analytical system for soil analysis (**b**) Spectral curve of soil added some heavy metals in 270~850 nm

the signal is weak and unstable at low concentrations. Besides, some trace elements in the soil are below the detection limit of LIBS, and other elements are distributed outside the effective band of the spectrometer, so their stable characteristic lines cannot be detected under these experimental conditions.

3. Applications of LIBS in Soil Sensing.

The common nutrition elements in the soil are C, N, P, K, Si, S, Ca, Mg, etc. These elements promote the healthy growth of plants and are also a basic guarantee for maintaining normal physiological activities of crops. Therefore, the content of these elements determines the level of soil fertility.

(i) Detection of C Content in Soil.

Carbon (C) element is one of the most basic constituent elements of the soil. Its content is directly related to the water-holding capacity of the soil and reflects the fertility and other characteristics of soil. As a fast and nondestructive method of spectrochemical analysis, LIBS technology has attracted the attention of many researchers, letting them use it to analyze and detect carbon in soil.

Cremers et al. (2001) first applied LIBS spectroscopy to measure soil organic carbon content. A 1064 nm laser wavelength was used to detect soil organic matter in some farms and woodlands in Colorado and New Mexico. The detection limit of LIBS is 300 mg·kg^{-1}, and the precision is 4~5%. With further research, Martin et al. (2003, 2010) explored the effect of key detection parameters, including laser wavelength and excitation energy, as well as univariate and multivariate methods on detection accuracy, in order to build a robust calibration model to predict soil organic carbon concentration. The carbon signal of LIBS at 247.8 nm measured on 20 pellets from each homogenized soil sample was shown to be highly correlated (coefficient of determination, $R^2 = 0.962$) with the organic carbon content measured by dry combustion using an elemental analyzer. Glumac et al. (2010) successfully explored a method to avoid the interference of neutral and single ionized Fe lines to the standard detection line of LIBS at 247.8 nm. A low-power Nd:YAG laser with a wavelength of 532 nm was used to optimize the high dispersion of the LIBS signal and time-gating strategy to minimize interference signals and maintain a high signal-to-noise ratio. Martin et al. (2013) used LIBS technology combined with multivariate data analysis methods to distinguish total carbon (TC), inorganic carbon (IC), and organic carbon (OC) in 58 soil samples from 5 places. The results showed that the correlation coefficients of TC, IC, and OC contents predicted by LIBS are 0.91, 0.87, and 0.91, respectively. Izaurralde et al. (2013) used LIBS technology, diffuse reflectance Fourier transform infrared spectroscopy (DRIFTS), and inelastic neutron scattering (INS) methods to determine the carbon content of field soil, and these three methods have achieved ideal measurement results.

(ii) Detection of Kalium Content in Soil.

Kalium (K) is one of the important nutrients in the soil and plays a significant role in plant growth. The nutritional functions of K on plants include promoting the activation of various enzymes in plants; improving photosynthesis, sugar metabolism, and protein synthesis; and enhancing the plant's ability to resist drought, cold, and pests. Dong et al. (2013a, b) analyzed the farmland soil with K content between 8.74 and 34.56 g·kg^{-1} by using the LIBS technique at 766.49 nm spectral line and established a quantitative model for predicting K content in soil. The correlation coefficient of the quantitative model is 0.935, and the predicted standard deviation is 9.26%. Meng et al. (2014) used a pulsed laser with a wavelength of 1046 nm as the excitation light source to study the spectral characteristics of potassium in soil. A spectral line of 769.9 nm was used as the analysis line of potassium. The optimal detection delay was 1 μs and the optimal gate width was 5.2 μs. The prediction curve of the soil K was obtained, and the relative error between the predicted value

and the true value was less than 5%. The results of this study provide a theoretical foundation for rapid and on-site quantitative detection of K element in soil.

In order to meet the urgent needs of online detection of soil K nutrients in the field, Zhang et al. (2014) designed a system for online detection of soil nutrients based on LIBS (Fig. 3.6) and carried out an experimental study of rapid determination of soil nutrients. The results showed that the characteristic absorption spectrum of soil potassium was at the wavelengths of 766.49 nm and 769.90 nm. The potassium nutrient content was positively correlated with the intensity of the specific wavelength, but when the mass fraction of potassium was greater than 0.3%, there was a significant self-absorption, and the relationship between potassium content and spectral intensity became nonlinear. The determinate coefficient of the model was 0.9337, the root mean square error was only 0.2761, and the minimum detection limit of soil potassium nutrients was 212 μg/g, which met the requirements for online detection of soil potassium nutrients.

(iii) Detection of Other Elements in Soil.

For other nutritional elements, such as N, P, and Ca, researchers have also obtained rich research findings using LIBS technology. Lu et al. (2013) used the calibration curve method to establish the relationship model between the intensity of LIBS spectrum and the contents of total nitrogen (TN) and total phosphorus (TP) in soil, indicating that there is a close correlation between them: the correlation coefficient of TN is 0.981, and the correlation coefficient of TP is 0.868. Dong et al. (2013a, b) studied the characteristics of N element with LIBS spectrum. The laser energy had an influence on the detection results, and the correlation coefficient between N content and the intensity of LIBS spectral lines is 0.996. Hussain et al. (2007) conducted a study on the distribution of nutrient elements in greenhouse soils using LIBS technology. Using the calibration curve method, the content of Ca,

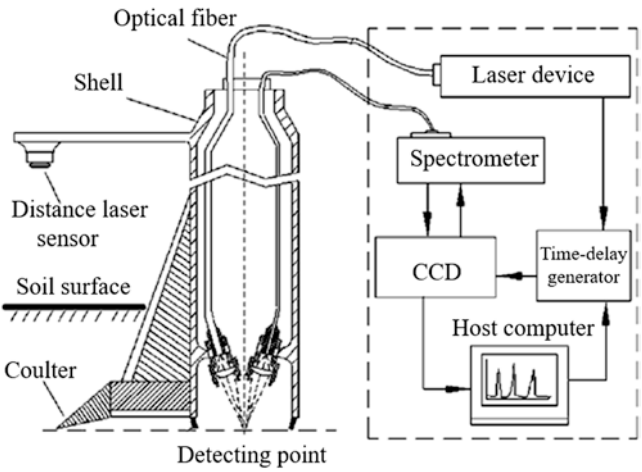

Fig. 3.6 Structure of soil nutrient detection system of LIBS. (Zhang et al. 2014)

K, P, Mg, Fe, S, Ni, and Ba in the soil samples was measured as 12, 9, 7, 9, 7, 10, 8, and 12 $mg \cdot kg^{-1}$, respectively. Wang et al. (2017) used LIBS technology to quantitatively detect nutrients in soil. An Nd:YAG pulsed laser with an output wavelength of 1064 nm and a pulse width of 5.82 ns was used as the light source. Based on the traditional LIBS system, a beam expander system and a real-time monitoring system were added; as a result, a cage-type LIBS system was developed to optimize the laser focus position of the beam expander system in the cage structure, and an optimal laser focus position of 0.2 cm was obtained. The contents of Cu, Mn, Mg, and K in the soil were quantitatively analyzed. Their detection limits were 0.42×10^{-6}, 13.2×10^{-6}, 38.5×10^{-6}, and 62×10^{-6}, respectively, which was better than that of the traditional LIBS systems. The mass fractions of Cu, Mn, Mg, and K elements in the soil were predicted, and the average relative errors of their predicted values were 9.2%, 9.6%, 8.5%, and 10.9%, respectively.

LIBS method has the advantages of short analysis time, acceptable detection limit and high accuracy, etc. However, the effects of different soil properties, such as texture, carbonate, total soil C, moisture, clay mineralogy, and silicon content on LIBS measurements, should be studied more extensively. In addition, the potential of field portable LIBS instruments to measure soil nutrients in situ and in complete soil profiles should be explored in future studies to expand the applicability of LIBS detection to soil nutrients.

3.2.4 Multispectral and Hyperspectral Imaging Sensing Technology for Soil Nutrients

Vis/NIR spectroscopy has been rapidly popularized to detect soil properties, because it can not only detect the organic components of the soil but also identify the mineral components and the texture of the soil; meanwhile, the detection speed is much faster than traditional methods. However, the spectral analysis technology can only obtain the point spectral information of the sample, and the spectral information acquired is not comprehensive. Hyperspectral imaging technology has the dual advantages of both spectral analysis and image analysis technologies and can obtain the spectral information, planar information, and spatial information of the detection object simultaneously. It can accurately collect information of each pixel at a minimum of nanometer level, and the information obtained is more comprehensive, specific, and accurate.

Sorenson et al. (2018) used a SisuROCK automated hyperspectral imaging system in laboratory to detect soil organic carbon (SOC) and total nitrogen (TN) content in discrete, intact, and unground soil and evaluated the potential of spectral imaging technology to replace traditional chemical analysis for predicting spatial distributions of soil components. After completing the spectral detection, soil samples were analyzed for SOC and TN concentrations by dry combustion. Spatial variation of carbon and nitrogen was determined using Moran's I and comparisons

of spatial variations among soil types. The TN in turn showed more aggregation for all soil types and horizons compared to SOC. In this study, imaging spectroscopy was successfully used to measure and characterize the spatial variability of SOC and TN at the soil aggregate scale.

Hyperspectral remote sensing technology has been applied to soil detection due to its extremely high spectral resolution. Qualitative and quantitative detection on soil nutrient using remote sensing technology began in the 1960s. Various components in the soil have characteristic absorptions in the range of the solar reflection spectrum, so the relationship between soil components and absorption spectra can be used to predict the material composition in soil. The development of spectral remote sensing makes it possible to quickly and widely obtain soil physical and chemical information. Zhang et al. (2019a, b) used remote sensing methods to determine spatial distribution of soil total nitrogen (STN). A random forest (RF) model was used to estimate the spatial distribution of STN content by combining 21 prediction factors such as the original band (O), the normal spectral index (S), the red edge index (R), and the environmental variable (E). The results indicated that the best prediction performance can be obtained by combining the RF model with the original band, normal spectral index, red edge index, and environmental variable (O + S + E + R). The RF-based remote sensing method proposed in this research can accurately capture the change of STN, and the performance of the prediction model can be improved by providing appropriate prediction factors. Lu et al. (2018) evaluated the detection method of organic matter (SOC) based on remote sensing imaging from land satellites, and the spatial distribution and dynamic changes of organic matter were analyzed using random forest (RF) and geographic weighted regression (GWR). The results show that the root mean square error of RF was 4.6 g/kg in 2008 and 4.4 g/kg in 2013, which is better than the GWR prediction model.

3.3 Instruments of Soil Nutrient Detection

Applying spectroscopic techniques to detect physical and chemical parameters of soil can not only reduce the time and cost of analysis but also realize the in situ and real-time detection of soil information, which is conducive to promote the application of precision agriculture. At present, scientists engaged in the research of soil fertility management and agricultural information technology have developed various forms of soil testing instruments based on spectral technology, such as portable, vehicle-mounted, and remote sensing devices. Through these devices, it is convenient to implement comprehensive, full-range, all-weather, and real-time monitoring of soils from three spatial dimensions of ground, air, and satellite, providing a prerequisite for intelligent on-demand variable operations and ensuring increased grain production and efficiency.

3.3.1 Portable Instruments of Soil Nutrient Detection

Vis/NIR spectroscopy is efficient to detect the soil temperature, humidity, organic matter, nitrogen, phosphorus, potassium, and other components. Based on the spectroscopy, various portable soil devices have been extensively researched, which can realize an in situ and real-time detection of soil parameters. Sudduth and Hummel (1993) developed a portable real-time soil sensor, which was mainly used to measure the organic matter content in the soil surface. Figure 3.7 shows the structure diagram of the portable instrument, which is mainly composed of three parts: light source, beam splitting, and measurement unit. The light source consists of a light bulb and a focusing lens, where the light bulb is an iodine tungsten lamp and can stably provide light source of Vis/NIR. The main components of the beam splitting are an entrance slit, a focusing lens, a filter disk, an angle sensor, and an optical fiber entrance port. Among them, the key component is the filter disk, which can be rotated by a drive motor to continuously produce rays of 1650~2600 nm, and the

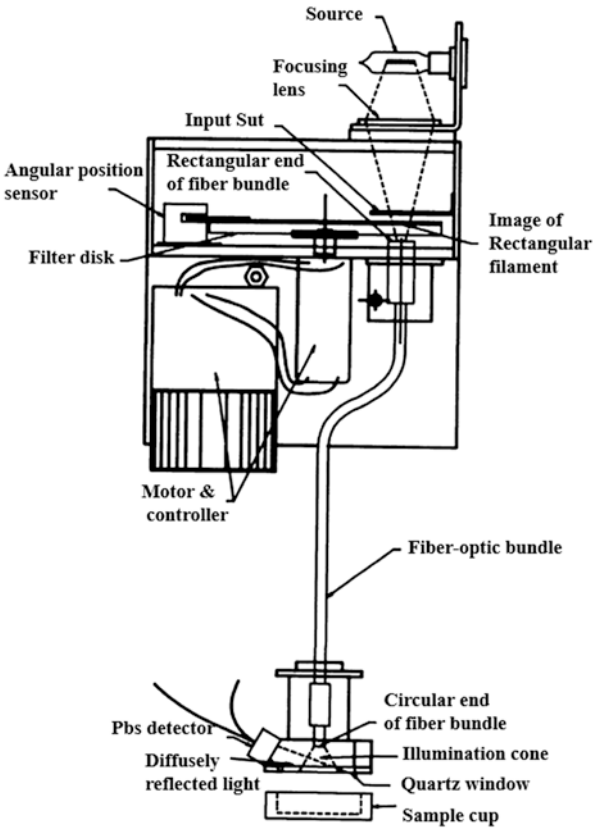

Fig. 3.7 Portable soil sensor. (Sudduth and Hummel 1993)

spectral resolution is below 55 nm. The measurement unit mainly includes an exit port of optical fiber, quartz plates, a sample box, and a photosensor. The photosensor provides stable photoelectric response in a wide spectral range of visible and near infrared, which is used to obtain the soil reflective spectrum and then achieve the prediction of soil organic matter content.

Li et al. (2010) developed a portable device for organic matter measurement, which could detect soil organic matter up to a depth of 30 cm. This measuring instrument was mainly composed of an optical module and an electronic module. The optical module included a light source, an optical signal transmission fiber, and a photoelectric conversion device. The electronic module included a driving circuit of light source, an amplifying circuit, an A/D conversion circuit, a liquid crystal display, a storage circuit of U disk, etc. (Fig. 3.8). The device used 850 nm LED as the light source. In order to minimize the energy consumption of incident and reflected light, a Y-type glass fiber was designed for input and output of the light source. When working, the probe was inserted into the soil to form a closed space, and then the rays from the light source was transmitted to the top of the probe and illuminated the soil around. The diffuse reflection rays from the soil were transmitted to the photoelectric conversion device, and the generated current was sent to the circuit unit for amplification, filtering, and storage. Under the condition of natural soil samples (about 20% moisture content), the coefficient of determination between the spectral absorbance and the content of soil organic matter was 0.950, and as for dry soil samples, the coefficient of determination was 0.982.

Based on the measurement device of soil organic matter above, An et al. (2012) developed a portable soil analyzer to obtain nitrogen content. The number of wavelengths used was increased from 1 to 7 wavelengths: 1550, 1450, 1300, 1200, 1100, 1050, and 940 nm. Its schematic diagram is shown in Fig. 3.9. When it is working, the probe is inserted into the soil and the code disk rotates sequentially to get the soil

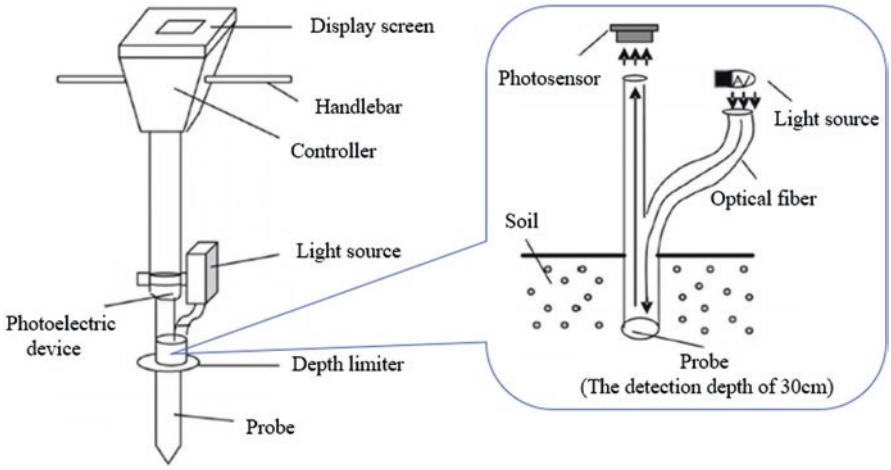

Fig. 3.8 Structure of soil detection device for organic matter. (Li et al. 2010)

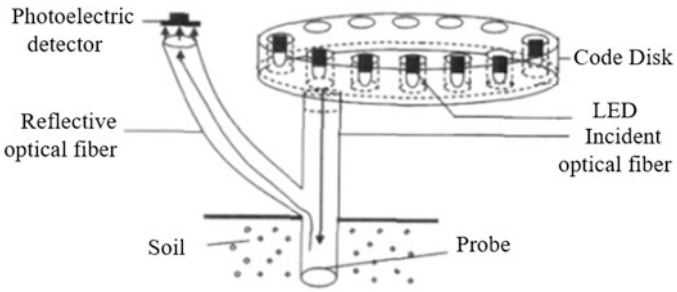

Fig. 3.9 Schematic diagram of portable tester for soil nitrogen content. (An et al. 2012)

Table 3.1 Measurement result using ASD and portable detection equipment. (Zhang 2015)

ASD instrument	Method	Wave number	Modeling set		Prediction set		
	SPA-LS-SVM	5	R^2	RMSEP	R^2	RMSEP	RPD
			0.80	0.0038	0.80	0.0031	2.26
Portable detection equipment	Method	Wave number	Modeling set		Prediction set		
	SPA-LS-SVM	15	R^2	RMSEP	R^2	RMSEP	RPD
			0.63	0.0079	0.62	0.0080	1.57

reflectance at 7 wavelengths, and then the total soil nitrogen content was obtained according to the established prediction model of soil nitrogen. The experimental results showed that the correlation coefficients of calibration and prediction for soil total nitrogen were 0.81 and 0.80, respectively.

Zhang (2015) developed a set of portable detection equipment for soil nutrient using hyperspectral analysis of Vis/NIR. The hardware part of the equipment is composed of the chassis shell, optical fiber, voltage conversion module, light source, drive circuit, integrated development board, power supply, touch screen, etc. The software part consists of the function loading module, spectrum acquisition module, data preservation module, display module, and parameter setting module. The core hardware component of the soil detection device is a USB4000 spectrometer. The optical fiber used for data collection is a Y-shaped optical fiber, which can also be replaced by two independent optical fibers (one for collecting data and one for receiving data). Then, a quantitative prediction model of near-infrared spectrum for soil total nitrogen (STN) content was established based on characteristic wavelengths. The results of portable instrument and ASD instrument to detect STN were shown in Table 3.1. The accuracy of portable instruments is inferior to ASD (350~2500 nm wavelength range) instruments, which is largely due to the size of the core component USB4000 which is only about a quarter of the ASD spectrometer, and the noise of the spectral data collected by the USB4000 spectrum is significantly greater than the spectral data obtained by the ASD.

3.3.2 *Airborne Equipment of Soil Nutrient Detection*

The UAVs (unmanned aerial vehicles) combined with remote sensing technology can quickly obtain the spectral data of soil and plants and achieve a monitoring of soil nutrients or plant growth information in large scale. UAVs can be classified as multi-rotor drones, fixed-wing drones, and helicopters according to the types of the flying platform (Fig. 3.10a). Multi-rotor drones have the most applications in soil remote sensing due to their simple control, no need for special runways to take off and land, and capability of hovering in the air after takeoff. In the field of consumer drones, the companies such as DJI and Parrot already have mature flight control platforms of multi-rotor drones, which can be conveniently equipped with various airborne cameras for remote sensing of soil nutrients. In addition, the drones gather spectral data by push broom scanning or hovering. In the push broom scanning mode, the drone takes continuous images of the soil while flying. After the acquisition is completed, image stitching and correction are conducted to complete a remote sensing image. In this mode, the data collection efficiency is high, but the data processing is troublesome. Under the hovering mode, the drone hovering in the air obtains a whole spectral image of the soil directly and does not require complex splicing in subsequent research work. However, its image acquisition efficiency is relatively low compared to the drone of push broom scanning (Fig. 3.10b).

In the actual soil information detection, the corresponding airborne equipment should be selected for remote sensing tasks according to the target component of the soil. RGB camera can be used to detect soil texture, type, organic matter, and other components. Vis/NIR camera can detect soil nitrogen, phosphorus, potassium, calcium, magnesium, aluminum, and other components. Thermal infrared camera can detect the surface temperature and humidity of soil, and Lidar can analyze the texture and terrain of the soil in three dimensions. Guo et al. (2019) used Vis/NIR remote sensing technology combined with partial least square regression model to predict the soil organic matter composition and obtained high prediction accuracy.

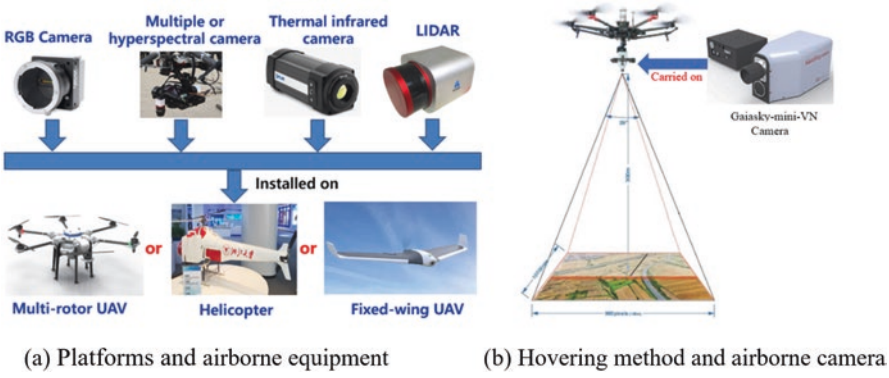

Fig. 3.10 Remote sensing based on UAVs for soil nutrient detection (**a**) Platforms and airborne equipment (**b**) Hovering method and airborne camera

Quebrajo et al. (2018) applied drone thermal infrared remote sensing technology to detect the water content of the soil, demonstrating the technological feasibility for the intelligent irrigation of sugar beets.

3.3.3 Satellite-Based Equipment for Soil Nutrient Detection

A satellite remote sensing system usually consists of satellites in the space and ground stations and client applications in the ground. The satellites are used to collect spectral information from Earth's surface at large scale and send the data to the ground stations. After that, the data are transmitted to the users by the ground station and then are processed and analyzed for obtaining remote sensing images. Satellite-based equipment is a key instrument for sensing soil nutrients. There are many forms of equipment that can be mounted on satellites, such as visible, NIR, and MIR cameras, multispectral scanners, and microwave radiometers. At present, satellite-based sensors are developing in the direction of multi-spectrum, multi-polarization, miniaturization, and high resolution.

Countries around the world have launched their own remote sensing satellites. Typical satellites that can be used for agricultural remote sensing are shown in Table 3.2. These satellites are equipped with Vis/NIR bands that can be used to detect soil nutrients or other soil properties. The spatial resolution is 10~30 m, and the revisit period is 4~44 days, which meets the needs for a wide range of soil monitoring. Zhai (2019) used GF-1 and Landsat 8 satellites to detect the organic content of soil. The results show that the reflectance of remote sensing images in the visible and NIR bands is significantly related to soil organic matter, and remote sensing images from Landsat 8 and GF-1 have similar prediction capabilities for organic matter. However, considering that GF-1 has higher spatial resolution and shorter revisit periods, it can replace the commonly used Landsat 8 to detect soil organic matter content. Zhang et al. (2019a, b) applied five satellites to observe soil moisture, which not only improved the spatial coverage of daily observations but also improved the accuracy of predicting soil moisture: the accuracy of soil moisture detection increased by 57.7% in Anhui Province, China, and 9.1% in Central Tibet, China.

Table 3.2 Parameters of main satellites

Model	Spatial resolution (m)	Waveband (nm)				Revisit period (day)	Country
		Blue	Green	Red	NIR		
GF-1	16	450 ~ 520	520 ~ 590	630 ~ 690	770 ~ 890	4	China
Landsat 8	30	450 ~ 515	525 ~ 600	630 ~ 680	845 ~ 885	16	USA
SPOT-5	10	/	495 ~ 605	617 ~ 687	780 ~ 893	26	France
JERS-1	18	/	520 ~ 660	630 ~ 690	760 ~ 860	44	Japan

Due to the influence of atmospheric conditions, data quality, and applicability of inversion models, it is difficult to achieve a prediction accuracy of more than 90% with only one satellite for the detection of soil parameters. Integrating multiple satellites to detect soil nutrients is one of the methods to improve the detection accuracy. In addition, in the study of satellite remote sensing for soil information, more research should be focused on parameter optimization and calibration methods of inversion models in order to further improve the sensing accuracy of soil by satellites.

3.3.4 Sensors in Internet of Things of Soil Nutrient Detection

Sensors, such as moisture, temperature, and nutrient sensors, are commonly used for monitoring soil characteristics in Internet of Things (IoT). The soil information monitored is transmitted to the cloud via wireless networks of Zigbee, Bluetooth, or WIFI, and then users can remotely retrieve soil data in cloud for obtaining the soil moisture and nutrient content to develop irrigation and fertilization strategies (Fig. 3.11).

In the detection of soil information, there is a requirement for monitoring soil moisture in real time and around the clock. Zhang et al. (2009) used Zigbee to connect soil moisture sensors and meteorological sensors to the network and developed an automatic monitoring and irrigation system for soil management based on fuzzy control algorithm. The wireless sensor network system is shown in Fig. 3.12. The system obtains real-time humidity of the soil and meteorological information such as ambient light, temperature, and wind speed. The established mathematical model calculates the moisture evaporations of soil and farmland, and then the intelligent

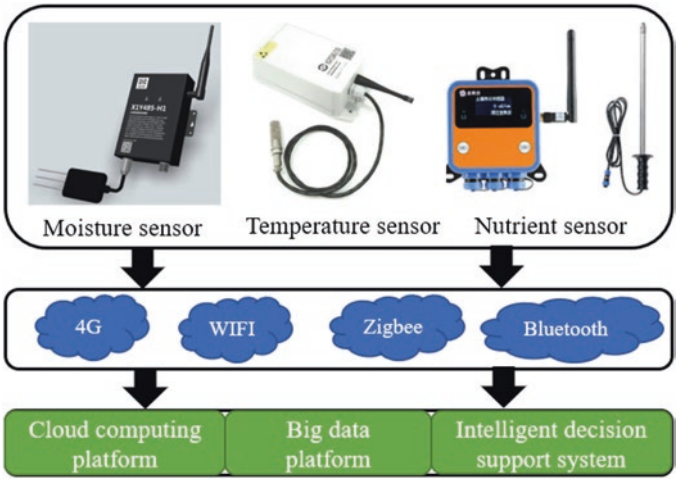

Fig. 3.11 Soil sensors of IoT

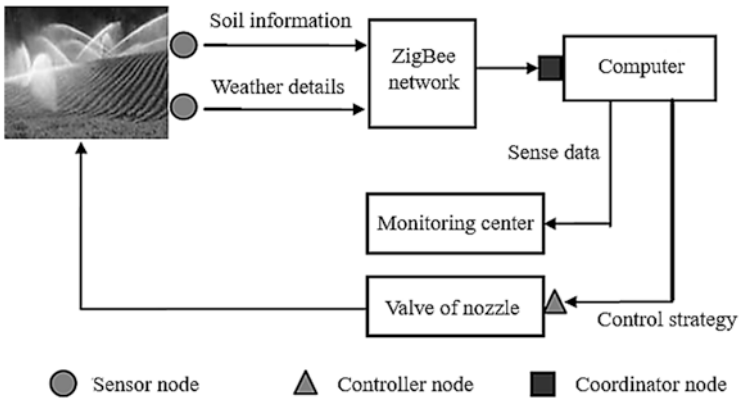

Fig. 3.12 Information flowchart of wireless sensor network system. (Zhang et al. 2009)

decision-making system takes the two evaporation values as the input parameters of irrigation system to spray the crops on demand. Its saving effect of water is significant.

3.4 Summary

The detection method of Vis/NIR spectroscopy has achieved high accuracy for predicting soil nutrients such as nitrogen, phosphorus, potassium, and organic matter content. Therefore, developing portable soil detectors as well as airborne- and satellite-based sensors based on Vis/NIR spectroscopy for rapidly detecting soil nutrients will play an important role in the extension of precision fertilization by soil testing. LIBS has a strong ability of detecting heavy metals in soil and is therefore a promising technique for soil nutrient detection. Revealing the absorption characteristics of LIBS under different soil types, structures, and components is the research focus that needs to be carried out.

References

Alexander DR, Poulain DE, Ahmad MU, Kubik RD, Cespedes ER (1994) Environmental monitoring of soil contaminated with heavy metals using laser-induced breakdown spectroscopy. In: International geoscience and remote sensing symposium, Pasadena, 1994. IEEE, New Jersey, p 767

An X, Li M, Zheng L, Liu Y, Zhang Y (2012) Performance of portable soil TN detector based on NIR spectroscopy. Trans Chin Soc Agric Mach 43(Z1):283–288

An X, Li M, Zheng L, Liu Y, Sun H (2013) Effect of soil moisture on prediction of soil total nitrogen using NIR spectroscopy. Spectrosc Spectr Anal 33(3):677–681

Baldock JA, Hawke B, Sanderman J, Macdonald LM (2013) Predicting contents of carbon and its component fractions in Australian soils from diffuse reflectance mid-infrared spectra. Soil Res 51(7&8):577–595

Cremers DA, Ebinger MH, Breshears DD, Unkefer PJ, Kammerdiener SA, Ferris MJ, Catlett KM, Brown JR (2001) Measuring total soil carbon with laser-induced breakdown spectroscopy (LIBS). J Environ Qual 30(6):2202–2206

Dong DM, Zhao CJ, Zheng WG, Zhao XD, Jiao LZ (2013a) Spectral characterization of nitrogen in farmland soil by laser-induced breakdown spectroscopy. Spectrosc Lett 46(6):421–426

Dong D, Zheng W, Zhao C, Zhao X, Jiao L, Zhang S (2013b) Determination of potassium in farmland soil using laser-induced breakdown spectroscopy. Spectrosc Spectr Anal 33(3):78–82

Glumac NG, Dong WK, Jarrell WM (2010) Quantitative analysis of soil organic carbon using laser-induced breakdown spectroscopy: an improved method. Soil Sci Soc Am J 74(6):1922–1928

Guo L, Zhang H, Shi T, Chen Y, Jiang Q, Linderman M (2019) Prediction of soil organic carbon stock by laboratory spectral data and airborne hyperspectral images. Geoderma 337:32–41

Hussain T, Gondal MA, Yamani ZH, Baig MA (2007) Measurement of nutrients in green house soil with laser induced breakdown spectroscopy. Environ Monit Assess 124(1–3):131–139

Izaurralde RC, Rice CW, Wielopolski L, Ebinger MH, Reeves JB III, Thomson AM, Harris R, Francis B, Mitra S, Rappaport AG, Etchevers JD, Sayre KD, Govaerts B, McCarty GW (2013) Evaluation of three field-based methods for quantifying soil carbon. PLoS One 8(1):e55560

Janik LJ, Skjemstad JO, Shepherd KD, Spouncer LR (2007) The prediction of soil carbon fractions using mid-infrared-partial least square analysis. Aust J Soil Res 45(2):73–81

Jia X, Chen S, Yang Y, Zhou L, Yu W, Shi Z (2017) Organic carbon prediction in soil cores using VNIR and MIR techniques in an alpine landscape. Sci Rep 7(1):2144

Li M, Pan L, Zheng L, An X (2010) Development of a portable SOM detector based on NIR diffuse reflection. Spectrosc Spectr Anal 30(4):1146–1150

Li M, Zheng L, An X, Sun H (2013) Fast measurement and advanced sensors of soil parameters with NIR spectroscopy. Trans Chin Soc Agric Mach 44(3):73–87

Lu C, Wang L, Hu H, Zhuang Z, Wang Y, Wang R, Song L (2013) Analysis of total nitrogen and total phosphorus in soil using laser-induced breakdown spectroscopy. Chin Opt Lett 11(5):053004

Lu W, Lu D, Wang G, Wu J, Huang J, Li G (2018) Examining soil organic carbon distribution and dynamic change in a hickory plantation region with Landsat and ancillary data. Catena 165:576–589

Martin MZ, Wullschleger SD, Garten CT Jr, Palumbo AV (2003) Laser-induced breakdown spectroscopy for the environmental determination of total carbon and nitrogen in soils. Appl Opt 42(12):2072–2077

Martin MZ, Labbé N, André N, Wullschleger SD, Harris RD, Ebinger MH (2010) Novel multivariate analysis for soil carbon measurements using laser-induced breakdown spectroscopy. Soil Sci Soc Am J 74(1):87–93

Martin MZ, Mayes MA, Heal KR, Brice DJ, Wullschleger SD (2013) Investigation of laser-induced breakdown spectroscopy and multivariate analysis for differentiating inorganic and organic C in a variety of soils. Spectrochim Acta B 87:100–107

Meng D, Zhao N, Liu W, Ma M, Wang Y, Yu Y, Fang L, Hu L, Zhang D, Yang R, Wang J, Liu J (2014) Quantitative measurement and analysis of potassium in soil using laser-induced breakdown spectroscopy. Chin J Lasers 42(5):0515003

Quebrajo L, Perez-Ruiz M, Pérez-Urrestarazu L, Martínez G, Egea G (2018) Linking thermal imaging and soil remote sensing to enhance irrigation management of sugar beet. Biosyst Eng 165:77–87

Sorenson PT, Quideau SA, Rivard B (2018) High resolution measurement of soil organic carbon and total nitrogen with laboratory imaging spectroscopy. Geoderma 315:170–177

Sudduth KA, Hummel JW (1993) Portable, near-infrared spectrophotometer for rapid soil analysis. Trans ASAE 36(1):185–193

Sun JY, Li MZ, Zheng LH, Hu YG, Zhang XJ (2006) Real-time analysis of soil moisture, soil organic matter, and soil total nitrogen with NIR spectra. Spectrosc Spectr Anal 26(3):426–429
Sun JY, Li MZ, Tang N, Zheng LH (2007) Spectral characteristics and their correlation with soil parameters of black soil in Northeast China. Spectrosc Spectr Anal 27(8):1502–1505
Wang J, Yan H, Zheng P, Tan G (2017) Quantitative detection of nutrient elements in soil based on laser induced breakdown spectroscopy. Chin J Lasers 44(11):1111002
Yu K (2016) Detection of physical-chemical information of soil using laser-induced breakdown spectroscopy technology. Doctor thesis, Zhejiang University
Yu F, Min S, Ju X, Zhang F (2002) Determination the content of nitrogen and organic substance in dry soil by using near infrared diffusion reflectance spectroscopy. Chin J Anal Lab 21(3):49–51
Yu K, Zhao Y, He Y, He D (2019) Response surface methodology for optimizing LIBS testing parameters: a case to conduct the elemental contents analysis in soil. Chemom Intell Lab Syst 195:103891
Zhai M (2019) Inversion of organic matter content in wetland soil based on Landsat 8 remote sensing image. J Vis Commun Image Represent 64:102645
Zhang H (2015) Soil nutrition content and type measurement based on NIR spectrum and hyper spectra image technology and design portable instrument. Doctor thesis, Zhejiang University
Zhang W, He Y, Qiu Z, Cao J, Qian S, Lu J, Jin J (2009) Design of precision irrigation system based on wireless sensor network and fuzzy control. Trans Chin Soc Agric Eng 25(Supp.2):7–12
Zhang J, Fang X, Zhang X, Yuan Y, Zhou L, Wu H (2014) Detection of soil potassium content based on laser-induced breakdown spectroscopy. Trans Chin Soc Agric Mach 45(10):294–299
Zhang K, Chao L, Wang Q, Huang Y, Liu R, Hong Y, Tu Y, Qu W, Ye J (2019a) Using multi-satellite microwave remote sensing observations for retrieval of daily surface soil moisture across China. Water Sci Eng 12(2):85–97
Zhang Y, Sui B, Shen H, Ouyang L (2019b) Mapping stocks of soil total nitrogen using remote sensing data: a comparison of random forest models with different predictors. Comput Electron Agric 160:23–30
Zhu D, Wu D, Song H, He Y (2008) Determination of organic matter contents and pH values of soil using near infrared spectroscopy. Trans Chin Soc Agric Eng 24(6):196–199

Chapter 4
Application of Soil Sensing in Precision Agriculture

Sakae Shibusawa, Masakazu Kodaira, Eiji Morimoto, and Minzan Li

Abstract Soil mapping technologies are required to visualize spatial and temporal variability between fields or within field. Proximal and nondestructive soil sensing coupled with GPS using visible and near-infrared (Vis-NIR) spectroscopy or electrical conductivity sensor (soil EC) is a promising approach. A series of tractor-mounted soil-analyzing systems based on Vis-NIR spectroscopy were developed. The structure of the systems is mainly composed of a connection unit (three-point hitch structure), a sensing unit, and a soil penetration part. In the sensing unit, a Vis-NIR spectrometer (NIR enhanced: 310–1100 nm, 3.1 nm/pixel interval), a halogen lamp, thermometers, and a personal computer are installed. The load cell provides cutting resistance measurement and automatic retreat function of the soil-penetrating part due to overloading. In the sensor probe box, a color microcamera head, a radiation/light-concentrating fiber, a displacement meter, and an air blow head are equipped. Estimation models of 33 soil parameters, including moisture content, total carbon, total nitrogen, and soil organic matter, were established with the spectral reflectance data obtained by the tractor-mounted soil-analyzing systems. The result shows the higher multiple calibration accuracy. A smart rice transplanter was developed, which could measure soil EC (apparent electrical conductivity) and topsoil depth. The fertility of the soil varies due to uneven distribution of compost or soil conditioner, and these variations will result in crop lodging at harvest time. The smart rice transplanter developed solves this lodging problem with soil EC data and performs real-time variable fertilizer application.

Keywords Proximal soil sensing · Vis-NIR spectroscopy · Soil mapping · Soil electrical conductivity · Soil sensor

S. Shibusawa · M. Kodaira (✉)
Tokyo University of Agriculture and Technology, Tokyo, Japan
e-mail: kodaira@cc.tuat.ac.jp

E. Morimoto
Tottori University, Tottori, Japan

M. Li
China Agricultural University, Beijing, China

M. Li et al. (eds.), *Soil and Crop Sensing for Precision Crop Production*,
Agriculture Automation and Control, https://doi.org/10.1007/978-3-030-70432-2_4

4.1 Tractor-Mounted Soil Analysis System Based on Vis-NIR Spectroscopy

4.1.1 Soil Sensing Instruments Based on Vis-NIR Spectroscopy

Precision agriculture (PA) aims to improve agricultural profitability and productivity (yield, quality, farming, etc.), as well as protecting environment. It has been enabled by the rapid development and spread of GNSS (Global Navigation Satellite System), GIS (Geographic Information System), and ICT (Information and Communications Technology).

To practice PA, the required technologies include field mapping technology to visualize spatial and temporal variability between fields or within field, variable-rate technology to perform farming work corresponding to the variability, and decision support system to solve complex problems and requirements. Especially, field mapping technology is the basis of PA. The technological feature of PA is to accurately record the spatial and temporal variability of soil, crop, yield, etc., to realize site-specific field management at low cost using field maps.

In terms of soil analysis, soil samples are collected from the field and analyzed by official method. The problems are the cost, analysis period, and labor for a large number of soil samples with location information collected for analysis of multiple properties to support the PA practice, and few growers are willing to adopt soil analysis for each cropping. The analysis period has been shortened compared to the official method by the development of a simple soil analysis method, which contributed to the improvement of soil analysis business. However, when crops with a short period from harvesting to sowing were cultivated in same field, it was difficult to plan and distribute fertilizer based on the soil analysis result using soil samples collected after harvest. The problems of labor and cost consuming on the grower side have not been improved.

To overcome these problems, development of soil sensing devices has been carried out using electrical, electromagnetic, acoustic, pneumatic, and optical technologies. It has been reported that spectroscopic technology using visible (Vis), near-infrared (NIR), and infrared (IR) soil reflectance is nondestructive, rapid, and cost-effective, with high accuracy compared to other soil sensing technologies (Adamchuk et al. 2004). The purpose to introduce spectroscopic technology in soil analysis is to improve price-performance ratio, which has more rapid and higher efficiency than the official and simple soil analytical method. In addition, the predicted values are required to be absolute quantitative values, with the accuracy at a level equivalent to the official method. The mainstream of soil spectroscopic analysis is to measure the soil diffuse reflectance spectra using a spectrophotometer installed in laboratory. As a result, the problems on the analysis business side have been improved. But the problems on the grower side, such as labor consuming in soil sampling with location information and sample drying and 2 mm sieving pretreatment work, have not yet been considered. The new problems are that the instrument is expensive, and it is necessary to analyze regression coefficient for each soil

type and each soil property. The number of soil properties is limited, and accuracy is low for nitrogen, phosphorous, and potassium which are required for fertilization design (Dalal and Henry 1986; Matsunaga and Uwasawa 1992a, b, 1993; Chang et al. 2001; Viscarra Rossel et al. 2006).

In order to measure a large amount of soil diffuse reflectance spectra with position information using a spectrophotometer without soil sample collection, field measurement-type (field-type hereinafter) spectrophotometers have been developed which can simultaneously measure the soil diffuse reflectance and position information in a field. When measuring raw soil sample spectra, the difference in water content greatly influences the spectra in the infrared region. Therefore, the field-type spectrophotometers have been developed which equipped with spectroscopic sensors sensitive in Vis-NIR wavelength range that is less affected by soil moisture (Shibusawa et al. 2000a, b; Mouazen et al. 2007; Christy 2008). As a result, the problems on both grower and analysis business sides have been improved. However, as "new problems" to the laboratory spectrophotometer, the countermeasures for that the field-type spectrophotometer cannot be used in fields such as slope, orchards, and forest have not been considered. In field measurement, diffuse reflectance spectra from other substances than soil, such as gravel and crop residues, may cause prediction errors. In addition, the soil diffuse reflectance spectra used to estimate the regression coefficient in previous studies were measured from dried and 2 mm sieved soil. The diffuse reflectance spectra of raw soil measured in a field have to be analyzed using a moisture correction coefficient (Christy 2008; Mouazen et al. 2014). In addition, the estimation errors of the regression coefficient and the moisture correction coefficient have been the factors that reduced the prediction accuracy.

The field-type spectrophotometer is useful as the field soil mapping technology. But the mainstream is to use interpolation methods in commercially available software such as GIS and Excel and the visualization method by grid-like soil mapping (Shibata 1999; Toriyama 2001; Umeda et al. 2011; Kuang and Mouazen 2013). However, the software installation/maintenance is expensive, and data transfer, conversion, and the setting process to display soil map are complicated. The variability status of multiple soil properties is difficult to confirm with growers immediately after the field observation, so it is lack in speed and convenience.

The soil property analyses for soil mapping are soil diagnostic properties (chemical, physical, and biological) that are necessary for crop production. There are more than 20 chemical properties including general properties, trace elements, and nitrogen. In terms of physical properties, besides soil dry density which is important in fertilization design, soil textures (sand, silt, and clay) are indispensable for determining soil fertility. The biological properties have microorganisms and nematodes which are useful information. But types of them are countless, and the analytical method and cultivation guideline are not established. The microorganism in soil decompose organic component into nutrients that can be used by crops and prevent failures, improve physicochemical and biological properties of soil, improve crop productivity and quality, and purify the soil. Therefore, it is becoming an important farming decision information after the chemical fertilizer. In general, the purpose of soil analysis is to estimate the input of chemical fertilizer necessary for crop

production while reducing the environmental impact, and three properties, nitrogen, phosphorous, and potassium, are the target properties. The reason why multi-property soil analysis is recommended is due to the fact of "Dobeneck's barrel" (Hans Arnold von Dobeneck) which proposed that crop growth is governed by the scarcest resource. Or the "Liebig's law of the minimum" by Justus von Liebig, which suggests that crop growth rate and yield are dictated not by total nutrients available but only affected by the scarcest nutrient that provided to the crop (limiting factor). In addition, the absorption of nutrients by crops is a synergistic effect promoted by other nutrients (when present in an appropriate amount), or when a certain nutrient is excessive, it may be an antagonist that suppresses or inhibits the absorption of other coexistence nutrients. These effects are also necessary to be considered. If it becomes possible to provide high-resolution soil maps rapidly with multiple properties, field management using right material with right amount at right time and location will be possible, which will be the basis for preventing excessive application of agricultural materials. Also, since various types of soil property maps are required according to the cultivation purposes of growers, the nondestructive prediction technology based on soil diffusion reflection spectra, which can provide multiple prediction values from a single measurement, is indispensable in soil sensing device.

The results of soil sensing are not only used as field mapping technology for PA but also contribute to soil/field management in good agricultural practice (GAP) which established standards and procedures for food security and provide field information for integration/aggregation, consolidation of fields, and reuse of abandoned land. The 70% use of total freshwater in agriculture is an urgent need for improvement, and soil maps of moisture and physical property are used as consensus building information to allocate freshwater resources efficiently and effectively (Hedley and Yule 2009; Mouazen et al. 2014). This is a contribution to the Sustainable Development Goals (SDGs: 1, 2, 12, 13, and 15) to realize a sustainable world (Ministry of Foreign Affairs of Japan 2018). As one of the countermeasures against global warming, the carbon farming (Australian Government 2011) assesses the ability of soil carbon sequestration. The carbon credit trading conducted by the Chicago Climate Exchange based on Clean Development Mechanism (CDM) is expected to be a source of income of growers.

4.1.2 Tractor-Mounted Soil Analysis Systems

There are potable and tractor-/vehicle-mounted devices that can predict physiochemical soil properties from diffuse reflectance spectra measured in a field. It was USDA (US Department of Agriculture) (Sudduth and Hummel 1993) that made it possible to continuously measure diffuse reflectance spectra in a field by installing a spectrophotometer on a tractor or vehicle and after that the Tokyo University of Agriculture and Technology (TUAT, Japan) in 1999 (Shibusawa et al. 1999) and Catholic University of Leuven (CU of Leuven, Belgium) (Mouazen et al. 2005) in

2005. Veris Technologies (USA) in 2008 (Christy 2008), Poznan University in 2013 (Poland) (Wojciechowski and Czechlowski 2013), Jacto (Brazil) in 2013, and University of Bonn (Germany) in 2015 (Rodionov et al. 2015) developed the test device, as shown in Table 4.1.

The measurement wavelength range of the USDA's device was 1630–650 nm, the observation depth was 0.35–0.50 m, the observation speed was 0.65 m/s, and the method to estimate regression coefficients was partial least square regression (PLSR). The target soil properties were cation exchange capacity (CEC), organic matter (organic carbon), and soil water content. The prediction accuracy by laboratory measurement (using dry and moist soil) was R^2 = 0.85–0.96. But the accuracy

Table 4.1 Comparison of tractor-/vehicle-mounted spectrophotometer

Authors	Equipment (spectrometer)	Field measurement		Spectra data for calibration		Multivariate analysis software
		Soil depth (m)	Speed (m/s)	Measurement location	Soil condition	
Sudduth and Hummel (1993), USDA	Prototype portable NIR spectrophotometer	0.035~0.05	0.65	Lab	Dry	The Unscrambler
Shibusawa et al. (1999, 2000a, b) and Imade Anom et al. (2001), TUAT	RTSS-01 (MMS 1 and MMS)	0.15, 0.20~0.25	0.28 0.28	Field	Fresh	The S-Plus data analysis
Mouazen et al. (2005, 2007), CU of Leuven	Fiber-type NIR spectrophotometer (Corona 45: MMS 1 and MMS)	0.15	0.42	Lab	Day	The Unscrambler Ver.7.8
Christy (2008), Veris Technologies	On-the-go spectrophotometer (NIR-128L-1.7-USB)	0.07	1.67	Lab	Dry	LabVIEW
Marín González et al. (2013)	Fiber-type NIR spectrophotometer (AgroSpec: MMS 1 and MMS)	0.15	0.83	Lab	Dry	The Unscrambler Ver.7.8
Wojciechowski and Czechlowski (2013), Poznan University	The combined soil measurement system (AgroSpec: MMS 1 and MMS)	–	–	Lab	Dry	The Unscrambler X
Jacto	Jacto Soil Sensor (Corona 45: MMS 1 and MMS)	–	–	Field	Fresh	The Unscrambler Ver.9.8
Rodionov et al. (2015), University of Bonn	Mobile measuring chamber (AgroSpec)	0.05	0.83	Lab	Dry	ParLes 3.1

extremely decreased when measured in a field while moving. It has been reported that the cause was due to the variations in the height of the observation surface and the sensor during the measurement. The purpose of raw soil diffuse reflectance spectra measurement is to obtain prediction values of soil physicochemical properties to create soil maps. However, there was no mechanism equipped to link the location information to the measured data, which did not lead to soil mapping.

The measurement wavelength range of the TUAT's device was 400–1700 nm, the observation depth was 0.30 m, and the observation speed was 0.05 m/s. The soil at the spot where the soil diffuse reflectance spectra were measured in the field was collected, and the reflectance spectra of the raw soil were measured in laboratory using a spectrophotometer (Shimadzu, UV3100). The equivalence of the two measurements was confirmed with correlation coefficient $R = 0.98$. The target properties were electric conductivity (EC), pH, nitrate nitrogen, soil water content, and soil organic matter. The method to estimate regression coefficient adopted single regression, and the accuracy from the spectra measured while moving was $R = 0.44–0.93$. Toward the problems of the USDA's device, Shibusawa et al. (1999) combined the tip of a subsoiler, which could reduce soil resistance and stably operate even at high speeds, with a chisel which was superior in penetration and crushing even in hard field and equipped with a sensor head. The variation in the height of the observation surface and the sensor was suppressed, and stable diffuse reflectance spectra acquisition was successfully conducted. In addition, RTK-GPS (Real-Time Kinematic-Global Positioning System) was installed to link "time and location" to "diffuse reflectance spectra." This made it possible to link position information to the prediction value calculated from the raw soil diffuse reflectance spectra. Since then, the developed devices have been equipped with DGPS (differential GPS) system in addition to the RTK-GPS system.

The measurement wavelength range of the CU of Leuven's device was 306.5–1710.9 nm, the observation depth was 0.15 m, the observation speed was 0.33 m/s, and the regression coefficients were estimated by PLSR (Mouazen et al. 2005, 2007). The target property was soil water content, with $R = 0.98$. For the regression coefficient estimation, a total of six types of soil diffuse reflection spectra were measured by adding water to dry soil from 0 to 0.25 kg/kg (0.05 kg/kg interval). The soil diffuse reflection spectra measured from a field were not used in the estimation of regression coefficient.

The measurement wavelength range of the Veris Technologies' device was 950–1650 nm (Christy 2008), the observation depth was 0.07 m, the observation speed was 1.67 m/s, and the regression coefficients were estimated by principal component regression (PCR). The target soil properties were lime, organic carbon, exchangeable potassium, LBC (lime buffer capacity), soil water content, magnesium, manganese, available phosphorus, pH, and zinc. The soil diffuse reflectance spectra used in the regression coefficient estimation were based on dry soil spectra measured in laboratory. The highest prediction accuracy was organic carbon with $R^2 = 0.67$. For the diffuse reflectance spectra measured in a field, they reduced the prediction error caused by moisture variation by previously analyzing a moisture correction model based on spectra difference between dry soil and moist soil.

The measurement wavelength range of the Poznan University's device was 400–1270 nm; the observation depth was 0.05 m; the observation speeds were 0.05, 0.07, and 0.1 m/s; and the regression coefficient was estimated by PLSR (Wojciechowski and Czechlowski 2013). The target property was soil water content. The accuracies were R^2 = 0.87–0.89 at constant and mixing speed.

The measurement wavelength range of the Jacto's device was 400–700 nm, the observation depth was 0.06 m, the observation speed was 0.56 m/s, and the regression coefficients were estimated by PLSR. The target soil properties were pH, CEC, exchangeable potassium, exchangeable calcium, and available phosphorous.

The measurement range of the University of Bonn's device was 410–2300 nm, the observation depth was 0.05 m, the observation speed was 0.83 m/s, and the regression coefficients were estimated by PLSR (Rodionov et al. 2015). The target soil properties were soil organic carbon and soil water content. The R^2 were 0.84 and 0.96, respectively. Although the observation speed was the highest, the moving was temporarily stopped when measuring the diffuse reflectance spectra.

The most used field spectrometers in the devices were MMS and MMS1 (Table 4.1). The highest observation speed at the maximum observation depth of 0.15 m was 0.83 m/s. The diffuse reflectance spectra used to estimate the regression coefficient were mostly based on dry soil in laboratory. The Unscrambler was used as the multivariate analysis software, and PLSR was used as the analysis method. The target soil properties in previous studies included nitrogen, phosphorus, and potassium. But the ranks of the regression coefficient were low, at C and D. The ranks were A and B only for soil water content, soil organic matter, and organic carbon (Table 4.2).

The commercialization of TUAT's device was performed by the Shibuya Machinery Co., Ltd. (Shibuya Seiki Co., Ltd. at present). The measurement properties were soil water content, soil organic matter, total nitrogen, and EC. The general regression coefficient (which does not depend on the soil type and various component concentrations) was not provided. The device commercialized by the Veris Technologies can perform soil mapping for soil organic matter and soil physical properties.

The problem is that it is necessary to analyze moisture correction equation when estimating regression coefficient using the diffuse reflectance spectra of dry soil. Moreover, high-accuracy, multi-property regression coefficient estimation has not been achieved.

4.1.3 Soil Analysis System (SAS) Series

The development of real-time subsoil optical sensor was started in 1997, and joint research was started in 1998 between the TUAT and Omron Corporation, Japan. The prototype was completed in 1999. A 01 model equipped with two spectrometers of Vis-NIR range was developed in 2001, and 02 model of nine-wavelength spectroscopic types (552, 651, 738, 811, 926, 1003, 1303, 1457, 1650 nm) was

Table 4.2 Properties and prediction accuracy of tractor-/vehicle-mounted spectrophotometer

Items	Wavelength (nm)	Analysis method (F)	*N*	RMSE	R^2	RPD	Rank	Authors
pH	400–1700	SMLR	15	0.16	0.58	1.25	E	Imade Anom et al. (2001)
	306–1710	PLSR (12)	295	0.22	0.71	2.14	C	Mouazen et al. (2007)
	920–1718	PCR	106	0.44	0.62	1.64	D	Christy (2008)
	400–2100	PLSR	160	0.40	0.79	2.16	C	Marín González et al. (2013)
Available phosphorus	920–1718	PCR	116	30.0	0.80	2.24	C	Christy (2008)
	306–1710	PLSR (9)	175	1.35	0.69	1.80	D	Mouazen et al. (2007)
Exchangeable potassium	920–1718	PCR	106	107	0.60	1.54	D	Christy (2008)
Exchangeable magnesium	920–1718	PCR	107	85.0	0.73	2.07	C	Christy (2008)
	400–2100	PLSR	160	0.38	0.69	2.44	C	Marín González et al. (2013)
Exchangeable calcium	920–1718	PCR	105	750	0.82	2.32	C	Christy (2008)
	400–2100	PLSR	160	22.1	0.89	0.83	E	Marín González et al. (2013)
Soluble zinc	920–1718	PCR	93	0.62	0.48	1.37	E	Christy (2008)
Easily reducible manganese	920–1718	PCR	110	34.0	0.40	1.27	E	Christy (2008)
Nitrate nitrogen	400–1700	SMLR	15	4.74	0.54	1.83	D	Imade Anom et al. (2001)
Cation exchange capacity	1630–2650	PLSR (10)	30	3.91	0.85	–	–	Sudduth and Hummel (1993)
	400–2100	PLSR	160	1.77	0.58	1.54	D	Marín González et al. (2013)
Electrical conductivity	400–1700	SMLR	15	41.7	0.65	1.10	E	Imade Anom et al. (2001)
Moisture content	1630–2650	PLSR (10)	30	1.69	0.96	–	–	Sudduth and Hummel (1993)
	400–1700	SMLR	15	3.11	0.66	1.83	D	Imade Anom et al. (2001)
	306–1710	PLSR	348	0.02	0.89	3.00	B	Mouazen et al. (2007)
	920–1718	PCR	105	2.80	0.65	1.75	D	Christy (2008)
	400–2170	PLSR	–	2.24	0.89	–	–	Wojciechowski and Czehlowski (2013)
	410–2300	PLSR	120	1.99	0.96	5.03	A	Rodionov et al. (2015)

(continued)

Table 4.2 (continued)

Items	Wavelength (nm)	Analysis method (F)	*N*	RMSE	R^2	RPD	Rank	Authors
Soil organic matter	400–1700	SMLR	15	0.56	0.65	1.86	D	Imade Anom et al. (2001)
	920–1718	PCR	106	0.40	0.80	2.20	C	Christy (2008)
Total carbon	306–1710	PLSR	173	0.27	0.73	1.92	D	Mouazen et al. (2007)
Soil organic carbon	1630–2650	PLSR (10)	30	0.26	0.85	–	–	Sudduth and Hummel (1993)
	410–2300	PLSR	120	0.73	0.84	2.53	B	Rodionov et al. (2015)

N number of samples, *PCR* principal component regression, *RMSE* root mean square error, *RPD* residual prediction deviation (standard deviation/RMSE). Rank (Kuang et al. 2012): A (excellent), B (good), C (approximate quantitative prediction), D (distinguish between high and low), E (not usable)

developed in 2002 (Shibusawa et al. 2000a, b; Bodun et al. 2000; Imade Anom et al. 2001; Kaho et al. 2004; Shibusawa et al. 2005; Roy et al. 2006). Patents associated with the device development (Japanese Patent Application No. Hei10-108862, No.2000-604663, No. 2001-322755, and No. 2002-169192) were transferred from the Omron Corporation to TUAT, and the license and technology were transferred to the Shibuya Machinery Corporation. In 2004, a promotion model of the tractor-mounted soil analysis system (SAS1000[1]) (Fig. 4.1) was developed (Shibuya Machinery Co. Ltd. 2004; Shibusawa et al. 2010; Kodaira and Shibusawa 2013, 2016). SAS is custom-made systems, which have specification for large-scale field (SAS2000), specification for paddy field (SAS2500) (Fig. 4.2) (Kodaira and Shibusawa 2018), specification for woodlot (SAS2600), and specification with self-propelled lightweight (SAS3000) (Fig. 4.3). Since no regression coefficient was provided for soil property, the challenge is to secure human resources who can measure soil diffuse reflectance spectra and physicochemical properties and introduce and operate software such as multivariate analysis and soil mapping.

(1) SAS1000

SAS1000 (Fig. 4.1) is composed of a connection unit (three-point hitch structure), a sensing unit, and a soil penetration part (Fig. 4.1b), and the weight is 550 kg. In the sensing unit, Carl Zeiss's Vis-NIR spectrometers (MMS1 NIR enhanced: 310–1100 nm, 3.1 nm/pixel interval), a halogen lamp (Ushio Electric Co., Ltd., JCR15V150WBAL), thermometers (external air, spectrometer, control panel), and a personal computer (PC) are installed. The soil penetration part has vertical and horizontal cutting blades for soil cutting and removal and a chisel plow with a

[1] *Disclaimer*: Commercial products are referred to solely for the purpose of clarification and should not be construed as being endorsed by the authors or the institution with which the authors are affiliated.

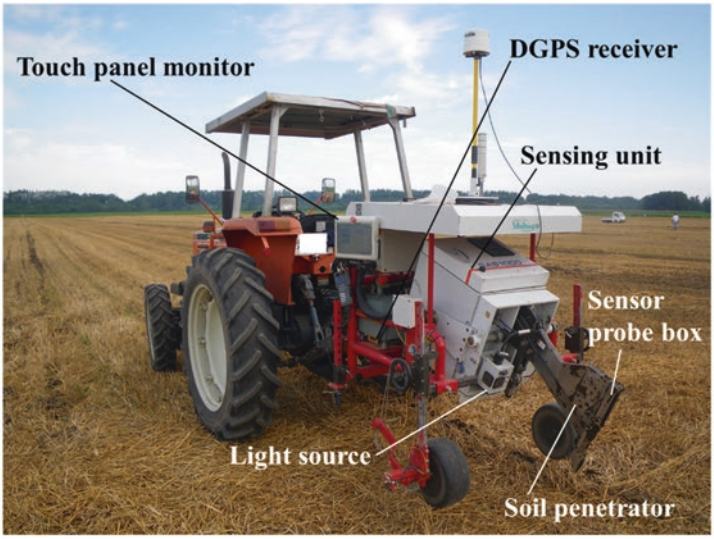

(a)

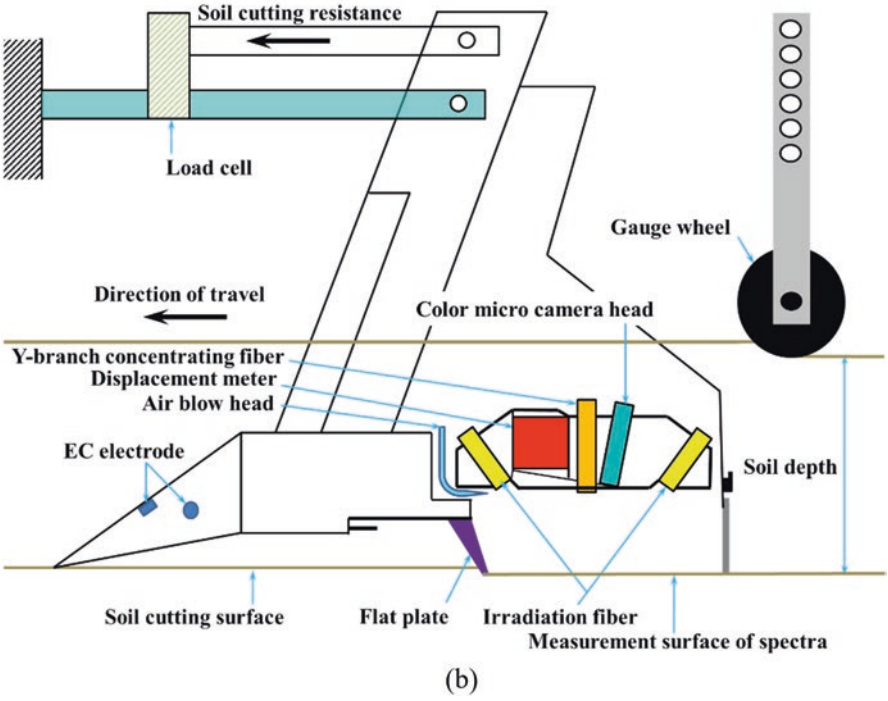

(b)

Fig. 4.1 Soil analysis system SAS1000 (**a**) SAS 1000 system, (**b**) Cross section of soil-penetrating part. (Shibusawa et al. 2010)

(a)

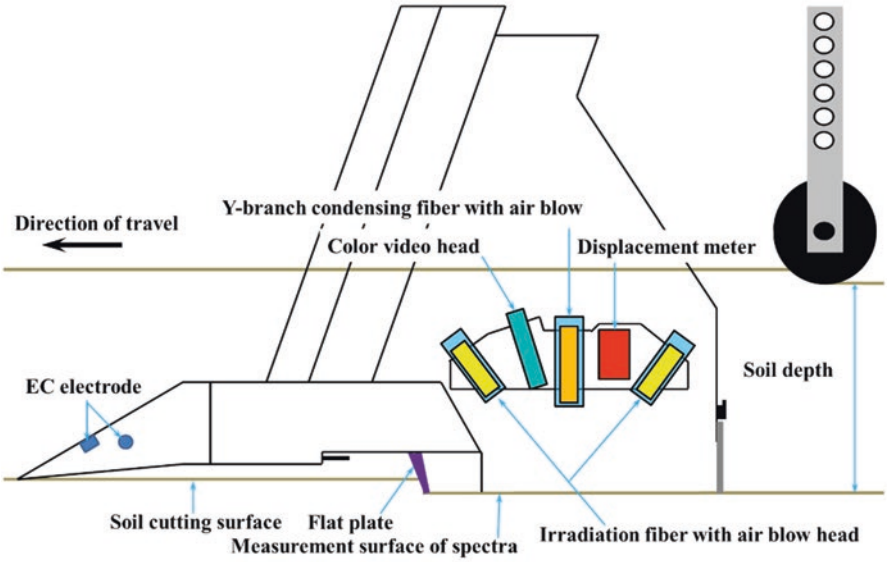

(b)

Fig. 4.2 Soil analysis system SAS2500 (**a**) System SAS2500 (**b**) Cross section of soil-penetrating part

Fig. 4.3 Soil analysis system SAS3000

sensor probe box. The load cell provides cutting resistance measurement and automatic retreat function of the soil-penetrating part due to overloading. In the sensor probe box, a color microcamera head (Toshiba Corporation, IK-UM44H), a radiation/light-concentrating fiber (Sumitomo Electric Industry Co., Ltd., GeO_2, F-doped quartz system), a displacement meter (Omron Corporation, ZX LD 100), and an air blow head are equipped. Image of the observation surface, Vis-NIR diffuse reflectance spectra, and distance to the observation surface can be obtained without contact with the soil. The soil penetration part is driven by a hydraulic system and a remote controller using tractor PTO as the power source. For location information, it was equipped with a DGPS receiver (Trimble Navigation Limited, DSM132) with horizontal measurement accuracy of less than 1 m. An inverter generator dedicated to SAS (Honda Motor Co., Ltd.) is installed on the tractor body. The observation speed is 0.28–1.12 m/s, the observation depth is 0.15–0.30 m (0.05 m interval), and the measurement interval can be arbitrarily set at 3 s and over (Shibuya Machinery Co. Ltd 2004; Shibusawa et al. 2010).

(2) SAS2500

SAS2500 (weight 660 kg) has been produced under the funding of a Japanese national grant program adopted in 2012 (Fig. 4.2). The different specifications from SAS1000 are that a radiation fiber with air blow head and a Y-branch light-concentrating fiber are used. The microcamera was changed to a video camera. The drive of the soil-penetrating part was changed to a hydraulic system (1 system, 3/8-inch coupler) (Fig. 4.2b), which can be operated by a switch in the tractor cab. The generator is mounted on the SAS body, because removability from the tractor is considered as important. The spectrometers were changed to C10083CAH (320–1100 nm, 0.3 nm/interval) and C9406GC (900–1700 nm, 1.6 nm/interval) produced by the Hamamatsu Photonics Co., Ltd. The halogen lamp was changed to JCR15V150W/AL produced by the Fuji Lamp Co., Ltd. The automatic retreat function of the soil penetration part was excluded, and it was changed to using a share

pin to prevent the soil penetration part from breakage. System updates and maintenance can be performed remotely via a communication line.

(3) SAS2600

SAS2600 (weight: 750 kg) was designed for a Japan's research project entitled with *Research and Development for Increased Woody Biomass Production through Genome Breeding and High Efficiency Forestry Operations* which was adopted in 2013 under the Development of Efficient Elemental Technologies for Biofuel Production funded by the New Energy and Industrial Technology Development Organization (NEDO). The prototype was produced with specification determined for Brazil's woodlot.

The system configuration is the same as SAS2500, and improvements and changes were made to reinforce the frame strength to approximately 1.2 times in deflection amount of SAS2500 (steel thickness 4.5–6 mm) and were equipped with a beam knife, as a countermeasure for eucalyptus plant's residual and hard soil. The DGPS receiver was changed to the model SPS351 (Nikon Trimble Co., Ltd.)

(4) SAS3000

SAS3000 was produced under a research project entitled the special scheme project on regional developing strategy (project ID14526726 and 16781474) by the NARO Bio-oriented Technology Research Advancement Institution (Fig. 4.3). The system configuration is the same as SAS2500, and improvements and changes were made by permanently installing a touch panel in the tractor cab, which enables one operation for the SAS setting. The observation speed is 0.28–1.68 m/s, and the weight was reduced to 510 kg. The DGPS receiver was changed to model SPS351 (Nikon Trimble Co., Ltd.).

4.1.4 Analysis of Calibration Model for Multiple Soil Properties

(1) Absorption Wavelength and Regression Coefficient Estimation

The moisture content (MC), humic acid (total carbon (TC), total nitrogen (TN)), soil organic matter (SOM), clay (CL, 1:1 type and 1:2 type), available silicate (SiO), and free iron oxide (Fe) have the absorption wavelength in the analysis wavelength range. Therefore, the regression coefficients can be estimated, and the negative peak waveform of the regression coefficient matches the absorption wavelength for each property (in the case of second-order differential absorbance).

Soil properties with no absorption wavelength within the analytical wavelength range (available phosphorus (P-a), exchangeable potassium (K), exchangeable calcium (Ca), exchangeable magnesium (Mg), exchangeable sodium (Na), ammonia nitrogen (N-a), nitrate nitrogen (N-n), hot-water-extractable nitrogen (N-h), hot water soluble boron (B), soluble zinc (Zn), soluble copper (Cu), easily reducible manganese (Mn), exchange acidity (y1), phosphate absorption coefficient (PAC),

pH, EC, CEC, 2:1-type minerals CL and sand (S), silt (SL), dry density (ρd), calcium/magnesia ratio (Ca/Mg), magnesium/potassium ratio (Mg/K), base saturation percentage (BSP), calcium saturation percentage (CSP), sodium ratio (Na-r), and carbon-nitrogen (C/N) ratio) correlated with the analysis values of organic, inorganic substances whose absorbance wavelength has been confirmed within the analytical wavelength range (Matsunaga and Uwasawa 1992b; Clark et al. 1987; Umeda et al. 2001; Zornoza et al. 2008). In the case of raw soil, the regression coefficients can be estimated due to the spectra variation caused by the hydration phenomenon of inorganic ion component and binding with organic molecules. The negative peak waveform of the regression coefficient was consistent with the absorption wavelength of the correlated properties.

The possibility of regression coefficient estimation can be evaluated from the correlation between soil analysis values, which is based on the evaluation and classification using correlation coefficient (R). The classification methods include Pearson product-moment correlation (interval and ratio scale data) and Spearman's rank correlation (rank scale data). In addition, Pearson product-moment correlation was adopted (Table 4.3).

To confirm the correlation and reliability of regression coefficients, it was confirmed that the obtained regression coefficient for each property used the absorption wavelength or absorption wavelength band, by confirming that the negative absorption peak of each regression coefficient for each property from 1 to selected F (PLSR factor) value was in agreement with the absorption wavelength or exists in the absorption wavelength band. When the fluctuation of the spectra is large due to the hydration phenomenon of the inorganic ion and binding with organic molecules, it may not completely match due to the wave number shift.

(2) Evaluation/Classification Methods of Regression Coefficient and Prediction Values

The evaluation indexes of regression coefficient estimation accuracy of soil are R^2, RPD, range error ratio (RER), and evaluation index (EI). There are several guidelines for the evaluation and classification based on R^2 and RPD. Here, guidelines for evaluation/classification without over-/under-evaluation are presented.

Table 4.3 Evaluation and classification of the correlation between soil analysis values using correlation coefficient

Evaluation	Classification				
Full correlation			$\|R\|$	=	1
Highly correlated	0.7	<	$\|R\|$	<	1
Correlated	0.4	<	$\|R\|$	≦	0.7
Low correlation	0.2	<	$\|R\|$	≦	0.4
Almost no correlation	0	<	$\|R\|$	≦	0.2
No correlation	0	=	$\|R\|$		

The possibility of estimation of regression coefficient for properties whose absorption wavelength is not confirmed in the analysis wavelength region is based on the correlation between soil analysis values. Therefore, in the correlation coefficient classification method shown in Table 4.4, the R range from 0.7 to 1.0, which is "highly correlated," is divided into four threshold values "0.95, 0.9, 0.8, and 0.7." Squaring each of the value, R then becomes "0.90, 0.81, 0.64, and 0.49," and R^2 threshold values are obtained. It has been decided to classify R^2 using these threshold values. This classification method is consistent with ranks "B, C, and D" of Malley et al. (2004). Ranks "A and D" are consistent with Kuang et al. (2012). Therefore, it is an intermediate classification between the two methods. The RPD used middle of Kuang et al. (2012), RER used Malley et al. (2004), and EI used Mizuno et al. (1987).

The evaluation and classification method using the combination of R^2 and RPD is to evaluate the availability of the estimated regression coefficients and the prediction values. Further, the combinations of R^2 and RER and R^2 and EI are to evaluate whether the estimated regression coefficients are composed of an enough range. In each combination, if they did not belong to the same rank, lower rank was selected.

(3) An Example of Regression Coefficient Estimation (Paddy Field)

(i) Test Fields

The test fields were agricultural production corporation Denpata (sandy clay loam, S = 64.6%, SL = 14.6%, CL = 20.8%) and Yokota farm (light clay, S = 52.8%, SL = 17.3). The test devices were SAS2500 and SAS3000. The sampling interval was 3 s. The observation speed was 0.28 m/s. The observation depth was 0.10 m determined by the grower. As the soil characteristics, the ratio of CL in Yokota farm was high, and the retainability of fertilizer was high. An overview of the analysis database is summarized in Table 4.5. The data collection for the test field was at 5 times in 3 years, from 48 fields. The total number of the collected data was 552, but 406 data for pH and EC, exchangeable sodium, and sodium ratio and 364 data for S, SL, CL, available silicate, and free iron oxide were used to estimate regression coefficient.

Table 4.4 Evaluation and classification methods using R^2 with RPD, RER, and EI

Evaluation	R^2	RPD	RER	EI (%)	Rank
Excellent	0.90<	3.0<	20<	≦12.4	A
Good	0.81-0.90	2.5-3.0	15-20	12.5-24.9	B
Approximate quantitative prediction	0.64-0.81	2.0-2.4	10-15	25.0-37.4	C
Distinguish between high and low	0.49-0.64	1.5-1.9	8-10	37.5-49.9	D
Not usable	<0.49	<1.5	<8	50.0≦	E

※Rank is classified into A–E, as "regression coefficient, prediction value": A, excellent; B, good; C, approximate quantitative prediction; D, distinguish between high and low; E, not usable

Table 4.5 Database for analysis

Implementation date	Location	Test field	Equipment	Number of test fields	Field size (ha)	Number of data
2013.12.06	Fukushima Prefecture	Denpata Farm	SAS2500	4	1.0	188
2014.09.23~24			SAS2500	4	1.2	118
2014.11.13~15	Ibaraki Prefecture	Yokota Farm	SAS2500	5	6.4	100
2015.10.25~27			SAS3000	10	10	120
2015.12.15~17			SAS3000	25	24	26
Total				48	42	552

(ii) Determination of Validation Method

The requirements to divide the dataset into calibration set and prediction set are pluralities of the same data that exist, with an unbiased frequency distribution, while a rectangular-shape distribution is expected (Akitomo and Shimamura 1998). The obtained distribution in this study was close to normal distribution, and the shape with two peaks also existed. The requirements of dividing for calibration set and prediction set were not satisfied. Therefore, full cross-validation was applied.

(iii) Correlation Between Analysis Values

For properties whose absorption wavelength was not confirmed in the analysis wavelength range, correlation coefficients between soil analysis values were obtained, and the correlations were summarized in Table 4.6 according to the classification in Table 4.3. Positive correlations are shown in black, and negative correlations are shown in red. "Correlation" (gray highlight) or "high correlation" (yellow highlight) with properties that have absorption wavelength in the analysis wavelength range are counted as direct correlation. "Correlation" and "high correlation" were counted as indirect correlation between the properties whose absorption wavelength has not been confirmed in the analysis wavelength range. Properties with many direct correlations have strong collinearity between analysis values of properties that have absorption wavelength in the analysis range, and the possibility to estimate regression coefficients is also high. Indirect correlations are less collinear than direct correlations, and the possibility to estimate regression coefficient is less than the direction correlation. But the possibility varies depending on the total number of correlations and the concentration distribution of the analysis values.

Twenty-two properties whose absorption wavelength has not been confirmed in the analysis wavelength range had correlation with eight properties that have an absorption wavelength (blue font in Table 4.6). The properties that have no direct correlation were base saturation, lime saturation, sodium ratio, and soluble zinc. The property that has no indirect correlation was soluble zinc. Therefore, it was 33 properties that could explain that the regression coefficients could be estimated by the correlation between the analysis values. The estimation of regression coefficient of soluble zinc could not be explained by the correlation with the analysis values.

Table 4.6 Correlation coefficient between analysis values

項目	N-a	N-h	N-n	N-t	P-a	SiO	K	Ca	Mg	Na	Fe	Cu	Zn	B	Mn	EC	CEC	Ca/Mg	Mg/K	BSP	CSP	ESP	HR	SOM	C-t	C/N	pH	yl	PAC	MC	ρd	S	SL	CL
N-a	1.000	—	—	—	—	—	—	—	—	—	—	—	—	—	—	—	—	—	—	—	—	—	—	—	—	—	—	—	—	—	—	—	—	—
N-h	-0.014	1.000	—	—	—	—	—	—	—	—	—	—	—	—	—	—	—	—	—	—	—	—	—	—	—	—	—	—	—	—	—	—	—	—
N-n	0.331	0.301	1.000	—	—	—	—	—	—	—	—	—	—	—	—	—	—	—	—	—	—	—	—	—	—	—	—	—	—	—	—	—	—	—
N-t	0.171	0.731	0.514	1.000	—	—	—	—	—	—	—	—	—	—	—	—	—	—	—	—	—	—	—	—	—	—	—	—	—	—	—	—	—	—
P-a	-0.583	-0.112	-0.579	-0.457	1.000	—	—	—	—	—	—	—	—	—	—	—	—	—	—	—	—	—	—	—	—	—	—	—	—	—	—	—	—	—
SiO	0.460	0.149	0.141	0.338	-0.298	1.000	—	—	—	—	—	—	—	—	—	—	—	—	—	—	—	—	—	—	—	—	—	—	—	—	—	—	—	—
K	0.572	0.196	0.354	0.402	-0.701	0.426	1.000	—	—	—	—	—	—	—	—	—	—	—	—	—	—	—	—	—	—	—	—	—	—	—	—	—	—	—
Ca	0.537	0.389	0.564	0.688	-0.770	0.283	0.742	1.000	—	—	—	—	—	—	—	—	—	—	—	—	—	—	—	—	—	—	—	—	—	—	—	—	—	—
Mg	0.666	0.155	0.491	0.444	-0.821	0.322	0.834	0.888	1.000	—	—	—	—	—	—	—	—	—	—	—	—	—	—	—	—	—	—	—	—	—	—	—	—	—
Na	0.550	0.260	0.411	0.449	-0.819	0.440	0.619	0.635	0.738	1.000	—	—	—	—	—	—	—	—	—	—	—	—	—	—	—	—	—	—	—	—	—	—	—	—
Fe	0.633	0.297	0.448	0.550	-0.765	0.457	0.742	0.832	0.829	0.690	1.000	—	—	—	—	—	—	—	—	—	—	—	—	—	—	—	—	—	—	—	—	—	—	—
Cu	0.141	0.343	0.514	0.545	-0.578	0.289	0.293	0.498	0.360	0.441	0.404	1.000	—	—	—	—	—	—	—	—	—	—	—	—	—	—	—	—	—	—	—	—	—	—
Zn	-0.029	0.007	-0.018	-0.005	-0.115	-0.085	0.022	0.077	0.027	0.068	0.096	0.184	1.000	—	—	—	—	—	—	—	—	—	—	—	—	—	—	—	—	—	—	—	—	—
B	0.191	0.563	0.482	0.714	-0.428	0.231	0.273	0.564	0.304	0.374	0.433	0.606	0.114	1.000	—	—	—	—	—	—	—	—	—	—	—	—	—	—	—	—	—	—	—	—
Mn	0.561	0.140	0.499	0.490	-0.879	0.493	0.692	0.800	0.817	0.793	0.826	0.680	0.143	0.484	1.000	—	—	—	—	—	—	—	—	—	—	—	—	—	—	—	—	—	—	—
EC	-0.271	0.057	-0.206	-0.000	0.135	-0.602	-0.078	-0.019	-0.104	-0.349	-0.417	-0.202	0.025	0.014	-0.064	1.000	—	—	—	—	—	—	—	—	—	—	—	—	—	—	—	—	—	—
CEC	0.446	0.457	0.683	0.780	-0.865	0.317	0.659	0.916	0.916	0.712	0.788	0.663	0.045	0.652	0.374	-0.126	1.000	—	—	—	—	—	—	—	—	—	—	—	—	—	—	—	—	—
Ca/Mg	-0.573	0.075	-0.361	-0.091	0.732	-0.191	-0.709	-0.517	-0.799	-0.676	-0.551	-0.271	-0.016	-0.064	-0.654	0.200	-0.540	1.000	—	—	—	—	—	—	—	—	—	—	—	—	—	—	—	—
Mg/K	0.485	0.109	0.504	0.375	-0.700	0.012	0.319	0.692	0.752	0.575	0.525	0.385	0.060	0.302	0.667	-0.058	0.709	-0.613	1.000	—	—	—	—	—	—	—	—	—	—	—	—	—	—	—
BSP	0.370	-0.114	-0.205	-0.284	-0.144	-0.002	0.343	0.241	0.334	0.120	0.214	-0.329	0.084	-0.230	0.161	0.439	-0.115	-0.220	0.117	1.000	—	—	—	—	—	—	—	—	—	—	—	—	—	—
CSP	-0.139	-0.260	-0.322	-0.286	0.131	-0.055	0.064	0.077	0.031	-0.120	0.073	-0.398	0.100	-0.207	-0.066	0.443	-0.294	0.169	-0.092	0.913	1.000	—	—	—	—	—	—	—	—	—	—	—	—	—
ESP	0.487	-0.246	-0.069	-0.241	-0.395	0.159	0.276	-0.011	0.273	0.619	0.091	-0.041	0.053	-0.188	0.297	-0.613	-0.049	-0.527	0.168	0.387	0.162	1.000	—	—	—	—	—	—	—	—	—	—	—	—
HR	0.278	0.664	0.563	0.968	-0.573	0.290	0.508	0.814	0.600	0.498	0.649	0.563	0.018	0.706	0.600	-0.034	0.874	-0.229	0.515	-0.181	-0.233	-0.223	1.000	—	—	—	—	—	—	—	—	—	—	—
SOM	0.525	0.517	0.611	0.850	-0.717	0.467	0.642	0.870	0.750	0.626	0.810	0.625	0.031	0.684	0.780	-0.100	0.909	-0.426	0.608	-0.069	-0.203	-0.093	0.909	1.000	—	—	—	—	—	—	—	—	—	—
C-t	0.278	0.664	0.563	0.968	-0.573	0.290	0.508	0.814	0.600	0.498	0.649	0.563	0.018	0.706	0.600	-0.034	0.874	-0.229	0.515	-0.181	-0.233	-0.223	1.000	0.909	1.000	—	—	—	—	—	—	—	—	—
C/N	0.493	0.301	0.532	0.594	-0.739	0.100	0.601	0.863	0.796	0.473	0.741	0.500	0.071	0.492	0.724	-0.162	0.837	-0.497	0.713	0.098	-0.058	-0.133	0.765	0.795	0.765	1.000	—	—	—	—	—	—	—	—
pH	0.410	-0.085	0.139	0.142	-0.463	0.426	0.326	0.391	0.455	0.458	0.445	0.293	0.132	0.318	0.517	-0.213	0.558	-0.254	0.393	0.073	-0.010	0.460	0.205	0.267	0.205	0.377	1.000	—	—	—	—	—	—	—
yl	0.353	0.177	0.403	0.288	-0.499	-0.101	0.424	0.425	0.455	0.310	0.439	0.374	-0.003	0.285	0.417	-0.074	0.487	-0.465	0.353	-0.078	-0.255	0.017	0.387	0.458	0.387	0.537	-0.193	1.000	—	—	—	—	—	—
PAC	0.664	0.304	0.490	0.613	-0.718	0.498	0.793	0.873	0.855	0.599	0.887	0.445	0.023	0.451	0.785	0.044	0.799	-0.347	0.563	0.241	0.049	0.033	0.718	0.864	0.718	0.778	0.242	0.468	1.000	—	—	—	—	—
MC	-0.055	0.630	0.327	0.823	-0.344	0.323	0.364	0.524	0.314	0.485	0.462	0.433	0.035	0.580	0.388	0.192	0.613	-0.088	0.236	-0.240	-0.246	-0.087	0.775	0.670	0.775	0.385	0.103	0.185	0.425	1.000	—	—	—	—
ρd	-0.268	-0.572	-0.576	-0.801	0.598	-0.416	-0.607	-0.736	-0.606	-0.588	-0.694	-0.613	-0.015	-0.636	-0.631	0.010	-0.626	0.404	-0.440	0.185	0.309	0.130	-0.823	-0.837	-0.823	-0.621	-0.109	-0.410	-0.708	-0.751	1.000	—	—	—
S	0.320	-0.419	-0.218	-0.572	0.279	-0.581	-0.563	-0.533	-0.502	-0.397	-0.642	-0.276	0.013	-0.381	-0.484	-0.848	-0.516	0.183	-0.136	-0.014	0.026	0.113	-0.565	-0.709	-0.565	-0.394	0.369	-0.179	-0.720	-0.452	0.630	1.000	—	—
SL	0.413	0.294	0.005	0.362	0.047	0.322	0.287	0.175	0.130	0.125	0.286	0.093	-0.043	0.208	0.164	-0.734	0.149	0.111	-0.153	-0.027	0.009	-0.096	0.294	0.390	0.294	0.036	0.358	-0.088	0.404	0.295	-0.362	-0.809	1.000	—
CL	0.539	0.401	0.335	0.581	-0.474	0.457	0.631	0.680	0.669	0.511	0.755	0.350	0.017	0.414	0.613	-0.713	0.676	-0.380	0.342	0.045	-0.049	-0.093	0.627	0.769	0.627	0.582	0.415	0.353	0.775	0.450	-0.670	-0.864	0.403	1.000
D.C.[*1]	4	6	5	6	6	3	7	7	6	8	7	6	0	7	7	2	6	2	4	0	0	0	6	7	6	6	3	2	8	6	8	8	2	7
I.C.[*2]	14	4	13	15	17	9	13	17	16	16	20	10	0	10	17	5	17	14	16	2	2	5	16	19	16	16	6	11	18	9	17	10	4	16
Total	18	10	18	21	23	12	20	24	22	24	27	16	0	17	24	7	23	16	20	2	2	5	22	26	22	22	9	13	26	15	25	18	6	23

*1 ; Direct correlation · Correlation with properties whose absorption wavelength exist in the analysis wavelength range, and the value is more than "correlated"
*2 ; Indirect correlation · Correlation with properties whose absorption wavelength do not exist in the analysis wavelength range, and the value is more than "correlated"
Grey highlight ; $|R|>0.4$ 「Correlated」, Yellow highlight ; $|R|>0.7$ 「Highly correlated」

[a]**Direct correlation:Correlation with properties whose absorption wavelength exist in the analysis wavelength range, and the value is more than "correlated"**

[b]Indirect correlation:Correlation with properties whose absorption wavelength do not exist in the analysis wavelength range, and the value is more than "correlated"

Grey highlight; $|R|>0.4$ 「Correlated」, Yellow highlight; $|R|>0.7$ 「Highly correlated」

(iv) PLSR Results

According to the absorbance in the analysis database (Fig. 4.4a), the spectra change is large at 350–400 nm, and it has a peak of positive waveform at 1400 nm and baseline shift. According to second-derivative absorbance of the S-G (Savitzky-Golay) method with smoothing point (SP) = 41 (Fig. 4.4b), which has the highest smoothing effect, four data were confirmed as outliers which had negative peaks at 600–700 nm. But the absorption wavelength of humic acid is 620 nm. According to the frequency distribution of humic acid shown in Fig. 4.4c, since about 14% of the analysis values were higher than others, they were not excluded.

Table 4.7 and 4.8 summarizes the estimation results of regression coefficients obtained through repeatedly running PLSR algorithm by excluding data with the largest prediction residual (outlier) at each run. Table 4.7 shows the statistical values of each property, and Table 4.8 shows the accuracy, evaluation, and classification of each regression coefficient. The accuracy of each property satisfies the condition of R^2>0.9 and $F \leqq 10$. In addition, since the evaluation/classification of calibration was Rank_{RPD} = A, the reliability of regression coefficient was obtained. The Rank_{RPD} = C was obtained for exchangeable magnesia, S, and CL in evaluation/classification of validation. To improve the reliability of the prediction value to "Rank_{RPD}=B," it is necessary to reanalyze by adding data.

To evaluate the range of database that constitutes the regression coefficient, the classification using RER and EI can be considered. Since RER is more strict evaluation of the 34 properties, they were evaluated by RER. The RER results were Rank_{cal}=C for available phosphorus, exchangeable potassium, exchangeable sodium, free iron oxide, soluble zinc, easily reducible manganese, EC, CEC, lime/magnesia ratio, magnesia/potassium ratio, soil organic matter, C/N, pH, exchange acidity, and ρd. It is necessary to add data in the range not possessed and re-analyze.

(v) Soil Analysis and Regression Coefficient

To show the detail of the database that constitutes the regression coefficients for each estimated property, scatter plots of analysis values and prediction values and regression coefficients are summarized, and several examples are shown in Fig. 4.5. The reference range of soil analysis (Agricultural Product Chemical Research Laboratory 2001; Yamazaki 2008) was described (Table 4.9). However, the reference range differs according to location, crop, and variety (Ministry of Agriculture Forestry and Fisheries 2008b, 2016a). For exchangeable calcium, the analysis value corresponding to the lime saturation of 40–60% is within the appropriate range and can be calculated from Eq. (4.1):

$$\text{Calcium saturation percentage} = \text{Ca}_{\text{me}} / \text{CEC} \times 100 \tag{4.1}$$

$$\text{Ca}_{\text{me}} = \text{Ca} / 28.04$$

The reference range for CEC and humic acid differs with soil type. The reference range of phosphate absorption coefficient is for dry field farming in Hokkaido, and the estimated phosphate utilization rate for crops is less than 700 (20–30%),

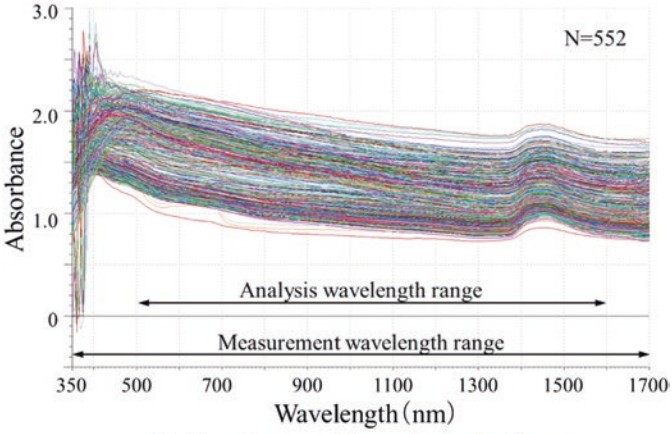

(a) Absorbance of the analysis database

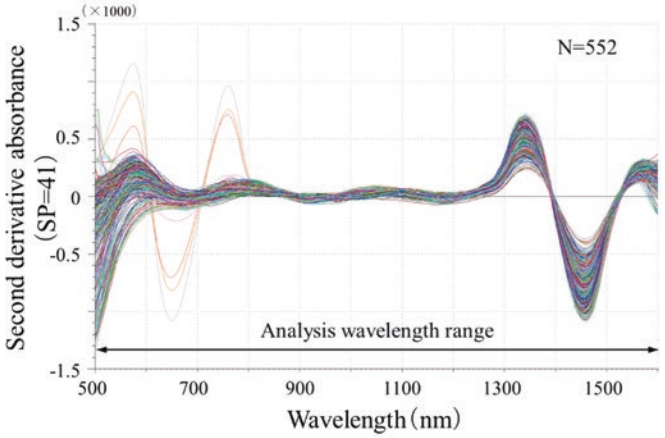

(b) Second derivative absorbance of the analysis database

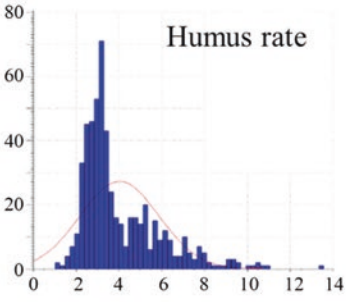

(c) Scatter plots of humus rate

Fig. 4.4 An example of PLS regression coefficient estimation (**a**) Absorbance of the analysis database (**b**) Second-derivative absorbance of the analysis database (**c**) Scatter plots of humus rate

Table 4.7 Thirty-four properties' regression coefficient estimation accuracy and evaluation/classification results (statistics)

Property	Unit	N_{Cal}|N	Range				S.D.	SDP		RMSE	
			Min	Max	Min_{Cal}	Max_{Cal}		Cal	Val	Cal	Val
N-a	mg/100 g	349|552	0.26	8.30	0.30	2.99	0.47	0.148	0.182	0.148	0.182
N-h	mg/100 g	287|552	2.18	14.7	2.18	6.91	0.74	0.234	0.250	0.234	0.250
N-n	mg/100 g	292|552	0.00	3.85	0.00	0.93	0.19	0.059	0.062	0.059	0.062
N-t	%	338|552	0.07	0.58	0.07	0.26	0.03	0.009	0.010	0.009	0.010
P-a	mg/100 g	538|552	1.54	34.4	1.54	34.3	9.94	3.096	3.301	3.094	3.298
SiO	mg/100 g	225|364	12.5	103	14.4	73.5	9.88	3.052	4.255	3.045	4.264
K	mg/100 g	462|552	1.69	52.6	5.38	28.4	5.22	1.645	1.797	1.643	1.795
Ca	mg/100 g	538|552	44.3	668	44.3	614	112	35.22	40.37	35.18	40.33
Mg	mg/100 g	535|552	3.52	180	3.52	148.0	29.9	9.424	12.37	9.415	12.36
Na	mg/100 g	270|364	0.58	26.3	0.58	15.0	3.79	1.192	1.275	1.189	1.273
Fe	mg/100 g	320|364	0.04	3.10	0.22	2.68	0.68	0.215	0.244	0.215	0.244
Cu	ppm	335|552	0.81	15.0	3.24	10.9	1.33	0.420	0.489	0.419	0.488
Zn	ppm	272|552	2.56	62.5	3.01	5.56	0.57	0.179	0.211	0.178	0.211
B	ppm	351|552	0.41	1.70	0.41	1.37	0.14	0.045	0.054	0.045	0.054
Mn	ppm	526|552	3.59	266	3.59	218	63.6	20.07	22.71	20.05	22.69
EC	mS/cm	363|406	0.01	0.09	0.01	0.06	0.02	0.005	0.006	0.005	0.006
CEC	me/100 g	551|552	7.18	42.3	7.18	42.3	8.96	2.833	3.056	2.831	3.053
Ca/Mg	E.R	459|552	1.91	9.05	1.91	6.45	1.24	0.391	0.408	0.391	0.407
Mg/K	E.R	387|552	2.95	20.5	3.62	11.8	1.85	0.578	0.657	0.577	0.656
BSP	%	358|552	19.9	114	43.1	102	9.37	2.960	3.322	2.956	3.318
CSP	%	315|552	17.6	84.9	32.7	68.9	5.90	1.865	2.216	1.862	2.213
ESP	%	212|364	0.18	5.38	0.45	2.41	0.35	0.119	0.137	0.110	0.128
HR	%	505|552	1.02	13.6	1.02	8.82	1.46	0.459	0.570	0.459	0.570
SOM	%	502|552	4.61	19.0	4.74	15.3	2.43	0.766	0.838	0.765	0.837
C-t	%	485|552	0.59	7.88	0.59	4.78	0.77	0.237	0.287	0.237	0.286
C/N	–	551|552	6.73	16.7	9.00	16.7	1.75	0.547	0.621	0.546	0.621
pH	–	288|406	5.61	6.76	5.74	6.49	0.17	0.043	0.048	0.054	0.067
y1	–	277|552	0.06	2.50	0.19	1.00	0.18	0.058	0.065	0.057	0.065
PAC	–	537|552	8.00	1518	8.00	1509	297	89.37	103.7	89.29	103.6
MC	–	288|552	28.3	115	30.7	53.3	4.17	1.314	1.424	1.312	1.422
DD	g/cm^3	389|552	0.61	1.03	0.76	1.00	0.06	0.018	0.021	0.018	0.021
S	%	250|364	18.4	75.5	29.5	72.2	7.78	2.586	3.659	2.047	3.014
SL	%	240|364	5.68	47.8	8.44	30.5	3.84	1.201	1.551	1.198	1.548
CL	%	290|364	13.2	51.1	18.2	43.2	4.96	1.562	2.259	1.529	2.144

E.R equivalence ratio

700–1500 (15–20%), and 1500–2000 (10%–15%) and more than 2000 (6–10%). The reliable range of the prediction values using the regression coefficients of 34 properties is the range of the analysis values in the scatter plots. For hot water extractable nitrogen, the range was 2.2–6.9 mg/100 g, including the reference range. But it cannot be used in soil analysis for high concentration data because it is not

Table 4.8 Thirty-four properties' regression coefficient estimation accuracy and evaluation/classification results (accuracy/evaluation/classification)

			R^2		RPD		$Rank_{RPD}$		RER		$Rank_{RER}$		EI		$Rank_{EI}$	
Property	SP	*F*	Cal	Val	Cal	Val	Cal	Val	Cal	Val	Cal	Val	Cal	Val	Cal	Val
N-a	7	7	0.90	0.85	3.17	2.57	A	B	18.2	14.7	B	C	11.0	13.6	A	B
N-h	17	6	0.90	0.89	3.17	2.97	A	B	20.2	18.9	A	B	9.9	10.6	A	A
N-n	13	4	0.90	0.89	3.17	3.00	A	B	15.8	14.9	B	B	12.7	13.4	B	B
N-t	7	6	0.90	0.87	3.18	2.76	A	B	20.5	17.8	A	B	9.8	11.3	A	A
P-a	7	5	0.90	0.89	3.21	3.01	A	B	10.6	9.93	C	C	18.9	20.2	B	B
SiO	7	8	0.90	0.82	3.25	2.32	A	B	19.4	13.9	B	C	10.3	14.4	A	B
K	15	8	0.90	0.88	3.18	2.91	A	B	14.0	12.8	C	C	14.3	15.6	B	B
Ca	17	9	0.90	0.87	3.18	2.77	A	B	16.2	14.1	B	C	12.4	14.2	A	B
Mg	3	8	0.90	0.83	3.18	2.42	A	C	15.4	11.7	B	C	13.0	17.1	B	B
Na	21	6	0.90	0.89	3.18	2.97	A	B	12.2	11.4	C	C	16.5	17.6	B	B
Fe	9	5	0.90	0.87	3.18	2.81	A	B	11.5	10.1	C	C	17.5	19.8	B	B
Cu	3	5	0.90	0.87	3.18	2.73	A	B	18.2	15.7	B	B	11.0	12.8	A	B
Zn	15	9	0.90	0.86	3.19	2.70	A	B	14.3	12.1	C	C	14.1	16.6	B	B
B	7	7	0.90	0.86	3.17	2.65	A	B	21.4	17.9	A	B	9.34	11.2	A	A
Mn	7	5	0.90	0.87	3.17	2.80	A	B	10.7	9.45	C	C	18.7	21.2	B	B
EC	7	5	0.90	0.88	3.17	2.85	A	B	10.6	9.60	C	D	18.8	20.9	B	B
CEC	21	8	0.90	0.88	3.17	2.94	A	B	12.4	11.5	C	C	16.1	17.4	B	B
Ca/Mg	15	6	0.90	0.89	3.17	3.04	A	B	11.6	11.1	C	C	17.2	18.0	B	B
Mg/K	11	8	0.90	0.87	3.21	2.82	A	B	14.1	12.4	C	C	14.2	16.2	B	B
BSP	15	9	0.90	0.88	3.17	2.83	A	B	20.0	17.8	A	B	10.0	11.2	A	A
CSP	9	8	0.90	0.86	3.17	2.67	A	B	19.5	16.4	B	B	10.3	12.2	A	A
ESP	15	7	0.90	0.87	3.18	2.74	A	B	17.8	15.3	B	B	12.1	14.0	A	B
HR	7	8	0.90	0.85	3.18	2.56	A	B	17.0	13.7	B	C	11.8	14.6	A	B
SOM	9	5	0.90	0.88	3.18	2.90	A	B	13.9	12.7	C	C	14.4	15.8	B	B
C-t	7	7	0.91	0.86	3.25	2.69	A	B	17.7	14.6	B	C	11.3	13.7	A	B
C/N	9	6	0.90	0.88	3.21	2.83	A	B	14.1	12.4	C	C	14.2	16.2	B	B
pH	9	8	0.90	0.85	3.17	2.58	A	B	13.9	11.3	C	C	11.4	12.8	A	B
y1	7	4	0.90	0.87	3.20	2.84	A	B	14.1	12.5	C	C	14.2	16.0	B	B
PAC	15	10	0.91	0.88	3.32	2.86	A	B	16.8	14.5	B	C	11.9	13.8	A	B
MC	9	4	0.90	0.88	3.17	2.93	A	B	17.2	15.8	B	B	11.7	12.6	A	B
DD	7	6	0.90	0.87	3.18	2.76	A	B	13.3	11.6	C	C	15.0	17.3	B	B
S	9	10	0.93	0.85	3.80	2.58	A	B	20.9	14.2	A	C	12.1	17.1	A	B
SL	11	9	0.90	0.84	3.21	2.48	A	B	18.4	14.2	B	C	10.9	14.1	A	B
CL	9	10	0.90	0.81	3.25	2.31	A	C	16.3	11.7	B	C	12.5	18.1	B	B

included in the regression coefficient database. The available phosphorus database included the reference range of 10–30 mg/100 g, so it can be used in the soil analysis. However, since data at 10–20 mg/100 g is missing, additional data and reanalysis in this range are required. Exchangeable magnesia, exchangeable sodium, and C/N also need reanalysis with intermediate data added. The ideal database of

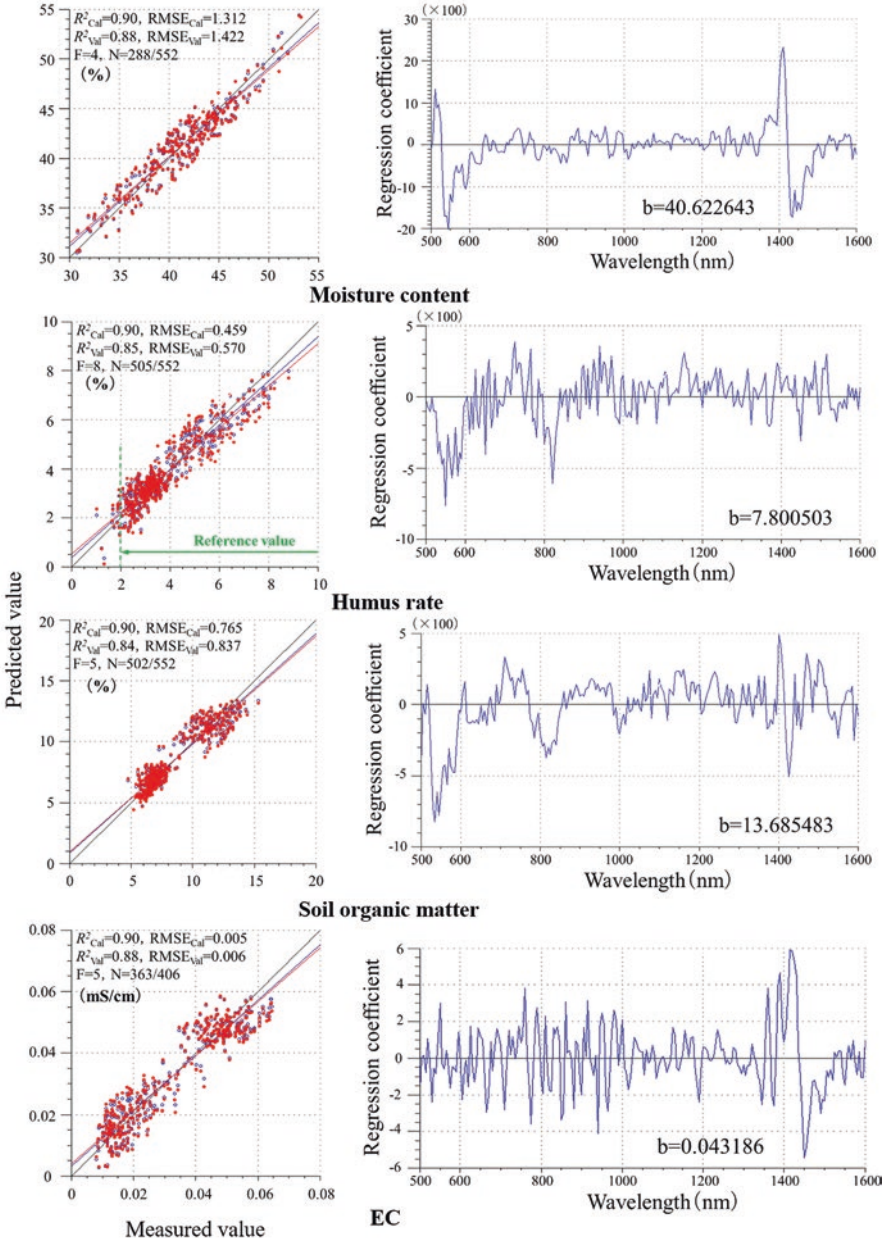

Fig. 4.5 Scatter plots of analysis and prediction values and regression coefficient

Table 4.9 Reference value of soil analysis

Property	Unit	Reference value			Property	Unit	Reference value		
pH	–	5.5	~	6.5	PAC	–	–	~	–
P-a	mg/100 g	10	~	30	CEC	me/100g	20	~	30
K	mg/100 g	15	~	30	HR	%	2	~	
Mg	mg/100 g	25	~	45	EC	mS/cm	0.4	~	0.6
Mg/K	E.R.	2	~		y1	–	–	~	–
Ca/Mg	E.R.		~	6	SOM	%	3	~	
Ca	mg/100 g	200	~	300	C-t	%	–	~	–
CSP	%	40	~	60	C/N	–	15	~	30
BSP	%	60	~	80	SiO	mg/100g	15	~	30
Cu	ppm	0.5	~	8.0	Fe	%	0.8	~	4.0
Zn	ppm	2	~	40	Na	mg/100g		~	15
Mn	ppm	50	~	500	ESP	%		~	20
B	ppm	0.5	~	1.0	MC	%	–	~	–
N-h	mg/100 g	5	~	7	DD	g/cm3	–	~	–
N-t	%	–	~	–	S	%	–	~	–
N-n	mg/100 g	–	~	–	SL	%	–	~	–
N-a	mg/100 g	–	~	–	CL	%	–	~	–

analysis and prediction values for the purpose of soil analysis were CEC, exchangeable calcium, base saturation, lime saturation, and free iron oxide.

(vi) Regression Coefficient and Absorption Wavelength

As the regression coefficient of each property has been applied with second derivative, the negative coefficient is almost the same with the peak waveform of the absorption wavelength. In soil water content whose absorption wavelength exists in the analysis wavelength region, the negative peak matches the water's absorption wavelength (1450 nm) (Fig. 4.5). In addition, the negative peak near 550 nm coincides with the green wavelength band, which is the complementary color of red, and it is necessary to consider the analysis wavelength region because of the effect of soil color. Furthermore, the regression coefficient waveform of soil water content has almost the same shape with the second-derivative absorbance spectra. Moreover, the regression coefficients in 600–1350 nm, which are not directly related to the absorption wavelength, seem to eliminate the baseline noise of the second-derivative absorbance. The negative peaks of soil organic matter, humus rate, total carbon, and total nitrogen were consistent with the absorption wavelength of humic acid (570 nm, 620 nm, 1100–1600 nm). The negative peaks of available silicate coincided with the absorption wavelength (930 nm, 1000 nm), and negative peaks were also confirmed at 570 nm and 620 nm because of its correlation with the organic content. Two negative peaks were observed in free iron oxide absorption band (1380–1410 nm), and a large negative peak was observed at 530 nm in the Fe^{3+} absorption band (500–800 nm). Although the absorption wavelength of CL is 1400 nm, no negative peak was observed in the regression coefficient. This is because when transforming to absorbance, 1400 nm was the conversion point

between the positive and negative peaks before and after 1400 nm, that is, zero. Since CL is composed of elements such as silicon and iron, multiple negative peaks of the regression coefficient were confirmed in the absorption wavelength of silicic acid and free iron oxide. The correlations between the analysis values of CL and free iron oxide and available silicate were “high correlation” and “correlation.” As examples of regression coefficient estimation based on correlation with properties whose absorption wavelength exists, ammonia nitrogen has no correlation with the analysis value of total nitrogen, but its correlation with organic content was confirmed. Hot water extractable nitrogen was highly correlated with total carbon, total nitrogen, and humus rate. Nitrate nitrogen was correlated with total nitrogen, total carbon, and humus rate. Negative peaks were observed in the absorption wavelength of humic acid in each property.

The obtained regression coefficient for each property is a local regression coefficient corresponding to the database that consists of the analysis value range of the 34 properties used in the regression coefficient estimation. Moreover, it cannot satisfy all soil conditions as general purpose regression coefficient.

4.2 Application of Tractor-Mounted Soil Analysis System in Precision Agriculture

4.2.1 Site-Specific Soil Mapping and Interpretation of Agricultural Fields

(1) Soil Observation Preparation/Data Collection/Analysis/Visualization Process

The items of SAS setting before soil observation are observation speed (0.28–1.68 m/s), sampling period of diffuse reflectance spectra (3–10 s, 1 s interval), and observation depth (0.10–0.30 m, 0.05 m interval). The data acquisition interval in the direction of measurement is determined by observation speed and sampling period. But the data acquisition interval may not match the calculated value according to the soil conditions. If the observation speed is not constant, the measurement area of diffuse reflectance spectra and the soil sampling interval will be different. So, it will not be changed during the operation. By adjusting the gauge wheel to the track of the tractor’s rare wheel, extra pitching fluctuation was avoided. The observation depth is the distance from the contact surface of the gauge wheel to the soil measurement surface leveled with a flat plate. When changing the observing depth, the top link was adjusted to ensure the SAS body’s frame horizontal. Setting the observation depth deeply increases the traction resistance, so the tractor’s drive condition and the model selection are important. In order to avoid the influence of tractor pitching, the draft control and position control of the tractor’s three-point link hitch were not functioned, while a free suspension system was adopted.

The observation setting items before soil observation are the determination of number of observation lines and the endpoints of field where the shape of the field

can be easily understood. The number of observation lines and the interval between the observation lines are determined according to the grower's purpose of use of the soil map. For example, in the case of using the soil map for pest control and fertilization by a boom sprayer with one wing of 12 m, the first observation line was determined at 12 m from the field edge, and the second and later were determined at 24 m intervals. A glass pole was set at the field end in the traveling direction to improve the visibility of straight traveling. In the case of one-plot management, the field was firstly divided into three parts, and the observation lines were around the middle of each part. If there was no request from the grower, the least common multiple of the working width of the working machine owned by the grower was used. The settings of the observation line that have been requested in the past were the harvesting width of yield combined, the spray width of boom sprayer and broadcaster, and the width of planting line of rice transplanter.

After the SAS's power was turned on, it was waited about 15 min to stabilize the output of the halogen lamp. Before observing the first line of each plot, SRS40 was installed to the calibration jig set (Fig. 4.6b) in the soil penetration part to obtain white reference and dark reference data.

The position of soil samples, which were the objective variables for estimating the regression coefficient, was firstly confirmed by the alarm from the sensor when collecting spectra data and then marked on the soil surface by a half-split chopstick, while the data number was confirmed from the touch panel monitor simultaneously with the spectra data collection. The area was excavated by a shovel where the chopstick was placed at a wider area than the spectra measured area but did not disturb the observation surface of SAS. The residues and gravel were then removed. After that, using a stainless steel scoop, the soil at a depth with several centimeters from the observation surface with about 0.3 m in width and the surrounding soil with the same depth of the observation surface were collected and packed into a sealable plastic bag with a zip (Asahi Kasei Home Products Co. Ltd., Ziplock® Double zipper). About 1 kg was placed in the plastic bag, and it was closed by confirming that the zip did not bite the soil particles while the air was sufficiently pushed out. On the plastic bag, the symbol with field name, observation line number, and diffuse reflectance spectra number was recorded.

Two sets of soil samples were prepared at each sampling position, one set was analyzed at the Tokyo University of Agriculture and Technology (TUAT) and the other set was analyzed at the Agricultural Product Chemical Research Laboratory

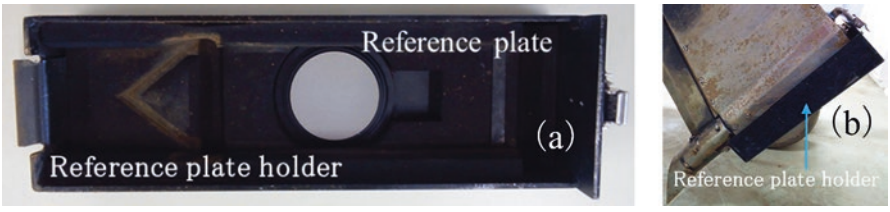

Fig. 4.6 Reference data acquisition method

(APCRL: Federation of Tokachi Agricultural Cooperative Association, Hokkaido, Japan). The soil samples were transported in refrigerators (0–10 °C) to restrain chemical composition change due to microbial activity. The soil samples sent to TUAT were stored in a refrigerator at 5 °C. Properties that could not be analyzed in TUAT were requested to be analyzed by APCRL. Properties that could not be analyzed in APCRL were analyzed by the Sumika Chemical Analysis Service, (SCAS) Ltd., using surplus dry soil samples used by APCRL. The analyzed values were not rounded by significant digits, but the display values of the weighing meter and measuring device and the total number of digits recorded on the recording medium of the device were used.

Once the soil analysis values were obtained, they were linked to the diffuse reflectance spectra, and a database for estimating the regression coefficients was constructed. The database was subjected to spectra preprocessing and PLSR analysis using multivariate analysis software (the Unscrambler Ver.9.8, CAMO Analytics AS). The prediction values were linked with position information and were visualized on a soil map. The visualization methods can be provided according to the grower's request, including interpolation map using the application software ArcMap of ArcGIS (ESRI Japan Co., Ltd.). The grid map divides a plot of field into grids with the mean, maximum, and minimum values shown in each grid. The dot map shows only the measurement point with dot of any size. When regression coefficient estimation is necessary, the black arrow and green arrow processes in Fig. 4.7 are necessary. When regression coefficient estimation is not required, blue arrow and green arrow processes are used to determine soil maps immediately after field observation.

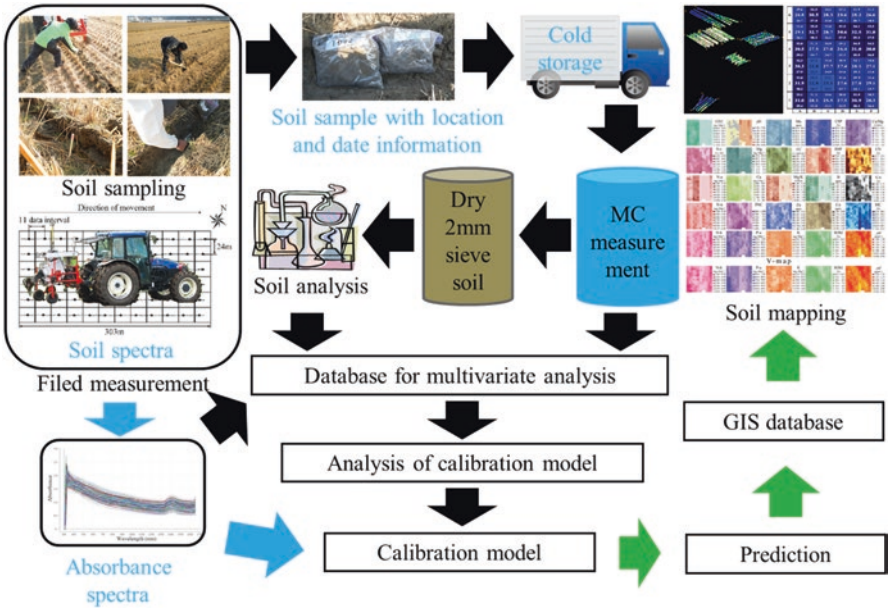

Fig. 4.7 Processes from field observation to soil mapping

(2) Soil Map

The soil map is defined as a spatial (or stratified) information at a certain date and time, with a high-resolution visualization of regional area, between fields or within field. Focusing on the plow layer, the soil map describes the information of soil physicochemical properties, biological properties, soil productivity (crop productivity such as yield), and soil fertility (conditions that support the root of crop and the ability of soil to supply the necessary amount of water and nutrients through the root according to the crop growth).

The purpose of creating a soil map is the management of local production area with group of crop cultivation fields or regional area and the soil management of grower-owned fields. In the management of local or regional area, the public infrastructure and environment necessary for crop cultivation and management are efficiently used, and profits are maximized by selecting crops and varieties. Higher efficiency in farm management requires the consolidation and accumulation of fields. The soil map is used as a source of information for decision-making and consensus building, such as improving workability by consolidating fields with similar fertility and reusing abandoned fields. The visualization method of one value per plot of field is the lowest resolution. The soil management of field owned by growers is based on the use of soil maps as a source of information on improving yield and quality as well as reducing production cost and environmental load through variable-rate work and crop or variety selection according to the variability between or within fields. The resolution of visualization varies according to the purpose of growers and their methods used in the farm management work.

The soil visualization information includes the terrain classification map, surface geological map, soil map, and groundwater map of the National Land Information Division, Ministry of Land, Infrastructure, Transport and Tourism, which were mainly used as sources of information for disaster countermeasures and building construction (Ministry of Land Infrastructure, Transport and Tourism 2018). Specialized for farmland use are soil profile map, fertility conservation soil map, and farmland soil map. The soil profile data is not used to directly control crop productivity, but the soil layer sequence that appears in the soil profile is the history of soil layer differentiation and shows whether the soil layer is going to maturity in the future. Therefore, it is an important information for reclamation of farmland and continuous design support on agricultural management. The problem is how to conduct soil survey up to 1 m soil depth and how to collect soil sample (Ministry of Agriculture Forestry and Fisheries 2016b). For the purpose of land use and farming guidance at municipal level, there are fertility conservation soil map data (Japan Soil Association) and farmland soil map data (Japan Soil Inventory, National Agriculture and Food Research Organization: NARO), which were compiled into database with physicochemical properties of the plow layer that cover the whole country. The farmland soil map is developed based on the data from the Fertilization Improvement Survey Project of the Ministry of Agriculture, Forestry and Fisheries, Fundamental Soil Survey for Fertility Conservation, Fundamental Soil-Environmental Survey, and Soil-Functional Monitoring Survey (about one point in

25 ha of soil profile survey in the farmland of Japan from 1953 to 2003) and the fertility conservation soil data. Seventeen properties were provided including thickness of plow layer (first layer), soil hardness (all soil layers hereinafter), bulk density, three phases (gas, liquid, solid), pF, water content, pH, exchange acidity, EC, total carbon, total nitrogen, base exchange capacity, exchangeable base, available phosphorus, available nitrogen, and suppliable silicic acid. The mean, median, standard deviation, and number of samples of each property were recorded for each of 60 soil groups. The scales of the farmland soil map are 1:200,000 and 1:50,000, and soil classification and soil temperature can also be viewed (Takada et al. 2013). The Agricultural Basic Law was enacted in 1961 which defined 0.3 ha as the standard plot (rice cultivation) in the field renovation project and was started in 1963 (Hirota 1999). The farmland soil map is composed of 1 data point per 83 plots (25 ha/0.3 ha). In addition, the cultivated area per management body is 2.87 ha (2017) (Ministry of Agriculture Forestry and Fisheries 2017), and ten agricultural management entities are displayed with same soil classification. Therefore, it is difficult to use the soil map in the measured resolution for regional or local management, soil management of grower's field, and land use and farming guidance at municipal level. Moreover, some growers bring soil from other places to improve the soil. Moreover, creating soil maps based on soil analysis for each plot of field becomes a subject.

The most popular visualization method is GIS software interpolation. The feature is that an arbitrary virtual data point is placed in the unmeasured area between measured data, and an estimated value calculated by interpolation methods, such as Kriging, natural neighbor, spline, and inverse distance weighting (IDW), is utilized to the virtual point, while a map drawn with smooth contour lines can be obtained. In past studies, Kriging and IDW have been often used, which are effective to grasp the variability.

IDW assumes that there are many sample points with regular arrangement, and the effect of variable decreases as the distance from the sample position increases. Then the effect of the sample data on the interpolation data is isotropic and inversely proportional to the distance.

Kriging (ordinary and universal) assumes that the distance or direction between sample points reflects a spatial correlation that can be used to explain variation in the surface. The Kriging tool fits a mathematical function to a specified number of points, or all points within a specified radius, to determine the output value for each location. It includes exploratory statistical analysis of the data, variogram modeling, creating the surface, and (optionally) exploring a variance surface. Kriging is selected when there is a spatially correlated distance or directional bias in the data.

Kriging is similar to IDW in that it weights the surrounding measured values to derive a prediction for an unmeasured location. The general formula for both interpolations is formed as a weighted sum of the data (Eq. 4.2):

$$\hat{Z}(S_0) = \sum_{i=1}^{N} \lambda_i Z(S_i) \tag{4.2}$$

where
$Z(s_i)$ is the measured value at the ith location.
λ_i is an unknown weight for the measured value at the ith location.
S_0 is the prediction location.
N is the number of measured values.

In IDW, the weight λ_i depends solely on the distance to the prediction location. However, with the Kriging method, the weights are based not only on the distance between the measured points and the prediction location but also on the overall spatial arrangement of the measured points. To use the spatial arrangement in the weights, the spatial autocorrelation must be quantified. The weight λ_i depends on a fitted model to the measured points, the distance to the prediction location, and the spatial relationships among the measured values around the prediction location (ESRI Japan 2016; Shoji and Koike 2007).

The requirement for soil map, which is as important as understanding of variability, is providing information in a classification method capable of instantaneous decision-making. Although the interpolation method is effective for grasping variability, the interpolation methods must be determined according to the spatial arrangement of the measurement data. Also, it is hard to determine the farm work range and work amount. For the paid GIS software, the costs of introduction and maintenance are problems, and the operation procedures from converting measured data to GIS readable format for display are operational issues.

Soil mapping methods include GIS software interpolation map, gird map, and dot map. Each visualization method has its characteristics, and it is necessary to select the visualization method according to the purpose of use of the soil map. However, the purpose of use of soil map varies with growers and field managers, while some may not have a purpose of use. In addition, there are no growers who divide one plot into multiple parts and perform soil analysis and mapping according to the number of divisions. Moreover, agricultural support system for guidance and fertilization design based on high-resolution soil map has not been established.

The first use of high-resolution soil map in such situation is to grasp the variability and record the grower's awareness to facilitate the grower's decision-making. It is necessary to provide field mapping technology to provide soil maps immediately after the field observation that enables the dialogue with grower and extension instructors. If the soil map can be provided on-site, and if it can share awareness of growers, provide advice from extension instructors, and create a database of grower's decision; it will be possible to serve as a part of decision support system. Therefore, a simple GIS display function (dot map) has been developed which shows the properties requested in the visualization methods and enabled soil mapping on-site.

(3) IDW Interpolation Map

The interpolated soil map is characterized by the fact that the status of variability can be drawn with clear contour line according to the classification, so the feature can be understood immediately. But there are problems with the introduction and

maintenance cost of GIS software and the operability of the mapping procedures. ArcCatalog in ArcGIS (V10.2.2 ESRI Inc., USA), map layout software ArcMap, and extension products (Spatial Analyst et al.) were used to create interpolation map. The feature of spatial data measured by SAS is that there are plenty of data collected from one plot and there are no scattered measurement positions or extreme inhomogeneities. Therefore, the effect on the interpolation point between the measured data is assumed to be smaller as the distance from the measured data point increases, and the influence of the data acquisition location on the interpolated value is isotropic. Therefore, IDW (ESRI Japan Co. Ltd 2002) is appropriate to be adopted due to its characteristics of that the influence of the data acquisition location on the interpolation result is inversely proportional to the distance. In IDW, the output cell size, power, and search radius can be set arbitrarily, but the automatic set values by the software were used. In the interpolation method, the inner area of a point with value and location information is visualized. In order to visualize the entire field inside the boundary, it is essential to record the field edge with values (analyzed and predicted values) and location information. Since no analysis value or spectra data were acquired at the field edge, soil maps were created by replacing the value with the data point closest to the field edge based on the characteristics of IDW. In addition, to distinguish among field end points and data points, data points were indicated by " · ," and the field end points were indicated by "+" (Fig. 4.8a).

(4) Grid Map

The grid map can facilitate efficient soil management when the purpose and method of use of the soil map are determined. For example, when variable-rate spraying is manually performed using a working machine such as a broadcaster or a boom sprayer, after determination of work width of the machine, the number of travel lines, the travel route, the start and stop positions of fertilizer application, and the number of grids in the travel direction, the center of the working width is measured with SAS. The average, minimum, and maximum values are shown for each grid, and the average value is used for classification. By showing the minimum and maximum values, it is possible to grasp the variability range and check for outlier (Fig. 4.8b).

For variable-rate work based on the grid map, a fertilization map can be created with manure increasing/decreasing zones determined based on cultivation calendar and cultivation guidelines.

(5) Simple GIS display function (Dot map)

The simple GIS display function (Fig. 4.9) is a visualization method that classifies and displays measurement points with color dots. Optional features include dot size, field outline, dot color, and threshold values of up to five divisions. When the pointer cursor is placed on the memorized reference value of each soil property, statistical value (average, maximum, minimum, and coefficient of variation), and acquired data points, the absorbance, second-derivative absorbance, and prediction value are displayed. In this way, it can be determined whether a sample for soil analysis needs to be collected and whether there is an abnormal spectrum. In

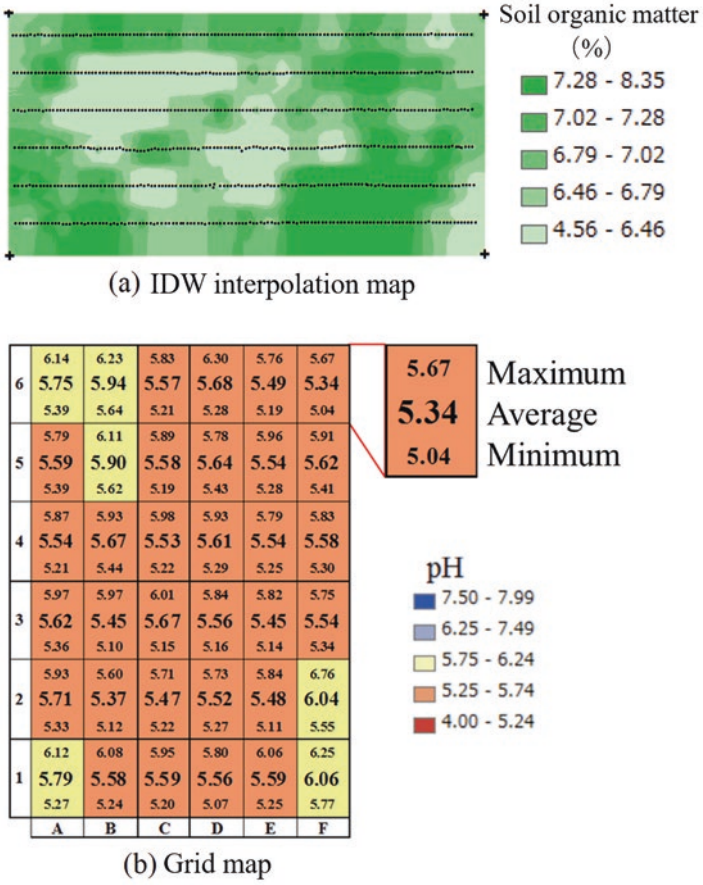

Fig. 4.8 Soil maps (**a**) IDW interpolation map (**b**) Grid map

addition, to display one plot of field or group of fields on the map, the map can display an arbitrary range by zooming. By registering the position information of the field edge and the entrance of working machine, it became easy to grasp the field direction when displaying complicated shapes or multiple fields. The title of the regression coefficient is composed of identification character, property, accuracy, and range of database, to prevent selection miss and grasp reliability of the prediction value. By registering the regression coefficient for each property, it is possible to display the dot map immediately after field observation and reduce the cost of GIS software's introduction, which makes it possible for the growers to understand their field and make decisions on-site. The simple GIS display function has been jointly developed with the Shibuya Seiki Co., Ltd.

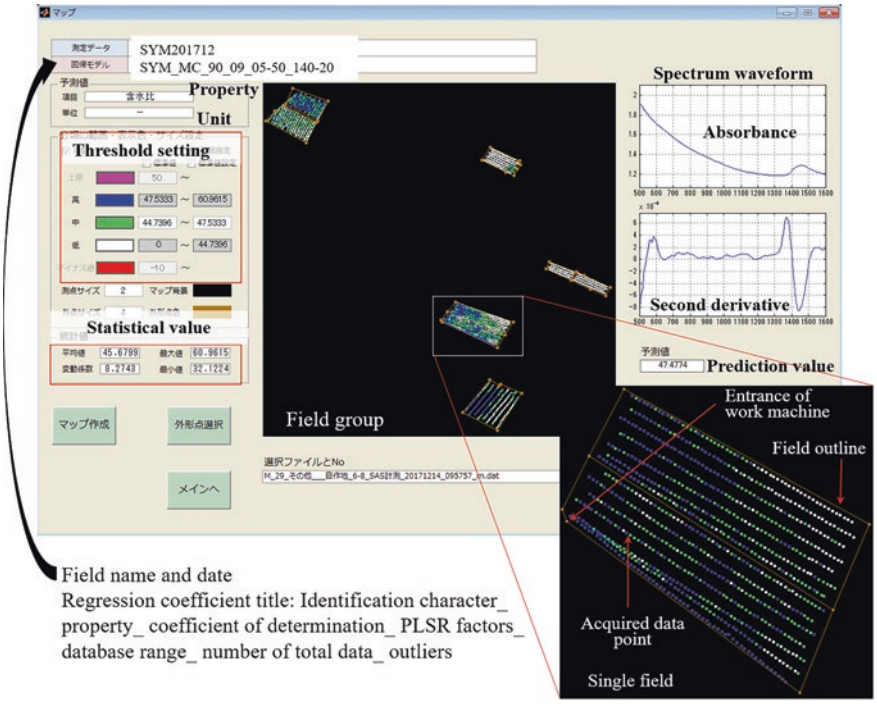

Fig. 4.9 Simple GIS display function (dot map)

4.2.2 Decision-Making for Crop Precision Farming

(1) Variable-Rate Application

(i) Test Fields, Device, and Methods

The test field was a rotation cropping field (4.43 ha, 303 m long side × 146 m short side) in Memuro-cho, Kasai-gun, Hokkaido, Japan. The test device was SAS1000, and the observation speed was 0.56 m/s, the observation depth was 0.15 m, the sampling period was 4 s, and the data measurement interval was 2.24 m. The field observation line interval was 24 m, which was the same with the pest control line. Field observations of the same field and the same line were conducted in October 2007, November 2008, and November 2010, and pH soil maps (Fig. 4.10) were provided to growers.

(ii) Make Decision by Growers

In the pH map after harvesting wheat in autumn 2007 and after harvesting sugar beet in 2008, a location with high pH value was confirmed on the south side (Fig. 4.10a, b). The grower decided to improve the soil condition before soybean

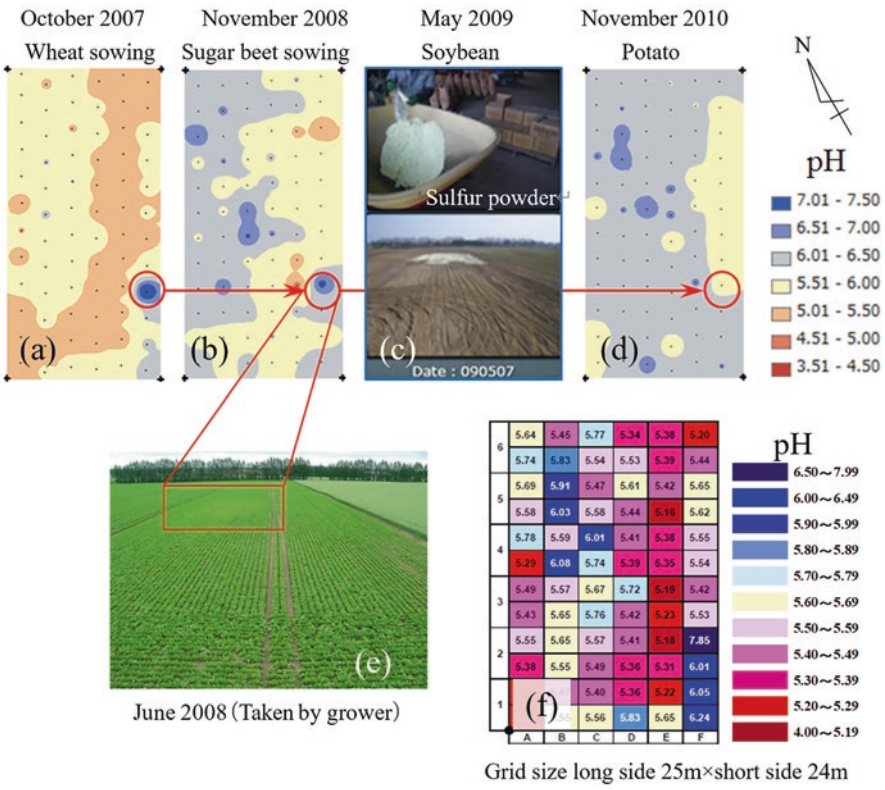

Fig. 4.10 Variable-rate application utilizing soil pH map

sowing in May 2009 and sprayed 360 kg/10a of sulfur powder by a broadcaster (Fig. 4.10c).

(iii) Reasons, Background, and Results

The high pH on the south side was because of overflowing with a large amount of lime cake (processed residue from refined sugar beet). The grower's rotation system was "wheat-sugar beet-soybean-potato-green manure," which was five crops in five years. If the pH value exceeds 6.5, potato and sugar beet may suffer disease of common scab, so the solution has been considered. In the growing season, symptoms such as slow growth and withering were visually observed in the place with high pH, and in the surrounding area, the location can be identified until harvest (Fig. 4.10e). After the harvest, the trace disappeared, and no solution was taken.

When the location with high pH can be identified from location information recorded in SAS and the grid map for easy manual variable-rate application can also be created, the grid map as shown in Fig. 4.10f can be provided. The size of the grid was determined by checking the distance over which the grower could manually adjust the spray amount. As a result of sulfur powder spraying, the field observation

after potato harvest in November 2010 confirmed that the pH dropped to 5.5–6.0 (Fig. 4.10d).

(2) Plan for Agricultural Work

(i) Test Fields, Device, and Methods

The test field was a taro rotation field (0.32 ha, 60 m long side × 54 m short side) in Aoyagi, Sayama City, Saitama Prefecture, Japan. The test device was SAS3000, and the observation speed was 0.28 m/s, the sampling period was 3 s, the observation depth was 0.15 m, and the data measurement interval was 0.84 m. For the purpose of visualizing the inside of the field with high resolution, the observation line was set at 3 m interval, to ensure that the tractor's wheel may not cover the observation line, because the interval between the taro planting rows was about 1 m and the width of the rare wheel of the tractor was 1.2 m. Field observation was conducted after taro harvest in February and December 2017. To estimate the regression coefficient for each property, a database of 100 samples for the analysis was used, which were collected in February 2017 from 10 plots of fields of 3 taro farmers in the Sayama area. For soil mapping, the soil maps with the data range divided according to the reference value of soil analysis were first provided to the grower, and then three equal division soil maps were provided.

(ii) Make Decision by Growers

The growers found that hot water extractable nitrogen and available phosphorus were below the reference value, and the exchangeable potassium was within the reference value in the divided interpolation methods (Fig. 4.11a) observed in February. It was considered that this was the topdressing effect of potassium fertilizer. From the soil map of the three equal division interpolation methods (Fig. 4.11b) observed in February, the grower changed the planting row direction from east-west to north-south.

(iii) Reasons, Background, and Work Results

The grower used sulfated potassium fertilizer as additional fertilization of the taro cultivation. The residual amount of exchangeable potassium was higher than hot water extractable nitrogen and available phosphorus, which agreed with the work of adding additional fertilizer.

According to the growers, they remembered that red soil was added to the east half of the field in the past. Also, the western taro was found to be smaller overall. The growers changed the planting row direction from east-west to north-south in consideration of cultivation management from work efficiency and soil property distribution. As a result of field observation after changing the planting row direction and after harvesting taro in December, hot water extractable nitrogen and available phosphorus were higher in the east half, while exchangeable potassium had a lower content (Fig. 4.12).

(3) Selection of Varieties Based on Differences Between Fields

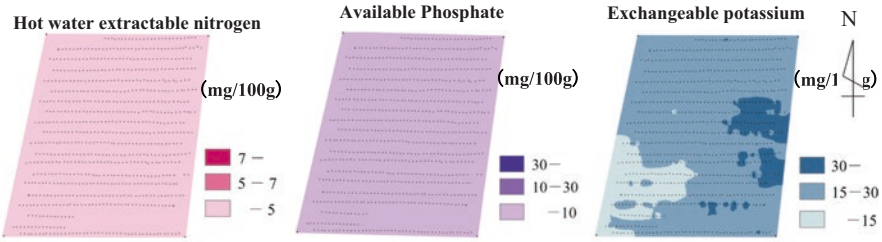

(a) Reference value division interpolation method observed in February

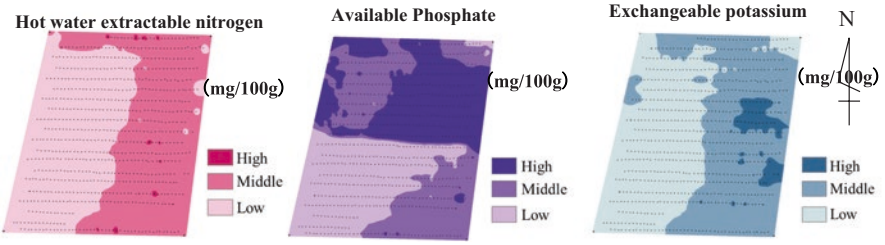

(b) Three equal division interpolation method observed in February

Fig. 4.11 Soil maps with data range (**a**) Reference value division interpolation method observed in February (**b**) Three equal division interpolation method observed in February

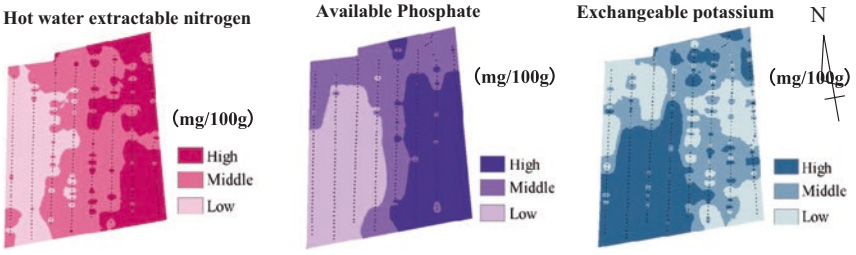

Fig. 4.12 Three equal division interpolation methods observed in December

(i) Test Fields, Device and Methods

The test fields were two plots of field (0.12 ha, 45 m long side × 30 m short side (trapezoid) and 0.16 ha, 55 m long side × 30 m short side (trapezoid)) in Aoyagi, Sayama City, Saitama Prefecture, Japan. The test device was SAS3000. The observation speed was 0.28 m/s, the sampling period was 3 s, the observation depth was 0.15 m, and the data measurement interval is 0.84 m. The interval between observation lines was 3 m; the observation line direction coincided with the direction of leveling, in north-south that crosses the direction of planting. There were factories and buildings on the west and north sides, and the location information at the end of the upper left of the two plots could not be captured accurately. Field observation was conducted after soil leveling (December 2017). To estimate the regression

coefficient for each property, the database was used in which 100 samples were collected in February 2017 at 10 plots from 3 taro farmers in the Sayama area. The soil map was confirmed with the grower after the field observation using dot maps based on the simple GIS display function of SAS3000 (Fig. 4.13).

(ii) Make Decision by Growers

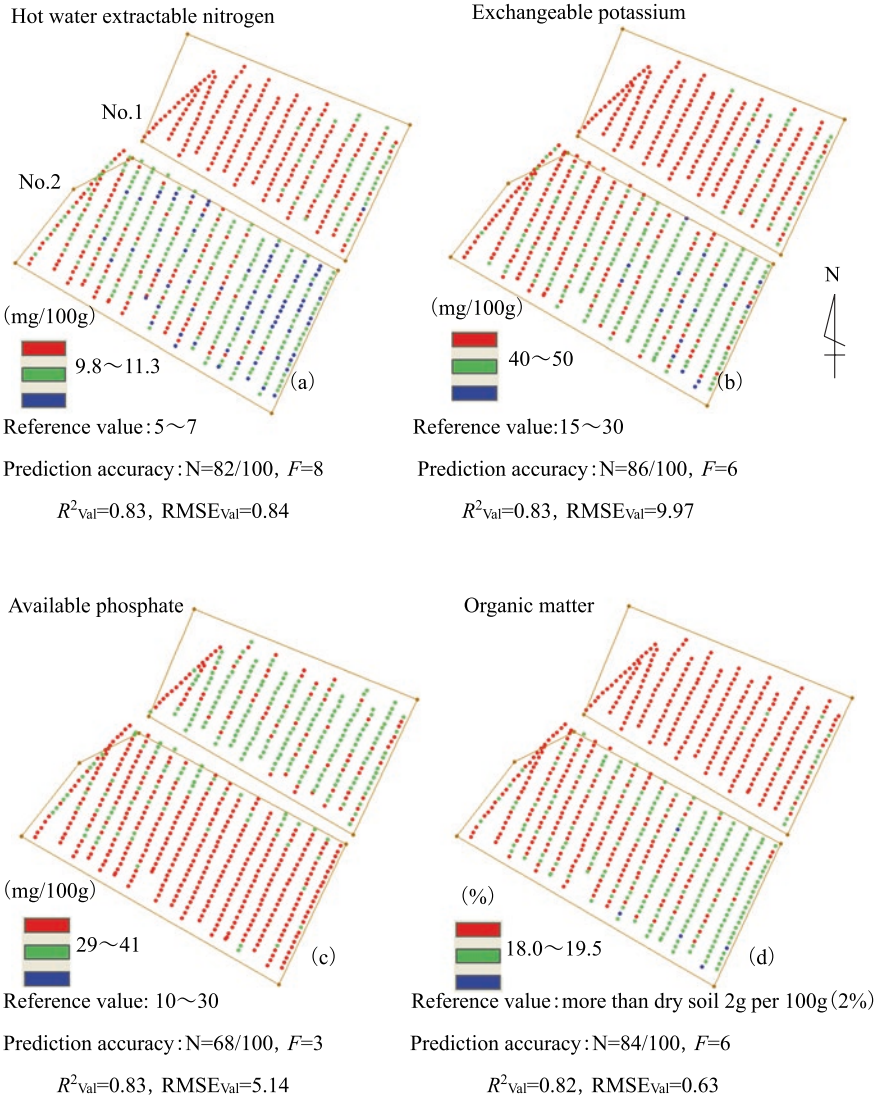

Fig. 4.13 Comparison between fields using dot map

The growers planned to cultivate Dodare (taro variety) in No. 1 field and lotus leaf in No. 2 field. But they switched the two cultivation varieties after referring to the soil maps of hot water extractable nitrogen, available phosphorus, and exchangeable potassium. So far, 2 tons of chicken manure compost has been put into the two plots of field, but it has been reduced to 1 ton.

(iii) Reasons, Background and Results

According to the growers, when the Dodare variety is cultivated in soil that is rich in nitrogen, the plant height and leaves and the mother taro tubers grow dramatically, while the secondary taro tubers tend to be small. According to the hot water extractable nitrogen soil map (Fig. 4.13a), the residual amount of both plots was higher than the reference value range, and No. 1 was higher than that of No. 2. Therefore, No.1 was planted with lotus leaves which are less affected by nitrogen.

In addition to the hot water extractable nitrogen, the residual amount of exchangeable potassium and available phosphorus in the two plots also exceeded the reference value range (Fig. 4.13b, c). Since the organic matter satisfied the condition of the standard level of 2 g per 100 g (2%) of dry soil (Ministry of Agriculture Forestry and Fisheries 2008a), the chicken manure compost input was reduced to half 1 ton.

4.3 Measurement and Application of Soil EC in Precision Agriculture

4.3.1 Soil EC Measurement: Theory and Method

Precision agriculture differentiates agriculture management based on the soil nutrient status and crop growth conditions of different locations in the farmland and can increase yield with less input. Rapid and accurate access to soil parameters is one of the bases of precision agriculture. The most informative, simple, least expensive, and accurate map of soil variability across the field is made using measurements of soil electrical conductivity (EC). Soil is an electrical conductor and soil EC is an important soil parameter. It has a relationship with several soil properties such as soil moisture, soil salinity (the amount of salt in the soil), soil texture (the percentage of sand, silt, and clay), cation exchange capacity (CEC), and organic carbon content. The measurements of the soil EC can reflect the soil status and provide a basis for implementing precision agriculture.

Soil EC is the most common measure of soil salinity and many nutrients are salts—a source of salinity. It is helpful to farmers to use soil EC to evaluate soil nutrient level. On the other hand, the nutrient accumulation, poor drainage, salt water intrusion in coastal areas, and saline irrigation water can lead to the unwanted buildup of salinity in soil, which is typically not beneficial to crops, grasses, or the microbial community in the soil. Soil salinity also affects the soil hydrology. Plant diseases and pathogens, reduced crop yields, or even crop failures may occur from

excessive soil salinity; therefore, the proper monitoring of soil salinity will help ensure the health of crops. Soil EC can change dramatically with water content and can be affected by the quality of the irrigation water, fertilization, drainage, and other natural processes. Compaction, clay content, and organic matter can influence moisture holding trends over time, also affecting EC capacities in soil.

As we know, electrical conductivity (EC), as well as its inverse electrical resistivity, is a fundamental property of a material or an object that quantifies how strongly it conducts or resists electric current. Electrical resistance is often used in electrical engineering and has the following relationship with electrical resistivity if the shape of the object is regular (Eq. 4.3):

$$R = \rho \frac{L}{S} \tag{4.3}$$

where R is electrical resistance (Ω), L is the length of the object (m), S is the cross-sectional area of the object (m^2), and ρ is the electrical resistivity (Ω·m).

Similarly, electrical conductance has the following relationship with electrical conductivity (Eq. 4.4):

$$G = \sigma \frac{S}{L} \tag{4.4}$$

where G is electrical conductance (Siemens, S), S is the cross-sectional area of the object (m^2), L is the length of the object (m), and σ is the electrical conductivity (S/m). It is obvious that $G = (1/R)$ and $\sigma = (1/\rho)$.

From Eqs. (4.3) and (4.4), it can be seen that if the cross-sectional area and length of the measured conductor are determined, the EC of the conductor can be easily obtained. However, the soil is a half-open and infinite measuring object and is just a complex measuring object with uncertain cross-sectional area and length for the measurement of the Earth conductivity. It is impossible to measure soil EC with Eqs. (4.3) and (4.4) directly.

Soil EC depends on the concentration of conductive ions in the soil. Therefore, it can be represented by measured ion concentration in soil solution, which has linear relationship with EC of soil solution. Pore water EC or soil water EC (EC_w or σ_w) is the electrical conductivity of the water in the soil pores. In order to simply measure the EC of pore water in situ, the tiny sensors would have to be inserted into microscopic water-filled pores. Obviously, it is impossible to measure the EC of water on that scale. In fact, it is feasible to extract a soil water sample and measure the EC of that sample.

Meanwhile, saturation extract EC (EC_e or σ_e) is measured by taking a soil sample, making a saturated paste of soil and deionized water, extracting the water, and then measuring the EC of the extracted solution. However, it is not easy to measure soil EC_w or soil EC_e in a field. A soil solution method is recommended. The soil solution is prepared as following.

The soil samples collected from a farmland are air-dried, smashed, and sieved (1 mm). Then, a certain weight of air-dried soil sample is weighed and added into a test tube or measuring cup, and five times of the weight of distilled water is added into the soil sample according to the water soil ratio of 5:1. After shaking the soil water solution on an oscillator for 30 min, and then standing for 30 min, the clear soil solution or the soil solution filtered by filter paper can be directly extracted for measurement of EC. The EC of the soil solution is usually measured by electrode method. The measured EC data of soil solution is called EC_w, and the EC data measured by aforementioned method can be also called as $EC_{1:5}$, which means that the soil solution is prepared by the water soil ratio of 5:1.

Soil $EC_{1:5}$ is widely used to analyze soil salinity (He et al. 2012). Soil salinity or sodicity is thought a major impediment to sustainable agriculture, worldwide. The Songnen Plain is the second largest plain of China after and also one of the five largest salt-affected soil regions in China. Therefore, soil $EC_{1:5}$ was used to characterize the salinity and sodicity of the salt-affected soils in the Songnen Plain, China, and determine the relationships between salinity, sodicity, and cation concentrations of 1:5 extracts (Chi and Wang 2010). One hundred and twenty-one soil samples were selected to determine chemical characteristics of soil using 1:5 extraction method. All samples were air-dried and passed through a 2 mm sieve, and then 4 g of soil was taken from each sample and put into a 100 ml bottle with 20 ml distilled water. After agitated and filtered, the $EC_{1:5}$ value of the soil solution was determined by a DDS-307 conductivity meter (Shanghai Precision Scientific Instrument Co., Ltd., China). The cations Na^+, K^+, Ca^{2+}, and Mg^{2+} were determined by using inductively coupled plasma mass spectroscopy (GBC, Scientific Equipment Pty Ltd., Australia). The TCC, total cation concentration (or total soluble salt concentration) ($mmol_c$ L^{-1}), was calculated as

$$\mathrm{TCC} = \mathrm{Na}^+ + \mathrm{K}^+ + \mathrm{Ca}^{2+} + \mathrm{Mg}^{2+} \tag{4.5}$$

Another soil salinity parameter, sodium adsorption ratio (SAR) $(mmol_c\ L^{-1})^{1/2}$, was calculated as

$$\mathrm{SAR} = \mathrm{Na} / \sqrt{\left(\mathrm{Ca}^2 + \mathrm{Mg}^{2+}\right)/2} \tag{4.6}$$

The analysis results showed that the coefficients of determination (R^2) between $EC_{1:5}$ and TCC and between $EC_{1:5}$ and SAR were 0.99 and 0.87, respectively, and $EC_{1:5}$ value had higher correlation with soil parameters, TCC and SAR, and could be used to well evaluate soil salinity and sodicity.

Although soil solution EC (EC_w), including $EC_{1:5}$ and $EC_{1:1}$, can describe soil EC level to a certain extent, it cannot replace soil EC since soil in farmland is a porous medium and has three phases of solid, liquid, and gas. The EC in soil is more complex than it is in soil solution. Therefore, the bulk soil electrical conductivity (EC_b or σ_b) is proposed and applied, which is also called soil apparent electrical conductivity (EC_a or σ_a). Soil EC_a (afterward, soil EC is used instead of soil EC_a) is the

electrical conductivity of the soil/water/air matrix combined and is measured by soil sensors from the undisturbed status.

The most popular measurement method of soil EC is four-electrode method. Figure 4.14 shows the typical pattern of the four-electrode method. Two electrodes (J and K) are connected with a constant electric current source, while the other two electrodes (M and N) are connected with a voltage meter. The constant electric current is injected into soil from J and K, and then a voltage drop between M and N is detected. Using the voltage drop, the soil EC can be measured (Telford et al. 1976; Sun and Wang 2001).

Using the four-electrode method shown in Fig. 4.14, the soil EC can be calculated as the following:

$$\sigma_b = \frac{\left(\frac{1}{L_{JM}} - \frac{1}{L_{JK}}\right) - \left(\frac{1}{L_{KM}} - \frac{1}{L_{KN}}\right)}{2\pi} \frac{I}{\Delta V_{MN}} \tag{4.7}$$

where σ_b is the soil EC; L_{JM}, L_{JK}, L_{KM}, and L_{KN} are the distances between J and M, J and K, K and M, and K and N respectively; I is the electric current between J and K; and ΔV_{MN} is the voltage drop between M and N.

When $L_{JM} = L_{MN} = L_{KN} = a$, the structure of soil EC measurement method shown in Fig. 4.14 is called Wenner array, and Eq. (4.8) can be simplified as

$$\sigma_b = \frac{1}{2\pi a} \frac{I}{\Delta V_{MN}} \tag{4.8}$$

When $L_{JK} = 2a$ and $L_{MN} = b$, the structure of soil EC measurement method shown in Fig. 4.14 is called Schlumberger array, and Eq. (4.9) can be simplified as

$$\sigma_b = \frac{1}{\pi\left(\frac{a^2}{b} - \frac{b}{4}\right)} \frac{I}{\Delta V_{MN}} \tag{4.9}$$

A portable soil EC detector was developed (Li et al. 2006; Li and Li 2011). The EC detector adopts a four-electrode method and consists of three parts: a probe with four electrodes, a control and display unit, and the data processing software. The probe injects a constant electrical current into soil and detects the voltage drop

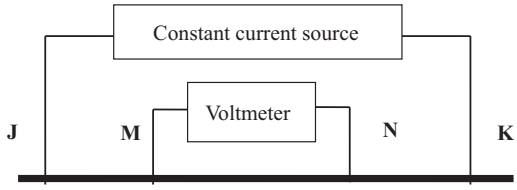

Fig. 4.14 Structure of soil EC measurement method based on four-electrode method

between two output electrodes. The voltage drop is then used to estimate the soil EC. The correlation analysis was performed between soil EC value and soil ammonium content, and higher correlation result was obtained ($R^2 = 0.9297$).

4.3.2 On-the-Go Measurement System of Soil EC

Soil EC, as an important parameter of soil characteristics, is of great significance to the precision management and fertilization in farmland. Precision agriculture is a differential management based on the temporal and spatial variation of agricultural parameters on the field scale. It needs modern agricultural machineries to perform the site-specific crop management. Therefore, as the one of the essential information of precision agriculture, soil EC measurement needs to be conducted rapidly, accurately, and real time. Thus, it is necessary to use the vehicle-mounted (on-the-go) measurement system to achieve the requirements of efficiency and accuracy.

(1) EM-38 Soil EC Mapping System Based on Electromagnetic Induction

The on-the-go measurement methods of the soil EC can be broadly classified into two categories, electromagnetic induction (EMI) method and aforementioned four-electrode method. EMI method is a noncontact type of method and the principal component is shown in Fig. 4.15. The instrument based on EMI method is composed of a transmitter and a receiver, placed about 1 m apart. Inside the transmitter, an alternating current (A/C) is applied to a copper coil to induce an electromagnetic wave, known as the primary magnetic field (H_T). When this magnetic field comes into contact with the conductive material such as soil, an eddy current in the soil matrix will be created. This new eddy current will generate a secondary magnetic field (H_I). Both H_T and H_I are measured by the receiver as a reinforced magnetic field (H_R). The measured response is a function of soil EC and is used to evaluate soil (Robinson et al. 2003).

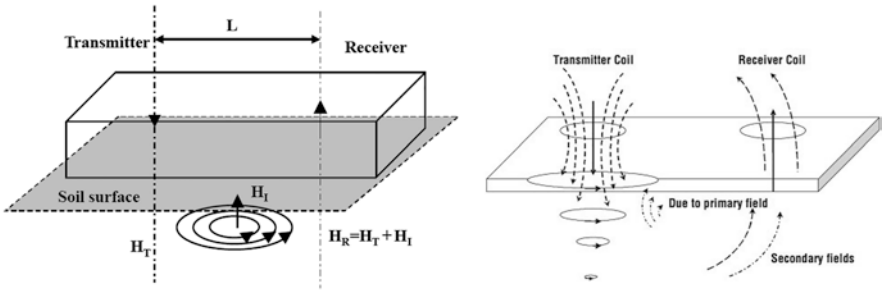

Fig. 4.15 Principal component of the EMI method

EM38 series of ground conductivity meter (Geonics Limited, Ontario, Canada)[2] is a typical soil EC measuring and mapping system. It can be used in handheld pattern and also in on-the-go pattern (vehicle-mounted) when it is equipped with a vehicle or tractor. The standard EM 38 - MK 2 includes two receiver coils, separated by 1 m and 0.5 m from the transmitter, providing data from effective depth ranges of 1.5 m and 0.75 m, respectively, when positioned in the vertical dipole orientation, and 0.75 m and 0.375 m, respectively, when in the horizontal dipole orientation, while the EM38-MK2-1 model includes one receiver coil only, at 1 m from the transmitter. The operating frequency is 14.5 kHz and measuring range is 0~1000 mS/m. External power sources can be connected to the instrument for extended field operations. When it is used in on-the-go pattern, a protective capsule, constructed of durable plastic materials, is available as an option.

A mobile data acquisition system for soil EC was developed using the Geonics EM38 sensor in order to investigate the correlation between topsoil depth and soil EC for precision agriculture (Sudduth et al. 2001). Topsoil depth is an important factor related to within-field productivity differences. The EM38 sensor was mounted on a wooden cart pulled behind a vehicle to form the mobile system with a GPS receiver and data collection computer. The test results showed that the soil EC provided the best estimates of topsoil depth and the relation between them followed the power function as Eq. (4.10):

$$y = \frac{1}{\sigma_b^{\alpha}} + \beta \tag{4.10}$$

where y is the topsoil depth (cm), σ_b is the soil EC (mS/m), and α and β are the constants. The experiments were conducted in several farms and the model for each farm got high coefficient of determination (R^2), R^2 = 0.84~0.95. If α is taken as 1, the model will become easy to be applied but the accuracy will go down a little.

(2) Veris Series of Soil EC Mapping System Based on Four-Electrode Method

One widely used device to measure soil EC in the field is the Veris 3100 (3105) Soil EC Mapping System (manufactured by the Veris Technologies in Salina, Kansas), which is manufactured based on four-electrode method. The Veris 3100 EC unit (Fig. 4.16) has six disks mounted on a toolbar to act as electrodes and records soil EC readings from two different depths every second. One pair of disk electrodes induces current into the soil. The change in voltage is measured across the other two pairs of disk electrodes resulting in simultaneous EC measurements for the top 30 cm of soil (two center disk electrodes) and the top 90 cm of soil (two outside disk electrodes). A Global Positioning System (GPS) receiver is mounted on

[2] *Disclaimer*: Commercial products are referred to solely for the purpose of clarification and should not be construed as being endorsed by the authors or the institution with which the authors are affiliated.

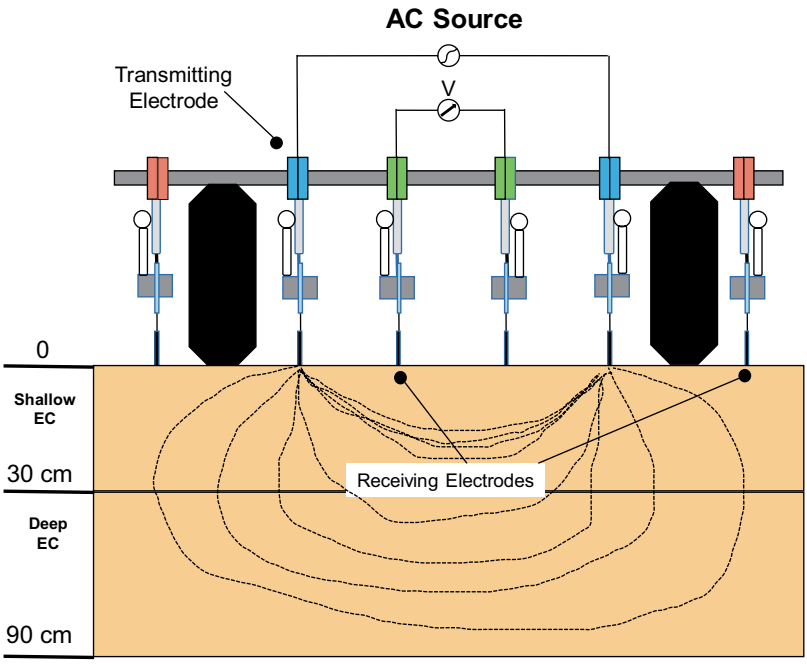

Fig. 4.16 Veris 3100 soil EC mapping system. (*Disclaimer:* Commercial products are referred to solely for the purpose of clarification and should not be construed as being endorsed by the authors or the institution with which the authors are affiliated)

the Veris unit to record the location of each soil EC measurement point in the field. All soil EC data and GPS data can be used to create a soil EC map of a field.

The differences between the soil EC zones in a field are caused by differences in the soil parameters, such as soil salinity, soil texture, soil organic matter (SOM) content, soil water content, and soil structure. It is shown that in most fields, zones with higher EC values have higher clay and organic matter content than lower EC zones. Farmers want to know the soil texture so that they can apply the correct amount of seeds, fertilizers, and irrigation to each section of their field. After understanding the pattern of soil composition across the field, farmers can make their soil and crop management decisions to fit the soil pattern rather than assuming that the whole field has a uniform composition. Soil EC maps have many economic and agronomic advantages to be used as a guide to make better management decisions. Examples of the most immediate uses of soil EC measurement and mapping are (Farahani et al. 2011) the following:

- Rapid identification of farm field variability
- Guidance to smart soil sampling as opposed to random- or grid-based soil sampling
- Logical placement and interpretation of on-farm tests

- Development of potential "management zones" for variable-rate seeding and chemical application
- Identification of coarse-textured zones within the field that are susceptible to leaching
- Identification of coarse-textured zones within the field that have low water-holding capacity and thus susceptible to crop water stress
- Identification of crop productivity zones based on relative clay and organic matter contents

Precision agriculture (site-specific management) demands the identification of subfield regions with homogeneous characteristics (management zones). However, determining subfield areas is difficult because of complex correlations and the spatial variability of soil properties and nutrient concentrations, responsible for variations in crop yields within the field. Soil EC is thought to be a potential estimator of soil properties and nutrients and a tool for the delimitation of homogeneous zones.

A Veris 3100 on-the-go soil sensing system was utilized to improve field management zone definition (Gunzenhauser et al. 2012). The Veris system with GPS is thought better to produce the dense mapping coverage needed to better define soil boundaries and improve the delineation of management zones.

Peralta and Costa (2013) also utilized a Veris 3100 on-the-go soil sensing system to delineate management zones with soil EC to improve nutrient management of crops in Argentina. The EC measurements to 0–90 cm are used because they are more stable over time than the EC measurements to 0–30 cm (Sudduth et al. 2003). The Veris 3100 sensor was pulled by a pickup truck, taking simultaneous and georeferenced EC data in real time with a DGPS to take a satellite position once per second. Average travel speeds ranged between 7 and 11 kmh^{-1}, corresponding to about 2–3 m spacing between measurements in the direction of travel. Meanwhile, soil properties and nutrients were analyzed by means of soil sampling, including SOM, CEC, pH, NO_3^--N content, P, Zn^{+2}, Ca^{+2}, Mg^{+2}, Mn^{+2}, Na^+, K^+, Fe^{+2}, Cu^{+2}, and SO_4^{-2}. The result of PCA and ANOVA revealed that soil EC measurements successfully delimited two homogeneous soil zones associated with the spatial distribution of soil properties and some nutrients (Na^{+2}, Mg^{+2}, Mn^{+2}, Cu^{+2}, Ca^{+2}, Zn^{+2}, Fe^{+2}). These results suggest that field-scale soil EC maps have the potential to design sampling zones to implement site-specific management strategies.

Greater understanding of soil EC can offer useful information for crop management decisions. A research team at Clemson University has identified the role of soil EC in production agriculture after several years of study (Wiatrak et al. 2009). Soil texture relates to factors that have a major impact on productivity. For example, irrigation scheduling is closely related to soil type and water-holding capacity of the soil. Yield potential of sandy soils generally is less than clay soils. Variations of soil texture within a field can also have an effect on tillage decisions and pest management. Since nematode densities were highly correlated to soil texture as measured by soil EC, soil EC can be effectively used for variable-rate applications of nematicides in production fields.

It was reported that variable-depth tillage could be used to significantly reduce fuel requirements for tillage operations. Soil compaction management relies heavily on the use of annual deep tillage, usually to a uniform depth throughout the field. Soil EC data were good estimates of the topsoil thickness, and the predicted tillage depths were inversely correlated to the soil EC (Wiatrak et al. 2009).

4.3.3 Application of Soil EC in Precision Agriculture

(1) *Smart Rice Transplanter Based on Soil EC*

Smart rice transplanter is the first agricultural machine in the world to analyze soil after puddling. The smart rice transplanter could measure soil EC (apparent electrical conductivity) and topsoil depth as measurement parameters. It is very important to determine the measurement method of soil EC, soil depth, and variability map of each parameter to the smart transplant. Figure 4.17 illustrates the smart rice transplanter. The prototype was applied in eight-row-type rice transplanter (NP80, Iseki).

On-the-go measurement of soil EC is also shown in Fig. 4.17. The soil EC sensor could measure bulk electrical conductivity during rice transplanting (Morimoto et al. 2013; Morimoto and Hayashi 2017). The soil EC sensor consisted of a pair of wheel-type electrode stainless steel sensors.

Since the two electrodes of the soil EC sensor are mounted on the front wheels, the distance between the electrodes is always the same at 1.1 m. Alternative current

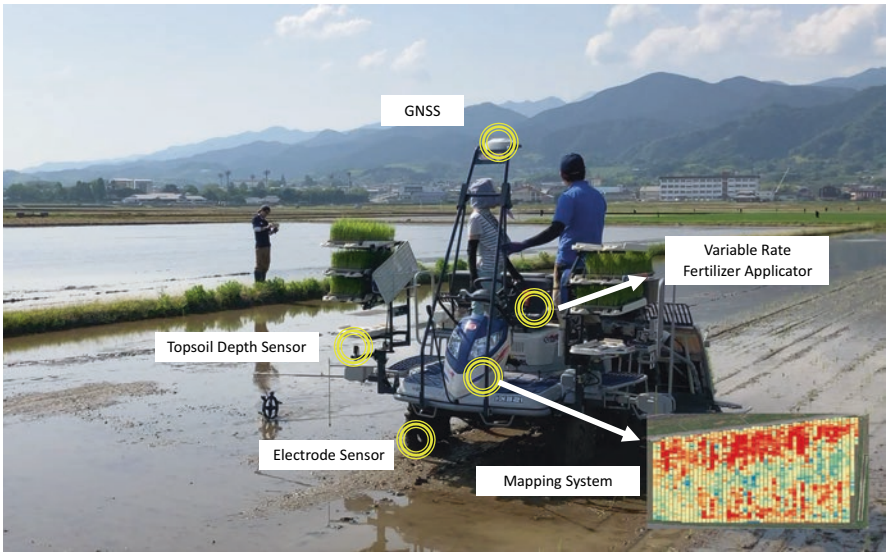

Fig. 4.17 Smart rice transplanter (Morimoto et al. 2013; Morimoto and Hayashi 2017)

of 1 kHz frequency was flowing between front wheels. Soil EC was affected by the soil moisture content and soil temperature. Since the moisture content of soil was close to 100% and solid-liquid ratio is almost 1.0 due to puddling operation, it could be measured without being affected by moisture content. In order to compensate temperature, a platinum resistance thermometer (E52, Omron) was applied. This thermometer was installed under the float of the rice transplanter to measure soil surface temperature. The interval of measurement was 1 s and the EC value was compensated to 25 °C by using Eq. (4.11):

$$\lambda_{25} = \frac{\lambda_t}{1 + 0.02(t - 25)} \tag{4.11}$$

where t is soil surface temperature (°C), λ_{25} is EC value at 25 °C (mS), and λ_t is measured electrical conductivity (mS).

Topsoil depth of paddy fields seems to be uniform, but the topsoil depth varies due to turning by agricultural machineries such as heading area. It is also known that the fertility of the soil varies due to uneven distribution of compost or soil conditioner, and these variations will result in crop lodging at the harvest time. The smart rice transplanter introduced in this section solves this lodging problem with a soil sensor and performs real-time variable fertilizer application. Topsoil depth was measured by ultrasonic distance sensor (USS, Model E4PA-LS200-MI-N, Omron). A couple of USS set in front of the rice transplanter at a height of 850 mm from the ground was shown in Fig. 4.18. Topsoil depth was calculated from a fixed height (i.e., 850 mm) minus the average of two sensor data as given by Eq. (4.12):

$$\mathrm{TD} = 850 - \frac{\left(D_{\mathrm{left}} + D_{\mathrm{right}}\right)}{2} \tag{4.12}$$

where TD is the topsoil depth and D_{left} and D_{right} are the distance from left and right sensors to soil surface (mm), respectively. USS could be measured with 5 Hz interval, provided average data per five datasets.

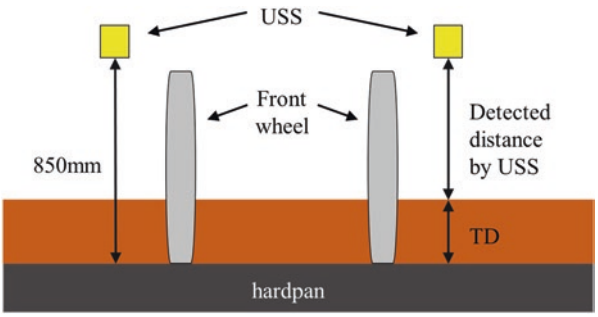

Fig. 4.18 Schematic diagram of topsoil depth sensing

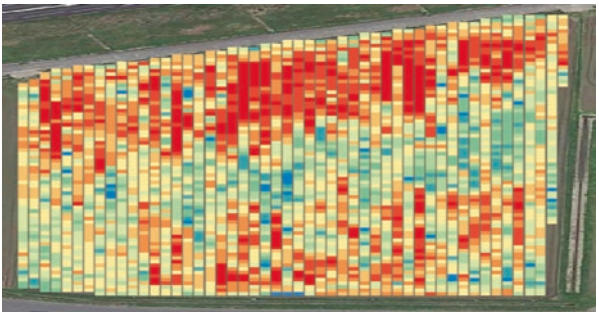

Fig. 4.19 Variability maps of soil EC (Morimoto et al. 2013; Morimoto and Hayashi 2017)

Fig. 4.20 Autonomous measurements of the soil EC based on electromagnetic induction

Figure 4.19 shows the soil EC map collected by the smart rice transplanter. Sensing and variable fertilizer application can be performed at the same time while planting rice and can be confirmed on a map immediately after the work is done. Also, as mentioned earlier, the system measures the electrical conductivity between the front wheels, so it can scan the entire field of soil. In the case of a 100 ha-scale farmhouse, a database of 1,000,000 points can be built in one year, and the number of data will increase dramatically compared to the conventional soil sampling method. It is expected that it will become the standard specification of the field with information on rice cultivation in the near future.

(2) *Topsoil Mapper Based on Soil EC*

A kind of precision agriculture equipment, Topsoil Mapper (Geoprospectors GmbH, Traiskirchen, Austria),[3] has been developed and brought to market from 2015 (http://www.geoprospectors.com/gb/). As a soil sensing product, the Topsoil Mapper (TSM) can conduct autonomous measurements of the soil EC based on electromagnetic induction as shown in Fig. 4.20. In precision agriculture,

[3] *Disclaimer*: Commercial products are referred to solely for the purpose of clarification and should not be construed as being endorsed by the authors or the institution with which the authors are affiliated.

differences in soil as well as varying yield capacities within a field are taken into account during the cultivation process in order to use operating materials efficiently, conserve resources, and increase agricultural yields. Using TSM, the inhomogeneity in the soil for a large area and comprehensively map soil parameters, such as soil type, water saturation, and compaction, can be obtained from the measured soil EC data. These soil parameters can then be used in real time for variable machine control.

TSM can be installed on any towing vehicle and supply exact data about soil properties. It is made of robust, entirely nonconductive material. On any towing vehicle, the TSM can be used regardless of weather and vegetation.

TSM has two working modes, BASIC and PRO.

Basic: TSM is capable of recording the depth of compaction, relative water content, and soil type automatically by using a motor during agricultural operations. In the Basic version, the user uploads the collected data via storage medium to the Data Box (cloud solution). Three maps are then produced using the parameters listed above. The data is managed centrally on the server and is available to the user at any time.

Pro: With the Pro version, the measured data is sent in real time to the terminal in the driver's cabin. In this way, the driver can immediately see, for example, the depth of compaction zones. The information is provided directly to the soil tilling machine in the form of a rule-based control. Working depth is set automatically, such that interaction with the machine's operator is not required. The advantages of this mode of operation are saving fuel and working time and reduce wear and tear due to optimized working depth.

TSM has three application possibilities, as shown in Fig. 4.20.

(i) Contact-Free Analysis of Soil Parameters

In *Basic* mode, the system can be mounted on any towing vehicle to conduct autonomous measurements of the soil EC without contacting the soil. Maps with the soil parameters for compaction, type of soil, and water saturation can be determined from the measured data. The farmers then have the option of integrating this data with other data for their farm management system and generating application maps from the results. As a rule, farmers use these maps in combination with the site-specific control of their agricultural equipment, as well as for planning of further agricultural operations.

(ii) Variable Control of Agricultural Machines in Real Time

As an alternative to asynchronous usage, the soil information can be used in *Pro* mode in combination with the appropriate agricultural equipment so that the latter can be controlled flexibly in real time. This allows two processes (acquisition and application) to be combined into one work step. When using the TSM for cultivation, the soil parameters determined by the system will be integrated into the calculation of the ideal depth of cultivation in real time. The parameters will be transferred as control parameters to the appropriate machine, while simultaneously

implementing data acquisition during the soil cultivation process. Depending on the cultivation strategy (shallow cultivation, subsoiling, or contour tracking), corresponding settings can also be modified on the terminal software so that additional information about the field will be taken into consideration.

(iii) Sensor-Supported Seed Control in Real Time

The application of sensor-supported real-time control, which can be realized with the TSM, also presents a huge potential for optimization in other areas, such as seed drilling. With this system, it is possible to adapt sowing to varying site conditions (soil type, soil moisture) in real time.

The TSM system also includes a Topsoil Visualizer (TSV), a Topsoil Data Box (TSDB), and a Topsoil Data Analyzer (TSDA).

The role of the TSV is to automatically process the recorded soil data and to calculate certain soil parameters such as compaction or water saturation. The information can then be passed directly to the implement, which automatically sets the tilling depth or controls the sowing quantity, allowing two steps to be performed simultaneously.

By the TSDB, the web portal of Geoprospectors GmbH (http://www.geoprospectors.com/gb/) allows field-related visualization of the soil parameters recorded, with the user being able to select different map displays. Output is also available as a geo-referenced dataset for further processing in the company's internal geo-information system.

The TSDA is a desktop software, which can be used to transfer the collected data to the laptop immediately and then analyze them automatically. The raw data and the processed data are displayed as maps within a few seconds. Consequently, for example, soil samples can be taken immediately and directly based on the zone maps determined on-site.

References

Adamchuk VI, Hummel JW, Morgan MT, Upadhyaya SK (2004) On-the-go soil sensors for precision agriculture. Comput Electron Agric 44:71–91

Agricultural Product Chemical Research Laboratory (2001) Soil diagnosis sheet (for field soil). https://www.nokyoren.or.jp/assay/assay-soil/. Accessed 24 Oct 2019 (In Japanese)

Akitomo I, Shimamura S (1998) Estimation of soil chemical content by near infrared spectroscopy. Bull Zootech Exp Stat Prefecture Yamaguchi Japan 14:111–117. (In Japanese)

Australian Government (2011) Carbon Credits (Carbon Farming Initiative) Act 2011. https://www.legislation.gov.au/Series/C2011A00101/Amendments. Accessed 5 May 2018

Bodun PO, Shibusawa S, Sasao A, Sakai K, Nonaka H (2000) Dredged sludge moisture prediction by textural analysis of the surface image. J Terrramech 37:3–20

Chang CW, Laird DA, Mausbach MJ, Hurburgh CR Jr (2001) Near-infrared reflectance spectroscopy-principal components regression analysis of soil properties. Soil Sci Soc Am J 65:480–490

Chi CM, Wang ZC (2010) Characterizing salt-affected soils of Songnen Plain using saturated paste and 1:5 soil-to-water extraction methods. Arid Land Res Manag 24:1–11. https://doi.org/10.1080/15324980903439362

Christy CD (2008) Real-time measurement of soil attributes using on-the-go near infrared reflectance spectroscopy. Comput Electron Agric 61:10–19
Clark DH, Mayland HF, Lamb RC (1987) Mineral analysis of forages with near infrared reflectance spectroscopy. Agron J 79(3):485–490
Dalal RC, Henry RJ (1986) Simultaneous determination of moisture, organic carbon, and total nitrogen by near infrared reflectance. Soil Sci Soc Am J 50:120–123
ESRI Japan (2016) An overview of the interpolation toolset. http://desktop.arcgis.com/ja/arcmap/10.3/tools/spatial-analyst-toolbox/an-overview-of-the-interpolation-tools.htm. Accessed 18 Nov 2017
Farahani HJ, Khosla R, Buchleiter GW (2011) Field EC mapping a new tool to make better decisions. Colorado State University Extension, Fact Sheet No. 0.568
Gunzenhauser B, Shanahan J, Lund E (2012) Utilizing on-the-go soil sensing devices to improve field management zones definition. Crop Insights 19(15):1–4
He YB, DeSutter T, Prunty L, Hopkins D, Jia XH, Wysocki DA (2012) Evaluation of 1:5 soil to water extract electrical conductivity methods. Geoderma 185–186:12–17
Hedley CB, Yule IJ (2009) Soil water status mapping and two variable-rate irrigation scenarios. Precis Agric 10:342–355
Hirota J (1999) Change of agricultural structure in rice farming and development of farmland consolidation style. J Agric Eng Soc Jpn 67(9):963–968
Imade Anom SW, Shibusawa S, Sasao A, Hirako S (2001) Soil parameters maps in paddy field using the real time soil spectrophotometer. JSAM J 63(3):51–58
Kaho T, Shibusawa S, Morimoto E, Hirako S, Ohtomo A (2004) Stability and availability of real-time soil spectrophotometer. J Jpn Soc Agric Machine 66(6):113–121. (In Japanese)
Kodaira M, Shibusawa S (2013) Using a mobile real-time soil visible-near infrared sensor for high resolution soil property mapping. Geoderma 199:64–79
Kodaira M, Shibusawa S (2016) Multivariate regression model estimation and soil mapping of multiple soil properties by using a tractor-mounted soil analyzing system. J Jpn Soc Agric Machine Food Eng 78(5):401–415. (In japanese)
Kodaira M, Shibusawa S (2018) Development of calibration model for SiO_2, Fe_2O_3, and Na_2O using subsurface diffuse reflectance spectra. J Jpn Soc Agric Machine Food Eng 80(2):114–122. (In japanese)
Kuang B, Mouazen AM (2013) Effect of spiking strategy and ratio on calibration of on-line visible and near infrared soil sensor for measurement in European farms. Soil Tillage Res 128:125–136
Kuang B, Mahmood HS, Quraishi MZ, Hoogmoed WB, Mouazen AM, van Henten EJ (2012) Sensing soil properties in the laboratory, in situ, and on-line: a review. Adv Agron 114:155–223
Li A, Li MZ (2011) Development of a ZigBee-based wireless sensor network for soil EC sensing. In: CIGR International Symposium 2011 (CIGR2011), September 19–23, 2011, Tokyo, Japan
Li M, Wang M, Wang Q (2006) Development and performance test of a portable soil EC detector. Appl Eng Agric 22(2):301–307
Malley D, Martin P, Ben-Dor E (2004) Application in analysis of soils. In: Roberts C, Workman J, Reeves III J (eds). Near infrared spectroscopy in agriculture. A Three Society Monograph (ASA, SSSA, CSSA), Madison, pp 729–784
Marín González O, Kuang B, Quraishi MZ, Munoz-Garcıa MA, Mouazen AM (2013) On-line measurement of soil properties without direct spectral response in near infrared spectral range. Soil Tillage Res 132:21–29
Matsunaga T, Uwasawa M (1992a) Near infrared diffuse reflectance spectra of the upland soils in Japan. Jpn J Soil Sci Plant Nutr 63(4):403–410. (In Japanese)
Matsunaga T, Uwasawa M (1992b) Application of near infrared spectrometry to quantitative analysis of soil physical and chemical properties. Jpn J Soil Sci Plant Nutr 63(6):712–714. (In Japanese)
Matsunaga T, Uwasawa M (1993) Near infrared diffuse reflectance spectra of clay minerals. Jpn J Soil Sci Plant Nutr 64(3):329–331. (In Japanese)

Ministry of Agriculture Forestry and Fisheries (2008a) Fundamental guidelines for fertility improvement. http://www.maff.go.jp/j/seisan/kankyo/hozen_type/h_dozyo/pdf/chi4.pdf#search=%27%E5%9C%B0%E5%8A%9B%E5%A2%97%E9%80%B2%E6%B3%95%E3%81%A8%E3%81%AF%27. Accessed 21 May 2017 (In Japanese)
Ministry of Agriculture Forestry and Fisheries (2008b) Aomori Prefecture Healthy soil making technology manual (2) Method and utilization of soil diagnosis. http://www.maff.go.jp/j/seisan/kankyo/hozen_type/h_sehi_kizyun/pdf/tuti12.pdf. Accessed 21 July 2017 (In Japanese)
Ministry of Agriculture Forestry and Fisheries (2016a) Prefectural fertilizer standards, etc.- When using fertilizer standards-. http://www.maff.go.jp/j/seisan/kankyo/hozen_type/h_sehi_kizyun/index.html. Accessed 12 Sept 2017 (In Japanese)
Ministry of Agriculture Forestry and Fisheries (2016b) Soil survey and soil collection method. http://www.maff.go.jp/j/seisan/kankyo/hozen_type/h_sehi_kizyun/pdf/gum21.pdf#search=%27%E5%9C%9F%E5%A3%8C%E8%A9%A6%E6%96%99%E6%8E%A1%E5%8F%96%E6%96%B9%E6%B3%95%27. Accessed 3 May 2018 (In Japanese)
Ministry of Agriculture Forestry and Fisheries (2017) Statistics on farmland. http://www.maff.go.jp/j/tokei/sihyo/data/10.html. Accessed 18 Nov 2017 (In Japanese)
Ministry of Foreign Affairs of Japan (2018) Sustainable Development Goals (SDGs). https://www.mofa.go.jp/mofaj/gaiko/oda/sdgs/pdf/about_sdgs_summary.pdf. Accessed 18 May 2018
Ministry of Land, infrastructure, Transport and Tourism (2018) National Land Survey (basic land survey, basic water survey) homepage. http://nrb-www.mlit.go.jp/kokjo/inspect/inspect.html. Accessed 3 May 2018 (In Japanese)
Mizuno K, Ishiguri T, Kondo T, Mizuno K (1987) Prediction of forage compositions and sheep responses by near infrared reflectance spectroscopy I. Evaluation of accuracy. Bull Natl Grassl Res Inst 38:35–47. (In Japanese)
Morimoto E, Hayashi K (2017) Design of smart agriculture Japan model. Adv Anim Biosci Precision Agric (ECPA) 8(2):713–717
Morimoto E, Hirako S, Yamasaki H, Izumi M (2013) Development of on-the-go soil sensor for rice transplanter. Eng Agric Environ Food 6(3):141–146
Mouazen AM, Baerdemaeker JD, Ramon H (2005) Towards development of on-line soil moisture content sensor using a fibre-type NIR spectrophotometer. Soil Tillage Res 80:171–183
Mouazen AM, Maleki MR, De Baerdemaeker J, Ramon H (2007) On-line measurement of some selected soil properties using a VIS-NIR sensor. Soil Tillage Res 93:13–27
Mouazen AM, Alhwaimel SA, Kuang B, Waine T (2014) Multiple on-line soil sensors and data fusion approach for delineation of water holding capacity zones for site specific irrigation. Soil Tillage Res 143:95–105
Peralta NR, Costa JL (2013) Delineation of management zones with soil apparent electrical conductivity to improve nutrient management. Comput Electron Agric 99:218–226
Robinson DA, Lesch SM, Lebron I, Shouse P (2003) Minimizing drift in electrical conductivity measurements in high temperature environments using EM-38. Soil Sci Soc Am J 68(2):339–345
Rodionov A, Welp G, Damerow L, Berg T, Amelung W, Pätzold S (2015) Towards on-the-go field assessment of soil organic carbon using Vis–NIR diffuse reflectance spectroscopy: developing and testing a novel tractor-driven measuring chamber. Soil Tillage Res 145:93–102
Roy SK, Shibusawa S, Okayama T (2006) Monitoring of topsoil characteristics using field-airborne hyperspectral signatures and underground soil images from real-time soil spectrophotometer (RTSS). J JSAM 68(2):50–62
Shibata Y (1999) Site-specific crop management for large size paddy field in Japan. J Jpn Soc Agric Machine 61(4):14–19. (In Japanese)
Shibusawa S, Hirako S, Otomo A, Li M (1999) Real-time underground soil spectrophotometer. Jpn Soc Agric Machine 61(3):131–133. (In Japanese)
Shibusawa S, Hirako S, Otomo A, Sakai K, Sasao A, Yamazaki K (2000a) Real-time soil spectrophotometer for in-situ underground sensing. Jpn Soc Agric Machine 62(5):79–86. (In Japanese)

Shibusawa S, Sato H, Hirako S, Otomo A, Sasao A (2000b) A revised soil spectrophotometer. IFAC Proc 33(29):231–236

Shibusawa S, Ehara K, Okayama T, Umeda H, Hirako S (2005) A real-time multi-spectral soil sensor: predictability of soil moisture and organic matter content in a small field. Precision Agriculture '05. Wageningen Academic Publishers, The Netherlands, pp 495–502

Shibusawa S, Kodaira M, Ninomiya K, Hirako S (2010) Commercialization of tractor-mounted soil analysis system. J Industry Acad Govern Collab 6(3):32–33. (In Japanese)

Shibuya Machinery Co. Ltd (2004) World's first new product development tractor-mounted soil analysis system. http://www.shibuya.co.jp/outline/ir/NewsReleasePDF/news20041125-1.PDF. Accessed 12 Sept 2015

Shoji T, Koike K (2007) Lecture note: Geostatistics Kring-estimation of spatial data taking account of error. J Geother Res Soc Jpn 29(4):183–194. (In Japanese)

Sudduth KA, Hummel JW (1993) Soil organic matter, CEC, and moisture sensing with a portable NIR spectrophotometer. Trans ASAE 36(6):1571–1582

Sudduth KA, Drummond ST, Kitchen NR (2001) Accuracy issues in electromagnetic induction sensing of soil electrical conductivity for precision agriculture. Comput Electron Agric 31:239–264

Sudduth KA, Kitchen NR, Bollero GA, Bullock DG, Wiebold WJ (2003) Comparison of electromagnetic induction and direct sensing of soil electrical conductivity. Agron J 95:472–482

Sun YR, Wang MH (2001) A mathematical model and its experimental study for a kind of measurement method of soil electric conductivity. Trans Chin Soc Agric Eng 17(2):20–23

Takada Y, Reon A, Nakai M, Obara H, Kohyama K (2013) Estimation of carbon and nitrogen content in surface horizon using "soil information web viewer". J Jpn Soc Soil Phys 123:117–124. (In Japanese)

Telford WM, Geldart L, Sheriff R (1976) Applied geophysics. Cambridge University Press, Cambridge, pp 633–640

Toriyama K (2001) Soil and plant nutrition science now developed from field study: acquisition and analysis of data from the new view point: growth of rice plant in the large size paddy field and the variability in soil nitrogen fertility. Jpn J Soil Sci Plant Nutr 72(3):483–458. (In Japanese)

Umeda T, Koyama F, Takamuku K (2001) Determination of mineral concentrations of beefs cattle manure with near infrared reflectance spectroscopy. Bull Fukuoka Agric Res Center 20:105–108. (In Japanese)

Umeda H, Shibusawa S, Okayama T, Sakuma DY, Kaho T, Ninomiya K (2011) Study of the precision farming with soil maps describing environmental load using a real-time soil sensor. J Jpn Soc Agric Machine 73(1):37–44. (In Japanese)

Viscarra Rossel RA, Walvoort DJJ, McBratney AB, Janik LJ, Skjemstad JO (2006) Visible, near infrared, mid infrared or combined diffuse reflectance spectroscopy for simultaneous assessment of various soil properties. Geoderma 131:59–75

Wiatrak P, Khalilian A, Mueller J, Henderson W (2009) Applications of soil electrical conductivity in production agriculture. Better Crops 93(2):16–17

Wojciechowski T, Czechlowski M (2013) Proximal soil sensing unit for cereal combine harvesters. Proc Inst Vehic 4(95):179–188

Yamazaki S (2008) Soil diagnosis guide. National Federation of Agricultural Cooperative Associations. Fertilizer pesticide department, Tokyo, pp 2–27. https://www.zennoh.or.jp/activity/hiryo_sehi/pdf/gijyutu_1-01b.pdf (In Japanese)

Zornoza R, Guerrero C, Mataix-Solera J, Scow KM, Arcenegui V, Mataix-Beneyto J (2008) Near infrared spectroscopy for determination of various physiCalibration, chemiCalibration and biochemiCalibration properties in Mediterranean soils. Soil Biol Biochem 40:1923–1930

Chapter 5
Theories and Methods for Spectroscopy-Based Crop Nutrient Sensing

Yan Zhu, Jun Ni, and Lili Yao

Abstract The monitoring of crop growth can provide timely information for precision field management and the basis for early crop yield estimation. Spectral analysis technology, remote sensing image technology, digital image processing technology, plant electrical signal detection, and other means can obtain crop growth information and analyze crop nutritional status without destructing plants. All of the above technologies have been widely used in crop growth monitoring, and the related fast acquisition sensing systems of crop nutrition have been developed. Chlorophyll and nitrogen concentrations of plants can be estimated with nondestructive remote sensing techniques. Based on canopy spectral characteristics of plants, several vegetation indices, such as ratio vegetation index (RVI), difference vegetation index (DVI), and normalized difference vegetation index (NDVI), were developed for detecting nutrient status of plants. Several specific spectral parameters of plant canopy are effective in the diagnosis of crop nutrient status, which are nutrient balance parameter, nitrogen sufficiency index (NSI), nitrogen response index (NRI), nitrogen nutrition index (NNI), and indicator difference method. Ground-based, UAV (unmanned aerial vehicle)-borne, and satellite remote sensing can be used to obtain above vegetation indices and spectral parameters for diagnosis of crop nutrient status, which will play a more and more important role in precision crop nutrient management.

Keywords Crop nutrient sensing · Plant canopy · Spectroscopy · Vegetation index · NDVI · Remote sensing

Y. Zhu · J. Ni (✉) · L. Yao
Nanjing Agricultural University, Nanjing, China
e-mail: nijun@njau.edu.cn

M. Li et al. (eds.), *Soil and Crop Sensing for Precision Crop Production*,
Agriculture Automation and Control, https://doi.org/10.1007/978-3-030-70432-2_5

Crop growth can be described by the characteristics of individual plants or group plants. The group composed of robust individual plants is called a good growing crop area. The monitoring of crop growth can provide timely information for precision field management and provide basis for crop early yield estimation. A variety of biological parameters closely related to crop growth are used to describe crop growth, including crop nutrition parameters (e.g., chlorophyll content, nitrogen content, and crop water content) and plant morphological parameters (e.g., leaf area, plant height, and coverage). It is the basis of precision agriculture to monitor the growth parameters of various crops.

The traditional monitoring methods of crop nutritional status mainly depend on the experience accumulated by farmers in the long-term agricultural life. According to the appearance changes of plant leaves and plant colors caused by the lack or excess of some nutrient elements, farmers can make their decision of fertilization. For example, when the crops are short of nitrogen, they will grow slowly and look light green, and the leaves are yellow or brown when they are dry. When the crops are short of potassium, the old leaves turn yellow along the edge. Especially when they are serious, the edges of the leaves look like being burnt, and the green among the veins is lost. When the crops are short of phosphorus, the leaves and plants become dark and gradually appear red or purple patches. In addition, when the crops are short of sulfur, magnesium, iron, and other elements, the leaves also represent different characteristics. However, because the growth of crops in the field is affected by many factors at the same time, the method of observation based on experience is limited by the difference of experience cognition and evaluation standard of the observer, which is prone to misjudgment or late judgment, affecting the field management decision-making.

The modern chemical experiment methods to analyze the leaves, leaf sheaths, stems, or the whole plant of the crops can extract the concentration of some nutrients in the crops, so as to realize the determination of the level of abundance and deficiency of corresponding elements. Those methods are accurate and repeatable and become a routine detection method. However, because of the need of sampling and measurement, the operation of the test process is complex, and the consumption of reagents and time is large; thus, it cannot meet the needs of rapid, simple, and nondestructive field crop growth detection for precision agriculture.

With the development of computer technology and advanced sensor technology, it is possible to obtain crop growth information accurately and quickly. Spectral analysis, remote sensing technology, digital image processing, plant electrical signal detection, and other means can obtain crop growth information and analyze crop nutritional status without destructing plants. All of the above technologies have been widely used in crop growth monitoring research, and the related fast acquisition sensing systems of crop nutrition have been developed.

5.1 Spectral Characteristics and Vegetation Indices of Crop Nutrients

5.1.1 Canopy Spectral Characteristics of Crop Nutrients

Nitrogen (N) in cereal crops is a main element for maintaining growth status and enhancing grain yield. Leaf N accumulation (LNA), as a product of leaf N content and leaf weight, reflects not only information on leaf N status but also vegetation coverage during crop growth. Therefore, quick, nondestructive, and accurate acquisition of LNA becomes a key technique for population growth diagnosis and precision N management in modern crop production (Hansen and Schjoerring 2003), which is of significant importance for precision diagnosis, real-time fertilization, and productivity prediction. Research in the past decades has shown that remote sensing technology offers the only practical alternative to the complicated, slow, and expensive chemical methods for estimating foliar chemical concentrations over large geographic areas (Sahoo et al. 2015). The existing reports indicated that it is feasible to estimate N accumulation in plant by spectroscopic means. However, further investigations are needed to explore consistent feature bands and construct simpler spectral parameters and to develop more accurate monitoring models with wider applicability of crop N accumulation estimation based on hyperspectral sensing information. Figure 5.1 shows the spectral reflectance of green plants.

In the visible waveband (400–700 nm), absorption by leaf pigments is the most important process leading to low reflectance and transmittance values. The main

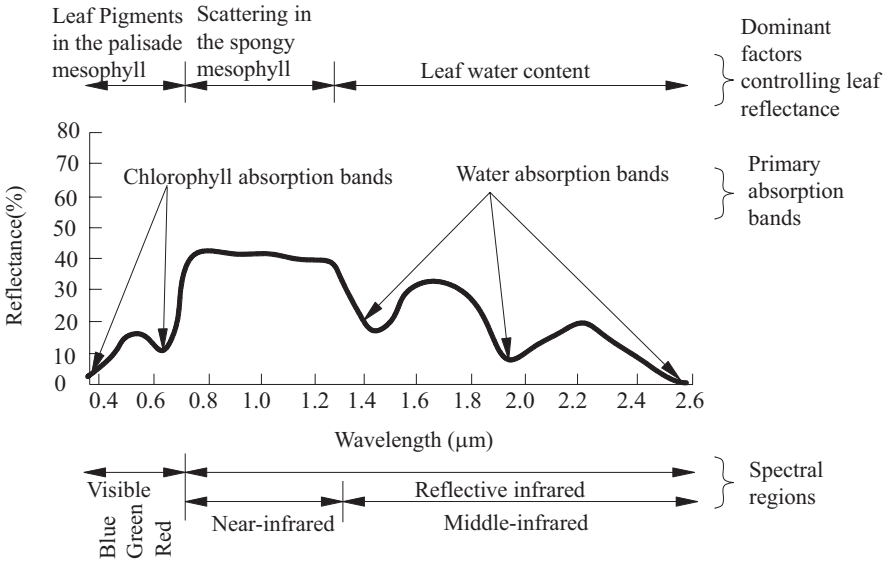

Fig. 5.1 Spectral reflectance of green plants

light-absorbing pigments are chlorophylls a and b (Chl a and Chl b), carotenoids, xanthophylls, and polyphenols, and all pigments have overlapping absorption features. Chl a displays maximum absorption in the 410–430 nm and 600–690 nm regions, whereas Chl b shows maximum absorption in the 450–470 nm range. These strong absorption bands induce a reflectance peak in the green domain at about 550 nm. Carotenoids absorb most efficiently between 440 and 480 nm.

In the near-infrared (NIR) waveband (700–1300 nm), leaf pigments and cellulose are almost transparent, so that absorption is very low and reflectance and transmittance reach their maximum values. This is caused by internal scattering at the air-cell-water interfaces within the leaves. Scattering occurs mainly due to multiple refractions and reflections at the boundary between the hydrated cellular walls and air spaces.

In the middle-infrared waveband, also called shortwave-infrared waveband (SWIR: 1300–2500 nm), leaf optical properties are mainly affected by water and other foliar constituents. Water largely influences the overall reflectance in the SWIR band effectively trapping the radiation, resulting in absorption that exceeds scattering processes. Protein, cellulose, lignin, and starch also influence leaf reflectance in the SWIR.

5.1.2 Vegetation Indices of Crop Nutrients

Plant nitrogen concentration can also be estimated with nondestructive remote sensing techniques since chlorophyll content is closely linked to nitrogen status. Based on canopy spectral characteristics of plants, several vegetation indices, such as simple ratio and normalized difference indices, were developed for detecting nutrient status of the plants.

1. Ratio Vegetation Index (RVI)

Ratio vegetation index (RVI), also known as greenness, is the ratio of two spectral reflectance, which can better reflect the difference of vegetation coverage and growth status, especially suitable for vegetation monitoring with vigorous growth and high coverage. RVI can be calculated as Eq. (5.1):

$$RVI = \rho_{NIR} \Big/ \rho_{\mathrm{R}} \tag{5.1}$$

where ρ_{NIR} is the spectral reflectance of the crop canopy at NIR band and ρ_{R} is the spectral reflectance of the crop canopy at red band. RVI is a sensitive indicator parameter of green plants, which has a high correlation with leaf area index (LAI), biomass dry matter (DM), and chlorophyll content. The RVI of the area covered by green and healthy vegetation is far greater than 1, while the RVI of nonvegetation-covered areas (bare soil, artificial buildings, water, dead vegetation, or serious insect pests) is near 1, and the RVI of vegetation is usually greater than 2. Vegetation

coverage affects RVI. When the vegetation coverage is high, RVI is very sensitive to vegetation. When the vegetation coverage is less than 50%, the sensitivity decreases significantly. The RVI is also affected by atmospheric conditions, which greatly reduces the sensitivity of vegetation detection, so atmospheric correction is needed before calculation.

2. Difference Vegetation Index (DVI)

Difference vegetation index (DVI) is probably the simplest vegetation index. It can be calculated as Eq. (5.2):

$$DVI = \rho_{NIR} - \rho_{\mathrm{R}} \tag{5.2}$$

DVI can well reflect the change of vegetation coverage, but it is sensitive to the change of soil background. When the vegetation coverage is 15~25%, DVI increases with the increase of biomass, and when the vegetation coverage is more than 80%, the sensitivity of DVI to vegetation decreases.

3. Normalized Difference Vegetation Index (NDVI)

The normalized difference vegetation index (NDVI) is used to detect vegetation growth state and vegetation coverage and eliminate some radiation errors. NDVI can be calculated as Eq. (5.3):

$$\mathrm{NDVI} = \frac{\left(\rho_{NIR} - \rho_{\mathrm{R}}\right)}{\left(\rho_{NIR} + \rho_{\mathrm{R}}\right)} \tag{5.3}$$

The value range of NDVI is −1~1. A negative value indicates that the ground is covered with clouds, water, snow, etc., which highly reflects the visible light. A value close to 0 indicates that there is rock, bare soil, etc., and the reflectance data at NIR and R bands are approximately equal. A positive value indicates vegetation coverage and increases with the increase of coverage, and the range of general green vegetation area is 0.2~0.8.

NDVI is the most widely used one of more than 40 vegetation indexes (Bannari et al. 1995; Tian and Min 1998). Although NDVI is sensitive to the change of soil background, it can eliminate most of the changes of irradiance related to instrument calibration, solar angle, terrain, cloud shadow, and atmospheric conditions and enhance the response ability to vegetation.

The limitation of NDVI is that the contrast of NIR and R reflectance is enhanced by nonlinear stretching. For the same image, when calculating RVI and NDVI separately, it can be found that the increasing speed of RVI value is higher than that of NDVI value, that is, NDVI has low sensitivity to high vegetation area. The treatment of atmospheric interference is insufficient, and atmospheric residual noise has a serious impact on NDVI index. It is easy to be disturbed by the soil background, especially in the middle vegetation coverage area. When the soil background becomes dark, NDVI index tends to increase.

4. Soil-Adjusted Vegetation Index (SAVI)

To overcome the limitations of NDVI, some new indexes were proposed to modify NDVI. Soil-adjusted vegetation index (SAVI) is one of those indexes and was designed to minimize soil brightness influences (Huete 1988). SAVI can be calculated as Eq. (5.4):

$$\mathrm{SAVI} = \frac{\left(\rho_{NIR} - \rho_{\mathrm{R}}\right)}{\left(\rho_{NIR} + \rho_{\mathrm{R}} + L\right)}\left(1 + L\right) \tag{5.4}$$

where L is a soil adjustment factor and the value range of L is 0~1. If the value of L is zero, the SAVI is equal to the NDVI. When $L = 1$, it means that the impact of soil background is zero and the vegetation coverage is very high. When $L = 0.5$, it permits the best adjustment to minimize the secondary backscattering effect of canopy-transmitted soil background reflected radiation.

Based on red edge bands, several simple ratio and normalized difference indices were developed for estimating Chl a concentration in plant leaves, for example, red edge ratio indices including Vogelmann index a (VOGa) (Vogelmann et al. 1993), GM-2 and simple ratio index (SR705, RI) (Gitelson and Merzlyak 1998), red edge normalized difference indices including Vogelmann indices b and c (VOGb and VOGc) (Zarco-Tejada et al. 2001), normalized difference 705 index (ND705) (Gitelson and Merzlyak 1994), modified simple ratio 705 (mSR705), and modified normalized difference index (mND705) (Sims and Gamon 2002). Ratio and normalized difference indices composed of red and NIR bands such as pigment-specific simple ratio (PSSR) and pigment-specific normalized difference (PSND) were also designed to assess Chl a and Chl b status in different deciduous tree leaves (Blackburn 1998).

5.2 Estimation of Leaf Nitrogen Accumulation in Wheat Based on Hyperspectral Sensing

5.2.1 Analysis of Canopy Spectral Characteristics

The studies focused on the hyperspectral sensing were conducted from five different N rates (0 kg N ha^{-1} (N0), 75 kg N ha^{-1} (N1), 150 kg N ha^{-1} (N2), 225 kg N ha^{-1} (N3), and 300 kg N ha^{-1} (N4)) and six wheat cultivars in three consecutive growing seasons to develop a new methodology for systematic exploration of novel sensitive bands and simple spectral indices to estimate LNA in wheat (Yao et al. 2010). The data were used to test the derived model equations, and the estimated results were compared with the measurements to evaluate reliability and accuracy of the equation output under independent cultural conditions. Besides R^2, the relative root mean square error (RRMSE) and slope were used to evaluate the fitness between the predicted and observed data, along with 1:1 plotting of the two sets of values. The RRMSE is calculated with the equation (Zhu et al. 2006).

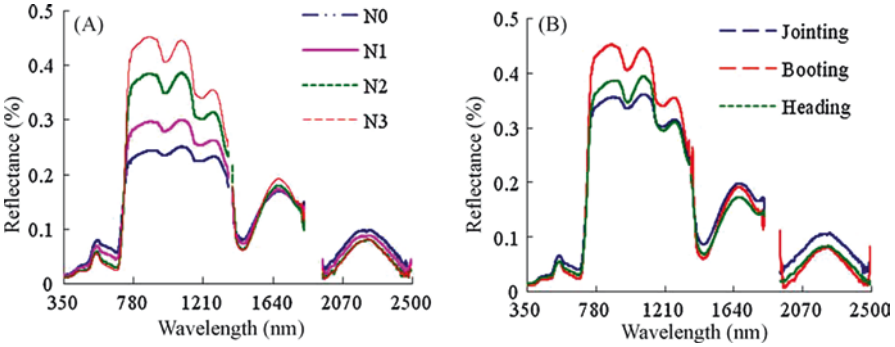

Fig. 5.2 Changes of canopy spectral reflectance with varied nitrogen rates and growth stages in Yumai 34 wheat (**a**) At booting stage (**b**) Under N3 of N rate

With the data from Yumai 34 in Exp. 1 as an example, Fig. 5.2 illustrates the dynamic change patterns of canopy hyperspectral reflectance with varied N rates at booting and with growth stages at N3. It can be seen that different N rates markedly influenced the characteristics of spectral reflectance of wheat canopy, with different spectral responses in the various waveband regions (Fig. 5.2a). With increasing N rates, the canopy spectral reflectance decreased in the range of visible bands and elevated in the NIR range with obvious differences among four N rates. This implied that these spectral regions are relatively sensitive to growth status of wheat under varied N levels. The similar spectral responses were observed at different growth stages and marked differences located in the visible and NIR regions (Fig. 5.2b). This is likely because wheat canopy structure and plant biochemical components experienced sharp changes at different growth stages and under varied N rates, thus influencing the properties of spectral reflectance. As a whole, under higher N rates and more vigorous growth stages, the canopy reflectance in the visible range was lower than under lower N rates and earlier growth stages, and the opposite pattern was seen in the NIR region.

With the observed data, the reduced sampling method was firstly adopted to analyze the functional relationships of LNA to $NDSI(R_{\lambda 1}, R_{\lambda 2}) = (R_{\lambda 1} - R_{\lambda 2})/(R_{\lambda 1} + R_{\lambda 2})$ at 10 nm interval using a combination of two random bands (λ_1 and λ_2) from 350 to 2500 nm based on the original spectra and to identify the sensitive band ranges with greater R^2 values. The regression analyses revealed that there were highly significant correlations between LNA and NDSI in two spectral ranges of visible bands and NIR bands, whether the function was linear or power or exponential form. The R^2 values were largely greater than 0.80 with linear regression based on the NDSI of 710–730 nm and 930–1010 nm, greater than 0.90 with power regression based on NDSI of 700–730 nm and 820–960 nm, and greater than 0.90 with exponential regression based on NDSI of 500–580 nm and 830–1010 nm. Then, through precise sampling on those sensitive spectral ranges, more detailed results of R^2 values between LNA and NDSI at 1 nm interval were obtained in three different functional forms.

5.2.2 *Spectral Monitoring Models for Crop Nutrients*

According to R^2 and standard error (SE), it can be seen that among the selected NDSI groups, for linear equation, the best performance was based on NDSI (R_{968}, R_{720}) (R^2 of 0.81 and SE of 1.31) (Fig. 5.3a); for power equation, the best result was from NDSI (R_{860}, R_{720}) (R^2 of 0.90 and SE of 1.33) (Fig. 5.3b); and for exponential equation, the best result was from NDSI (R_{940}, R_{570}) (R^2 of 0.90 and SE of 1.20) (Fig. 5.3c). In particular, the power equation from NDSI (R_{860}, R_{720}) and the exponential equation from NDSI (R_{940}, R_{570}) markedly enhanced the accuracy of LNA monitoring in wheat.

The above results indicated that the well-performed spectral indices and monitoring equations were all based on the sensitive bands from visible to NIR ranges, whether derived from linear or nonlinear equations. Among them, three NDSI models such as linear, power, and exponential functions exhibited exceptional predictability (R^2>0.81, SE<1.33).

With the well-performed spectral indices NDSI (R_{860}, R_{720}), the bandwidths were expanded from 1 to 100 nm gradually at the interval of 1 nm, and then the corresponding LNA monitoring models with varied bandwidths were established based on the two spectral indices.

Comparing the values of R^2 and SE of the calibration, it can be seen that NDSI (R_{860}, R_{720}) showed similar change patterns in validation. With the increased bandwidths, for NDSI (R_{860}, R_{720}), R^2 ascended firstly and then descended after 37 nm, although SE increased gradually. Analyzing the bandwidth impaction on validation performance of NDSI (R_{860}, R_{720}), the results showed that R^2 decreased but RRMSE increased gradually for NDSI (R_{860}, R_{720}). The result indicated that the monitoring model exhibited apparent difference after the bandwidth of NDSI (R_{860}, R_{720}) was over 33 nm.

The independent dataset was used to test the model for LNA estimation in wheat. Three statistics of R^2, RRMSE, and slope between the observed and estimated values were considered comprehensively for evaluating the performance of established

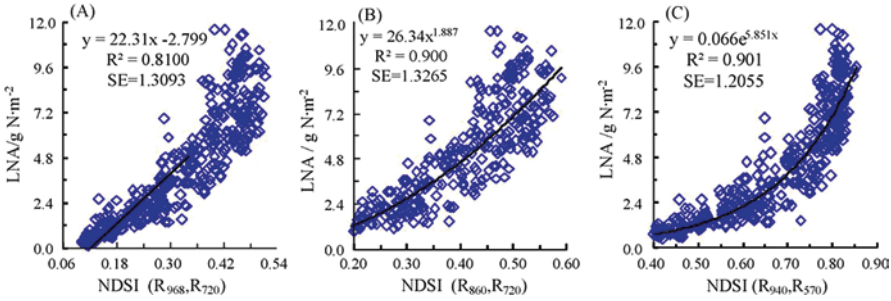

Fig. 5.3 Quantitative relationships of LNA to spectral indices in wheat (n = 402) (**a**) NDSI(R_{968}, R_{720}) (**b**) NDSI(R_{860}, R_{720}) (**c**) NDSI(R_{940}, R_{570})

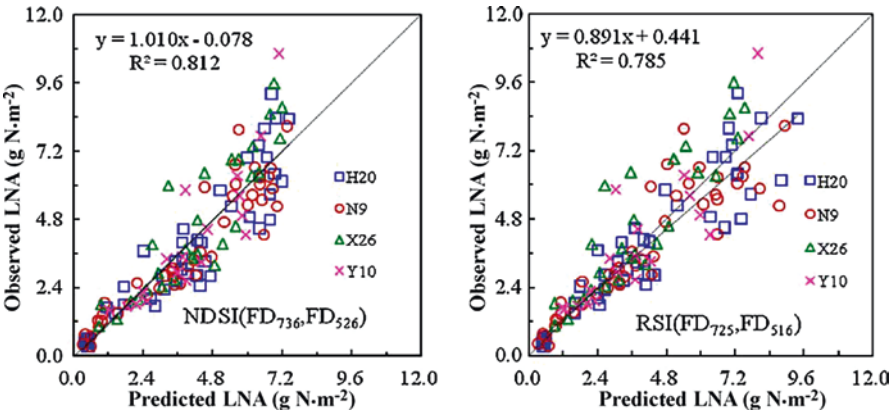

Fig. 5.4 1:1 relationship between the predicted and observed LNA in wheat from two models based on NDSI (R_{860}, R_{720}) (n = 134)

models. It can be seen that the overall performance was excellent with all estimation models on LNA.

The monitoring models derived with NDSI (R_{860}, R_{720}) had good performance with R^2 of 0.83, RRMSE of 0.25, and slope of 0.93, respectively. The 1:1 plotting with the observed and predicted values well exhibited the reliability and accuracy of the derived models, as shown in Fig. 5.4.

5.3 Real-Time Diagnosis of Crop Growth

5.3.1 Diagnosis of Crop Nutrient Status Based on Nutrient Balance Principle

The principle of fertilization application based on nutrient balance was first proposed by the famous American soil chemist Truog E. at the Seventh International Soil Society in 1960 (Truog 1960) and then developed and applied to crop production by Stanford (1973). The nutrient balance method is also called the target yield method. The target yield-based fertilization model is a typical representative of the soil test fertilization model. The core of the target yield method is to calculate the amount of fertilizer applied under the specific yield, ecological area, and cultivation conditions according to the balance of nutrient input and output. The target yield method is developed from the traditional nutrient balance method, which is one of the most commonly used methods all over the world (Du et al. 2012). The principle is that the nutrients absorbed by crops come from soil and fertilizer, and the difference between the total fertilizer requirement of the crop and the amount of fertilizer supplied by the soil is the amount of fertilizer to achieve the target yield (Eq. 5.5):

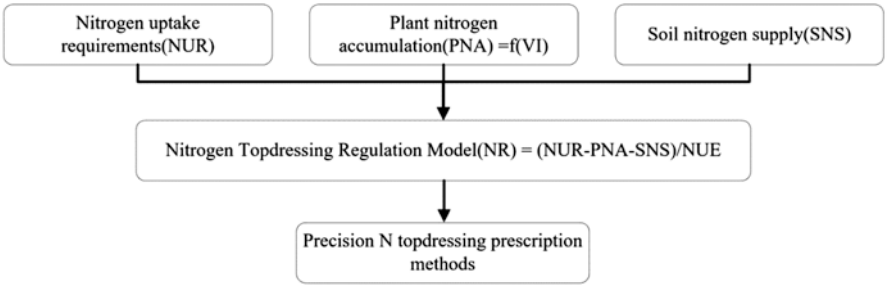

Fig. 5.5 Precision topdressing nitrogen technology based on nutrient balance method

$$\text{Topdressing N rate} = \frac{\left(\begin{array}{c}\text{N uptake per unit yield} \times \text{Yield goal} - \\ \text{Soil N supply} \times 2.25 \times \text{Correction coefficient}\end{array}\right)}{\left(\text{Nutrient concentration of N fertilizer} \times \text{Inseason N use efficiency}\right)} \tag{5.5}$$

The target yield is the planned yield, which is the fundamental basis for determining the amount of fertilization. The design of the target yield is the premise and basis for achieving quantitative crop management. The current target yield design in production mainly includes "determining yield by land," "determining yield by water," or setting the average yield in the past three years or revising the production potential of light and temperature as the target yield. The supply of a certain nutrient in the soil is obtained by converting the soil test value, and the correction coefficient of the effective soil nutrient is obtained through field experiments. The test shows that the correction coefficient is not a fixed value. It has a significant negative correlation with the soil test value and has a great relationship with the soil type and texture. In the early 1980s, the Shanghai Research Institute of Chemical Industry introduced the "soil effective nutrient correction coefficient" from the Indian literature (Ramamoorthy 1967). The corrected soil nutrient measured values were used instead of field test to calculate soil supply, which promoted the nutrient balance method in the south of the Yangtze River Region. The National Engineering and Technology Center for Information Agriculture of Nanjing Agricultural University has constructed a crop growth diagnosis and regulation model based on the principle of nutrient balance method (Fig. 5.5; Zhang et al. 2020). The experiments show that when using the nutrient balance method to recommend fertilization, the coefficients in the calculation (such as the effective nutrient correction factor for the soil, and the utilization rate of the fertilizer in the season) use general constants. Research shows that each parameter changes dynamically under different conditions. Only through scientific experiments to find the quantitative relationship between each subitem and the measured value of soil nutrients can we get the appropriate recommended fertilization amount.

5.3.2 Diagnosis of Crop Nutrient Status Based on Nitrogen Index Method

1. Nitrogen Sufficiency Index

Nitrogen sufficiency index (NSI) is defined as the ratio of the chlorophyll meter reading of a field to the chlorophyll meter reading of the well-fertilized field. When the nitrogen sufficiency index is less than 0.95, it is considered that the crop nitrogen status is deficient, and then fertilizer should be added. When the index is greater than 0.95, it is considered that the crop nitrogen status is sufficient and no topdressing nitrogen is required. This nitrogen nutrition diagnosis method based on NSI eliminates the influence caused by different varieties, growth and climatic conditions, plant diseases, and other factors on chlorophyll meter readings through normalization. However, there are still two problems that need to be further studied when applying the NSI concept to nitrogen nutrition diagnosis: for different crops in different regions or growth periods, when the NSI means nitrogen deficiency or surplus, as shown in Table 5.1, which lists the research results of some scholars on NSI. If a nitrogen deficiency has been determined, it is necessary to determine the amount of nitrogen fertilizer that is applied to achieve the maximum yield.

2. Nitrogen Response Index

Johnson and Raun (2003) proposed the application of the nitrogen response index (NRI) to guide the management of nitrogen fertilizer. This index is essentially the reciprocal of the nitrogen sufficiency index (NSI). Therefore, to calculate this index, the well-fertilized plots are set as the reference fields. The results of the study suggest that if the response of crops to the nonnitrogen limitation plots is obvious compared to other plots, the NRI value should be relatively high. There is a greater chance of indicating a nitrogen response during the crop growing season, otherwise in contrast. Some studies have pointed out that it is not necessary to add any nitrogen fertilizer when NRI is 1, because this means that the target field has the same nitrogen nutrition status as the reference field. However, is a NRI value greater than 1 signifies a nitrogen deficiency? For different crops in different regions or growth periods of the same crop, the threshold of nitrogen response index needs to be further studied to better diagnose the nitrogen nutrition status during the crop growing season.

Table 5.1 Previous studies about nitrogen sufficiency index (NSI)

Crop	Threshold	Growth stages	Topdressing N/(kg/ha)	Reference
Maize	0.95	V6-VT, one time a week	22	Peterson (1993)
	0.97	V10-VT	30–100	Sawyer et al. (2011)
Rice	0.90	14 days after transplanting to flowering stage, one time a week	30	Hussain et al. (2000)

3. Nitrogen Nutrition Index

Plant nitrogen-based critical concentration index represents the minimum nitrogen concentration required to obtain the maximum aboveground biomass under specific time and soil types. More and more studies proved that plant nitrogen concentration decreases when there is an increase of aboveground biomass, and the relationship of these two indexes can be described by the dilution curve $N = aW-b$ during the crop growth period. In this equation, W represents the aboveground biomass of the plant (Mg/ha), N means the aboveground plant nitrogen concentration (%), a is the nitrogen concentration when the aboveground biomass is 1 Mg/ha, and b represents the dilution factor of this curve.

According to the correlation diagram between plant nitrogen and aboveground biomass, if the crop is short of nitrogen under a certain amount of biomass, the actual plant nitrogen concentration should be less than the critical nitrogen concentration of plants and located below the critical nitrogen concentration dilution curve. On the contrary, the actual plant nitrogen concentration should be greater than the critical nitrogen concentration and located above the curve. Researchers developed the concept of the nitrogen nutrition index (NNI) based on this rule, which means the ratio of the actual plant nitrogen concentration to the critical one. When NNI is equal to 1, it means that nitrogen application is appropriate. When NNI is less than 1, it means insufficient, and when NNI is greater than 1, it means excessive.

In recent years, NNI has been considered as the best indicator to diagnose the nitrogen nutrition status of plants (Lemaire et al. 2008; Tremblay et al. 2011), which can accurately diagnose the nitrogen nutrition status of crops. Nevertheless, since the determination of NNI needs to be obtained through destructive field sampling, it is not suitable for real-time nitrogen nutrition diagnosis. Many scholars estimate NNI accurately based on the nondestructive remote sensing technology (Mistele and Schmidhalter 2008), which has laid a solid foundation for nondestructive and real-time nitrogen nutrition diagnosis. However, the critical nitrogen concentration dilution curves of crops were variable for different regions (environment conditions such as climate) and even for different varieties of the same crop (Yao et al. 2014), which requires the establishment of critical nitrogen concentration dilution curve suitable for the local climate conditions and varieties before applying NNI as a nitrogen nutrition diagnosis. Otherwise, the diagnosis result based on the NNI will not accurately reflect the nitrogen nutrition status of the crop.

About the recommended fertilization algorithm based on NNI, the deficiency or the topdressing nitrogen amount is calculated by the correlation between NNI and the nitrogen application amount, and NNI also shows an upward trend with the increase of nitrogen application amount (Xue and Yang 2008). However, in this algorithm, the calculation of NNI is not determined by measuring the ratio of the actual plant nitrogen concentration to the critical one, but through the ratio between the NDVI values obtained from plots in need of topdressing and plots without nitrogen fertilizer restriction, which is consistent with the concept of the sufficient index described above. Xue and Yang (2008) analyzed the correlation at the stage of young panicle differentiation between the change amount of NNI and the nitrogen fertilizer variable (the amount of nitrogen fertilizer increased and decreased compared with the standard nitrogen treatment), which showed that the relationship

conformed to the exponential growth model ($Y = a \times (1-bX)$), and determination coefficient is as high as 0.92, based on which nitrogen fertilizer can be recommended. However, the model is only based on one-year data in 2004 and needs to be refined over many years' data.

Scientists all over the world have established the critical nitrogen concentration dilution curves of different crops in different regions; thus, the NNI of different crops can be calculated, and the remote sensing technologies of different scales have been applied directly or indirectly to estimate NNI (Cao et al. 2013); the next step is to develop nitrogen fertilizer recommendation algorithms based on NNI.

5.3.3 Diagnosis of Crop Nutrient Status Based on Indicator Difference Method

The index difference method is a method to diagnose the growth and nutritional status of crops after comparing the observed values of the indicators with the ideal values of the indicators (Fig. 5.6). When the degree of the difference exceeds a certain range, it is necessary to carry out corresponding management and regulation of crop growth through fertilization or irrigation.

5.3.3.1 Dynamic Changes of Leaf Area Index

Leaf area index (LAI) is an important parameter which is necessary for studying crop photosynthesis, transpiration, the relationship between photosynthesis and transpiration, water use, and forming the basis of productivity. During the whole growing period, the LAI dynamics gradually increased with the progress of the growing process, reached the maximum at the booting stage, and then slowly decreased. At different yield levels, as the yield increased, the LAI of wheat continued to increase. The suitable maximum LAI of typical varieties is different at different ecological points and varies due to differences in various characteristics and climatic conditions. The dynamics of a suitable LAI of the same variety at the same ecological point increases with the increase of yield levels. Wood et al. (2003) developed a management strategy for variable fertilization based on crop canopy

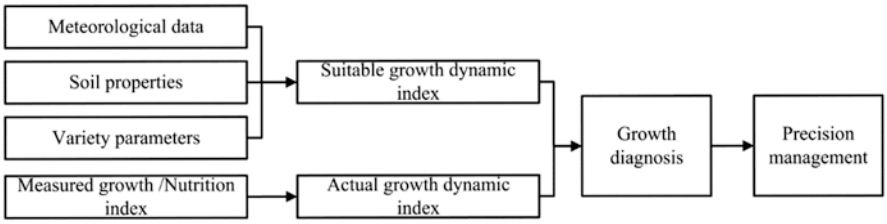

Fig. 5.6 Crop growth diagnosis technology based on indicator difference method

size, that is, the green area index (GAI), based on the experience of high-yield wheat cultivation in the UK. If the current crop GAI is greater than the target value, the fertilization amount is lower than the standard amount or no fertilization. If the current crop GAI is less than the target value, the fertilization amount is higher than the standard amount. The amount of dietary supplement is equal to the product of the amount of nitrogen required per unit of GAI, and the value of GAI increases or decreases. The specific calculation steps are as follows:

1. Set the target value of the GAI, such as GAI = 6.5.
2. Determine the current GAI of the crop, such as GAI = 2.5.
3. Calculate the difference between the target value and the current value, such as 6.5−2.5 = 4.0.
4. Assume that for each unit of GAI produced, the crop canopy nitrogen requirement (CNR) is 30 kg N ha^{-1}.
5. Calculate the amount of nitrogen fertilizer required to reach the target GAI, which is 4.0 × 30 = 120 kg N ha^{-1}.
6. Determine the soil inorganic nitrogen supply (e.g., 75 kg N ha^{-1}), and subtract the soil supply from the total nitrogen fertilizer requirement, which is 120−75 = 45 kg N ha^{-1}.
7. Assuming that the average recovery rate of nitrogen fertilizer is 60%, in order for crops to absorb 45 kg N ha^{-1} nitrogen fertilizer, 90 kg N ha^{-1} nitrogen fertilizer is required.

Wood et al. (2003) showed that applying the abovementioned fertilization recommendation algorithm to variable fertilization instead of the traditional uniform fertilization can not only reduce the nitrogen surplus but also increase economic benefits. Xue and Yang (2008) further developed a rice nitrogen fertilizer recommendation algorithm based on the LAI according to the GAI method. However, the application of the above algorithm needs to accurately estimate the GAI or LAI based on remote sensing technology. In addition, it is also critical to accurately estimate the amount of nitrogen fertilizer required for each unit of GAI or LAI produced.

5.3.3.2 Dynamic Changes of Spectral Index

With the growth process moving forward, the agronomy indicators that describe the growth of plants changed. The change of those indicators usually goes through a slow grow period, a relatively stable period, and then a slow decline period, and its dynamic change can be simulated by quadratic polynomial, ratio model, modified Gaussian model, lognormal model, beta equation, logistic equation, and modified logistic equation.

Spectral indices, which indicate the variability regulation of vegetation in some way, are the different waveband constitutions of linear or nonlinear combination or spatial transformation of satellite remote sensing and other multispectral data, like NDVI and RVI. Spectral indices can be used for quantitative monitoring of crop population size, growth status, nutritional status, etc., and change along with the

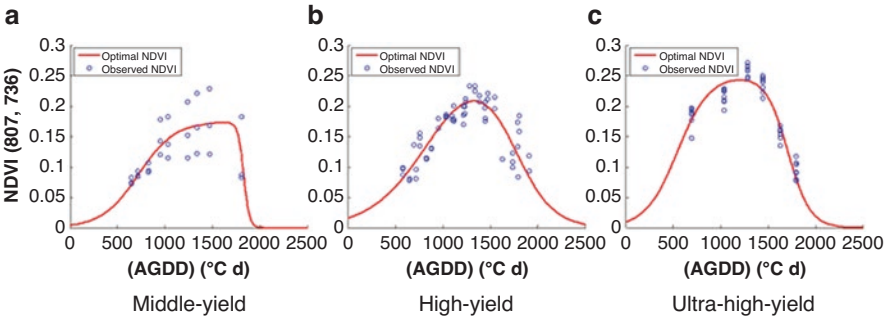

Fig. 5.7 Dynamic changes of nitrogen uptake vegetation index NDVI (807, 736) of wheat plants under different yield levels (**a**) Middle-yield (**b**) High-yield (**c**) Ultra-high yield. (Yao 2012)

Table 5.2 Model parameters of NDVI (807, 736) double logistic model under different yield levels

Yield levels	y_{max}	k_g/(m^{-2} °C^{-1} d^{-1}) (×10^{-3})	t_g/(°C d)	k_s/(m^{-2} °C^{-1} d^{-1}) (×10^{-3})	t_s (°C d)	R^2	RMSE
Middle yield	0.17	5.19	720.92	2.09	1841.95	0.989	0.0018
High yield	0.25	3.74	786.76	5.40	1786.92	0.937	0.0044
Ultrahigh yield	0.25	5.48	542.66	8.42	1706.41	0.981	0.0048

growth stage. Logistic model and Richard model function are used to fit the dynamic change of spectral indices in order to simulate the growth status of different crop groups and then provide theoretical guidance for subsequent growth diagnosis and fertilizer regulation.

Figure 5.7 shows the dynamic changes of nitrogen uptake-sensitive vegetation index NDVI (807, 736) of wheat plants under different yield levels (Yao 2012). As seen from the figure, with the increase of AGDD (accumulated growing degree day), the NDVI (807, 736) at various yield levels showed a change law of first increase and then decreased. At the same time, they are combined with the growth law of crops and dynamic changes based on dual logistic model fitting. Table 5.2 shows the fitted NDVI (807, 736) double logistic model coefficients at different output levels (Yao 2012). It can be known from Table 5.2 that with the increase of the output level, the model parameter y_{max} shows an increasing trend and reaches a stable maximum under ultrahigh production. The maximum speed k_g during crop growth also reached a maximum under ultrahigh yield, and the corresponding maximum speed k_s during fading also appeared in the case of ultrahigh yield. After further comparing the inflection point times t_g and t_s of NDVI (807, 736), the earliest time for growth and fading inflection points was found under ultrahigh yield, indicating that the crop growth process is fastest under ultrahigh yield and the crop's ultrahigh yield mainly depends on its faster growth rate. However, the growth inflection point of NDVI (807, 736) plants in mid-production was earlier than that of high yield, but the appearance of decline inflection point was later than that of high yield, which indicates that the longer growth process of high-yield fields makes their yields higher than normal midfield.

At the same time, according to the statistical indicators of the fitted model, it can be known that the dual logistic model for fitting the change of nitrogen absorption index of the plant has high accuracy, and the R^2 of the model is greater than 0.93, and the RMSE is less than 0.005 (Table 5.2).

The appropriate crop growth curve is a useful tool for scientific crop management. Under the three divided yield levels, a suitable dynamic change model of the plant nitrogen uptake index NDVI (807, 736) was fitted by a dual logistic model, and the results showed that the model had higher fitting accuracy. Through the established model, the users can obtain the appropriate NDVI value at each time point in the crop growth process according to the different target yields, which can be compared with the actually measured vegetation index. Then the nitrogen fertilizer control measures can be taken. By using AGDD as a time axis to build a model, the effects of different years and ecological points on wheat growth can be eliminated. At the same time, the model has fewer parameters and has practical biological significance.

Some studies take rice as the research object and have established a high-yield rice population dynamic model based on NDVI value to achieve a real-time diagnosis of the dynamics of high-yield population indicators (Liu et al. 2017). Figure 5.8a, b shows the dynamic changes of rice canopy NDVI under different nitrogen fertilizer treatments. The canopy NDVI value of rice varies similarly with variety and nitrogen levels. The NDVI value rises rapidly before reaching its peak and slowly rises as it approaches the summit. These values stabilize after reaching a peak and then gradually decrease. Both rice varieties reached the maximum NDVI value at the booting stage.

The relative NDVI (RNDVI) dynamic model of japonica and indica rice at different production levels was constructed using the double logistic method (Fig. 5.8c, d; Liu et al. 2017). The NDVI dynamic determination coefficients (R^2) of the two types of rice were above 0.86. RNDVI dynamic models of indica and japonica rice at different yield levels showed similar trends. However, there are some differences in the simulation dynamics of NDVI. The more significant the output potential, the higher the rising rate before the NDVI peak, the longer the NDVI peak platform, and the lower the falling rate after the peak.

5.4 Ground-Based, UAV-Borne, and Satellite Remote Sensing for Crop Nutrient Management

5.4.1 Ground-Based Monitoring Systems for Crop Nutrient Management

Nanjing Agricultural University in Nanjing, China, developed a crop growth sensor based on crop spectral properties (Ni et al. 2018). The crop growth sensor uses sunlight as a light source and is structurally divided into an upward light sensor and a

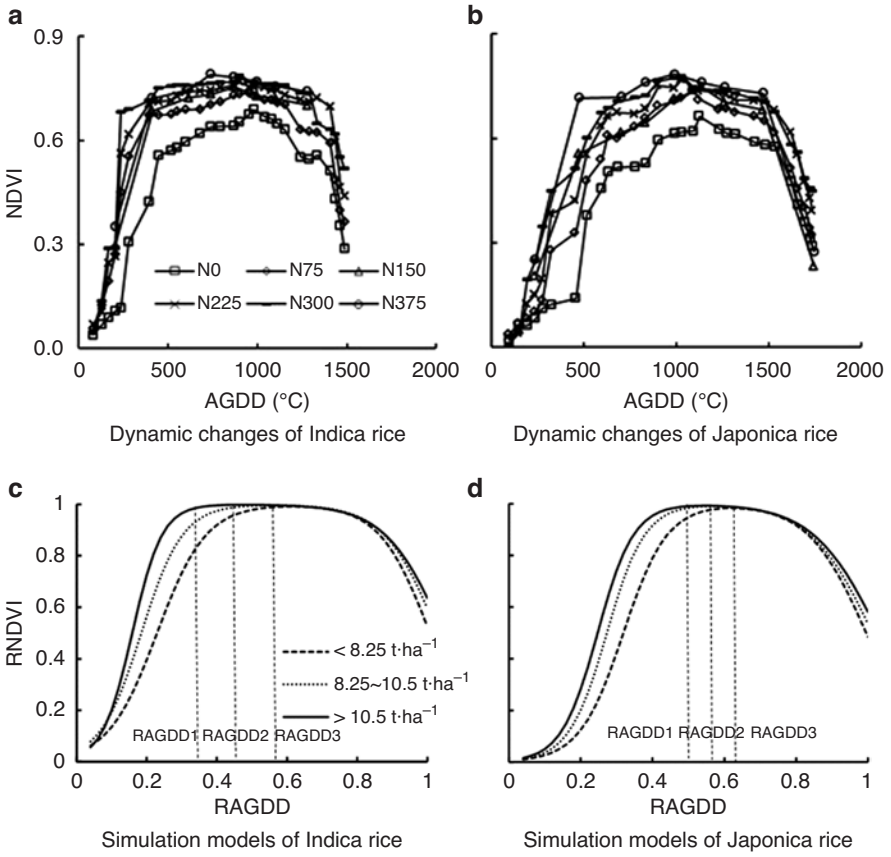

Fig. 5.8 Dynamic changes and simulation models of canopy NDVI under different nitrogen treatments (**a**) Dynamic changes of Indica rice (**b**) Dynamic changes of Japonica rice (**c**) Simulation models of Indica rice (**d**) Simulation models of Japonica rice. (Liu et al. 2017)

downward light sensor. The upward light sensor is used to receive the radiation information of sunlight at 720 nm and 810 nm bands, and the downward light sensor is used to receive the reflected light radiation information of the crop canopy in the corresponding band. Then the information is converted into an electrical signal by a photodetector for processing to obtain the characteristics of the crop canopy spectral reflectance. Based on canopy reflectance and coupled with a crop growth model, the crop growth information such as leaf nitrogen content, LNA, LAI, and leaf dry weight can be obtained (Ni et al. 2013). The sensor device adopts an integrated design, which is convenient for integration and transplantation and suitable for field test environments. As shown in Fig. 5.9, the portable crop growth monitoring sensor consists of a multispectral sensor, a signal processing circuit, a processor system, a sensor support, a spirit level, a support rod, and other components.

Fig. 5.9 Outlook of crop growth monitoring sensor. (Ni et al. 2018)

The key components of the crop growth monitoring sensor include two systems, signal conditioning system and signal processing system.

1. Signal Conditioning System

The electric signals transmitted by the optical signal sensing system are converted, amplified, filtered, etc., so that they can meet the requirements to be processed by the subsequent microcontroller. By selecting the appropriate electronic components and designing suitable circuits based on the performance parameters of the photoelectric converter and the output signal characteristics of the multispectral sensor, the amplification and filtering of weak signals can be achieved.

2. Signal Processing System

The signal transmitted by the first amplifier is processed to obtain the reflectance data. The realization of the final reflectance depends on the microprocessor, and the primary considerations in the selection are low power consumption, small size, and suitable for signal acquisition and processing.

The multispectral sensor is a critical part of the system. The narrowband interference filter is used as the spectral filter. The material is optical glass, the center wavelength is the characteristic wavelength ±2 nm, the center wavelength transmission is 65–70%, the peak transmission is 65–70%, the bandwidth is 9 nm, and the cutoff rate is less than 0.00001%. It can not only dramatically inhibit the spectral information of other bands from entering the detection lens and improve the measurement accuracy of the sensor but also ensure the consistency of sensor sensitivity. The

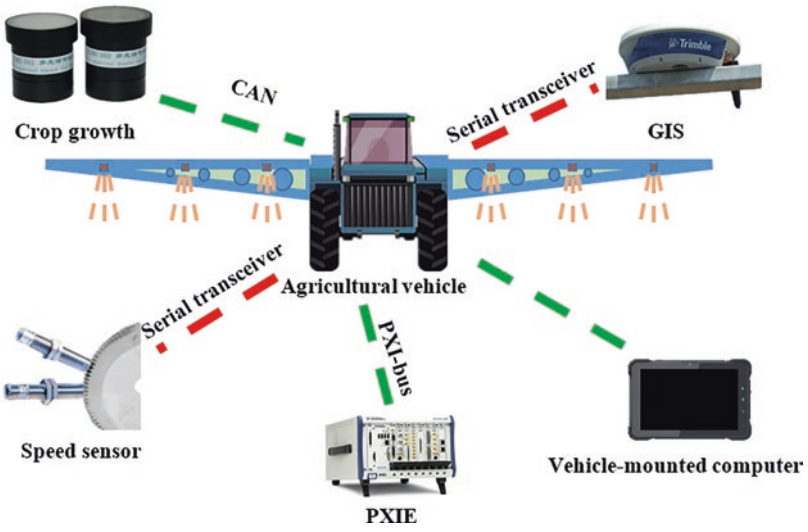

Fig. 5.10 Schematic diagram of the vehicle-mounted crop growth monitoring system

photodetector is a photodiode with a spectral response range of 400–1100 nm, a sensitivity of 0.55 A/W, and a maximum short-circuit current of 120 μA. The two photodetectors are packaged on the same base, which enhances the reliability of the system.

Compared to the portable sensors, the vehicle-mounted crop growth monitoring system has the advantages of full coverage, high throughput, and rapid information acquisition. It can acquire real-time crop growth information through the different sensors mounted on the vehicle. After calculation and calibration, the information will be used to support crop field management, such as fertilization and irrigation.

Figure 5.10 shows the overall structure of a vehicle-mounted crop growth monitoring system, which can work based on real-time online field sensing, data analysis, and guidance variable fertilization requirements. The information sensing part includes crop growth sensors, speed sensors, and GPS. The data acquisition and processing part includes signal conditioning modules, data processing modules, data transmission modules, and the monitoring software system. The signal conditioning module, data processing module, and data transmission module are integrated into a sensing node. The measured object is converted into an electrical signal by the sensor. Various types of data are summarized to the data node for processing through the transmission network and finally sent to the upper layer software system for human-machine interaction. The data during the collection process will be stored in a third-party database.

The vehicle-mounted system is equipped with a passive light source crop growth multispectral sensor. It obtains the crop canopy reflection information at two sensitive bands, 730 nm and 815 nm. It uses the sensing hardware to perform photoelectric conversion to generate an electrical signal that indirectly reflects the crop growth

information. It is necessary to extract and further optimize the signal content according to the needs and obtain useful information. Through algorithmic calculations, various parameters that respond to crop growth, such as NDVI, can reflect the crop growth information directly.

Due to various equipment on the vehicle platform, electrical isolation between the instruments and equipment is needed to avoid the impact of agricultural machinery vibration on the sensing signals. The acquisition and stable transmission of field crop growth information require multisensor parallel transmission and reception without interference from each other to ensure the information network. In response to these problems, the CAN (Controller Area Network) bus transmission scheme is used to design a vehicle-mounted information network, which has the advantages of high accuracy, good stability, low power consumption, low cost, long transmission distance, and fast speed.

Wireless sensor networks (WSN) are self-organized into a multi-hop monitoring network by wireless communication in a large number of inexpensive miniature sensor nodes deployed in the monitoring area. Based on the actual needs of farmland information collection, a fast and real-time, nondestructive, large-scale acquisition system of crop growth information (leaf dry weight, LAI, leaf layer nitrogen content, and nitrogen accumulation) and environmental data (canopy temperature, canopy humidity, canopy carbon dioxide concentration, soil temperature, and soil water content) was developed (Pang 2014). It can collect environmental parameters that affect the growth of crops, as well as the growth parameters of the crops themselves so that more accurate plant diagnosis and regulation can be carried out to help farmers scientifically improve overall agricultural benefits.

Considering the wide area, openness, harsh environment, and inconvenient maintenance of farmland, the designed collection node must be able to communicate wirelessly, and it must be less affected by the environment and low power consumption and can work stably for a long time. The hardware structure of the collection node is shown in Fig. 5.11a.

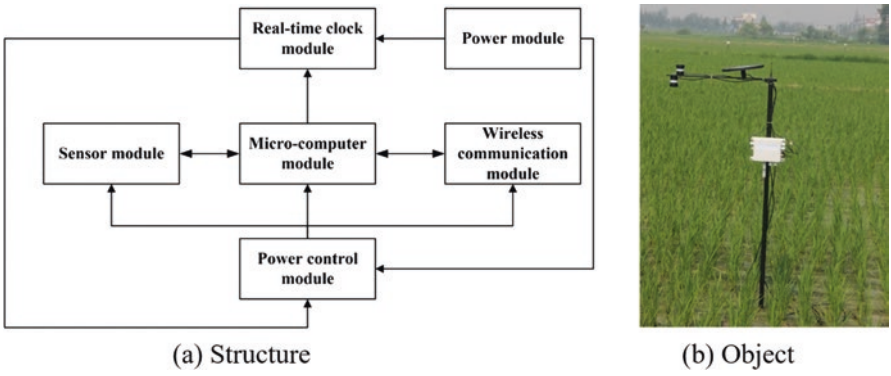

Fig. 5.11 Wireless crop growth information sensor node (**a**) Structure (**b**) Object. (Pang 2014)

A SHT71 digital integrated temperature and humidity sensor is selected in the collection node. The SHT71 integrates functions such as humidity detection, temperature detection, signal conditioning, 14-bit A/D, and heater on a single chip. It adopts unique industrial CMOS (complementary metal-oxide semiconductor) technology to ensure extremely high reliability and long-term stability. The soil moisture sensor chooses HL-TR01, which is a high-precision, high sensitivity soil moisture sensor based on the principle of frequency domain reflection and manufactured using high-frequency electronic technology. By measuring the dielectric constant of the soil, it can directly and stably reflect the volume percentage of real moisture in different types of soils.

The soil temperature sensor is packaged by a single-wire digital temperature sensor DS18B20 produced by the American DALLAS Semiconductor Company with an external 1.5-meter cable. DS18B20 can achieve temperature measurement in the range of −55–125 °C, and the error is within ±0.5 °C. The calculated value of the field temperature is transmitted through serial communication, which can fluctuate in the range of 3~5.5 V. The CO_2 module uses the MH-Z14 nondispersive infrared sensor. It combines mature infrared absorption gas detection technology with precise optical path design and sophisticated circuit design to create a general-purpose infrared gas sensor. Using nondispersive infrared (NDIR) principle to detect CO_2 in the air, it has good selectivity, no oxygen dependence, and long life. The assembled crop growth information sensor is shown in Fig. 5.11b.

5.4.2 UAV-Borne Monitoring System for Crop Nutrient Management

As a new remote sensing platform, the unmanned aerial vehicle (UAV) has its unique advantages in flexibility and resolution compared with traditional satellite and aviation remote sensing, and the data has higher accuracy. The application of UAV-borne technology in remote sensing meets the needs of information acquisition and application in modern agriculture, improves the spatial-temporal dimension of remote sensing technology, and provides technical support for various agricultural information acquisitions and decision-making.

A UAV-borne multispectral crop growth sensor is developed by Nanjing Agricultural University in China (Ni et al. 2017; Yao et al. 2019). After investigating the monitoring method of the UAV-borne sensor based on its spectral monitoring mechanism and structural design features, and analyzing the spatial distribution characteristics of the airflow field under the low-altitude hovering operation of the UAV, the UAV-borne crop growth monitoring system is built to achieve high-throughput and real-time access to rice and wheat growth information.

The multispectral crop growth sensor is equipped with a dual-band detection lens, uses sunlight as the light source, and has a test field of view of 27°. It is packaged in a nylon case and weighs 11.34 g. The crop canopy ratio vegetation index

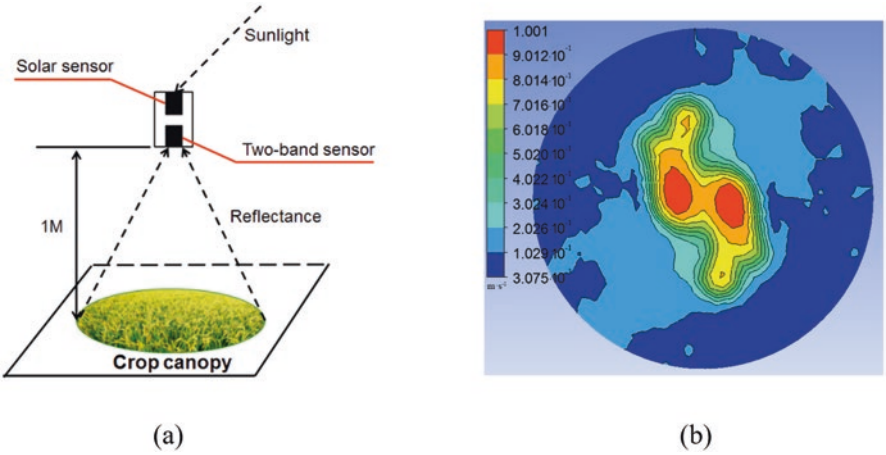

Fig. 5.12 UAV-borne multispectral crop growth sensor (**a**) Multispectral crop growth sensor test (**b**) Ground velocity nephogram distribution. (Ni et al. 2017)

(RVI) can be an output in real time. The utility model utilizes a photosensitive element to realize high-fidelity energy conversion of light energy to electric energy, and the structure can be divided into an upward light sensor and a downward light sensor. The upward light sensor is used to acquire radiation information of sunlight at wavelengths of 730 nm and 815 nm, and the downward light sensor is configured to receive crop canopy-reflected light radiation information of a corresponding wavelength. The test needs to be carried out in clear, windless, and cloudless weather. The test height needs to be maintained at 1.0~1.5 m above the crop canopy. The test field of view is aimed vertically downward, and the crop canopy remains relatively static. The test schematic is shown in Fig. 5.12a. The physical parameters such as the UAV flight area, rotor rotation speed, and rotor rotation direction were set by CFD (computational fluid dynamic) software, and the UAV hovering-operation-state simulation analysis was carried out. In the grid simulation area with a diameter of 1.2 m and a height of 1.85 m, the velocity of each grid node is composed of the transverse velocity component, the longitudinal velocity component, and the axial velocity component. The flying height of the UAV was set to 1 m from the ground, and the ground velocity nephogram distribution result was displayed by CFX's own post-processing module, as shown in Fig. 5.12b.

The velocity intensity in Fig. 5.12b was analyzed. The results of the combined velocity nephogram distribution show that, due to the opposite rotation of the two pairs of rotors of the quadrotor UAV, the forward-rotating rotors generate a downwash flow, so the region with the highest wind speed is distributed directly below the two forward-rotating rotors, and the wind speed gradually decreases toward the periphery and is also distributed in an elliptical shape. The long semiaxis of the region is about 0.35 m, and the short semiaxis is about 0.3 m.

According to the CFD numerical simulation analysis and the actual test results of the three-dimensional airflow field, combined with the test field of view of the multispectral crop growth sensor, when the multispectral crop growth sensor was

deployed 60 cm away from the rotors of the UAV, the test area of the crop canopy retained Lambert characteristics, and measurement results were not affected by the airflow field, enabling normal testing. Therefore, a carbon fiber support with a length of 60 cm was designed; one end of the support was fixed to the UAV, and the other end was equipped with a sensor, and they were connected by a cantilever beam structure.

In order to avoid the vibration impact of the high-speed rotation of the rotors on the multispectral crop growth sensor and the support during the flight, a damping rod was designed to provide shock absorption in order to maintain the stable state of the support and the multispectral crop growth sensor. The support and the damping rod were fixed by a triangular structure to improve the overall stability and shock resistance. The angle between the support and the damping rod is very important for the stability of the structure and the balance performance of the aircraft. Therefore, the optimal value of the angle was calculated by static equation analysis.

Taking the sensor support as the research object, the analysis diagram of the force sustained by the support is shown in Fig. 5.13a, b. AB is the sensor support,

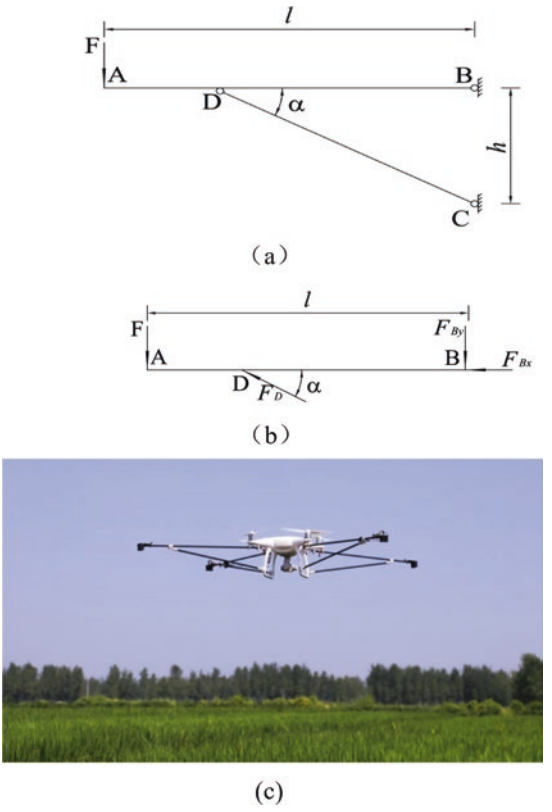

Fig. 5.13 Analysis of the force sustained by UAV sensor support (**a**) Schematic diagram of the structure of support and damping rod (**b**) Analysis of the force sustained by each part of the support (**c**) UAV-borne spectroscopy sensor with the support rod. (Yao et al. 2019)

CD is the support damping rod, points C and D are the fixed points of the sensor support and the damping rod at the end of the UAV, and the force sustained by the sensor support is analyzed by static equations:

$$F = -F_{By} + F_D \sin\alpha \tag{5.6}$$

$$F_D \cos\alpha = -F_{Bx} \tag{5.7}$$

$$Fl = F_D \sin\alpha \cdot \frac{h}{\tan\alpha} \tag{5.8}$$

Simultaneous calculations were performed on Eqs. (5.6), (5.7), and (5.8) to obtain the following:

$$F_D = \frac{Fl}{h\cos\alpha} \tag{5.9}$$

$$F_{Bx} = -\frac{Fl}{h} \tag{5.10}$$

$$F_{By} = F\left(\frac{l}{h}\tan\alpha - 1\right) \tag{5.11}$$

In Eqs. (5.8, 5.9, 5.10, and 5.11), F_D is the internal force of CD; F_{Bx} and F_{By} are the reaction forces in the horizontal and vertical directions of fixed point B, respectively; α is the angle between AB and CD; h is the height difference between fixed points B and C; and l is the length of AB.

When the length of the UAV support is 60 cm, the value of α ranges from 9.5° to 90°. Since a certain length of the support needs to be used for fixing the UAV and multispectral crop growth sensor, the actual value range of α is 13°–90°. From the derivation results of Eqs. (5.9, 5.10 and 5.11), it can be seen that F_D and F_{By} decrease with the decrease of α, and the smaller the values of F_D and F_{By}, the more stable the force sustained by the support structure. Therefore, the optimal angle between the sensor support and the damping rod is 13°. Figure 5.13c shows the field operation of the UAV-borne spectroscopy sensor.

5.4.3 *Satellite-Based Remote Sensing Systems for Crop Nutrient Management*

Since the twentieth century, satellite remote sensing technology has been widely used in many fields for practical applications. Agriculture is one of the most important fields in the application of remote sensing technology. As China's agricultural production shifts toward intensification, there is an urgent need for spatial

information, especially for dynamic, large-scale, fast, and timely remote sensing information during crop production. The application of agricultural remote sensing in China mainly involves the establishment of a remote sensing monitoring platform for agricultural conditions, the inversion of farmland radiation and remote sensing of agronomic parameters, crop remote sensing classification and identification, crop yield and quality prediction, agricultural remote sensing monitoring systems, model and application, and so on. With the development of space science and technology, agricultural remote sensing has gradually formed a development trend of combining low-level, medium-level, high-level, and multilevel and static and dynamic mechanism and application and the widespread use of remote sensing and information technology. Promote the development of agricultural production management in the direction of quantification, precision, and intelligence, and the level of agricultural science and technology is gradually increasing.

With the development of space detection technology, the performance of optical sensors has been continuously improved, and satellite imaging systems with higher spatial resolution and faster return periods have been launched in succession. In recent years, satellites such as Sentinel-2 A/B, GF-1 A/B/C/D, and Planet have appeared. The temporal, spatial, and spectral resolutions of Earth observation satellites have been improved to varying degrees to obtain crop growth. The ability of information is gradually strengthened, and there is a trend of free data. The number of high-scoring images has proliferated in a short period. The traditional crop growth monitoring model has been completely subverted, and crop growth monitoring has begun to enter the era of big data. It is foreseeable that shortly satellite-based crop growth monitoring technology will certainly usher in new development opportunities.

Satellites are the most effective remote sensing platform for large-scale Earth observation. Since the launch of the first land resource satellite, Landsat-1, in 1972, the number of satellite images has a trend of explosive growth. The emergence of massive satellite image data has provided new development opportunities for large-scale crop growth monitoring. Remote sensing image data obtained through different satellite platforms have been widely used in crop identification, crop growth parameter estimation, and many other fields. The transformation of agricultural modernization has played a huge role. Land resource satellites have multiple classification methods. According to the imaging principle, the most commonly used land resource satellites currently include two types: optical and radar satellites. According to spatial resolution, land resource satellites mainly include three types of high spatial resolution, medium spatial resolution, and low spatial resolution (Mulla 2013; Onojeghuo et al. 2018).

Affected by the periodic growth of crops, the main factors hindering their widespread application in agriculture are the spatial-temporal resolution and difficulty of acquiring terrestrial resources. Moreover, the challenge of acquiring satellite images is closely related to the level of their spatial-temporal resolution. High spatial resolution satellite images (referred to as high-scoring images) have prominent spatial details, which can more realistically reflect the spatial distribution characteristics of farmland and is of great significance for crop growth monitoring in small and

broken fields. Unfortunately, most of the high-scoring satellites currently use commercial operations. These methods have some common problems. For example, images must be acquired in a predetermined way through programming, the acquiring period is not fixed, the time resolution is low, and the price is high. The problem is particularly serious in the acquisition of submeter high-scoring images such as WorldView-2/3 and Pleiades. However, with the enhancement of space observation capabilities, many problems in the acquisition of high-resolution images are greatly improved. The high-resolution images from high-resolution satellites, GF-1, GF-2, GF-6, and other meter/submeter satellites, can be quickly released in a short period with the Internet. We can use a variety of channels to restrict the acquisition of meter-level images in the target area. The cost of acquiring meter-level images has dropped significantly. The ground observation capabilities of such satellites have been revolutionarily improved, making these images grow in crops. The monitoring field shows great application potential (Chen et al. 2019). Although medium and low spatial resolution satellite images (referred to as low- and medium-resolution images) show many disadvantages in terms of space, such satellites have a short return period, a fixed imaging period, and more precious spectral information. The official websites of the US Geological Survey (USGS) and European Space Agency (ESA) and other sites have free access to low- and medium-resolution satellite images such as Landsat-8 and Sentinel-2. The advantages of data acquisition and spectral information overcome some of the disadvantages of spatial resolution. They are making such images widely used in crop identification, growth parameter monitoring, productivity estimation, and other fields, which provide reliable data support for the development and improvement of crop growth monitoring (Xu et al. 2018).

Remote sensing is a data acquisition process from surface information (multidimensional, infinite real bodies) to remote sensing information (two-dimensional, limited, discrete analog information). Satellite remote sensing images are digital responses of features such as the spectrum of the ground and space. Quickly and effectively extracting satellite image information and accurately converting it into crop growth information is the purpose of crop growth monitoring using satellite images. The technology of satellite image information extraction mainly includes image preprocessing, spectral calculation, and feature transformation.

Satellite image preprocessing mainly includes radiation calibration, atmospheric correction, and image calibration. Using the calibration tools included in remote sensing image processing software such as ENVI, the head file information of the remote sensing image is automatically analyzed for radiation calibration, and the original digital value is converted into the radiation brightness value. Atmospheric correction tools such as FLAASH are used to eliminate the effects of the atmosphere and other factors through the radiative transfer model. At the same time, the radiance value is converted to surface reflectance to improve the accuracy and consistency of remote sensing images. Based on ground control points, different images are registered to eliminate geographic deviations, and finally a high-quality satellite image dataset is constructed (Deng 2010).

The vegetation index is one of the most commonly used characteristic parameters in the field of crop growth monitoring. It refers to a variety of parameters that have a certain indication of vegetation composed of a linear or nonlinear combination of spectral data. Spectral, texture, and spatial features are the three most commonly used features in satellite remote sensing images. Both single band reflectance and vegetation index belong to the category of spectral characteristics. The texture and spatial features can directly reflect the organizational structure of the image surface. The texture features can be extracted by statistical methods, signal processing methods, model methods, and structural methods (Liu and Kuang 2009), and the spatial features can be analyzed by object-oriented image analysis. Technology for mining, texture, and spatial characteristics are important information in crop classification and crop growth monitoring, and they are of great significance to the improvement of crop identification and growth monitoring accuracy. The textures and spatial features obtained by different platforms and different algorithms can effectively mine the information in the satellite image, to provide the basis for the next step in crop identification or the construction of agronomic parameter models.

Using the extracted spectrum, texture, phenology, and other information from remote sensing data, you can quickly and efficiently monitor the planting area and spatial distribution of major crops and further extract crop nitrogen nutrition and other information. Real-time monitoring of crop nitrogen content can guide variable fertilization. Monitoring on-time series can analyze crop growth changes and even affect crop yield. The principle of remote sensing estimation of crop nitrogen content is that with a certain irradiation intensity, under the action of electromagnetic waves, the nitrogen bonds of the crop chemical constituent molecules generate vibration and forming differences in spectral absorption and reflection in certain bands, showing different reflectance. These special bands are crop nitrogen-sensitive bands. By analyzing the correlation between the spectral reflectance of these sensitive bands and the crop nitrogen content, remote sensing monitoring and estimation of crop nitrogen content can be achieved.

Current research on crop nitrogen nutrition index monitoring has achieved remarkable results. However, there are still some problems to be solved urgently:

1. Improving the universality of satellite remote sensing inversion models. Among existing remote sensing estimation models, the inversion of indicators based on statistical models is relatively simple. Therefore, inversion models are often unstable and not universal. Models are often affected by crop types and local environments and need to be adjusted or even remodeled. On the one hand, the sensitive band analysis should start from the crop growth mechanism. On the other hand, the inversion method can be combined with the mechanical advantages of the physical model. Because the physical model describes the radiative transmission mechanism of light in the vegetation-soil system, the universality is relatively high, but the model is complex (Cheng et al. 2018). How to combine the advantages of the two to construct a remote sensing inversion model with high universality needs further research.

2. The fusion of multisource remote sensing data. Different remote sensing data complement each other. Real-time obtaining remote sensing data of the crop during each growth period is conducive to timely grasp of crop growth status and provides a basis for formulating field management strategies (Wang et al. 2014).

Wang et al. (2012) used the SPOT-5 HRV on March 19, 2009, and the HJ-1B CCD remote sensing image on March 22, 2009, in Anyang County, Henan Province, in conjunction with the synchronous ground sampling test. The spectral response, the accuracy of the monitoring model, and the spatial distribution of leaf nitrogen content were analyzed in three aspects. The remote sensing image monitoring effect of nitrogen in winter wheat was analyzed and evaluated. The results show that the three bands of reflectance and vegetation index of the two types of remote sensing images are closely related to the nitrogen content of wheat leaves. Among them, the optimal model vegetation index for SPOT-5 images is green NDVI (GNDVI), and the optimal model vegetation index of the HJ-1B image is NDVI. SPOT-5 image is better than the HJ-1B image in monitoring accuracy, but the difference is not large. The spatial distribution chart (Fig. 5.14) shows that the nitrogen content of winter wheat leaves in Anyang County is low in the west and high in the east, which is consistent with the actual survey and the distribution of yield levels. From the comparison of the left and right figures, the nitrogen content of wheat leaves obtained by using SPOT-5 GNDVI is slightly higher than that obtained by using HJ-1B NDVI, and it is most obvious in the central and western parts of Anyang County. Decided by the degree of fragmentation, in the case of the same degree of fragmentation, the lower the spatial resolution of the remote sensing image is, the more pixels are mixed. However, on the whole, the spatial distribution of nitrogen content in wheat leaves retrieved from the HJ-1B image is consistent with the SPOT-5 image. The SPOT-5 image inversion distribution map results are closer to the ground measurement results.

In conclusion, due to the limitation of satellite remote sensing technology, there is still a lack of remote sensing data with both high spatial resolution and high

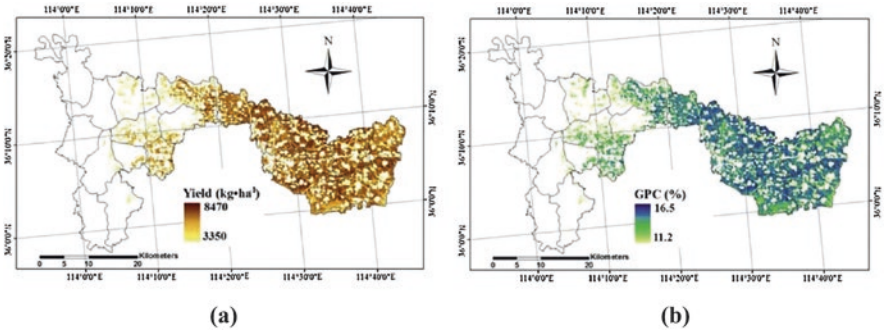

Fig. 5.14 Spatial distribution of nitrogen content in winter wheat leaves in Anyang County, Henan Province, based on SPOT-5 and HJ-1B satellite images (**a**) SPOT-5 (**b**) HJ-1B satellite images. (Wang et al. 2011)

temporal resolution, and at the same time, it is necessary to meet the needs of field crop dynamic monitoring. On the one hand, due to complex geographical conditions and the generally small scale of crop production, China has a large number of fragment fields, which makes it difficult for remote sensing images to identify different fields. Affected by the revisited period, the cloud and rain climate, high cost, etc., a limited number of effective high spatial resolution images can be obtained during the crop growth period, which makes it difficult to achieve continuous dynamic monitoring of crop growth. With the ever-increasing variety and number of ground observation platforms and remote sensing sensors, multiband, multi-polarization, and multi-scale remote sensing data sources are continuously produced. How to achieve effective fusion between multisource remote sensing data, thereby increasing the value of data utilization, and digging new information from multisource fusion data, has become a hot issue in the field of remote sensing (Huang and Zhao 2017). Therefore, multisource remote sensing data fusion is needed and then applied to crop nitrogen nutrition monitoring.

References

Bannari A, Morin D, Bonnr F, Huete AR (1995) A review of vegetation indices. Remote Sens Rev 13(1–2):95–120

Blackburn GA (1998) Quantifying chlorophylls and carotenoids at leaf and canopy scales: an evaluation of some hyperspectral approaches. Remote Sens Environ 66(3):273–285

Cao Q, Miao Y, Wang H, Huang S, Cheng S, Khosla R, Jiang R (2013) Non-destructive estimation of rice plant nitrogen status with Crop Circle multispectral active canopy sensor. Field Crops Res 154:133–144

Chen Z, Hao P, Liu J, An M, Han B (2019) Technical demands of agricultural remote sensing satellites in China. Smart Agri 1(1):32–42

Cheng T, Zhu Y, Li D, Yao X, Zhang K (2018) Hyperspectral remote sensing of leaf nitrogen concentration in cereal crops. In: Thenkabail P, Lyon J, Huete A (eds) Hyperspectral remote sensing of vegetation, second edition, four volume set, volume 2. CRC Press, Boca Raton

Deng SB (2010) ENVI Remote sensing image processing method. Sciences Press, Beijing

Du J, Bai YL, Yang LP, Lu YL, Wang L, Wang H, Wang ZY (2012) Application of nutrient balance method in soil fertilization recommendation for winter wheat. Soil Fertil Sci China 1:7–13

Gitelson AA, Merzlyak MN (1994) Spectral reflectance changes associated with autumn senescence of *Aesculus hippocastanum* L. and *Acer platanoides* L. Leaves. Spectral features and relation to chlorophyll estimation. J Plant Physiol 143(3):286–292

Gitelson AA, Merzlyak MN (1998) Remote sensing of chlorophyll concentration in higher plant leaves. Adv Space Res 22(5):689–692

Hansen PM, Schjoerring JK (2003) Reflectance measurement of canopy biomass and nitrogen status in wheat crops using normalized difference vegetation indices and partial least squares regression. Remote Sens Environ 86:542–553

Huang B, Zhao YQ (2017) Research status and prospects of spatiotemporal fusion of multi-source satellite remote sensing images. J Surv Mapp 46(10):1492–1499

Huete AR (1988) A soil-adjusted vegetation index (SAVI). Remote Sens Environ 25:295–309

Hussain F, Bronson K, Peng S (2000) Use of chlorophyll meter sufficiency indices for nitrogen management of irrigated rice in Asia. Agron J 92:875–879

Johnson G, Raun W (2003) Nitrogen response index as a guide to fertilizer management. J Plant Nutr 26:249–262

Lemaire G, Jeuffroy M-H, Gastal F (2008) Diagnosis tool for plant and crop N status in vegetative stage. Eur J Agron 28:614–624
Liu L, Kuang GY (2009) Survey of image texture feature extraction methods. J Image Gr 14(4):622–635
Liu X, Ferguson R, Zheng H, Cao Q, Tian Y, Cao W, Zhu Y (2017) Using an active-optical sensor to develop an optimal NDVI dynamic model for high-yield rice production (Yangtze, China). Sensors 17(4):672
Mistele B, Schmidhalter U (2008) Estimating the nitrogen nutrition index using spectral canopy reflectance measurements. Eur J Agron 29:184–190
Mulla DJ (2013) Twenty-five years of remote sensing in precision agriculture: key advances and remaining knowledge gaps. Biosyst Eng 114(4):358–371
Ni J, Yao X, Tian YC, Cao WX, Zhu Y (2013) Design and test of portable crop growth monitoring diagnostic instrument. Trans Chin Soc Agri Eng 29(6):150–156
Ni J, Yao L, Zhang J, Cao W, Zhu Y, Tai X (2017) Development of an unmanned aerial vehicle-borne crop-growth monitoring system. Sensors 17(3):502
Ni J, Zhang J, Wu R, Pang F, Yan Z (2018) Development of an apparatus for crop-growth monitoring and diagnosis. Sensors 18(9):3129
Onojeghuo A, Blackburn G, Huang J, Kindred D, Huang W (2018) Applications of satellite 'hyper-sensing' in Chinese agriculture: challenges and opportunities. Int J Appl Earth Obs Geoin 64:62–86
Pang FR (2014) Research on automatic acquisition of farmland information based on wireless sensor network. PhD thesis, Nanjing Agricultural University
Peterson TA (1993) Using a chlorophyll meter to improve N management. Cooperative Extension, Institute of Agriculture and Natural Resources, University of Nebraska-Lincoln, Lincoln
Ramamoorthy B (1967) Fertilizer application for specific yield targets of Sonara-64. Indian Farm 16(4):46–49
Sahoo RN, Ray SS, Manjunath KR (2015) Hyperspectral remote sensing of agriculture. Curr Sci 108(5):848–859
Sawyer JE, Lundvall J, Hawkins JS, Barker DW (2011) Sensing nitrogen stress in corn. Agriculture and Environment Extension Publications
Sims DA, Gamon JA (2002) Relationships between leaf pigment content and spectral reflectance across a wide range of species, leaf structures and developmental stages. Remote Sens Environ 81(2–3):337–354
Stanford G (1973) Rationale for optimum nitrogen fertilization in corn production. J Environ Qual 2(2):159–165
Tian QJ, Min XJ (1998) Advances in study on vegetation indices. Adv Earth Sci 13(4):327–333
Tremblay N, Fallon E, Ziadi N (2011) Sensing of crop nitrogen status: opportunities, tools, limitations, and supporting information requirements. HortTechnology 21:274–281
Truog E (1960) Fifty years of soil testing. Madison, WISC. USA. In: 7th International congress of soil science, 1960, IV(7), 46
Vogelmann JE, Rock BN, Moss DM (1993) Red edge spectral measurements from sugar maple leaves. Int J Remote Sens 14(8):1563–1575
Wang L, Wang B, Feng W, Zheng T, Feng X, Zheng G (2011) Comparative analysis of monitoring winter wheat nitrogen with SPOT-5 and HJ image. J Triticeae Crops 31:331–336
Wang L, Tian Y, Zhu Y, Yao X, Zheng G, Cao W (2012) Estimation of winter wheat leaf area index based on fusion of remote sensing data with different spatiotemporal resolutions. Trans Chin Soc Agri Eng 28(17):117–124
Wang L, Tian Y, Yao X, Zhu Y, Cao W (2014) Predicting grain yield and protein content in wheat by fusing multi-sensor and multi-temporal remote-sensing images. Field Crops Res 164:178–188
Wood GA, Welsh JP, Godwin RJ, Taylor JC, Earl R, Knight SM (2003) Real-time measures of canopy size as a basis for spatially varying nitrogen applications to winter wheat sown at different seed rates. Biosyst Eng 84:513–531

Xu X, Ji X, Jiang J, Yao X, Tian Y, Zhu Y, Cao W, Cao Q, Yang H, Shi Z, Cheng T (2018) Evaluation of one-class support vector classification for mapping the paddy rice planting area in Jiangsu Province of China from Landsat 8 OLI imagery. Remote Sens 10:546

Xue L, Yang L (2008) Recommendations for nitrogen fertiliser topdressing rates in rice using canopy reflectance spectra. Biosyst Eng 100:524–534

Yao X (2012) Non-destructive monitoring and precise regulation of plant nitrogen nutrition in wheat. PhD dissertation of Nanjing Agricultural University

Yao X, Zhu Y, Tian YC, Liu XJ, Cao WX (2010) Exploring hyperspectral bands and estimation indices for leaf nitrogen accumulation in wheat. Int J Appl Earth Obs Geoin 12(2):89–100

Yao X, Ata-Ul-Karim ST, Zhu Y, Tian Y, Liu X, Cao W (2014) Development of critical nitrogen dilution curve in rice based on leaf dry matter. Eur J Agron 55:20–28

Yao L, Wang Q, Yang J, Zhang Y, Zhu Y, Cao W, Ni J (2019) UAV-borne dual-band sensor method for monitoring physiological crop status. Sensors 19:816

Zarco-Tejada PJ, Miller JR, Noland TL, Mohammed GH, Sampson PH (2001) Scaling-up and model inversion methods with narrowband optical indices for chlorophyll content estimation in closed forest canopies with hyperspectral data. IEEE Trans Geosci Remote Sens 39(7):1491–1507

Zhang K, Yuan Z, Yang T, Lu Z, Tian Y, Zhu Y, Cao Q, Liu X (2020) Chlorophyll meter-based nitrogen fertilizer optimization algorithm and nitrogen nutrition index for in-season fertilization of paddy rice. Agron J 112:288–300

Zhu Y, Li Y, Feng W, Yao X, Cao W (2006) Monitoring leaf nitrogen in wheat using canopy reflectance spectra. Can J Plant Sci 86:1037–1046

Chapter 6
Remote Sensing Technologies for Crop Disease and Pest Detection

Chenghai Yang

Abstract Remote sensing has long been used for the detection and management of crop plant diseases and insect pests. This chapter presents an overview of major remote sensing platforms and systems commonly used for crop disease and pest detection. Specifically, remote sensors mounted on satellites, manned aircraft, and unmanned aircraft systems (UAS) are discussed and applications on the use of these imaging sensors for detecting and mapping crop diseases and insect pests are reviewed. Cotton root rot is used as a practical example to illustrate how airborne and satellite imagery can be integrated with variable rate technology for crop disease detection, site-specific fungicide application, and performance evaluation. Some of the challenges and future directions are briefly discussed. The overview and methodologies presented in this chapter should provide researchers, extension personnel, growers, crop consultants, and farm equipment and chemical dealers with practical guidelines for remote detection and effective management of some crop diseases and insect pests.

Keywords Crop disease · Insect pest · Airborne imagery · Satellite imagery · Prescription map · Variable rate application

6.1 Introduction

Plant diseases and pests reduce crop yield, degrade product quality, and cause worldwide economic losses. It is estimated that yield losses at a global scale range from 10% to 40% for five major food crops (i.e., wheat, rice, maize, potato, and soybean) based on a survey from crop health experts in 67 countries (Savary et al.

C. Yang (✉)
Agricultural Research Service, United States Department of Agriculture, College Station, TX, USA
e-mail: chenghai.yang@usda.gov

M. Li et al. (eds.), *Soil and Crop Sensing for Precision Crop Production*, Agriculture Automation and Control, https://doi.org/10.1007/978-3-030-70432-2_6

2019). This study also identified 137 individual pathogens and pests and documented the losses to them associated with each of the five crops.

Timely detection of crop diseases and pests is critical to their control and management with appropriate crop protection measures. Traditionally, the identification and classification of common plant diseases and pests are based on field surveys and the knowledge of the grower or the crop consultant. However, for new and emerging pathogens and pests, the use of microscopic, serological, and DNA-based technologies in conjunction with the knowledge of experts is usually required (Oerke 2019). Because these techniques are expensive and time-consuming, these are only used for special purposes.

Farmers generally have the knowledge of the approximate time and extent of the incidences of common diseases and pests in their fields, even though these incidences are commonly heterogeneous in time and space. Some diseases and pests (e.g., soilborne) tend to be patchy and relatively stable, while others (e.g., airborne) can change in time and space within the growing season. In this regard, traditional uniform pesticide application is probably adequate for most airborne diseases and pests, while variable rate technology or site-specific application is more appropriate for soilborne diseases and pests in order to reduce pesticide use and minimize the negative environmental impact. However, in either case, information on the distribution and severity of any disease or pest in fields and across a farm or a region is needed for more effective control and management. The spatial and temporal incidence data acquired during the growing season can be used not only for within-season management but also for the control of recurring diseases and pests in following seasons.

Direct detection of pathogens and pests over a large area is very difficult and may not be necessary in many practical applications. As a large majority of them can cause damage to crop plants and/or fruits, detection of their damage and effects to the plants may be more practical and effective. Any disease or pest that can cause enough morphological and physiological changes in crop plants is a good candidate for remote sensing. As an early example, a film-based camera mounted on an airplane was used to take aerial photographs of cotton fields infested by cotton root rot, a soilborne disease caused by the fungus *Phymatotrichopsis omnivora* (Taubenhaus et al. 1929). This work stimulated extensive experiments to examine spectral reflectance characteristics of healthy and stressed plants and to use aerial photography for identifying various crop diseases (airborne, insect-borne, seed-borne, and soilborne) (Colwell 1956; Myers 1983; Ryerson et al. 1997). Although film-based aerial photography is no longer used today, it had been a primary remote sensing tool until early 2010s when satellite and airborne imagery completely replaced it.

Both airborne and satellite images have been successfully used to detect and map many crop diseases and pests, but early detection remains a challenge. In most cases, by the time remote sensing imagery can reveal any plant canopy symptoms, damage may have already been done to the crop. This delayed detection may be early enough to reduce further damage with certain measures for some crops; for others, it may be too late to stop the infection or infestation for the current growing season. For example, once the plant is infected with cotton root rot, it will die within a week or so. In fact, remote sensing has been commonly used to assess the extent

and severity of the damage caused by a disease or a pest. Moreover, imagery obtained in the present growing season can be used for the management of recurring diseases, such as cotton root rot, in future growing seasons.

Pesticides are widely used for disease and insect pest control to reduce crop yield loss and quality degradation. Uniform pesticide application has been commonly used since many diseases and pests tend to spread quickly across the field. However, site-specific and variable rate applications can be more effective for the management of some diseases and pests that are stable either within the season or across different seasons. If a disease or pest tends to occur in similar areas within the field across different seasons, site-specific application can be made before the initiation of the disease or pest based on the infestation maps from previous years. Cotton root rot is one such disease that has affected the cotton industry for over a century. Yang et al. (2016) started to collect airborne imagery to monitor the distribution and severity of cotton root rot in south Texas in 1999 and in central Texas in 2010. The time series images showed that this disease tends to occur in a similar area within fields across different years. The recurrent pattern of the disease provides a strong evidence to use historical imagery for creating prescription maps.

This chapter presents an overview of major remote sensing platforms and systems commonly used for the detection and management of crop plant diseases and insect pests. Specifically, remote sensors mounted on satellites, manned aircraft, and unmanned aircraft systems (UAS) are discussed and applications on the use of these imaging sensors for detecting and mapping crop diseases and insect pests are reviewed. Cotton root rot is used as a practical example to illustrate how airborne and satellite imagery can be integrated with variable rate technology for crop disease detection, site-specific fungicide application, and performance evaluation. Some of the challenges and future directions are briefly discussed. The overview and methodologies presented in this chapter should provide researchers, extension personnel, growers, crop consultants, and farm equipment and chemical dealers with practical guidelines for remote detection and effective management of some crop diseases and insect pests.

6.2 Remote Sensing Platforms and Systems for Disease and Pest Detection

Remote sensing employs a sensor to measure and record the reflected and emitted electromagnetic radiation from the target area in the field of view of the sensor. Sensors used in remote sensing, or simply called remote sensors, have two broad categories: non-imaging (e.g., spectroradiometers) and imaging (e.g., cameras). Imaging sensors are typically carried on earth-orbiting satellites and manned aircraft, while non-imaging sensors can be handheld or mounted on ground-based vehicles. Recently, UAS have emerged as a popular remote sensing platform to fill the gap between manned and ground-based platforms due to their low cost and low-flying altitude for high spatial resolution imagery.

Imaging sensors are designed to provide nadir views of a target area from vertical perspectives. Depending on the source of energy, imaging sensors can be grouped into passive and active sensors. Passive remote sensors, represented by electro-optical sensors and passive microwave, detect reflected sunlight or emitted thermal infrared and microwave energy from the surface. Active remote sensors, such as imaging radar (radio detecting and ranging), provide their own energy source to a target and record the reflected energy from the target. Passive sensors can be easily affected by the time of the day and weather conditions, while active sensors have the advantage to obtain measurements anytime, regardless of the time of day.

Electro-optical sensors as the main imaging sensors use detectors to convert the reflected and/or emitted radiation from a ground target to electrical signals proportionally, which are then recorded on magnetic, optical, and/or solid-state media for viewing and processing on a computer. Based on remote sensing applications, detectors are designed with sensitivities for spectral regions across the electromagnetic spectrum, including the near ultraviolet (UV, 0.3–0.4 μm), visible (0.4–0.7 μm), near-infrared (NIR, 0.7–1.0 μm), shortwave infrared (SWIR, 1–3 μm), mid-wave infrared (MWIR, 3–5 μm), and thermal infrared or longwave infrared (LWIR, 7–14 μm). Although there are variations on the definitions of the spectral regions, these wavelength ranges are commonly used in most imaging sensors. The total span of the wavelengths that can be detected by electro-optical detectors extends from 0.3 to 15 μm and the reflective spectrum extends from about 0.38 to 3.0 μm (Campbell 2002). The sensors operating in the visible to SWIR region can only be used under sunlit conditions, while MWIR and LWIR sensors can be used during the day or night.

Remote sensors used on satellites, manned aircraft, and UAS are predominantly electro-optical sensors. In the following sections, the three different platforms and commonly used imaging sensors are discussed and the applications of these platforms for disease and pest detection are briefly reviewed.

6.2.1 Satellite Sensors for Disease and Pest Detection

Traditional satellite sensors such as Landsat and SPOT have long been used for disease and pest detection over large geographic areas. Since 1972, eight Landsat satellites have been launched to provide uninterrupted images of the earth's surface. Landsat 9 is scheduled to be launched in late 2020 to replace Landsat 7 in orbit that was launched in 1999. Landsat 8, launched in 2013, is currently providing image data and will continue to have some overlap with the new satellite. Landsat 8 acquires about 740 scenes a day with a size of 185 km × 180 km and a repeat cycle of 16 days. It captures 12-bit image data in one panchromatic band at 15-m spatial resolution, eight spectral bands (coastal, blue, green, red, NIR, SWIR 1, SWIR 2, and Cirrus) at 30 m, and two thermal bands (LWIR 1 and LWIR 2) at 100 m. Landsat 9 will provide data in the same spectral bands as Landsat 8 with an improved 14-bit radiometric resolution.

Despite its coarse spatial resolution and relatively long revisit time, Landsat imagery has been successfully used to monitor crop disease and pest conditions and map severe infestations at regional scale. Chen et al. (2007) detected the take-all disease infestation in wheat using Landsat 5 Thematic Mapper (TM) imagery. Mirik et al. (2011) distinguished areas infested with wheat streak mosaic from noninfested areas using TM images in two counties of the Texas Panhandle over multiple crop years. Zhang et al. (2014) evaluated 30-m HJ-CCD satellite imagery for monitoring powdery mildew of winter wheat. It is always a challenge to discriminate diseases and pests co-occurring at the same time and space as they could cause similar symptoms during certain crop growth periods. Combined use of image data and crop phenological and environmental information can help improve the accuracy for discriminating coexisting crop diseases and/or pests. Ma et al. (2019) discriminated winter wheat powdery mildew and aphid infestations during a co-epidemic outbreak of the disease and the insect pest in northeast China based on temporal Landsat 8 imagery integrated with crop growth and environmental parameters.

Recent advances in high-resolution satellite sensors have significantly narrowed the gaps in spatial and temporal resolutions between traditional satellite sensors and airborne imaging sensors. Since IKONOS, the first commercial high-resolution satellite sensor, was successfully launched in 1999 to provide multispectral imagery at 4-m spatial resolution, dozens of such satellite systems with spatial resolutions of 10 m or finer have been launched. The short revisit time and fast data delivery combined with their large ground coverage make high-resolution satellite imagery attractive for many applications, including disease and pest detection and other precision agriculture operations that require high-resolution image data.

Most high-resolution satellite sensors offer panchromatic imagery with submeter resolution and multispectral imagery in four spectral bands (blue, green, red, and NIR) with spatial resolutions of 1–4 m. Such sensors include IKONOS, QuickBird, GeoEye-1, Pléiades 1A and 1B, SkySat-1 and -2, Gaofen-2, TripleSat, Cartosat-2C and -2D, GaoJing-1, and WorldView-4. A few other satellite sensors offer more spectral bands such as WorldView 2 and 3. WorldView 2 provides eight bands in the visible to NIR region at 1.24 m, while WorldView 3 offers a total of 28 bands, including the same eight spectral bands at 1.24 m, eight SWIR bands (1195–2365 nm) at 3.7 m, and 12 spectral bands (405–2245 nm) at 30 m. Other satellite sensors offer multispectral imagery with 5- to 10-m spatial resolutions, such as RapidEye (6.5 m), SPOT 6 and 7 (6 m), and Sentinel-2A and -2B (10 m). It is worth noting that Sentinel-2A and -2B imagery is freely available to users. Some of the earlier satellites such as IKONOS and QuickBird were deactivated or retired, but archived images from these satellites are still available. Yang (2018) provided a review of over two dozen high-resolution satellite sensors and their applications for precision agriculture.

Satellite remote sensing is rapidly advancing with many countries and commercial firms launching new satellite sensors every year. Planet Labs, Inc. (San Francisco, California, USA), currently operates three different Earth-imaging constellations, PlanetScope, RapidEye, and SkySat. PlanetScope consists of over 120 satellites to provide either RGB (red, green, blue) frame images or split-frame images with half RGB and half NIR at 3-m spatial resolution. RapidEye has five

satellites collecting multispectral imagery in five spectral bands (blue, green, red, red edge, and NIR) with 6.5-m nominal resolution, which is resampled to 5 m at delivery. SkySat with a constellation of 14 satellites captures submeter panchromatic imagery and 1-m multispectral imagery in four standard bands (blue, green, red, and NIR). The complete PlanetScope constellation of approximately 130 satellites can image the entire land surface of the earth every day.

Due to the high spatial resolution and short revisit time, the new generation of satellite sensors has been increasingly used for precision agriculture applications, including crop disease and pest detection. Franke and Menz (2007) used QuickBird imagery for detecting powdery mildew and leaf rust in winter wheat and achieved high accuracies with severe infections at late growth stages. Santoso et al. (2011) also used QuickBird imagery to map and identify basal stem rot in oil palms. SPOT 6 satellite imagery was used for mapping powdery mildew in winter wheat at multiple regions (Yuan et al. 2016). Li et al. (2015) examined the feasibility of WorldView 2 imagery for the detection of Huanglongbing, also known as citrus greening. Yang et al. (2018) used GeoEye-1 imagery to map cotton root rot and create prescription maps for site-specific fungicide application for the management of the disease. Song et al. (2017) evaluated Sentinel-2 imagery and compared it with airborne imagery for mapping cotton root rot. Abdel-Rahman et al. (2017) explored the possibility of using RapidEye data to assess stem borer larva densities in maize fields and found that the densities could only be predicted during the middle growing season. The literature on the use of satellite imagery for disease and pest monitoring and detection will continue to expand as low-cost and no-cost satellite imagery is becoming more available.

6.2.2 Manned Aircraft-Based Imaging Systems for Disease and Pest Detection

Airborne imaging systems are commonly referred to as imaging systems carried on manned aircraft, so imagery obtained from manned aircraft is known as airborne or aerial imagery. Cameras or imaging systems used on manned aircraft are generally not restricted by their size and weight and they need to be operated or triggered by the pilot or a camera operator on the aircraft. A typical airborne multispectral or hyperspectral imaging system consists of one or more cameras and a computer with a monitor for data acquisition and real-time visualization.

Depending on the types of remote sensors being carried, a designated remote sensing aircraft is specially outfitted with camera holes or ports in the underside of the aircraft. However, cameras that are light, not sophisticated, and remotely triggerable can be simply attached to the landing gear or hung out a door window of an aircraft using simple mounts. Most aircraft for remote sensing fly below altitudes of 3000 m above mean sea level (MSL) where no oxygen mask or cabin pressurization is needed. Common fixed-wing, propeller-driven aircraft such as Cessna 206, 182, and 172 belong to this class, which is widely used throughout the world.

Agricultural aircraft are a special class of manned aircraft used for aerial application. There are thousands of agricultural aircraft used to apply crop production and protection materials in the United States alone. These aircraft can be equipped with one or multiple cameras to monitor crop growing conditions; detect and map infestations of crop weeds, diseases, and insect pests; and assess the performance and efficacy of ground and aerial application treatments. This additional imaging capability will also increase the utility of agricultural aircraft and help aerial applicators generate additional revenue with remote sensing services.

Light sport aircraft (LSA) are a fairly new category of small, lightweight aircraft that are simple to fly. Different countries have their own specifications and regulations for LSA. In the United States, several distinct groups of aircraft may be flown as LSA. The US Federal Aviation Administration (FAA) defines a LSA as an aircraft, other than a helicopter or powered lift, that meets certain requirements, including a maximum gross takeoff weight of 600 kg, a maximum stall speed of 83 km/h, and a maximum speed in level flight of 220 km/h among others. LSA aircraft have great potential as a flexible and economical platform for aerial imaging. They are less expensive than other manned aircraft, but they do not have many of the restrictions UAS have.

6.2.2.1 Multispectral Imaging Systems Based on Industrial Cameras

Multispectral imaging systems typically employ two or more industrial cameras and spectral filters to obtain images in multiple bands. For example, a typical four-band imaging system consists of four identical cameras equipped with four different bandpass filters to obtain blue, green, red, and NIR band images. The composite image of red, green, and blue bands forms the normal color or RGB image, while the composite image of NIR, red, and green bands forms the color-infrared (CIR) image.

Among the advantages of airborne imaging systems are their relatively low cost, high spatial resolution, and real-time/near-real-time availability of imagery for visual assessment and their ability to obtain data in narrow spectral bands in the visible to LWIR region of the spectrum. Over the years, numerous commercial and custom-built multispectral imaging systems have been developed and used for diverse remote sensing applications, including disease and pest detection. Most airborne multispectral imaging systems can provide 8- to 16-bit image data with submeter resolution at 3–12 narrow spectral bands in the visible to NIR region of the spectrum (Everitt et al. 1998; Escobar et al. 1998; Gorsevski and Gessler 2009; Yang 2012).

Monochrome charge-coupled device (CCD) sensors have been typically used in industrial cameras, though complementary metal oxide semiconductor (CMOS) sensors have been increasingly displacing CCD sensors in recent years because of their lower cost and less power consumption. Each camera in a multispectral system is usually equipped with a different bandpass filter. This approach allows each

camera to be individually adjusted for optimum settings, but it requires that the individual band images be properly aligned with each other even if the cameras are well aligned. Another approach is to use a beam splitting prism and multiple sensors built in one single camera to achieve multispectral imagery. One such system is the CS-MS1920 multispectral 3-CCD camera (Teledyne Optech, Inc., Vaughan, Ontario, Canada), which uses a beam splitting prism and three CCD sensors to acquire images in 3–5 spectral bands within the 400–1000 nm spectral range. The advantage of this approach is that the band images are optically and mechanically aligned.

The US Department of Agriculture-Agricultural Research Service's (USDA-ARS) Aerial Application Technology Research Unit in College Station, Texas, has devoted considerable efforts to the development and evaluation of airborne imaging systems for agricultural applications. Figure 6.1 presents a four-camera multispectral imaging system (lower left) along with three other imaging systems developed/assembled at the ARS location. The four-camera imaging system consists of four monochrome CCD cameras and a ruggedized PC equipped with a frame grabber and image acquisition software (Yang 2012). The cameras are sensitive in the 400–1000 nm spectral range and provide 2048 × 2048 active

Fig. 6.1 A four-camera imaging system (lower left) mounted along with a hyperspectral camera (upper left), a thermal camera (upper right), and a multispectral imaging system based on two consumer-grade cameras (central to lower right) owned by the USDA-ARS at College Station, Texas

pixels with 12-bit data depth. The four cameras are equipped with blue (430–470 nm), green (530–570 nm), red (630–670 nm), and NIR (810–850 nm) bandpass interference filters, respectively.

Many commercial companies offer different types of multispectral imaging systems. Airborne Data Systems, Inc. (Redwood Falls, Minnesota, USA), offers several multispectral camera systems for airborne remote sensing.[1] The SpectraView is an airborne multispectral camera system designed to accommodate up to eight different cameras. The cameras can vary in size, format, and wavelength from UV to LWIR. The system is designed with a fully integrated global positioning system/inertia navigation system (GPS/INS) unit providing precise, automated georegistration of the images.

Tetracam's multispectral imaging systems come in two product families (Tetracam, Inc., Chatsworth, California, USA). Each system in the agricultural digital camera (ADC) family consists of a single camera equipped with fixed filters at green, red, and NIR wavelengths. Systems in the multiple-camera array (MCA) family contain 4, 6, or 12 registered and synchronized cameras to simultaneously capture user-specified band images in visible to NIR wavelengths. Tetracam's Micro-MCA systems can also be configured with one or two FLIR TAU thermal sensors (FLIR Systems, Inc., Nashua, New Hampshire). FLIR's thermal cameras come in many series with sensor arrays up to 1280 × 1024 pixels in typical spectral ranges of 1–5 μm, 3–5 μm, and 7.5–13 μm. The thermal camera shown in Fig. 6.1 is a FLIR model SC640 thermal imaging camera sensitive in the 7.5–13 μm spectral range. It captures 14-bit thermal images with 640 × 480 pixels. ITRES Research Ltd. (Calgary, Alberta, Canada) offers the TABI-1800 thermal camera that captures 14-bit broadband images with a swath of 1800 pixels, the industry's widest array in the 3.7–4.8 μm spectral range.

Phase One Industrial (Copenhagen, Denmark) provides high-end aerial imaging products. The Phase One 150MP 4-Band aerial system consists of two synchronized 150-megapixel (150-MP) iXM-RS150F cameras (RGB and achromatic) mounted side by side, a Somag CSM40 modular stabilizer, an Applanix GPS/inertial measurement unit (IMU), an iX Controller computer, and the iX Capture software. Each camera has a pixel array of 14,204 × 10,652 pixels. The software performs pixel alignment between the RGB and NIR images. The other similar configuration is the Phase One 100MP 4-Band aerial system with two 100MP iXM-RS100F cameras. Phase One is also offering an advanced large-format 190MP 4-Band system with two RGB cameras and one NIR camera to allow faster and more efficient execution of aerial imaging projects.

[1] *Disclaimer*: Commercial products are referred to solely for the purpose of clarification and should not be construed as being endorsed by the authors or the institution with which the authors are affiliated.

6.2.2.2 Multispectral Imaging Systems Based on Consumer-Grade Cameras

Recently, consumer-grade digital cameras have been increasingly used as a remote sensing tool. The main advantage is that one single consumer-grade camera can capture RGB images directly. Moreover, it can be modified to capture images in one single NIR band or in a combination of two visible bands and one NIR band. However, image quality from modified cameras may not be as good as that from the individual industrial cameras.

A consumer-grade camera fitted with either a CCD or CMOS sensor employs a Bayer color filter mosaic to obtain true-color RGB images using one single sensor (Bayer 1976; Hirakawa and Wolfe 2008). A Bayer filter mosaic is a color filter array for arranging RGB color filters on the pixel array of the sensor. Since each pixel is filtered to record only one of the three primary colors, various demosaicing algorithms are used to interpolate a set of complete red, green, and blue values for each pixel. Although pixel interpolation lowers the effective spatial resolution of the band images, the three band images are perfectly aligned. Consequently, consumer-grade digital color cameras have been increasingly used by researchers for agricultural applications (Sakamoto et al. 2012; Akkaynak et al. 2014; Yang et al. 2014; Song et al. 2016).

Images with visible and NIR bands are commonly used in remote sensing. Many vegetation indices such as the normalized difference vegetation index (NDVI) require spectral information in NIR and red bands. Since most consumer-grade cameras only provide the three broad RGB bands, NIR filtering techniques can be used to convert an RGB color camera to a NIR camera. Two of the companies that offer infrared camera conversion services are Life Pixel Infrared (Mukilteo, Washington, USA) and LDP LLC (Carlstadt, New Jersey, USA). The NIR blocking filter is typically replaced by a 720-nm or 830-nm long-pass filter. Since the Bayer filter mosaic is fused to the sensor substrate, the transmission profiles of the Bayer color channels remain when using RGB cameras with the long-pass NIR filter. All three channels in the converted camera only record NIR radiation. Although any of the three channels can be used as the NIR channel, the red channel usually has the best sensitivity. Studies have been conducted on the use of NIR-converted digital cameras for monitoring plant conditions and results from these studies support their use as simple and affordable tools for plant stress detection and crop monitoring (Nijland et al. 2014; Rabatel et al. 2014; Zhang et al. 2016; Wu et al. 2017).

In the last few years, several single- and dual-camera imaging systems based on consumer-grade cameras have been developed for use on any traditional aircraft or agricultural aircraft at USDA-ARS, College Station, Texas (Yang et al. 2014; Yang and Hoffmann 2015). The original USDA-ARS single-camera imaging system consisted of a Nikon D90 digital CMOS camera with a Nikon AF Nikkor 24 mm f/2.8D lens (Nikon Inc., Melville, New York, USA) to capture the color image with up to 4288 × 2848 pixels, a Nikon GP-1A GPS receiver (Nikon Inc., Melville, New York, USA) to geotag the image, an AUVIO 7″ portable LCD video monitor (Ignition L.P., Dallas, Texas, USA) to view the live image, and a Vello FreeWave wireless

remote shutter release (Gradus Group LLC, New York, New York, USA) to trigger the camera.

To assemble a dual-camera system, a second identical Nikon D90 camera was modified to a NIR camera. To trigger the two cameras simultaneously, one hahnel Giga T Pro II wireless timer remote receiver (hahnel Industries Ltd., Bandon, Co., Cork, Ireland) was attached to each camera and one single hahnel remote transmitter was used to start and stop image acquisition. The remote control allows the user to take images automatically at set time intervals between consecutive shots. Since the NIR image has the same center GPS coordinates as the RGB image, only one GPS receiver is needed. The two cameras can be attached via a mount to an aircraft with minimal or no modification to the aircraft. Both the single- and dual-camera systems have been evaluated for crop disease and pest detection and crop-type identification (Yang and Hoffmann 2015; Zhang et al. 2016).

Two other systems with higher-end consumer-grade cameras were also developed at USDA-ARS, College Station, Texas. One system, as shown in Fig. 6.1, consisted of two Canon EOS 5D Mark III digital cameras with 5760 × 3840 pixels (Canon USA Inc., Lake Success, New York, USA). One camera captured normal RGB color images, while the other camera was equipped with an 830-nm long-pass filter to obtain NIR images. The other consisted of two Nikon D810 digital cameras with 7360 × 4912 pixels. Similarly, one camera captured RGB color images, while the other camera was equipped with an 830-nm long-pass filter to obtain NIR images. These two imaging systems have the same sensor size (36 mm × 24 mm) and focal length (20 mm). The dimension of the images from each system is 1.8 by 1.2 times the flight height. At a flight height of 1000 m AGL, the image covers a ground area of 1800 m × 1200 m with a pixel size of 31 cm for the Canon system and 24 cm for the Nikon system. The two-camera systems have also been evaluated for crop disease and pest detection (Yang et al. 2014; Wu et al. 2017).

6.2.2.3 Hyperspectral Cameras

Hyperspectral imaging sensors or imaging spectrometers collect image data in tens to hundreds of very narrow, continuous spectral bands throughout the visible to thermal infrared region of the spectrum. Imagery from hyperspectral sensors contains more spectral details than imagery from multispectral sensors and has the potential for better differentiation and estimation of biophysical attributes for remote sensing applications.

Many commercial airborne hyperspectral sensors have been developed and used for various remote sensing applications since the late 1980s. The Airborne Visible/Infrared Imaging Spectrometer (AVIRIS) was the first hyperspectral imaging sensor that delivered calibrated images of upwelling spectral radiance in 224 contiguous spectral bands with wavelengths from 400 to 2500 nm. AVIRIS was developed by the Jet Propulsion Laboratory (JPL) (Pasadena, California, USA) and has been collecting hyperspectral images for scientific research and applications since 1987 (http://aviris.jpl.nasa.gov/). The pixel size and swath width of the AVIRIS data

depend on the altitude from which the data are collected. When collected at 20 km above sea level, imagery has a pixel size of 20 m and a ground swath of 11 km. When collected at 4 km above the ground, the pixel size is 4 m and the swath is 2 km wide. The AVIRIS system has been upgraded and improved in a continuous effort to meet the requirements of investigators using AVIRIS spectral images for scientific research and applications.

HyMap is an airborne hyperspectral imaging sensor developed and manufactured by Integrated Spectronics Pty. Ltd. (Sydney, Australia). After the first sensor became operational in 1996, the HyMap series of airborne hyperspectral scanners have been deployed in many countries in North America, Europe, Africa, and Australasia. The initial HyMap sensor had 96 channels in the 550–2500 nm range and was designed primarily for mineral exploration (Cocks et al. 1998). The current HyMap sensor, operated by HyVista Corporation Pty. Ltd. (Sydney, Australia), provides 128 bands in the 450–2500 nm spectral range. The sensor can be configured to capture images with 512 pixels with a spatial resolution of 3–10 m for different environmental, agricultural, and urban applications (Dehaan and Taylor 2002; Galvao et al. 2004; Schiefer et al. 2006).

The Compact Airborne Spectrographic Imager (CASI) was first introduced in 1989 by ITRES Research Ltd. (Calgary, Alberta, Canada). Currently, ITRES offers a suite of airborne hyperspectral sensors covering the visible to thermal spectral range. The CASI-1500H captures 14-bit hyperspectral images at up to 288 bands in the 380–1050 nm spectral range with 1500 across-track pixels. The SASI-1000A offers images with 1000 pixels at 200 bands in 950–2450 nm to allow continuous VNIR-SWIR coverage together with the CASI-1500H. The MASI-600 is the first commercially available MWIR airborne hyperspectral sensor with 600 pixels and 64 bands in a spectral range of 3–5 μm. The TASI-600 is the airborne hyperspectral thermal sensor with 600 spatial pixels and 32 bands in a spectral range of 8–11.5 μm.

More commercial airborne hyperspectral imaging sensors have become available in recent years with improved spatial and spectral resolutions and high-performance GPS/INS units for increased position accuracy. The Specim's AISA hyperspectral systems (Spectral Imaging Ltd., Oulu, Finland) cover VNIR (380–1000 nm), SWIR (1000–2500 nm), and thermal LWIR (7.7–12.3 μm) spectral ranges. The family of the airborne hyperspectral systems includes AisaKESTREL 10 in 400–1000 nm, AisaKESTREL 16 in 600–1640 nm, AisaFENIX and AisaFENIX 1K in 380–2500 nm, and AisaOWL in 7.7–12.3 μm. The AisaFENIX sensor can capture images with a swath of 384 pixels at up to 348 VNIR bands and 274 SWIR bands, while the AisaFENIX 1K sensor can capture images with a swath of 1024 pixels at up to 348 VNIR bands and 256 SWIR bands. The AisaOWL can obtain images with a 384-pixel swath at 96 bands. All the sensors are equipped with a GPS/INS unit for monitoring the aircraft position and attitude.

Headwall Photonics, Inc. (Fitchburg, Massachusetts, USA), is another hyperspectral instrument manufacturer that currently offers a suite of hyperspectral sensors covering the spectral range of 250–2500 nm. Separate hyperspectral imaging sensors are available for UV to visible (250–500 nm), VNIR (380–1000 nm), NIR (900–1700 nm), and SWIR (950–2500 nm) spectral ranges. It also offers a

co-registered VNIR-SWIR imaging sensor with full hyperspectral coverage from 400 to 2500 nm. Headwall's sensors can be configured to capture images with a swath of up to 1600 pixels at hundreds of bands. Similarly, a high-accuracy GPS/INS unit is integrated into each hyperspectral sensor. As an example, the hyperspectral imaging system at USDA-ARS in College Station, Texas, consists of a Headwall HyperSpec VNIR E-Series imaging spectrometer (upper left of Fig. 6.1), an integrated Applanix APX-15 GPS/IMU, and a hyperspectral data processing unit. The spectrometer can capture 16-bit images with up to 923 spectral bands and a swath of 1600 pixels in the wavelength range of 380–1000 nm. At 1000 m AGL, the hyperspectral camera covers a swath of 615 m with a pixel size of 38 cm.

Airborne multispectral and hyperspectral imaging systems have been used for detecting and mapping crop insect pests and diseases for decades. Past research has shown that CIR aerial photography can be used to remotely detect sooty mold deposits on citrus foliage caused by the honeydew-producing insects, brown soft scale, and citrus blackfly (Hart and Myers 1968; Hart et al. 1973; Everitt et al. 1994). Nuessly et al. (1987) evaluated CIR aerial photography for detecting sooty mold growing on honeydew secreted by sweetpotato whiteflies on cotton plants in the Imperial Valley of California. Everitt et al. (1996) described the application of airborne videography with GPS and GIS technologies for detecting and mapping silverleaf whitefly (also known as sweetpotato whitefly B-biotype) infestations in cotton in the Rio Grande Valley of Texas. Fletcher (2005) evaluated simulated QuickBird imagery derived from high-resolution airborne CIR imagery for detecting sooty mold-affected citrus orchards in the Rio Grande Valley of Texas.

The feasibility of airborne CIR videography was demonstrated for detecting Phymatotrichum root rot in cotton (Nixon et al. 1987) and root-knot nematodes in kenaf (Cook et al. 1999). Airborne digital multispectral imagery was evaluated for detecting Phytophthora foot rot in citrus orchards (Fletcher et al. 2001), mapping late blight in tomato fields (Zhang et al. 2005), and mapping cotton root rot in cotton fields (Yang et al. 2005). Airborne hyperspectral imagery was evaluated for identifying yellow rust in wheat (Huang et al. 2007), grapevine leafroll virus (MacDonald et al. 2016), and yellow leaf curl on tomatoes (Lu et al. 2018). Airborne multispectral and hyperspectral imaging techniques were jointly used for detecting citrus greasy spot (Du et al. 2004), cotton root rot (Yang et al. 2010), and citrus greening (Kumar et al. 2012; Li et al. 2014).

6.2.3 Unmanned Aircraft-Based Imaging Systems for Disease and Pest Detection

UAS as an emerging remote sensing platform are gaining popularity in recent years. There are two major types of UAS used today, rotary and fixed-wing. A rotary UAS has the capability to take off and land vertically and hover in place, but it has a short flight time and slow speed. In contrast, a fixed-wing UAS can be hand-launched or

requires a launcher to take off and a runway to land, but it can fly at a longer time with faster speed. Small UAS are generally powered by batteries which typically have a flight time of 10–30 min. The flight range of a UAS also limits the radius that can be covered during each flight.

Most small UAS can only carry a small payload that restricts the type of cameras to be used. More importantly, the imaging systems used on UAS should have the capability to be triggered remotely or automatically by the control system on the UAS. Therefore, most of the imaging systems used for manned aircraft cannot be directly used for UAS imaging. Nevertheless, some systems such as the single- and dual-camera systems based on consumer-grade cameras can be directly mounted on UAS for aerial imaging. Moreover, many multispectral and hyperspectral camera manufacturers are providing cameras for UAS. MicaSense, Inc. (Seattle, Washington, USA), is a good example and has provided several lines of multispectral camera products, including the 5-band RedEdge 3, the 5-band RedEdge-MX, the 6-band Altum, and the 10-band dual-camera system. ITRES offers smaller versions of the hyperspectral sensors for use on UAS. Specim's AisaKESTREL 10 and AisaKESTREL 16 hyperspectral cameras can also fit to a UAS platform. Headwall's VNIR and SWIR hyperspectral sensors or coaligned VNIR-SWIR sensors can be mounted on high-performance UAS with a choice of GPS/IMU.

UAS can capture images at very high spatial resolution, making it possible to assess crop disease and pest conditions at leaf and plant levels. In the last few years, UAS-based remote sensing has been increasingly used for crop phenotyping to estimate plant growth parameters (Varela et al. 2017; Roth et al. 2018; Hassan et al. 2019). Like airborne and satellite imagery, UAS imagery has become an important data source to assess crop diseases and insect pests. Garcia-Ruiz et al. (2013) compared a UAS-based and a manned aircraft-based imaging platform for identification of Huanglongbing-infected citrus trees. Albetis et al. (2017) evaluated the feasibility of detecting the *Flavescence dorée* grapevine disease using UAS multispectral imagery. Cao et al. (2018) used UAS-based RGB and thermal imagery to detect a fungal disease on oilseed rape leaves. Mattupalli et al. (2018) used UAS-based RGB imagery to assess root rot infestations in alfalfa fields. Heim et al. (2019) evaluated a MicaSense RedEdge 3 multispectral camera mounted on a UAS for detection of myrtle rust on a lemon myrtle plantation. Vanegas et al. (2018) used UAV-based multispectral and hyperspectral data for detecting grape phylloxera infestation in vineyards.

Despite their widespread use and fast-growing popularity, UAS have many flight restrictions due to their safety threat to the air space. Each country has its own rules and regulations pertaining to UAS operations. The safety concerns of commercial pilots, especially aerial applicators and other pilots operating in low-level airspace, need to be addressed. In the United States, UAS pilots must follow the Part 107 guidelines set up by the US FAA (https://www.faa.gov/uas/commercial_operators/). Some of the important operation restrictions include the following: (1) The unmanned aircraft with all payload must weigh less than 55 lbs. (25 kg), (2) the flight must be conducted within visual line of sight only, (3) the maximum allowable altitude is 400 ft (122 m) above ground level (AGL), (4) the maximum ground

speed is 100 mph (161 km/h), and (5) operations in Class B, C, D, and E airspace are allowed with the required air traffic control permission. The person operating a small UAS must either hold a remote pilot airman certificate or be under the direct supervision of a certified person. There are many other restrictions, though some of the restrictions can be waived if a certificate of waiver is granted.

Due to the current aviation regulations and their own limitations, UAS have been mainly used for image acquisition over research plots and relatively small crop areas. Until some of the UAS restrictions are changed for commercial applications, conventional manned aircraft remain to be an effective and versatile platform for airborne remote sensing. High-resolution satellite imagery is becoming more available at lower cost with large coverage and short revisit time. Farmers nowadays have more choices of image data than even before.

6.3 Practical Methodologies for Crop Disease Detection and Management

A variety of remote sensors mounted on different platforms have been successfully used to detect and map many crop diseases and pests. Depending on the specific disease or pest to be detected, the type of imagery and the type of platforms to be selected are different. As discussed previously, if the disease or pest is stable in the present season or recurs at similar areas in the following season, the imagery taken in the current season can be used for site-specific management either within the season or after the season. In this section, cotton root rot is used as an example to illustrate the practical procedures and methodologies for remote detection and site-specific management of the disease.

Cotton root rot is a destructive soilborne cotton disease that has plagued the cotton industry for more than a century (Pammel 1888; Uppalapati et al. 2010). The fungus spreads from plant to plant either through root contact or by slow growth of mycelial strands through the soil (Smith et al. 1962). Infected plants turn yellow and then wilt and die within a week. Plants infected earlier in the season will die before bearing fruit, whereas later infection will reduce cotton yield and lower lint quality (Ezekiel and Taubenhaus 1934; Yang et al. 2005).

Despite decades of research efforts, effective practices for the control of this disease were lacking until Topguard® Terra fungicide (FMC Corporation, Philadelphia, Pennsylvania, USA) was registered by the US Environmental Protection Agency in 2015. Since the fungicide is not effective once the plant is infected, it is usually applied at planting or shortly before planting or after plant emergence. Thus, aerial imagery taken in the current season cannot be used for the management of this disease for the season. Historical airborne images have shown that this disease tends to occur in similar areas within fields across different years (Yang et al. 2016). Therefore, site-specific fungicide application can be made at planting or before the initiation of the disease based on the infestation maps from

previous years. Three years of field experiments were conducted to demonstrate how to implement site-specific fungicide application using historical imagery and variable rate technology for the management of this disease (Yang et al. 2018).

In this section, the methodologies for image acquisition and processing, prescription map creation, variable rate application, and performance evaluation will be discussed to demonstrate how remote sensing and variable rate technology can be used for the detection and management of cotton root rot. Hopefully, these procedures can be used or provide some guidance for similar crop diseases and pests.

6.3.1 Image Selection and Acquisition for Crop Disease Detection

Remote sensing is the most practical means for accurately detecting and mapping cotton root rot because of the large numbers of infested areas and their irregular shapes within fields. Both airborne and satellite images have been successfully used to map the extent of cotton root rot infestations near the end of the growing season when the damage is fully pronounced (Yang et al. 2005, 2010). Airborne imagery has fine spatial resolution, but its availability varies by location and year. Even if airborne imagery is available for your fields, it may not be very useful if taken early in the season. Satellite imagery provides an alternative data source because of its short repeat cycle and large ground coverage. The traditional Landsat imagery is freely available, but it may be only good to map severe infestations with large areas. High-resolution satellite sensors with spatial resolutions of 5 m or less, such as GeoEye-1, WorldView-3 and -4, and GaoJing-1, would be more appropriate. If such imagery is not available, imagery with resolutions of 5–10 m, such as RapidEye, SPOT 6 and 7, and Sentinel-2, can be used with the possibility that small infested areas may not be detected.

Several airborne imaging systems (i.e., three-, four-, and two-camera) and two satellite sensors (Geoeye-1 and Sentinel-2) had been used for image acquisition for the cotton root rot project in the last two decades. The three-camera imaging consisted of three digital cameras, which were filtered for in the green (560 ± 5 nm), red (630 ± 5 nm), and NIR (851 ± 6 nm) bands, respectively, to obtain 8-bit images with 1024 × 1024 pixels (Everitt et al., 1998). The four-camera imaging system used was the one shown in Fig. 6.1. Several versions of two-camera systems were used, including the Canon camera-based system shown in Fig. 6.1 and two others based on two different types of consumer-grade Nikon cameras. One such system consisted of two identical Nikon D810 cameras with 7360 × 4912 pixels. One camera was used to obtain RGB images, while the second camera was modified to capture NIR images with an 830-nm long-pass filter. A Cessna 206 aircraft equipped with two camera ports was used for image acquisition at altitudes of approximately 1525–3050 m (5000–10,000 ft) above ground level. All airborne images were taken between 1030 and 1500 h

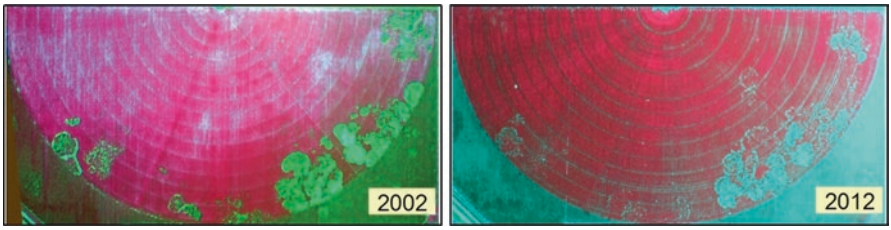

Fig. 6.2 Airborne color-infrared images for a 97-ha cotton field infested with cotton root rot in south Texas in 2002 and 2012. (Yang et al. 2016)

under sunny weather conditions. Pixel size for images captured at 3050 m was 1.3 m, 1.0 m, and 0.8 m for the three-, four-, and two-camera systems, respectively. GeoEye-1 satellite imagery contained blue, green, red, and NIR bands with a spatial resolution of 2 m, while Sentinel-2 imagery had the four standard bands at 10-m resolution.

Figure 6.2 presents the airborne CIR images acquired from a 94-ha irrigated cotton field in south Texas shortly before cotton harvest in 2002 and 2012. Areas with noninfected plants had pinkish or reddish color, while infested areas exhibited a greenish or light blue tone. The circular wheel tracks caused by the center-pivot system can be clearly seen on the images. Some differences in infestations existed between the 2 years, but the overall spatial patterns looked similar. Image classification results showed that percentage infestation areas for the field were 11.7% in 2002 and 8.7% in 2012. The smaller area in 2012 was because some of the infested areas in 2002 were not fully pronounced in 2012, even though there were a few newly infested areas. Nevertheless, cotton root rot occurred in the same general areas within the field and this recurrent pattern was also found in other infested cotton fields.

6.3.2 Image Processing and Prescription Map Creation for Crop Disease Management

Satellite imagery is usually rectified to a known coordinate system at delivery, while airborne imagery needs to be preprocessed and georeferenced before further analysis. The individual band images from any of the multicamera systems were aligned to each other using an image-to-image registration procedure and were then stacked as a multiband composite image. The aligned images were rectified to the Universal Transverse Mercator (UTM), World Geodetic System 1984 (WGS-84), coordinate system based on a set of ground control points. All procedures for image registration and rectification were performed using ERDAS Imagine (Intergraph Corporation, Madison, Alabama, USA) or ENVI (Research Systems, Inc., Boulder, Colorado, USA).

If a large number of mages were collected over a whole farm or a large geographic region along multiple flight lines, Pix4DMapper (Pix4D SA, Lausanne, Switzerland) was used to automatically convert the band images or RGB/NIR images into 2D orthomosaics and 3D digital surface models (DSMs). The band images from different cameras were automatically aligned and georeferenced during the image mosaicking process with 10–20 ground control points. The individual band mosaics were then staked as a composite image for further analysis.

Most image processing software packages such as Erdas Imagine and ENVI can be used to classify the image and then create the prescription map for use by a variable rate control system. Moreover, other less expensive farm software products such as Farmer Pro and Adviser Prime (Trimble Inc., Sunnyvale, California, USA) and SMS Advanced (AgLeader, Ames, Iowa, USA) can be used for this purpose. In addition, QGIS (https://qgis.org/en/site/) is a free software package that can perform image processing and create prescription maps.

Numerous classification techniques have been evaluated to distinguish cotton root rot-infested areas from airborne multispectral imagery. Yang et al. (2005) applied the Iterative Self-Organizing Data Analysis (ISODATA) unsupervised classification technique to CIR imagery to accurately detect and map root rot infestations within cotton fields in south Texas. Yang et al. (2010) compared airborne multispectral and hyperspectral imagery for mapping root rot areas and their results showed that both types of imagery could accurately identify root rot-infested areas, even though hyperspectral imagery could be used to assess the severity level of the infestation. Yang et al. (2016) evaluated and compared two unsupervised methods (ISODATA applied to imagery or to NDVI) and six supervised classification methods, including minimum distance, Mahalanobis distance, maximum likelihood, spectral angle mapper (SAM), neural network, and support vector machine (SVM). They concluded that all these methods were almost equally accurate, but the unsupervised methods could be easily implemented and therefore were recommended for cotton root rot classification. To consider the potential expansion of the disease and the size of the tractor-applicator system, a 3–10 m buffer should be added around the infested areas as part of the treatment zone in the prescription map (Yang et al. 2018).

Figure 6.3 shows an airborne CIR image, the unsupervised classification map from the NDVI image, and the prescription map with a 5-m buffer for an 11-ha cotton field near San Angelo, Texas. The classification map effectively separated cotton root rot-infested areas within the field. About 37% of the field was infested based on the classification map, while 63% of the field needed to be treated based on the prescription map with the 5-m buffer. The polygons in the prescription map were assigned application rates of 0 for noninfested areas and 46.8 L ha^{-1} (5 gal ac^{-1}) for infested areas. The prescription map was converted to a shapefile that a variable control system could accept.

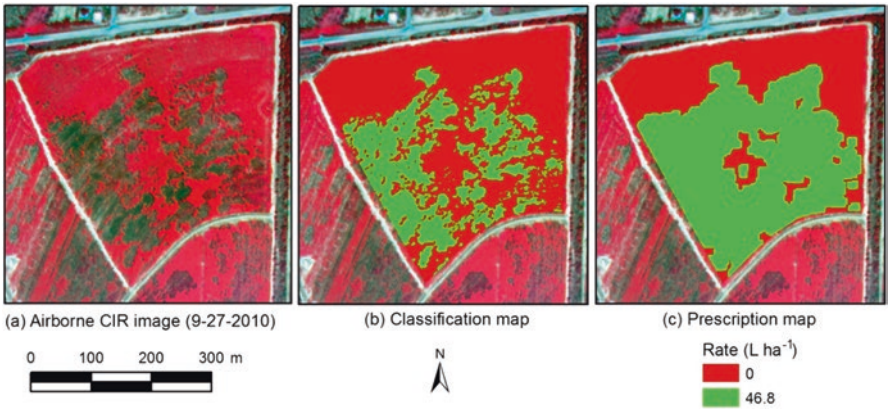

Fig. 6.3 Process of classifying an airborne CIR image and then creating a prescription map with a 5-m buffer for an 11-ha cotton field near San Angelo, Texas. The green areas in the prescription map were treated with Topguard fungicide with 46.8 L ha^{-1} of water. (Yang et al. 2018)

6.3.3 Site-Specific Fungicide Application for Crop Disease Management

Pesticides (i.e., fungicides and insecticides) are widely used to control crop diseases and insect pests to minimize yield loss and quality reduction in crop production. Traditional uniform pesticide application is effective for most diseases and pests, but variable rate application may be more appropriate and economical for the management of some stable infestations. Variable rate application does not change the basic functionality of existing applicators, but it does require the addition of a control system that can read a prescription map to adjust application rate automatically. Different control systems are available for variable rate application, but flow-based control systems are simple and commonly used to deliver the desired rate across the boom or swath with an electronic controller.

For Topguard Terra fungicide application, two flow-based control systems, a John Deere controller (Deere & Company, Moline, Illinois, USA) and a Trimble controller (Trimble Inc., Sunnyvale, California, USA), were selected. The John Deere control system consisted of a controller, a servo valve, a flowmeter, and a shutoff valve. The system was added to a John Deere tractor owned by a producer near Edroy, Texas. The Trimble system with similar components was adapted to a John Deere tractor owned by a producer in San Angelo, Texas. Both tractors were already equipped with the StarFire RTK GPS receiver. The John Deere system required a John Deere GreenStar display and the Trimble system required a Trimble FMX Display. Both displays were already integrated on the respective tractors for automatic guidance and other field operations. The prescription maps in shapefile format were uploaded to the displays and each system was calibrated for desired rates before fungicide application over multiple fields owned by the two producers in 2015–2017.

6.3.4 *Performance and Efficacy Evaluation for Crop Disease Management*

The performance and efficacy of a variable rate application can be evaluated using as-applied maps and post-application aerial imagery along with ground observations. A series of small rectangular areas is recorded in an as-applied map during field application. The actual rate and the target rate for each rectangular area included in the as-applied map can be used for application accuracy assessment, while aerial imagery taken during the growing season can be used to detect any root rot infestation from the treated fields. Figure 6.4 shows a pretreatment CIR image taken in 2010, the as-applied map overlaid on the CIR image, and a posttreatment CIR image taken shortly before harvest in 2015 for the 11-ha cotton field. A close examination of the as-applied map revealed that the application system missed only a few small areas and did not turn on or off exactly when entering or exiting treatment zones. Nevertheless, the control system generally accurately applied the product to the prescribed areas. Spatial analysis showed that the actual treatment area was only 1.4% larger than the target treatment area, while the actual application rate was 1.5% lower than the desired rate for the field (Yang et al. 2018). Results from other test fields had similar results, indicating both types of the control systems performed well and could be used for implementing site-specific fungicide application.

By comparing the CIR image with natural infestation in 2010 and the CIR image taken after treatment in 2015, it was clear that the fungicide effectively controlled the disease in the treated areas, even though root rot occurred at a number of small areas shortly before harvest. This late infestation caused hardly any yield loss because most of the bolls were already fully developed by that time. The dullness of

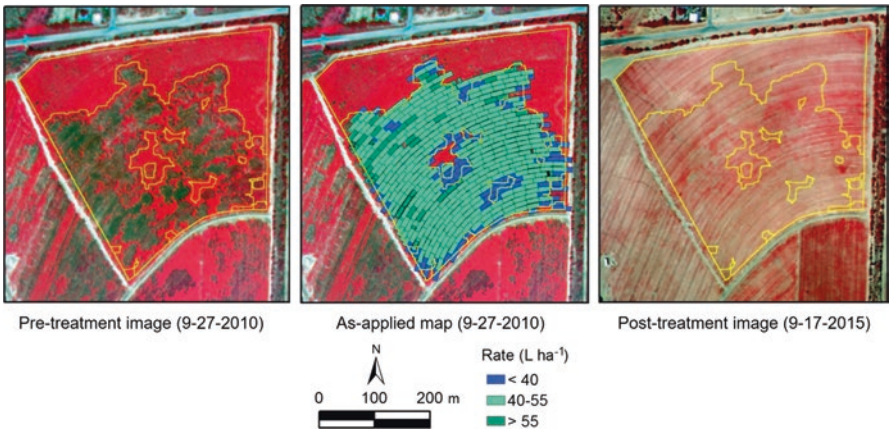

Fig. 6.4 Comparison of airborne image acquired in 2010 with natural infestation (left), as-applied map (center), and airborne image acquired in 2015 with site-specific treatment of Topguard Terra fungicide for an 11-ha cotton field near San Angelo, Texas. (Yang et al. 2018)

the image in 2015, caused by small plant size and low canopy cover, made it a little difficult to see the late infestation in the treated areas. In fact, canopy cover for much of the field was less than 50–60% due to the dry weather and limited irrigation for the season.

For the control of cotton root rot, Topguard Terra fungicide is the only choice and it is very expensive. The cost at full application rate is $124 per hectare ($50 per acre). For example, if the whole 11-ha field (actual area was 11.3 ha) were treated uniformly at full rate, the fungicide cost for the field would have been $1401 (11.3 ha × $124/ha). As only 63% of the field were treated, the savings on fungicide was about $518 or 37% over uniform treatment. Clearly, for large fields with the same percentage of infestations, the savings would be more significant. For example, if only 20% of the 97-ha field shown in Fig. 6.2 needed treatment, the savings on fungicide use would amount to $9622 (97 ha × $124/ha × 80%) for the filed in one season alone. The cost to add a variable rate control system to the existing tractor or planter was about $4000–$5000. This initial investment can be recouped if the treatment area is reduced by 32–40 ha in one single year. Our aerial surveys indicate that most fields with a history of cotton root rot infestations contain 20–40% infested areas, even though some fields could reach 75% (Yang et al. 2018). Therefore, there is a great potential for significant savings with site-specific fungicide application for the management of cotton root rot.

6.4 Challenges and Future Development

This chapter presented an overview of remote sensing technologies commonly used for the detection and management of crop diseases and insect pests. Specifically, ground-based sensors and remote sensors mounted on satellites, manned aircraft, and UAS were discussed. Practical examples were provided to illustrate how these sensors can be integrated with variable rate technology for crop disease detection and site-specific management. Diseases and pests that can cause distinctive plant symptoms (e.g., color change, defoliation, and sooty mold deposit) are good candidates for remote sensing, but it can be very difficult to distinguish the damage by a certain disease or pest when multiple biotic and abiotic conditions coexist. However, in many cases, there is only one dominant disease or pest and remote sensing can be used to map and quantify the extent and severity of the infestation as demonstrated by many studies discussed above. Otherwise, advanced sensors and image analysis techniques (e.g., machine leaning and deep learning) should be evaluated to differentiate the infestations with other confounding factors.

The availability of diverse remote sensing systems today presents both tremendous opportunities and great challenges to remote sensing practitioners and end users. Some of the challenges include platform selection (i.e., UAS, manned aircraft, and satellite), type of images to collect (e.g., multispectral, hyperspectral, and thermal), image acquisition timing, image conversion to information, and practical use of the image products. To select an appropriate platform and/or imaging system,

various factors (e.g., area size, image type and resolution requirements, and time and cost constraints) need to be considered for a specific application. In general, UAS will be more appropriate if very-high-resolution imagery is needed for a small area, while manned aircraft will be more effective for large fields or at a farm level. If manned aircraft is not available, satellite imagery will be a good choice as it can cover a large area with relatively fine spatial resolution.

For crop disease and pest detection, multispectral imagery with RGB and NIR bands is usually sufficient. Hyperspectral or thermal imagery is only needed when visible and NIR imagery cannot meet the requirement. The timing of image collection is critical for disease and pest detection to minimize or stop further crop damage. It is necessary to identify the optimum image acquisition window for different diseases and pests. Converting imagery into useable maps and information for disease or pest control is not always easy, even though numerous image processing techniques are available to convert imagery into classification maps and vegetation index maps. More research is needed to develop operational procedures for transforming image classification maps to applications maps. Each disease or pest has its own characteristics and requires different procedures for detection and management, though the cotton root rot project presented in this chapter should provide some guidance. For diseases and pests that tend to recur year after year at similar areas, historical imagery can be used to document the spatial and temporal consistency and variation of the infestation.

Variable rate application has great potential to reduce pesticide use and increase profitability as demonstrated by the cotton root rot project. Although the individual technologies required to implement site-specific pesticide application are available, it still presents a great challenge for many farmers to integrate all the technologies into a disease or pest management system. Not all diseases and pests are good candidates for variable rate application and traditional uniform application remains an effective approach. More research is needed to identify relevant diseases and pests for which site-specific management will be both technically feasible and economically profitable.

Disclaimer Mention of trade names or commercial products in this chapter is solely for the purpose of providing specific information and does not imply recommendation or endorsement by the US Department of Agriculture. The USDA is an equal opportunity provider and employer.

References

Abdel-Rahman EM, Landmann T, Kyalo R, Ong'amo G, Mwalusepo S, Suleiman S, Le Ru BP (2017) Predicting stem borer density in maize using RapidEye data and generalized linear models. Int J Appl Earth Obs Geoinf 57:61–74. https://doi.org/10.1016/j.jag.2016.1012.1008

Akkaynak D, Treibitz T, Xiao B, Gürkan UA, Allen JJ, Demirci U, Hanlon RT (2014) Use of commercial off-the-shelf digital cameras for scientific data acquisition and scene-specific color calibration. J Opt Soc Am 31:312–321

Albetis J, Duthoit S, Guttler F, Jacquin A, Goulard M, Poilvé H, Féret JB, Dedieu G (2017) Detection of Flavescence dorée grapevine disease using unmanned aerial vehicle (UAV) multispectral imagery. Remote Sens 9:308. https://doi.org/10.3390/rs9040308

Bayer BE (1976) Color imaging array. US Patent 3971065. Eastman Kodak Company, Rochester/New York

Campbell JB (2002) Introduction to remote sensing, 3rd edn. The Guilford Press, New York

Cao F, Liu F, Guo H, Kong W, Zhang C, He Y (2018) Fast detection of *Sclerotinia sclerotiorum* on oilseed rape leaves using low-altitude remote sensing technology. Sensors 18:4464

Chen X, Ma J, Qiao H, Cheng D, Xu Y, Zhao Y (2007) Detecting infestation of take-all disease in wheat using Landsat Thematic Mapper imagery. Int J Remote Sens 28(22):5183–5189

Cocks T, Jenssen R, Stewart A, Wilson I, Shields T (1998) The HYMAP airborne hyperspectral sensor: the system, calibration and performance. In: Proceedings of the 1st EARSeL workshop on imaging spectroscopy. Remote Sensing Laboratories, University of Zurich, Zurich

Colwell RN (1956) Determining the prevalence of certain cereal crop diseases by means of aerial photography. Hilgardia 26:223–286

Cook CG, Escobar DE, Everitt JH, Cavazos I, Robinson AF, Davis MR (1999) Utilizing airborne video imagery in kenaf management and production. Ind Crop Prod 9:205–210

Dehaan RL, Taylor GR (2002) Field-derived spectra of salinized soils and vegetation as indicators of irrigation-induced soil salinization. Remote Sens Environ 80:406–417

Du Q, French JV, Skaria M, Yang C, Everitt JH (2004) Citrus pest stress monitoring using airborne hyperspectral imagery. In: Proceedings of the international geoscience and remote sensing symposia, vol VI. IEEE, Piscataway, pp 3981–3984

Escobar DE, Everitt JH, Noriega JR, Cavazos I, Davis MR (1998) A twelve-band airborne digital video imaging system (ADVIS). Remote Sens Environ 66:122–128

Everitt JH, Escobar DE, Summy KR, Davis MR (1994) Using airborne video, global positioning system, and geographic information system technologies for detecting and mapping citrus blackfly infestations. Southwest Entomol 19:129–138

Everitt JH, Escobar DE, Summy KR, Alaniz MA, Davis MR (1996) Using spatial information technologies for detecting and mapping whitefly and harvester ant infestations in south Texas. Southwest Entomol 21(4):421–432

Everitt JH, Escobar DE, Noriega JR, Cavazos I, Davis MR (1998) A three-camera multispectral digital video imaging system. Remote Sens Environ 54:333–337

Ezekiel WN, Taubenhaus JJ (1934) Cotton crop losses from Phymatotrichum root rot. J Agric Res 49(9):843–858

Fletcher RS (2005) Evaluating high spatial resolution imagery for detecting citrus orchards affected by sooty mould. Int J Remote Sens 26(3):495–502

Fletcher RS, Skaria M, Escobar DE, Everitt JH (2001) Field spectra and airborne digital imagery for detecting Phytophthora foot rot infections in citrus trees. HortScience 36(1):94–97

Franke J, Menz G (2007) Multi-temporal wheat disease detection by multi-spectral remote sensing. Precis Agric 8:161–172

Galvao LS, Ponzoni FJ, Epiphanio JCN, Rudorff BFT, Formaggio AR (2004) Sun and view angle effects on NDVI determination of land cover types in the Brazilian Amazon region with hyperspectral data. Int J Remote Sens 25:1861–1879

Garcia-Ruiz F, Sankaran S, Maja JM, Lee WS, Rasmussen J, Ehsani R (2013) Comparison of two aerial imaging platforms for identification of Huanglongbing-infected citrus trees. Comput Electron Agric 91:106–115

Gorsevski PV, Gessler PE (2009) The design and the development of a hyperspectral and multispectral airborne mapping system. ISPRS J Photogramm Remote Sens 64:184–192

Hart WG, Myers VI (1968) Infrared aerial photography for detection of populations of brown soft scale in citrus groves. J Econ Entomol 61:617–624

Hart WG, Ingle SJ, Davis MR, Mangum C (1973) Aerial photography with infrared color film as a method of surveying for citrus blackfly. J Econ Entomol 66:190–194

Hassan MA, Yang M, Rasheed A, Yang G, Reynolds M, Xia X, Xiao Y, He Z (2019) A rapid monitoring of NDVI across the wheat growth cycle for grain yield prediction using a multispectral UAV platform. Plant Sci 282:95–103

Heim RHJ, Wright IJ, Scarth P, Carnegie AJ, Taylor D, Oldeland J (2019) Multispectral, aerial disease detection for myrtle rust (*Austropuccinia psidii*) on a lemon myrtle plantation. Drones 3:25

Hirakawa K, Wolfe PJ (2008) Spatio-spectral sampling and color filter array design. In: Lukac R (ed) Single-sensor imaging: methods and applications for digital cameras. CRC Press, Boca Raton, pp 137–151

Huang W, Lamb DW, Niu Z, Zhang Y, Liu L, Wang J (2007) Identification of yellow rust in wheat using in-situ spectral reflectance measurements and airborne hyperspectral imaging. Precis Agric 8(4–5):187–197

Kumar A, Lee WS, Ehsani MR, Albrigo LG, Yang C, Mangan RL (2012) Citrus greening disease detection using aerial hyperspectral and multispectral imaging techniques. J Appl Remote Sens 6:063542

Li H, Lee WS, Wang K, Ehsani R, Yang C (2014) Extended spectral angle mapping (ESAM) for citrus greening disease detection using airborne hyperspectral imaging. Precis Agric 15:162–183

Li X, Lee WS, Li M, Ehsani R, Mishra AR, Yang C, Mangan RL (2015) Feasibility study on Huanglongbing (citrus greening) detection based on WorldView-2 satellite imagery. Biosyst Eng 132:28–38

Lu J, Zhou M, Gao Y (2018) Using hyperspectral imaging to discriminate yellow leaf curl disease in tomato leaves. Precis Agric 19:379–394

Ma H, Huang W, Jing Y, Yang C, Han L, Dong Y, Ye H, Shi Y, Zheng Q, Liu L, Ruan C (2019) Integrating growth and environmental parameters to discriminate powdery mildew and aphid of winter wheat using bi-temporal Landsat-8 imagery. Remote Sens 11:846

MacDonald SL, Staid M, Staid M, Cooper ML (2016) Remote hyperspectral imaging of grapevine leafroll-associated virus 3 in cabernet sauvignon vineyards. Comput Electron Agric 130:109–117

Mattupalli C, Moffet CA, Shah KN, Young CA (2018) Supervised classification of RGB aerial imagery to evaluate the impact of a root rot disease. Remote Sens 10:917. https://doi.org/10.3390/rs10060917

Mirik M, Jones DC, Price JA, Workneh F, Ansley RJ, Rush CM (2011) Satellite remote sensing of wheat infected by wheat streak mosaic virus. Plant Dis 95:4–12. https://doi.org/10.1094/PDIS-04-10-0256

Myers VI (1983) Remote sensing applications in agriculture. In: Colwell RN (ed) Manual of remote sensing. American Society of Photogrammetry, Falls Church, pp 2111–2228

Nijland W, de Jong R, de Jong SM, Wulder MA, Bater CW, Coops NC (2014) Monitoring plant condition and phenology using infrared sensitive consumer grade digital cameras. Agric For Meteorol 184:98–106

Nixon PR, Escobar DE, Bowen RL (1987) A multispectral false-color video imaging system for remote sensing applications. In: Proceedings of the 11th biennial workshop on color aerial photography and videography in the plant sciences and related fields, vol 295–305. American Society for Photogrammetry and Remote Sensing, Bethesda, p 340

Nuessly GS, Meyerdirk DE, Hart WG, Davis MR (1987) Evaluation of color-infrared aerial photography as a tool for the identification of sweetpotato whitefly induced fungal and viral infestations of cotton and lettuce. In: Proceedings of the 11th biennial workshop on color aerial photography and videography in the plant sciences and related fields. American Society of Photogrammetry and Remote Sensing, Bethesda, pp 141–148

Oerke EC (2019) Precision crop protection systems. In: Stafford J (ed) Precision agriculture for sustainability. Burleigh Dodds Science Publishing, pp 347–397

Pammel LH (1888) Root rot of cotton, or "cotton blight", Annual Bulletin 4. Texas Agricultural Experimental Station, College Station, pp 50–65

Rabatel G, Gorretta N, Labbé N (2014) Getting simultaneous red and near-infrared band data from a single digital camera for plant monitoring applications: theoretical and practical study. Biosyst Eng 117:2–14

Roth L, Aasen H, Walter A, Liebisch F (2018) Extracting leaf area index using viewing geometry effects – a new perspective on high-resolution unmanned aerial system photography. ISPRS J Photogramm Remote Sens 141:161–175

Ryerson RA, Curran PJ, Stephens PR (1997) Applications: agriculture. In: Philipson WR (ed) Manual of photographic interpretation. American Society for Photogrammetry and Remote Sensing, Bethesda, pp 365–397

Sakamoto T, Gitelson AA, Nguy-Robertson AL, Arkebauer TJ, Wardlow BD, Suyker AE, Verma SB (2012) An alternative method using digital cameras for continuous monitoring of crop status. Agric For Meteorol 154–155:113–126

Santoso H, Gunawan T, Jatmiko RH, Darmosarkoro W, Minasny B (2011) Mapping and identifying basal stem rot disease in oil palms in North Sumatra with QuickBird imagery. Precis Agric 12:233–248

Savary S, Willocquet L, Pethybridge SJ, Esker P, McRoberts N, Nelson A (2019) The global burden of pathogens and pests on major food crops. Nat Ecol Evol 3:430–439. https://doi.org/10.1038/s41559-018-0793-y

Schiefer S, Hostert P, Damm A (2006) Correcting brightness gradients in hyperspectral data from urban areas. Remote Sens Environ 101:25–37

Smith HE, Elliot FC, Bird LS (1962) Root rot losses of cotton can be reduced, Publication No. MP361. Texas A&M Agricultural Extension Service, College Station

Song H, Yang C, Zhang J, Hoffmann CW, He D, Thomasson JA (2016) Comparison of mosaicking techniques for airborne images from consumer-grade cameras. J Appl Remote Sens 10(1):016030

Song X, Yang C, Wu M, Yang G, Hoffmann WC (2017) Evaluation of sentinel-2A imagery for mapping cotton root rot. Remote Sens 9:206

Taubenhaus JJ, Ezekiel WN, Neblette CB (1929) Airplane photography in the study of cotton root rot. Phytopathology 19:1025–1029

Uppalapati SR, Young CA, Marek SM, Mysore KS (2010) Phymatotrichum (cotton) root rot caused by *Phymatotrichopsis omnivora*: retrospects and prospects. Mol Plant Pathol 11(3):325–334

Vanegas F, Bratanov D, Powell K, Weiss J, Gonzalez F (2018) A novel methodology for improving plant pest surveillance in vineyards and crops using UAV-based hyperspectral and spatial data. Sensors 18:260

Varela S, Assefa Y, Prasad PVV, Peralta NR, Griffin TW, Sharda A, Ferguson A, Ciampitti IA (2017) Spatio-temporal evaluation of plant height in corn via unmanned aerial systems. J Appl Remote Sens 11(3):036013

Wu M, Yang C, Song X, Hoffmann WC, Huang W, Niu Z, Wang C, Wang L (2017) Evaluation of orthomosics and digital surface models derived from aerial imagery for crop type mapping. Remote Sens 9:239

Yang C (2012) A high resolution airborne four-camera imaging system for agricultural applications. Comput Electron Agric 88:13–24

Yang C (2018) High resolution satellite imaging sensors for precision agriculture. Front Agric Sci Eng 5(4):393–405

Yang C, Hoffmann WC (2015) Low-cost single-camera imaging system for aerial applicators. J Appl Remote Sens 9:096064

Yang C, Fernandez CJ, Everitt JH (2005) Mapping Phymatotrichum root rot of cotton using airborne three-band digital imagery. Trans ASABE 48(4):1619–1626

Yang C, Fernandez CJ, Everitt JH (2010) Comparison of airborne multispectral and hyperspectral imagery for mapping cotton root rot. Biosyst Eng 107:131–139

Yang C, Westbrook JK, Suh CP, Martin DE, Hoffmann WC, Lan Y, Fritz BK, Goolsby JA (2014) An airborne multispectral imaging system based on two consumer-grade cameras for agricultural remote sensing. Remote Sens 6:5257–5278

Yang C, Odvody GN, Thomasson JA, Isakeit T, Nichols RL (2016) Change detection of cotton root rot infection over 10-year intervals using airborne multispectral imagery. Comput Electron Agric 123:154–162

Yang C, Odvody GN, Thomasson JA, Isakeit T, Minzenmayer RR, Drake DR, Nichols RL (2018) Site-specific management of cotton root rot using airborne and high resolution satellite imagery and variable rate technology. Trans ASABE 61(3):849–858

Yuan L, Pu R, Zhang J, Wang J, Yang H (2016) Using high spatial resolution satellite imagery for mapping powdery mildew at a regional scale. Precis Agric 17:332–348

Zhang M, Qin Z, Liu X (2005) Remote sensed spectral imagery to detect late blight in field tomatoes. Precis Agric 6:489–508

Zhang J, Pu R, Yuan L, Wang J, Huang W, Yang G (2014) Monitoring powdery mildew of winter wheat by using moderate resolution multi-temporal satellite imagery. PLoS One 9(4):e93107. https://doi.org/10.1371/journal.pone.0093107

Zhang J, Yang C, Song H, Hoffmann WC, Zhang D, Zhang G (2016) Evaluation of an airborne remote sensing platform consisting of two consumer-grade cameras for crop identification. Remote Sens 8:257

Chapter 7
Plant Phenotyping

Quan Qiu, Man Zhang, Ning Wang, Ruicheng Qiu, and Yanlong Miao

Abstract Breeding is thought to be one of the most effective ways to solve the problem of food crisis. However, traditional phenotyping in breeding is time consuming and laborious, and the database is insufficient to meet the requirements of plant breeders, hindering the development of breeding. Accordingly, innovations in phenotyping are urgent to solve this bottleneck. The morphometric and physiological parameters of plants are particularly of interest to breeders. Numerous sensors have been employed and novel algorithms have been proposed to collect data on such parameters. These sensors and sensing techniques used in phenotyping include color digital cameras, Lidar or laser sensors, range cameras, spectral sensors and cameras, thermography, fluorescence sensors, and X-ray computed tomography (CT) techniques. In addition, remote-sensing technologies, three-dimensional (3D) imaging techniques, reverse engineering, and virtual plant techniques can also provide the basis for phenotyping. Some parameters that have been measured in phenotyping include plant height, leaf parameters, in-plant space, chlorophyll, water stress, biomass, and characteristics of plant roots. In plant phenotyping, different types of platforms are employed to meet the requirements of different plant phenotyping scenarios. Indoor phenotyping equipment, in-field sensor networks, ground mobile platforms, phenotyping towers, field-scan platforms, unmanned aerial vehicles (UAVs), airplanes, and even satellites can all implement plant phenotyping. In order to extract features of plants and reveal corresponding traits of interests in plant phenotyping, different mathematical tools and algorithms are employed to process the data, including data preprocessing algorithms, traditional statistical tools, and machine learning algorithms.

Q. Qiu
National Engineering Research Center for Information Technology in Agriculture, Beijing, China

M. Zhang (✉) · R. Qiu · Y. Miao
China Agricultural University, Beijing, China
e-mail: cauzm@cau.edu.cn

N. Wang
Oklahoma State University, Stillwater, OK, USA

M. Li et al. (eds.), *Soil and Crop Sensing for Precision Crop Production*,
Agriculture Automation and Control, https://doi.org/10.1007/978-3-030-70432-2_7

Keywords Plant phenotype · Morphometric parameters · Physiological parameters · Sensors · Lidar · Phenotyping platform

7.1 Introduction

Food security means that all people, at all times, have physical, social, and economic access to sufficient, safe, and nutritious food that meets their food preferences and dietary needs for an active and healthy life. The rapid increase of the world population, alongside the decrease in cultivated land area, intensification of global climate change, and exacerbation of water resource shortage, is posing a tremendous challenge to the agricultural sector, which is facing the growing problem of food security (Großkinsky et al. 2015).

The most effective way to solve the food crisis is to increase grain yield. Plants are influenced by both self-genome and external environment conditions. For example, plants are more frequently subjected to unprecedented extreme weather (e.g., gale, drought, and waterlogging). Thus, breeding new plant varieties capable of withstanding complex and varied environmental conditions is necessary.

In the past decades, significant progress has been made in the field of plant breeding. Particularly, advances in plant functional genomics and gene technologies have deepened the understanding on plant genomes (Yang et al. 2013). Currently, genetically modified technologies have become an attractive subject and are regarded as the effective and expedient solution to increase grain yield. With the development of plant genotyping, breeders intend to research on the nature of the genotype through environment interactions. Phenotype, which is the external expression of plant genetics, results from the interaction of the genotype and environment. Consequently, understanding the relationship between genotype and phenotype and linking them to the physiology at the cellular and tissue levels are becoming more significant than ever (Großkinsky et al. 2015; Cobb et al. 2013). Breeders pay attention to both the final grain yield and the entire process of plant growth. As an organ develops, some plant traits and phenotypic parameters that vary in space and time need to be monitored and measured for a considerable time to cultivate excellent varieties. However, this task is formidable because numerous parameters are measured manually and the methods employed are outdated, laborious, costly, and time consuming. As a result, current manual measurement approaches cannot be used in large-scale breeding production to acquire phenotypic information (Yang et al. 2013). Owing to the lack of phenotypic data, phenotyping has superseded genotyping as the major operational bottleneck and funding constraint of genetic analyses and breeding research (Cobb et al. 2013). Thus, applying new techniques and methods to relieve this bottleneck is both urgent and promising.

In recent years, innovations in electronics, computer science, and sensor technologies have promoted the development of phenotyping, and novel methods

specific to the measurement of phenotypic parameters have been put forward. Since 2010, rapid high-throughput plant phenotyping methods, which exhibit great potential to enhance selection efficiency for plant breeding, have been discussed (Sankaran et al. 2015). All types of existing sensors and technologies have been implemented and integrated. Some precision agriculture technologies, which have been studied for many years, can also be implemented in phenotyping. In addition, sensor technologies, remote-sensing technologies, three-dimensional (3D) imaging techniques, reverse engineering, and virtual plant technique can provide the basis for phenotyping. Such measuring methods can be carried out in the field or the laboratory to collect massive data, thereby facilitating high-throughput phenotyping.

Therefore, phenotyping allows the measurement of the morphometric and physiological parameters of plants in a rapid, nondestructive, accurate, and high-throughput manner. It can help breeders analyze and screen the salt resistance, drought resistance, and insect resistance of different varieties. Currently, the measured objects in plant phenotyping are conventional food and economic crops, such as wheat, maize, sorghum, barley, tomato, bean, and grape. These plants have significant practical and economic values for agricultural development. Measurement usually focuses on some crop stand parameters. These parameters can be divided into morphometric and physiological parameters. The morphometric parameters, including plant height, stem diameter, leaf area or leaf area index, leaf angle, stalk length, and root traits, and the physiological parameters, such as chlorophyll, photosynthetic rate, water stress, biomass, salt resistance, and leaf water content, which can all influence or represent the growth of a plant.

The objectives of this chapter are to summarize and analyze the existing sensing methods and sensors according to the related morphometric and physiological parameters in high-throughput plant phenotyping and discuss the obstacles encountered in this field.

7.2 Sensing Instruments for Plant Phenotyping

7.2.1 Overview

The phenotypic parameters that must be measured are numerous, and thus various sensors and sensing techniques are used in phenotyping, including color digital cameras, Lidar or laser sensors, range cameras, spectral sensors and cameras, thermography, fluorescence sensors, and X-ray computed tomography (CT) technique. Several typical sensors that have been extensively implemented in plant phenotyping are described in the following part, and related representative products are listed in Table 7.1.

Color digital cameras, which are mostly made up of charge-coupled device (CCD) silicon sensors or complementary metal oxide semiconductors, are the most conventional and simplest sensors in the machine vision field. They can collect the

Table 7.1 Typical devices in plant phenotyping measurement[a]

Sensor	Sensor model	Manufacturer
Color digital camera	–	Canon, Tokyo, Japan
		Nikon, Tokyo, Japan
Lidar/laser sensor	LMS series	Sick AG, Waldkirch, Germany
	VLP-16, HDL-32E	Velodyne Acoustics, California, USA
Range camera	CamCube 3.0	PMD, Germany
	SR4000	MESA AG, Switzerland
	Kinect 2.0	Microsoft, Washington, USA
Spectral sensor	GreenSeeker RT 100, 200	Trimble, California, USA
	Crop Circle ACS 210, 430, 470	Holland Scientific, Lincoln, USA
	N-Sensor	Yara International ASA, Oslo, Norway
Thermography	FLIR T-series	FLIR, Oregon, USA
Fluorescence sensor	Multiples 2, 3	FORCE-A, Orsay, France

[a]*Disclaimer*: Commercial products are referred to solely for the purpose of clarification and should not be construed as being endorsed by the authors or the institution with which the authors are affiliated

visible-band radiation of an object and present its color and texture information with similar wavelengths to human eyes. Plant 3D structure can be reconstructed with many images captured by the stereo vision system. It consists of one or more color digital cameras, which make it possible for color digital cameras to measure more phenotypic parameters.

Lidar sensors, which emit infrared or visible wavelength pulses, have been extensively used in agricultural studies since the 1980s (Lee et al. 2010) and are mostly based on the time-of-flight (ToF) principle, interferometry, or triangulation. Lidar sensors based on ToF are suitable to measure long ranges, while the others are used to measure short ranges (Dworak et al. 2011). Lidar sensors output discrete point cloud data containing the distance information between the object and the sensors. Based on the structures, Lidar can be divided into two-dimensional (2D) Lidars and 3D Lidars. Two-dimensional Lidars detect an object through sector scanning and generate point cloud data in a plane. Three-dimensional Lidars can present the point cloud data of the object surface features with high accuracy and high resolution, as well as more easily acquire morphological and structural data (Gai et al. 2015). Besides the common Lidar sensor just for measuring distances, full-waveform (FWF) Lidar and hyperspectral Lidar were also implemented in plant phenotyping. FWF Lidar contains all the return information of a laser pulse in a unique waveform shape. FWF Lidar makes it easier to distinguish diverse objects (Lin 2015). Hyperspectral Lidar is able to add the spectral response characteristics of a plant to multiple wavelengths to point data, which help to diagnose the vigor of the plant.

Range cameras can provide real-time depth information and images simultaneously. These cameras are mostly based on the ToF principle, structured light and light coding, ordinarily return depth, amplitude, and intensity images. The depth

image contains the Z coordinate of the scene, and the amplitude image can evaluate the quality of depth information, and the intensity image is simply a grayscale image (Kazmi et al. 2014). As a new kind of range cameras, RGB-D cameras equipped with RGB (red, green, and blue) cameras, depth sensors, and infrared emitters have been developed at low cost, which can simultaneously provide color information and depth information of an object. Kinect (Microsoft, WA, America) and Xtion (Asus, Taipei, Taiwan) are regarded as representatives of such cameras and are used extensively in numerous applications, including its primary application of plant measurement (Xia et al. 2015).

Spectral sensors usually detect the reflected information of a visible spectrum (400–700 nm) and a near-infrared (NIR) spectrum (700–1200 nm) and can be used to explore some specific characteristics of objects. Some commercial agricultural products, such as GreenSeeker (Trimble, California, USA), ASD FieldSpec (Analytical Spectral Devices, Boulder, USA), N-Sensor ALS (Yara International ASA, Oslo, Norway), and Crop Circle (Holland Scientific, Lincoln, USA), have been widely implemented by researchers.

These spectral devices usually measure crop or soil spectral reflectance at multiple wavelengths and provide classic vegetation indices. In addition, spectral cameras, including multispectral and hyperspectral cameras, can acquire spectral images that record the reflections in a broad range of wavelengths of an object. Compared with spectral sensors, spectral cameras combine spectral information with every pixel and contribute to reducing the background interference and making spectral information more accurate (Shakoor et al. 2017; Yang et al. 2017).

Thermography detects and visualizes the infrared radiation of an object in line with its temperature. The sensitive spectral band of thermography is 3–14 μm, and the most common wavelengths are 3–5 μm and 7–14 μm (Li et al. 2014a). Thermography is able to detect early heat generation in stressed plants, especially leaves (Kwon et al. 2015). Thermal images can represent the surface temperature of a plant objectively.

Fluorescence sensors measure plants in a unique and active manner. In general, the chlorophyll of a plant is the fluorescent part. External light is absorbed and utilized by the chlorophyll for photosynthesis, where a proportion of the absorbed light is converted into heat, while the other proportion is reflected back in the form of fluorescence. Numerous plant traits, particularly some parameters related to the photosynthesis of the plant, can be acquired by detecting the fluorescence.

Many other sensors, such as ultrasonic sensors, thermometers, and X-ray computer tomography (CT), are also used in phenotype measurement.

Phenotype measurement can be conducted in an indoor or outdoor measurement environment. Measurement types mainly include handheld, vehicle-based, and unmanned aerial vehicle (UAV)-based measurements. The characteristics of the common sensors are listed in Table 7.2, and a detailed information about these sensors are discussed in the following sections.

Table 7.2 Advantages and disadvantages of common sensors implemented in phenotyping

Sensors	Advantages	Disadvantages
Stereo vision system	Low cost	Heavy computation
	High resolution	Sensitive to ambient light
	Suitable for UAV	Subject to the uniform texture
Lidar/laser sensor	Long measurement range	High cost
	Suitable for spatial classification	Limited information on occlusions and shadows
	Spectral information can be retrieved from reflection	
	Suitable for UAV	
Range camera	Provide depth images to process	Low resolution
		Sensitive to ambient light
		Short measurement range
Spectral sensor	Wide commercial applications and technology maturity	Small measurement region
		Background interference
Spectral camera	Abound spectral information	High cost
	Remove background interference	Large image data and heavy computation
	Suitable for UAV	Sensitive to ambient conditions
Thermography	Large measurement region	Sensitive to ambient conditions
	Remove background interference	Require extensive calibration
	Suitable for UAV	
Fluorescence sensor	Sensitive to chlorophyll and water stress	Small field of view
		Require intensive illumination
Ultrasonic sensor	Low cost	Short measurement range
	High sampling rate	Sensitive to surface
	Process data easily	
Thermometer	Low cost	Affected by ambient temperature
	Impervious to sunlight	Soil background interference
X-ray CT	Visualize the interior of objects	High cost
	Provide 3D information with high resolution	Require complex instruments

7.2.2 Sensing Instrumentation for Plant Canopy

Several phenotypic parameters are closely related to the plant canopy, including plant height, leaf parameters, chlorophyll, and water stress.

7.2.2.1 Plant Height Measurement

Plant height is a vital morphological parameter that can be used to describe the architecture of the plant canopy. Plant height at the seedling growth stage can represent plant vigor, which is closely related to the final grain yield.

Conventional measurement is performed manually with a meter stick and is thus subject to human error, especially when the plant is higher than the human measuring it. Color digital cameras have been used to measure plant height. However, this method requires known objects as reference. It is difficult to realize high-throughput measurement rapidly through this method. An accurate and acceptable method that can determine plant height is the difference method, wherein the difference between the canopy height and the surface is calculated (Grenzdörffer 2014). Novel systems or sensors, such as stereo vision systems, Lidar or laser sensors, ultrasonic sensors, and range cameras, have also been utilized to measure plant height.

The current types of high-throughput measurement methods for plant height are vehicle-based and UAV-based (Grenzdörffer 2014; Gao et al. 2015; Jiang et al. 2016; Sharma et al. 2016). Each measurement type has its pros and cons. Vehicle-based measurement can acquire relatively accurate raw data owing to its close-up sampling, making it possible to obtain individual plant height. Conversely, UAV-based measurement is performed at a distance from the canopy and is capable of measuring considerable plant height (Shi et al. 2016).

Plant Height Measurement Based on Stereo Vision Systems

With stereo vision systems, high-resolution images of a plant can be obtained and 3D models can be generated by fusing images of different perspectives to measure plant height. Typically, fused images are collected from several different cameras or a moving camera (Fig. 7.1), and 3D models are established based on the relative positions of cameras. Chen et al. (2011) adopted binocular

Fig. 7.1 Plant height measurement. (**a**) Several different cameras (Nguyen et al. 2015). (**b**) A moving camera

stereovision to monitor maize in the fields and then reconstructed the images in 3D to calculate plant height. Many algorithms were put forward to make it possible to measure plant height with a single camera. Jay et al. (2015) estimated plant height with a single-color camera and constructed a 3D model of the plant using the Structure-from-Motion (SFM) algorithm, and both color and 3D information were used to derive plant height. A camera was also installed on a UAV to collect images from a large field of maize and sorghum (Shi et al. 2016), and the digital surface model was calculated with SFM to estimate plant height, but the results were not satisfactory, which may be caused by the insufficient images. High-resolution and considerable overlap images are of great importance. Santos and Rodrigues (2016) employed the patch-based multiple-view stereo algorithm (PMVS) to reconstruct the 3D point of maize and estimated plant height by computing the distance between the farthest point and the fitting ground plane, and the measuring error was inferior to 1%. Nonetheless, the accuracy and speed of the processing algorithms for stereo vision systems need to be improved. Binocular stereo vision is positively correlated with measuring distances, and SFM is sensitive to wrong registration. Stereo vision systems are also not robust against natural illumination due to the limitations of color digital cameras, which restricts the outdoor applications of these systems.

Plant Height Measurement Based on Lidar Sensors

Lidar or laser sensors have been used to measure plant height because they present good adaptation to illumination and provide considerable data. Some studies have selected vehicle-based measurement and installed Lidar to measure plant height. Plant height can be derived from the point cloud data of Lidar, including distance information collected from the plant canopy or plant side. Chatzinikos et al. (2013) used a laser scanner to measure the properties of three plants. Saeys et al. (2009) adopted 2D Lidar to measure wheat and used the histogram method to estimate plant density. Zhang and Grift (2012) used 2D Lidar to detect the stem height of *Miscanthus giganteus*. Given the measurement errors introduced by the inclination angles resulting from the installation of the sensor or the undulation of the ground, Zhang and Grift (2012) analyzed and developed a correction algorithm based on the difference between the maximum and minimum ordinates. However, both travel speed and natural wind affected the aforementioned studies, because high speed can diminish the data volume as a result of the 2D line scan nature. On the other hand, 2D Lidars are not robust in measuring the occlusion of plant organs, such as overlapping leaves and branches (Kazmi et al. 2014). Owing to their ability to handle this situation, 3D Lidars have been mounted at certain heights to observe plants in some studies (Hoffmeister et al. 2015; Weiss and Biber 2011). Because the measurement error increases with the increase of the measurement distance, the appropriate distance and installation position of the 3D laser radar should be determined. To address this issue, the related tests and

analysis were conducted by Ehlert and Heisig (2013). The results showed that plant surface generated based on point cloud becomes steeper with an increase in scan angle. The accuracy of the point cloud data was highest when 3D Lidars scanned small plants vertically, and the front angle represented the best angle for high plants. Different from 2D Lidars, 3D Lidars were unaffected by a wide speed range, and the velocity of a vehicle had a negligible effect on the measurement results (Selbeck et al. 2010).

Novel Lidars with preferable performances have also been introduced to measure plant height. A 3D Lidar with four layers was adopted to measure the height of wheat and maize (Selbeck et al. 2010; Ehlert et al. 2010). The Lidar emits a pulse, and four photodiodes at different heights receive the return signals. As a result, a pulse can acquire four echo signals, and the accuracy and data volume can be improved. Gao et al. (2015) likewise adopted an airborne FWF Lidar system to extract maize height through a UAV-based measurement. Unlike Lidar point clouds, which recorded limited strong peaks, a FWF contained all the return signals of a laser pulse (Gao et al. 2015), and different signals could be combined and analyzed. UAV-based measurement can build a digital terrain model to improve measurement accuracy. Plant height can be acquired by taking the difference between the digital terrain model and the current UAV surface model (Bendig et al. 2013, 2014, 2015), thus generating crop surface models.

Plant Height Measurement Based on Ultrasonic Sensors

The measuring principle of ultrasonic sensors is similar to that of Lidars. Although the spatial resolutions of ultrasonic sensors are lower than Lidars, the prices are relatively low. The ultrasonic sensors are also not influenced by natural conditions because of its wavelengths; therefore, they are extensively used for outdoor measurement. Plant height can be calculated by ultrasonic sensors using the difference method. Sui et al. (2012, 2013) utilized ultrasonic sensors for vehicle-based measurement coupled with a global positioning system (GPS) to measure the height of cotton plants and generate the height distribution maps. Sharma et al. (2016) used ultrasonic sensors mounted on a two-wheel bicycle to measure maize height for yield estimation. However, ultrasonic sensors are likely to be divergent and damped. Their scanning accuracy is susceptible to the orientation and roughness of the sensing surface that data are easily lost. The sensors are usually installed perpendicular to the ground to ensure precision, but the movement of upright leaves with wind will lead to different readings (Dworak et al. 2011). All of these factors result in the fact that ultrasonic sensors are not suitable for long-range measurement. Recently, the acoustic spectrum in a wide frequency range was applied, and the quality of the ultrasonic signals were significantly improved (Finkelshtain et al. 2016), which might promote its application. To improve measurement accuracy, ultrasonic sensors can be also combined with Lidars (Pittman et al. 2015).

Plant Height Measurement Based on Range Cameras

Range cameras measure plant height based on its depth information. An autonomous field robot mounted with a depth camera from PMD technologies AG in Germany was developed, and the plant height was monitored by calculating the histogram of distances (Klose et al. 2012). However, the cameras are usually disturbed by natural illuminations, and the pixels of the images are low (e.g., 204 × 204 pixels for PMD CamCube).

Besides depth information, color information provided by RGB-D cameras makes it easier to remove background interference and identify plants. Azzari et al. (2013) used Kinect to characterize the vegetation structure, and the normalized root-mean-squared error of plant height ranged from 2.7% to 19.1%. Gai et al. (2015) used Kinect to recognize plants and calculate their heights, and the measuring error of maize was within 2 cm. Andújar et al. (2016) applied Kinect to estimate the height of cauliflower, and the deviation from the ground truth was less than 2 cm. Kinect provides high-resolution images (e.g., 640 × 480 pixels and up to 1920 × 1080 pixels) even if its cost is lower than the aforementioned sensors. In addition, the latest Kinect is robust against natural illuminations, and its applications in plant phenotyping are promising.

Comparison and Analysis of Plant Height Measurements

Compared with other sensors, the measurement accuracy of Lidars is the highest because of the considerable amounts of data acquired (Shi 2009). However, the Lidars are costly. Although ultrasonic sensors have a price advantage, only few studies use these sensors because they generate huge amounts of invalid data. Stereo vision systems require image calibration, and range cameras possess low resolution, so that the data may be lost after data processing. Illumination also has an effect on the measurement accuracy of both stereo vision systems and range cameras. With the improved performance and algorithm, aside from its low cost and high accuracy, Kinect may be a good choice for plant height measurement.

7.2.2.2 Leaf Parameter Measurements

A leaf is one of the important parts of a plant canopy. It plays a significant role in plant growth because its growing status affects the efficiency of the direct solar energy utilization of the plant. Therefore, the leaf is a vital parameter in plant phenotyping. Numerous morphological parameters are associated with leaves, which are frequently measured in phenotyping and include leaf inclination angle (LIA) or leaf angle distribution (LAD), leaf area (LA), and leaf area index (LAI). LIA refers to the angle between the zenith and the leaf surface normal and determines the quality of plant light interception. LAD has an

influence on the LAI measurement and represents the water stress of a plant (Zou et al. 2014). LA refers to the area of a single leaf, and its estimation is significant to the biometrical observation (geometric features) of a plant. LAI indicates the ratio of the summation of plant LAs per unit ground area. LAI represents the vitality of a plant group and the canopy architecture, which results in photosynthesis and plant water use. The aforementioned parameters are relevant to a plant in terms of biological and physical processes, such as photosynthesis, respiration, transpiration, and water use, as well as to grain yield. LIA can be measured manually using a protractor. Compared with that of LIA, the measurement methods of LAI and LA are complicated and arduous. A leaf needs to be painted with paper in unit cells, and the number of cells can then be counted to obtain the area.

A few sensors and techniques for measuring leaves have been developed and implemented gradually for phenotyping to save time and minimize labor.

Leaf Parameter Measurement Using Color Digital Cameras and Stereo Vision System

A color digital camera is a low-cost imaging device and extensively used in various fields, including measuring plant leaves. Specifically, the color images of leaves are captured and processed with morphological operations, which can be used to calculate the parameters of LIA, LA, and LAI.

Color digital cameras can be mounted on a UAV to measure plant canopy. Ribera et al. (2016) estimated traits of sorghum, and the images were mosaicked and segmented to verify plant center location and assess leaf numbers and LA. But the plant leaves that connected to each other led to the failure to evaluate individual plants. It is a significant task to handle occlusion and intersection problems in color images and segment individual plants or leaves. Color images are able to estimate the green cover fraction, and previous studies have shown that there is a relationship between the plant coverage and LAI. Liu and Pattey (2010) used top-of-canopy color images over a plant to estimate LAI, and a model was built based on gap fraction, which was linearly related with LAI2000.

Stereo vision systems are also introduced to measure leaf features. Yeh et al. (2014) developed a system which consisted of two off-the-shelf cameras with parallel optical axes. Images were rectified and registered, and the corresponding pointes were detected and matched. Plants were segmented and LA was calculated by counting the pixels. Leemans et al. (2012) used stereoscopic images to build a model with distance information, and LAI was segmented and calculated in the field. Multiple cameras can be used to construct a multi-view stereo vision system. Zhang et al. (2016) combined four images taken at different positions with the SFM algorithm to reconstruct paprika plant in 3D and accurately estimated leaf lengths and widths, which could be used to measure LA (Bazaza et al. 2011; Oner et al. 2011).

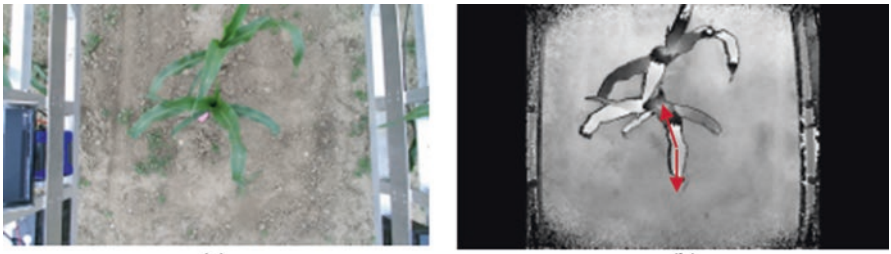

Fig. 7.2 Leaf parameter measurement by range cameras. (**a**) RGB image of maize. (**b**) Angles of leaves in the depth image

Leaf Parameter Measurement Using Range Cameras

Range cameras were tested to analyze the parameters of leaves, and the depth images of a leaf captured by PMD and SwissRanger SR4000 cameras were analyzed and compared under indoor (room) and outdoor (shadow and sunlight) conditions (Kazmi et al. 2014). The results showed that determining the best possible integration times for each condition was necessary. Depth information offered by range cameras was widely used to extract plants and leaves. Song et al. (2014) combined stereo and ToF images and conducted a localized search to find the boundary of leaves. Chéné et al. (2012) proposed a segmentation algorithm of depth images captured by Kinect to extract leaf and measured its azimuth and zenith angles for plant phenotyping, as shown in Fig. 7.2. Additionally, Andújar et al. (2016) separated crops from ground based on both the height difference and colors. Plant leaves were extracted and reconstructed in 3D. Point cloud data were meshed and smoothed, and then LAD, LAI, and LA were successfully estimated (Song et al. 2014; Paulus et al. 2014a, b).

Leaf Parameter Measurement Using Spectral Sensors and Cameras

A few vegetation indices can generally be derived based on the spectral responses of the plant canopy. In particular, nondestructive methods can be used to invert some parameters and indirectly calculate LAI, and typically, the most common parameter used to invert LAI is the normalized difference vegetation index (NDVI) (Huete and Jackson 1988). New parameters were also presented in recent studies. Hasegawa et al. (2010) combined the hotspot-dark spot index and the NDVI, both of which are related closely with LAI, and proposed a normalized hotspot-signature vegetation index (NHVI) to build the relationship with LAI. The results showed that NHVI has better performance in estimating LAI than NDVI. In general, the spectral information in the visible and NIR bands is used to build LAI models. Neinavaz et al. (2016a, b) conducted some research in the thermal infrared region (TIR). Spectrometer was implemented to measure the spectral information of plants in the TIR. In the region, spectra mostly came from the emissivity of plants rather than their reflectance. Radiometric calibration was carried out to the measurement. They

found that the canopy emissivity spectra increased with rising LAI (Neinavaz et al. 2016a). PLSR and ANN were applied to analyze the spectral data, and the results indicated that the spectrum in TIR was able to retrieve LAI, but it was necessary to conduct further study in field conditions (Neinavaz et al. 2016b). LAI also can be evaluated according to the plant coverage calculated from spectral images. Dammer et al. (2016) used a multispectral camera to collect the plant reflections of light at red and infrared wavelengths. Schirrmann et al. (2016) gathered images from the red and NIR wavelength range of plants, and then NDVI images based on red and NIR images were calculated. NDVI images were processed to extract plants and calculate the plant coverage, and then LAI was estimated according to the coverage.

Leaf Parameter Measurement Using Lidar/Laser Sensors

Special attention is increasingly given to Lidar to measure leaf features (Kempthorne et al. 2014). Lidar can rapidly acquire the point cloud data of a leaf surface by using sensors to scan the plant canopy and leaves. Plant architecture can thus be generated under indoor or field conditions.

Considerable research on plant 3D visualization and virtual plants has also been conducted for many years. The 3D point cloud data and growth rules (e.g., L system) are applied to modeling, and some leaf parameters are calculated and extracted in this way. All the results provide the basis for the following Lidar measurement. For Lidar measurement, LIA, LA, and LAI can be obtained by surface computation. Multi-view or multi-frame Lidar data need to be registered and matched (Garrido et al. 2015) and then can be used to reconstruct leaves in 3D (Fig. 7.3). Hosoi et al.

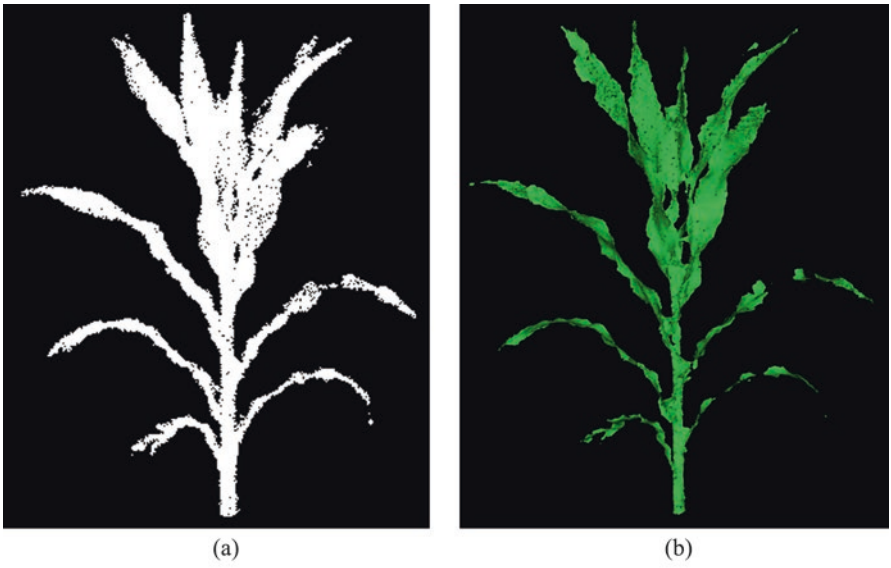

Fig. 7.3 Leaf parameter measurement by laser sensors. (**a**) Point cloud data of the maize plant. (**b**) 3D reconstruction of each leaves

(2011) used Lidar to scan tomato plants and extract corresponding points and then to estimate LA, LAI, and LIA. In terms of field measurement, Gebbers et al. (2011) designed vehicle-based Lidar sensors to analyze the relationship between LAI and plant height. Consequently, a regression model was built to estimate LAI rapidly.

Comparison and Analysis of Leaf Parameter Measurements

The abovementioned measurement methods can be divided into two types according to the measurement principle of leaves. Color digital cameras, stereo vision systems, range cameras, and Lidar can measure or estimate leaf features by segmenting and reconstructing the leaf and calculating its actual values. Spectral sensors and cameras can acquire leaf features through inferring on the basis of related parameters. Compared with the inference method, reconstruction is more complicated and has costly computation operation. However, the measurement accuracy of reconstruction is generally higher than that of inference.

Several problems have been encountered in practice that cause the measurement methods of LIA, LA, and LAI to be incomplete. On the one hand, accomplishing the measurement of leaves according only to the single-perspective data is difficult. Multi-perspective measurement is needed to reduce deviations. On the other hand, leaves of the same plant or adjacent plants will block and overlap each other. Current methods have difficulty classifying all leaves and settling this situation. Consequently, measurement results usually tend to be underestimated. Potentially, it is possible to extract leaves using deep learning techniques.

7.2.2.3 Chlorophyll Measurements

Chlorophyll is the organic molecule of plant leaves and is regarded as one of the key components in plant photosynthesis. Plant leaf nitrogen cannot be synthesized without chlorophyll. Some studies have found a high relationship between leaf nitrogen and chlorophyll because pigments determine most spectral features between 400 and 700 nm in a spectrum (Ulissi et al. 2011). Moreover, reflection from this wave band primarily depends on the chlorophyll content of leaves and has a negative correlation with leaf nitrogen content (Lamb et al. 2002). The nutritional and physiological statuses of a plant can be effectively estimated based on chlorophyll content. Measuring chlorophyll is crucial for monitoring plant growth, promoting nitrogenous fertilizer usage, and guaranteeing high yield.

The Kjeldahl method has the highest accuracy among chlorophyll measurement methods and is deemed the most commonly used method to measure chlorophyll. However, it necessitates a complex and time-consuming chemical analysis. Leaves are also destroyed in the process of measurement, and the plant growth will be affected. Rapid, nondestructive, and cost-effective measurement methods are, therefore, necessary.

As an alternative, spectral technology has been applied to analyze the chemical components of plants because of its rapid and nondestructive advantages. Various spectral sensors and cameras have been developed to measure plant chlorophyll. In addition, researchers have acknowledged that fluorescence technology can measure chlorophyll according to the response of leaves to light. Some Lidars or laser sensors with specific wavelengths and the capability to measure chlorophyll have also been developed.

Chlorophyll Measurement Based on Spectral Sensors

The development of spectral technology has resulted in an increasing number of mature products being introduced in the market. Spectral sensors are the most frequently used instruments to assess vegetation status with visible and NIR light. Many studies have also been carried out using some typical spectral sensors that are passive type or active type to measure chlorophyll. Conventionally, some spectral vegetation indices have also been calculated based on spectral information in several different wavelengths to invert chlorophyll, which are revealed to be slightly superior to NDVI.

The passive-type sensors usually capture the reflectance spectrum of a plant to solar radiation, so these sensors are susceptible to ambient light and recommended to be used around noon under clear-sky conditions. Bai et al. (2016) mounted NDVI sensors and portable spectrometers on a field platform to measure chlorophyll. The sensors and spectrometers all consisted of an up-looking unit to measure solar radiation and a downlooking unit to detect reflected spectrum. Uplooking values and downlooking values were integrated to calculate NDVI and then to estimate plant chlorophyll. As a representative of passive-type sensors, Yara N-Sensor is widely used in measuring chlorophyll, which provides multispectral reflection of a plant. There is also a sky pointing spectrometer to correct for the fluctuation in light intensity. Raper and Varco (2015) analyzed the multispectral reflectance and provided a simplified canopy chlorophyll content index to detect cotton chlorophyll, which indicated that reflectance in the red edge region strongly related with the leaf nitrogen status. ASD FieldSpec is also a portable device, whose wavelength is in the domain of 350–2500 nm and is also capable of providing hyperspectral data. Based on the hyperspectral reflectance data obtained through ASD, He et al. (2016) estimated the nitrogen status of wheat by proposing the multi-angle vegetation index and pointed out that taking the measuring angle into account is very important. Thorp et al. (2015) estimated leaf chlorophyll with the partial least squares regression (PLSR) approach, and the results showed that the performance was better than NDVI and the physiological reflectance index. Inoue et al. (2016) compared the canopy chlorophyll of different plant types and regional scales and found that the ratio of the spectral index with the reflectance at 815 nm and 704 nm was robust to predict canopy chlorophyll content.

Conversely, GreenSeeker, Crop Circle, and other devices equipped with active spectral sensors have been widely used in agriculture, because they can tolerate severe environments. The active sensors usually emit amber or red and NIR waveband light due to their link to chlorophyll (Samborski et al. 2015) and record the reflectance of several wavebands to calculate some vegetation indices to measure chlorophyll, primarily NDVI. Barker et al. (2016) used GreenSeeker and Crop Circle mounted on field-based phenotyping platforms to measure plant chlorophyll, and the change in NDVI from night to the brightest noon was 0.046 for GreenSeeker and 0.0013 for Crop Circle, which indicated that they were all not significantly affected by ambient light. Kipp et al. (2014a) developed a method for measuring the early chlorophyll in winter wheat with the use of multispectral active sensors, including GreenSeeker and Crop Circle. They also used RGB image analysis as a reference method and proposed a novel index, the early plant vigor index (EPVI), using single wavelength values (670 nm, 750 nm, and 862 nm) to evaluate early plant vigor. Samborski et al. (2015) used the GreenSeeker Model 505 (red at 656 nm and NIR at 774 nm) and Crop Circle ACS-210 (amber at 590 nm and NIR at 880 nm) to collect red and amber canopy NDVI values of winter wheat at three growth stages and found that the genotype had an effect on both the red and amber NDVI values at Zadoks 37 to 39 growth stages and only on amber NDVI values at 55 to 71 growth stages. Taskos et al. (2015) compared Crop Circle ACS-210 and ACS-430 (red at 630 nm, red edge at 730 nm, and NIR at 780 nm), and calculated and analyzed different NDVI values in each individual waveband. The results demonstrated that ACS-430 indices and red edge-based indices were more strongly correlated with leaf chlorophyll of vineyards. The new Crop Circle ACS-470 provided filters to select different wavelengths and vegetation indices were also highly related to plant nitrogen (Padilla et al. 2014), and the red edge-based indices performed better than the NDVI and ratio vegetation index (Taskos et al. 2015). But plant height, measuring distance, temperature, and reflectance from soil or adjacent rows affect the performance of active sensors. The optimal measuring distance should be adjusted depending on canopy architecture and the growth stage, and the distance of sensors beyond 40 cm from the canopy is appropriate (Li et al. 2014b; Kipp et al. 2014b; Raper et al. 2013; Stamatiadis et al. 2010). In addition, reflectance indices were less sensitive at the late growth stages of plants with the reduction in the NIR reflectance from the canopy (Samborski et al. 2015; Padilla et al. 2014).

Among all the active- and passive-type spectral sensors, GreenSeeker, Crop Circle, and N-Sensor are most commonly used for on-the-go real-time measurement of plant chlorophyll, all of which could be mounted on a platform and suitable for high-throughput phenotyping. Raper et al. (2013) tested N-Sensor, GreenSeeker Model 505, and Crop Circle ACS-210 and found that N-Sensor and Crop Circle ACS-210 were less sensitive than GreenSeeker Model 505 at the early growth stage of pants when NDVI values were small, while N-Sensor and Crop Circle ACS-210 had better performance than GreenSeeker Model 505 at the late growth stages when NDVI values were higher than 0.6.

Chlorophyll Measurement Based on Spectral Cameras

Unlike common spectral sensors, multispectral or hyperspectral cameras can measure canopy spectral reflectance in wide wavebands with high spatial resolution images, making it possible to extract plant from background with image processing and derive numerous vegetation indices exactly. Based on these advantages, spectral cameras have been extensively applied to estimate and predict plant chlorophyll.

Spectral cameras can capture visible and NIR spectra and are suitable for vehicle-based, UAV-based, and satellite-based measurement. However, radiometric and geometric corrections, as well as atmospheric corrections, are needed. Similar to spectral sensors, NDVI is also the most frequently derived vegetation index to measure chlorophyll. Bourgeon et al. (2016) mounted a visible and NIR multispectral camera on a tractor to assess vineyard. Considering ambient light variation, a calibration method was proposed for multispectral images to produce reflectance images. A color chart was used as a radiometric reference in RGB and NIR images, and red and NIR spectral channels were chosen to calculate NDVI values and generate NDVI images. Then the segmentation algorithm was applied to NDVI images in order to distinguish leaves from background. The average NDVI value of leaves was calculated as a spatial representation of the region. In recent years, more and more researchers apply multispectral cameras and hyperspectral cameras on UAV to capture canopy reflectance data to measure plant chlorophyll. Moreover, the radiometric correction was done firstly to convert the raw digital numbers to radiance values. Then, the atmospheric correction, namely, the Fast Line-of-Sight Atmosphere Analysis of Spectral Hypercubes (FLAASH), was carried out to remove the atmospheric effects of absorption and scattering. Finally, the geometric correction was applied to correct the offset between the airborne data and ground spectra (Leblanc et al. 2014). The spatial resolution of images can achieve at decimeter level, and all of the images can be also mosaicked for a better understanding of the measured region (Elarab et al. 2015; Zaman-Allah et al. 2015). Elarab et al. (2015) calculated the vegetation indices, selected LAI, NDVI, and thermal and red bands as inputs of relevance vector machine algorithms to spatially estimate oat chlorophyll with a root-mean-squared error of 5.31 μg/cm^2. Kalacska et al. (2015) developed a model that comprised a continuous wavelet transform with a neural network to predict chlorophyll with R^2 value ranging from 0.8 to 0.9.

Satellite spectral imagers can provide spectral images that cover large-sized plots, but the spatial resolution is lower and the sample period is longer than vehicle-based and UAV-based measurements. Houborg et al. (2016) analyzed hyperspectral images from the Earth Observing-1 satellite with a 30-m ground resolution. Images were radiometrically and geometrically corrected, and atmospheric correction was also carried out with the FLAASH algorithm to retrieve water vapor and correct adjacency effects. Then vegetation indices were calculated for multiple-parameter regression to assess chlorophyll. Some indices, particularly in the red-edge bands, played an important role in improving the robustness of chlorophyll retrieval.

Chlorophyll Measurement Based on Fluorescence Sensors

Chlorophyll fluorescence (ChlF) is emitted by chlorophyll shortly after plants absorb light. It mainly comes from photosystem II, which offers a promising method for measuring plant chlorophyll content. ChlF signals can be divided into the red fluorescence (RF) and the far-red fluorescence (FRF). The ChlF ratios of RF and FRF are usually used to estimate plant chlorophyll.

ChlF measurements contain active fluorescence-based measurement and passive reflectance-based measurement. Active fluorescence-based measurement takes the basis of the pulse-amplitude modulation or the laser-induced fluorescence (LIF) transient method, and the measuring range can reach up to several meters. Passive reflectance-based measurement derives ChlF with the use of the sun-induced fluorescence (SIF) method (Cendrero-Mateo et al. 2015). Active fluorescence-based measurement has advantage over passive reflectance-based measurement in tolerating ambient light; therefore, many researchers apply this measurement.

LIF is an active sensing technique wherein leaves are excited by laser sensors and then reemit fluorescence, which is widely used in measuring chlorophyll. Yang et al. (2015, 2016) used the ultraviolet (UV) laser to induce fluorescence and measured the intensity of fluorescence peaks at 685 m and 740 nm to estimate paddy rice nitrogen content with back-propagation neural network (BPNN) and support vector machine (SVM) models. They found that the intensity of fluorescence peaks was more sensitive and accurate than the fluorescence ratios in estimating nitrogen content. Agati et al. (2013, 2015) and Longchamps and Khosla (2014) used the multiplex fluorescence sensors to measure the nitrogen status. The sensors provided the flavonol, chlorophyll, and nitrogen balance indices (NBI) that were calculated based on the ratio of the RF and FRF induced by UV, red, green, or blue light. One of the NBI was highly related to leaf nitrogen content and not affected by seasons (Agati et al. 2015). Longchamps and Khosla (2014) also conducted some tests to verify the fact that the fluorescence sensors could measure the variation of chlorophyll at the early stage of plant development. Soil has less impact on the measurement if plant height is higher than 20 cm. In order to investigate the influence of light intensity and temperature, Thoren et al. (2010) tested LIF measurements under field and controlled laboratory conditions. Studies showed that the chlorophyll content of plant leaves was strongly related to the ratio of the two peaks of ChlF at 690 nm and 730 nm, and the ratio decreased linearly with an increase in light intensity up to 23 °C.

Chlorophyll Measurement Based on Lidar/Laser Sensors

Blue and red light are essential partners for plant photosynthesis, which are absorbed by chlorophyll and carotenoids, and most green light is reflected. Some research has proved that the reflectance of green light is sensitive to the variation in plant chlorophyll, and the canopy reflectance at 550 nm will increase with the reduction of chlorophyll (Daughtry et al. 2000). Based on research, Eitel et al. (2010, 2011,

2014a, b) conducted many studies on the use of a green (532 nm) laser sensor to measure leaf chlorophyll and nitrogen. The reflectance intensity values were recorded to calculate chlorophyll. However, there are many factors that influence the measurement accuracy. In order to improve the measurement accuracy, Eitel et al. (2011) proposed the following process. First, the laser reference intensity was normalized using a white reference panel to correct the drift of laser intensity. Second, the soil and edge returns were removed based on an intensity threshold. Third, the distance between the laser sensor and plant constant was kept. The results indicated that green laser intensity was strongly correlated with chlorophyll and nitrogen content. Furtherly, a multi-wavelength laser system was tested and the ratio of green and red laser return intensities was used to measure plant nitrogen. However, the results were not significantly improved compared with previous research, which might be caused by aggravating the leaf angle effects.

With the development of Lidars, the hyperspectral Lidar was introduced to measure plant chlorophyll or nitrogen. This kind of Lidar works based on wide-spectrum emission and is able to produce point cloud data with spectral information (Behmann et al. 2016). Sun et al. (2017) compared the performance of ASD FieldSpec, multispectral Lidar, and hyperspectral Lidar, and the results demonstrated that hyperspectral Lidar had the best performance in estimating plant nitrogen. Nevalainen et al. (2014) used hyperspectral Lidar to estimate leaf-level chlorophyll. Points that had low NDVI values were filtered and vegetation indices were calculated for linear regression analysis to estimate chlorophyll. The results demonstrated that the modified chlorophyll absorption ratio index (MCARI), which was calculated by using reflectance at 750 nm and 705 nm, had the best performance in measuring needle-leaf chlorophyll. Du et al. (2016a) recorded the reflectance intensity of a hyperspectral Lidar and selected characteristic wavelengths to estimate nitrogen contents with SVM regression. They proposed that considering more wavelengths as inputs in the regression can significantly improve measurement accuracy. Furthermore, they combined hyperspectral Lidar data and LIF data to detect nitrogen (Du et al. 2016b). With the use of SVM regression, PLSR, and two artificial neutral networks (ANNs), the determination coefficients were high. In addition, it was also found that the reflectance spectrum performed less well in predicting plant chlorophyll content when the leaf nitrogen content was high.

Recently, Ounis et al. (2016) described a new Lidar system combing LIF and SIF, which might help measure chlorophyll content in the future.

Comparison and Analysis of Chlorophyll Measurements

Chlorophyll measurement has always been the priority of considerable research, and the related spectral products and sensors have been widely implemented for such task. Spectral measurement is usually disturbed by ambient conditions, especially sun illumination, and the performance of active sensors is better than that of passive sensors. Previous studies have demonstrated that the reflected spectral information from soil can affect the spectral determination of chlorophyll at the early

stages of plant growth because soil coverage is low at such an early development stage (Kipp et al. 2014a). Owing to the abundant spectral information, hyperspectral or multispectral sensors and cameras can probably eliminate background interference by deducing some vegetation indices. Hyperspectral or multispectral cameras can be used on both ground vehicles and UAV or satellite, making it possible to realize large-scale measurement by mosaicking multi-frame images. Image processing methods can be applied to extract vegetation and remove background interference. But the volume of data captured by spectral cameras is tremendously large due to the high data rate, especially in the UAV measurement, which needs laborious offline processing. ChlF measurement is more sensitive to the variation of chlorophyll than vegetation indices. Compared to spectral sensors like GreenSeeker or Crop Circle, the field of view of a multiplex fluorescence sensor is smaller. Reflectance almost comes from plant vegetation, which gives rise to the ChlF measurement, independent of distance and soil. In addition, the intensities of fluorescence at about 690 nm and 740 nm are largely used to analyze and estimate plant chlorophyll.

The measurement accuracy of laser sensors mainly depends on the reflectance intensity that is affected by various factors, such as temperature, leaf edge, measuring angle, and leaf roughness. Hyperspectral Lidar provides help for us to measure chlorophyll in spatial and temporal scales and broadens the potential application of Lidars.

7.2.2.4 Water Stress Measurements

Global warming and water resource shortage have resulted in the inevitable reduction of grain yield. In the increasingly crucial task of conducting research on the water use efficiency of plants, water stress is an important parameter for assessing plant water status. Stomatal conductance and leaf water potential (LWP) are vital indictors of plant water stress, and canopy temperature is a surrogate for stomatal conductance (Prashar and Jones, 2016). Crop water stress index (CWSI) is successfully related to LWP (Bellvert et al. 2015). Generally, water stress can be measured by two methods, one based on canopy or vegetation temperature and the other based on canopy or vegetation reflectance. Thermal infrared techniques are an effective method to investigate canopy temperature. Spectral techniques are widely used to measure canopy reflectance. Typically, thermometers, thermography, spectral sensors, and cameras are implemented to evaluate water stress.

Water Stress Measurement Based on Thermometers

Thermometers can be mounted on some phenotyping platforms to monitor plant canopy temperature (Bai et al. 2016; Barker et al. 2016), whose measuring region is concentrated and small to reduce interference. Although ambient light does not affect thermometers due to their measured radiations in the long-infrared spectrum,

ambient temperature has a significant effect on thermometer reading. Tests conducted by Barker et al. (2016) showed that thermometer reading was higher than the surface temperature when the ambient temperature was high, and the thermometer would underestimate the actual temperature when the ambient temperature was low. Therefore, they put forward a correction method based on the ground truth measurement with the use of thermocouples to reduce the measurement error.

Vegetation temperature is usually lower than ambient temperature, but when the vegetation fraction is small, especially at the early stage of plant development, soil temperature is higher than ambient temperature during middays that disturbs the measurement. In order to reduce the influence of soil, Rischbeck et al. (2016) used two thermometers to measure canopy temperature with the opposed oblique views at an angle of 45° from the nadir. This measurement was capable of increasing the biomass proportion in the field of view. The actual, lowest, and highest canopy temperatures were used to calculate CWSI. Besides, some researchers collected ambient temperature to correct thermometer values. Ni et al. (2015), Kim et al. (2015), and Bai et al. (2016) regarded the difference between canopy temperature and air temperature as an indicator of water stress to assess plant growth.

Water Stress Measurement Based on Thermography

Infrared thermography is considered a high-throughput tool for measuring plant temperature to estimate the plant water stress, which provides great help for us to evaluate the spatial and temporal water variability of plants.

Thermal images captured by thermography usually contain canopy temperature and background temperature, and it is a critical problem to eliminate the background noises of thermal images. Normally, one empirical method based on the temperature differences between canopy and background is used to separate canopy. Measuring time during the day should be taken into account due to the variable environment. In the morning, the temperature difference between soil and canopy is small, the leaf water potential is unstable, and the solar angle is not optimal. Conversely, LWP is more stable due to stomatal closure and most leaves are exposed to sunlight around midday, and the thermal images containing the highest temperature differences are suitable to assess the canopy water stress (Bellvert et al. 2014). The other method used to separate the canopy from the background is to simultaneously collect thermal and color images of the canopy (Cohen et al. 2015; Zia et al. 2013; Grant et al. 2016). Thermal and color images are aligned, and then the canopy can be extracted based on segmentation algorithms of color image processing. The method is able to handle situations wherein it is difficult to identify the leaves and shaded soil just on the basis of temperature and improve the measuring efficiency of canopy temperature. In addition, thermal image resolution plays an important role in eliminating inaccurate temperatures, especially the temperatures correlated to the edge pixels that contain both canopy and background (Prashar and Jones 2016).

Infrared thermography can be applied on vehicle-based platforms (Cohen et al. 2015), UAV (Bellvert et al. 2015; Gago et al. 2015), and greenhouse (Mangus et al.

2016). Thermal images of plant and environmental parameters were collected synchronously, and thermal images needed to be calibrated with radiometric correction. After canopy temperatures were calculated, CWSI, LWP, vapor pressure deficit (VPD), and other parameters would be applied to evaluate plant water stress.

Water Stress Measurement Based on Spectral Sensors and Cameras

Buitrago et al. (2016) conducted research to investigate the changes in the thermal infrared spectra of plants caused by water or temperature stress and found that water stress and temperature stress created a similar spectral response, and the emissivity in the mid-infrared spectrum decreased with water loss. Further, many spectral sensors were applied to measure the canopy temperature or water stress of plants. Elsayed et al. (2015) tested a hyperspectral passive sensor, a hyperspectral active sensor, an active flash sensor, a Crop Circle, and a GreenSeeker to assess the normalized relative canopy temperature (NRCT) that was similar to the CWSI introduced by Rischbeck et al. (2016), and the spectral indices of all sensors were strongly correlated with NRCT.

Assessing the water stress of plants based on spectral indices is a principle method for spectral sensors and cameras, but the internal structure of the leaf affects the sensitivity of these indices. Taking advantage of the spectral reflectance at specific wavelengths collected by a spectrometer, Bandyopadhyay et al. (2014) proposed and calculated different water stress indices to characterize the water stress of wheat. Winterhalter et al. (2011) evaluated a series of spectral indices to estimate the canopy water mass of maize and the global coefficients of determination of several indices were over 0.70. In addition, a hyperspectral camera was also used. Moshou et al. (2014) extracted spectral features from hyperspectral images to detect the water stress of wheat. They applied least squares SVM to analyze spectral data and selected six indices whose central wavelengths were at 503 nm, 545 nm, 566 nm, 608 nm, 860 nm, and 881 nm, respectively. Rossini et al. (2013) acquired hyperspectral data from airborne imagery and verified that the photochemical reflectance index had good performance in measuring water stress.

Comparison and Analysis of Water Stress Measurements

The measuring region of thermometers is small and the measurement accuracy depends on the vegetation. Thermography is able to provide temperatures within a region, offering an opportunity to directly monitor the global variations, especially in the measurement of UAV. However, the thermography's region of interest is often determined manually (Mangus et al. 2016), and the sensor's field of view also affects the measurement of the canopy temperature (Prashar and Jones 2014) and the thermal resolution needs to be improved. Although some spectral indices are closely related to water potential and stomatal conductance, canopy temperature

and relevant parameters are still recommended as the best indicators of water stress (Rossini et al. 2013; Zarco-Tejada et al. 2012).

The measurement of water stress still presents some problems that need to be solved. First, thermal measurement is easily affected by dynamic variations in environmental factors, including solar radiation, cloud cover, wind speed, air temperature, humidity, and VPD (Tattaris et al. 2016), and the time of measurement also influences the results; all of these interferences should be taken into account. Second, canopy temperature changes vary with canopy architecture, plant height, soil coverage, leaf angle, and other factors, all of which need to be considered. Combining different sensors or parameters together to measure water stress is feasible in order to improve the accuracy. Besides, fluorescence is also put forward to measure water stress, which is more sensitive to water stress (Rischbeck et al. 2016; Cerovic et al. 1996).

7.2.3 Sensing Instruments for Biomass

Plant biomass is defined as the total fresh or dry weight of plant, including the above-ground and below-ground parts. Plant biomass is an important ecological indicator for various aspects, such as plant architecture, photoabsorption, and carbon assimilation. Since measurement of the below-ground biomass is difficult, most studies focus on measuring the above-ground biomass. On the one hand, the above-ground biomass can demonstrate the nutritional status and nitrogen utilization of a plant. On the other hand, breeders generally regard the above-ground biomass as a reference to estimate the growth of plant root.

In general, the above-ground biomass can be estimated using destructive, nonspectral, or spectral methods (Tucker 1980). Destructive methods need to harvest, prune, dry, and weigh plants. This process is complicated and time consuming, but the results are usually served as criteria for the latter two methods. Nonspectral and spectral methods mostly measure certain plant parameters and develop prediction models to estimate the above-ground biomass.

7.2.3.1 Biomass Measurement Using the Nonspectral Method

The nonspectral method focuses on measuring the plant height. Similar to the trunk in trees, the plant stem accounts for the majority of the entire plant weight (Silva et al. 2015; Andújar et al. 2015). Given that plant height is basically up to the stem height, the stem height is one of the significant parameters for an above-ground biomass prediction model in a few studies (Ehlert et al. 2008, 2009; Marshall and Thenkabail 2015; Tilly et al. 2015a). Lidar was adopted to measure the heights of rice, oilseed rape, winter rye, winter wheat, and grassland. Linear regressions were conducted, and the results demonstrated high coefficients of determination between above-ground biomass and plant height in the range of 0.60–0.99 (Ehlert et al. 2009;

Tilly et al. 2015a). Fricke et al. (2011) installed an ultrasonic sensor on a vehicle to measure sward height. The results were used as the input data to predict forage biomass, and the mean residuals ranged between 0.893 and 1.672. Notably, the accuracy was high if no mixture was present in the sward. Estimating biomass based on plant height is promising but further improvements are needed. Vegetation coverage should be considered (Marshall and Thenkabail 2015), especially at the early growth stage of plants. The Chinese Academy of Science (Li et al. 2015a, b) used airborne Lidar to derive the LAI and height of maize in northwest and north China, and then estimated biomass to improve measurement accuracy and efficiency.

7.2.3.2 Biomass Measurement Using the Spectral Method

Spectral methods mostly measure certain vegetation indices and nitrogen content of a plant using spectral sensors or cameras. Nitrogen status is a primary component of plants and plays a vital role in contributing to biomass. Biomass accumulation is strongly related to nitrogen application rates (Serrano et al. 2000). NIR spectral data are applied to measure nitrogen and estimate biomass. SPAD and ASD FieldSpec were widely used, and prediction models were developed based on the hyperspectral reflectance of a plant canopy (Fricke and Wachendorf, 2013; Gao et al. 2013; Winterhalter et al. 2012). Gnyp et al. (2014a, b) proposed a vegetation index with the use of a multiband combination in the NIR and short-wave infrared domains to develop a biomass model, which could improve the estimation of above-ground biomass. Furthermore, Mistele and Schmidhalter (2008, 2010) conducted a few vehicle-based measurement studies by using spectral sensors. Erdle et al. (2011) compared a bidirectional passive radiometer and three active sensors (Crop Circle, GreenSeeker, and an active flash sensor) and calculated several vegetation indices. The results demonstrated that the active sensor was more flexible. Parameters related with nitrogen, such as NDVI and simple R780/R740 ratio (Mistele and Schmidhalter, 2008, 2010; Erdle et al. 2011), are strongly related to plant biomass. Considerable research also showed that the canopy architecture had an effect on the estimation of biomass, and the correlation coefficient between LAI and biomass was 0.96 (Erdle et al. 2011), and the vertical biomass distribution of maize was a bell shape. Hence, the canopy parameters are necessary to estimate plant biomass (Winterhalter et al. 2012).

7.2.3.3 Combined Method for Biomass Measurement

The potential of combining the nonspectral and spectral methods to estimate above-ground biomass is currently being explored. Plant height and several indices related with nitrogen content are being used to refine the prediction models and improve the estimation of above-ground biomass. At the early stage of maize, Montes et al. (2011) employed light curtain and spectral reflectance sensor to estimate biomass with SVM regression from the V4 (collar of 4th leaf unfolded) to V8 (collar of 8th

leaf unfolded) stage. The results showed very high values of repeatability. Freeman et al. (2007) used GreenSeeker to collect NDVI and combined it with plant height to predict biomass during the V8 to V10 (collar of 10th leaf unfolded) stage of maize. Hyperspectral measurement with ASD FieldSpec can be used to calculate vegetation indices, such as NDVI, normalized reflectance index, renormalized difference vegetation index, and red edge inflection point. These indices fused with plant height derived from Lidar or ultrasonic sensors can be used to estimate biomass (Fricke and Wachendorf 2013; Tilly et al. 2015b).

7.2.3.4 Comparison and Analysis of Biomass Measurements

Studies have shown that plant height is a significant parameter for estimating plant biomass. This parameter is also the measurement key of the nonspectral method. The water and nitrogen concentration of plants will affect the estimation of biomass. These two parameters can be measured by spectral methods, but the results will be disturbed by weather, vegetation coverage, and soil. Plant height and nitrogen and water concentrations are regarded as the fundamental parameters for estimating plant biomass. These parameters can be combined to estimate plant fresh weight and dry weight and thus to improve the accuracy and robustness of measurement.

7.2.4 Sensing Instrument for Plant Roots

The root is an essential plant organ below ground and directly influences the absorption and usage of nutrient and water, which provides the basics of plant growth naturally. In general, plants represent different responses to ambient biotic and abiotic stresses based on their root system architecture (RSA), especially under drought stress; an appropriate RSA can greatly promote the adaptation of plants against various extreme weather and the impact of climate change. There are four primary roots that consist of RSA, which are coarse or taproots (first root to emerge from the seed), lateral roots (any root branching from another root), shoot-borne roots (roots that arise from shoot tissues), and basal roots (develop from the hypocotyl), respectively. The significant parameters of roots are total root lengths, primary root lengths, number of lateral roots, network width, root volume, root surface areas, and so on (Wasaya et al. 2018; Han and Yan 2018; Lee 2016). Selecting plants based on the RSA is a significant option for breeders to cultivate new species. However, how to measure and evaluate RSA is a challenge. The tough fact is that most roots are hidden by soil and not visible. People have to shovel out plant roots and clear the incidental soil and then manually measure some morphologic parameters to evaluate RSA (Trachsel et al. 2011). This method would interrupt the growth of plants and cannot realize dynamic measurement. More attention should be focused on evaluating RSA in a high-throughput and nondestructive way.

Currently, root phenotyping is conducted under two conditions, controlled conditions and field conditions. As an alternative, it is feasible to visualize RSA by changing the growth conditions of roots. In the controlled conditions, plants were usually cultivated using containers that were made of glasses, papers, gels, and others, so almost completed roots could be monitored. It is incontestable that there are some small distinctions between the controlled roots and natural roots due to unexplained factors. After all, soil should be the growth medium for roots to develop. Therefore, many researchers seek to explore plant RSA under field conditions using sensors that are able to detect roots over time in soil.

Several sensors and techniques were applied for monitoring RSA, such as color digital cameras, X-ray CT, magnetic resonance imaging (MRI), and neutron-computed tomography (Adu et al. 2014; Adu, 2014). Specific to the controlled conditions, color digital cameras are commonly used to obtain root images in various perspectives and extract root traits. In terms of the field conditions, X-ray CT was frequently applied to measure roots in root phenotyping.

7.2.4.1 Plant Root Measurement Based on Color Digital Cameras

Color digital cameras or scanners are able to measure plant roots at many growth stages and situations, especially under controlled conditions. They are widely implemented in conjunction with soil-free techniques, such as hydroponics, aeroponics, gel plates, and growth pouches (Atkinson et al. 2019).

Some researchers applied a color digital camera to evaluate the seminal roots of plant seeds. First, seeds were germinated using wet seed germination paper (Adu et al. 2015) or growth pouches (Richard et al. 2015). Then, seeds were placed on a clear flat and images of seeds were acquired. Finally, images were processed and the angle, number, and length of seminal roots were calculated. Slovak et al. (2014) also developed a scalable open-source pipeline, which could extract 16 traits of seed roots.

A lot of papers reported that plants were cultivated in cylinder tubes (Slota et al. 2016; Nakini and DeSouza 2014) or square chambers under controlled conditions (Jia et al. 2019), and the roots were able to grow and spread with the support of gels or nutrient solutions. Moreover, plant roots were visible and root images can be captured.

Two tasks need to be finished when using color images to analyze RSA. One is a fundamental step to segment roots from the background, which is not difficult because most growth mediums are transparent to visible light. The other is classifying the primary roots and numerous lateral roots, detecting their tips, and tracing root skeletons so as to extract more root traits. Region growing algorithms are widely applied to settle this issue. Notably, color images have been broadly used in root phenotyping, and many software packages are available to process root images and extract root traits, such as EZ-Rhizo, Smart Root, WinRhizo, ImageJ, IJ_Rhizo, Root System Analyzer, and Root Trace (Wasaya et al. 2018). Root length, tip angle, number of crown and lateral roots, surface area, and other root traits can be

calculated automatically using the software (Slota et al. 2016; Adu et al. 2014; Clark et al. 2013). Besides, researchers also developed many platforms or software for specific issues, for example, RhizoVision Crown aimed at evaluating root crown traits (Seethepalli et al. 2019), and MyROOT combined a bottom-up root tracking approach with a hypocotyl detection algorithm to obtain the root traits of wheat and barley (Betegón-Putze et al. 2019). Kumar et al. (2014) applied a statistical learning method to discriminate primary roots and lateral roots and detect their tips successfully.

Three-dimensional reconstruction of roots can be accomplished using several 2D side-view images that were obtained at various angles, and RSA can be analyzed in a novel way. Han et al. (2018) developed a 3D imaging system using simple space carving to quantify the RSA of rice. It is essential to segment root portions from the 3D model of root and deep learning techniques (Wang et al. 2019a) or software. For example, RootReader 3D (Pineros et al. 2016) and DynamicRoots (Jiang et al. 2018; Symonova et al. 2015) could be used to decompose the 3D root system into individual branches and then extracted root traits.

7.2.4.2 Plant Root Measurement Based on X-Ray CT

CT, as a radiation-based technique, enables the visualization of the interior of solid objects, and X-ray is widely selected as its energy source (Mooney et al. 2012). The application of CT in root phenotyping is a nondestructive measurement based on the principle of attenuations of roots and soil at an electromagnetic wave, and the 3D architecture of soil and roots can be generated with high resolution (Adu 2014). Using contrasts in X-ray attenuation between growth medium solids, air-filled pores, soil water, and plant material makes it possible to sense plant roots under field conditions (Mooney et al. 2012). Maenhout et al. (2019) tested a method to segment large mature maize roots from X-ray CT images. The method is able to remove the soil particles around plant roots and extract root volumes. In practice, the most frequently applied segmentation algorithm is still the region growing algorithm, and the "top-down process" method is always used to track roots. Many software packages are available to process CT images, like RootViz, RooTrak, and VGstudio Max (Maenhout et al. 2019; Pfeifer et al. 2015; Zappala et al. 2013). In addition, Mairhofer et al. (2013) extended RooTrak, making it possible to extract plagiotropic roots.

However, there are several factors that impact the measurements when using CT images to assess plant roots. First, the medium plays a great important role in segmenting roots from CT images. X-ray attenuation values vary with soil type, soil moisture content, air-filled pores, root water status, root material, and age, which lead to the fact that roots cannot be extracted accurately just using threshold-based methods (Rogers et al. 2016; Mooney et al. 2012; Mairhofer et al. 2013). Second, there are some organic matters in soil that will be mixed with plant roots, and the attenuation values of the soil and roots overlap. More information or prior knowledge needs to be considered to develop novel approaches and improve the accuracy of segmentation.

7.2.4.3 Plant Root Measurement Using Other Sensing Techniques

Similar to X-ray CT, MRI is an alternative option, which is able to visualize the 3D structure of plant roots under field conditions (Koch et al. 2019). Dusschoten et al. (2016) estimated the RSA of maize and quantified the growth of roots using MRI. Pflugfelder et al. (2017) tested and analyzed the affections of natural soil substrates and soil moisture on MRI root image qualities, and the results showed that the two factors have no effect on image qualities in the range of 50%–80% water holding capacity.

Besides aforementioned techniques, novel techniques and approaches were explored and developed to measure RSA. Kalogiros et al. (2016) put forward a model based on the analysis of RSA traits, which can output elongation rate, branching rate, and gravitropic without measuring individual roots. Schlüter et al. (2018) proposed a root distance model to describe root growth throughout all stages and estimate the rhizosphere volumes. Those models can help us to estimate root growths, improve measure efficient, and provide references for breeding. Sometimes the color contrast between roots and soil is poor; Bodner et al. (2018) used a hyperspectral camera to scan the root system of *Triticum durum* and extracted feature wavelengths to segment roots from soil. In terms of 3D root measurement, Prince et al. (2018) directly installed a laser stripe, instead of a color camera, to scan plant roots grown in gel medium and captured 3D cloud point data of roots. In addition, Corona-Lopez et al. (2019) pointed out that electrical impedance tomography (EIT) could also help us to obtain 3D roots and had the potential to be used as a low-cost tool for root phenotyping, but the limited resolution of EIT needed to be improved.

Recently, Truong et al. (2018) introduced an ultra-wideband frequency system to nondestructive imaging RSA, and Wang et al. (2019a, b) used the microelectrode ion flux estimation method to assess the oxidative stress tolerance of barley roots. Both of them offered new prospects to estimate RSA, though more work should be done to improve their performances.

7.2.4.4 Comparison and Analysis of Plant Root Measurements

It is a challenging task to measure and assess RSA, due to the complicated, opaque, and heterogeneity growth environment of plant roots. Specific sensing techniques and approaches should be taken into consideration to promote root phenotyping. In controlled conditions, color digital cameras are able to capture root images and extract root traits with high resolution and low cost. But color cameras are incapable of monitoring RSA under field conditions, so that X-ray CT imaging is applied to solve the issue as a powerful tool. However, the costs of the facilities are usually high and the instruments are sophisticated, making it unable for CT imaging to be largely used in the field (Zhang and Zhang 2018). MRI has the same problems as X-ray. Novel sensing techniques have been explored and tested to evaluate RSA, but currently only primary roots can be measured, and in most cases, small roots are misclassified. Although those techniques cannot provide precise measurement

because of their low resolutions and interference noises, they provide an extension to root phenotyping.

7.3 Platforms for Plant Phenotyping

Breeding scientists use plant phenotyping to collect various plant and environment information, from shape to nutrient content, from a single plant to a large plant group(s), and from near-range observation to space observation. As a result, different types of platforms are employed to meet the requirements of different plant phenotyping scenarios. Indoor phenotyping equipment, in-field sensor networks, ground mobile platforms, phenotyping tower, field-scan platforms, unmanned aerial vehicles (UAVs), airplanes, and even satellites can all implement plant phenotyping. Plant phenotyping platforms can be grouped into three categories: ground-based platforms, aerial platforms, and indoor platforms.

7.3.1 Ground-Based Platforms

In-field sensor networks, ground mobile platforms, phenotyping towers, and field-scan platforms are categorized as ground-based platforms.

7.3.1.1 In-Field Sensor Networks

Even though sensor networks can be wired or wireless, it is better to consider the in-field sensor networks as wireless sensor networks (WSNs) in precision agriculture applications. With its features of low power consumption and low cost, WSNs have advantages in collecting environmental information at a large amount of in-field spots over a long time span. Environmental information and their changing trends are important components of plant phenotyping under generalized definition. Breeding scientists need both environmental information and plant information to conduct phenomic analysis to find traits to improve crop yield and environmental adaption (Reynolds et al. 2019).

Various environmental information can be collected by the in-field sensor networks (Aqeer-ur-Rehman et al. 2014; Ojha et al. 2015; Jawad et al. 2017), such as conditions of light, wind, air, and soil. For light information, solar radiation and light intensity are the main parameters. For wind conditions, wind speed and direction are the corresponding data of targets. Air humidity, temperature, atmospheric pressure, and rainfall are often collected and monitored. Soil moisture, temperature, dielectric permittivity, pH, conductivity, and salinity are collected to evaluate soil conditions. Meanwhile, plant information can also be collected by in-field sensor networks directly (Ojha et al. 2015; Jones et al. 2018). Sensors for photosynthesis, carbon dioxide (CO_2) concentration, hydrogen, leaf wetness, leaf temperature, leaf

area index (LAI), canopy conductance, evaporation rate, and stem moisture have been used as stationary nodes of in-field sensor networks.

Although great efforts have been put on WSNs for in-field monitoring, there are still challenges on node deployment, energy saving, and routing protocol (Al-Turjman 2019). Different deployment strategies of sensor nodes can bring different network performances on connectivity, coverage, and reliability. Existing 2D deployment strategies cannot meet the requirements of plant phenotyping, which may cause time-variable 3D coverage problems. As a result, new 3D deployment strategies for wireless sensor nodes need to be developed. Meanwhile, the rules to determine the density and location of sensor nodes on a WSN should be developed with the expertise of agronomists and crop scientists. For plant phenotyping, the WSNs need to collect throughout-season or year-round data, thus requiring the strategies of energy-saving and uses of long-term sensors. To enhance sensor nodes' energy efficiency, researchers are working on relevant topics, such as node sleep/active mode switching strategy, distributed asynchronous medium access control (MAC) protocol, and end-to-end encryption and authentication. Routing is another factor that has a strong influence on the data collection performances of WSNs. The key point of routing is to search for the most stable and effective routine for every transmission, so that the sensing data can be collected correctly with minimum dropping rate. In plant phenotyping scenarios, the routing protocol should also be able to handle energy-hungry multimedia exchange over a long time span. Therefore, alternative optimal routines have to be chosen for new transmission tasks, avoiding repeated heavy energy cost on a single node.

7.3.1.2 Ground Mobile Platforms

A ground mobile platform is another branch of ground-based platforms as shown in Fig. 7.4, which is a very popular topic in plant phenotyping. Ground mobile platforms employ signals from the global navigation satellite system (GNSS) to localize themselves and obtain plant phenotyping data together with corresponding localization information. Compared with other platforms, a ground mobile platform has two distinguishing features: high mobility and high flexibility. These features endow it with the best data collection power among all outdoor platforms. With high mobility, the ground mobile platform can scout a large area and collect phenotyping data for a large plant group in a relatively short time duration. This makes it a hot research topic for high-throughput phenotyping (HTPP). Meanwhile, high flexibility lets ground mobile platforms move in-field smartly and carry various sensors to take close observation for crops. Close observation consists of both top-view and side-view observations for crops. Other than commonly used top-view observations among all platforms, close side-view observations on ground mobile platforms can get under-canopy sights. Under-canopy observation in the natural growing environment is very important for plant phenotyping, which can intensively reflect the crop responses to complex natural climatic, meteorological, and edaphological processes.

Fig. 7.4 Ground mobile phenotyping platforms (*Disclaimer*: Commercial products are referred to solely for the purpose of clarification and should not be construed as being endorsed by the authors or the institution with which the authors are affiliated)

Based on different power sources and control patterns, ground mobile platforms have different variants, such as trolley cart-based platforms (Crain et al. 2016), tractor-based platforms (Baker III et al. 2016), and mobile robot-based platforms (Cousins 2015; Mueller-Sim et al. 2017; Young et al. 2018; Bao et al. 2019). Trolley cart-based platforms are constructed on specially selected or designed trolley carts, whose widths are multiples of crop row spacing. Therefore, they can let the wheels move on the terrain between two adjacent crop lines and carry different sensors to collect plant phenotyping information. To be noted, trolley cart-based platforms are driven manually. As a result, their payload, endurance time, and coverage area will be much smaller than engine-driven platforms. Many researchers still choose trolley cart-based platforms, because they are easy to build and operate.

Tractor-based platforms are developed by adding different plant phenotyping sensors on engine-driven agricultural machinery. Since many agricultural machines usually do not have phenotyping sensors on board, specially designed brackets for different sensors need to be added on agricultural machinery for plant phenotyping. With powerful engine, tractor-based platforms can carry more sensor/battery payloads and have longer endurance time and larger scouting coverage area. But they still need a driver behind the steering wheel, which makes their working time heavily depend on the driver situations.

Mobile robot-based platforms employ mobile robots as sensor carriers (Cousins 2015; Mueller-Sim et al. 2017; Young et al. 2018; Rouphael et al. 2018; Bao et al. 2019). They do not require a driver and can scout the crop field autonomously or controlled remotely. There are different configurations for the mobile robots. Some small robots can run between two adjacent crop rows. Others may run over multiple

crop rows. By cruising autonomously, mobile robot-based platforms can work day and night to collect plant phenotyping information. Even if their moving speed is not higher than tractor-based or aerial platforms, their longer working time can still guarantee a large coverage in a relatively short time duration. This feature makes mobile robot-based platform another hot topic for HTPP (Qiu et al. 2019).

The other forms of ground-based platforms for plant phenotyping include tripods (Friedli et al. 2016), field scan platforms (Virlet et al. 2017), and phenotyping towers (Naito et al. 2017).

On a tripod platform, the sensors are mounted on tripods to collect plant phenotyping information or meteorological information. As the structures of tripods are not sturdy enough, this type of platforms are not suitable for long-term observation. Meanwhile, big and heavy sensors cannot be mounted on tripods. Usually, tripods will be dispatched at different locations on the field manually. After finishing data collection tasks at one spot, they can be moved to another spot easily. Sometimes one tripod platform will be moved to different adjacent positions to generate multiple-view observations because of their lightweight feature. Researchers from Switzerland (Friedli et al. 2016) employed tripods to get crop height information using periodically terrestrial laser scanning. White spherical targets were dispatched at fixed locations to help calibrate and match scan data from different laser scans. Maize, soybean, and wheat were the crop targets. Plant architecture, height growth during the season, and short-term growth fluctuation were compared and analyzed.

Field scan platforms can be regarded as moving phenotyping towers. Some review papers categorize this type of platforms as mobile robotic platforms. But there is an obvious difference between field scan platforms and mobile robot platforms: field scan platforms move on rails, so that the location and length of the rails limit the coverage of field scan platforms. The advantage of field scan platforms is controllable and stable moving speeds due to their movement on rails. This brings the possibility of collecting plant phenotyping information in an intensive scanning mode. Some field scan platforms have lift arms, which can carry plenty of sensors to obtain crop observations from different heights and viewpoints. Researchers from UK mounted a camera box on a field scan platform to conduct high-throughput phenotyping tasks (Virlet et al. 2017). With a maximum payload of 500 kg, the camera box carried one chlorophyll fluorescence imager, two hyperspectral mirror scanners, one visible camera, one thermal infrared camera, two 3D laser scanners, one hyperspectral system, and NDVI sensor, which formed a big and heavy sensor array. This platform can take crop growth measurements, help to identify key growth stages of crops, and produce detailed descriptions of canopy development across the entire life cycle.

Phenotyping towers are tower-based platforms for carrying different plant phenotyping sensors. Compared with tripods, they have stronger structures and fixed locations. Strong structures endow them with powerful payloads/sensor-carrying capabilities. Multiple sources of sensor data can be collected during each trial or data collection circle. Strong structures also help to take long-term phenotyping observations, for example, multi-year-round observations. At the same time, strong structures determine that towers cannot move flexibly and have to stay at fixed

locations, which limits the coverage area of phenotyping towers. To solve this problem, researchers use multiple towers to obtain larger crop area coverage. Naito et al. (2017) used two phenotyping towers together and each tower carried two cameras and captured rice field images with different pitch and yaw angles over three years. Captured images were analyzed to obtain several vegetation indices (VIs), such as simple ratio (SR), NDVI, and transformed vegetation index (TVI). Then the correlations between different VIs and grain yields were conducted and SR showed the best performance in estimating grain weight.

7.3.2 Aerial Platforms

Compared with ground-based platforms, aerial platforms have much stronger capabilities on monitoring speed and area coverage. As a result, many researchers choose to collect plant phenotyping data with aerial platforms (Atkinson et al. 2018). There are different types of aerial platforms for plant phenotyping, including UAVs (Sankaran et al. 2015; Yang et al. 2017), blimps (Liebisch et al. 2015), manned aircraft (Gonzalez-Dugo et al. 2015), and satellites (Lobell et al. 2015). Different types of aerial platforms have different features and advantages. UAVs can get high-resolution data, and manned aircraft have high scouting speeds. Satellites have large monitoring coverage, while blimps can conduct low-speed monitoring at higher altitudes. But they are all sensitive to weather conditions, such as strong wind, heavy cloud, and rainstorm. Furthermore, airspace regulations constrain the application area of most aerial platforms.

7.3.2.1 Unmanned Aerial Vehicles (UAVs)

Among all aerial platforms, UAVs are the most popular platforms in the research area of plant phenotyping (Sankaran et al. 2015; Yang et al. 2017). They have distinguishing features, such as low cost, low flying altitude, easy deployment, timely data collection, and high data accuracy. Compared with other types of aerial platforms, UAVs can obtain high-resolution plant trial images, 0.05–0.15 m^2 per pixel (Atkinson et al. 2018). Multi-rotors (Fig. 7.5), helicopters, and fixed-wing UAVs are commonly used variants for plant phenotyping.

Now, multi-rotors or drones bring the most active research topic in aerial platforms for plant phenotyping. With the rapid development of drones in recent years, the flight control system, configuration design, and component materials have all been greatly upgraded. They share all the advantages of aerial platforms and play to the extreme. The price of a commercial drone product can be less than 400 dollars. Most drones can fly stably at low altitudes under the help of on-board flying control systems. With the "ready-to-fly" function, a drone can take off, fly, and land by itself following the commands from a person without any drone flying experiences. The operators can even use their smart phone to control the drones. Due to the flexible

Fig. 7.5 Multi-rotor package for plant phenotyping (Yang et al. 2017): (**a**) an eight-rotor UAV, (**b**) flight control system, (**c**) remote controller, (**d**) gimbal, (**e**) user interface

access to the field, drones can timely collect plant phenotyping data with high scouting frequency. Furthermore, drones can hover at a stable position and take specific observations for a selected field area, which perfectly fits the application scenarios in plant phenotyping. On the other hand, drones also have short points to be improved. First, battery is the key bottleneck problem for drones. The capacity of current batteries can only support a flying duration of less than 30 min. Second, small payload is another drawback of drones. Heavy and big sensors cannot be used on them. Third, the flying stability of drones drops down rapidly in strong wind and rainstorm weather, which leads to low quality of plant phenotyping monitoring data. Fourth, the high frequency and low-amplitude vibration caused by turning rotors introduce noise into sensor data, which requires the application of new anti-shake technologies to calibrate the collected data.

The helicopter is another variant of UAVs for plant phenotyping. The early application of helicopters in agriculture is known as aerial spraying for crop protection. Helicopter spraying systems from Yamaha was employed to conduct aerial spraying in Japan since the 1990s. To be noted, aerial spraying and aerial scouting are similar tasks for helicopters. Researchers replace sprayers on helicopters with cameras and use them as platforms for plant phenotyping data collection (Chapman et al. 2014). Compared with multi-rotors, helicopters have two main different features: gas engine and main rotor. Helicopters use gas engines as the power sources of their rotors, while multi-rotors use batteries to drive their rotors. Gas engines endow

helicopters with a higher average payload capacity. As a result, heavier sensors such as Lidars can be mounted on helicopters, but rarely on multi-rotors. Meanwhile, gas engines lead to heavier shaking problem and louder noise, compared with electrical motors. To lift the helicopters, main rotors are big and powerful. The strong airflow caused by the main rotor will disturb the stable state of crops and bring trouble to the data collection task. Therefore, helicopters need to take observations at higher altitude than multi-rotors. The unstable dynamic pattern coming from the main rotor structure also increases the operation difficulty, which requires skilled operators or complex flight control strategies. For a safe and successful plant phenotyping trial, a skilled support team is recommended to stand by for helicopters, while multi-rotors seldom need it.

Besides multi-rotors and helicopters, fixed-wing UAVs are also common plant phenotyping platforms (Shi, et al. 2016). They are well known in the areas of model airplane competition and geographic survey, before showing their potential in plant phenotyping. Compared with rotors, they have a higher flying speed but lack hover capability (Sankaran et al. 2015; Han et al. 2018). High speed makes fixed-wing UAVs have larger scouting area. At the same time, high speed also results in blurred sample images. Lack of hover capability means that they cannot take close and intensive observations for specific areas. Poor weather conditions such as strong wind and rainstorm also limit the application of fixed-wing platforms. Another application barrier for fixed-wing UAVs is the complex takeoff operations and wild landing manner. There are two takeoff strategies: run-up and hand launching. Run-up takeoff requires a long and flat track, which is hard to find on farmland. As a result, hand launching is more popular for plant phenotyping applications, which needs skilled operators to increase the takeoff success rate and protect the on-board sensors from takeoff accidents. The only landing manner for fixed-wing platforms is to keep landing gesture and slow down. The impact during the landing process is inevitable especially on the uneven farmland. Therefore, sensors mounted on fixed-wing platforms should be equipped with anti-shock and secure brackets.

The limited payload and high phenotyping expectations claim critical requirements for the on-board sensors of UAV platforms: lightweight, high accuracy, compact package, and low power consumption (Yang et al. 2017). Based on these features, researchers select digital camera, multispectral/hyperspectral camera, infrared thermal imager, Lidar, 3D camera, and synthetic aperture radar (SAR) as the main on-board sensors. Researchers from Washington State University, Oregon State University, and USDA (Sankaran et al. 2015) conducted a comprehensive survey on the typical sensors of UAVs. Digital cameras are convenient to obtain and use and the grayscale or colored images coming from digital cameras on UAVs can be used to analyze visible phenotyping parameters, such as outer defects, greenness, and plant growth. Multispectral sensors can detect more visible light bands and the collected data can be employed to analyze the crop responses to nutrient deficiency, water stress, and diseases (Mahlein et al. 2012). Hyperspectral sensors enjoy a higher band resolution than multispectral sensors and can also help to conduct product quality control and yield estimation. Infrared thermal sensors can generate images with temperature information on each pixel. Under the help of temperature

information, researchers can induce stomatal conductance information and analyze plant responses to water stress and diseases. Lidar and 3D camera are both ranging sensors. A 3D camera can generate depth image with distance information for each pixel. With lower accuracy, they can obtain plant height and canopy density information. Lidar has a higher measurement accuracy and can carry out precise estimations for plant height and volume. SAR can obtain high-resolution radar images under low-visibility weather conditions, which are helpful for crop acreage monitoring, key crop trait estimation, and yield prediction.

7.3.2.2 Blimps

Blimps are widely used for advertising, by towing large flag banners. Researchers also use them as plant phenotyping platforms (Sankaran et al. 2015). They can fly at low speed and hover to obtain high-resolution images of field crops. Bigger and heavier sensors can be mounted on blimps. However, launching a blimp-based field trial is not an easy task. Because of its massive body shape, it is hard for blimps to move from one spot to another, and they cannot give good flight performances under windy weather conditions. The cost of using blimps is also much higher than that of UAVs. A good example for blimp-based plant phenotyping platforms is Zeppelin NT. The highest speed of a blimp is 20 km/h and it can work when the wind speed is under 25 m/s. It can obtain high-resolution thermal images (10 cm × 10 cm/pixel). Field tests proved that the Zeppelin platform is capable of monitoring crops throughout the season, giving robust image segmentation and identifying individual plots. Equipped with three different cameras, canopy cover and NDVI value can be deduced for maize plants.

7.3.2.3 Manned Aerial Vehicles

Manned aerial vehicles are popular platforms for geographic survey and agricultural tasks. In the USA, thousands of manned aircraft are being used for crop protection. By carrying different kinds of sensors, manned aerial vehicles can be used to monitor crop growing conditions, detect crop loss (weeds, diseases, and insect damage), and assess the performance of ground/aerial treatments (Yang 2016). As a result, researchers also employ manned aircraft as plant phenotyping platforms (Gonzalez-Dugo et al. 2015). Manned aerial vehicles have much larger payload capacity than UAVs. Hence, a wide variety of sensors can be equipped on a manned aircraft, including multispectral imaging sensors, hyperspectral imaging sensors, thermal cameras, consumer-grade cameras, and Lidars. Manned aerial vehicles take observations at higher altitude than UAVs. Their flying altitude ranges from a hundred-meter level to a thousand-meter level (Yang 2016). Meanwhile, they have a much higher flying speed than UAVs and blimps. With these advantages, they can carry all needed sensors and collect large-area phenotyping data in one flight. But high speed and high altitude also result in lower resolution and blurred airborne images. The

resolution of aircraft-mounted sensors is around 1 m^2/pixel, compared with 0.05 m^2/pixel to 0.15 m^2/pixel for drones (Atkinson et al. 2018). Furthermore, the data collection trials based on manned aerial vehicles are not easy to launch. Skilled pilots and nearby airports are two essential requirements that are often hard to meet.

7.3.2.4 Satellites

Satellites have been used for remote sensing imagery in agriculture since Landsat 1 (Earth Resources Technology Satellite 1) was launched in 1972 (Mulla 2013). With the rapid development of sensing technologies in the last decade, the resolution and visit frequency of satellite remote sensing have been greatly improved. The panchromatic and multispectral pixel sizes of high-resolution satellite sensors range from 0.31 to 1 m and 1.24 to 3.28 m, respectively. One-day revisit is also not an impossible mission for new satellites (Yang 2018). High sensing resolution and high visit frequency make satellites become good sensing platforms for precision agriculture. A large number of literature reported the applications of satellite remote sensing on crop growth and yield, irrigation, and crop losses (Karthikeyan et al. 2020). The images taken by satellites cover far more bigger areas than those taken by other aerial platforms. As platforms in space orbits, satellites have limited onboard sensor types and fixed sampling periods. Similar to other aerial platforms, satellite remote sensing is also sensitive to cloudy weather. Furthermore, satellite remote sensing can only obtain spectral indices rather than true plant phenotyping parameters. Because of these disadvantages, the plant phenotyping information collected by satellites is limited and high-frequency data collection is also impossible. Some researchers think that satellites are not ideally suited for plant phenotyping (Atkinson et al. 2018), even if they are cheap data sources and have space resolution up to m^2/pixel level. However, some other researchers think that satellite imagery has good potential in analyzing soil moisture and drought risk (Martínez-Fernández et al. 2016), predicting regional crop yield (Lobell et al. 2015), and detecting crop diseases (Yuan et al. 2017).

7.3.3 Indoor Platforms

Both ground-based and aerial platforms are designed for field-based plant phenotyping, which are mainly nondestructive and remote sensing solutions for crop groups. The information collected by field-based plant phenotyping can reflect the growth status of crops under natural environment conditions (climate, weather, and soil), but lack precise and microscopical details, which need close, multiview, and even destructive observations. These details are important to reveal the truth of crop growth and environmental stresses. In addition, field-based plant phenotyping has many uncontrollable environment parameters. As a result, determining the relationships between environmental stresses and crop responses becomes a difficult task.

To tackle these issues, researchers also pay attention to indoor platforms (Zhao et al. 2019). Indoor platforms have distinguished advantages in obtaining precise and intensive measurements. First, indoor platforms do not need to meet the requirements of in situ measurements, which are common requirements for field-based platforms. Therefore, operators have enough time to conduct sample preparations, such as surface cleaning and stem cutting. Meanwhile, operators have more available resources to improve measurement conditions, such as adjusting light conditions and sample gestures and view angles. All these help to obtain more precise and detailed measurements. Second, indoor platforms are in a space with more controllable environment parameters. Thus, researchers can design specific environment stresses for crops and observe their responses with indoor platforms, which can reveal the relationships between stresses and crop responses directly.

According to the observation scales, indoor platforms can be categorized into three types: tissue-level platforms, organ-/single plant-level platforms, and group-level platforms.

7.3.3.1 Tissue-Level Platforms

Tissue-level platforms usually need measurement targets destructively prepared, by taking them apart from the whole plants. Thus, the targets can be placed onto or into the platforms where precise and intensive measurements are taken. With these phenotyping information from tissue-level platforms, 3D tissue structures can be rebuilt and tissue nutrition contents can be analyzed. A good example for tissue-level platforms is the micro-CT platform. This platform is widely used for the 3D structure detection of small objects, including mechanical parts, animal organs, and plant tissues. Agricultural researchers employ it as a plant phenotyping platform. Researchers from Beijing Research Center for Information Technology in Agriculture use this platform to reconstruct the 3D anatomical models of maize organs (stem, root, and leaf). Based on the proposed "sample preparation protocol," 31 phenotypic traits for stem, 33 phenotypic traits for leaves, the volume and surface area for roots can be extracted from micro-CT collected data (Zhang et al. 2018).

7.3.3.2 Organ-/Single Plant-Level Platforms

Organ-/single plant-level platforms can precisely extract the phenotypic traits without destructive sampling. They usually have one single type of sensors, cameras, or laser scanners. Two-/three-dimensional models can be constructed based on sensing data. For 2D modeling, a sensor holder and a sample container are enough to set up a simple platform, such as a 2D root structure phenotyping solution from Georgia Institute of Technology and Pennsylvania State University (Bucksch et al. 2014). Three-dimensional models are constructed by merging multiview observations.

There are different solutions for multiview observation, among which the turning stand and flexible manipulator are the most popular ones. For a turning-stand-based platform, the target will be placed on a turning stand and one or more cameras will take pictures from different directions. The turning stand solutions can be used for all plant organs, including stems, leaves, and even roots. The root trait extraction is taken as an example, and the solution has three main components: a transparent container with rooted plant and nutrient solution inside, a turning stand under the container, and cameras (Clark et al. 2011). For a flexible-manipulator-based platform, the sensor is mounted on the manipulator as an end effector. The manipulator will move around the plant, letting the sensor take multiview observations (Paulus et al. 2014a, b).

7.3.3.3 Group-Level Platforms

Tissue- and organ-/single plant-level platforms mainly focus on measurement accuracy, while measuring speed is also very important to plant phenotyping. With the growing demands for selecting traits with good resistances among massive quantity of samples, high-throughput phenotyping for advanced breeding is more and more popular. Group-level indoor platforms are good examples for high-throughput phenotyping. Although the crops growing indoor (in greenhouse in fact) cannot encounter the same natural challenges as those growing in an open field, and researchers can set specific microclimate conditions to observe the corresponding crop responses. Indoor group-level platforms can conduct high-throughput phenotyping without sacrificing measurement accuracy, because the sensor carriers for indoor group-level platforms are powerful enough to carry various sensors, which can take close and multiview observations.

There are two typical forms of group-level indoor platforms: assemble line and moving crane. The major difference between the two forms is the dynamic states of the sensors. For assemble line platforms, various sensors are mounted at static sensing stations, such as RGB cameras, RGB-D cameras, infrared cameras, multispectral cameras, hyperspectral cameras, chlorophyll fluorescent cameras, and laser range finders. All sensors are static and the crop samples will be transported to different sensing stations by a conveyor belt or similar mechanisms. “Conveyor Scanalyzer” from “LemnaTec” (Choudhury et al. 2018) and high-throughput rice phenotyping facility (HRPF) from China (Yang et al. 2014) are good examples for this type of platforms.

For moving crane platforms, all plants in greenhouse are static, while the moving cranes will carry various sensors to collect phenotyping information for different cultivation areas. As sensors are mounted on the cranes, this type of platforms mainly deliver top-view observations. There are several good examples for indoor moving crane, such as the “Canopy Scanalyzer” from “LemnaTec” (https://www.lemnatec.com/products/canopy-scanalyzer/) and Crop 3D from China (Guo et al. 2016).

7.4 Data Analytics for Plant Phenotyping

The aim of plant phenotyping is to collect features, parameters, and states of crops as many as possible. Therefore, various sensors are introduced into this research field and plenty of plant targets are observed under different conditions. Hence, plant phenotyping often encounters data diversity of formats, noise, errors, and physical characteristics. In addition, the volume of data grows rapidly with the development of new high-throughput phenotyping technologies. All the abovementioned reasons heavily increase the difficulty of data analysis, to extract features of plant and reveal corresponding traits of interests. As shown in Fig. 7.6, in order to tackle this problem, different mathematical tools and algorithms are employed to process the data, including data preprocessing algorithms, traditional statistical tools, and machine learning algorithms.

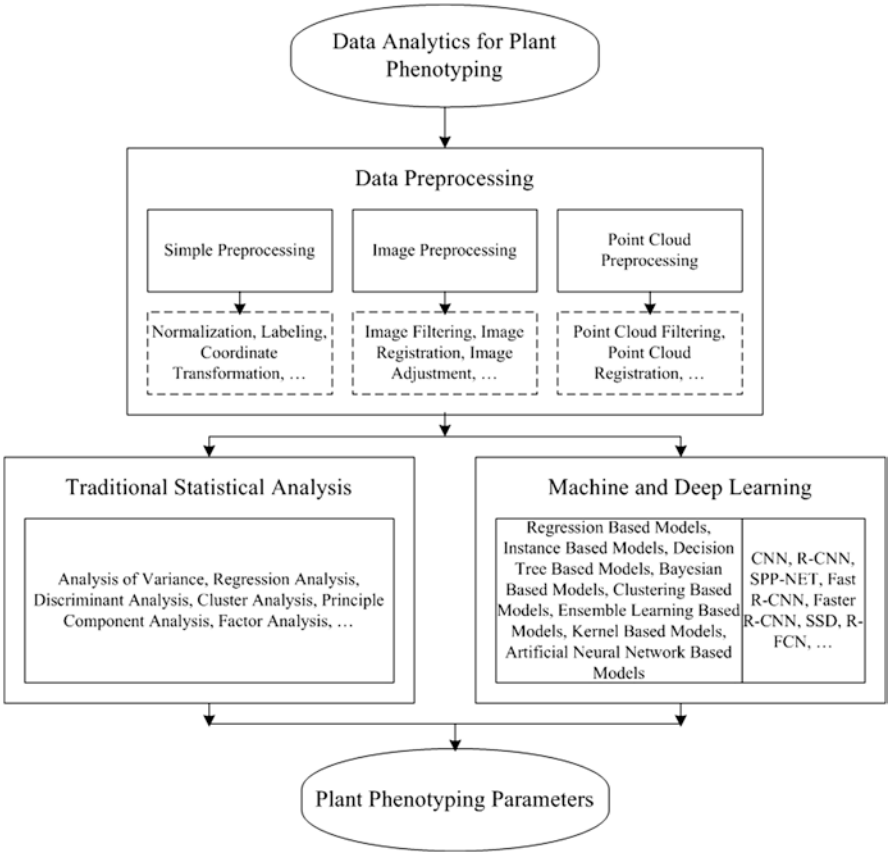

Fig. 7.6 Flowchart for data analytics in plant phenotyping

7.4.1 Data Preprocessing

7.4.1.1 Overview

For most cases, plant phenotyping data are collected under natural crop growing conditions. The collected data suffers from multiple sources of noise and errors, such as changing lighting intensity, water mist, dust, self-occlusion of leaves/branches, sensor vibrations, and incorrect sensing operations. As a result, the raw data need to be preprocessed in order to be ready for further analysis. According to the complexity of the preprocessing methods, data preprocessing operations for plant phenotyping can be grouped into simple preprocessing, image preprocessing, and point cloud preprocessing, respectively. Simple preprocessing includes general methods including normalization, labeling, and coordinate transformation. Image preprocessing algorithms consist of filters, registration algorithms, and image adjustment algorithms. Point cloud preprocessing algorithms consist of filters and registration algorithms.

Normalization adjusts data types of different scales into the same normal scale, for example, an interval of [0, 1]. After normalization, the dimensional data become dimensionless data and modeling errors coming from unbalanced scales are greatly reduced. Labeling is an important preprocessing step for machine learning algorithms. The supervised learning algorithm needs labeled training and testing data to build and verify the learning models. Although there are automatic labeling algorithms reported in literature, manual labeling assisted by labeling software is still the main labeling method. Coordinate transformation solves the data localization problem of inconsistent coordinate systems. Under many situations, data analysis needs position information as data identities or reflecting data relationships. Inconsistent coordinate systems lead to wrong localization and gesture priors, or unit priors. An example for coordinate transformation is transforming GPS data from (longitude, latitude) to local X–Y coordinates.

7.4.1.2 Image Preprocessing

There are plenty of image processing techniques, such as domain transform, encoding and compression, enhancement and recovery, and segmentation. For the image preprocessing problems in plant phenotyping, image adjustment, image registration, and image filtering are widely used.

Images have different displaying solutions. Some plant phenotyping traits are obvious under specific displaying solutions. For these cases, image adjustment can help to find the proper displaying solutions for trait extraction. Color space transformations and histogram building are commonly used image adjustment techniques. RGB, CMY, HSV, HSI, Lab, and YUV are common color spaces. Each color space has its own features and advantages. Although RGB space is the most popular one for saving images on computers, it is not the favorite of scientists. RGB space

combines hue, intensity, and saturation together, which makes digital adjustments for image details a difficult mission. CMY space is widely used in printing industry. C, M, and Y stand for the color of corresponding ink cartridges. YUV space employs intensity and chromatic aberration to describe different colors. It is widely used for image encoding, such as JPEG (Joint Photographic Experts Group) and MPEG (Moving Picture Experts Group). HSV and HSI are similar spaces. They share two common components – hue and saturation – which are very important in plant organ detection. Lab space is good at describing human vision aesthesis. It can be used for color balancing according to the entry of "CIELAB color space" on Wikipedia. In plant phenotyping applications, researchers often transform RGB data to HSV, his, or Lab data, hoping to make phenotyping traits easy to detect. As fruit surfaces usually have a higher saturation level in images, HSV and HSI transforms can be employed to preprocess images for fruit detection tasks. Histograms are built from grayscale images. Histogram building is a preprocessing step for image segmentation algorithms, such as the well-known Otsu segmentation algorithm (Otsu 1979).

To obtain comprehensive plant phenotyping data, multiview image data collection is a popular strategy. Thus, image registration is essential for multiview matching and fusion. There are two main categories for image registration: area-based registration and feature-based registration. Area-based registration registers images based on their overlapped windows. To achieve the best registration results, sliding windows are employed to search the overlapped windows. The similarity of overlapped windows is calculated based on pixel-level attributes. Area-based registration has obvious disadvantages in registering images with view rotations, which results in low registration accuracy for multiview registration problems. As a result, area-based registration is seldom found in plant phenotyping literature. On the other hand, feature-based registration is capable of registering images with view rotations and is widely used in plant phenotyping. Harris corner detector, features from accelerated segment test (FAST) corner detector, scale-invariant feature transform (SIFT) detector, and speeded up robust features (SURF) detector are typical feature-based registration algorithms in plant phenotyping. Harris corner detector uses low-level and local features to register images. It can generate a large amount of corner points and cause heavy computational loads. In addition, it suffers from ghost when obvious rotate transform exists. FAST corner detector employs local intensity discrepancy to detect corner points. It is fast and suitable for real-time image processing applications. Threshold selection of FAST is the key point for good detection performances. SIFT supplies a feature abstracting strategy that is invariant to scale and rotation transforms. Furthermore, the strategy enjoys high tolerance to lighting changing, viewpoint changing, affine transformation, and noise. It also suffers from high computational load. SURF is regarded as an upgraded version of SIFT. It is a detector based on interest point detection and descriptor. SURF inherits the long points of SIFT and greatly cuts down the computational load. There are a large quantity of literature about image registration in plant phenotyping, such as employing SIFT to detect legume leaf features (Larese and Granitto 2015) and using SURF to fuse UAV-based hyperspectral images (Habib et al. 2016).

During the data collection process of plant phenotyping, cameras are sensitive to environmental conditions and plant self-occlusions, which may introduce different kinds of noise. As a result, getting rid of noise and outliers with image filtering techniques is a necessary step. There are plenty of image filtering techniques, including Gaussian filters, mean/median filters, and bilateral filters. Gaussian filter's impulse response obeys a Gaussian function. With this feature, it can suppress noise and smooth images. An example of Gaussian filter is filtering the noise of hyperspectral images for maize seedlings (Yang et al. 2019b). Mean/median filters use mean or median pixel values of the smooth window to conduct the filtering operation. Mean filters are typical linear filters, which blur the image details while getting rid of noise. Median filters are nonlinear filters, which are good at filtering impulse noise and protecting sharp image edges. Fernandez-Gallego et al. (2018) employ a median filter to reduce the noise of RGB images for wheat ear counting. Bilateral filters are nonlinear filters. They replace the selected pixel value with the weighted average value of its surrounding pixels, and the weighted value is based on a Gaussian distribution. The most important feature of bilateral filters is that they take not only Euclidean distance, but also radiation difference under consideration. An example of bilateral filter is employing it to cut down the noise influences in RGB images of white chrysanthemums (Yang et al. 2019a).

7.4.1.3 Point Cloud Preprocessing

There are two main point cloud preprocessing techniques: point cloud registration and point cloud filtering.

(1) Point Cloud Registration

Point cloud registration algorithms can be divided into two groups: exhaustive method-based registration and feature-based registration. Exhaustive method-based registration traverses the whole registration space to minimize the error function or maximize the number of matched point pairs. RANSAC (random sample consensus) and 4PCS (4-point congruent set) are two good algorithms for exhaustive method-based registration. Feature-based registration searches for matched point pairs under the help of morphological features, for example, FPFH (Fast Point Feature Histograms) descriptor. SAC-IA (Sample Consensus Initial Alignment) and ICP (Iterative Closest Point) are two typical algorithms for feature-based registration. These four algorithms are representative ones in plant phenotyping.

RANSAC is an iterative registration algorithm, whose core ideas are randomness and hypothesis. Randomness is helpful to cut down computational loads, and hypothesis means regarding randomly selected points as inlier points and using them to compute other inliers. RANSAC assumes that models are formed by the inliers, and the outliers cannot fit the models. Thus, it can carry out model parameter estimation robustly. However, optimal models can only be obtained with infinite iterations. Furthermore, the setting of thresholds counts a lot to the registration accuracy. 4PCS is based on the RANSAC framework and speeds up the registration

process through building and matching congruent four-point pairs. With the help of affine invariance constrains and largest common point-set strategy, 4PCS can give the best registration for input point cloud pairs of arbitrary shapes. SAC-IA employs FPFH features to search the correspondence point pair between two point clouds. The optimal transformation matrix is determined through rigid transformation and calculation of distance error functions. SAC-IA suffers from heavy computational loads when registering large point clouds. Thus, downsampling is required for large point clouds, which will lose part of the feature points and lower the registration accuracy. ICP is a popular registration algorithm based on the least squares method. It employs an iterative strategy to find the optimal rotation matrix R and translation vector T for point cloud registration. Most of the ICP's computational load comes from searching for the closest point pairs of two point clouds in each iteration. Although bad initial R and T settings will easily let the algorithm hit a local maximum, ICP is still widely used because of its strong noise tolerance capability. More and more researchers start to apply point cloud registration in plant phenotyping, such as plant detection and mapping with RANSAC (Weiss and Biber 2011), plant height and spacing abstraction for maize with SAC-IA and ICP as shown in Fig. 7.7

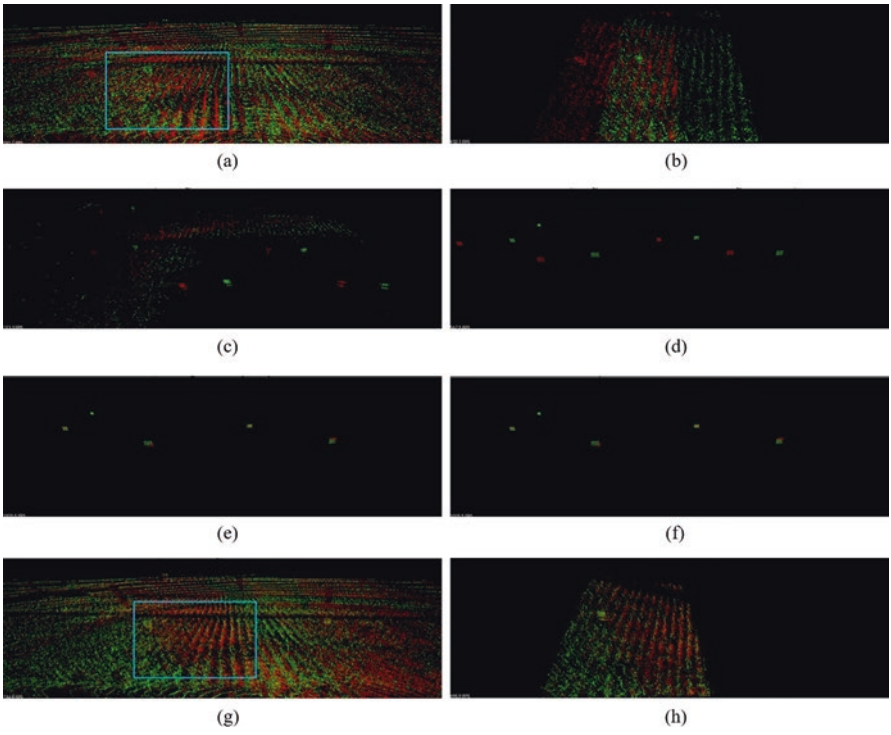

Fig. 7.7 Parcel-level point cloud registration for maize with SAC-IA and ICP (Qiu et al. 2019). (**a**) Unregistered two clouds. (**b**) Magnified view of the blue rectangle area in (**a**). (**c**) Cutting off most plant points. (**d**) DBSCAN abstracted landmarks. (**e**) SAC-IA registered result. (**f**) ICP registered result. (**g**) Merged two clouds. (**h**) Magnified view of the blue rectangle area in (**g**)

(Qiu et al. 2019), and 3D reconstruction for maize plant with ICP (Garrido et al. 2015).

(2) Point Cloud Filtering

Point cloud filtering is employed to get rid of noise and outliers. There are different filters working for point clouds, including pass-through filters, conditional filters, radius filters, statistical filters, and voxel filters. Pass-through filters are simple filters and can get rid of the points that are not located in a preset region on a given dimension. They are often employed to crop expected point cloud subsets, for example, specific height pass filters for cropping plant point clouds above the terrain surface. Similar to pass-through filters, conditional filters also help to crop subsets. However, it can get rid of unexpected points depending on flexible conditions, which can be designed according to various features of the target point cloud. Radius filters employ a radius to filter out the points lying within low point density areas. If the nearby circle/sphere area of a point has less points than a preset threshold, the point will be filtered. Radius filters run fast and retain the high point density area. But its performance heavily depends on the preset radius and threshold. Voxel filters divide the 3D space into bounding boxes called voxels. They can filter out noise and outliers according to the point density in voxels. On the other hand, they can also carry out downsampling tasks for high-density point clouds while preserving the geometrical information as much as possible. There are many application examples for point cloud filtering in plant phenotyping, such as filtering the 3D maize plant point cloud with a statistical filter (Lu et al. 2017), filtering the point cloud of clustered leaves with a radius filter (Li et al. 2019), and downsampling the grape point cloud with a voxel filter (Mack et al. 2017).

7.4.2 Traditional Statistical Analysis

Before the appearance of machine learning algorithms, plant phenotyping researchers employ traditional statistical analysis to handle the collected data and make conclusions. Even though machine learning is widely used for plant phenotyping data analysis nowadays, researchers still prefer statistical analysis for small data set analysis. Traditional statistical analysis belongs to multivariate statistical analysis. It is an important branch of mathematical statistical analysis and a common name for a group of comprehensive analysis methods. These methods can find the statistical laws among correlated multiple targets and parameters, which just hits the point of the data analysis tasks for plant phenotyping. The plant phenotyping data come from selected samples and can never cover the whole experimental crop group. This natural attribute determines that the plant phenotyping data have variability and randomness. Additionally, the measurement process also introduces noise and error. As a result, making conclusions depending on raw plant phenotyping data cannot work. Based on the data from a sample population, tradition statistical analysis can infer the attributes and traits of the whole sample population, help make conclusions

with high confidence and solid theoretical support, and offer precise plant phenotyping data for good trait screening during crop breeding. There are several common methods for traditional statistical analysis, including analysis of variance, regression analysis, discriminant analysis, cluster analysis, principal component analysis, and factor analysis.

(1) Analysis of Variance

Analysis of variance is a common model in data analysis. Mean value, variance, and covariance are basic elements in analysis of variance. Mean value shows the middle position of a sample set. Variance shows the deviation of a random variable to its mean value. Covariance shows the distribution density of a sample set. For plant phenotyping applications, the mean value, variance and covariance will work together to carry out the multivariate analysis tasks. Through analyzing the contributions of different variation sources on the total variation, analysis of variance can figure out the influence levels of definite and controllable factors on the results. In analysis of variance, factors are named with control variables, and results are named with observation variables. According to the number of control variables and their controllability, analysis of variance methods can be categorized into three groups, one-factor analysis of variance, multifactor analysis of variance, and analysis of covariance. For both one-factor and multifactor analysis, control variables are controllable. As a result, the influence of one factor can be observed by keeping other factors constant. Meanwhile, multifactor analysis can also observe the correlation influences of two or more factors on observation variables. Taking the influences of different varieties and fertilizing quantities on crop yield as an example, varieties and fertilizing quantities can be taken as control variables, and yield can be taken as the observation variable. Either the best variety or the best fertilizing quantity for crop yield can be obtained, by keeping the other factor constant. Furthermore, the best combination of variety and fertilizing quantity can be determined through testing the yield distribution under different combinations. For crop yield, there are also uncontrollable variables, such as weather and soil conditions. To solve this problem, weather and soil conditions are introduced as covariates. Thus, analysis of covariance can be employed to evaluate the significant influences from controllable variables. An application example for analysis of variance on plant phenotyping is analyzing the relationship between different genotypes and nitrogen fertilizer demands (Kefauver et al. 2017).

(2) Regression Analysis

Regression analysis is a collection of statistical methods for determining the quantitative relationships between two or more than two groups of variables. For big data analysis, it is a modeling technique for prediction, which mainly focuses on predicting the dependent variables with independent variables. The common regression analysis methods consist of linear regression, logistic regression, polynomial regression, stepwise regression, and ridge regression. Linear regression is one of the most well-known modeling tools. It builds prediction models based on linear functions, by determining the coefficients with regression estimation. Logistic

regression is used to compute the probabilities of true or false for events. An obvious feature of logistic regression is the Boolean dependent values, yes or no, true or false, and 1 or 0. Logistic regression needs a large sample set to guarantee the estimation accuracy. When the index of independent variables in the regression function is an integer larger than 1, the regression is called polynomial regression. Polynomial regression is capable of fitting polynomial functions. For the regression problems of functions with multiple independent variables, stepwise regression is also a good choice. It can build models by adding or deleting covariates according to specified standards, aiming to maximize the prediction power with minimum independent variables. Ridge regression is a biased estimation method for data sets suffering from multicollinearity. It adds a degree of bias to the least square regression estimates, in order to reduce the standard errors. Regression analysis can be used for different plant phenotyping applications, such as crop yield and quality prediction (Magney et al. 2016) and disease-related genotype detection (Yu et al. 2018).

(3) Discriminant Analysis

Discriminant analysis is a set of multivariable classification methods based on interval predictors or independent variables. The purpose of discriminant analysis is building the discriminant functions of a combination of feature values, which can discriminate instants from different categories. There are two main types of discriminant functions, linear discriminant functions and canonical discriminant functions. To conduct discriminant analysis, the discriminant variables are required to meet three assumptions. First, none of the discriminant variables is a combination of others. Second, the covariance matrices of instance groups are equal to each other. Third, the discriminant variables obey a multivariate normal distribution. In other words, each discriminant variable obeys a normal distribution when other discriminant variables are constant. There are four main variants for discriminant regression, including maximum likelihood estimation-based discriminant regression, distance-based discriminant regression, Fisher discriminant regression, and Bayes discriminant regression. Discriminant regression is also a common tool for plant phenotyping applications, such as seed classification (Elmasry et al. 2019) and nutrient absorption estimation (Kenobi et al. 2017).

(4) Cluster Analysis

Cluster analysis is the process of categorizing the physical or abstracted objects into several groups, whose members are similar to each other. Cluster analysis employs two types of descriptors to reflect the correspondence or relational closeness between two instances or variables. The first type uses the proximity level of a pair of variables as the descriptor, for example, distance. The common distance definitions are Euclidean distance, Manhattan distance, Chebyshev distance, and chi-squared distance. The second type uses the similarity level of a pair of variables as the descriptor, for example, the correlation coefficient. The most popular correlation coefficient is Pearson correlation coefficient. Researchers proposed a large variety of clustering algorithms, such as hierarchical clustering, K-means clustering,

density-based clustering, model-based clustering, and grid-based clustering. Hierarchical clustering categorizes objects on different layers. A tree graph will be built after hierarchical clustering. K-means clustering is the most well-known clustering algorithm. It categorizes all samples into K groups according to the Euclidean distance between two sample points. Density-based clustering can search for the high-density areas segmented by low-density areas. It can find clusters of different shapes, while distance-based clustering can only find spherical clusters. Model-based clustering assumes all samples obey a series of implicit probability distributions. As a result, samples obeying the same distribution will go to the same cluster. Grid-based clustering divides the attribute space into finite grids, and samples are categorized according to their space locations. For plant phenotyping, cluster analysis usually works together with other analysis methods. For example, cluster analysis and discriminant analysis are employed to classify grape varieties based on their reflectance spectra (Rustioni et al. 2013).

(5) Principal Component Analysis

Principal component analysis (PCA) transforms the original correlated variable set into an independent variable set. The new variables are linear combinations of original variables, and they are obtained with orthogonal transform. Theoretically, principal analysis can find infinite new components. However, only few of them contains valuable and dominant information of the original variable set. These components are called principal components. PCA brings at least four benefits for data analysis. First, it carries out dimensionality reduction, which uses fewer principal components to hold the dominant information of the original variable set. Second, it brings a graphic expression for the data distribution. By taking each principal component as an axis, all samples can be located in an orthogonal coordinate system, which clearly shows the standing of each sample and lets the outliers become explicit. Third, it helps to build regression models. Principal components can act as variables for the new regression models. Fourth, it helps to select dominant factors. PCA can sort the new components in a descending order according to their covariance values. The selected principal components can be recognized as dominant factors for the sampled data set. Researchers often employ PCA to analyze the relationships between genotypes and plant phenotypes, such as selecting good genotypes for black raspberry (Yazdanpour et al. 2018).

(6) Factor Analysis

The idea of factor analysis is categorizing the variables into different groups based on their correlation status. After categorizing, variables in the same group have high correlation, while variables in different groups are independent or have low correlation. Factor analysis assumes that high-dimensional samples are generated with Gaussian distribution, linear transformation, and error disturbance. As a result, high-dimensional samples can be expressed by low-dimensional samples, and dimensional deduction can be achieved. Factor analysis is quite different from PCA. PCA abstracts principal components by building linear combinations of original variables, while factor analysis finds factors by decomposing original variables

into several linear combinations. Factor analysis has advantages in determining the influences on plant phenotypes, coming from genotypes, fertilizers, or environmental conditions. Some researchers employ multifactor analysis to estimate and validate the drought tolerance of maize (Dias et al. 2018).

7.4.3 Machine Learning and Deep Learning

7.4.3.1 Machine Learning

(1) Overview

Statistical analysis is good at analyzing the data with obvious statistical and low-dimensional features. However, most plant phenotyping data are collected under complex agricultural scenarios. The features to be extracted might be strongly coupled, heavily distorted, and high dimensional and hence are difficult to be modeled with traditional statistical tools or explicit equations. To solve this problem, researchers introduce machine learning (ML) algorithms. Machine learning algorithms have advantages in building black-box models, which can infinitely approach the true models with more and more training. This idea avoids the tough modeling topic and finds the feature patterns approximately. Meanwhile, machine learning algorithms are capable of describing the implied relationships among multiple inputs and multiple outputs. This capability helps to extract the tightly related features simultaneously (Singh et al. 2016).

Machine learning algorithms are a set of computerized mathematical solutions for feature extracting and modeling. They can search for patterns automatically from given data sets, instead of selecting the most fitted models manually with traditional statistical methods. The common modeling process for machine learning consists of three main parts: data preparation, model training, and model testing. Before model training starts, a data set will be given and divided into two sets, one for training and the other for testing. After data preparation is ready, the machine learning model will be trained with the training data. Then, testing data will be applied on the trained model to verify the training achievements. If the testing accuracy reaches a preset level, the trained model is ready for use. Otherwise, another training and testing loop should be launched with adjusted settings. The loops will not stop until the preset accuracy level is reached. To be noted, not all machine learning algorithms require labeled training and testing data. Based on the learning manners, machine learning algorithms can be roughly divided into four categories: supervised learning, unsupervised learning, semi-supervised learning, and reinforcement learning (Dey 2016). Only supervised learning strictly requires all training and testing data should be labeled.

(2) Machine Learning Models

As a large number of machine learning algorithms have been proposed, it is difficult to give a comprehensive description for the whole research field. Categorizing

the algorithms into several groups can help to take a quick glance and select the right algorithms in application. Other than choosing proper machine learning tools based on learning manners, researchers prefer to select the suitable algorithms according to their model characteristics, which can imply their advantages in handling specific data sets. There are several commonly used models, such as regression-based models, instance-based models, decision tree-based models, Bayesian-based models, clustering-based models, ensemble learning-based models, kernel-based models, and artificial neural network-based models (Liakos et al. 2018).

(3) Regression-Based Models

Regression-based models mainly focus on revealing the relationships between variables, especially the influencing mechanisms of input variables on outputs. These groups of algorithms belong to the supervised learning category, meaning that they require all training and testing data labeled. In addition, they are sensitive to outliers. Linear regression and logistic regression are the most famous examples for regression-based models. There are also more powerful variants, such as ordinary least squares regression, multivariate adaptive regression splines, and multiple linear regression. LemnaTec GmbH employed a prediction regression model to solve leaf-counting problems (Pape and Klukas 2015).

(4) Instance-Based Models

K-nearest neighbor (KNN) is the most famous example for instance-based models. It combines training and testing steps together by adjusting the K value, distance definitions, and decision-making rules. For each new instance to be classified or predicted, K-nearest neighbor will calculate the distances between it and all training instances, find the K-nearest instance subset, and make decisions based on voting results of K-nearest instances. K-nearest neighbor has advantages on multiple-target classification problem. However, it is not capable of dealing with big data sets, because its computation load increases heavily if the data volume grows. For plant phenotyping, an example is grading the maturity of blueberry fruits (Tan et al. 2018).

(5) Decision Tree-Based Models

A decision tree is a simple machine learning idea based on tree structures. It can give classification or regression decisions/labels at the leaf nodes by following a series of decision rules on a binary tree. The tree graph has three basic elements: root node, attribute node, and leaf node. The root node contains all the featured data, the attribute node contains the decision rules, and leaf nodes are the category labels. Under the help of the tree graph, decision tree-based models can achieve satisfying accuracy for big data problems after quick training and are capable for multi-classification problems. On the other hand, they are easily overfitted and often ignore the correlations among different attributes. Decision tree (DT) and classification and regression trees (CART) are the most popular decision tree-based models. A plant phenotyping example for decision tree-based models is evaluating the canopy coverage ratio of paddy field (Guo et al. 2017).

(6) Bayesian-Based Models

These models are based on the Bayesian theorem, which assumes all characteristics are independent. The assumption helps to build simple and effective models. In the learning process, Bayesian-based models are robust to missing data attributes and tolerant of small training data sets. Meanwhile, they are capable of handling multi-classification problems. However, the independence hypothesis is not valid in most practical applications and correlated attributes are prone to reduce the model performances. Bayesian-based models have different variants, including native Bayes, mixture of Gaussians, and Bayesian belief network. An instance for the application of Bayesian-based models on plant phenotyping is weed classification. A native Bayes-based classifier is built and trained to recognize two kinds of weeds (Ahmad et al. 2018).

(7) Clustering-Based Models

The idea of clustering-based models is gathering the similar instances into corresponding clusters. They are typical unsupervised learning algorithms. In the clustering process, the meaning or name for each cluster is not taken under consideration, which implies the training data are unlabeled. If the rules for similarity calculation are ready, the clustering-based models are ready to work. K-means algorithm is a classic example of clustering-based models. It can group N instances into K clusters. The selection of K value is important to the performances of the algorithm. K-means algorithm is also sensitive to noise and isolated instances. Researchers from Iowa State University employ the K-means algorithm to detect single plants among 3D point clouds obtained in a growth chamber (Bao et al. 2018).

(8) Ensemble Learning-Based Models

In fact, ensemble learning-based models do not have unique mathematical models. The idea of ensemble learning is combining weak learning models to form powerful learning strategies. Each selected weak model will be trained independently. In the prediction step, the results from weak models are fused to give more accurate and robust performances. The key point of these strategies is how to select the proper weak models and fuse their results. Common ensemble learning-based models are Boosting, AdaBoost, and Random Forest (RF). Some researchers use RF to detect *Septoria tritici* blotch, a disease in wheat (Odilbekov et al. 2018).

(9) Kernel-Based Models

Kernel-based models have distinguishing advantages in solving nonlinear classification and prediction problems. Kernel functions can project the models from low-dimension spaces to high-dimension spaces. Thus, some linear indivisible problems can be transformed to linear separability problems in high-dimension spaces, and instances from two different categories can be easily recognized. Support vector machine (SVM) is the most famous kernel-based learning algorithm. It is good at handling nonlinear and high-dimensional problems. As its optimizing target is minimizing the structured risks, SVM has a strong generalization power

and can reach satisfying accuracy with a small training data set. This feature makes it popular in agriculture applications, because it is difficult to obtain a large quantity of training data for most agricultural cases (high data collection cost and critical data collection conditions). SVM is widely used for plant phenotyping, such as plant growth prediction (Qiu et al. 2017), disease detection (Nagasubramanian et al. 2018), and canopy coverage estimation (Yu et al. 2017).

(10) Artificial Neural Network-Based Models

Artificial neural networks (ANNs) are inspired by the structure and working mechanism of the human brain. With hundreds of variants, ANNs are the most active branch in machine learning. A typical ANN has three layers of neurons: input layer, middle/hidden layer, and output layer. The numbers of neurons for input and output layers are fixed according to the numbers of input/output parameters. The number of neurons for the hidden layer can be selected freely. Each neuron in the hidden layer and output layer is connected to all neurons in the last layer by weighted connections, which will be calibrated during the training process. A sum operation is embedded in every neuron of hidden and output layers to fuse all the information from the last layer. For the hidden layer, each neuron also has an active function to handle the sum result. ANN is capable of modeling nonlinear and complex systems, and this feature makes it a good choice for plant phenotyping applications. An example for the application of ANN in plant phenotyping is recognizing different tobacco variants with hyperspectral plant leaf images (Seiffert et al. 2010). There are different topology structures for different ANNs, such as feedforward network, feedback network, self-organizing map neural network, and convolutional neural network. A convolutional neural network (CNN) is the most famous network for deep learning, which is the most popular machine-learning topic in recent years. An introduction especially about deep learning in plant phenotyping will be given in the following part.

7.4.3.2 Deep Learning

The most popular basic network for deep learning is CNN (LeCun et al. 1989). The first successful application of CNN was the recognition of handwritten numbers (LeCun et al. 1998). In this application, the pooling layer was introduced and the structure of modern CNN was established. The hidden layers of CNN are divided into three categories: convolutional layer, pooling layer, and fully connected layer. Convolutional layers and pooling layers are placed alternatively and appear in pairs. They play different roles in the feature extracting process: convolutional layers abstract the local features, while pooling layers help to get rid of the redundant features and endow the algorithm with translation invariance. With different convolutional-pooling layer pairs, CNN can abstract features of different dimensions. A fully connected layer is used to combine all the abstracted features and fulfill the learning purposes. In 2012, Hinton and his students greatly improved the image classification accuracy in the ImageNet challenge (Krizhevky et al. 2012) with a new proposed CNN variant, AlexNet. AlexNet is regarded as the milestone

for the new rapid development period of deep learning. A large number of deep learning (DL) algorithms were presented after that, including R-CNN, SPP-NET, Fast R-CNN, Faster R-CNN, SSD, and R-FCN. Now, deep learning algorithms become powerful tools in the field of image processing and natural language processing. With these advantages, deep learning is drawing more and more attention of plant phenotyping researchers. A number of successful deep learning algorithms for image processing are employed to extract plant phenotyping traits. Researchers from Iowa State University conducted a survey about the published papers of ML-based and DL-based plant phenotyping (Singh et al. 2018). It shows that the portion of DL-based plant phenotyping solutions in ML-based ones grows rapidly since 2017, from 1/10 in 2017 to 5/6 in 2018. The plant phenotyping applications of deep learning cover a variety of topics, such as plant recognition (Šulc and Matas 2017), leaf counting (Ubbens et al. 2018), plant stalk counting and width estimating (Baweja 2018), bloom detection (Xu et al. 2018), disease detection (Toda and Okura 2019), and stress identification (Ghosal et al. 2018).

7.5 Summary

More recently, special attention were focused on plant phenotyping, measuring morphologic and physiological parameters of various plants, and fewer attention were drawn to sensing soil and environment conditions. It is significant to monitor the ambient growth conditions of plants, such as soil nutrient, ambient temperature and humidity, and solar radiation.

Plant growth is susceptible to numerous factors, and plant phenotype is the specific characteristics that are deemed to the results from the interaction of its genetic properties and external environment conditions (Uchiyama et al. 2014). A plant acquires primary water and nutrition from soil resources and collects light, carbon dioxide, oxygen, and others to finish assimilation and catabolism. Phenotyping is a dynamic measurement process and changing along with plant growth. Simultaneously, soil and ambient environmental conditions also vary with time. Nitrogen, light, humidity, and other factors at different levels will contribute to variations in measurement results (Uchiyama et al. 2014; York and Lynch 2015). Therefore, it is necessary and essential to sense soil and environment over a long time, build a corresponding database for analyzing the relationship between phenotype and genotype of plants, further provide more information for breeders to assess species, and identify ideotypes.

References

Adu MO (2014) Variations in root system architecture and root growth dynamics of Brassica rapa genotypes using a new scanner-based phenotyping system. PhD thesis, The University of Nottingham

Adu MO, Chatot A, Wiesel L, Bennett MJ, Broadley MR, White PJ, Dupuy LX (2014) A scanner system for high-resolution quantification of variation in root growth dynamics of Brassica rapa genotypes. J Exp Bot 65(8):2039–2048

Adu MO, Wiesel L, Bennett MJ, Broadley MR, White PJ, Dupuy LX (2015) Scanner-based time-lapse root phenotyping. Bio-protocol 5(6):e1424

Agati G, Foschi L, Grossi N, Guglielminetti L, Ceovic ZG, Volterrani M (2013) Fluorescence-based versus reflectance proximal sensing of nitrogen content in Paspalum vaginatum and Zoysia matrella turfgrasses. Eur J Agron 45:39–51

Agati G, Foschi L, Grossi N, Volterrani M (2015) In field non-invasive sensing of the nitrogen status in hybrid bermudagrass (Cynodon dactylon × C. transvaalensis Burtt Davy) by a fluorescence-based method. Eur J Agron 63:89–96

Ahmad J, Muhammad K, Ahmad I, Ahmad W, Smith ML, Smith LN, Jain DK, Wang HX, Mehmood I (2018) Visual features based boosted classification of weeds for real-time selective herbicide sprayer systems. Comput Ind 98:23–33

Al-Turjman F (2019) The road towards plant phenotyping via WSNs: an overview. Comput Electron Agric 161:4–13

Andújar D, Fernández-Quintanilla C, Dorado J (2015) Matching the best viewing angle in depth cameras for biomass estimation based on poplar seedling geometry. Sensors 15(6):12999–13011

Andújar D, Dorado J, Fernández-Quintanilla C, Ribeiro A (2016) An approach to the use of depth cameras for weed volume estimation. Sensors 16(7):972–982

Aqeer-ur-Rehman, Abbasi AZ, Islam N, Shaikh ZA (2014) A review of wireless sensors and networks' applications in agriculture. Comput Stand Interfaces 36:263–270

Atkinson JA, Jackson RJ, Bentley AR, Ober E, Wells DM (2018) Field phenotyping for the future. Annu Plant Rev Online 3

Atkinson JA, Pound MP, Bennett MJ, Wells DM (2019) Uncovering the hidden half of plants using new advances in root phenotyping. Curr Opin Biotech 55:1–8

Azzari G, Goulden M, Rusu R (2013) Rapid characterization of vegetation structure with a Microsoft Kinect sensor. Sensors 13(2):2384–2398

Bai G, Ge Y, Hussain W, Baenziger PS, Graef G (2016) A multi-sensor system for high throughput field phenotyping in soybean and wheat breeding. Comput Electron Agric 128:181–192

Baker J III, Zhang NQ, Sharon J, Steeves R, Wang X, Wei Y, Poland J (2016) Development of a field-based high-throughput mobile phenotyping platform. Comput Electron Agric 122:74–85

Bandyopadhyay KK, Pradhan S, Sahoo RN, Singh R, Gupta VK, Joshi DK, Sutradhar AK (2014) Characterization of water stress and prediction of yield of wheat using spectral indices under varied water and nitrogen management practices. Agric Water Manag 146:115–123

Bao Y, Shah D, Tang L (2018) 3D perception-based collision-free robotic leaf probing for automated indoor plant phenotyping. Trans ASABE 61(3):859–872

Bao Y, Tang L, Breitzman MW, Fernandez MGS, Schnable PS (2019) Field-based robotic phenotyping of sorghum plant architecture using stereo vision. J Field Robot 36:397–415

Barker J, Zhang N, Sharon J, Steeves R, Wang X, Wei Y, Poland J (2016) Development of a field-based high-throughput mobile phenotyping platform. Comput Electron Agric 122:74–85

Baweja H (2018) StalkNet: a deep learning pipeline for high-throughput measurement of plant stalk count and stalk width. In: Field and service robotics, Springer proceedings in advanced robotics, vol 5. Springer, pp 271–284

Bazaza A, Farimana Z, Bannayanb M (2011) Modeling individual leaf area of basil (Ocimum basilicum) using different methods. Int J Plant Prod 5(4):439–447

Behmann J, Mahlein AK, Paulus S, Dupuis J, Kuhlmann H, Oerke EC, Plümer L (2016) Generation and application of hyperspectral 3d plant models: methods and challenges. Mach Vis Appl 27(5):611–624

Bellvert J, Zarco-Tejada PJ, Girona J, Fereres E (2014) Mapping crop water stress index in a 'pinot-noir' vineyard: comparing ground measurements with thermal remote sensing imagery from an unmanned aerial vehicle. Precis Agric 15(4):361–376

Bellvert J, Marsal J, Girona J, Zarco-Tejada PJ (2015) Seasonal evolution of crop water stress index in grapevine varieties determined with high-resolution remote sensing thermal imagery. Irrig Sci 33(2):81–93

Bendig J, Bolten A, Bareth G (2013) UAV-based imaging for multi-temporal; very high resolution crop surface models to monitor crop growth variability. Photogramm Fernerkund Geoinf 6:551–562

Bendig J, Bolten A, Bennertz S, Broscheit J, Eichfuss S, Bareth G (2014) Estimating biomass of barley using crop surface models (CSMs) derived from UAV-based RGB imaging. Remote Sens 6(11):10395–10412

Bendig J, Yu K, Aasen H, Bolten A, Bennertz S, Broscheit J, Gnyp ML, Bareth G (2015) Combining UAV-based plant height from crop surface models; visible; and near infrared vegetation indices for biomass monitoring in barley. Int J Appl Earth Obs Geoinform 39:79–87

Betegón-Putze I, González A, Sevillano X, Blasco-Escámez D, Caño-Delgado AI (2019) MyROOT, a method and software for the semiautomatic measurement of primary root length in Arabidopsis seedlings. Plant J 98:1145–1156

Bodner G, Nakhforoosh A, Arnold T, Leitner D (2018) Hyperspectral imaging: a novel approach for plant root phenotyping. Plant Methods 14:84

Bourgeon MA, Paoli JN, Jones G, Villette S, Gée C (2016) Field radiometric calibration of a multispectral on-the-go sensor dedicated to the characterization of vineyard foliage. Comput Electron Agric 123:184–194

Bucksch A, Burridge J, York LM, Das A, Nord E, Weitz JS, Lynch JP (2014) Image-based high-throughput field phenotyping of crop roots. Plant Physiol 166:470–486

Buitrago MF, Groen TA, Hecker CA, Skidmore AK (2016) Changes in thermal infrared spectra of plants caused by temperature and water stress. ISPRS J Photogramm Remote Sens 111:22–31

Cendrero-Mateo MP, Moran MS, Papuga SA, Thorp KR, Alonso L, Moreno J, Ponce-Campos G, Rascher U, Wang G (2015) Plant chlorophyll fluorescence: active and passive measurements at canopy and leaf scales with different nitrogen treatments. J Exp Bot 67(1):275–286

Cerovic ZG, Goulas Y, Gorbunov M, Briantais JM, Camenen L, Moya I (1996) Fluorosensing of water stress in plants: diurnal changes of the mean lifetime and yield of chlorophyll fluorescence, measured simultaneously and at distance with a τ-LIDAR and a modified PAM-fluorimeter, in maize, sugar beet, and kalanchoë. Remote Sens Environ 58(3):311–321

Chapman SC, Merz T, Chan A, Jackway P, Hrabar S, Dreccer MF, Holland E, Zheng BY, Ling TJ, Jimenez-Berni J (2014) Pheno-copter: a low-altitude, autonomous, remote-sensing robotic helicopter for high-throughput field-based phenotyping. Agronomy 4(2):279–301

Chatzinikos A, Gemtos T, Fountas S (2013) The use of a laser scanner for measuring crop properties in three different crops in Central Greece. In: Precision agriculture '13: proceedings of the 9th European conference on Precision agriculture, Lleida, Catalonia, Spain. Wageningen Academic Publishers, Wageningen, pp 129–136

Chen B, He C, Ma Y, Bai Y (2011) 3D image monitoring and modeling for corn plants growth in field condition. Trans CSAE 27(S1):366–372. (in Chinese)

Chéné Y, Rousseau D, Lucidarme P, Bertheloot J, Caffier V, Morel P, Belin É, Chapeau-Blondeau F (2012) On the use of depth camera for 3D phenotyping of entire plants. Comput Electron Agric 82:122–127

Choudhury SD, Bashyam S, Qiu YM, Samal A, Awada T (2018) Holistic and component plant phenotyping using temporal image sequence. Plant Methods 14:35

Clark RT, MacCurdy RB, Jung JK, Shaff JE, McCouch SR, Aneshansley DJ, Kochian LV (2011) Three-dimensional root phenotyping with a novel imaging and software platform. Plant Physiol 156:455–465

Clark RT, Famoso AN, Zhao K, Shaff JE, Craft EJ, Bustamante CD, McCouch SR, Aneshansley DJ, Kochian LV (2013) High-throughput two-dimensional root system phenotyping platform facilitates genetic analysis of root growth and development. Plant Cell Environ 36:454–466

Cobb JN, DeClerck G, Greenberg A, Clark R, McCouch S (2013) Next-generation phenotyping: requirements and strategies for enhancing our understanding of genotype–phenotype relationships and its relevance to crop improvement. Theor Appl Genet 126(4):867–887

Cohen Y, Alchanatis V, Sela E, Saranga Y, Cohen S, Meron M, Bosak A, Tsipris J, Ostrovsky V, Orolov V, Levi A, Brikman R (2015) Crop water status estimation using thermography: multi-year model development using ground-based thermal images. Precis Agric 16(3):311–329

Corona-Lopez DDJ, Sommer S, Rolfe SA, Podd F, Grieve BD (2019) Electrical impedance tomography as a tool for phenotyping plant roots. Plant Methods 15:49

Cousins D (2015) Bosch Bonirob robot set to make field work easier for farmers. Farmers Weekly 1052:7

Crain JL, Wei Y, Barker J III, Thompson SM, Alderman PD, Reynolds M, Zhang NQ, Poland J (2016) Development and deployment of a portable field phenotyping platform. Crop Sci 56(3):965–975

Dammer K, Dworak V, Selbeck J (2016) On-the-go phenotyping in field potatoes using camera vision. Potato Res 59(2):113–127

Daughtry CST, Walthall CL, Kim MS, Colstoun EBD, McMurtrey JE (2000) Estimating corn leaf chlorophyll concentration from leaf and canopy reflectance. Remote Sens Environ 74(2):229–239

Dey A (2016) Machine learning algorithms: a review. Int J Comput Sci Inf Technol 7(3):1174–1179

Dias KODG, Gezan SA, Guimarães CT, Nazarian A, da Costa e Silva L, Parentoni SN, de Oliveira Guimarães PE, de Oliveira Anoni C, Pádua JMV, de Oliveira Pinto M, Noda RW, Ribeiro CAG, de Magalhães JV, Garcia AAF, de Souza JC, Guimarães LJM, Pastina MM (2018) Improving accuracies of genomic predictions for drought tolerance in maize by joint modeling of additive and dominance effects in multi-environment trials. Heredity (Edinb) 121(1):24–37

Du L, Gong W, Shi S, Yang J, Sun J, Zhu B, Song S (2016a) Estimation of rice leaf nitrogen contents based on hyperspectral LIDAR. Int J Appl Earth Obs Geoinform 44:136–143

Du L, Shi S, Yang J, Sun J, Gong W (2016b) Using different regression methods to estimate leaf nitrogen content in rice by fusing hyperspectral Lidar data and laser-induced chlorophyll fluorescence data. Remote Sens 8(6):526–539

Dusschoten DV, Metzner R, Kochs J, Postma JA, Pflugfelder D, Bühler J, Schurr U, Jahnke S (2016) Quantitative 3D analysis of plant roots growing in soil using magnetic resonance imaging. Plant Physiol 170(3):1176–1188

Dworak V, Selbeck J, Ehlert D (2011) Ranging sensors for vehicle-based measurement of crop stand and orchard parameters: a review. Trans ASABE 54(4):1497–1510

Ehlert D, Heisig M (2013) Sources of angle-dependent errors in terrestrial laser scanner-based crop stand measurement. Comput Electron Agric 93:10–16

Ehlert D, Horn HJ, Adamek R (2008) Measuring crop biomass density by laser triangulation. Comput Electron Agric 61:117–125

Ehlert D, Adamek R, Horn HJ (2009) Laser rangefinder-based measuring of crop biomass under field conditions. Precis Agric 10(5):395–408

Ehlert D, Heisig M, Adamek R (2010) Suitability of a laser rangefinder to characterize winter wheat. Precis Agric 11(6):650–663

Eitel JUH, Vierling LA, Long DS (2010) Simultaneous measurements of plant structure and chlorophyll content in broadleaf saplings with a terrestrial laser scanner. Remote Sens Environ 114(10):2229–2237

Eitel JUH, Vierling LA, Long DS, Hunt ER (2011) Early season remote sensing of wheat nitrogen status using a green scanning laser. Agric For Meteorol 151(10):1338–1345

Eitel JUH, Magney TS, Vierling LA, Brown TT, Huggins DR (2014a) Lidar based biomass and crop nitrogen estimates for rapid; non-destructive assessment of wheat nitrogen status. Field Crop Res 159:21–32

Eitel JUH, Magney TS, Vierling LA, Dittmar G (2014b) Assessment of crop foliar nitrogen using a novel dual-wavelength laser system and implications for conducting laser-based plant physiology. ISPRS J Photogramm Remote Sens 97:229–240

Elarab M, Ticlavilca AM, Torres-Rua AF, Maslova I, McKee M (2015) Estimating chlorophyll with thermal and broadband multispectral high resolution imagery from an unmanned aerial system using relevance vector machines for precision agriculture. Int J Appl Earth Obs Geoinform 43:32–42

Elmasry G, Mandour N, Wagner MH, Demilly D, Verdier J, Belin E, Rousseau D (2019) Utilization of computer vision and multispectral imaging techniques for classification of cowpea (Vigna unguiculata) seeds. Plant Methods 15:24

Elsayed S, Rischbeck P, Schmidhalter U (2015) Comparing the performance of active and passive reflectance sensors to assess the normalized relative canopy temperature and grain yield of drought-stressed barley cultivars. Field Crop Res 177:148–160

Erdle K, Mistele B, Schmidhalter U (2011) Comparison of active and passive spectral sensors in discriminating biomass parameters and nitrogen status in wheat cultivars. Field Crop Res 124(1):74–84

Fernandez-Gallego JA, Kefauver SC, Gutiérrez NA, Nieto-Taladriz MT, Araus JL (2018) Wheat ear counting in-field conditions: high throughput and low-cost approach using RGB images. Plant Methods 14:22

Finkelshtain R, Bechar A, Yovel Y, Kósa G (2016) Investigation and analysis of an ultrasonic sensor for specific yield assessment and greenhouse features identification. Precis Agric 17:1–16

Freeman KW, Girma K, Arnall DB, Mullen RW, Martin KL, Teal RK, Raun WR (2007) By-plant prediction of corn forage biomass and nitrogen uptake at various growth stages using remote sensing and plant height. Agron J 99(2):530–536

Fricke T, Wachendorf M (2013) Combining ultrasonic sward height and spectral signatures to assess the biomass of legume-grass swards. Comput Electron Agric 99:236–247

Fricke T, Richter F, Wachendorf M (2011) Assessment of forage mass from grassland swards by height measurement using an ultrasonic sensor. Comput Electron Agric 79:142–152

Friedli M, Kirchgessner N, Grieder C, Liebisch F, Mannale M, Walter A (2016) Terrestrial 3D laser scanning to track the increase in canopy height of both monocot and dicot crop species under field conditions. Plant Methods 12:9

Gago J, Douthe C, Coopman RE, Gallego PP, Ribas-Carbo M, Flexas J, Escalona J, Medrano H (2015) UAVs challenge to assess water stress for sustainable agriculture. Agric Water Manag 153:9–19

Gai J, Tang L, Steward B (2015) Plant recognition through the fusion of 2D and 3D images for robotic weeding. In: Proceedings of the 2015 ASABE annual international meeting, New Orleans, LA, USA, 26–29 July, Paper No. 152181371

Gao S, Niu Z, Huang N, Hou X (2013) Estimating the leaf area index; height and biomass of maize using HJ-1 and RADARSAT-2. Int J Appl Earth Obs Geoinform 24:1–8

Gao S, Niu Z, Sun G, Zhao D, Jia K, Qin Y (2015) Height extraction of maize using airborne full-waveform LIDAR data and a deconvolution algorithm. IEEE Geosci Remote Sens Lett 12(9):1–5

Garrido M, Paraforos DS, Reiser D, Arellano MV, Griepentrog HW, Valero C (2015) 3D maize plant reconstruction based on georeferenced overlapping LiDAR point clouds. Remote Sens 7(12):17077–17096

Gebbers R, Ehlert D, Adamek R (2011) Rapid mapping of the leaf area index in agricultural crops. Agron J 103(5):1532

Ghosal S, Blystone D, Singh AK, Ganapathysubramanian B, Singh A, Sarkar S (2018) An explainable deep machine vision framework for plant stress phenotyping. Proc Natl Acad Sci U S A 115(18):4613–4618

Gnyp ML, Bareth G, Li F, Lenz-Wiedemann VIS, Koppe W, Miao Y, Hennig SD, Jia L, Laudien R, Chen X, Zhang F (2014a) Development and implementation of a multiscale biomass model using hyperspectral vegetation indices for winter wheat in the North China Plain. Int J Appl Earth Obs Geoinform 33(12):232–242

Gnyp ML, Miao Y, Yuan F, Ustin SL, Yu K, Yao Y, Huang S, Bareth D (2014b) Hyperspectral canopy sensing of paddy rice aboveground biomass at different growth stages. Field Crop Res 155:42–55

Gonzalez-Dugo V, Hernandez P, Solis I, Zarco-Tejada PJ (2015) Using high-resolution hyperspectral and thermal airborne imagery to assess physiological condition in the context of wheat phenotyping. Remote Sens 7:13586–13605

Grant OM, Ochagavía H, Baluja J, Diago MP, Tardáguila J (2016) Thermal imaging to detect spatial and temporal variation in the water status of grapevine (*Vitis vinifera* L.). J Hortic Sci Biotechnol 91(1):43–54

Grenzdörffer GJ (2014) Crop height determination with UAS point clouds. Int Arch Photogramm Remote Sens Spat Inf Sci XL-1:135–140

Großkinsky DK, Svensgaard J, Christensen S, Roitsch T (2015) Plant phenomics and the need for physiological phenotyping across scales to narrow the genotype-to-phenotype knowledge gap. J Exp Bot 66(18):5429–5440

Guo Q, Wu F, Pang S, Zhao X, Chen L, Liu J, Xue B, Xu G, Li L, Jing H, Chu C (2016) Crop 3D: a platform based on LiDAR for 3D high-throughput crop phenotyping. Scientia Sinica Vitae 46(10):1210–1221

Guo W, Zheng BY, Duan T, Fukatsu T, Chapman S, Ninomiya S (2017) EasyPCC: benchmark datasets and tools for high-throughput measurement of the plant canopy coverage ratio under field conditions. Sensors 17:798

Habib A, Han Y, Xiong WF, He FN, Zhang Z, Crawford M (2016) Automated ortho-rectification of UAV-based hyperspectral data over an agricultural field using frame RGB imagery. Remote Sens 8(10):796

Han T, Yan FK (2018) Developing a system for three-dimensional quantification of root traits of rice seedlings. Comput Electron Agric 152:90–100

Han XZ, Thomasson JA, Bagnall GC, Pugh NA, Horne DW, Rooney WL, Jung J, Chang AJ, Malambo L, Popescu SC, Gates IT, Cope DA (2018) Measurement and calibration of plant-height from fixed-wing UAV images. Sensors 18(12):4092

Hasegawa K, Matsuyama H, Tsuzuki H, Sweda T (2010) Improving the estimation of leaf area index by using remotely sensed NDVI with BRDF signatures. Remote Sens Environ 114(3):514–519

He L, Zhang HY, Zhang YS, Song X, Feng W, Kang GZ, Wang CY, Guo TC (2016) Estimating canopy leaf nitrogen concentration in winter wheat based on multi-angular hyperspectral remote sensing. Eur J Agron 73:170–185

Hoffmeister D, Waldhoff G, Korres W, Curdt C, Bareth G (2015) Crop height variability detection in a single field by multi-temporal terrestrial laser scanning. Precis Agric 17(3):296–312

Hosoi F, Nakabayashi K, Omasa K (2011) 3-D modelling of tomato canopies using a high-resolution portable scanning Lidar for extracting structural information. Sensors 11(12):2166–2174

Houborg R, McCabe MF, Angel Y, Middleton EM (2016) Detection of chlorophyll and leaf area index dynamics from sub-weekly hyperspectral imagery. In: Proceedings of SPIE remote sensing for agriculture, ecosystems, and hydrology XVIII, p 999812

Huete A, Jackson R (1988) Soil and atmosphere influences on the spectra of partial canopies. Remote Sens Environ 25(1):89–105

Inoue Y, Guérif M, Baret F, Skidmore A, Gitelson A, Schlerf M, Darvishzadeh R, Olioso A (2016) Simple and robust methods for remote sensing of canopy chlorophyll content: a comparative analysis of hyperspectral data for different types of vegetation. Plant Cell Environ 39(12):2609–2623

Jawad HM, Nordin R, Gharghan SK, Jawad AM, Ismail M (2017) Energy-efficient wireless sensor networks for precision agriculture: a review. Sensors 17:1781

Jay S, Rabatel G, Hadoux X, Moura D, Gorretta N (2015) In-field crop row phenotyping from 3D modeling performed using structure from motion. Comput Electron Agric 110:70–77

Jia Z, Liu Y, Gruber BD, Neumann K, Kilian B, Graner A, von Wirén N (2019) Genetic dissection of root system architectural traits in spring barley. Front Plant Sci 10:400

Jiang Y, Li C, Paterson AH (2016) High throughput phenotyping of cotton plant height using depth images under field conditions. Comput Electron Agric 130:57–68

Jiang N, Floro E, Bray AL, Laws B, Duncan KE, Topp CN (2018) High-resolution 4D spatiotemporal analysis of maize roots. BoioRxiv

Jones HG, Hutchinson PA, May T, Jamali H, Deery DM (2018) A practical method using a network of fixed infrared sensors for estimating crop canopy conductance and evaporation rate. Biosyst Eng 165:59–69

Kalacska M, Lalonde M, Moore TR (2015) Estimation of foliar chlorophyll and nitrogen content in an ombrotrophic bog from hyperspectral data: scaling from leaf to image. Remote Sens Environ 169(4):270–279

Kalogiros DI, Adu MO, White PJ, Broadley MR, Draye X, Ptashnyk M, Bengough AG, Dupuy LX (2016) Analysis of root growth from a phenotyping data set using a density-based model. J Exp Bot 67(4):1045–1058

Karthikeyan L, Chawla I, Mishra AK (2020) A review of remote sensing applications for food security: crop growth and yield, irrigation, and crop losses. J Hydrol 586:124905

Kazmi W, Foix S, Alenyà G, Andersen HJR (2014) Indoor and outdoor depth imaging of leaves with time-of-flight and stereo vision sensors: analysis and comparison. ISPRS J Photogramm Remote Sens 88:128–146

Kefauver SC, Vicente R, Vergara-Diaz O, Fernandez-Gallego JA, Kerfal S, Lopez A, Melichar JPE, Serret Molins MD, Araus JL (2017) Comparative UAV and field phenotyping to assess yield and nitrogen use efficiency in hybrid and conventional Barley. Front Plant Sci 8:1733

Kempthorne DM, Turner IW, Belward JA, Mccue SW, Barry M, Young J (2014) Surface reconstruction of wheat leaf morphology from three-dimensional scanned data. Funct Plant Biol 42(5):444

Kenobi K, Atkinson JA, Wells DM, Gaju O, De Silva JG, Foulkes MJ, Dryden IL, Wood ATA, Bennett MJ (2017) Linear discriminant analysis reveals differences in root architecture in wheat seedlings related to nitrogen uptake efficiency. J Exp Bot 68(17):4969–4981

Kim M, Kim S, Kim Y, Choi Y, Seo M (2015) Infrared estimation of canopy temperature as crop water stress indicator. Korean J Soil Sci Fertil 48(5):499–504

Kipp S, Mistele B, Baresel P, Schmidhalter U (2014a) High-throughput phenotyping early plant vigour of winter wheat. Eur J Agron 52:271

Kipp S, Mistele B, Schmidhalter U (2014b) The performance of active spectral reflectance sensors as influenced by measuring distance; device temperature and light intensity. Comput Electron Agric 100:24–33

Klose R, Scholz C, Ruckelshausen A (2012) 3D time-of-flight camera-based sensor system for automatic crop height monitoring for plant phenotyping. In: Proceedings of the CIGR-AgEng 2012 international conference of agricultural engineering, Valencia, Spain, 8–12 July, pp 55–60

Koch A, Meunier F, Vanderborght J, Garré S, Pohlmeier A, Javaux M (2019) Functional–structural root-system model validation using a soil MRI experiment. J Exp Bot 70(10):2797–2809

Krizhevky A, Sutskever I, Hinton GE (2012) ImageNet classification with deep convolutional neural networks. In: Proceedings of the annual conference on neural information processing systems, Cambridge, USA, pp 1097–1105

Kumar P, Huang C, Cai J, Miklavcic SJ (2014) Root phenotyping by root tip detection and classification through statistical learning. Plant Soil 380:193–209

Kwon T, Kim K, Yoon H, Lee S, Kim B, Siddiqu ZS (2015) Phenotyping of plants for drought and salt tolerance using infra-red thermography. Plant Breed Biotech 3(4):299–307

Lamb DW, Steyn-Ross M, Schaare P, Hanna MM, Silvester W, Steyn-Ross A (2002) Estimating leaf nitrogen concentration in ryegrass (Lolium spp.) pasture using the chlorophyll red-edge: theoretical modelling and experimental observations. Int J Remote Sens 23(18):3619–3648

Larese MG, Granitto PM (2015) Finding local leaf vein patterns for legume characterization and classification. Mach Vis Appl 27(5):709–720

Leblanc G, Kalacska M, Soffer R (2014) Detection of single graves by airborne hyperspectral imaging. Forensic Sci Int 245:17–23

LeCun Y, Boser B, Denker JS, Henderson D, Howard RE, Hubbard W, Jackel LD (1989) Backpropagation applied to handwritten zip code recognition. Neural Comput 1:541–551

LeCun Y, Bottou L, Bengio Y, Haffner P (1998) Gradient-based learning applied to document recognition. Proc IEEE 86(11):2278–2324

Lee N (2016) High-throughput phenotyping of above and below ground elements of plants using feature detection, extraction and image analysis techniques. PhD thesis, Iowa State University
Lee WS, Alchanatis V, Yang C, Hirafuji M, Moshou D, Li C (2010) Sensing technologies for precision specialty crop production. Comput Electron Agric 74:2–33
Leemans V, Dumont B, Destain M, Vancutsem F, Bodson B (2012) A method for plant leaf area measurement by using stereo vision. In: Proceedings of the CIGR-AgEng 2012 international conference of agricultural engineering, Valencia, Spain, 8–12 July
Li F, Miao Y, Feng G, Yuan F, Yue S, Gao X, Liu Y, Liu B, Ustin SL, Chen X (2014a) Improving estimation of summer maize nitrogen status with red edge-based spectral vegetation indices. Field Crop Res 157:111–123
Li L, Zhang Q, Huang D (2014b) A review of imaging techniques for plant phenotyping. Sensors 14(11):20078–20111
Li W, Niu Z, Huang N, Wang C, Gao S, Wu C (2015a) Airborne Lidar technique for estimating biomass components of maize: a case study in Zhangye City, Northwest China. Ecol Indic 57(2):486–496
Li W, Niu Z, Wang C, Huang W, Chen H, Gao S, Li D, Muhammad S (2015b) Combined use of airborne Lidar and satellite GF-1 data to estimate leaf area index; height; and aboveground biomass of maize during peak growing season. IEEE J Sel Top Appl Earth Obs Remote Sens 8(9):4489–4501
Li D, Cao Y, Shi G, Cai X, Chen Y, Wang S, Yan S (2019) An overlapping-free leaf segmentation method for plant point clouds. IEEE Access 7:129054–129070
Liakos KG, Busato P, Moshou D, Pearson S, Bochtis D (2018) Machine learning in agriculture: a review. Sensors 18:2674
Liebisch F, Kirchgessner N, Schneider D, Walter A, Hund A (2015) Remote, aerial phenotyping of maize traits with a mobile multi-sensor approach. Plant Methods 11:9
Lin Y (2015) Lidar: an important tool for next-generation phenotyping technology of high potential for plant phenomics. Comput Electron Agric 119:61–73
Liu J, Pattey E (2010) Retrieval of leaf area index from top-of-canopy digital photography over agricultural crops. Agric For Meteorol 150(11):1485–1490
Lobell DB, Thau D, Seifert C, Engle E, Little B (2015) A scalable satellite-based crop yield mapper. Remote Sens Environ 164:324–333
Longchamps L, Khosla R (2014) Early detection of nitrogen variability in maize using fluorescence. Agron J 106(2):511
Lu H, Tang L, Whitham SA, Mei Y (2017) A robotic platform for corn seedling morphological traits characterization. Sensors (Basel) 17(9):2082
Mack J, Lenz C, Teutrine J, Steinhage V (2017) High-precision 3D detection and reconstruction of grapes from laser range data for efficient phenotyping based on supervised learning. Comput Electron Agric 135:300–311
Maenhout P, Sleutel S, Xu H, Hoorebeke LV, Cnudde V, Neve SD (2019) Semi-automated segmentation and visualization of complex undisturbed root systems with X-ray μCT. Soil Till Res 192:59–65
Magney TS, Eitel JUH, Huggins DR, Vierling LA (2016) Proximal NDVI derived phenology improves in-season predictions of wheat quantity and quality. Agric For Meteorol 217:46–60
Mahlein AK, Oerke EC, Steiner U, Dehne HW (2012) Recent advances in sensing plant diseases for precision crop protection. Eur J Plant Path 133(1):197–209
Mairhofer S, Zappala S, Tracy S, Sturrock C, Bennett MJ, Mooney SJ, Pridmore TP (2013) Recovering complete plant root system architectures from soil via X-ray μ-computed tomography. Plant Methods 9:8
Mangus DL, Sharda A, Zhang N (2016) Development and evaluation of thermal infrared imaging system for high spatial and temporal resolution crop water stress monitoring of corn within a greenhouse. Comput Electron Agric 121:149–159
Marshall M, Thenkabail P (2015) Developing in situ non-destructive estimates of crop biomass to address issues of scale in remote sensing. Remote Sens 7(1):808–835

Martínez-Fernández J, Gonázlez-Zamora A, Sánchez N, Gumuzzio A, Herrero-Jiménez CM (2016) Satellite soil moisture for agricultural drought monitoring: assessment of the SMOS derived soil water deficit index. Remote Sens Environ 177:277–286

Mistele B, Schmidhalter U (2008) Spectral measurements of the total aerial N and biomass dry weight in maize using a quadrilateral-view optic. Field Crop Res 106(1):94–103

Mistele B, Schmidhalter U (2010) Tractor-based quadrilateral spectral reflectance measurements to detect biomass and total aerial nitrogen in winter wheat. Agron J 102(2):499

Montes JM, Technow F, Dhillon BS, Mauch F, Melchinger AE (2011) High-throughput non-destructive biomass determination during early plant development in maize under field conditions. Field Crop Res 121:268–273

Mooney SJ, Pridmore TP, Helliwell J, Bennett MJ (2012) Developing X-ray computed tomography to non-invasively image 3-D root systems architecture in soil. Plant Soil 352(1):1–22

Moshou D, Pantazi X, Kateris D, Gravalos I (2014) Water stress detection based on optical multisensor fusion with a least squares support vector machine classifier. Biosyst Eng 117:15–22

Mueller-Sim T, Jenkins M, Abel J, Kantor G (2017) The Robotanist: a ground-based agricultural robot for high-throughput crop phenotyping. In: 2017 IEEE international conference on robotics and automation (ICRA), Singapore, May 29–June 3, pp 3634–3639

Mulla DJ (2013) Twenty five years of remote sensing in precision agriculture: key advances and remaining knowledge gaps. Biosyst Eng 114:358–371

Nagasubramanian K, Jones S, Sarkar S, Singh AK, Singh A, Ganapathysubramanian B (2018) Hyperspectral band selection using genetic algorithm and support vector machines for early identification of charcoal rot disease in soybean stems. Plant Methods 14:86

Naito H, Ogawa S, Valencia MO, Mohri H, Urano Y, Hosoi F, Shimizu Y, Chavez AL, Ishitani M, Selvaraj MG, Omasa K (2017) Estimating rice yield related traits and quantitative trait loci analysis under different nitrogen treatments using a simple tower-based field phenotyping system with modified single-lens reflex cameras. ISPRS J Photogramm Remote Sens 125:50–62

Nakini TKD, DeSouza GN (2014) Distortion correction in 3D-modeling of roots for plant phenotyping. In: European conference on computer vision (ECCV) workshop on computer vision for plant phenotyping, Sept. Zurich, Switzerland

Neinavaz E, Darvishzadeh R, Skidmore AK, Groen TA (2016a) Measuring the response of canopy emissivity spectra to leaf area index variation using thermal hyperspectral data. Int J Appl Earth Obs Geoinform 53:40–47

Neinavaz E, Skidmore AK, Darvishzadeh R, Groen TA (2016b) Retrieval of leaf area index in different plant species using thermal hyperspectral data. ISPRS J Photogramm Remote Sens 119:390–401

Nevalainen O, Hakala T, Suomalainen J, Mäkipää R, Peltoniemi M, Krooks A, Kaasalainen S (2014) Fast and nondestructive method for leaf level chlorophyll estimation using hyperspectral Lidar. Agric For Meteorol 198-199:250–258

Nguyen TT, Slaughter DC, Max N, Maloof JN, Sinha N (2015) Structured light-based 3d reconstruction system for plants. Sensors 15(8):18587–18612

Ni Z, Liu Z, Huo H, Li ZL, Nerry F, Wang Q, Li X (2015) Early water stress detection using leaf-level measurements of chlorophyll fluorescence and temperature data. Remote Sens 7(3):3232–3249

Odilbekov F, Armonien R, Henriksson T, Chawade (2018) Proximal phenotyping and machine learning methods to identify Septoria tritici blotch disease symptoms in wheat. Front Plant Sci 9:685

Ojha T, Misra S, Raghuwanshi NS (2015) Wireless sensor networks for agriculture: the state-of-art in practice and future challenges. Comput Electron Agric 118:66–84

Oner F, Odabas MS, Sezer I, Odabas F (2011) Leaf area prediction for corn (Zea mays L.) cultivars with multiregression analysis. Photosynthetica 49(4):637–640

Otsu N (1979) A threshold selection method from gray-level histograms. IEEE Trans Syst Man Cybern 9(1):62–66

Ounis A, Bach J, Mahjoub A, Daumard F, Moya L, Goulas Y (2016) Combined use of LIDAR and hyperspectral measurements for remote sensing of fluorescence and vertical profile of canopies. Span Assoc Remote Sens 45:87–94

Padilla FM, Teresa P-FM, Gallardo M, Thompson RB (2014) Evaluation of optical sensor measurements of canopy reflectance and of leaf flavonols and chlorophyll contents to assess crop nitrogen status of muskmelon. Eur J Agron 58:39–52

Pape J, Klukas C (2015) Utilizing machine learning approaches to improve the prediction of leaf counts and individual leaf segmentation of rosette plant images. In: Proceedings of the computer vision problems in plant phenotyping workshop. BMVA Press, pp 3.1–3.12

Paulus S, Behmann J, Mahlein A, Plümer L, Kuhlmann H (2014a) Low-cost 3D systems: suitable tools for plant phenotyping. Sensors 14(2):3001–3018

Paulus S, Dupuis J, Riedel S, Kuhlmann H (2014b) Automated analysis of barley organs using 3D laser scanning: an approach for high throughput phenotyping. Sensors 14:12670–12686

Pfeifer J, Kirchgessner N, Colombi T, Walter A (2015) Rapid phenotyping of crop root systems in undisturbed field soils using X-ray computed tomography. Plant Methods 11:41

Pflugfelder D, Metzner R, Dusschoten DV, Reichel R, Jahnke S, Koller R (2017) Non-invasive imaging of plant roots in different soils using magnetic resonance imaging (MRI). Plant Methods 13:102

Pineros MA, Larson BG, Shaff JE, Schneider DJ, Falcão AX, Yuan L, Claik RT, Craft EJ, Davis TW, Pradier P, Shaw NM, Assaranurak I, Couch SR, Sturrock C, Bennett M, Kochian LV (2016) Evolving technologies for growing, imaging and analyzing 3D root system architecture of crop plants. J Integr Plant Biol 58(3):230–241

Pittman J, Arnall D, Interrante S, Moffet C, Butler T (2015) Estimation of biomass and canopy height in bermudagrass; alfalfa; and wheat using ultrasonic; laser; and spectral sensors. Sensors 15(2):2920–2943

Prashar A, Jones HG (2014) Infra-red thermography as a high-throughput tool for field phenotyping. Agronomy 4(3):397–417

Prashar A, Jones HG (2016) Assessing drought responses using thermal infrared imaging. Methods Mol Biol 1398:209–219

Prince S, Das NTK, Murphy M, Valliyodan B, DeSouza GN, Nguyen HT (2018) Prediction of soybean root response in the field using nondestructive seedling three-dimensional root features. Plant Phenome J 1:180003

Qiu Q, Zheng C, Wang W, Qiao X, Bai H, Yu J, Shi K (2017) A new strategy in observer modeling for greenhouse cucumber seedling growth. Front Plant Sci 8:1297

Qiu Q, Sun N, Bai H, Wang N, Fan ZQ, Wang YJ, Meng ZJ, Li B, Cong Y (2019) Field-based high-throughput phenotyping for maize plant using 3D LiDAR point cloud generated with a "phenomobile". Front Plant Sci 10:554

Raper TB, Varco JJ (2015) Canopy-scale wavelength and vegetative index sensitivities to cotton growth parameters and nitrogen status. Precis Agric 16(1):62–76

Raper TB, Varco JJ, Hubbard KJ (2013) Canopy-based normalized difference vegetation index sensors for monitoring cotton nitrogen status. Agron J 105(5):1345

Reynolds D, Ball J, Bauer A, Davey R, Griffiths S, Zhou J (2019) CropSight: a scalable and open-source information management system for distributed plant phenotyping and IoT-based crop management. GigaScience 8:1–11

Ribera J, He F, Chen Y, Habib AF, Delp EJ (2016) Estimating phenotypic traits from UAV based RGB imagery. In: Proceedings of the 22nd ACM SIGKDD conference on knowledge discovery and data mining, San Francisco, CA, USA, 13–17 August

Richard C, Hickey LT, Fletcher S, Jennings R, Chenu K, Christopher JT (2015) High-throughput phenotyping of seminal root traits in wheat. Plant Methods 11(1):13

Rischbeck P, Elsayed S, Mistele B, Barmeier G, Heil K, Schmidhalter U (2016) Data fusion of spectral; thermal and canopy height parameters for improved yield prediction of drought stressed spring barley. Eur J Agron 78:44–59

Rogers ED, Monaenkova D, Mijar M, Nori A, Goldman DI, Benfey PN (2016) X-ray computed tomography reveals the response of root system architecture to soil texture. Plant Physiol 171:2028–2040

Rossini M, Fava F, Cogliati S, Meroni M, Marchesi A, Panigada C, Giardinoe C, Busettoa L, Migliavaccaaf M, Amaduccig S, Colomboa R (2013) Assessing canopy PRI from airborne imagery to map water stress in maize. ISPRS J Photogramm Remote Sens 86(3):168–177

Rouphael Y, Spíchal L, Panzarová K, Casa R, Colla G (2018) High-throughput plant phenotyping for developing novel biostimulants: from lab to field or from field to lab? Front Plant Sci 9:1197

Rustioni L, Basilico R, Fiori S, Leoni A, Maghradze D, Failla O (2013) Grape colour phenotyping: development of a method based on the reflectance spectrum. Phytochem Anal 24(5):453–459

Saeys W, Lenaerts B, Craessaerts G, Baerdemaeker JD (2009) Estimation of the crop density of small grains using Lidar sensors. Biosyst Eng 102:22–30

Samborski SM, Gozdowski D, Walsh OS, Lamb DW, Stępień M, Gacek ES, Drzazga T (2015) Winter wheat genotype effect on canopy reflectance: implications for using NDVI for in-season nitrogen topdressing recommendations. Agron J 107(6):2097

Sankaran S, Khot LR, Espinoza CZ, Jarolmasjed S, Sathuvalli VR, Vandemark GJ, Miklas PN, Carter AH, Pumphrey MO, Knowles NR, Pavek MJ (2015) Low-altitude, high-resolution aerial imaging systems for row and field crop phenotyping: a review. Eur J Agron 70:112–123

Santos TT, Rodrigues GC (2016) Flexible three-dimensional modeling of plants using low- resolution cameras and visual odometry. Mach Vis Appl 27(5):695–707

Schirrmann M, Hamdorf A, Garz A, Ustyuzhanin A, Dammer K (2016) Estimating wheat biomass by combining image clustering with crop height. Comput Electron Agric 121:374–384

Schlüter S, Blaser SRGA, Weber M, Schmidt V, Vetterlein D (2018) Quantification of root growth patterns from the soil perspective via root distance models. Front Plant Sci 9:1084

Seethepalli A, Guo H, Liu X, Griffiths M, Almtarfi H, Li Z (2019) RhizoVision Crown: an integrated hardware and software platform for root crown phenotyping. BioRxiv. 6 March

Seiffert U, Bollenbeck F, Mock H, Matros A (2010) Clustering of crop phenotypes by means of hyperspectral signatures using artificial neural network. In: Proceedings of 2nd workshop on hyperspectral image and signal processing: evolution in remote sensing, 14–16 June, Reykjavik, Iceland

Selbeck J, Dworak V, Ehlert D (2010) Testing a vehicle-based scanning lidar sensor for crop detection. Can J Remote Sens 36(1):24–35

Serrano L, Filella I, Penuelas J (2000) Remote sensing of biomass and yield of winter wheat under different nitrogen supplies. Crop Sci 40:723–731

Shakoor N, Lee S, Mockler TC (2017) High throughput phenotyping to accelerate crop breeding and monitoring of diseases in the field. Curr Opin Plant Biol 38:184–192

Sharma LK, Bu H, Franzen DW, Denton A (2016) Use of corn height measured with an acoustic sensor improves yield estimation with ground based active optical sensors. Comput Electron Agric 124:254–262

Shi Y (2009) Performance evaluation of off-shelf range sensors for in-field crop height measurement. Master's thesis, Oklahoma State University, Stillwater

Shi Y, Thomasson JA, Murray SC, Pugh NA, Rooney WL, Shafian S, Rajan N, Rouze G, Morgan CLS, Neely HL, Rana A, Bagavathiannan MV, Henrickson J, Bowden E, Valasek J, Olsenholler J, Bishop MP, Sheridan R, Putman EB, Popescu S, Burks T, Cope D, Ibrahim A, McCutchen BF, Baltensperger DD, Avant RV Jr, Vidrine M, Yang CH (2016) Unmanned aerial vehicles for high-throughput phenotyping and agronomic research. PLoS One 11(7):e0159781

Silva AGP, Görgens EB, Campoe OC, Alvares CA, Stape JL, Rodriguez LCE (2015) Assessing biomass based on canopy height profiles using airborne laser scanning data in eucalypt plantations. Sci Agric 72(6):504–512

Singh A, Ganapathysubramanian B, Singh AK, Sarkar S (2016) Machine learning for high-throughput stress phenotyping in plants. Trends Plant Sci 21(2):110–124

Singh AK, Ganapathysubramanian B, Sarkar S, Singh A (2018) Deep learning for plant stress phenotyping: trends and future perspective. Trends Plant Sci 23(10):883–898

Slota M, Maluszynski M, Szarejko I (2016) An automated, cost-effective and scalable, flood-and-drain based root phenotyping system for cereals. Plant Methods 12:34

Slovak R, Göschl C, Su X, Shimotani K, Shiina T, Busch W (2014) A scalable open-source pipeline for large-scale root phenotyping of arabidopsis. Plant Cell 26:2390–2403

Song Y, Glasbey CA, Polder G, Van Der Heijden GWAM (2014) Non-destructive automatic leaf area measurements by combining stereo and time-of-flight images. IET Comput Vis 8(5):391–403
Stamatiadis S, Taskos D, Tsadila E, Christofides C, Tsadilas C, Schepers JS (2010) Comparison of passive and active canopy sensors for the estimation of vine biomass production. Precis Agric 11(3):306–315
Sui R, Thomasson J, Ge Y (2012) Development of sensor systems for precision agriculture in cotton. Int J Agric Biol Eng 4(5):1–14
Sui R, Fisher DK, Reddy KN (2013) Cotton yield assessment using plant height mapping system. J Agric Sci 5(1):23–31
Šulc M, Matas J (2017) Fine-grained recognition of plants from images. Plant Methods 13:15
Sun J, Shi S, Gong W, Yang J, Du L, Song S, Chen B, Zhang Z (2017) Evaluation of hyperspectral Lidar for monitoring rice leaf nitrogen by comparison with multispectral Lidar and passive spectrometer. Sci Rep 7:40362
Symonova O, Topp CN, Edelsbrunner H (2015) DynamicRoots: a software platform for the reconstruction and analysis of growing plant roots. PLoS One 10(6):e0127657
Tan KZ, Lee WS, Gan H, Wang SW (2018) Recognising blueberry fruit of different maturity using histogram oriented gradients and colour features in outdoor scenes. Biosyst Eng 178:59–72
Taskos DG, Koundouras S, Stamatiadis S, Zioziou E, Nikolaou N, Karakioulakis K (2015) Using active canopy sensors and chlorophyll meters to estimate grapevine nitrogen status and productivity. Precis Agric 16(1):77–98
Tattaris M, Reynolds MP, Chapman SC (2016) A direct comparison of remote sensing approaches for high-throughput phenotyping in plant breeding. Front Plant Sci 7:1131
Thoren D, Thoren P, Schmidhalter U (2010) Influence of ambient light and temperature on laser-induced chlorophyll fluorescence measurements. Eur J Agron 32(2):169–176
Thorp KR, Gore MA, Andrade-Sanchez P, Carmo-Silva AE, Welch SM, White JW, French AN (2015) Proximal hyperspectral sensing and data analysis approaches for field-based plant phenomics. Comput Electron Agric 118:225–236
Tilly N, Hoffmeister D, Cao Q, Lenz-Wiedemann V, Miao Y, Bareth G (2015a) Transferability of models for estimating paddy rice biomass from spatial plant height data. Agriculture 5(3):538–560
Tilly N, Aasen H, Bareth G (2015b) Fusion of plant height and vegetation indices for the estimation of barley biomass. Remote Sens 7(9):11449–11480
Toda Y, Okura F (2019) How convolutional neural networks diagnose plant disease. Plant Phenomics 2019:9237136
Trachsel S, Kaeppler SM, Brown KM, Lynch JP (2011) Shovelomics: high throughput phenotyping of maize (Zea mays L.) root architecture in the field. Plant Soil 341:75–87
Truong T, Dinh A, Wahid K (2018) An ultra-wideband frequency system for non-destructive root imaging. Sensors 18:2438
Tucker C (1980) A critical review of remote sensing and other methods for non-destructive estimation of standing crop biomass. Grass Forage Sci 35(3):177–182
Ubbens J, Cieslak M, Prusinkiewicz P, Stavness I (2018) The use of plant models in deep learning: an application to leaf counting in rosette plants. Plant Methods 14:6
Uchiyama H, Sakurai S, Mishima M, Arita D, Okayasu T, Shimada A, Taniguchi R (2014) An easy-to-setup 3D phenotyping platform for KOMATSUNA dataset. ICCV workshop paper
Ulissi V, Antonucci F, Benincasa P, Farneselli M, Tosti G, Guiducci M, Tei F, Costa C, Pallottino F, Pari L, Menesatti P (2011) Nitrogen concentration estimation in tomato leaves by VIS-NIR non-destructive spectroscopy. Sensors 11(12):6411–6424
Virlet N, Sabermanesh K, Sadeghi-Tehran P, Hawkesford MJ (2017) Field scanalyzer: an automated robotic field phenotyping platform for detailed crop monitoring. Funct Plant Biol 44:143–153
Wang H, Shabala L, Zhou M, Shabala S (2019a) Developing a high-throughput phenotyping method for oxidative stress tolerance in barley roots. Plant Methods 15:12

Wang T, Rostamza M, Song Z, Wang L, McNickle G, Iyer-Pascuzzi A, Qiu Z, Jin J (2019b) SegRoot: a high throughput segmentation method for root image analysis. Comput Electron Agric 162:845–854
Wasaya A, Zhang X, Fang Q, Yan Z (2018) Root phenotyping for drought tolerance: a review. Agronomy 8(11):241
Weiss U, Biber P (2011) Plant detection and mapping for agricultural robots using a 3D LIDAR sensor. Robot Auton Syst 59(5):265–273
Winterhalter L, Mistele B, Jampatong S, Schmidhalter U (2011) High throughput phenotyping of canopy water mass and canopy temperature in well-watered and drought stressed tropical maize hybrids in the vegetative stage. Eur J Agron 35(1):22–32
Winterhalter L, Mistele B, Schmidhalter U (2012) Assessing the vertical footprint of reflectance measurements to characterize nitrogen uptake and biomass distribution in maize canopies. Field Crop Res 129:14–20
Xia C, Wang L, Chung B, Lee J (2015) In situ 3D segmentation of individual plant leaves using a RGB-D camera for agricultural automation. Sensors 15(8):20463–20479
Xu R, Li CY, Paterson AH, Jiang Y, Sun SP, Roberson JS (2018) Aerial images and convolutional neural network for cotton bloom detection. Front Plant Sci 8:225
Yang CH (2016) Aerial imaging with manned aircraft for precision agriculture. Resource: engineering and Technology for Sustainable. WORLD 23(4):25–27
Yang CH (2018) High resolution satellite imaging sensors for precision agriculture. Front Agric Sci Eng 5(4):393–405
Yang W, Duan L, Chen G, Xiong L, Liu Q (2013) Plant phenomics and high-throughput phenotyping: accelerating rice functional genomics using multidisciplinary technologies. Curr Opin Plant Biol 16(2):180–187
Yang W, Guo Z, Huang C, Duan L, Chen G, Jiang N, Fang W, Feng H, Xie W, Lian X, Wang G, Luo Q, Zhang Q, Liu Q, Xiong L (2014) Combining high-throughput phenotyping and genome-wide association studies to reveal natural genetic variation in rice. Nat Commun 5:5087
Yang J, Shi S, Gong W, Du L, Ma YY, Zhu B, Song SL (2015) Application of fluorescence spectrum to precisely inverse paddy rice nitrogen content. Plant Soil Environ 61(4):182–188
Yang J, Gong W, Shi S, Du L, Sun J, Song S, Chen B, Zhang Z (2016) Analyzing the performance of fluorescence parameters in the monitoring of leaf nitrogen content of paddy rice. Sci Rep 6:28787
Yang G, Liu J, Zhao C, Li Z, Huang Y, Yu H, Xu B, Yang X, Zhu D, Zhang X, Zhang R, Feng H, Zhao X, Li Z, Li H, Yang H (2017) Unmanned aerial vehicle remote sensing for field-based crop phenotyping: current status and perspectives. Front Plant Sci 8:1111
Yang Q, Luo S, Chang C, Xun Y, Bao G (2019a) Segmentation algorithm for Hangzhou white chrysanthemums based on least squares support vector machine. Int J Agric Biol Eng 12(4):127–134
Yang W, Yang C, Hao Z, Xie C, Li M (2019b) Diagnosis of plant cold damage based on hyperspectral imaging and convolutional neural network. IEEE Access 7:118239–118248
Yazdanpour F, Khadivi A, Etemadi-Khah A (2018) Phenotypic characterization of black raspberry to select the promising genotypes. Sci Hortic 235:95–105
Yeh YF, Lai T, Liu T, Liu C, Chung W, Lin T (2014) An automated growth measurement system for leafy vegetables. Biosyst Eng 117:43–50
York LM, Lynch JP (2015) Intensive field phenotyping of maize (Zea mays L.) root crowns identifies phenes and phene integration associated with plant growth and nitrogen acquisition. J Exp Bot 66(18):5493–5505
Young SN, Kayacan E, Peschel JM (2018) Design and field evaluation of a ground robot for high-throughput phenotyping of energy sorghum. Precis Agric 20(4):697–722
Yu K, Kirchgessner N, Grieder C, Walter A, Hund A (2017) An image analysis pipeline for automated classification of imaging light conditions and for quantification of wheat canopy cover time series in field phenotyping. Plant Methods 13:15
Yu K, Anderegg J, Mikaberidze A, Karisto P, Mascher F, McDonald BA, Walter A, Hund A (2018) Hyperspectral canopy sensing of wheat Septoria tritici blotch disease. Front Plant Sci 9:1195

Yuan L, Bao Z, Zhang H, Zhang Y, Liang X (2017) Habitat monitoring to evaluate crop disease and pest distributions based on multi-source satellite remote sensing imagery. Optik 145:66–73

Zaman-Allah M, Vergara O, Araus JL, Tarekegne A, Magorokosho C, Zarco-Tejada PJ, Hornero A, Albà AH, Das B, Craufurd P, Olsen M, Prasanna BM, Cairns J (2015) Unmanned aerial platform-based multi-spectral imaging for field phenotyping of maize. Plant Methods 11:35

Zappala S, Mairhofer S, Tracy S, Sturrock CJ, Bennett M, Pridmore T, Mooney SJ (2013) Quantifying the effect of soil moisture content on segmenting root system architecture in X-ray computed tomography images. Plant Soil 370(1–2):35–45

Zarco-Tejada PJ, González-Dugo V, Berni JAJ (2012) Fluorescence; temperature and narrow-band indices acquired from a UAV platform for water stress detection using a micro-hyperspectral imager and a thermal camera. Remote Sens Environ 117(1):322–337

Zhang L, Grift TE (2012) A LIDAR-based crop height measurement system for Miscanthus giganteus. Comput Electron Agric 85:70–76

Zhang Y, Zhang N (2018) Imaging technologies for plant high-throughput phenotyping: a review. Front Agric Sci Eng 5(4):406–419

Zhang Y, Teng P, Shimizu Y, Hosoi F, Omasa K (2016) Estimating 3D leaf and stem shape of nursery paprika plants by a novel multi-camera photography system. Sensors 16(6):874–891

Zhang C, Si Y, Lamkey J, Boydston RA, Garland-Campbell KA, Sankaran S (2018) High-throughput phenotyping of seed/seedling evaluation using digital image analysis. Agronomy 8(5):63

Zhao C, Zhang Y, Du J, Guo X, Wen W, Gu S, Wang J, Fan J (2019) Crop Phenomics: current status and perspectives. Front Plant Sci 10:714

Zia S, Romano G, Spreer W, Sanchez C, Cairns J, Araus JL, Müller J (2013) Infrared thermal imaging as a rapid tool for identifying water-stress tolerant maize genotypes of different phenology. J Agron Crop Sci 199(2):75–84

Zou X, Ttus MM, Tammeorg P, Torres CL, Takala T, Pisek J, Mäkelä P, Stoddard FL, Pellikka P (2014) Photographic measurement of leaf angles in field crops. Agric For Meteorol 184(2):137–146

Chapter 8
Crop Sensing in Precision Agriculture

Hong Sun, Minzan Li, and Qin Zhang

Abstract Precision agriculture or precision farming is a scientific management strategy based on the spatial and temporal variability of soil, crops, and the environment, and crop sensing is an effective technology to understand the variability. In the past decades, a number of crop sensors or instruments based on spectroscopy have been developed and applied to satisfy the requirements and solve detecting problems in the field. These instruments can be used in multiple types, such as handheld detection, vehicle-mounted diagnosis, and remote sensing by UAV or satellites. Typical sensors and specific applications are summarized to explain the application fundamental and potential of crop sensing. These spectral sensors include hyper-spectrometers, multiband sensors for vegetation indices, and imagery instruments using visible or extended spectral bands. Frontier research areas in sensor development are also introduced involving wireless sensor networks, integrated sensors for data fusion, and different methods for spectral imaging collection. In addition, applications of different sensors are reviewed including the recognition of crops and weeds, estimation of nutrients and growth status, and identification of disease and pests. A variable-rate fertilizer system controlled by crop sensors is also demonstrated to show how crop sensing technology could help precision management in the field. Crop sensing sensors and instruments will promote reliable predictions and operations in agriculture.

Keywords Crop Sensing · Crop sensor · Spectral instrument · Crop imagery · Precision agriculture

H. Sun (✉) · M. Li
China Agricultural University, Beijing, China
e-mail: sunhong@cau.edu.cn

Q. Zhang
Washington State University, Prosser, WA, USA

M. Li et al. (eds.), *Soil and Crop Sensing for Precision Crop Production*,
Agriculture Automation and Control, https://doi.org/10.1007/978-3-030-70432-2_8

8.1 Introduction

Precision agriculture (PA) or precision farming contributes to improving agronomic performance, saving resources, and protecting the environment. It is established as a management strategy that employs detailed, site-specific information to precisely manage production inputs based on variability to replace average inputs in the field. Besides 3S technology including the Global Navigation Satellite System (GNSS), Geographic Information Systems (GIS), and remote sensing (RS), many other technologies such as proximal imaging, spectroscopy, and wireless sensor network (WSN) are applied in PA (Jawad et al. 2017). They provide more efficient ways in crop management including real-time detection of crop growth, targeted analysis and decision-making of precision operation, and manual labor liberation by optimized tools.

In general, there are three main steps in precision crop management including soil and crop sensing, decision-making, and variable-rate application. One of the critical issues in precision agriculture is how to measure crop growth data noninvasively and efficiently. In the past decades, significant progress on optical instruments has been made in crop monitoring (Pallottino et al. 2019). A number of crop sensors and instruments have been developed and used to meet the requirements of PA and solve detecting problems in the field as shown in Fig. 8.1. They include RGB (red, green, blue) cameras, multispectral image sensors, hyper-spectrometers, unmanned aerial vehicles (UAVs), satellite remote sensors, thermographic imagers, and light detection and ranging (LiDAR). Most of them are developed based on the combination of spectroscopy, optical

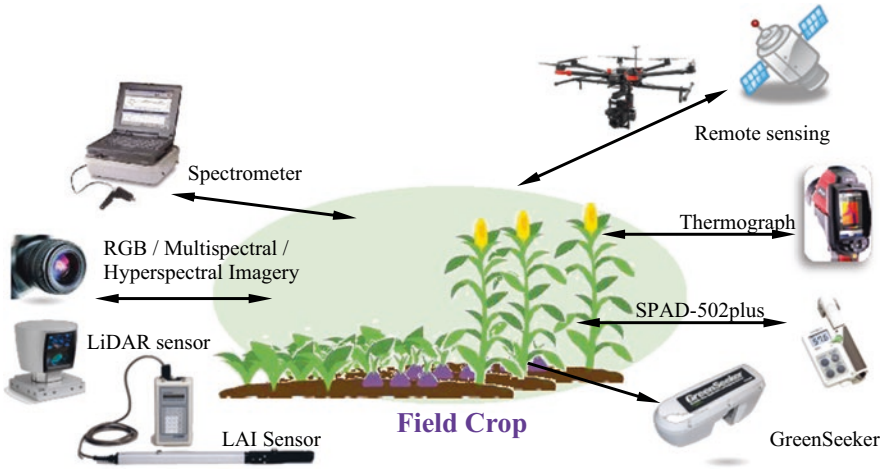

Fig. 8.1 Crop sensing instruments in precision agriculture (*Disclaimer*: Commercial products are referred to solely for the purpose of clarification and should not be construed as being endorsed by the authors or the institution with which the authors are affiliated)

principles, and photodetectors to measure the reflected electromagnetic energy. In a typical way, data are represented with energy intensity by line plots and two-dimensional (2D) and three-dimensional (3D) images and even presented as a data cube.

In most cases, crop information is captured by instruments through line scanning or digital photography. Then the data are analyzed using various specialized software applications, such as spectroscopy analysis and digital image processing. Spectroscopy uses the interaction of electromagnetic waves with an object to perform an analysis related to crop nutrient or biomass. Digital imaging is a set of computational techniques for analyzing, enhancing, compressing, processing, and reconstructing crop images. Both methods are widely used in crop recognition and parameter estimation.

Researchers have developed some new instruments and extended their applications in many scenarios, including handheld detection, vehicle-mounted diagnosis, and remote sensing by UAVs or satellites, to build reliable prediction models of complex and uncertain phenomena in agriculture. In order to explain the application fundamental and potential of crop sensing instruments in precision agriculture, sensors and the specific models from spectral and image sensing technologies are examined. Applications of crop sensing involve the recognition of crops and weeds, estimation of nutrient and growth status, identification of disease and pests, and detection of special crop fruits.

8.2 Spectroscopy-Based Sensing Instruments for Crop Monitoring

8.2.1 Foundation of Spectral Sensing and Vegetation Indices in Crop Sensing

According to the range of electromagnetic radiation at specific nanometer (nm) wavelength, crop sensing is generally referred to as ultraviolet (UV, 200–400 nm), visible (Vis, 400–760 nm), near-infrared and shortwave infrared (NIR and SWIR, 760–2500 nm) (Toth and Jóźkow 2016). The green plant typically displays low reflectance in the visible region, especially in the red band close to 650 nm due to strong absorbance by photosynthetic and accessory plant pigments. By contrast, the reflectance is usually high from the red-edge (680–760 nm) to the NIR (780–2500 nm) region because there is very little absorbance by subcellular particles or pigments and considerable scattering at mesophyll cell wall interfaces.

Since the changes in leaf pigments and biochemical components caused by nutrient stress or bio-infringement can influence the spectral characteristics of leaves, the spectral analysis can be used to monitor growing crops (Narvaez et al. 2017). Zhang et al. (2019a) reviewed that the spectral features used in plant monitoring was

Table 8.1 Spectral features for monitoring plant diseases and pests

Category	Feature type	Characteristics	Reference
VIS-NIR features	Original reflectance	Capture spectral variations caused by disease infection or pest infestation. The spectral features are capable of describing either variation of band reflectance intensity or changes in shape of spectral curves.	Sankaran et al. (2010), Huang et al. (2012), Xu et al. (2007), Zhang et al. (2012), Luo et al. (2013) and Zhang et al. (2014)
	Vegetation indices		
	Derivative spectral features		
	Continuous removal spectral features		
	Wavelet features		
Fluorescence and thermal parameters	Parameters derived from laser-induced fluorescence spectra, e.g., F686/F740	Presymptomatic indicators of plant diseases and pests. The fluorescence parameters measure changes in photosynthesis due to plant diseases and pests. The thermal parameters indicate changes in plant transpiration intensity.	Tartachnyk et al. (2006), Kuckenberg et al. (2009), Bauriegel et al. (2014), Stoll et al. (2008) and Calderón et al. (2013)
	Parameters associated with the saturation pulse method, e.g., Fv/Fm, NPQ, ΦPSII, and Fv′/Fm′		
	Absolute/relative temperature, e.g., Tleaf−Tair		

Note: The table is modified from Table 8.2 (Zhang et al. 2019a)

particularly affected by disease and pests. As shown in Table 8.1, spectral features of infected or damaged plants are highlighted including VIS-NIR spectral reflectance, fluorescence, and thermal features. Among those spectral features, band reflectance is the simplest form and can be transformed in different ways, such as spectral derivative, continuous removal transformation, and continuous wavelet transformation.

Spectral characteristics of vegetation can be analyzed based on sensitive reflectance and the vegetation index (VI). Sensitive wavelengths related to crop parameters are selected from the hyper-spectra to evaluate the vegetation vigor. A VI is a spectral transformation of two or more wavebands designed to enhance the contribution of vegetation properties and allows reliable spatial and temporal intercomparisons of terrestrial photosynthetic activity and canopy structural variations. Some VIs measured by specific bands are listed in Table 8.2, in which R_i is the reflectance at i nm or i band such as green, red, red edge, or NIR. Among these VIs, the Normalized Difference Vegetation Index (NDVI) is the most commonly used in crop monitoring. Large amounts of literature indicate that quantization parameters of spectra and vegetation indices are common methods in vegetation recognition, crop classification, and biomass estimation. Therefore, some sensors have been developed to measure VIs based on spectroscopy due to huge potentials of field applications.

Table 8.2 Vegetation indices measured by spectral reflectance

Name	Acronym	Formula	Application	Reference
Difference vegetation index	DVI	$R_{NIR} - R_{red}$	Disease (soybean rust)	Cui et al. (2009)
Ratio vegetation index	RVI	R_{NIR}/R_{red}	Disease (soybean rust), LAI (apple), yield (wheat), nitrogen (wheat)	Cui et al. (2009), Han et al. (2016), Zhang et al. (2019b) and Cao et al. (2012)
Normalized difference vegetation index	NDVI	$(R_{NIR} - R_{red})/(R_{NIR} + R_{red})$	Water (corn, soybeans), LAI (apple, potato), nitrogen (wheat)	Dejonge et al. (2016), Chen et al. (2005), Han et al. (2016) and Cao et al. (2013)
Normalized difference red edge	NDRE	$(R_{NIR} - R_{red\ edge})/(R_{NIR} + R_{red\ edge})$	Nitrogen (wheat, rice), chlorophyll (sorghum)	Cao et al. (2013) and Potgieter et al. (2017)
Green normalized difference vegetation index	GNDVI	$(R_{\text{nir}} - R_{\text{green}})/(R_{\text{nir}} + R_{\text{green}})$	Powdery mildew (wheat), aphid (wheat), leafhopper (cotton), water (corn, apple, potato)	Zhang et al. (2012), Luo et al. (2013), Prabhakar et al. (2011), Dejonge et al. (2016), Han et al. (2016) and Ray et al. (2006)
Green ratio vegetation index	GRVI	$(R_{NIR}/R_{green}) - 1$	LAI (apple)	Han et al. (2016)
Photochemical reflectance index	PRI	$(R_{531} - R_{570})/(R_{531} + R_{570})$	Disease (grape leafroll), LAI (potato)	Naidu et al. (2009) and Ray et al. (2006)
Red-edge vegetation stress index	RVSI	$(R_{714} + R_{752})/(2 - R_{733})$	Disease (grape leaf)	Naidu et al. (2009)
Soil-adjusted vegetation index	SAVI	$(R_{NIR} - R_{red})(1 + L)/(R_{NIR} + R_{red} + L)$	LAI (potato)	Ray et al. (2006)
Optimized soil-adjusted vegetation index	OSAVI	$1.16(R_{800} - R_{670})/(R_{800} + R_{670} + 0.16)$	Water (corn)	Dejonge et al. (2016)
Normalized difference water index	NDWI	$(R_{858} - R_{1640})/(R_{858} + R_{1640})$	Water (corn and soybeans)	Chen et al. (2005)

8.2.2 Spectral Sensing in Crop Monitoring

Spectral instruments with optical sensors are the fundamental tools to assess vegetation status. Three kinds of spectral instruments have been used including continuous spectrometers, vegetation index sensors, and imaging spectrometers. In general, spectrometers are used to measure continuous spectral reflectance of light over a specific portion of the electromagnetic spectrum, and vegetation index sensors measured by dual or multispectral bands. There are many commercially available

products of portable sensors for crop monitoring. They are generally defined as a passive type or an active type according to lighting strategies during the measurements. For example, the Soil Plant Analysis Development (SPAD) meter is a compact device with active lighting and transmittance measurement to determine the amount of chlorophyll in plant leaves at 650 and 940 nm. The GreenSeeker (Trimble Agriculture, Sunnyvale, CA, USA) gets NDVI with the active lighting module. Some applications of hyperspectral sensing and vegetation index sensing in crop monitoring are listed in Table 8.3, which include detections of chlorophyll content, nitrogen content, and sugar content and estimations of growth stages and yields, even weed identification.

Table 8.3 Spectral sensing applications in crop monitoring

Type	Describe	Application	Reference
Hyperspectral sensing	Vis-NIR, 350–1075 nm or 350–2500 nm, handheld or vehicle mounted	Chlorophyll content (maize), growth stages (potato), weeds	Liu et al. (2018a, b), Sun et al. (2019a, b) and Shirzadifar et al. (2018)
	Vis-NIR,190–900 nm, lab used	Sugar content (apple)	Zhang et al. (2015)
	Vis-NIR, 350–820 nm, portable	Chlorophyll (wheat)	Cheng et al. (2017)
Vegetation index sensing	Active light, 650 and 940 nm, transmittance, handheld	Chlorophyll, nitrogen (wheat, corn, coffee)	Uddling et al. (2007), Netto et al. (2005), Zhao et al. (2007) and Gholizadeh et al. (2017)
	Active light, 660 and 780 nm, handheld or vehicle mounted	Nitrogen (corn, wheat), yield (wheat), growth stages (corn)	Cao et al. (2012, 2017), Zhang et al. (2019b), Taskos et al. (2015), Singh et al. (2015) and Tremblay et al. (2009)
	Vis-NIR six bands (450, 550, 650, 670, 730, 760 nm), and three of these bands can be used at one time, handheld or vehicle mounted	Nitrogen (wheat), chlorophyll (grape)	Cao et al. (2013, 2017) and Taskos et al. (2015)
	550, 670, 700, 740, 780 nm, vehicle mounted	Nitrogen (wheat), growth stages (corn)	Singh et al. (2015), Tremblay et al. (2009)
	Active light, 670, 730 and 760 nm, handheld or vehicle mounted	Yield (grasses/ legumes)	Serrano et al. (2016)
	Active light, 730 and 808 nm, vehicle mounted	Growth stages (winter wheat)	Sharabian et al. (2013)
	Active light, 653 and 931 nm, transmittance, handheld	Nitrogen (grape)	Taskos et al. (2015)

8.2.2.1 Hyper-Spectrometers for Crop Sensing

Hyper-spectrometers are the most frequently used instruments especially during theoretical or mechanism analysis in crop sensing. Most of the instruments used in chemical detection are designed based on UV spectroscopy, which work under the principle of Beer Lambert's law. Zhang et al. (2015) used a UV-2450 spectrograph to measure the visible and NIR spectral reflectance of apple leaf samples within the 300–900 nm band, and such spectral information of apple tree leaves in different phenological phases could be used to predict fruit sugar content. According to the result of the two-dimensional correlation spectroscopic analysis on apple leaf reflectance with fruit sugar content as perturbation, it was observed that the autocorrelation peaks all appeared at the 530–570 nm and 700–720 nm wavebands in the synchronization spectrogram. The contribution proportion to fruit sugar content in different growth periods was investigated and then the support vector machine (SVM) model was established. The determination coefficient of the calibration model (R_c^2) of the SVM model reached 0.89, and the determination coefficient of validation (R_v^2) reached 0.88.

Compared with laboratory instruments, portable sensors are more flexible in the field. The devices could be selected by spectral range, resolution, usage requirements, and so on. For example, ASD FieldSpecHH[1] is a 512-element photodiode array spectroradiometer with a 325–1075 nm wavelength range. It uses a fixed concave holographic reflective grating that disperses the light onto a fixed photodiode array that has 512 individual detection points or "elements" in a line. Associated with each of these elements is a distinct signal whose magnitude is determined by the total integrated amount of light energy falling on that element. Then, each element is assigned to a position within 512 points. In this way, the analog signal is converted into digital signal. The instruments could be set to view traceable wavelength references such as emission source, reflectance standards, and the output of a triple monochromator. The output results are data points with known element-position and wavelength-channel coordinates.

Many of the current studies on crop monitoring involve portable spectrometers. The operation flow generally involves the control parameter setting, storage directory setting, dark noise measuring, reference calibration, sample detection, spectrum calculation, and display. The measured data are used to analyze and establish a specific model for crop monitoring purposes. Liu et al. (2018a, b) measured the spectral reflectance of maize canopy by using ASD FieldSpecHH to estimate the chlorophyll content. The data were processed following wavelet denoising and multivariate scatter correction (MSC) to reduce the noise influence. Then three spectral ranges were extracted by interval partial least squares (IPLS), including 525–549 nm, 675–749 nm, and 850–874 nm. The chlorophyll content estimation model was developed by using support vector regression (SVR). The calibration R_c^2 of the

[1] *Disclaimer*: Commercial products are referred to solely for the purpose of clarification and should not be construed as being endorsed by the authors or the institution with which the authors are affiliated.

model was 0.831, the RMSEC was 1.3852 mg/L, the validation R_v^2 was 0.809, and the RMSEP was 0.8664 mg/L. Using the same spectrometer, Sun et al. (2019a) explored the optimizing spectral features to identify the growth stages of potato plants. In general, the canopy spectral reflectance varied with the growth stages in the bands of 400–500 nm, 530–640 nm, 740–880 nm, and 910–960 nm. The classification accuracies of SVM models were 100% in the training set and 94.59% in the testing set, respectively.

8.2.2.2 Portable Sensors Used in Crop Monitoring

According to the specific features and VIs used in crop monitoring, some sensors are designed as portable with only several sensitive bands to reduce redundant spectra. These specific sensors are generally developed based on the red and NIR bands. Besides red and NIR bands, a red-edge band located in the range of 700–760 nm is also included in the instruments to increase the variables in detecting models. An instrument can be designed to measure the transmitted or reflected light from leaves and crop canopy. The light source in the measurement can be natural light (sunlight) or artificial light source (lamp) defined as a passive or active lighting. The instrument with active lighting is more robust in field application to improve the performances under the limitation of weather or time windows. A few portable (handheld) instruments could be used to evaluate the content of chlorophyll or nitrogen, LAI, and yield using the calculated VIs. Farmers can use them in precision agriculture according to the application cases, leaf, or canopy measurement.

Portable Sensors for Leaf Measurement

Portable or handheld instruments for leaf measurement have advantages of compact size and lightweight. Most of them are designed based on the transmittance with the active light source. One of the widely used leaf chlorophyll meter is probably the Soil and Plant Analyzer Development (SPAD) chlorophyll meter, such as SPAD-502 Plus (Konica Minolta Inc., Japan).

Uddling et al. (2007) reported that the readings from the SPAD-502 Plus could not only provide the measurement of chlorophyll content, but also provide the information for estimating nitrogen status as well as photosynthetic pigment content. Schepers et al. (1992) compared the corn leaf disk N concentrations and SPAD 502 chlorophyll meter readings from N rate studies at the silking stage for a variety of hybrids. Data indicated that chlorophyll meter readings correlated well with leaf N concentrations for a given hybrid and location. Netto et al. (2005) established a correlation between the photosynthetic pigment content extracted in dimethylsulfoxide, the total nitrogen content, and the chlorophyll fluorescence variables with the SPAD-502 readings in *Coffea canephora* Pierre leaves. If the SPAD-502 readings were lower than 40, it showed impairment in the photosynthetic process. In the study, total N concentration increased linearly with SPAD-502 readings. Meanwhile,

the relationship between the values obtained by the SPAD-502 and the chlorophyll fluorescence variables (F_0, F_m, and F_v/F_m) proved that the maximum quantum efficiency of the photosystem II, indicated by the F_v/F_m ratio, started to fall at around 40.

The measured values by SPAD meters have also been used in the fertilization guiding. Zhao et al. (2007) proposed a study on the relationship between SPAD chlorophyll meter readings and nitrogen content in leaves in order to determine the amount of nitrogen fertilization. Field experiments were conducted in three wheat growth duration stages from 2003 to 2006. Grain yields and soil NO_3-N contents were measured in all plots. The results indicated that the fertilizer application guided by the meter values reduced the spatial variability of wheat yield and had benefits of low soil residual NO_3-N content and NO_3-N leaching potential.

Gholizadeh et al. (2017) focused on the relationship between SPAD chlorophyll meter readings and N content in leaves during different growth stages. The research introduced the most suitable stage for the assessment of crop N and prediction of rice yield. Results implied that there was a better relationship between rice leaf N content ($R^2 = 0.93$) and yield ($R^2 = 0.81$), with SPAD readings at the panicle formation stage. Therefore, the SPAD-based evaluation of N status and prediction of rice yield is more reliable on this stage rather than at the booting stage.

Although SPAD readings have been widely used in the measurement of chlorophyll content, Xiong et al. (2015) indicated the relationship between chlorophyll content and leaf N content per leaf area, and the relationship between SPAD readings and leaf N content per leaf area varied widely among the species groups. A significant impact of light-dependent chloroplast movement on SPAD readings was observed under low leaf N supplementation in both rice and soybean but not under high N supplementation. Furthermore, the allocation of leaf N to chlorophyll was strongly influenced by short-term changes in growth light. It demonstrates that the relationship between SPAD readings and leaf N content per leaf area is profoundly affected by environmental factors and leaf features of crop species, which should be accounted for when using a chlorophyll meter to guide N management in agricultural systems.

Portable Sensors for Canopy Measurement

Instruments for canopy monitoring are generally designed to measure the reflected light related to typical VIs. Portable instruments, such as GreenSeeker, Crop Circle, and N-Sensor, are commonly used to get the NDVI in the field. For on-the-go applications, these sensors can also be mounted to vehicles to remotely sense plants while driving through a field.

According to the concept of the active crop canopy monitoring, an instrument emits a brief burst of red and infrared light and then measures the amount of each type of light that is reflected back from the plant. GreenSeeker sensors (Trimble Navigation Limited, Sunnyvale, CA, USA) are designed based on modulated red (650–670 nm) and NIR (755–785 nm) LEDs (light-emitting diode). Crop Circle devices (Holland Scientific Inc., Lincoln, Nebraska, USA) are equipped with

multispectral active sensors. The Crop Circle ACS-430 incorporates three optical measure channels, so that the sensor simultaneously measures crop/soil reflectance at 670, 730, and 780 nm. Moreover, the Crop Circle ACS-470 has six bands (450, 550, 650, 670, 730, 760 nm) and three of these bands can be used at one time to measure the radiative transfer and biophysical characteristics of plant canopies. Yara N-Sensor (Yara International ASA, Germany) is different from the active optical sensors mentioned above. It has a xenon flashlamp, which provides high-intensity multispectral light, so that it can measure and record the crop light reflectance in a waveband between 450 and 900 nm (Munoz-Huerta et al. 2013).

Several studies were conducted to detect crops based on portable sensors mentioned above. Cao et al. (2012) found that GreenSeeker-NDVI was exponentially related to N uptake in winter wheat, whereas the correlation between N uptake and RVI was linear. Zhang et al. (2019b) intended to expand the applicability of GreenSeeker in monitoring the growth status and predicting the grain yield of winter wheat (*Triticum aestivum* L.). Four field experiments with multiple wheat cultivars and N treatments were conducted during 2013–2015 to obtain NDVI and RVI synchronized with four agronomic parameters: LAI, leaf dry matter (LDM), leaf nitrogen concentration (LNC), and leaf nitrogen accumulation (LNA). Duration models indicated that NDVI and RVI explained 80%, 68–70%, 10–12%, and 67–73% of the variability in LAI, LDM, LNC, and LNA, respectively. Considering the variation among different wheat cultivars, the newly normalized VIs rNDVI (NDVI vs. the NDVI for the highest N rate) and rRVI (RVI vs. the RVI for the highest N rate) were calculated to predict the relative grain yield (RY, the yield vs. the yield for the highest N rate). rNDVI and rRVI explained 77–85% of the variability in RY.

In order to determine which VIs calculated from the Crop Circle sensor can perform the best estimation of rice N status, Cao et al. (2013) compared six VIs based on the green (550 ± 20 nm), red-edge (730 ± 10 nm), and NIR (>760 nm) bands. The results indicated that using the Normalized Difference Red Edge (NDRE) to predict plant N uptake had the highest coefficient of determination (R^2, 0.76) and the lowest root mean square error (RMSE, 17.00 kg N/ha). The second best-performing vegetation index was the Red-Edge Chlorophyll Index (CIRE), which performed similarly to NDRE. Crop Circle ACS-210 and ACS-430 (red at 630 nm, red edge at 730 nm, and NIR at 780 nm) were compared and different NDVI values were analyzed in each individual waveband (Taskos et al. 2015). The results demonstrated that ACS-430 and red-edge-based indices were more strongly correlated with leaf chlorophyll of vineyards.

Regarding the Yara N-Sensor (Yara International ASA, Germany), Singh et al. (2015) investigated the tractor-mounted N-Sensor to predict nitrogen (N) content for wheat crop under different nitrogen levels. It was observed that there was a strong correlation among sensor attributes (sensor value and sensor NDVI) and different N-levels. The Yara N-Sensor/FieldScan (Yara International ASA, Germany) was used to assess the status of N in spring wheat and corn (*Zea mays* L.) at specific growth stages (Tremblay et al. 2009). It was found that the Yara N-Sensor/FieldScan should be used before growth stage V5 in corn during the season if NDVI was used

to derive crop N requirements. Yara N-Sensor/FieldScan can also record spectral information from wavebands other than red and NIR, and more VIs can be derived that might relate better to the nitrogen status than NDVI.

Besides the instruments introduced above, there are similar systems such as OptRx Crop meter (Holland Scientific, USA), CropSpec sensor (Topcon Positioning Systems, USA), and CCM-200 and CCM 300 (Edaphic Scientific, Australia). They are also widely used in nitrogen and chlorophyll measurements (Serrano et al. 2016; Sharabian et al. 2013). Published reports indicate that each sensor has its own sensitivity characteristics, and the wavelengths around 550, 650, 766, and 850 nm are mostly selected according to different applications (Tremblay et al. 2009; Cao et al. 2017; Taskos et al. 2015). Meanwhile, the algorithms should be proposed to establish estimation models, so that the modeling results could indicate the operation in the field management.

8.2.3 Development of Spectroscopy-Based Systems for Crop Detection

The current trend in crop sensing is to integrate compact sensors and detecting models. In this sense, certain studies have been conducted to develop new systems to provide support in field management.

8.2.3.1 Development of Hyperspectral Sensors for Crop Monitoring

In order to predict the nutrient content of winter wheat nondestructively in the field, an integrated system was developed based on an STS-VIS sensor (Cheng et al. 2017). The STS-VIS sensor from Ocean Optics Inc., USA, is a compact sensor for portable application. It is a grating-based device with an advanced CMOS (complementary metal-oxide-semiconductor) 1024-element detector array to measure wavelengths in 350–850 nm. The USB output makes secondary development possible to satisfy online detection, typically by the software integration of established models. As shown in Fig. 8.2, the hardware of the integrated spectrometer consists of three parts of the optical system, the data storage module, and the controller. The optical sensor with a fiber is used to measure the reflected light from the leaf or canopy of the field crop. The controller could be connected to the sensor through USB2.0 or a wireless network. The supporting software installed on the PC or mobile controller helps to control the signal communication and processing. The setting parameters include the integration time, sampling frequency, and average number due to the effects of the ambient light intensity and the sampling requirements.

A software program was also developed to collect the spectral reflectance of winter wheat canopy in 350–820 nm. The calibration experiment was carried out to

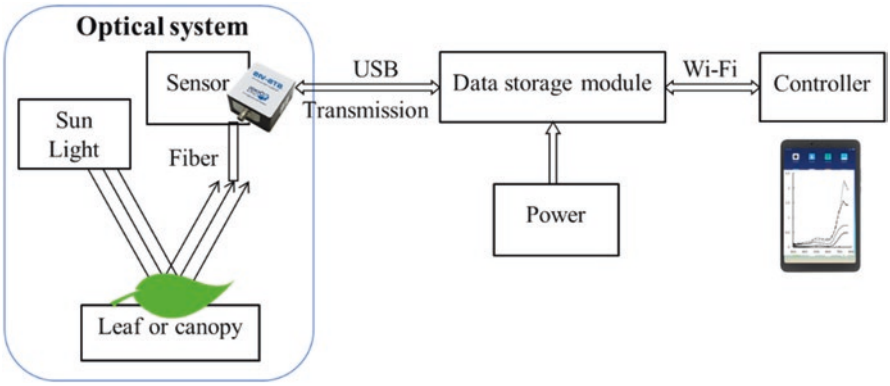

Fig. 8.2 Mechanical structure of the integrated spectrometer. (Cheng et al. 2017)

test the performance of the sensor by a gray calibration board with four different gray levels. The correlation coefficient between the sensor and ASD (Field Spec HandHeld2) showed that the average correlation coefficient was 0.94. Eight wavelengths, including 514, 527, 562, 572, 605, 705, 719, and 795 nm, were selected to detect the chlorophyll content using the random frog (RF) algorithm after spectral curve smoothing. The determination coefficient of the partial least squares (PLS) regression model was 0.69.

8.2.3.2 WSN-Based Sensors for Crop Monitoring

With the development of wireless sensor networks (WSNs), a novel system which contained one control unit and several optical sensor nodes for crop growth detection was developed by China Agricultural University (Zhong et al. 2014). Sensors, organized by ZigBee WSN, were designed to collect, amplify, and transmit the optical signals. A CS350 (Cilico Microelectronics Corp., Ltd., Xi'an, China) type of PDA (personal digital assistant) was selected as the coordinator of the whole wireless network to receive, display, and store all the data sent from different sensor nodes. Since wireless communication was applied, the PDA could be easily used, installed in the cab of the tractor, or hand-held by the operator.

Each sensor node was designed with four optical channels at the wavebands of 550, 650, 766, and 850 nm, respectively. Since the detection system used sunlight as the light source, besides the reflected light from crop canopy, the sunlight intensity was also measured as a reference as shown in Fig. 8.3. A full-function sensor node had to contain eight optical channels, the upward four for the sunlight measurement and the downward four for the reflected light measurement. A silicon photodiode was used to convert the light signal to current signal in each optical channel. A 4:1 time-sharing analog multiplex chip was applied to share the amplification unit and an OPA333 amplifier was chosen which had the properties of high precision, low quiescent current, and low power consumption. The weak signals were then

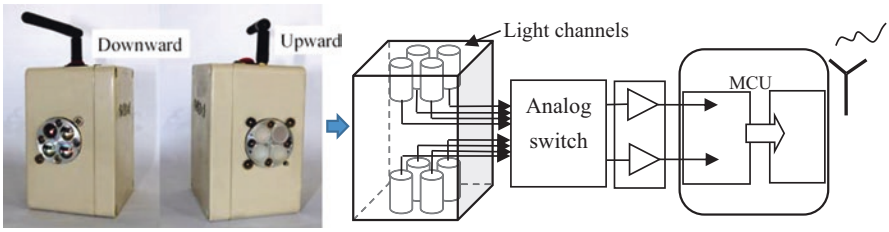

Fig. 8.3 Structure of the WSN-based sensor for crop monitoring. (Zhong et al. 2014)

amplified and transformed to voltage signals and subsequently read through A/D convertors in the microcontroller unit (MCU), which was a JN5139 wireless module (Jennic Co, UK). The measured data were wirelessly transmitted to the coordinator via an antenna.

Therefore, once started, the sensor was initialized and the data were collected automatically with a certain sampling frequency. By setting the address of analog switch, the data of each channel were repeated for ten times and then averaged. Sensors had different identification numbers, and the sampling frequency was adjustable according to different requirements.

In the field experiments, the optical sensors measured the spectral reflectance of the crop canopy with four channels at 550, 650, 766, and 850 nm separately. The transmission quality of the sensor nodes was evaluated at distances of 20, 40, 60, 80, and 100 m and the signals could be transmitted precisely without packet loss in all tests. Calibration experiments showed that the accuracy of the optical components was high enough for application. The results of the stationary field experiments showed that the detection system was capable of monitoring the spectral characteristics of the crop canopy. The correlation between chlorophyll content and NDVI was at an acceptable level, with R^2 of 0.681–0.718. The system provides a support for crop growth detection and a theoretical basis for further research on chlorophyll content prediction in the field.

8.2.3.3 An Integrated Sensor Based on Spectroscopy and Imagery

Furthermore, in order to monitor crop information more efficiently, a multi-fusion sensor was developed based on the combination of spectroscopy and imagery technology, as shown in Fig. 8.4 (Long 2020). The sensor was designed to collect the spectral reflectance and images of the crop canopy. It consists of three parts including sensors, a data processing unit, and a data transmission port. The spectral reflectance collected by an AS7263 sensor (ams AG, Premstaetten, Austria) involved six bands in the red and NIR ranges (610, 680, 730, 760, 810, and 860 nm), each of which had 20 nm of full-width half-max detection. The RGB image was captured to estimate the canopy coverage to help determine the location during field measurement. The data could be sent to a mobile phone remotely through a Wi-Fi module.

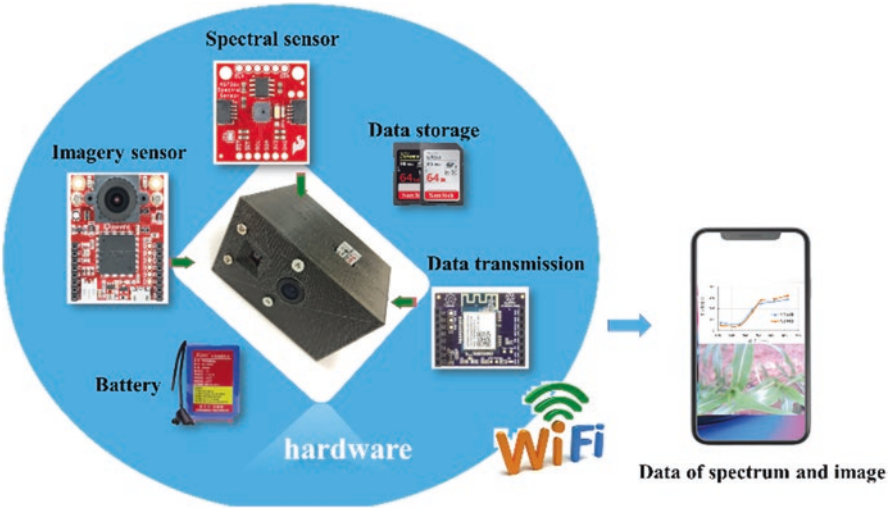

Fig. 8.4 Structure of the integrated sensor based on spectroscopy and imagery

The sensor application experiments were performed. The fusion data of spectral reflectance and images from the sensor were used to analyze the growth status of field corn with different levels of fertilizer. The adaptive boosting algorithms were used to model the chlorophyll content. The determination coefficient of the model was 0.859, which was higher than that just based on spectral data (0.829). The fusion of spectral reflectance and image data could improve the prediction accuracy of crop chlorophyll content. It provides a new tool for crop monitoring in the field.

8.3 Image Sensing for Crop Detection

8.3.1 Foundation of Crop Imaging and Feature Extraction

Optical imaging is one of the noninvasive methods for crop sensing. Similar to spectrometers, optical imaging uses the special properties of light and electromagnetic waves to obtain detailed images of leaves and plants, as well as canopy and even ecosystems. In a typical way, the data are represented with energy intensity in a line plot or 2D images. Recently, image sensing has resulted in many developments in agricultural information acquisition. A variety of imaging instruments are available such as monochrome and color digital cameras (RGB), depth and time-of-flight (ToF) cameras, multispectral and hyperspectral cameras, thermography, fluorescence sensors, and others (Yang et al. 2017; Li et al. 2014a, b).

New data sources and processing methods of 2D and 3D images and spectral data cubes significantly boom the research on crop recognition, plant positioning, and phenotype measurement. Lots of features can be extracted from images as

shown in Table 8.4, including color features, texture presentation, shape and spatial description, Vis-NIR spectral features, fluorescence, and thermal parameters (Mavridou et al. 2019; Ali et al. 2017).

In the last two decades, extensive research has been reported for image feature extraction and objective analysis. High-level image visuals are represented in the form of feature vectors that consist of numerical values. Research shows that there is a significant gap between image feature representation and human visual understanding (Latif et al. 2019). Thus, the feature selection in imaging systems is dependent on the requirements of crop monitoring; meanwhile, feature representation is another task in research.

Table 8.4 Image features in crop monitoring

Category	Feature type	Characteristics	Reference
Color	Morphological, gray level	Features are capable of describing greenness and color changes in leaves, plants, or canopy. They are used in crop and weed recognition, disease and pest identification, biomass and yield estimation, nutrient and growth status monitoring, etc.	Knoll et al. (2018), Jiang et al. (2018), Garcia et al. (2017), Liu et al. (2017), Ferreira et al. (2019) and Ali et al. (2017)
	RGB color space		
	HSV or HSI color space		
	CMY, YUV, etc.		
Texture	Local binary pattern (LBP)	Provides information in the spatial arrangement of colors or intensities. It indicates biomass, weeds, and structure changes	Waldchen et al. (2017) and Lowe (2004)
	Grey-level co-occurrence matrix (GLCM)		
	Wavelet texture		
Shape and spatial	Geometry, size, area, length, width	Features refer to appearance and help to measure phenotype, recognize objects, identify diseases or pests, and discriminate weeds	Barbedo (2016), Oppenheim et al. (2017), Priyankara and Withanage (2015) and Kebapci et al. (2011)
	Haar-like feature		
	Speeded up robust features (SURF)		
	Histogram of oriented gradients (HOG), scale-invariant feature transform (SIFT)		
VIS-NIR spectral features	Original reflectance	The spectral features are capable of describing either the variation of band reflectance intensity or changes in the shape of spectral curves used in nutrient estimation, disease detection, etc.	Liu et al. (2018a, b), Potgieter et al. (2017), Shirzadifar et al. (2018) and Cao et al. (2012, 2013, 2017)
	Vegetation indices		
	Derivative spectral features		
	Continuous removal spectral features		
	Wavelet features		
Thermal parameters	Absolute/relative temperature, e.g., Tleaf−Tair	The thermal parameters indicate transpiration intensity	Neinavaz et al. (2016)

Advances in automated and high-throughput imaging technologies have resulted in a deluge of high-resolution images and sensor data of plants. However, extracting patterns and features from this large amount of data requires the use of machine learning (ML) tools to enable data assimilation and feature identification for stress phenotyping (Waldchen and Mader 2018). ML approaches can be deployed in identification, classification, and prediction, such as SVM, neural networks (NNs), kernel methods, and instance-based approaches (Singh et al. 2016). Recently, deep learning (DL), a subset of ML approaches, has emerged as a versatile tool to assimilate large amounts of heterogeneous data and provide reliable predictions of complex and uncertain phenomena (Liu et al. 2017). These tools are increasingly being used in extracting crop features and identifying symptoms of crop growth status (Singh et al. 2018).

8.3.2 Imaging Technologies Used in Crop Detection

Imaging technologies play an important role in crop sensing. The great majority of the sensors are designed based on either solid-state technology, such as CCD (charge-coupled device) and CMOS (complementary metal-oxide-semiconductor) chips used in optical imagers, or avalanche photodiodes, like InGaAs (indium gallium arsenide) and single-photon avalanche diode (Toth and Jóźkow 2016). An appropriate equipment should be examined in order to satisfy the needs of each application. In general, the most important factors that need to be considered are the sensor resolution, frame rate, and price (Pajares et al. 2016).

Considering the diverse cameras that are available in the market, several images used are listed in Table 8.5. Imaging technologies used in near-ground crop detection can be divided into four types which are digital color imaging to capture RGB images, 3D imaging to measure depths or spatial distribution, and spectral and thermal imaging. A color image is simple and affordable, so that RGB images are extensively used in crop sensing tasks of recognizing weeds, measuring plants, and detecting diseases and pests in the field (Garcia et al. 2017; Yang et al. 2014; Jiang et al. 2018; Ferreira et al. 2019; Zong et al. 2019; Knoll et al. 2019).

Although a stereovision system could measure 3D data, the imaging methods by ToF are popular due to the robust environmental influences, such as LiDAR and photonic mixer devices (PMD) (Knoll et al. 2016a). A typical LiDAR sensor emits pulsed light waves into the surrounding environment. These pulses bounce off surrounding objects and return to the sensor and then the time for each pulse to return to the sensor is measured. The sensor uses the time to calculate the distance between the sensor and the object. Repeating this process millions of times per second creates a precise, real-time 3D map of the environment. The LiDAR sensors are used in phenotype measurement such as height and biomass (Tilly et al. 2015). Moreover, some low-cost 3D cameras are also applied in crop sensing such as Kinect (Microsoft, USA) and Real Sense (Intel., USA). They provide flexible tools in weed identification and fruit recognition (Sa et al. 2016; Kang and Chen 2020).

Table 8.5 Several images used in near-ground crop detection

Type	Describe	Application	Reference
Color images	RGB, handheld, 1280 × 720, 1920 × 1080, and 2048 × 1536	Pest distribution	Garcia et al. (2017)
	RGB, UAV, 7360 × 4912	Chlorophyll content (corn)	Qiao et al. (2019)
	RGB, handheld, 6000 × 4000	Classify carrot crop and weeds	Knoll et al. (2016b)
	RGB, handheld, 4608 × 3456	Weed recognition	Jiang et al. (2018)
	UAV, RGB, 4000 × 3000	Weed recognition	Ferreira et al. (2019)
	RGB, handheld, 2592 × 2048	Plant measurement (corn)	Zong et al. (2019)
	RGB, handheld, 3648 × 2736	Blueberry identification	Li et al. (2014a, b)
3D images	RGB, 1920 × 1080; depth, 512 × 424, 0.5–4.5 m	Weeds, fruit detection	Knoll et al. (2016b) and Sa et al. (2016)
	RGB, 1920 × 1080; depth, 1280 × 720, 0.105–10 m	Fruit detection	Kang and Chen (2020)
	Depth: 204 × 204, vehicle mounted	Weed detection	Knoll et al. (2016a),
	ToF LIDAR 16 lines, 100 m	Height and biomass (rice)	Tilly et al. (2015)
Multispectral images	470, 515, 550, 610, 656, 710, 760, 800, 830, 860, 900, and 950 nm, 12 bands, 1280 × 1024, UAV	Crop classification	Wang et al. (2019)
	RGB-NIR four bands,1296 × 964, vehicle mounted	Chlorophyll detection (corn), weed classification	Zhang et al. (2018) and Knoll et al. (2016b)
	Five bands, 475, 560, 668, 717, and 840 nm, 1280 × 960, UAV	LAI, nitrogen, chlorophyll content (sorghum)	Potgieter et al. (2017)
Hyperspectral images	900–1700 nm, 3.5 nm	Nitrogen detection (oilseed rape)	Zhu et al. (2019)
	369–988 nm, 1.2 nm	Chlorophyll and nitrogen detection (longan)	Yue et al. (2018)
	369–1042 nm,10 nm	Fruit recognition	Okamoto and Lee (2009)
	400–1000 nm, 4 nm, lab	Disease (rice), water content (maize)	Huang et al. (2017) and Liu et al. (2018a, b)
Thermal images	750–1350 nm, 640 × 512 pixels, UAV	Yield estimation (soybean)	Maimaitijiang et al. (2020)
	640 × 480 pixels, −40 °C to 150 °C, ±2%	Fruit detection	Gan et al. (2018)

Imaging spectrometers collect images as well as spectra from the observed crop. Nowadays, a wide range of imaging spectrometers have been used on different platforms including stationary or handheld near-ground platforms and unmanned aerial vehicle (UAV) platforms. Imaging spectral instruments have been widely used in crop detecting with crop classification, disease identification, nutrient estimation (chlorophyll, water, nitrogen content), and so on (Zhu et al. 2019; Yue et al. 2018; Huang et al. 2017; Liu et al. 2018a, b; Zheng et al. 2018). In addition, thermal sensors are also used in drought estimation because of close relationships among the temperature, water stress, and environment (Maimaitijiang et al. 2020).

8.3.3 Development of Imaging Systems for Crop Detection

The results of previous research studies have provided basic principles for the development of optical sensing to acquire the spectral information in the field. Spectroscopy analysis and image processing are applied as rapid, convenient, and nondestructive techniques for crop growth monitoring. The Research Center for Precision Agriculture at China Agricultural University (CAU) has developed three kinds of multispectral imagery systems for crop monitoring (Wu et al. 2015; Sun et al. 2019b; Liu et al. 2020). In general, each system includes a multispectral camera device and controlling software. The multispectral camera is designed with the capability to measure multispectral images of crop canopy in three visible bands (red [R], green [G], and blue [B]) and a NIR band. The software is developed to control the camera system. Furthermore, the estimating models of crop parameters should be embedded in the system. This way, it could provide an online device and method for crop sensing.

8.3.3.1 A Two-CCD-Based Imaging System for Crop Measurement

A two-CCD-based imaging system was designed for crop measurement, which included a multispectral image acquisition device, a communication protocol converter, and a controlling platform (Wu et al. 2015). A multispectral two-channel CCD camera (JAI Ltd., Denmark) was used, which included a splitter prism with two reflecting mirrors to split input light into visible and NIR bands. Two CCD sensors could obtain four images in three visible bands (400–700 nm, R, G, and B) and one NIR band (760–1000 nm) at the same time. The camera link communication protocol standard was adapted to output RGB and NIR images with 1024(h) × 768(v) active pixels per channel. The communication between the camera and computer was conducted by a QuadMVCL2GE converter (Beijing Microview Science and Technology Co., Ltd., China) to convert the output image from the camera link into the GigE Vision standard. The highest output bandwidth was 960 Mbps. In the research, a panel industrial control computer (PPC-3708, Beijing Weidatong Co., China) was used as the system platform. The main functions included a

Fig. 8.5 Multispectral images of tomato canopy (Sun et al. 2013). (**a**) Original RGB image (**b**) Original NIR image (**c**) Segmented RGB image (**d**) Segmented NIR image

multispectral camera control module, an image acquisition module, and a multispectral image processing module. When the system was connected, it could work following image acquisition, data conversion, and image display and storage. The multispectral image could be displayed and stored in RAW, BMP, and JPG format.

An image processing model was developed with three main functions: image enhancement, image segmentation, and parameter calculation (Sun et al. 2013). The developed system was applied in the chlorophyll content estimation of tomato. Multispectral images were collected and the SPAD values of tomato leaves were measured. More than 80 pairs of RGB and NIR images were acquired in the experiment. They were first processed by the median filtering algorithm to eliminate the noise and then segmented from the background. Figure 8.5a, b shows a pair of RGB and NIR images, and the segmented results are shown in Fig. 8.5c, d, respectively. The average gray values of each image were calculated to get the VIs of tomato canopy. The correlation analysis results indicated that the highest correlation coefficient was 0.7514 between RVI and SPAD values.

8.3.3.2 A Portable Binocular Sensor for Crop Monitoring

The NDVI calculated based on spectral reflectance is proved as one of the important parameters to estimate crop growth parameters quickly and nondestructively. Thus, the measurement of the NDVI distribution is one of important research directions for sensor development (Sun et al. 2019b). Unlike the two-CCD-based imaging system which could acquire the RGB and NIR images synchronously, some low-cost binocular vision systems could also be used in the collection of RGB and NIR images. The biggest challenge in using these kinds of binocular vision systems is image matching, so that the NDVI distribution and dynamics of crops could be monitored with high accuracy.

In order to develop a portable multispectral imaging system for crop monitoring, an FM830-5 M device (Shanghai Percipio Information Technology Co., Ltd., China), which had an RGB camera and two NIR cameras, was used to acquire RGB and NIR images of corn. The RGB and one of the NIR cameras were used to develop a binocular sensor for crop monitoring. Images of RGB and NIR were processed following preprocessing, image matching, segmentation, and image reflectance correction. The flowchart is shown in Fig. 8.6.

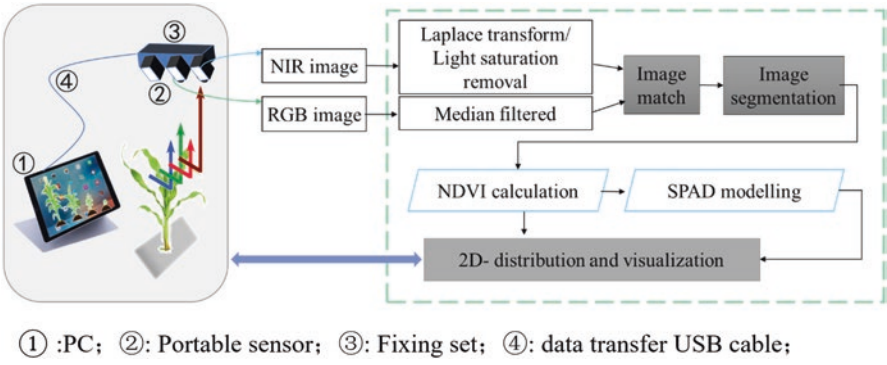

Fig. 8.6 Development of crop sensor using binocular stereo vision systems

The acquired images were calibrated and preprocessed. Firstly, the RGB image was preprocessed. The edge and texture of the RGB image were enhanced by Laplace transform. The light saturation removal (LSR) algorithm was used to improve the image quality. Secondly, the median filter was used to eliminate the salt and pepper noise of images.

In order to compare the performances of different image matching methods, 51 maize plants were collected synchronously by the binocular vision system at 90°, 54°, and 35°, respectively. Three algorithms, namely, SURF (Speeded-Up Robust Features), SIFT (Scale-Invariant Feature Transform), and ORB (Oriented Brief), were applied and discussed for RGB-NIR image matching. The optimal matching method was SURF, which was determined by matching time, PSNR (peak signal to noise ratio), MI (mutual information), and SSIM (structural similarity index).

The crops were segmented from the background by using the ExG (Extra Green) algorithm and maximum interclass variance algorithm (OTSU). The R, G, B, and NIR components of the segmented RGB images were extracted. Then, the NDVI of each pixel in the image was calculated, and the spatial distribution map of the crop VI was drawn. The SPAD values at pixel level were calculated. The regression model of SPAD values and NDVI showed that the determination coefficient was 0.619. The demonstration of the sensor application and results are shown in Fig. 8.7.

8.3.3.3 A Portable Multispectral Sensor for Crop Measurement

A 25-wavelength spectral imaging sensor (mode: XIMEAI-5 × 5-CMOS, Shanghai Branch of IMEC Microelectronics Co., Ltd., China) was used to develop a multi-spectral system for crop measurement, as shown in Fig. 8.8a (Liu et al. 2020). The filter of this sensor was processed on the wafer of a commercial application CMOS image capture chip that has a mosaic layout. There was a specific spectral filter on each pixel, and 25 wavelengths were placed on the COMSIS-CMV2000 sensor with two million pixels. This sensor was able to obtain spectral information of the

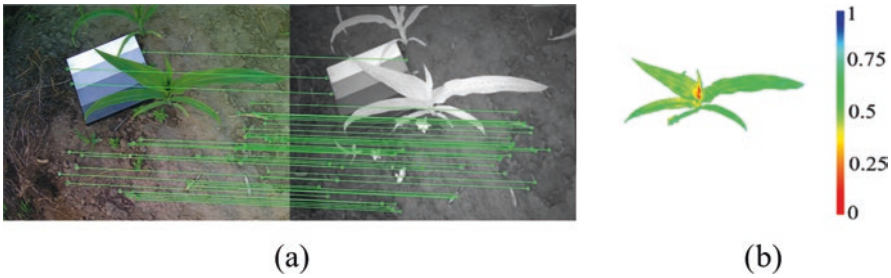

Fig. 8.7 Demonstration of the sensor application and results (Sun et al. 2019b). (**a**) Image matching (**b**) NDVI mapping

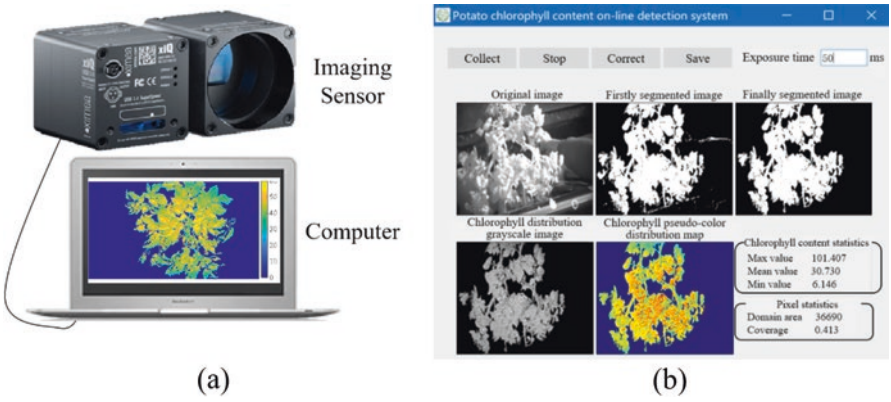

Fig. 8.8 Spectral sensor and control software of the detection system (Liu et al. 2020). (**a**) Spectral sensor (**b**) Control software interface

following 25 wavelengths: 666, 681, 706, 720, 732, 746, 759, 772, 784, 796, 816, 827, 837, 849, 859, 869, 887, 888, 902, 910, 920, 926, 935, 940, and 945 nm. The sensor had a field of view (FOV) of 50°. The image size of each wavelength was 409 pixels × 217 pixels, and the grayscale resolution was 10 bits.

In order to realize the real-time detection of SPAD values of potato plants in the field, a control software program was developed based on the Qt Creator 4.9.1 platform under a Windows operating environment. The user interface shown in Fig. 8.8b was designed based on the Qt Widgets application. The image processing functions were realized by calling the OpenCV libraries. The main functions of the software included the following: spectral image collection, exposure time adjustment, spectral image correction, SPAD value pseudo-color expression, SPAD value statistics, and image saving.

The spectral sensor and control software comprised the SPAD value real-time detection system. The reflectance of potato plants was extracted by the segmented mask images. The partial least squares (PLS) regression was employed to establish the SPAD value detection model based on sensitive variables selected using the

uninformative variable elimination (UVE) algorithm. So the visualization distribution map of SPAD values was drawn by pseudo-color processing technology.

8.4 Remote Sensing Platforms for Crop Monitoring

8.4.1 Remote Sensing Instruments Used in Crop Monitoring

Unlike spectral sensors introduced above, remote sensing spectrometers usually operate in Earth observation, capturing images as well as spectra from the observed materials. Images in wavebands make it possible to locate and extract plants from the background by image processing and derive numerous VIs. Great efforts have been made over the past decades to produce high-quality data in remote sensing by developing a wide range of imaging spectrometers placed on aerial/satellite platforms (Paoletti et al. 2019). Compared with near-ground platforms such as UAVs and stationary or handheld near-ground devices, which focus on specific fields or plants in small areas (Wang et al. 2019; Han et al. 2019), aerial and satellite remote sensing related to Earth observation is suitable for large farmland and ecosystem monitoring.

Efforts have been made over the past decades to produce high-quality data. These instruments could be classified into multispectral or hyperspectral devices according to the numbers of bands. A multispectral image contains from several to about a dozen bands, while a hyperspectral image (HSI) contains hundreds to thousands of contiguous wavelengths (Mishra et al. 2017). Several systems, shown in Table 8.6, are mostly used in aerial and satellite remote sensing. Similar to the spectral images mentioned before, the features extracted from remote sensing data include color features, texture presentation, shape and spatial description, and Vis-NIR spectral features.

8.4.2 Application of Multispectral Remote Sensing

Traditional satellite sensors such as SPOT and Landsat have long been used in crop sensing. The SPOT Vegetation sensor was carried aboard SPOT 4 and 5 which were launched in 1998 and 2002, respectively. It had the capability of imaging the entire Earth each day with IFOV (1.15 km) (https://eos.com/landsat-5-tm/). SPOT Vegetation collected data in four spectral bands in 0.43–0.47 μm, 0.61–0.68 μm, 0.78–0.89 μm, and 1.58–1.75 μm (Cayrol et al. 2000).

Landsat Thematic Mapper (TM) was a multispectral scanning radiometer that was carried on board Landsat 4 and 5. The TM sensors had provided nearly continuous coverage from July 1982 to June 2013. A TM scene had an instantaneous field of view (IFOV) of 30 m × 30 m in bands of visible (0.45–0.52 μm, 0.52–0.60 μm,

Table 8.6 Spectral imaging used in remote sensing

Type	Describe	Application	Reference
Multispectral remote sensing	SPOT 4 and 5, 0.40–0.89 μm, VIS/NIR/SWIR four bands	Yield (maize), grassland	Zhao et al. (2015) and Cayrol et al. (2000)
	Landsat 4 and 5, 0.45–2.35 μm, VIS/NIR/SWIR/thermal seven bands,	Yield (maize),	Zhao et al. (2015)
	Landsat 7, 0.45–2.35 μm, VIS/NIR/SWIR/thermal/PAN, eight bands	Yield (maize), crop classification	Zhao et al. (2015) and Zhong et al. (2019)
	Landsat 8, 0.43–2.29 μm, VIS/NIR/SWIR/thermal/PAN, nine bands	Crop classification, disease (wheat)	Zhong et al. (2019) and Ma et al. (2019)
	0.4–14.4 μm, 36 bands	Yield (wheat), Drought monitoring	Zhou et al. (2019) and Shen et al. (2019).
Hyper-spectral remote sensing	360–2450 nm, 224 bands, 10 nm	Disease (soybean)	Nagasubramanian et al. (2017)
	380–2510 nm, 430 bands, 5-nm interval	Crop classification	Salas et al. (2020)
	350–1050 nm, 288 bands	N stress (corn)	Goel et al. (2003)
	450–2500 nm, 125 bands	Nitrogen, disease (wheat)	Huang et al. (2004) and Mewes et al. (2011)

0.63–0.69 μm), NIR (0.76–0.90 μm), and SWIR (2.08–2.35 μm), while the band of 10.41–12.5 μm has an IFOV of 120 m × 120 m on the ground. The Landsat Enhanced Thematic Mapper Plus (ETM+) was introduced with Landsat 7 (https://eos.com/landsat-7/) and was built by Raytheon SBRS (Santa Barbara Remote Sensing), Goleta, CA. Except the visible and NIR bands of TM data, ETM also scans the bands of SWIR (1.57–1.75 μm, 2.09–2.35 μm), thermal infrared (10.40–12.50 μm), and a panchromatic (PAN) (0.52–0.90 μm).

The Operational Land Imager (OLI) and Thermal Infrared Sensor (TIRS) are instruments onboard the Landsat 8 satellite (https://eos.com/landsat-8/), in which OLI, built by the Ball Aerospace & Technologies Corporation, measures in the visible, NIR, and SWIR infrared portions of the spectrum. Therefore, Landsat 8 Instruments have nine spectral bands at 30-m spatial resolution including a PAN band: visible (0.43–0.45 μm, 0.450–0.51 μm, 0.53–0.59 μm), red (0.64–0.67 μm), NIR (0.85–0.88 μm), SWIR (1.57–1.65 μm, 2.11–2.29 μm), panchromatic (PAN) (0.50–0.68 μm), and cirrus (1.36–1.38 μm). It also has two thermal infrared sensors with bands of 10.6–11.19 μm and 11.5–12.51 μm at 100-m spatial resolution.

Using satellite remote sensing to understand maize yield gaps in the North China Plain with Quzhou County as an example, Zhao et al. (2015) used Landsat 5 TM, Landsat 7 ETM+, and SPOT 4 satellite data during the summer maize growing season from 2007 to 2013 with the exceptions of 2008 and 2011 when there was a lack of high-quality cloud-free images. In order to solve the spatial differences between SPOT 4 and Landsat data, Landsat images were resampled to 20-m resolution using

the nearest neighbor method. Results indicate that remote sensing can provide reasonably reliable estimates of maize yields in this region. In addition, the majority of yield gap is dominated by transient factors, and shrinking this gap may require high-quality forecasts to make informed optimal management decisions.

Satellite remote sensing also has been used in crop classification and disease monitoring. Zhong et al. (2019) used data from Landsat 7 ETM+ and Landsat 8 OLI at 3- m resolution to classify summer crops. Two types of deep learning models were designed using Landsat Enhanced Vegetation Index (EVI) time series. Three widely used classifiers were also tested for comparison, including a gradient boosting machine called XGBoost, Random Forest, and SVM. Among non-deep-learning classifiers, XGBoost achieved the best result with 84.17% accuracy and an F1 score of 0.69. The model employs EVI time series by examining shapes at various scales in a hierarchical manner. Ma et al. (2019) discriminated winter wheat powdery mildew and aphid infestations during a co-epidemic outbreak of the disease and the insect pest in northeast China based on temporal Landsat 8 imagery integrated with crop growth and environmental parameters.

Using satellite monitoring, the system notifies its users of critical changes in vegetation, sends real-time weather risk alerts, and automates the prioritization process within field work planning tasks. As a result, all of the abovementioned capabilities make it possible not to miss important points in the treatment of fields and to respond in a timely manner to any changes. So far, researchers have implemented agricultural projects for monitoring fields, classifying crops, identifying growth and stress status, and forecasting crop yields (Zhou et al. 2019; Shen et al. 2019).

8.4.3 Application of Hyperspectral Remote Sensing

Advances in sensing and computer technologies have achieved great improvement in hyperspectral image data acquisition. A number of HSI data missions for Earth Observation have been launched and provide new tools for satellite remote sensing, such as the NASA Hyperspectral Infrared Imager (HyspIRI), the Environmental Mapping and Analysis Program (EnMAP), and the Precursore IperSpettrale della Missione Applicativa (PRISMA) program (Paoletti et al. 2019). Meanwhile, several instruments are used in capturing great volumes of HSI data based on airborne remote sensing. As shown in Table 8.3, some of best-known spectrometers are available for crop sensing.

The Airborne Visible/Infrared Imaging Spectrometer (AVIRIS), developed by the Jet Propulsion Laboratory (JPL) (Pasadena, California, USA), was a hyperspectral imaging sensor that delivered calibrated images of upwelling spectral radiance in 224 contiguous spectral bands with wavelengths from 400 to 2500 nm (http://aviris.jpl.nasa.gov/). Moreover, the Airborne Visible Infrared Imaging Spectrometer-Next Generation (AVIRIS-NG) sensor samples 430 contiguous bands between 380 nm and 2510 nm at approximately 5-nm spectral resolution.

Nagasubramanian et al. (2017) identified the disease named charcoal rot in soybean crops using AVIRIS hyperspectral data. In the range of 383–1032 nm, they developed a 3D convolutional neural network (CNN) model for soybean charcoal rot disease identification. The classification accuracy was 95.73% and the infected class F1 score was 0.87. Salas et al. (2020) derived a set of narrow−/broadband indices from the AVIRIS-NG imagery to represent spectral variations and identify target classes and their distribution patterns. The results showed that the maximum entropy (MaxEnt) and generalized linear model (GLM) had strong discriminatory image classification abilities with area under the curve (AUC) values ranging between 0.75 and 0.93 for MaxEnt and between 0.73 and 0.92 for GLM. It was also found that the Photochemical Reflectance Index (PRI) and Moment Distance Ratio Right/Left (MDRRL) were important predictors for target classes such as wheat, legumes, and eggplant.

The Compact Airborne Spectrographic Imager 1500 (CASI 1500), designed by ITRES Research Ltd. (Calgary, Alberta, Canada), is a system that acquires data in 380–1050 nm and splits light into 288 discrete bands. It was used to obtain images over a field that had been set up to study the effects of various nitrogen application rates and weed control on corn (Goel et al. 2003). The results indicated that the reflectance of corn was significantly influenced ($\alpha = 0.05$) at certain wavelengths by the presence of weeds, the nitrogen rates, and their interaction. Differences in response due to nitrogen stress were most evident at 498 nm and in the band at 671 nm.

In addition, the HyMap scanner, built by Integrated Spectronics Pty Ltd. of Sydney, Australia, has four spectrometers in the interval of 450–2450 nm excluding the two major atmospheric water absorption windows. The research was conducted on estimating foliage nitrogen concentration from HyMap data using continuum-removal analysis (Huang et al. 2004). It identified the known nitrogen absorption features. The coefficient of determination increased from 0.65, using the standard derivative analysis, to 0.85 with the continuum-removal analysis. Mewes et al. (2011) indicted the potential to detect wheat disease induced by a pathogen infection. With the original spectral resolution of HyMap, the highest classification accuracy could be obtained by using 13 spectral bands with a Kappa coefficient of 0.59.

In summary, imaging spectrometers are of increasing importance for agricultural applications, particularly for the support of crop sensing that increases the productivity of crop stands (Zhou et al. 2019; Shen et al. 2019). However, to define an optimal sensor-based system or a data product designed for crop detection, it is necessary to know which spectral wavelengths are representative and which spectral resolution is needed. The methods of data processing also face the challenges from different instruments and requirements. Hence, research may involve data fusion and modelling supported by machine learning and even deep learning.

8.5 Precision Crop Management Based on Sensing Instruments

Spectroscopy and imaging sensors have been widely used to support precision agriculture by providing information for crop management (Zhang et al. 2018). It presents an automated solution of object recognition and detection in crop production, combined with technologies of machine vision and machine learning algorithms as well as deep learning systems (Gomes and Leta 2012; Kamilaris and Prenafeta-Boldú 2018). More and more agricultural robots have been developed based on crop sensing instruments and processing methods. They have been used in specific tasks that are traditionally performed manually in which manual methods have the disadvantages of being tedious and error-prone. Some recent advancements of crop sensors are applied in precision management in the field including variable sprayers for fertilizers and weed control and field-based crop phenotyping (Patricio and Rieder 2018).

8.5.1 Applications of Spectroscopy-Based Crop Sensors

8.5.1.1 Classification of Weeds and Damage Caused by Disease and Pests

Since reflectance of crops, weeds, and soil differs in the visual and NIR wavelengths, there is potential to distinguish them by spectral reflectance at different wavelengths. Vrindts et al. (2002) measured canopy reflectance of sugar beet, maize, and weeds with a line spectrograph (480–820 nm). Four wavelengths were selected to separate the sugar beet and weed plants including 572.7, 676.1, 801.4, and 814.6 nm. The overall classification accuracy was over 90%, while it had not shown good capability to classify maize and weeds with only 15% accuracy. Shirzadifar et al. (2018) selected bands around 1078, 1435, 1490, and 1615 nm to identify weeds of kochia, water hemp, and lamb's-quarters.

In order to design an optical weed sensor, sensitive wavelengths within the visible and NIR bands (496, 546, 614, 676, and 752 nm) were selected based on the spectral differences between stems and leaves of various crops and weeds (Wang et al. 2001). The partial least-squares (PLS) calibration model was established by the combination of these wavelengths and their VIs. The designed instrument with the embedded model could identify wheat, bare soil, and weeds with classification rates of 100%, 100%, and 71.6%, respectively, for the training data set when the weed density was above 0.02 plants/cm^2. Sui et al. (2008) developed a ground-based weed mapping system to measure weed intensity and distribution in a cotton field. It was used to directly output the canopy coverage and intensity ratio by connecting with a WeedSeeker sensor. The changes in leaf pigments and biochemical components caused by fungi infection or pest damage can influence the spectral characteristics of leaves, so that the spectral differences between healthy and damaged leaves

can be used to identify the plant health status. Various VIs are used in monitoring plant disease and pests such as NDVI, GNDVI, and OSAVI (Zhang et al. 2012, 2019a). Based on the fluorescence spectra, some studies applied the ratio of fluorescence (e.g., F686/F740) amplitude at fluorescence peaks to achieve presymptomatic detection for some pathogens (Bürling et al. 2012). Parameters associated with the saturation pulse method could be used to evaluate the changes of affected pigments, such as the maximum quantum efficiency of photosystem II (PSII) primary photochemistry (Fv/Fm), the maximum efficiency of PSII photochemistry in light-adapted material (Fv'/Fm′), and non-photochemical quenching (NPQ). Besides VIS-NIR and fluorescence spectroscopy, thermal observation provides an indicator to find the temperature changes of stressed symptoms from plant canopy.

The sensitive features are important for detection of diseases or pests. Naidu et al. (2009) discussed the spectral characteristics of grape infected by grapevine leafroll disease (GLD). The spectral differences between healthy and infected leaves are located around the green (near 550 nm), shortwave NIR (near 900 nm), and NIR (near 1600 and 2200 nm) bands. The classification models were built based on the sensitive wavelengths (531, 570, 752 nm, etc.) and VIs (NDVI, RVSI, PRI, etc.). Moreover, the results showed that compared with the linear regression result of 0.72 from RVSI, the accuracy increased to 0.78 when RVSI was combined with the reflectance in the blue band (470–490 nm) and 526 nm. In the same study, the classification accuracy was 0.75 by the variables that combined PRI with bands of 765–830, 970, and 684 nm.

Similarly, Annamalai and Lee (2004) investigated the spectral signatures of immature green citrus fruit and leaves for the purpose of developing a spectrally based fruit identification and early yield mapping system. Diffuse reflectance of fruit and leaf samples were measured in the range of 400–2500 nm, and two important wavelengths at 815 and 1190 nm were selected. A ratio of these two wavelengths was used to distinguish immature green fruit from leaves. Other researchers studying leaf miner damage, bacterial spots, and yellow rust of crop leaves had examined the sensitivity of spectral responses and characteristics and established identification models by partial least squares (PLS) regression, stepwise multiple linear regression (SMLR), support SVM, and so on (Moshou et al. 2014). Recently, more and more statistical analysis and machine learning modeling methods are applied. Deep learning, a part of machine learning, has also been applied to select the features or to build an end-to-end architecture for discriminant analysis.

8.5.1.2 Monitoring of Nutrient Content and Biomass Status

Crop growth status is generally evaluated by the nutrient content and biomass level, in which the contents of chlorophyll, nitrogen, and water are related to the nutrient level, and the biomass is generally estimated by the leaf area index (LAI) referred to a unit area or volume of habitat. The estimation of crop growth parameters using spectroscopy helps to guide the management of fertilizer and irrigation and predict the yield in the field.

The chlorophyll measurement has always been the priority of considerable research because chlorophyll is the organic molecule of plant leaves for photosynthesis and highly relates with leaf nitrogen in the 400–700 nm spectral range (Ulissi et al. 2011). Using the same spectral features shown in Table 8.1, a large number of researchers estimate the chlorophyll content by sensitive wavelengths, VIs, red-edge location, and others. Ciganda et al. (2009) constructed a red-edge chlorophyll index with red-edge (720–730 nm) and NIR (770–800 nm) spectral reflectance. Chen et al. (2010) proposed a new spectral indicator named Double-peak Canopy Nitrogen Index (DCNI) which was used for maize nitrogen estimation. Schlemmer et al. (2013) indicated that the chlorophyll content could be accurately retrieved using green and red-edge chlorophyll indices by the bands located in the NIR (780–800 nm) and either the green (540–560 nm) or red edge (730–750 nm). Rossini et al. (2012) estimated chlorophyll using a suite of VIs and found a high correlation of over 0.8 between leaf chlorophyll content and narrowband spectral indices. Sonobe et al. (2018) showed that shading treatment for a crop made the reflectance lower near the wavelengths of 550 and 740 nm. Two methods, machine learning algorithms and the inversion of a radiative transfer model, were evaluated using measurements from tea leaves. Overall, the kernel-based extreme learning machine had the highest performance with a root mean square error (RMSE) of 3.04 ± 0.52 μg cm^{-2} and the ratios of performance to deviation (RPD) from 3.38 to 5.92 for the test set.

The molecular absorption of hydrogen-containing groups (O-H, N-H, C-H) provides a potential to measure the moisture content nondestructively (Cheng et al. 2011). Although water absorption has been explored in the infrared region with spectral centers at 970, 1200, 1440, and 1950 nm (Palmer and Williams 1974), a series of researchers proposed different wavelengths due to the influences of species, phenology, environment stress, and so on. Dejonge et al. (2016) established a diagnosis model of corn water content to guide the field irrigation using the NDVI, OSAVI, and GNDVI. Among these VIs, the NDVI showed the best performance with highest R^2, slope almost equal to 1. So the vegetation ratios of water-stressed and non-stressed NDVI was set as an irrigation trigger with the threshold value of 0.93.

In addition, spectroscopy methods can be used to invert some biomass parameters and indirectly calculate LAI. Except the NDVI, other spectral indices have also been presented in recent research. Ray et al. (2006) found that VIs, NDVI, and SAVI (Soil-Adjusted Vegetation Index), calculated in the bands of 780–680 nm, produced the highest correlation coefficients with LAI. Han et al. (2016) built a model to predict the LAI of apple tree canopy by comparing SVM and random forest (RF) algorithms. Some VIs used in the RF regression model were in accordance with LAI in the full fruit period including GNDVI, NDIVI, RVI, and GRVI. Besides the VIS and NIR regions, Neinavaz et al. (2016) conducted some research in the thermal infrared region (TIR) and found that the canopy emissivity spectra increased with rising LAI.

In particular, the value of LAI could also be measured by an optical sensor, named LAI-2000 Plant Canopy Analyzer (LI-COR Biosciences, USA). It works by digital photography to show how canopy gap fraction measurements can be overestimated if measurements are taken when foliage is brightly lit (Han et al. 2016).

According to the studies mentioned above, the main methods include data preprocessing, sensitive parameter selection, and estimation modelling. The capabilities and performances of spectroscopy were explored for crop sensing. However, the methods used in data processing and the results were different, indicating that the sensors and algorithms used might influence the application significantly. Researchers will face further challenges on sensor integration and data fusion.

8.5.2 Applications of Imaging-Based Crop Sensors

8.5.2.1 Application of Ground-Based Imaging Instruments

Classification of Crops and Weeds

Focusing on the recognition of field weeds by different imaging sensors, Knoll et al. (2016a), used a time-of-flight (TOF) sensor, CamCube 3, to create depth images with a resolution of 204 × 204 pixels. In addition, more sensors were equipped on a field robot named *Bonirob*, including a Bispectral JAI camera, a Nikon D5300 camera, a Kinect II, and a laser scanner (Knoll et al. 2016b, c). The Bispectral JAI camera (JAI Ltd., Denmark) uses one lens for two cameras (RGB camera and IR camera) with 1296 × 966 pixels. The Nikon D5300 captures RGB images with a resolution of 6000 × 4000 pixels. Moreover, the Kinect II records a color image with the size of 1920 × 1080 pixels and an infrared image of 512 × 424 pixels. Meanwhile, the ToF technology allows a depth image of 512 × 424 pixels. In the research, the best performances were provided by the JAI camera and the Nikon camera. As a result, two VI determination methods based on RGB images were proposed by extracting color features of RGB and HSV (hue, saturation, value) (Knoll et al. 2016b).

However, the disturbances of results are the influences of, for example, weather, the various stages of growth, the large number of different weeds, and the different soil conditions. In order to eliminate these influences, a self-learning convolutional neural network was used for weed recognition in the field. This deep-learning approach achieved accuracy of over 98% (Knoll et al. 2018). Similarly, a classification model of weeds in organic carrot was proposed by using a convolutional neural network (CNN) to help in weed management (Knoll et al. 2019). Several proposed methods also indicated that deep learning could help to extract high-level features from images to improve the classification accuracy (Asad and Bais 2019; Peng et al. 2019).

Identification of Specialty Fruits

Harvesting of specialty fruits such as apples, citrus, cherries, and pears is highly labor intensive and is becoming less sustainable with increasing cost and decreasing availability of a skilled labor force (Gongal et al. 2015).

In order to help harvesting and yield prediction of specialty fruits, a digital SLR camera (EOS Rebel T2i, Canon Inc., Japan) with an 18–55 mm lens was used to collect the RGB images of field blueberry with 3648 × 2736 pixels. Li et al. (2014a, b) selected three color components, red (R), blue (B), and hue (H), to separate fruits of four maturity stages from background through different classifiers. The performances were discussed among the results of the K-nearest neighbor (KNN), naïve Bayesian classification (NBC), and supervised K-means clustering classifier (SK-means). In this work, the KNN classifier yielded the highest classification accuracy (85–98%) from the validation set.

In the immature green citrus fruit detection, Gan et al. (2018) built an imaging system to provide valuable information for yield estimation at earlier stages. The system consisted of two color cameras (USB 3.0, The Imaging Source, Charlotte, NC, USA) and a thermal camera (A655sc, FLIR, Wilsonville, OR, USA). Images from all three cameras had the same spatial resolution, 640 × 480 pixels, and very similar diagonal field of views of about 30°. A new Color-Thermal Combined Probability (CTCP) algorithm was created to effectively fuse information from the color and thermal images to classify potential image regions into fruit and non-fruit classes. The results present that the fusion of the color and thermal images effectively improved the accuracy of immature green citrus fruit detection. For the same aim, Okamoto and Lee (2009) used a hyperspectral camera of 369–1042 nm to acquire hyperspectral images of green fruits of three different citrus varieties (tangelo, Valencia, and Hamlin). Spatial image processing steps (noise reduction filtering, labeling, and area thresholding) were applied. The results of pixel identification tests showed that the detection success rates were 70–85%, depending on citrus varieties.

Measurement of Crop Growth Status

Three-dimensional cameras have been used to obtain the depth or position information. The Kinect camera has a normal webcam and a depth sensor which can provide RGB-D image. The depth sensor consisted of an infrared laser projector combined with a monochrome CMOS sensor that could detect the range of 0.8–4.0 m. Sa et al. (2016) used a Kinect camera to capture RGB and NIR images. A Faster Region-based CNN (Faster R-CNN) model was established to detect sweet peppers, which took into account both precision and recall performances improving from 0.807 to 0.838. Kang and Chen (2020) used a RealSense D-435 camera to collect RGB and depth images for apple detection in the orchard. From the experiment results, DaSNet-v2 with ResNet-101 achieved 0.868, 0.88, and 0.873 on recall and

precision of detection and accuracy of instance segmentation on fruits, respectively. In addition, it reached 0.794 on the accuracy of branch segmentation.

Although the measurement of plants is traditionally based on RGB images, the information of plant appearance is more accurately presented in 3D space, especially for geometry and topology. So the 3D imaging instruments are increasingly used in the crop phenotyping. LiDAR or laser sensors have been used to measure plant height and biomass because they present good adaptation to illumination and provide considerable data. LiDAR was adopted to measure the height and biomass of rice, oilseed rape, winter rye, winter wheat, and grassland (Tilly et al.,2015).

In order to estimate the nutrient content, an AD-130 GE bispectral camera (JAI Ltd., Denmark) was also used to capture multispectral images of RGB and NIR. Fifteen image parameters were extracted including the average gray values of images, the VIs (NDVI, NDGI, RVI, DVI), and image texture parameters (energy, moment of inertia, correlation, entropy, etc.). An SVM model was estimated to provide support for corn nutritional diagnosis and fertilization management decisions.

In order to evaluate the nitrogen content in oilseed rape (*Brassica napus* L.), Zhu et al. (2019) collected spectral images in 900–1700 nm wavebands using a hyperspectral camera, ImSpectorN17E (Spectral Imaging Ltd., Oulu, Finland). A fast nitrogen content grade classification method for oilseed rape canopy was established by employing a deep learning algorithm named stacked auto-encoders (SAEs). In this study, the SAE algorithm was introduced for the data dimensional reduction and feature extraction from hyperspectral images, and then the multiple classification models were applied for the feature testing and validation within the feature data under different camera angles with different feature units. Results showed that the best accuracy was presented by data captured under the 25° angle.

Hyper SIS (Zolix Instruments Co., Ltd., Beijing, China) is a hyperspectral camera to measure in the 369–988 nm band with a spectral resolution of 1.2 nm. It was used to detect the nitrogen detection of longan plants (Yue et al. 2018). The initial features were extracted using the principle component analysis (PCA) to identity a number of potential characteristic wavelengths (483, 518, 625, 631, 642, and 675 nm). Then the texture based on the gray-level co-occurrence matrix (GLCM) was extracted from those images. Combined with the state-of-the-art deep learning technology, a distribution model of chlorophyll content for longan leaves based on convolution neural networks (CNNs) and deep neural networks (DNNs) was proposed. As a result, the R^2 of the calibration and validation set were 0.84 and 0.82, respectively.

In the detection of rice panicle blast disease, Huang et al. (2017) measured images in the band of 400–1000 nm by using a Gaia Field-F-V10 (Spectral Imaging Ltd., Finland) spectrometer. A deep convolutional neural network model, Google Net, was used to learn the representation of hyperspectral image data. The proposed method achieved a classification accuracy of 92.0%. The same hyperspectral camera has also been used in the nutrient monitoring of water or chlorophyll content (Liu et al. 2018a, b; Zheng et al. 2018).

8.5.2.2 Application of UAV-Based Imaging Instruments

With the development of remote sensing technology, the advantages of UAVs acquiring farmland images are fast and convenient. Furthermore, the scope of acquisition is gradually becoming an important means and research hotspot for farmland information acquisition (Yang et al. 2014, 2017).

Different types of spectroscopic and image sensors for UAV have been developed, such as digital color sensors and multispectral/hyperspectral imaging sensors, further extending UAV-based remote sensing to various applications (Lu et al. 2019).

Crop Classification

Based on digital color cameras, Yang et al. (2014) designed a multispectral imaging system based on two identical consumer-grade cameras for agricultural remote sensing. The cameras are equipped with a full-frame CMOS sensor with 5616 × 3744 pixels. One camera captures normal color images, while the other is modified to obtain NIR images. Images are stored in 14-bit RAW and 8-bit JPEG files in CompactFlash cards. The system has been practically applied in estimating crop canopy cover, detecting cotton root rot, and mapping henbit and giant reed infestations.

In order to classify different crops, Ferreira et al. (2019) used a Phantom DJI 3 Professional drone (DJI Technology Co. Ltd., China) to collect RGB images with 4000 × 3000 pixels to train a model and achieved 97% accuracy in the discrimination of grass and broadleaf. Based on this goal, Wang et al. (2019) equipped a multispectral camera on a composite wing UAV to collect images of cotton, corn, and squash. A Micro MCA12 Snap (Tetracam, CA, USA) obtained images at 12 bands of 470, 515, 550, 610, 656, 710, 760, 800, 830, 860, 900, and 950 nm, with 1280 × 1024 pixels in each band. A CNN network was designed to extract features and classify crops. Compared with the SVM based on radial basis kernel function and the backpropagation neural network, the optimized CNN had the best effect and the highest classification accuracy of 97.75%.

Crop Detection

Due to the requirement of nutrient estimation, Qiao et al. (2019) estimated the chlorophyll content of maize. RGB images with a resolution of 7360 × 4912 pixels were collected by using ILCE-7R (Sony Corporation, Japan) equipped on a DJI M600 UAV platform. The parameters related to the color and texture features in the images were extracted after the canopy segmentation to reduce influences from the background. The established model had a determination coefficient of 0.76. The distribution map of chlorophyll content in field maize canopy was drawn based on a pseudo-color technique. It provided a tool to visually distinguish the field road and canopy area, showing the difference in chlorophyll distribution of the plot.

Potgieter et al. (2017) conducted the assessment of seasonal leaf area dynamics of sorghum breeding lines by using multispectral imaging from an UAV. A RedEdge™ narrowband multispectral camera (MicaSense Inc., USA) capturing five bands at specific nanometer (nm) wavelength peaks was fitted to the UAV platform. The bands captured were blue (B: 475 nm center wavelength, 20 nm bandwidth), green (G: 560 nm, 20 nm), red (R: 668 nm, 10 nm), red edge (RE: 717 nm, 10 nm), and near-infrared (NIR: 840 nm, 40 nm). The horizontal field of view was 47.2 degrees with a 5.5-mm focal length producing an image resolution of 1280 × 960 pixels. It was found that the good correlations between each VI (NDVI and EVI) and each growth parameter, such as plant number per plot, canopy cover, and LAI both during the vegetative growth phase (pre-anthesis) and at maximum canopy cover shortly after anthesis. The NDRE, which is used to estimate leaf chlorophyll content, was also the most useful in characterizing the leaf area dynamics/senescence patterns of contrasting genotypes.

Cen et al. (2019) discussed the use of a lightweight UAV with dual image-frame snapshot cameras to estimate aboveground biomass (AGB) and panicle biomass (PB) of rice at different growth stages with different nitrogen (N) treatments. An RGB camera (NEX-7 camera, Sony Corporation, Japan) with a spatial resolution of 6000 × 4000 pixels and a snapshot multispectral camera (CMV2 K CMOS, IMEC, Chatsworth, Leuven, Belgium) with a spatial resolution of 409 × 216 pixels coupled with a three-axis gimbal were mounted on the UAV. The multispectral camera contains 25 wavelengths in the spectral region of 600–1000 nm (679, 693, 719, 732, 745, 758, 771, 784, 796, 808, 827, 839, 84, 860, 871, 880, 889, 898, 915, 922, 931, 937, 944, 951, and 956 nm). It was found that the canopy height extracted from the crop surface model exhibited a high correlation with the ground-measured canopy height, and several VIs were highly correlated with AGB.

These applications show that imaging instruments are being widely used onboard UAVs for collecting spectral and spatial information that allows the generation of maps to indicate the aspects of the plant state. Due to the availability of NIR wavelengths in multispectral images, spectral images have also become an indispensable tool for evaluating the physiological- and biochemical-related parameters of plants, such as LAI, vegetation fraction, nitrogen (N) and chlorophyll status, net photosynthesis, and biomass.

8.5.3 Variable-Rate Fertilizer Management Based on Crop Sensors

8.5.3.1 Variable-Rate Fertilizer Mapping Based on Imaging Instruments

In order to further extend the functions of the crop growth detector, a WSN-based detection system was proposed to measure crop spectral characteristics on the go and in real time as shown in Fig. 8.9. The controller was an industrial personal computer (IPC) with an attached ZigBee wireless communication module (JN5139

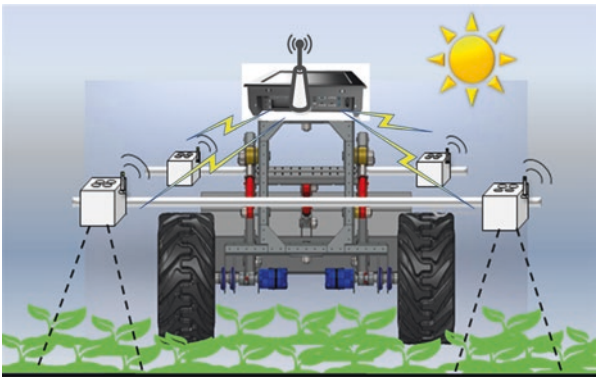

Fig. 8.9 Structure of the vehicle-mounted crop detection system

module). As the coordinator of the whole wireless network, it was used to establish the wireless network, waiting for sensor nodes to join in, and receiving, displaying, and storing all the data from different sensor nodes.

The measuring unit consisted of several optical sensors, and each optical sensor was used as a sensor node in this WSN. Each sensor node consisted of an optical part and a circuit part. The optical part contained eight optical channels at four wavebands. Since the detection system used sunlight as a light source, besides the reflected light from crop canopy, the sunlight intensity should also be measured as a reference. Therefore, two solutions were put forward:

1. A full-function sensor node had to contain eight optical channels, upward four for the sunlight and downward four for the reflected light.
2. As shown in Fig. 8.9, one sensor node was selected to measure the sunlight as the type I sensor, and other sensor nodes were used to measure the reflected light as the type II sensors.

As discussed above, the independence of the sensor (type I) was selected to measure the sunlight, and then the whole network shared the sunlight data. Under the premise of measurement precision, this type of design greatly reduced the cost of the system. Thus, sensors and the controller can set up a communication network in many ways. The networking mode between handheld and vehicle-mounted systems can be transformed into each other. The transmission distances can be up to hundreds of meters, which realized the real-time, continuous measurements of crops in the field. Furthermore, it increased the flexibility of the detector installation.

The new system increased the optical channels and was realized to measure the crop spectral characteristics on the go and in real time after being installed on an on-board mechanical structure (Zhong et al. 2014). Referring to the field test in Shaanxi Province, China, the distribution of the chlorophyll content of wheat detected by the new system is shown in Fig. 8.10a (Sun et al. 2015). In this way, it

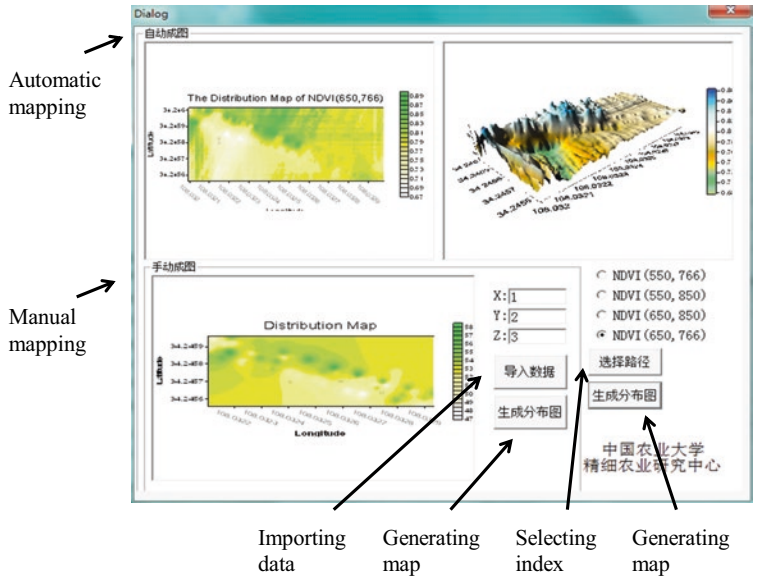

(a)

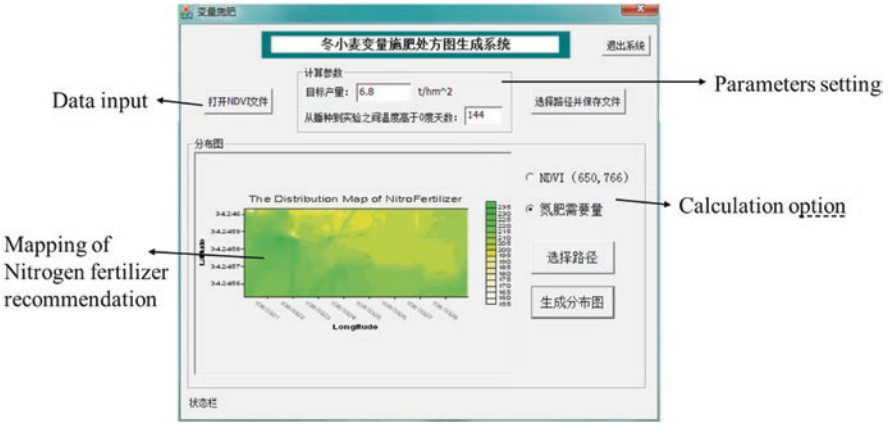

(b)

Fig. 8.10 Variable-rate fertilizer mapping based on imaging instruments (**a**) Distribution of chlorophyll content of wheat (Sun et al. 2015). (**b**) Fertilizer recommendation mapping

provides the automatic mapping of comprehensive growth status in the field. Combined with the fertilizer decision strategy such as the yield prediction method, the fertilizer recommendation map could also be used as an output as shown in Fig. 8.10b.

8.5.3.2 Variable-Rate Fertilizer Control Based on Crop Sensing

Variable-rate fertilization technology improves the operational efficiency and utilization rate of a fertilizer and accelerates the sustainable development of modern agriculture to promote high-yield, superior-quality production while ensuring sufficient environmental protection. The crop sensors discussed in this chapter show the great potential to control the fertilizer rate in the field. Therefore, lots of variable-rate fertilizer applicators or sprayers are developed based on those sensors.

Commercial products, such as GreenSeeker products (Trimble Navigation Limited, Sunnyvale, CA, USA), Crop Circle devices (Holland Scientific Inc., Lincoln, Nebraska, USA) and Yara N-Sensors (Yara International ASA, Germany), promote solutions for variable-rate fertilization. However, the models of crop estimation and fertilizer decision are fixed in such systems. Hence, it might limit the applications of specific requirements such as crop diversities or regions.

In order to provide a more flexible system for precision fertilization, the multi-fusion sensor which was developed based on the combination of spectroscopy and imagery technology was applied in a fertilizer sprayer by China Agricultural University (Sun et al. 2018). The sensor was designed to measure the spectral reflectance in the red and NIR ranges, such as 610, 680, 730, 760, 810, and 860 nm, each with 20 nm of full-width half-max detection. More than ten kinds of VIs could be calculated by these data for crop monitoring. It means that the sensor could provide more flexible and modifiable models for different requirements of crop estimation. The RGB image was captured to estimate the canopy coverage so as to help determine the location during field measurement. The transmission method had been modified from the Wi-Fi to the CAN-bus, which has the advantages of long data-transmitting distance, fast speed, reliable transmit, and low cost. The sensing system is shown in Fig. 8.11a. A GPS model helps to record the detecting location, one of the sensors is used to calibrate the changes of sunlight, and crop sensors transmit data to the IPC by CAN-bus.

Generally, as shown in Fig. 8.11b during the fertilization process, the NDVI values of the crop canopy are acquired in real time by crop sensors. These values are transmitted to the vehicle-mounted IPC terminal through the CAN-bus cable. A variable-rate fertilization expert decision system preset into the IPC is run based on the model to generate optimal fertilizer rate in real time.

In this chapter, sensing principles and applied sensors based on spectroscopy and imagery are reviewed. Some developed sensors have been introduced and demonstrated to show the frontier research in this area. Numerous researchers in the cited literature have documented the practical applications of these sensors in many scenarios, including handheld detection, vehicle-mounted diagnosis, and remote sensing by UAVs or satellites, to build reliable prediction models of complex and uncertain phenomena in agriculture. With the integration of variable-rate technology, more and more precision management measures can be taken based on crop sensing methods. Recently, more and more new sensors and machine learning methods are applied in crop monitoring. These applications show the new trends for crop sensing. Smart crop sensors with artificial intelligence (AI) processors or deep learning models should emerge soon to improve the sensing accuracy or broaden the applications in the future.

Fig. 8.11 Variable-rate fertilizer control based on crop sensing (**a**) Sensing system used in a fertilizer sprayer (**b**) Variable-fertilizer sprayer

References

Ali H, Lali MI, Nawaz MZ, Sharif M, Saleem BA (2017) Symptom based automated detection of citrus diseases using color histogram and textural descriptors. Comput Electron Agric 138:92–104

Annamalai P, Lee WS (2004) Identification of green citrus fruits using spectral characteristics, ASAE paper no. FL04-1001. ASAE, St. Joseph, Mich

Asad MH, Bais A (2019) Weed detection in canola fields using maximum likelihood classification and deep convolutional neural network. Information Processing in Agriculture. https://doi.org/10.1016/j.inpa.2019.12.002

Barbedo JG (2016) A review on the main challenges in automatic plant disease identification based on visible range images. Biosyst Eng 144:52–60

Bauriegel E, Brabandt H, Garber U, Herppicha WB (2014) Chlorophyll fluorescence imaging to facilitate breeding of *Bremia lactucae*-resistant lettuce cultivars. Comput Electron Agric 105:74–82

Bürling K, Hunsche M, Noga G (2012) Presymptomatic detection of powdery mildew infection in winter wheat cultivars by laser-induced fluorescence. Appl Spectrosc 66(12):1411–1419
Calderón R, Navas-Cortés JA, Lucena C, Zarco-Tejada PJ (2013) High-resolution airborne hyperspectral and thermal imagery for early detection of *Verticillium* wilt of olive using fluorescence, temperature and narrow-band spectral indices. Remote Sens Environ 139:231–245
Cao Q, Cui Z, Chen X, Khosla R, Dao TH, Miao Y (2012) Quantifying spatial variability of indigenous nitrogen supply for precision nitrogen management in small scale farming. Precis Agric 13:45–61
Cao Q, Miao Y, Huang S, Wang H, Khosla R, Jiang R (2013) Estimating rice nitrogen status with the crop circle multispectral active canopy sensor. In: Stafford JV (ed) Precision agriculture '13. Wageningen Academic Publishers, Wageningen, pp 95–101
Cao Q, Miao Y, Li F, Gao X, Liu B, Lu D, Chen X (2017) Developing a new crop circle active canopy sensor-based precision nitrogen management strategy for winter wheat in North China plain. Precis Agric 18(1):2–18
Cayrol P, Chehbouni A, Kergoat L, Dedieu G, Mordelet P, Nouvellon Y (2000) Grassland modeling and monitoring with SPOT-4 VEGETATION instrument during the 1997-1999 SALSA experiment. Agric For Meteorol 105(1–3):91–115
Cen H, Wan L, Zhu J, Li Y, Li X, Zhu Y, Weng H, Wu W, Yin W, Xu C, Bao Y, Feng L, Shou J, He Y (2019) Dynamic monitoring of biomass of rice under different nitrogen treatments using a lightweight UAV with dual image-frame snapshot cameras. Plant Methods 15(1). https://doi.org/10.1186/s13007-019-0418-8
Chen D, Huang J, Jackson TJ (2005) Vegetation water content estimation for corn and soybeans using spectral indices derived from MODIS near- and short-wave infrared bands. Remote Sens Environ 98(2):225–236
Chen PF, Haboudance D, Tremblay N, Wang JH, Vigneault P, Li BG (2010) New spectral indicator assessing the efficiency of crop nitrogen treatment in corn and wheat. Remote Sens Environ 114(9):1987–1997
Cheng T, Rivard B, Sanchez-Azofeifa A (2011) Spectroscopic determination of leaf water content using continuous wavelet analysis. Remote Sens Environ 115(2):659–670
Cheng M, Zhang J, Li M, Liu H, Sun H, Zheng T (2017) Chlorophyll content diagnosis model of winter wheat at heading stage applied in miniature spectrometer. Trans Chinese Soc Agric Eng 33(z1):157–163
Ciganda V, Gitelson A, Schepers J (2009) Non-destructive determination of maize leaf and canopy chlorophyll content. J Plant Physiol 166(2):157–167
Cui D, Zhang Q, Li M, Zhao Y, Hartman GL (2009) Detection of soybean rust using a multispectral image sensor. Sens & Instrumen Food Qual 3(1):49–56
Dejonge KC, Mefford BS, Chavez JL (2016) Assessing corn water stress using spectral reflectance. J Remote Sens 37(10):2294–2312
Ferreira AD, Freitas DM, da Silva GG, Pistori H, Folhes MT (2019) Unsupervised deep learning and semi-automatic data labeling in weed discrimination. Comput Electron Agric 165:104963
Gan H, Lee WS, Alchanatis V, Ehsani R, Schueller JK (2018) Immature green citrus fruit detection using color and thermal images. Comput Electron Agric 152:117–125
Garcia JA, Pope C, Altimiras F (2017) A distributed K-means segmentation algorithm applied to Lobesia botrana recognition. Complexity. https://doi.org/10.1155/2017/5137317
Gholizadeh A, Saberioon M, Borůvka L, Wayayok A, Soom MAM (2017) Leaf chlorophyll and nitrogen dynamics and their relationship to lowland rice yield for site-specific paddy management. Inform Process Agric 4(4):259–268
Goel PK, Prasher SO, Landry JA, Patel RM, Bonnell RB, Viau AA, Miller JR (2003) Potential of airborne hyperspectral remote sensing to detect nitrogen deficiency and weed infestation in corn. Comput Electron Agric 38(2):99–124
Gomes JFS, Leta FR (2012) Applications of computer vision techniques in the agriculture and food industry: a review. Eur Food Res Technol 235(6):989–1000

Gongal A, Amatya S, Karkee M, Zhang Q, Lewis K (2015) Sensors and systems for fruit detection and localization: a review. Comput Electron Agric 116:8–19

Han Z, Zhu X, Fang X, Wang Z, Wang L, Zhao G, Jiang Y (2016) Hyperspectral estimation of apple tree canopy LAI based on SVM and RF regression. Spectrosc Spectr Anal 36(3):800–805

Han L, Zhang Y, Qin Q (2019) Endmember extraction of farmland hyperspectral image using deep learning autoencoder and shuffled frog leaping algorithm. Trans Chinese Soc Agric Eng 35(6):167–173

Huang Z, Turner BJ, Dury SJ, Wallis IR, Foley WJ (2004) Estimating foliage nitrogen concentration from HYMAP data using continuum removal analysis. Remote Sens Environ 93(1):18–29

Huang J, Liao H, Zhu Y, Sun J, Sun Q, Liu X (2012) Hyperspectral detection of rice damaged by rice leaf folder (*Cnaphalocrocis medinalis*). Comput Electron Agric 82:100–107

Huang S, Sun C, Qi L, Ma X, Wang W (2017) Rice panicle blast identification method based on deep convolution neural network. Trans Chinese Soc Agric Eng 33(20):169–176

Jawad HM, Nordin R, Gharghan SK, Jawad AM, Ismail M (2017) Energy-efficient wireless sensor networks for precision agriculture: a review. Sensors 17(8):1781

Jiang H, Wang P, Zhang Z, Mao W, Zhao B, Qi P (2018) Fast identification of field weeds based on deep convolutional network and binary hash code. Trans Chinese Soc Agric Machin 49(11):30–38

Kamilaris A, Prenafeta-Boldú FX (2018) Deep learning in agriculture: a survey. Comput Electron Agric 147(1):70–90

Kang H, Chen C (2020) Fruit detection, segmentation and 3D visualisation of environments in apple orchards. Comput Electron Agric 171:105302

Kebapci H, Yanikoglu B, Unal G (2011) Plant image retrieval using color, shape and texture features. Comput J 54(9):1475–1490

Knoll FJ, Holtorf T, Hussmann S (2016a) Investigation of different plant root exit point vector search algorithms in organic farming. IEEE Trans Instrum Meas 65(5):1035–1041

Knoll FJ, Holtorf T, Hussmann S (2016b) Vegetation index determination method based on color room processing for weed control applications in organic farming. In: 2016 IEEE international instrumentation and measurement technology conference proceedings. https://doi.org/10.1109/I2MTC.2016.7520508

Knoll FJ, Holtorf T, Hussmann S (2016c) Investigation of different sensor systems to classify plant and weed in organic farming applications. SAI Comput Conference. https://doi.org/10.1109/SAI.2016.7556004

Knoll FJ, Czymmek V, Poczihoski S, Holtorf T, Hussmann S (2018) Improving efficiency of organic farming by using a deep learning classification approach. Comput Electron Agric 153:347–356

Knoll FJ, Czymmek V, Harders LO, Hussmann S (2019) Real-time classification of weeds in organic carrot production using deep learning algorithms. Comput Electron Agric 167:105097

Kuckenberg J, Tartachnyk I, Noga G (2009) Detection and differentiation of nitrogen-deficiency, powdery mildew and leaf rust at wheat leaf and canopy level by laser-induced chlorophyll fluorescence. Biosyst Eng 103(2):121–128

Latif A, Rasheed A, Sajid U, Ahmed J, Ali N, Ratyal NI, Zafar B, Dar SH, Sajid M, Khalil T (2019) Content-based image retrieval and feature extraction: a comprehensive review. Math Problems Eng:2019. https://doi.org/10.1155/2019/9658350

Li H, Lee WS, Wang K (2014a) Identifying blueberry fruit of different growth stages using natural outdoor color images. Comput Electron Agric 106:91–101

Li L, Zhang Q, Huang D (2014b) A review of imaging techniques for plant phenotyping. Sensors 14(11):20078–20111

Liu B, Zhang Y, He D, Li Y (2017) Identification of apple leaf diseases based on deep convolutional neural networks. Symmetry 2017:10(1). https://doi.org/10.3390/sym10010011

Liu H, Li M, Zhang J, Gao D, Sun H, Yang L (2018a) Estimation of chlorophyll content in maize canopy using wavelet denoising and SVR method. Int J Agric Biol Eng 11(6):132–137

Liu N, Wu L, Chen L, Sun H, Dong Q, Wu J (2018b) Spectral characteristics analysis and water content detection of potato plants leaves. IFAC-PapersOnLine 51(17):541–546
Liu N, Liu G, Sun H (2020) Real-time detection on SPAD value of potato plant using an in-field spectral imaging sensor system. Sensors 20(12):3430. https://doi.org/10.3390/s20123430
Long Y (2020) Development of crop condition detection system based on spectrum fusion. Master's thesis, China Agricultural University, Beijing, China
Lowe DG (2004) Distinctive image features from scale-invariant keypoints. Int J Comput Vis 60(2):91–110
Lu N, Zhou J, Han Z, Li D, Cao Q, Yao X, Tian Y, Zhu Y, Cao W (2019) Improved estimation of aboveground biomass in wheat from RGB imagery and point cloud data acquired with a low-cost unmanned aerial vehicle system. Plant Methods 15(1):17. https://doi.org/10.1186/s13007-019-0402-3
Luo J, Huang W, Zhao J, Zhang J, Zhao C, Ma R (2013) Detecting aphid density of winter wheat leaf using hyperspectral measurements. IEEE Journal of Selected Topics in Applied Earth Observations and Remote Sensing 6(2):690–698
Ma H, Huang W, Jing Y, Yang C, Han L, Dong Y, Ye H, Shi Y, Zheng Q, Liu L, Ruan C (2019) Integrating growth and environmental parameters to discriminate powdery mildew and aphid of winter wheat using bi-temporal Landsat-8 imagery. Remote Sens 11(7):846
Maimaitijiang M, Sagan V, Sidike P, Hartling S, Esposito F, Fritschi FB (2020) Soybean yield prediction from UAV using multimodal data fusion and deep learning. Remote Sens Environ 237(2):111599
Mavridou E, Vrochidou E, Papakostas GA, Pachidis T, Kaburlasos VG (2019) Machine vision systems in precision agriculture for crop farming. J Imag 5(12):89
Mewes T, Franke J, Menz G (2011) Spectral requirements on airborne hyperspectral remote sensing data for wheat disease detection. Precis Agric 12:795–812
Mishra P, Asaari MSM, Herrero-Langreo A, Lohumi S, Diezma B, Scheunders P (2017) Close range hyperspectral imaging of plants: a review. Biosyst Eng 164:49–67
Moshou D, Pantazi X, Kateris D, Gravalos I (2014) Water stress detection based on optical multisensor fusion with a least squares support vector machine classifier. Biosyst Eng 117:15–22
Munoz-Huerta RF, Guevara-Gonzalez RG, Contreras-Medina LM, Torres-Pacheco I, Prado-Olivarez J, Ocampo-Velazquez RV (2013) A review of methods for sensing the nitrogen status in plants: advantages, disadvantages and recent advances. Sensors 13(8):10823–10843
Nagasubramanian K, Jones S, Singh AK, Singh A, Ganapathysubramanian B, Sarkar S (2017) Explaining hyperspectral imaging based plant disease identification: 3D CNN and saliency maps. 31st Conference on Neural Information Processing Systems (NIPS 2017), Long Beach, CA, USA
Naidu RA, Perry EM, Pierce FJ, Mekuria T (2009) The potential of spectral reflectance technique for the detection of *grapevine leafroll-associated virus-3* in two red-berried wine grape cultivars. Comput Electron Agric 66(1):38–45
Narvaez FY, Reina G, Torres-Torriti M, Kantor G, Cheein FA (2017) A survey of ranging and imaging techniques for precision agriculture phenotyping. IEEE-ASME Trans Mechatron 222(6):2428–2439
Neinavaz E, Darvishzadeh R, Skidmore AK, Groen TA (2016) Measuring the response of canopy emissivity spectra to leaf area index variation using thermal hyperspectral data. Int J Appl Earth Obs Geoinform 53:40–47
Netto AT, Campostrini E, De Oliveira JG, Bressan-SmithR.E. (2005) Photosynthetic pigments, nitrogen, chlorophyll a fluorescence and SPAD-502 readings in coffee leaves. Sci Hortic 104(2):199–209
Okamoto H, Lee WS (2009) Green citrus detection using hyperspectral imaging. Comput Electron Agric 66(2):201–208
Oppenheim D, Edan Y, Shani G (2017) Detecting tomato flowers in greenhouses using computer vision. World Acad Sci Eng Technol/Int J Comput Electric Autom Contr Inform Eng 11(1):104–109

Pajares G, Garcia-Santillan I, Campos Y, Montalvo M, Guerrero JM, Emmi L, Romeo J, Guijarro M, Gonzalez-de-Santos P (2016) Machine-vision systems selection for agricultural vehicles: a guide. J Imag 2(4):34

Pallottino F, Antonucci F, Costa C, Bisaglia C, Figorilli S, Menesatti P (2019) Optoelectronic proximal sensing vehicle-mounted technologies in precision agriculture: a review. Comput Electron Agric 162:859–873

Palmer KF, Williams D (1974) Optical properties of water in the near infrared. J Opt Soc Am 64(8):1107–1110

Paoletti ME, Haut JM, Plaza J, Plaza A (2019) Deep learning classifiers for hyperspectral imaging: a review. ISPRS J Photogramm Remote Sens 158:279–317

Patricio DI, Rieder R (2018) Computer vision and artificial intelligence in precision agriculture for grain crops: a systematic review. Comput Electron Agric 153:69–81

Peng M, Xia J, Peng H (2019) Efficient recognition of cotton and weed in field based on faster R-CNN by integrating FPN. Trans Chinese Soc Agric Eng 35(20):202–209

Potgieter A, George-Jaeggli B, Chapman SC, Laws K, Suárez Cadavid LA, Wixted J, Watson J, Eldridge M, Jordan DR, Hammer GL (2017) Multi-spectral imaging from an unmanned aerial vehicle enables the assessment of seasonal leaf area dynamics of sorghum breeding lines. Front Plant Sci 8:1532

Priyankara HA, Withanage DK (2015) Computer assisted plant identification system for android. Moratuwa Engineering Research Conference. https://doi.org/10.1109/MERCon.2015.7112336

Qiao L, Zhang Z, Chen L, Sun H, Li M, Li L, Ma J (2019) Detection of chlorophyll content in maize canopy from UAV imagery. IFAC-Papers OnLine 52(30):330–335

Ray SS, Das G, Singh JP, Panigrahy S (2006) Evaluation of hyperspectral indices for LAI estimation and discrimination of potato crop under different irrigation treatments. Int J Remote Sens 27(24):5373–5387

Rossini M, Cogliati S, Meroni M, Migliavacca M, Galvagno M, Busetto L, Cremonese E, Julitta T, Siniscalco C, Morra di Cella U, Colombo R (2012) Remote sensing-based estimation of gross primary production in a subalpine grassland. Biogeosciences 9(7):2565–2584

Sa I, Ge ZY, Dayoub F, Upcroft B, Perez T, McCool C (2016) DeepFruits: a fruit detection system using deep neural networks. Sensors 16(8):122

Salas EAL, Subburayalu SK, Slater B, Zhao K, Bhattacharya B, Tripathy R, Das A, Nigam R, Dave R, Parekh P (2020) Mapping crop types in fragmented arable landscapes using AVIRIS-NG imagery and limited field data. Int J Image Data Fusion 11(1):33–56

Sankaran S, Mishra A, Ehsani R, Davis C (2010) A review of advanced techniques for detecting plant diseases. Comput Electron Agric 72(1):1–13

Schepers JS, Francis DD, Vigil M, Below FE (1992) Comparison of corn leaf nitrogen concentration and chlorophyll meter readings. Commun Soil Sci Plant Anal 23(17–21):2173–2187

Schlemmer M, Gitelson A, Schepers J, Ferguson R, Peng Y, Shanahan J, Rundquist D (2013) Remote estimation of nitrogen and chlorophyll contents in maize at leaf and canopy levels. Int J Appl Earth Obs Geoinf 25:47–54

Serrano JM, Shahidian S, da Silva JRM (2016) Monitoring pasture variability: optical OptRx ® crop sensor versus Grassmaster II capacitance probe. Environ Monit Assess 188(2):117

Sharabian VR, Noguchi N, Hanya I, Ishii K (2013) Evaluation of an active remote sensor for monitoring winter wheat growth status. Eng Agric Environ Food 6(3):118–127

Shen R, Huang A, Li B, Guo J (2019) Construction of a drought monitoring model using deep learning based on multi-source remote sensing data. Int J Appl Earth Obs Geoinf 79(7):48–57

Shirzadifar A, Bajwa S, Mireei SA, Howatt K, Nowatzki J (2018) Weed species discrimination based on SIMCA analysis of plant canopy spectral data. Biosyst Eng 171:143–154

Singh M, Kumar R, Sharma A, Singh B, Thind SK (2015) Calibration and algorithm development for estimation of nitrogen in wheat crop using tractor mounted N-sensor. Sci World J:163968. https://doi.org/10.1155/2015/163968

Singh A, Ganapathysubramanian B, Singh AK, Sarkar S (2016) Machine learning for high-throughput stress phenotyping in plants. Trends Plant Sci 21(2):110–124

Singh AK, Ganapathysubramanian B, Sarkar S, Singh A (2018) Deep learning for plant stress phenotyping: trends and future perspectives. Trends Plant Sci 23(10):883–898
Sonobe R, Sano T, Horie H (2018) Using spectral reflectance to estimate leaf chlorophyll content of tea with shading treatments. Biosyst Eng 175:168–182
Stoll M, Schultz HR, Baecker G, Berkelmann-LoehnertzB (2008) Early pathogen detection under different water status and the assessment of spray application in vineyards through the use of thermal imagery. Precis Agric 9(6):407–417
Sui R, Thomasson JA, Hanks J, Wooten J (2008) Ground-based sensing system for weed mapping in cotton. Comput Electron Agric 60(1):31–38
Sun H, Wu Q, Li M, Zhao R, Zheng L (2013) Development of crop monitoring system using 2-channel CCD image sensor. 2013 ASABE annual international meeting, Kansas City, Missouri, July 21, 2013, paper number: 131620020
Sun H, Zhang M, Pei X, Yang W, Wen Y, Zhao Y, Li M (2015) Development of a spectral measurement system for crop detection. 2015 ASABE annual international meeting, New Orleans, Louisiana, July 26-29, 2015, paper number: 152188957
Sun Z, Sun H, Liu H, Zhang J, Che L, Li M, Zheng L, Wang X (2018) Performance test and parameter optimization of variable spraying liquid fertilizer machine. IFAC-PapersOnLine 51(17):118–123
Sun H, Liu N, Xing Z, Zhang Z, Li M, Wu J (2019a) Parameter optimization of potato spectral response characteristics and growth stage identification. Spectrosc Spectr Anal 39(6):1870–1877
Sun H, Xing Z, Zhang Z, Ma X, Long Y, Liu N, Li M (2019b) Visualization analysis of crop spectral index based on RGB-NIR image matching. Spectrosc Spectr Anal 39(11):3493–3500
Tartachnyk II, Rademacher I, Kuhbauch W (2006) Distinguishing nitrogen deficiency and fungal infection of winter wheat by laser-induced fluorescence. Precis Agric 7(4):281–293
Taskos DG, Koundouras S, Stamatiadis S, Zioziou E, Nikolaou N, Karakioulakis K, TheodorouN (2015) Using active canopy sensors and chlorophyll meters to estimate grapevine nitrogen status and productivity. Precis Agric 16(1):77–98
Tilly N, Aasen H, Bareth G (2015) Fusion of plant height and vegetation indices for the estimation of barley biomass. Remote Sens 7(9):11449–11480
Toth C, Joźkow G (2016) Remote sensing platforms and sensors: a survey. ISPRS J Photogramm Remote Sens 115:22–36
Tremblay N, Wang Z, Ma B, Belec C, Vigneault P (2009) A comparison of crop data measured by two commercial sensors for variable-rate nitrogen application. Precis Agric 10(2):145–161
Uddling J, Gelang-Alfredsson J, Piikki K, Pleijel H (2007) Evaluating the relationship between leaf chlorophyll concentration and SPAD-502 chlorophyll meter readings. Photosynth Res 91(1):37–46
Ulissi V, Antonucci F, Benincasa P, Farneselli M, Tosti G, Guiducci M, Tei F, Costa C, Pallottino F, Pari L, Menesatti P (2011) Nitrogen concentration estimation in tomato leaves by VIS-NIR non-destructive spectroscopy. Sensors 11(6):6411–6424
Vrindts E, De Baerdemaeker J, Ramon H (2002) Weed detection using canopy reflection. Precis Agric 3(1):63–80
Waldchen J, Mader P (2018) Plant species identification using computer vision techniques: a systematic literature review. Arch Comput Methods Eng 25(2):507–543
Wang N, Zhang N, Dowell FE, Sun Y, Peterson DE (2001) Design of an optical weed sensor using plant spectral characteristics. Trans ASAE 44(2):409–419
Wang C, Zhao Q, Ma Y, Ren Y (2019) Crop identification of drone remote sensing based on convolutional neural network. Trans Chinese Soc Agric Machin 50(11):161–168
Wu Q, Sun H, Li M, Song Y, Zhang Y (2015) Research on maize multispectral image accurate segmentation and chlorophyll index estimation. Spectrosc Spectr Anal 35(1):178–183
Xiong D, Chen J, Yu T, Gao W, Ling X, Li Y, Peng S, Huang J (2015) SPAD-based leaf nitrogen estimation is impacted by environmental factors and crop leaf characteristics. Sci Rep 5(1):13389
Xu H, Ying Y, Fu X, Zhu S (2007) Near-infrared spectroscopy in detecting leaf miner damage on tomato leaf. Biosyst Eng 96(4):447–454

Yang C, Westbrook JK, Suh C, Martin DE, Hoffmann WC, Lan Y, Fritz BK, Goolsby JA (2014) An airborne multispectral imaging system based on two consumer-grade cameras for agricultural remote sensing. Remote Sens 6(6):5257–5278

Yang G, Liu J, Zhao C, Li Z, Huang Y, Yu H, Xu B, Yang X, Zhu D, Zhang X, Zhang R, Feng H, Zhao X, Li Z, Li H, Yang H (2017) Unmanned aerial vehicle remote sensing for field-based crop phenotyping: current status and perspectives. Front Plant Sci. https://doi.org/10.3389/fpls.2017.01111

Yue X, Ling K, Hong T, Gan M, Liu Y, Wang L (2018) Distribution model of chlorophyll content for Longan leaves based on hyperspectral imaging technology. Trans Chinese Soc Agric Machin 49(08):18–25

Zhang J, Pu R, Wang J, Huang W, Yuan L, Luo J (2012) Detecting powdery mildew of winter wheat using leaf level hyperspectral measurements. Comput Electron Agric 85:13–23

Zhang J, Yuan L, Pu R, Loraamm RW, Yang G, Wang J (2014) Comparison between wavelet spectral features and conventional spectral features in detecting yellow rust for winter wheat. Comput Electron Agric 100:79–87

Zhang Y, Zheng L, Li M, Deng X, Ji R (2015) Predicting apple sugar content based on spectral characteristics of apple tree leaf in different phenological phases. Comput Electron Agric 112:20–27

Zhang J, Li M, Sun Z, Liu H, Sun H, Yang W (2018) Chlorophyll content detection of field maize using RGB-NIR camera. IFAC-Papers OnLine 51(17):700–705

Zhang J, Huang Y, Pu R, Gonzalez-Moreno P, Yuan L, Wu K, Huang W (2019a) Monitoring plant diseases and pests through remote sensing technology: a review. Comput Electron Agric 165:104943

Zhang J, Liu X, Liang Y, Cao Q, Tian Y, Zhu Y, Cao W, Liu X (2019b) Using a portable active sensor to monitor growth parameters and predict grain yield of winter wheat. Sensors 19(5):1108

Zhao C, Jiang A, Huang W, Liu K, Liu L, Wang J (2007) Evaluation of variable-rate nitrogen recommendation of winter wheat based on SPAD chlorophyll meter measurement. N Z J Agric Res 50(5):735–741

Zhao Y, Chen X, Cui Z, Lobell DB (2015) Using satellite remote sensing to understand maize yield gaps in the North China plain. Field Crop Res 183:31–42

Zheng T, Liu N, Wu L, Li M, Sun H, Zhang Q, Wu J (2018) Estimation of chlorophyll content in potato leaves based on spectral red edge position. IFAC-Papers OnLine 51(17):602–606

Zhong Z, Sun H, Li M, Zhang F, Li X (2014) Development of a vehicle-mounted crop detection system. J Integr Agric 13(6):1284–1292

Zhong L, Hu L, Zhou H (2019) Deep learning based multi-temporal crop classification. Remote Sens Environ 221:430–443

Zhou L, Mu H, Ma H, Chen G (2019) Remote sensing estimation on yield of winter wheat in North China based on convolutional neural network. Trans Chinese Soc Agric Eng 35(15):119–128

Zhu Y, Cen H, El-manawy AI, Weng H, He Y (2019) A feature extraction method based on deep learning using hyperspectral imaging for the evaluation of oilseed grape canopy nitrogen content grades. 2019 ASABE annual international meeting, USA, Boston, Massachusetts July 7–10, 2019, paper number: 1900541

Zong Z, Zhao S, Liu G (2019) Coronal identification and centroid location of maize seedling stage. Trans Chinese Soc Agric Machin 50(S1):27–33

Chapter 9
Perspectives of Soil and Crop Sensing in Smart Agriculture

Liping Chen, Daming Dong, and Guijun Yang

Abstract Sensors, especially soil and crop sensors, play an important role in the development of smart agriculture. There are both opportunities and challenges in soil and crop sensor technologies. A typical problem faced is that most soil and crop sensors currently used in agriculture are industrial sensors, which cannot meet the requirements of agricultural production and agricultural environments. Many important parameters of soil and crops cannot be measured using current sensors. There is an urgent need to improve the accuracy, precision, and intelligence level for crop and soil sensors. Herein, the problems and challenges of modern soil and crop sensors are firstly proposed, and the indicators perceived in the future smart agriculture are analyzed. Then some advanced sensor techniques are introduced, which may inspire the novel sensor techniques for crop and soil sensing. These advanced sensors include most popular soil and crop sensors, from soil nutrient sensors to heavy metal sensors and from sensors used in crop phenotyping to hormone sensors for crops, electrochemical sensors, and optical sensors. A special type of satellite-based sensors for crops and soils is also discussed, which shares a similar principle with ground-based sensors, which work in quite different ways. Finally, the perspectives for further research and development of soil and crop sensors are proposed.

Keywords Soil sensor · Crop sensor · Remote sensing · Phenotyping · Optical sensors · Smart agriculture

L. Chen (✉) · D. Dong
National Engineering Research Center of Intelligent Equipment for Agriculture, Beijing, China
e-mail: chenlp@nercita.org.cn

G. Yang
National Engineering Research Center for Information Technology in Agriculture, Beijing, China

M. Li et al. (eds.), *Soil and Crop Sensing for Precision Crop Production*, Agriculture Automation and Control, https://doi.org/10.1007/978-3-030-70432-2_9

Sensors are very important in smart agriculture. The sensing of soil and crop information determines the process of fertilization, application of agricultural materials, field management, and decision-making for smart agriculture. Therefore, the development level of smart agriculture depends on the level of accuracy, precision, and intelligence of sensing technology for crops and soil. In the past 30 years, although the sensing technologies for crops and soil have made great progress, they still face several problems. A typical problem is that most soil and crop sensors currently used in agriculture are industrial sensors, rather than sensors specially designed for agriculture, and they cannot well meet the requirements of agriculture. This restricts the development of sensing technology for crops and soil. There are many difficulties and challenges in the field of crop and soil sensing, such as the complexity of the soil matrix and detection of many trace elements. On the other hand, the development of sensing technology is also an opportunity. The considerable progress of sensing technology for crops and soil will advance the development of smart agriculture. Thus, it is necessary to analyze the bottlenecks and problems of sensing technology for crops and soil in smart agriculture. The possible development of sensing technology for crops and soil in the future will be discussed through the review of sensing technology in the past 30 years.

9.1 Opportunities and Challenges of Sensing Technology for Crops and Soil

9.1.1 Limitations of Sensing Technology for Crops and Soil at Present

At the current stage, important progress has been made on comprehensive soil sensing under the development of transducing and measuring technology and the progress of physics, chemistry, biology, material science, and other technologies. In particular, significant accomplishments have been achieved using current technology to detect some specific soil and crop indicators. In terms of soil measurement, previous soil sensors mostly relied on simple physical principles. For example, soil moisture was detected by measuring the soil capacitance (Kojima et al. 2016) and soil temperature was detected by measuring the soil thermocouples (Qiu et al. 1998). Now, neutron scattering can be also used to measure moisture (Franz et al. 2016). The soil pollutants can be detected by a variety of different principles, including physical, chemical, and biological methods (Teng et al. 2014). In terms of crop sensing, many indicators can be measured using on-site and fast handheld sensors, which could not be measured by sensors before (Onwude et al. 2016). For example, chlorophyll was measured using spectrophotometry after grinding and extraction in the past (Onwude et al. 2016). But now, the content of various components of the leaves, including moisture, nitrogen, and chlorophyll, can be determined using the reflectivity of crop and laser-induced fluorescence (Onwude et al. 2016; Padilla

et al. 2018). The development of these technologies has promoted the advancement of modern agricultural technology. Compared with two or three decades ago, several indicators of crops and soil, whether beneficial or harmful, can be measured by sensors.

However, significant limitations of sensing technologies for crops and soil still exist at present (Tripodi et al. 2018). There are two main reasons for these limitations. One is the disconnection of professional skills between professionals of sensing technology and professionals of agronomy. The other is the gap in the development of technology itself.

The first limitation is that the measurement indicators of current sensors still need to be further improved. Many concerned indicators in crops and soil still cannot be obtained by sensors. For example, there are no commercial sensors on the market to rapidly measure crop hormones, and some soil nutrients cannot be measured by sensors at present. In fact, in these areas, some sensing technologies have potential. With the advancement of science and technology and the further integration of sensing technology and agriculture, a number of potential technologies will be applied to the measurement of crop and soil properties. The application of these technologies will broaden the sensing range and make it possible to sense an increasing number of precision indicators of crops and soil. Thereby the development of precision agriculture and smart agriculture will be further promoted.

The second significant limitation is that the precision of crop and soil sensors need to be further improved due to the unstructured nature of agriculture. For example, when measuring soil moisture using time domain reflectometry, the high-precision measurement result of soil moisture can be obtained under the condition of a very uniform soil structure, which has been proved in laboratory experiments (Stangl et al. 2009; Cristi et al. 2016). However, in actual measurement, the sensor needs to be recalibrated before each measurement due to the influence of soil particle size, compactness, type, texture, and other factors. In addition, most of the sensors currently used in agriculture are industrial sensors, which cannot meet the needs of agriculture in terms of measurement range, sensitivity, vegetation photosynthetic physiology probing and gross primary productivity (GPP) estimation. The sensitivity and measurement range of the sensor are contradictory. A lower detection limit often corresponds to a small range, while a large range will lead to decreased sensitivity. Therefore, the mature industrial sensors in market are not suitable for agricultural measurement. The sensitivity, measurement range, and other technical indicators of the sensor also need to be considered and weighed.

The third significant limitation is the poor environmental adaptability and reliability of the sensor. Although the high reliability of sensors is required in many industrial applications, the reliability of industrial sensors cannot meet the requirements of agricultural applications in the open field environment. It is difficult for sensors to work stably for a long time due to the many extreme sensor supplication conditions in agriculture (Lindblom et al. 2017). For example, in crop measurement, especially in the application of crop sensors in the greenhouse environment, sensors often face the effects of high temperature, high humidity,

Fig. 9.1 Complex application scenarios for agricultural environmental monitoring (high temperature, high humidity, strong radiation, dust pollution, and corrosion)

and high dew point, as shown in Fig. 9.1. The temperature sensors commonly used in industry can often be damaged within days due to the high-humidity environment when applied to facility agriculture. Therefore, how to develop sensors with high reliability and high environmental adaptability is still a technical problem to agricultural sensors.

9.1.2 Indicators Perceived in Smart Agriculture

With the development of various sensing technologies and the application of these sensing technologies in industrial, medical, environmental, and other fields, it is inevitable that several indicators can be monitored and sensed quickly in real time. Therefore, there will be an increasing number of sophisticated and diverse indicators to be detected and sensed in the future smart agriculture. Furthermore, crop sensing and soil sensing are some of its most important parts (Lindblom et al. 2017).

First, in the application of soil sensors, a number of physical parameters need to be detected, such as soil moisture profile and soil compactness. With the development of smart agriculture, the monitoring accuracy of these sensors needs to be further improved, such as the measurement of soil moisture. At present, most

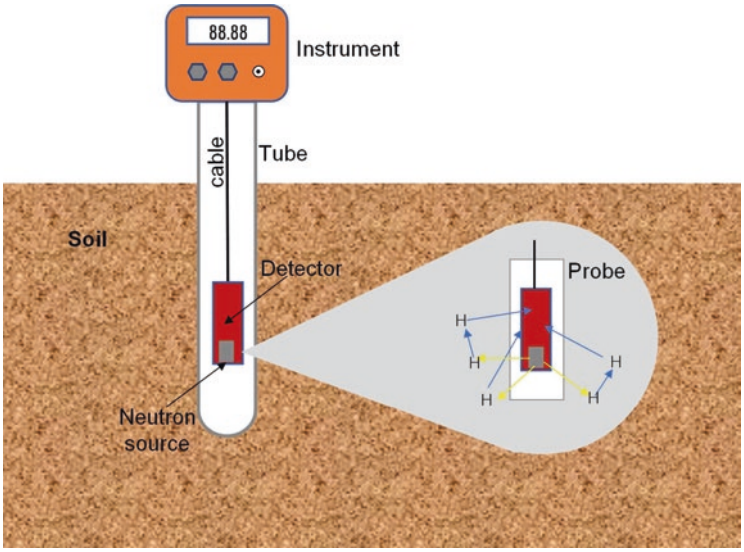

Fig. 9.2 Principles and applications of neutron soil moisture meter

sensors rely on the calibration to improve the accuracy. Although the neutron sensor has problems of radiation (Fig. 9.2), it is still more precise. With the development of technologies, the optics and electromagnetism will measure a number of soil indexes in a distributed, imaging manner. They can satisfy the sensing of soil moisture information at both a certain point and different points of a section and thus more elaborately guide agricultural production (Franz et al. 2016; Steven and Evett 2009).

The other important indexes are soil chemical parameters, especially soil nutrient parameters. The diagnosis of nutrient information will be the premise of the development of precision agriculture. Therefore, there will be a number of new technologies, such as infrared spectroscopy, laser spectroscopy, and nuclear magnetic resonance spectroscopy, for the measurement of soil nitrogen, phosphorus, and potassium, as well as other effective nutrients and trace elements. These sensors will further improve the efficiency of smart agriculture (Sinfield et al. 2010; Mukherjee and Laskar 2019). Another factor is the pollutant content in soil, including heavy metals and some persistent pollutants. Especially for persistent pollutants, there is no particularly suitable sensing method at present, but with the development of chemical sensing technology and biosensor technology, it will become possible to monitor persistent pollutants continuously and in real time (Baydarashvili et al. 2017; Meng et al. 2017). Due to the continuous integration of industry and agriculture, persistent pollutants will be a major crisis facing agriculture, so real-time and rapid monitoring of persistent pollutants is of great significance for agricultural development.

The sensing of biological substances in soil is a new challenge. In the past, few sensors were able to collect information in the soil such as microorganisms and humus. With the development of agriculture in the future, the content of

Table 9.1 Summary of indicators in soil

Indicator type	Soil parameters
Physical indicators	Color, texture, structure, porosity, compactness, permeability, bulk density, water content, field water capacity, volume capacity, temperature, infiltration, porosity
Chemical indicators	pH, electrical conductivity (EC), salinity, total N, available K, available P, total organic carbon (TOC), heavy metals, POPs, PAHs, fluoride, cation exchange capacity (CEC)
Biological indicators	Microbial biomass, enzyme activity, biochar to organic char ratio, soil respiration

Bünemann et al. (2018)

microorganisms and other biological substances will also be an indispensable part of soil sensing, because the contribution of microorganisms and other bioinformatics to the soil is considerable. Some advanced sensing methods, such as fluorescence spectroscopy, can reflect the content of microorganisms in soil (Stockdale and Brookes 2006). The indicators of soil properties and corresponding soil parameters are summarized in Table 9.1.

In recent years, most studies on crop sensing methods are focused on detecting some high-content information of crops, such as crop moisture, leaf canopy temperature, chlorophyll content, and nitrogen content (Onwude et al. 2016; Padilla et al. 2018). The development trend of crop sensors in the future will be higher precision and more flexibility in sensing high-content material information, such as using handheld or ground fixed-point observation, to quickly obtain these indicators whose accuracy needs to be further improved (Virlet et al. 2017). The other aspect is the measurement of some trace substances. A typical factor is hormones, the content of which in crops is very low. Hormone are a manifestation of the response of the crop to environmental stress. The standard process of enzyme-linked immunosorbent assay (ELISA) for hormone detection is shown in Fig. 9.3, which is complicated and time-consuming. Therefore, if some hormones can be accurately measured by a handheld sensor, they can easily reflect the ability of organisms to adapt to the environment and the response to environmental stress, so as to guide the process of fertilization and pesticide application (Tsai et al. 2015). On the other hand, the measurement of some substances related to crops and food safety will also be gradually realized by handheld sensors, such as the content of heavy metals and pesticide residue, as well as some gluten protein, fat, etc.

Phenotyping is more meaningful for crops, and so many indicators of phenotyping rely on the further development of sensor technology (Table 9.2). For example, information on plant height, leaf inclination, and 1000-grain weight are detected by sensors as the morphological information of crops. In terms of some internal components, leaf nitrogen, chlorophyll, and hormone content are also included in the scope of crop phenotypic studies. Hence, the development of sensors will further provide the tool support for the accurate measurement of crop phenotypes, so as to promote the in-depth integration of phenotyping and genomics, which will also be the forefront trend of the development of smart agriculture (Zhao et al. 2019).

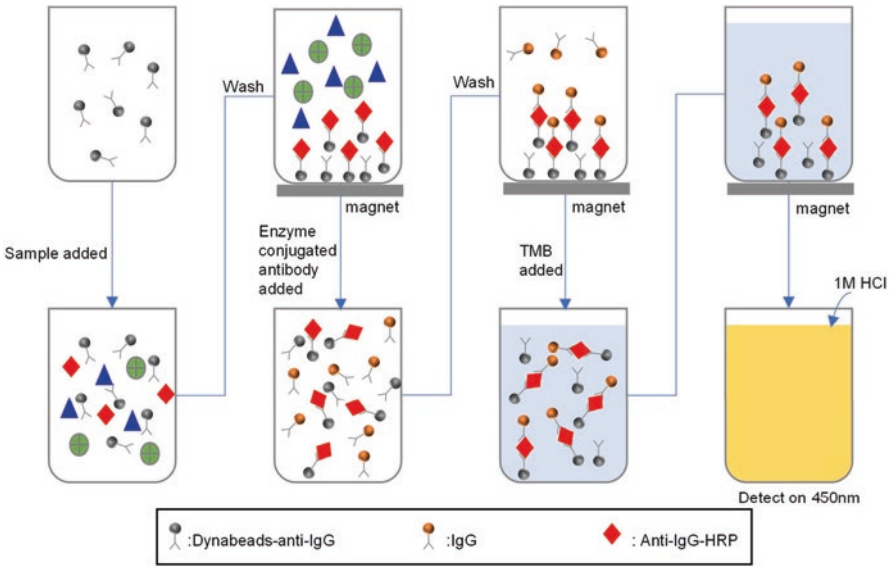

Fig. 9.3 Standard process of enzyme-linked immunosorbent assay(ELISA)for hormone detection

Table 9.2 Indicators of plant phenotype extraction

Types	Parameters
Indicators of high-throughput plant phenotyping platforms (HTPPs) in controllable environment	Plant morphology, color, and texture, multiple chlorophyll fluorescence, LAI, surface temperature, stomatal conductance, transpiration phenotype, canopy and leaf water status, seed composition, plant or organ morphology, morphology parameters, three-dimensional structure
Indicators of high-throughput plant phenotyping platforms (HTPPs) in filed environment	Ground cover, canopy height, plant geometry, growth and biomass, counting features, growth stages, vegetation indices, chlorophyll fluorescence parameters, leaf coverage, leaf inclination, light penetration depth, leaf N concentration
Plant micro-phenotypic indicators	Variation in cell size, number of cell files in the radial direction, percentage of aerenchyma, cell wall thickness, amount of cytoplasm and vacuole size, stalk diameter

Zhao et al. (2019)

9.1.3 From Field to Satellite Observation

Remote sensing makes observation take a giant leap from point to regional scale. It can monitor a regional area instantaneously or in a few seconds. We can find many new patterns we could not find before, such as spatial distribution and spatial and temporal variations. This new means surpass the cognitive limitations of humans, changes the conventional way of cognizing our earth, and provides a new vision for human and agriculture. Therefore, it has triggered the new application of sensors in the field plot scale or regional scale.

Table 9.3 Typical crop and soil parameters from remote sensing technology

Object	Level	Structural/physical	Physiological/chemical
Crop	Canopy	Green area index/leaf area index, canopy cover fraction, plant/canopy height, plant density, lodging, fPAR, albedo	CCC, CNC, WC, DM, biomass, yield, grain protein content, temperature
	Leaf	Leaf orientation, leaf area, leaf area density, leaf angle density	LCC, LNC, carotenoids, anthocyanin, WC, DM, phosphorus, color, soluble sugar and starch, etc.
Soil	Soil	Surface roughness, soil residue cover, electrical conductivity	Soil moisture, organic matter, soil nutrients (N, P, K, Ca, etc.), texture (clay, silt, and sand percentages), organic carbon content, pH, salinity, heavy metals, temperature, ET

Note: *CCC* canopy chlorophyll content, *CNC* canopy nitrogen content, *LCC* leaf chlorophyll content, *LNC* leaf nitrogen content, *DM* dry matter, *SSC* soluble solid content, *MC* moisture content, *TTA* titratable acidity, *TSS* total soluble solid, *WC* water content

Most remote sensing sensors rely on optical theories and convert electromagnetic radiation in different spectral wavelengths to electrical signal. Currently, various sensors are used in agriculture, including visual sensor (RGB), multispectral sensor, hyperspectral sensor, thermal infrared sensor, LiDAR, synthetic aperture radar (SAR), and fluorescence sensor (Weiss et al. 2019).

After 30–40 years of development, satellite remote sensing has made great progress in crop and soil monitoring. A large number of satellites, especially designed for vegetation and even agriculture, were launched, and many crop and soil parameters can be obtained from satellite remote sensing, as shown in Table 9.3.

However, remote sensing uses noncontact imaging sensors and has some inherent limitations, such as instantaneous rather than process observation (limited revisit time by satellite orbital constraints), poor penetration ability and just capturing top-surface information, easily affected by bad weather, and viewing from up to down. In addition, although many sensors work well when using proximal sensing in the lab or field, their accuracy drops when they are used in remote sensing. In contrast to field sensors, remote sensing faces more challenges. Since advances in proximal sensing have evolved much faster than in remote sensing, the technology gap still has to be bridged.

1. *Atmosphere effect*: The sensor will take an image at an altitude of hundreds of kilometers from space. The signal will be affected by the complex atmospheric environment. Especially, the land surface illumination from the sunlight is quite not stable. Radiometric calibration is needed to overcome these problems, also considering directional reflectance and topographic distortions.
2. *Geometric location*: Most remote sensing sensors are on mobile platform. And each pixel is expected to have accurate information about its geo-location. Typically, costly high-precision global navigation satellite system (GNSS) devices in combination with an inertial measurement unit (IMU) are required to obtain sensor location and orientation in most systems. For instance, the geometric position accuracy will be constrained by the GNSS, and the accuracy of point cloud will be constrained by the IMU.

3. *Scale problem*: Due to the spatial resolution of remote sensing, there are increased mixed pixels (mixed spectral), including shade, soil, crop, and other objects in one pixel. Different satellites with different spatial scales will make the situation more complex.
4. *More professional interpretation*: In most cases, the measurement result of the sensor is not the information we need directly. The original obtainment of the sensor is just the DN (digital number) value rather than agronomical variables, not even spectral reflection, scattering coefficient, or brightness temperature. Professional analysis or knowledge is required to interpret the imagery, such as a physical model for quantitative inversion and an image processing method.

9.2 Inspiration of Advanced Technology for Crop and Soil Sensing

9.2.1 Electrochemical Sensors

Electrochemical sensors are widely used in the fields of environmental protection, food processing, and industrial and agricultural production due to its low cost, high sensitivity, and convenient online measurement. Electrochemical sensors have the ability to detect numerous indicators, including most free ions, most inorganic molecules, and a large number of organic molecules (Hoekstra et al. 2018). Therefore, electrochemical sensors have good application prospects in detecting the chemical properties and composition in crops and soil. The electrochemical sensing technology is developing rapidly and showing many advantages, such as several detection indicators, lower limit of detection, and more convenient and efficient measurement methods. Especially in recent years, several new technologies in electrochemical sensing are developed, which will greatly expand the application in agriculture, especially in the fields of crop and soil detection (Ali et al. 2020).

First of all, a large number of advanced materials and process technologies are applied in the research and development of electrochemical sensors. For example, nanocomposite technology can improve the sensitivity and selectivity of electrochemical sensors and achieve multiobjective simultaneous measurement, which makes it possible to quantitatively measure some previously undetectable indexes, or greatly reduces the detection limit of some indexes (Lawal 2018). With its excellent electrochemical performance, graphene has been widely used as an electrode modifier to realize the sensing of analytes, which has become a research hotspot in recent years. Graphene-modified electrochemical sensors can detect extremely low-level cytochrome, organophosphorus, and antibiotics (Lawal 2018). Furthermore, graphene can be combined with various biomolecules to build electrochemical biosensors. For example, the immobilization of glucose oxidase in graphene and gold nanocomposites can realize the detection of glucose, and graphene and its derivatives can be combined with DNA or RNA to form a DNA biosensor, which can realize the detection of specific bacteria (Saidur et al. 2017). These new methods

have certain enlightenment significance for the rapid acquisition of the crop physiological state and soil physicochemical properties and components.

Miniaturization and on-chip technology is another development trend in electrochemical sensors. As a large number of microsensors have appeared at present, the consumption of samples and reagents can be greatly reduced, and ppb- or even ppt-level measurement can be achieved (Maduraiveeran et al. 2018). The stable, reliable, and shapeable sensor arrays can be cheaper and more productive as the sensitive electrodes and processing circuits are integrated on circuit boards of miniature sensors by using technologies such as etching, lithography, or printing generally. Since electrochemical microsensors can be integrated easily, a large number of different types of miniature sensors can be fixed on the surface of the chip to build a microsensing analysis system. This technology is called laboratory-on-a-chip, which can realize the analysis of inorganic ions, organic molecules, and others accurately and quickly (Economou et al. 2018). There is a wide range of applications of laboratory-on-a-chip in the biomedical and pharmaceutical fields. Combined with microfluidic technology, the detection and analysis of nucleic acids, proteins, and cells can be realized. The measurement of crop components and soil colony composition can be applied with the improvement and development of the laboratory-on-a-chip technology.

Wearable sensors have become another very obvious trend with the development of miniaturization and convenience of electrochemical sensors (Maduraiveeran et al. 2018). Generally, such sensors are designed based on flexible and stretchable electronic materials or integrated in electrochemical sensors in wearable devices such as smart watches and wristbands (Bandodkar and Wang 2014). For example, Electrozyme LLC (Boston, Massachusetts, United States) had developed a wristband product with a built-in biosensor, which can provide real-time monitoring of the content of various specific molecules (electrolyte, Na^{2+}, K^{+}, lactic acid, etc.) in sweat, so that users can view their physical conditions in real time (Economou et al. 2018). A type of biosensor gloves using extensible printed electrodes is developed by the University of California, San Diego, which rapidly detects organophosphorus pesticide residues on food surfaces (Amit et al. 2019). Wearable electrochemical sensors have very obvious advantages to monitor the biomass in the measured object in real time. After improvement and application, these technologies will have better application prospects in monitoring the biological reaction processes of crop growth or fruit ripening.

9.2.2 Optical Sensors

In recent years, optical sensors have gained unprecedented attention in many fields, due to the rapid development of related optical devices, such as photosensitive materials, lenses, refracting devices, and detectors. The development of optical sensors has also provided corresponding enlightenment for soil and crop perception.

First of all, the development of optical range sensors has been very rapid, which is mainly driven by market promotion. LiDAR is a good example and has been increasingly used in long-distance ranging. LiDAR sensors use the triangulation range imaging method, which has become the standard configuration in many automotive electronic systems. In the market, the number of manufacturers producing LiDAR with imaging-based ranging principles continues to expand, and the ranging precision has been improved but the cost is getting lower and lower. This method will also promote the development of LiDAR ranging technology in the agricultural field, especially for plant height measurement and other applications (Jimenez-Berni et al. 2018). When using lasers to measure micro-distances, laser sensors have very obvious advantages. The interference imaging of two lasers is used to measure small deformations, which is also very important in crop measurement. For example, using two laser beams to form a speckle displacement can measure some morphological changes on the crop surface (Ansari et al. 2018), which has more obvious advantages and potentials compared with current measurement methods.

Fluorescence sensing is the most likely technology for practical application in crop sensing. A schematic diagram of fluorescence, the electronic states of a fluorophore and the transitions between them, is shown in Fig. 9.4. Many studies are focusing on fluorescence spectrum sensing methods and its application in crop component measurement, especially in terms of chlorophyll measurement of leaves. Some fluorescent sensors can judge the chlorophyll and nitrogen contents of crops at short distance, while some sensors can achieve long-distance measurement of crops (Padilla et al. 2016). The load on some satellites can obtain the fluorescence induced by sunlight from crops through specific channels, and the analysis of fluorescence can be used for crop yield estimation food safety, air pollution, agricultural source gas emissions, water quality testing, and so on. Because crop components contain a large number of fluorophores, including chlorophyll a, chlorophyll b, and carotenoids, fluorescence sensors will be widely used in crop sensing. In soil measurement, the application of fluorescence sensors is relatively more difficult. However, with the continuous development of fluorescence sensing methods, such

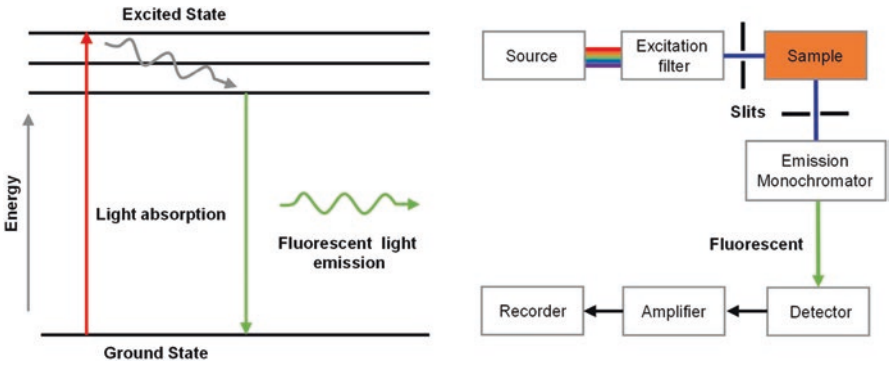

Fig. 9.4 Schematic diagram of fluorescence – the electronic states of a fluorophore and the transitions between them

as the development of time-resolved and three-dimensional fluorescence, fluorescence sensors are bound to play a more important role in crop and soil applications.

Optical scattering is a rapidly developing sensing method in recent years. There are two types of optical scattering sensors, elastic scattering without changing the laser wavelength and Raman scattering. Elastic scattering has been improved in recent years and is increasingly used in biomedicine. The scattering formed by some molecular clusters can also be used to measure trace components in crops, such as some hormones (Guerraf et al. 2019). On the other hand, elastic scattering has still not been used for crop component measurement, but it has potential in this field. Raman scattering has been used in medicine, biology, analytical chemistry, and other occasions in recent years because it can achieve molecular measurement. Figure 9.5 shows a Raman detector based on MEMS (M1S, CloudOptek Co., Ltd. Beijing, China.), which can detect various chemicals and medicines. Especially Raman scattering shows a great potential in tracing material and human metabolite analysis. However, applying Raman spectroscopy to crop measurement will first face a lot of fluorescence interferences; therefore, how to eliminate these fluorescence interferences and obtain Raman scattering signals of specific molecules in crop components is the main problem in the detection of crop component with Raman sensors.

Another kind of sensor with significant implications for the measurement of soil and crop components is the optical absorption sensor, which has increasing applications in several fields, including environmental security, food safety, air pollution, agricultural source gas emissions, water quality testing and so on. The absorption capacity, measuring methods, detector level, signal-to-noise ratio, and spectroscopic methods of optical sensors have been greatly developed with the development of these devices. Therefore, optical absorption sensors have great potential in soil and crop measurement. It should be noted that although near-infrared (NIR) and

Fig. 9.5 Raman detector based on MEMS (M1S, CloudOptek Co., Ltd.) (*Disclaimer:* Commercial products are referred to solely for the purpose of clarification and should not be construed as being endorsed by the authors or the institution with which the authors are affiliated.)

infrared optical absorption sensors are widely used in the measurement of soil component at present, many problems have still not been solved. The serious interference of soil organic matter leads to the bad specificity of absorption, and the transmissibility of many models is poor. But these problems will be gradually improved with the development of hardware and software technology. In terms of hardware, the absorption measurement of specific optical signals in different wavebands, including the development of tunable narrowband lasers, will gradually solve the matrix interference problems. Further, in terms of software, the ability and level of spectral processing will become increasingly intelligent due to the increasing applications of machine learning in spectral processing, which also can improve the detection ability of the model to some extent.

Furthermore, in addition to the enlightenment from the above optical sensing principles, we should also note another phenomenon, the implications of miniaturization of optical sensors. With the miniaturization of optical devices and the on-chip and integrated development of electronic devices, many optical systems can be made smaller and smarter. For example, the Raman spectrometer used to be a bulky system equipped with a laser, laser refrigeration system, grating spectrometer, and other modules. Thus, the volume was large and it was difficult to be applied in situ. But now the Raman spectrometer can be turned into a handheld device or even into a smart phone, which also provides the possibility for further application of optical sensing technology in the agricultural field. Many scattering and absorption sensors even can be put into the interior of the plant or the soil to achieve unprecedented simplified measurements due to the smaller and smaller volume and the on-chip characteristics of detectors. Figure 9.6 shows an example of a portable NIR module and structure (DLP NIRscan Nano EVM, Texas Instruments Incorporated, Dallas, Texas, USA). The supported wavelengths are from 900 to 1700 nm and the optical resolution is 10 nm, and the size is only 62 mm (length) × 58 mm (width) × 36 mm (height). It is because of the development of miniaturization of detectors that the

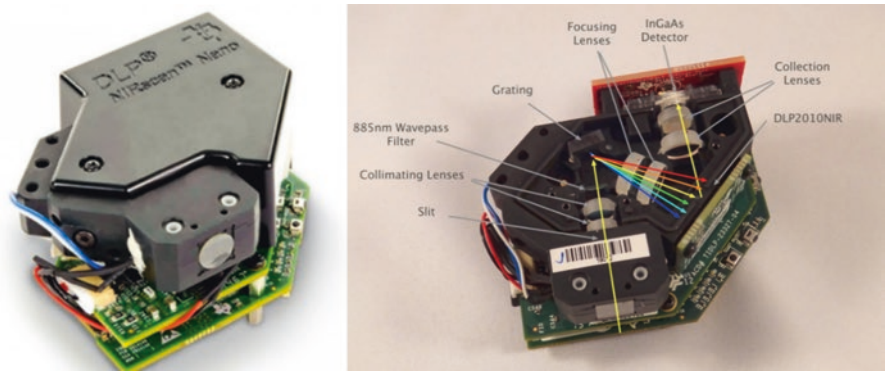

Fig. 9.6 Portable NIR module and structure (DLP NIRscan Nano EVM, Texas Instruments Incorporated, Dallas, Texas, USA) (*Disclaimer*: Commercial products are referred to solely for the purpose of clarification and should not be construed as being endorsed by the authors or the institution with which the authors are affiliated)

cost of sensing technology including optical scattering, fluorescence, absorption spectrum, and other principles will gradually decrease.

9.2.3 Other Advanced Sensors

In addition to electrochemical and optical sensors, other sensor technologies have important implications for agriculture, especially in soil and crop sensing. For example, the dielectric spectrum sensor can reflect the energy change and energy distribution between two electrodes by using the dielectric effect of materials. In the past, dielectric spectrum sensors have been widely used in biochemistry fields, as well as in the measurement of soil and rock in mountains (Cheng et al. 2014). It is of scientific significance to apply dielectric spectrum technology to soil and crop measurement. In recent years, some scientists and research institutions are trying to apply the dielectric spectrum sensor in agriculture, such as using the dielectric spectrum sensor to measure crop biomass and soil moisture (Fig. 9.7), but the current application is relatively rare. The application of the dielectric spectrum is not only limited to the measurement of the change of physical properties between two electrodes, but also to the detection of some chemical substances through the surface modification of electrode materials. It is believed that in the future, the dielectric spectrum sensors will also play an important role in the field of crop and soil sensing.

Other sensors based on electromagnetics will also have a very important application value in crop and soil measurement. For example, the nuclear magnetic spectrometer can measure the information of different substances and imaging information in the object, so it has produced very important applications in biology, medicine, flaw detection, petroleum, and other industries. However, the application of nuclear magnetic spectrometers in agriculture is still in its infancy, which is mainly determined by the irregularity of agricultural objects. In recent years, the development of nuclear magnetic spectrometers has been very rapid, especially in the measurement while drilling, which has gradually shown advantages. The

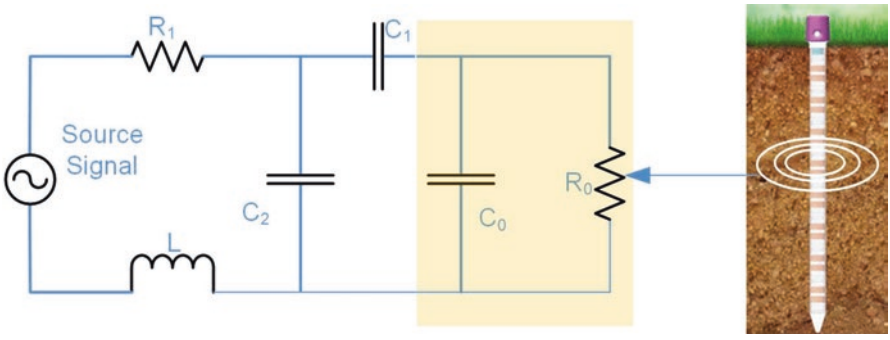

Fig. 9.7 Principle of a dielectric spectrum sensor for soil monitoring

technology is becoming increasingly advanced, and the cost has become decreasing. Therefore, it has great potential in crop water measurement and soil structure measurement. For example, the volume of nuclear magnetic resonance spectrometers is gradually decreasing, which can detect soil and crops in the field (Forouzangohar et al. 2015). It is believed that with the gradual development of magnet technology and the progress of image processing technology, nuclear magnetic spectrometers will have wider application in agriculture.

With the rapid development of sensor technology, sensors with different principles and different ways are developing very fast. It is hard to list them all in this section. It is necessary to pay attention to the development of new technologies at all times and apply some potential technologies for its transition to agriculture.

9.2.4 Lessons from Other Platforms and Missions

1. *Advanced Satellite and Ground Vehicle Platform*

Nanosatellites or CubeSats will become a trend due to their low cost and high revisit ability. A CubeSat consists of very small and lightweight units that can be joined together to form one satellite (Maes and Steppe 2019). In addition, it will be easy to establish a satellite constellation using multiple small satellites. For example, the SkySat constellation operated by Planet Labs is the very-high-resolution component of Planet's satellites. It has provided nearly daily multispectral imagery with 3-m resolution since 2016. In the future, small satellites and constellation will play an irreplaceable role in smart agriculture. In addition, UAVs and UGVs (unmanned ground vehicles) will be a promising platform (Kim et al. 2019). In recent years, UAVs show unlimited potential in agriculture, due to their low cost and high flexibility. Ground vehicles, such as tractor and robotics, as a platform of both observation and operation (spraying, harvest, etc.), will also be a promising platform.

2. *Future Satellite Mission for Earth*

The Earth Explorer-Fluorescence Explorer (FLEX) mission, a European Space Agency (ESA) future mission, will map vegetation fluorescence to quantify photosynthetic activity. The information from FLEX will lead to better insight into crop health and stress. In addition, GF and Sentinel series satellites will be improved to provide more available data. Soil Moisture Active Passive (SMAP), Soil Moisture and Ocean Salinity (SMOS), and other future satellite missions for global change monitoring, i.e., water and carbon cycle, will be launched in the future (Mohanty et al. 2017).

9.3 Prospects for Crop Sensor Technologies in Smart Agriculture

9.3.1 Crop Phenomics Sensor Technologies

As mentioned above, crop phenomics is one of the main trends in the development of modern agriculture. Thereby, new sensor technologies will play an increasingly important role in this field. Crop phenomics will step into the phase of multilevel observation (Zhao et al. 2019). New sensors can observe variables in-field from organ level to plant level and from group level to area level. Besides, the observation will be more comprehensive, more precise, and more accurate, which will be combined with metabonomics and genomics to improve the level of crop breeding in modernization and precision.

The application of new sensor technologies in crop phenomics is an important direction. There will be a rise in new sensors applied to the observation of crop phenomics, such as optical sensors and electrochemical sensors. An example is shown in Fig. 9.8 (Yuan et al. 2018). A ground-based multi-sensor phenotyping system equipped with ultrasonic sensors and light detection and ranging (LiDAR) was developed. Canopy heights of 100 wheat plots were estimated five times during a season by the ground phenotyping system and an unmanned aircraft system (UAS). The experimental results showed that the LiDAR provided the best results.

With these new sensors, the imperceptible variables before will become perceptible now, or the variables that could only be observed in the laboratory before can be observed in-field now, and the imprecise results before will become accurate now. For instance, it was difficult to observe the root systems decades ago. With the emergence of such sensors as ground-penetrating radar (GPR), the root systems can be detected accurately to meet the demands of simultaneous observation about overground and underground variables (Alani and Lantini 2020). Another example is plant hormones and diseases. In the past, detecting plant hormones and disease was difficult by sensors and usually was carried out in the laboratory. Now, some

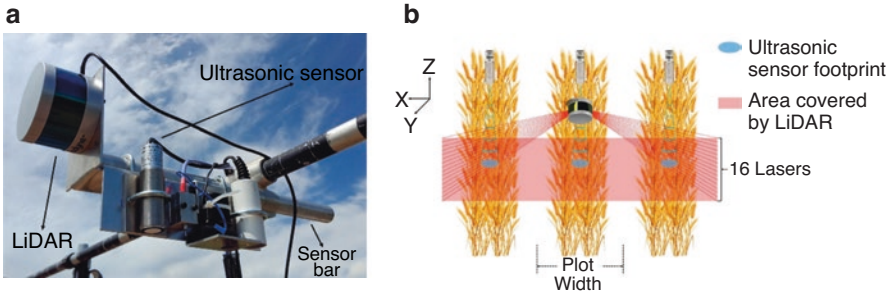

Fig. 9.8 Plant phenotypic information monitoring during the growth cycle. (Yuan et al. 2018)

spectroscopic methods and electrochemical methods will make it possible to observe them in-field. Thus, the new sensory models will be a great boost to crop phenomics.

Another important trend of crop phenotypic parameter field measurement is the study of noise reduction and elimination methods. Currently the crop phenotype measurement often depends on more diverse platforms. In the past, crop phenotypic measurement was often carried out indoors, using the pipeline method. With the development of technology, it becomes possible that the crop phenotypic measurement can be carried out in the field, such as through handheld sensors or mobile robots, to achieve rapid measurement, as shown in Fig. 9.9 (Zhao et al. 2016). This approach is an increasingly important trend. On the other hand, even if it is not obtained by moving and only by fixed-point observation, it is still subject to many noises in the field, such as the shelter of some leaves and the influence of light. Many important parameters can be measured in the laboratory without any problem, but in the field, the noise is very obvious. For example, for simple plant height and leaf inclination, the deviation of machine vision will be very small when measured in the laboratory by pipeline. However, since the outdoor environment is complex,

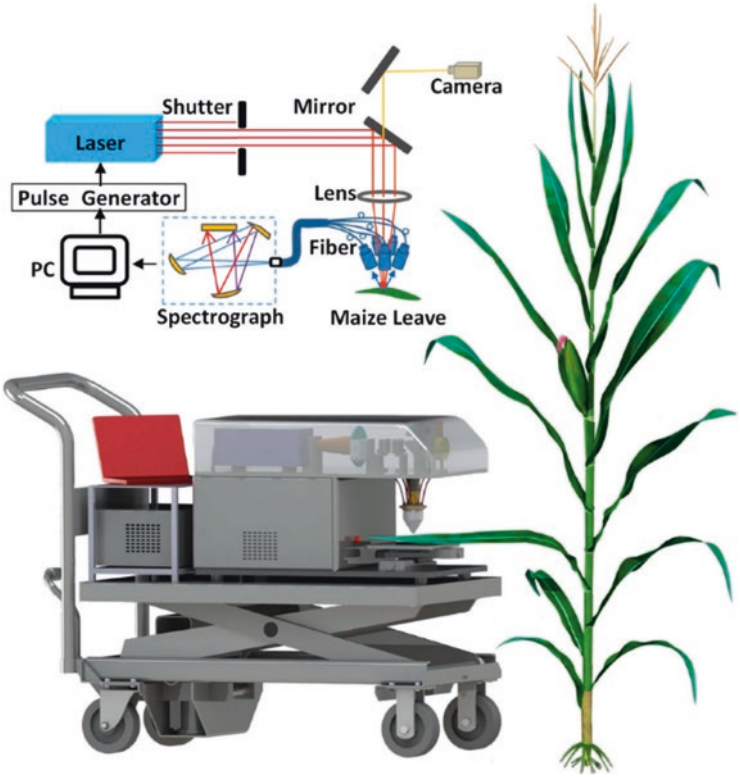

Fig. 9.9 Multiple elements of the three-dimensional distribution measurement using field robot and laser-induced plasma spectroscopy. (Zhao et al. 2016)

whether through fixed-point observation or moving observation, the visual error will cause the distortion of the phenotypic parameters, which makes it difficult for the measurement accuracy to meet the actual needs. Therefore, with the development of technology, it is very important to realize the field measurement of the crop phenotype in mobile environments. This is also an important technology development trend in the future.

9.3.2 Sensing for Crop Nutritional Status

The nutritional status of crops during growth is one of the important directions and trends of crop nutrition sensors. These nutritional statuses are mainly used to regulate precision agricultural operations, especially to guide irrigation and fertilization operations. The content of water and concentrations of nitrogen, phosphorus, and potassium are typical indicators. In the past, agricultural production was usually managed by fertilization and irrigation according to the instructions on the indicator map. For example, irrigation was carried out when soil moisture was relatively low and corresponding fertilizers were applied when soil nutrients were relatively deficient. However, farmers need to monitor the soil nutrition and understand the nutrition level of crops when they need to carry out fertilizing and irrigation in the ideal static working environment, so that the production will be more economical. Therefore, it is an important trend to realize the online fast perception of crop nutritional status. The existing sensing methods cannot fully and accurately realize the online fast perception of crop nutritional status. However, with the development of sensing technology, there will be an increase in the number of sensing methods applied to the exploration of crop nutritional status. For example, the diffuse reflectance spectrum of the crop canopy can be used to measure the content of chlorophyll and nitrogen in crop leaves (Wu et al. 2004). It is worth mentioning that the crop nutritional status must be distinguished from conventional elements. It is necessary to distinguish the status between all elemental forms and effective elemental forms when measuring the crop nutritional elements. For example, some specific nitrogen nutrients like nitrate nitrogen are usually more sensitive to the crop and they can reflect the crop nutritional status when measuring nitrogen levels. The meaning of total nitrogen is different from nitrate nitrogen. In the future development, it is necessary to consider the issue of effective nutrients when the sensory technology is applied to the measurement of crop nutritional elements.

With the development of modern agriculture and food science, the real-time perception of crop nutritional status is indispensable. With the improvement of people's living standard, the requirement of food quality will be higher and higher. Therefore, the nutrition of crops is not only to guide agricultural production, but also to be related to the quality of crops after harvest. Consumers have much higher concerns on the quality, safety, and nutrition of the crops after harvest. Therefore, sensors for online real-time measurement of nutrients in the production process are an

important trend in the future, and the detected indicators include selenium content, starch content, protein content, calories, etc.

9.3.3 *Sensing for Crop Pests*

Real-time measurement of crop diseases and pests in the field with sensors are extremely difficult. Although quite a few methods have been developed for the field observation of pests and diseases, most of them do not have market prospects. A more typical example is the use of images to achieve real-time measurement of crop pests and diseases. As shown in Fig. 9.10, the surface area and image characteristics of disease spots can be used to distinguish whether crops are suffering from diseases and what kind of diseases they are (Zhang et al. 2020). However, since the disease and pest images of many crops are very similar, it is difficult to use these machine vision methods to a large-scale area. Therefore, some methods use the biological effects of pathogens to achieve rapid measurement of crop pests and diseases through biosensors. However, at present these methods have not been directly applied in the field and often require plant sampling for culture in the laboratory before measurement, which is time-consuming and cannot be considered as online or in situ detection methods.

With the development of physical sensors, chemical sensors, and biosensors, these sensors will be further applied in the farm field. For example, the rapid pre-treatment of pathogens or the processing of some specific optical signals can be

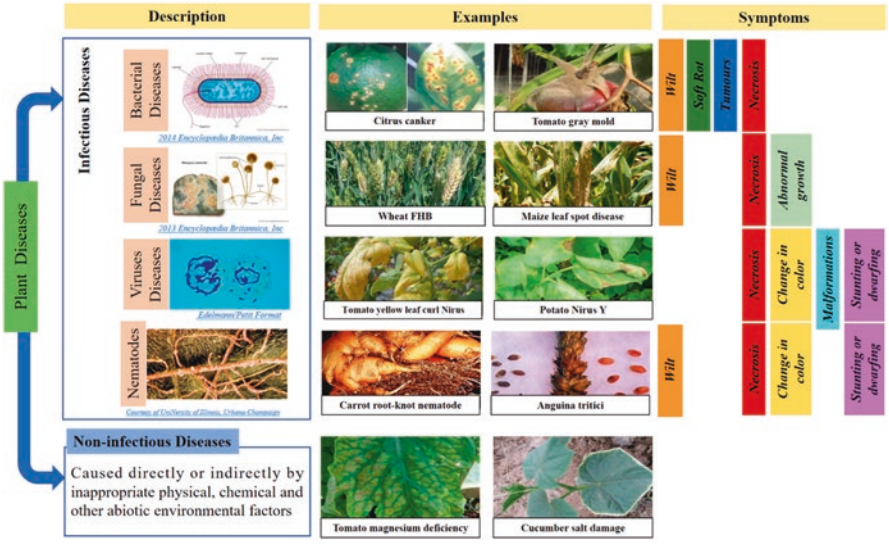

Fig. 9.10 Plant stress phenotyping isolation using the deep machine vision framework coupled with the DCNN. (Zhang et al. 2020)

used to realize the exact measurement and classification of diseases and pests in the field. This will be a huge challenge for sensor technology, and it will also have a very broad market application space.

9.3.4 Remote Sensing for Crops

For crop sensing in the future, remote sensing will inevitably step to the deeper interaction with agronomy. Many variables retrieved from remote sensing cannot directly serve or support the crop diagnosis and operation decisions. For instance, the amount of foliar chlorophyll content does not determine the definite diagnosis of nutritional stress because it is necessary to know the normal reference first. The decrease of soil moisture or foliar water content does not necessarily indicate the occurrence of agricultural drought or even water stress. Since crop is a living life, it can self-regulate to adapt to the environment and change quickly during its entire life cycle. Therefore, the water and nutrition status of crops are different based on different components (i.e., leaf position, canopy layer) at different growing stages. Particularly, many issues in smart agriculture, such as early diagnosis of nutrient/water stress, early warning of diseases and pests, distinguishing different stresses, early prediction of crop yield and quality, and quantitative assessment of agricultural disaster loss, cannot be addressed just by remote sensing. Only when integrated with agronomy knowledge, remote sensing can transfer from data to information and further to agronomical decisions. One of the potential solutions is the integration of remote sensing observation into the crop growth model. It expands the agronomy knowledge from site to regions and also expands the remote sensing observation from instantaneous monitoring to dynamical monitoring, which will help the early prediction of yield/quality and crop stress diagnosis.

Another trend will be expected from the improvement of remote sensing technology itself as described below.

1. *Integration of multi-platforms and multi-sensors.* Increasing observation dimension will help to improve the accuracy of estimated agronomical variables. And different physiological parameters are required to support crop stress diagnosis. It should be focused to exploit the complementarity of different platforms and different sensors. Satellites are the most stable and efficient platform, while UAV is the most flexible platform. Ground platforms (e.g., vehicle, tractor, or robotics) provide data with the highest resolution and accuracy, while sensor networks provide the best continuity in time. Hyperspectral sensors or multispectral sensors have the advantage in sensing pigment content, while thermal sensors are sensitive to water, and LiDAR can easily obtain the 3D structure information of crops. Future studies will therefore focus on the improved sensing integration from hybrid platforms using scaling-based approaches in order to increase the data accessibility and make optimal use of all available data sources (Latif 2018).

2. *Universally applicable models*. Extensive empirical models were developed in the past years. However, the models developed from one region may not be available in another region. It is important to develop universally applicable crop models. Physically based models, such as radiative transfer models, will help to improve the understanding of the interaction mechanism between electromagnetic wave at different spectral bands and nutritional pigment (or water content) in the leaf scale, together with physiological/structural parameters in the canopy scale. In addition, prior knowledge in this field or contextual information should be explored to constrain the estimated results.
3. *Translating scientific results into common practice*. The current requirement of practical and technical expertise for data processing hampers the routine application of remote sensing in smart agriculture. There is a clear need to standardize and harmonize the processing pipeline and to include this in commercial sensors and processing software.
4. *Cutting-edge sensing technologies*. Some new sensors have emerged in recent years, such as chlorophyll fluorescence, multispectral or hyperspectral LiDAR, miniSAR, and terahertz imaging. They are promising but problems of miniaturization and cost need to be addressed before they can be used in more remote sensing platforms.

9.4 Prospects for Soil Sensing Technology in Smart Agriculture

9.4.1 Soil Nutrient Sensors

Nutrient information in farmland soil is an important factor affecting crop growth. It is very important to master the distribution of nutrient information in soil (such as total nitrogen and organic matter) to guide agricultural production (Sinfield et al. 2010). Laboratory methods are often used to measure soil nutrients of farmland in the past, which have a long measuring period and complex process. Although the accuracy is high, it cannot meet the requirements of fast and real-time information in precision agriculture. Most of the measurement results by rapid detection methods have deviations compared with measurement in the laboratory. Besides, most of the rapid detection methods can only realize fixed-point measurement and have some disadvantages, such as time-consuming and costly, which hinders their widespread application (Mukherjee and Laskar 2019). Therefore, how to obtain and analyze nutrient information accurately in real time is the first problem to be solved in the research of smart agriculture.

Although many promising technologies have been applied to soil nutrient sensing so far, the problem of in situ soil nutrient measurement has not been solved. Therefore, soil nutrient sensing is still one of the key directions for the development of agricultural sensing technology in the next decade or even two. Many methods,

such as NIR spectroscopy, mid-infrared (MIR) spectroscopy, and ion-selective electrodes (ISE), have been applied to soil sensing, but none of them have been widely used in agricultural practice (Wang et al. 2018). Very low soil nutrient content and overly complex soil collectives are the main reasons that make soil nutrient sensing difficult. For example, the concentration of nitrate nitrogen is only about 10 ppm. However, a lot of irrelevant elements, such as soil moisture, have spatial-temporal changes that interfere with the very small amounts of nutrient information. Therefore, it is difficult for the sensor to measure the soil nutrient in situ in the field.

Further, some new technologies such as laser-induced breakdown spectroscopy (LIBS) have gradually attracted people's attention. For example, on a Mars exploration vehicle, NASA and European Space Agency use intense lasers to ablate Martian soil and rocks to generate plasma and then use plasma emission spectroscopy to measure different elements in soil and rocks, as shown in Fig. 9.11. Based on this work, researchers in the agricultural field use LIBS to detect elements in the soil. But there are still many issues that need to be solved. In addition, some new technologies such as nanotechnology, new electrochemical technology, and new nano-modified electrochemical materials are gradually being used to solve the rapid measurement of soil nutrients from different perspectives. Therefore, the rapid measurement of soil nutrients will get new development opportunities, and a number of new technologies will be integrated to produce revolutionary results.

It can be predicted that with the development of these methods, the rapid measurement of farmland soil will usher in rapid progress. Soil nutrient measurement will gradually develop from the laboratory to the field, from single measurement to compound measurement, from human measurement to machine measurement, and

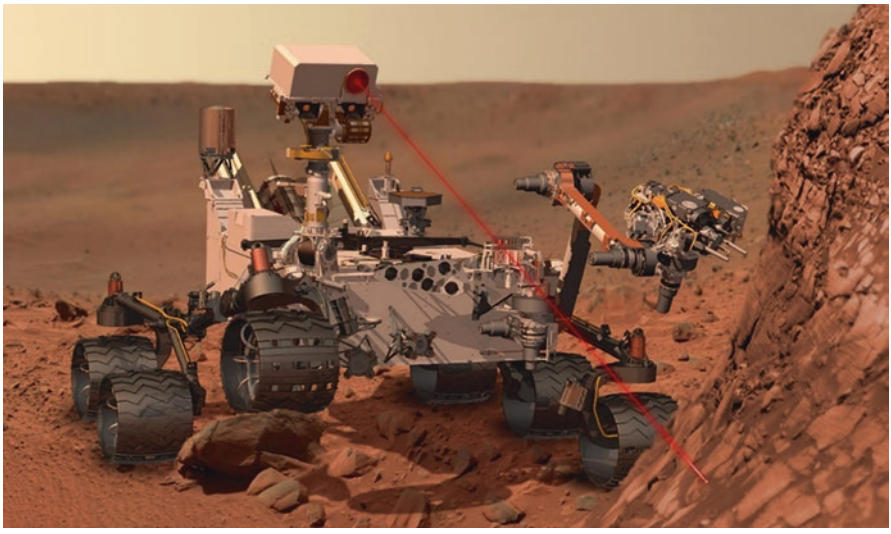

Fig. 9.11 Composition investigating the rock surface using a LIBS instrument installed on Chemistry and Camera. (https://www.jpl.nasa.gov/spaceimages/details.php?id=PIA14760)

from single-point measurement to area array measurement. These developments will promote the progress of precision agriculture and smart agriculture.

9.4.2 Soil Heavy Metal Sensors

In addition to soil nutrient information, heavy metal information is also important, and sensors of heavy metals in soil have a very important market prospect. Because of the rapid development of agriculture in the world, the pollution of heavy metals from industrial sources to agricultural sources is becoming increasingly serious, which has seriously threatened the safety level of agricultural products. It is of great significance to carry out rapid and on-site measurement of heavy metals in soil. The traditional method of soil heavy metal detection, with a series of chemical means and then a detection of large analytical instruments, is time-consuming, laborious, and expensive, which seriously restrict the development of large-scale farmland environmental monitoring.

X-ray fluorescence, as shown in Fig. 9.12, is a feasible method for the rapid measurement of soil heavy metals in recent years, but the detection limit of X-ray fluorescence still cannot meet the demands and can only be used as a qualitative measurement. With the development of new technologies, the fluorescence intensity, safety, and detection ability of X-ray fluorescence will be further developed,

Fig. 9.12 Handheld X-ray fluorescence (XRF) for soil heavy metal detection. (James Hutton Institute, https://www.hutton.ac.uk/research/groups/environmental-and-biochemical-sciences/analysis-equipment/chemical) (*Disclaimer:* Commercial products are referred to solely for the purpose of clarification and should not be construed as being endorsed by the authors or the institution with which the authors are affiliated)

which will promote the application of X-ray fluorescence in the rapid field detection of soil heavy metals (Singh et al. 2017). Furthermore, other new technologies including electrochemistry and nanometer materials will also propose new methods for detecting soil heavy metals. In any case, the detection limit is still the most important issue in soil heavy metal detection. Because the content of various heavy metals in the soil is very low, even at very low doses, it still poses a serious hazard to agricultural products. Therefore, how to quickly detect very low content of heavy metals will be the main bottleneck, and new technologies in the future will continue to work in this direction.

For physical methods such as X-ray fluorescence and laser-induced breakdown spectroscopy, the main method to improve the detection ability lies in the improvement of the physical mechanism. For example, the enhancement of the spectral signal through the confocal action of two lasers, improvement of the sensitivity, and reduction of the detection limit will make it possible to measure the heavy metals with low dose in soil. For electrochemistry and other methods, it is actually the measurement of heavy metals in the dissolved soil. Although the detection ability is sufficient, it is still needed to measure the untreated soil directly in the field. Therefore, besides the sensitivity, electrochemical sensors have to deal with the problem of how to extract the ion quickly, especially when ions exchange at very low water content. With the rapid development of new material technology, these ideas will no longer be impossible.

9.4.3 Soil Physical Parameter Sensors

Soil physical properties are also important information, including moisture, temperature, compactness, and granularity. That information represents the absorbable nutrition level and the arability level of the soil. With the development of precision agriculture and smart agriculture, in-field and fast measurement of soil physical properties is also required.

Measurement of soil physical properties should rely on the physical theories and physical characteristics, such as electrical properties, the absorption of microwave, and the reflection of an electrical signal. However, the methods become diverse and are not limited in the ordinary theories with the emergence of the new techniques. GPR is a simple example in soil detection (Wijewardana and Galagedara 2010). The sensitivity and spatial resolution of the radar is improved due to the progress in the electromagnetic field. GPR was only used in detection of the very strong root systems in the past, while it can measure root systems for density, granularity, and other properties more precisely now. Plane detection is the main difference in sensory mechanisms between GPR and conventional radar which can measure soil in large areas and multilayers in real time harmlessly. Hereby, it has obvious advantage over conventional methods. Meanwhile, other sensory mechanisms and methods, such as microwave and nuclear magnetic resonance (NMR), also measure many soil physical properties. But those methods are still limited in volume, accuracy, price, and

other aspects. Those methods will be improved and merged with the requisition of precision agriculture and the increase of additional value on farm products.

9.4.4 Prospective of Soil Sensing by Remote Sensing

In the future, remote sensing will mainly play a role in soil moisture and soil nutrition.

1. *Soil moisture*: Due to its poor penetration depth, remote sensing can only "see" the top surface of the soil or some millimeters in depth, which leads to an incomplete picture of the soil moisture profile. The potential solution may be integration with hydrological models. The surface soil moisture will be extended to the deeper soil, even the soil vertical profile in the root zones. Another obstacle is that, for most cases, agricultural soil fields are under crop cover. It is necessary to remove the vegetation effect when using remote sensing. Microwave or SAR sensors will be a promising choice. Microwave sensors are sensitive to moisture and have high penetration ability. In addition, soil moisture is a highly temporal variable and spatially heterogeneous, with varying land use having very significant differences in behavior. Ground network sensors or meteorological data should be combined since sub-daily or hourly records are needed for an accurate application of soil moisture.
2. *Soil nutrition*: Currently, soil nutrition is frequently investigated using spectral remote sensing by different researchers, include nitrogen, phosphorus, organic matter, texture (clay, silt, and sand percentage), and even heavy metals (Ladoni et al. 2010). However, it is a global challenge for real-time in situ soil measurement, even if using proximal sensing. There is a long way to really serve smart agriculture. Here some perspectives are provided. (a) Since the accurate soil mapping cannot be achieved without exhaustive soil sample collection, remote sensing will be used to guide sampling rather than predict soil properties. Remote sensing will be the auxiliary means, working together with other tools, i.e., geostatistics method. (b) Crop status will be a proxy indicator for detecting soil nutrition stress. (c) Remote sensing should be integrated with pedology and other information, such as fertilizer management, to predict soil nutrition variation (Mulder et al. 2011).
3. *Universal models*: One of the common issues in detecting soil nutrition and water by remote sensing is the model's accuracy and robustness. Apparently, the biggest obstacle is inconsistency of models obtained from different studies at different locations. Using local or regional correlation approaches may not scale for operational use over vast areas, since large variations exist among soil spectra due to soil genesis and soil formation. One possible solution to this problem is to collect an exhaustive number of soil samples from around the world, establish a global soil spectral library, and develop a universal model (Ge et al. 2011).

4. *New cutting-edge sensing technology*: In addition to SAR, gamma-ray spectrometry is another technology suitable to exploring soil texture, water, and fertilizers. Gamma-ray spectrometry can provide information down to 1 m in peaty soils and 30–60 cm in mineral soils. Airborne gamma-ray spectrometry (airplane or UAV) can provide valuable data sets (Mohanty et al. 2017). Moreover, GPS receivers can sense soil moisture fluctuations over an area of 1000 m^2 and thus are a potential source of soil moisture in regions (Chew et al. 2016).

References

Alani AM, Lantini L (2020) Recent advances in tree root mapping and assessment using non-destructive testing methods: a focus on ground penetrating radar. Surv Geophys 41:605–646

Ali MA, Dong L, Dhau J, Khosla A, Kaushik A (2020) Perspective – electrochemical sensors for soil quality assessment. J Electrochem Soc 167:37550

Bandodkar JA, Wang J (2014) Non-invasive wearable electrochemical sensors: a review. Trends Biotechnol 32(7):363–371

Amit M, Mishra RK, Hoang Q, Galan AM, Wang J, Ng TN (2019) Point-of-use robotic sensors for simultaneous pressure detection and chemical analysis. Mater Horizons 6(3):604–611

Ansari MZ, Mujeeb A, Nirala AK (2018) Assessment of biological leaf tissue using biospeckle laser imaging technique. Laser Phys 28(6):65608

Baydarashvili M, Shrednik N, Spasovskaia A (2017) Detection method of pollution with heavy metals ions of the soil. Proc Eng 189:630–636

Bünemann EK, Bongiorno G, Bai Z, Creamer RE, De Deyn G, de Goede R, Fleskens L, Geissen V, Kuyper TW, Mder P (2018) Soil quality – a critical review. Soil Biol Biochem 120:105–125

Cheng Q, Sun YR, Xue XZ, Guo J (2014) In situ determination of soil freezing characteristics for estimation of soil moisture characteristics using a dielectric tube sensor. Soil Sci Soc Am J 78(1):133–138

Chew C, Small EE, Larson KM (2016) An algorithm for soil moisture estimation using GPS-interferometric reflectometry for bare and vegetated soil. GPS Solutions 20:525–537

Cristi F, Fierro V, Suárez F, Muñoz JF, Hausner MB (2016) A TDR-waveform approach to estimate soil water content in electrically conductive soils. Comput Electron Agric 121:160–168

Economou A, Kokkinos C, Prodromidis M (2018) Flexible plastic, paper and textile lab-on-a chip platforms for electrochemical biosensing. Lab Chip 18(13):1812–1830

Forouzangohar M, Baldock JA, Smernik RJ, Hawke B, Bennett LT (2015) Mid-infrared spectra predict nuclear magnetic resonance spectra of soil carbon. Geoderma 247–248:65–72

Franz TE, Wahbi A, Vreugdenhil M, Weltin G, Heng L, Oismueller M, Strauss P, Dercon G, Desilets D (2016) Using Cosmic-ray neutron probes to monitor landscape scale soil water content in mixed land use agricultural systems. Appl Environ Soil Sci 2016:1–11

Ge Y, Thomasson JA, Sui R (2011) Remote sensing of soil properties in precision agriculture: a review. Front Earth Sci 5(3):229–238

Guerraf AE, Aouzal Z, Bouabdallaoui M, Ben JS, El Jaouhari A, Wang R, Bazzaoui M, Bazzaoui EA (2019) Electrochemically roughened silver surface versus fractal leaf-shaped silver crystals for surface-enhanced Raman scattering investigation of polypyrrole. J Solid State Electrochem 23:1811–1827

Guo YQ, Yano T, Momii K (1998) An improved methodology to measure evaporation from bare soil based on comparison of surface temperature with a dry soil surface. J Hydrol 210:93–105

Guo GM, Niu GH, Shi Q, Lin QY, Tian D, Duan YX (2019) Multi-element quantitative analysis of soils by laser induced breakdown spectroscopy (LIBS) coupled with univariate and multivariate regression methods. Anal Methods 11(23):3006–3013

Hoekstra R, Blondeau P, Andrade, FJ (2018) Distributed electrochemical sensors: recent advances and barriers to market adoption. Analytical and Bioanalytical Chemistry 410(17):4077–4089
Jimenez-Berni JA, Deery DM, Rozas-Larraondo P, Condon AG, Rebetzke GJ, James RA, Bovill WD, Furbank RT, Sirault XR (2018) High throughput determination of plant height, ground cover, and above-ground biomass in wheat with LiDAR. Front Plant Sci 9:237
Kim J, Kim S, Ju C, Son HI (2019) Unmanned aerial vehicles in agriculture: a review of perspective of platform, control, and applications. IEEE Access 7:105100–105115
Kojima Y, Shigeta R, Miyamoto N, Shirahama Y, Nishioka K, Mizoguchi M, Kawahara Y (2016) Low-Cost Soil Moisture Profile Probe Using Thin-Film Capacitors and a Capacitive Touch Sensor. Sensors 16(8)
Ladoni M, Ladoni M, Bahrami HA, Bahrami HA, Alavipanah SK, Norouzi AA (2010) Estimating soil organic carbon from soil reflectance: a review. Precis Agric 11:82–99
Latif MA (2018) An agricultural perspective on flying sensors: state of the art, challenges, and future directions. IEEE Geosci Remote Sens Magaz 6(4):10–22
Lawal AT (2018) Progress in utilisation of graphene for electrochemical biosensors. Biosens Bioelectron 106:149–178
Lindblom J, Lundstr MC, Ljung M, Jonsson A (2017) Promoting sustainable intensification in precision agriculture: review of decision support systems development and strategies. Precis Agric 18(3):309–331
Maduraiveeran G, Sasidharan M, Ganesan V (2018) Electrochemical sensor and biosensor platforms based on advanced nanomaterials for biological and biomedical applications. Biosens Bioelectron 103:113–129
Maes WH, Steppe K (2019) Perspectives for remote sensing with unmanned aerial vehicles in precision agriculture. Trends Plant Sci 24(2):152–164
Meng D, Zhao N, Wang Y, Ma M, Fang L, Gu Y, Jia Y, Liu J (2017) On-line/on-site analysis of heavy metals in water and soils by laser induced breakdown spectroscopy. Spectrochim Acta B Atomic Spectrosc 137:39–45
Mohanty BP, Cosh MH, Lakshmi V, Montzka C (2017) Soil moisture remote sensing: state-of-the-science. Vadose Zone J 16(1):1–9
Mukherjee S, Laskar S (2019) Vis–NIR-based optical sensor system for estimation of primary nutrients in soil. J Opt 48:87–103
Mulder VL, de Bruin S, Schaepman ME, Mayr TR (2011) The use of remote sensing in soil and terrain mapping – a review. Geoderma 162(1-2):1–19
Onwude DI, Hashim N, Chen G (2016) Recent advances of novel thermal combined hot air drying of agricultural crops. Trends Food Sci Technol 57:132–145
Padilla FM, Peña-Fleitas MT, Gallardo M, Thompson RB (2016) Proximal optical sensing of cucumber crop N status using chlorophyll fluorescence indices. Eur J Agron 73:83–97
Padilla FM, Gallardo M, de Souza R, Thompson RB (2018) Proximal optical sensors for nitrogen management of vegetable crops: a review. Sensors 18:2083
Pasquale T, Daniele M, Accursio V, Teodoro C (2018) Sensing technologies for precision phenotyping in vegetable crops: current status and future challenges. Agronomy 8(4):57
Qiu GY, Yano T, Momii K (1998) An improved methodology to measure evaporation from bare soil based on comparison of surface temperature with a dry soil surface. Journal of Hydrology 210(1-4):93–105
Rafael H, Pascal B, Andrade FJ (2018) Distributed electrochemical sensors: recent advances and barriers to market adoption. Anal Bioanal Chem 410:4077–4089
Saidur MR, Aziz ARA, Basirun WJ (2017) Recent advances in DNA-based electrochemical biosensors for heavy metal ion detection: a review. Biosens Bioelectron 90:125–139
Sinfield JV, Fagerman D, Colic O (2010) Evaluation of sensing technologies for on-the-go detection of macro-nutrients in cultivated soils. Comput Electron Agric 70(1):1–18
Singh V, Joshi GC, Bisht D (2017) Energy dispersive X-Ray fluorescent analysis of soil in the vicinity of industrial areas and heavy metal pollution assessment. J Appl Spectrosc 84:306–311

Stangl R, Buchan GD, Loiskandl W (2009) Field use and calibration of a TDR-based probe for monitoring water content in a high-clay landslide soil in Austria. Geoderma 150(1-2):23–31
Steven R, Evett RCSJ (2009) Soil profile water content determination: spatiotemporal variability of electromagnetic and neutron probe sensors in access tubes. Vadose Zone J 8(4):926–941
Stockdale EA, Brookes PC (2006) Detection and quantification of the soil microbial biomass – impacts on the management of agricultural soils. J Agric Sci 144(4):285–302
Teng Y, Wu J, Lu S, Wang Y, Jiao X, Song L (2014) Soil and soil environmental quality monitoring in China: a review. Environ Int 69:177–199
Tripodi P, Massa D, Venezia A Cardi T (2018) Sensing Technologies for Precision Phenotyping in Vegetable Crops: Current Status and Future Challenges. Agronomy-Basel 8(4.
Tsai H, Lu Y, Liao H, Wu S, Yu F, Fuh CB (2015) Detection of rabbit IgG by using functional magnetic particles and an enzyme-conjugated antibody with a homemade magnetic microplate. Chem Central J 9:8
Virlet N, Sabermanesh K, Sadeghitehran P, Hawkesford MJ (2017) Field Scanalyzer: an automated robotic field phenotyping platform for detailed crop monitoring. Funct Plant Biol 44:143
Wang B, Liu C, Chen YW, Dong FQ, Chen S, Zhang D, Zhu JP (2018) Structural characteristics, analytical techniques and interactions with organic contaminants of dissolved organic matter derived from crop straw: a critical review. RSC Adv 8:36927–36938
Weiss M, Jacob F, Duveiller G (2019) Remote sensing for agricultural applications: a meta-review. Remote Sens Environ 236:111402
Wijewardana YGNS, Galagedara LW (2010) Estimation of spatio-temporal variability of soil water content in agricultural fields with ground penetrating radar. J Hydrol 391(1-2):24–33
Wu BF, Zhang F, Liu CL, Zhang L, Luo ZM (2004) An integrated method for crop condition monitoring. J Remote Sens 8(6):498–514
Yuan W, Li J, Bhatta M, Shi Y, Baenziger PS, Ge Y (2018) Wheat height estimation using LiDAR in comparison to ultrasonic sensor and UAS. Sensors 18:3731
Yuki K, Ryo S, Naoya M, Yasutomo S, Kazuhiro N, Masaru M, Yoshihiro K (2016) Low-cost soil moisture profile probe using thin-film capacitors and a capacitive touch sensor. Sensors-Basel 16(8):1292
Zhang N, Yang G, Pan Y, Yang X, Chen L, Zhao C (2020) A review of advanced technologies and development for hyperspectral-based plant disease detection in the past three decades. Remote Sens 12:3188
Zhao CJ, Dong DM, Du XF, Zheng WG (2016) In-field, in situ, and in vivo 3-dimensional elemental mapping for plant tissue and soil analysis using laser-induced breakdown spectroscopy. Sensors (Basel, Switzerland) 16(10):1764
Zhao C, Zhang Y, Du J, Guo X, Fan J (2019) Crop phenomics: current status and perspectives. Front Plant Sci 10:714

Index

M. Li et al. (eds.), *Soil and Crop Sensing for Precision Crop Production*,
Agriculture Automation and Control, https://doi.org/10.1007/978-3-030-70432-2